

**COMPARATIVE STUDIES ON FLOW SEPARATION DELAY OF GENERIC  
SUBSONIC AIRFOIL AND FLOW INJECTION APPROACH**

Thesis Submitted for the Award of the Degree of

**DOCTOR OF PHILOSOPHY**

**in**

**(Aerospace Engineering)**

**By**

**Ms K. Sai Priyanka(41900443)**

**Supervised By**

**Name of Supervisor(UID)**

Jv mlaljeyan(22724)

**Name of Department (Designation)**

Aerospace Engineering

(Professor)**Supervisor Affiliation**

Lovely Professional University



**LOVELY PROFESSIONAL UNIVERSITY, PUNJAB**

**2024**

## **DECLARATION**

I, hereby declared that the presented work in the thesis entitled “Comparative Studies On Flow Separation Delay Of Generic Subsonic Airfoil And Flow Injection Approach” in fulfillment of degree of Doctor of Philosophy (Ph. D.) is outcome of research work carried out by me under the supervision J V M Lal Jeyan working as Professor, in the Aerospace engineering of Lovely Professional University, Punjab, India. In keeping with general practice of reporting scientific observations, due acknowledgements have been made whenever work described here has been based on findings of other investigator. This work has not been submitted in part or full to any other University or Institute for the award of any degree.



**(Signature of Supervisor)**

Name of the scholar: K.Sai Priyanka

Registration No.:41900443

Department/school: Aerospace Engineering

Lovely Professional University,

Punjab, India

**CERTIFICATE**

This is to certify that the work reported in the Ph. D. thesis entitled “Comparative Studies On Flow Separation Delay Of Generic Subsonic Airfoil And Flow Injection Approach” submitted in fulfillment of the requirement for the reward of degree of **Doctor of Philosophy (Ph.D.)** in the Aerospace Engineering is a research work carried out by K.Sai Priyanka, 41900443, is bonafide record of his/her original work carried out under my supervision and that no part of thesis has been submitted for any other degree, diploma or equivalent course.



**(Signature of Supervisor)**

Name of supervisor: Dr. J V Muruga Lal Jeyan

Designation: Professor

Department/school: Aerospace Engineering

University: Lovely Professional University

# ABSTRACT

As it involves several technical calculations and tests, designing an aircraft is a complex procedure. One must consider various elements relating to aerodynamics, structural flexibility, and rigidity of each component of the aircraft to design and manufacture a working airplane. The same goes for building a wing to match the necessary viewpoints to make the aircraft airworthy, and several airfoils are thoroughly investigated by predicting various design characteristics of the wings. Many elements, including wing span, wing position, angle of incidence, and others, are considered when building an aircraft wing that will work. Any aircraft's design process is complicated by the airfoil specifics and wing and fuselage designs. While discussing wings, boundary layer separation is a topic that is frequently brought up. This is a crucial aspect that should be carefully considered when constructing the wing. This theory is put to use in the computation of the skin-friction drag experienced by a body as it passes through a fluid. Events and studies in a compressible flow's boundary layer are now the focus of in-depth research. A boundary layer separates when it separates from a surface and enters a wake and separation visible through the abundant region of a streamlined path, with flow slowing down as pressure increases. This border gap significantly hampers the functioning of a wing. Throughout the modern era, numerous theoretical and experimental studies were carried out to stop or fix this boundary layer separation. There were numerous strategies put out to reduce and prevent boundary layer separation. This delay is one such approach. Experimental and computational research identified a practical and simple strategy to postpone the separation from a standard airfoil, we used passive flow separation techniques such as placing a vent close to a wing's trailing edge. This study focuses on a fictitious report on boundary layer separation delay that incorporates techniques using passive stream separation approaches. The flow control boundary layer technique is covered in full in this report, which also covers regulating boundary layer detachment. Research on flow separation delay in various special airfoils is guided by varying speed, vent design, and vent alignment along the chord. We started by modeling 2D conventional airfoils and performing computational analysis on them using the ANSYS program by adjusting the airfoil's velocity and vent angle. After receiving the desired outcomes, we created 3D models of the relevant NACA 5 series airfoils. These NACA 5 series airfoil specifications were downloaded from reliable website, and Fusion 360 software was used to construct the 3D models. Different vent designs were suggested, such as circular, elliptical, rectangular, cubic, hexagonal, pentagonal, and triangular holes spaced 45mm apart from airfoil leading edge throughout the length of wing, with an equal 50 mm space between them. So, we choose to focus on the elliptical holes. The circular holes were placed where they should be on the corresponding NACA 5

series 3D models. Then, at a 5-degree spacing, these models were positioned 0 to 25 degrees. To test every potential solution, the hole placements were also changed. The completed models were then uploaded into ANSYS and computationally examined to determine drag and lift coefficients. ANSYS Fluent was used to calculate the CL, CD. for velocities from 5 to 50 m/s, laminar model, Spalart-Allmaras, and K-epsilon and K-omega were used. The airfoil with vents as well as the regular airfoil design yielded results. The findings obtained from vented airfoils were compared to those obtained from conventional ones. Upon comparison, we discovered that L, D factors on corresponding wings varied according to environments in which they were used. At initial conditions like 0,5,10,15,20,25 degrees and 5–15 m/s, it was frequently seen that there would be a slight drop of L and an rise in drag. In the later part, where the velocity varied from 15 to 25m/s at angles between 15 and 25degrees,we also discovered an improvement in the performance of the vented wing compared to the conventional ones. We can conclude from the results that vented airfoils per form impressively at highest AOA and speed, which is helpful for us in constructing a more sophisticated aircraft that can operate at higher altitudes and angles of attack. for this report, an experimental technique chosen to compare the computational data with the real data. First, teak wood and other 3Dfabricating materials were used to create a few models of the required wings (the desired wings were changed to NACA airfoils). The vent position, angle, and other desired qualities were considered when creating both the conventional and vented wings. After completion, these models were evaluated in a wind tunnel for drag, lift, CL&CD. The results were first contrasted between models with conventional and vented wings. When the required outcomes were attained, they were compared between the outcomes acquired experimentally and computationally. By comparing the data, we can conclude that the experimental and computational results were very close, with an error margin of 3-5percent. Plots between CL and CD, CL and Alpha, and CD and Alpha were created from the results. Both the conventional and vented wing results from the experimental and computational study were presented in these graphs. We may deduce from the plots and findings that the vented wing per forms worse than the conventional one sat the beginning of the process. Later, when the velocity and attack angle rise, the vented wings per form better than the conventional ones because they exhibit a situation known as a delayed boundary layer separation.

**KEYWORDS :** Flow re-attachment, Delay stall, Aerodynamics

## Acknowledgement

I'd would like to use this chance to express my heartfelt thanks and appreciation to a lot of wonderful people in my life. I could not have been who I am now without their incredible advice, mentorship, assistance, care, and love. Firstly, I want to convey my heartfelt gratefulness and sincere admiration to my research supervisor, Dr. JVM Lal, for his persistent support, advice, inspiration, and encouragement throughout the years. He picked me as his Ph.D. student. He has been invaluable in developing my research skills. I recall how he pushed me when I needed it and coached me in all technical aspects, such as strengthening my communication and technical writing abilities for publications. He has strengthened my confidence on several occasions and has never failed to keep my optimism alive. I can't thank him enough for his faith in the face of disappointment. He's certainly one of the most animated and enthusiastic persons I've ever met. I consider myself privileged to have him as my counselor. I'd also want to thank Dr. Amit Kumar Thakur, my supervisory group, for his invaluable guidance, hold, and constructive input throughout the years. I'd like to use this chance to thank him. They have also assisted me in broadening my horizons, and I thank the Aerospace Engineering department professors and non-teaching staff members for their invaluable assistance over the course of my research work. Finally, and most importantly, Thanks, my parents for giving me motivation at low times and making my journey memorable.

<b>CHAPTER1 .....</b>	<b>1</b>
<b>INTRODUCTION.....</b>	<b>1</b>
1.1    INTRODUCTION.....	1
1.2    FUNDAMENTAL FORCESACTINGONTHEOBJECTINFLIGHT.....	1
<b>CHAPTER2 .....</b>	<b>10</b>
<b>LITERATUREREVIEW .....</b>	<b>10</b>
2.1    REVIEWOF LITERATURE.....	10
<b>CHAPTER3 .....</b>	<b>37</b>
<b>DESIGNINGMODEL.....</b>	<b>37</b>
3.1    RESEARCH GAP FROM THE FINDINGS AND DESIGN IMPLEMENTATION BY USING THE AIRFOIL CO- ORDINATEVALUES .....	37
3.2    CATIADESIGNINGTOOLSOFTWARE .....	37
<b>CHAPTER4 .....</b>	<b>57</b>
<b>CFDPROCEDURE .....</b>	<b>57</b>
4.1    INTRODUCTIONTOCOMPUTATIONALFLUIDDYNAMICS.....	57
<b>CHAPTER5 .....</b>	<b>67</b>
<b>RESULTANDDISCUSIONOFCFDANALYSIS.....</b>	<b>67</b>
5.1    RESULTSANDDISCUSSIONS.....	67
5.2    ZEROATTACK ANGLE : .....	67
5.3    FIVE M/S.....	68
5.4    TEN M/S.....	68
5.5    15M/s.....	69
5.6    TWENTY M/S .....	70
5.7    25M/s.....	70
5.8    THIRTY M/S .....	71
5.9    FIFTY M/S.....	72
5.10    FIVEATTACK ANGLE : .....	74
5.11    FIVE M/S.....	74
5.12    TEN M/S.....	75
5.13    FIFTEEN M/S .....	76
5.14    TWENTY M/S .....	76
5.15    TWENTY FIVE M/S.....	78
5.16    THIRTY M/S .....	78
5.17    FIFTY M/S.....	79
5.18    TENDEGREE ATTACK ANGLE : .....	80
5.19    5M/s .....	80
5.20    TWENTY-FIVE M/S.....	83
5.21    THIRTY M/S .....	84
5.22    FIFTY M/S.....	85
5.23    FIFTEENATTACK ANGLE : .....	86
5.24    FIVE M/S.....	86

5.25	TEN M/S.....	87
5.26	FIFTEEN M/S.....	88
5.27	TWENTY FIVE M/s.....	89
5.28	THIRTY M/S.....	90
5.29	FIFTY M/S.....	91
5.30	TWENTYATTACK ANGLE : .....	92
5.31	FIVE M/S.....	92
5.32	TEN M/S.....	93
5.33	FIFTY M/S.....	96
5.34	GRAPHS : - FOR23015 FOR BOTH VENT ANDWITHOUT VENT .....	98
5.35	FIVE M/S.....	98
5.36	TEN M/S.....	99
5.37	FIFTEEN M/S.....	100
5.38	TWENTY M/S.....	101
5.39	TWENTY-FIVE M/S.....	102
5.40	THIRTY M/S.....	103
5.41	FIFTY M/S.....	103
5.42	FIVE M/S.....	105
5.43	TEN M/S.....	105
5.44	FIFTEEN M/S.....	106
5.45	TWENTY M/S.....	107
5.46	TWENTY FIVE M/s.....	108
5.47	THIRTY M/S.....	108
5.48	FIFTY M/S.....	109
5.49	FIVEATTACK ANGLE : .....	111
5.50	FIVE M/S.....	111
5.51	TWENTY M/S.....	113
5.52	TWENTY FIVE M/s.....	114
5.53	10ATTACK ANGLE : .....	117
5.54	FIVE M/S.....	117
5.55	TEN M/S.....	117
5.56	FIFTEEN M/S.....	118
5.57	TWENTY M/S.....	119
5.58	TWENTY FIVE M/s.....	120
5.59	THIRTY M/S.....	121
5.60	THIRTY M/S.....	121
5.61	FIFTY M/S.....	121
5.62	FIFTEENATTACK ANGLE : .....	123
5.63	FIVE M/S.....	123
5.64	TEN M/S.....	124
5.65	FIFTEEN M/S.....	124
5.66	TWENTY M/S.....	125
5.67	TWENTY FIVE M/s.....	126
5.68	THIRTY M/S.....	127
5.69	FIFTY M/S.....	128
5.70	TWENTYATTACK ANGLE : .....	129
5.71	FIVE M/S.....	129



5.72	TEN M/S.....	130
5.73	FIFTEEN M/S.....	131
5.74	TWENTY M/S.....	132
5.75	TWENTY-FIVE M/S.....	132
5.76	THIRTY M/S.....	133
5.77	FIFTY M/S.....	134
5.78	CHARTS : - FOR23021AIRFOIL.....	135
5.79	FIVE M/S.....	135
5.80	TEN M/S.....	136
5.81	FIFTEEN M/S.....	137
5.82	TWENTY M/S.....	138
5.83	TWENTY-FIVE M/S.....	138
5.84	THIRTY M/S.....	139
5.85	FIFTY M/S.....	140
5.86	FIVE M/S.....	141
5.87	TEN M/S.....	142
5.88	FIFTEEN M/S.....	142
5.89	TWENTY-FIVE M/S.....	144
5.90	THIRTY M/S.....	145
5.91	FIVEATTACK ANGLE.....	147
5.92	FIVE M/S.....	147
5.93	TEN M/S.....	147
5.94	FIFTEEN M/S.....	148
5.95	TWENTY M/S.....	149
5.96	TWENTY FIVE M/s.....	150
5.97	THIRTY M/S.....	150
5.98	FIFTY M/S.....	151
5.99	TENATTACK ANGLE : .....	153
5.100	FIVE M/S.....	153
5.101	TEN M/S.....	154
5.102	TWENTY M/s.....	155
5.103	THIRTY M/S.....	157
5.104	FIFTY M/S.....	157
5.105	15ATTACK ANGLE : .....	159
5.106	FIVE M/S.....	159
5.107	TEN M/S.....	160
5.108	FIFTEEN M/S.....	160
5.109	TWENTY M/s.....	161
5.110	THIRTY M/S.....	163
5.111	FIFTY M/S.....	164
5.112	TWENTY ATTACK ANGLE : .....	165
5.113	FIVE M/S.....	165
5.114	FIFTEEN M/S.....	166
5.115	TWENTY M/s.....	167
5.116	TWENTY FIVE M/s.....	168
5.117	THIRTY M/S.....	169
5.118	FIFTY M/S.....	170

5.119	CHARTS : - FOR24015.....	171
5.120	FIVE M/S.....	171
5.121	TEN M/S.....	172
5.122	FIFTEEN M/S.....	173
5.123	TWENTY M/S.....	174
5.124	TWENTY-FIVE M/S.....	175
5.125	THIRTY M/S.....	176
5.126	FIFTY M/S.....	177
5.127	FIVE M/S.....	178
5.128	TEN M/S.....	179
5.129	FIFTEEN M/S.....	180
5.130	TWENTY M/S.....	181
5.131	TWENTY FIVE M/s.....	181
5.132	THIRTY M/S.....	182
5.133	FIFTY M/S.....	183
5.134	FIVEATTACK ANGLE : .....	184
5.135	FIVE M/S.....	184
5.136	TEN M/S.....	185
5.137	FIFTEEN M/S.....	186
5.138	TWENTY M/S.....	187
5.139	TWENTY-FIVE M/S.....	187
5.140	THIRTY M/S.....	188
5.141	FIFTEEN M/S.....	189
5.142	TENATTACK ANGLE : .....	191
5.143	FIVE M/S.....	191
5.144	TEN M/S.....	192
5.145	FIFTEEN M/S.....	193
5.146	TWENTY M/S.....	193
5.147	TWENTY FIVE M/s.....	194
5.148	THIRTY M/S.....	195
5.149	FIFTY M/S.....	196
5.150	FIVEATTACK ANGLE : .....	198
5.151	FIVE M/S.....	198
5.152	TEN M/S.....	199
5.153	FIFTEEN M/S.....	199
5.154	TWENTY M/S.....	200
5.155	TWENTY FIVE M/s.....	201
5.156	THIRTY M/S.....	202
5.157	FIFTY M/S.....	203
5.158	TWENTYATTACK ANGLE : .....	204
5.159	FIVE M/S.....	204
5.160	TEN M/S.....	205
5.161	FIFTEEN M/S.....	205
5.162	TWENTY M/S.....	206
5.163	TWENTY FIVE M/s.....	207
5.164	THIRTY M/S.....	208
5.165	FIFTY M/S.....	208

5.166	FIFTY M/S.....	208
5.167	CHARTS : .....	210
5.168	FIVE M/S.....	210
5.169	TEN M/S .....	211
5.170	FIFTEEN M/S.....	212
5.171	TWENTY M/S.....	213
5.172	TWENTY FIVE M/S.....	214
5.173	THIRTY M/S .....	214
5.174	FIFTY M/S.....	215
<b>CHAPTER6 .....</b>		<b>229</b>
<b>EXPERIMENTALANALYSISWITHWINGMODELS .....</b>		<b>229</b>
6.1	EXPERIMENTALBOUNDARYCONDITIONS .....	229
<b>CHAPTER7 .....</b>		<b>251</b>
<b>RESULTS ANDDISCUSSION .....</b>		<b>251</b>
7.1	RESULTSANDDISCUSSIONS .....	251
<b>CHAPTER8 .....</b>		<b>253</b>
<b>CONCLUSION.....</b>		<b>253</b>
8.1	CONCLUSION.....	253
8.2	FUTUREPERSPECTIVE .....	253
<b>ANNEXURES .....</b>		<b>255</b>

## Listoftables

TABLE1 : DRAG AND LIFT FORCE VALUES,23015AIRFOILATZEROAOA.....	73
TABLE2 : DRAG AND LIFT FORCE VALUES,23015AIRFOILATZEROAOA.....	73
TABLE3 : DRAG AND LIFT FORCE VALUES,23015AT 5°AOA .....	80
TABLE4 : DRAG AND LIFT FORCE VALUES,23015AT 5°AOA .....	80
TABLE5 : DRAG AND LIFT FORCE VALUES FOR23015AT10°.....	86
TABLE6 : DRAG AND LIFT FORCE VALUES FOR23015AT10° .....	86
TABLE7 : DRAG AND LIFT FORCE VALUES,23015AT 15°.....	91
TABLE8 : DRAG AND LIFT FORCE VALUES,23015AT 15°.....	92
TABLE9 : DRAG AND LIFT FORCE,23015AT20°AOA .....	97
TABLE10 : DRAG AND LIFT FORCE,23015AT20°AOA.....	97
TABLE11 : DRAG AND LIFT FORCE,23021 .....	110
TABLE12 : DRAG AND LIFT FORCE,23021 .....	110
TABLE13 : DRAG AND LIFT FORCE VALUES,23021 .....	116
TABLE14 : DRAG AND LIFT FORCE VALUES,23021 .....	116
TABLE15 : DRAG AND LIFT FORCE VALUES,23021AT10°AOA.....	122
TABLE16 : DRAG AND LIFT FORCE VALUES,23021AT10°AOA.....	123
TABLE17 : DRAG AND LIFT FORCE VALUES,23021AT15AOA.....	129
TABLE18 : DRAG AND LIFT FORCE VALUES,23021AT15AOA .....	129
TABLE19 : DRAG AND LIFT FORCE VALUES,AT20° .....	135
TABLE20 : DRAG AND LIFT FORCE VALUES,AT20° .....	135
TABLE21 : DRAG AND LIFT FORCE VALUES,24015AT0°AOA.....	146
TABLE22 : DRAG AND LIFT FORCE VALUES,24015AT0°AOA.....	146
TABLE23 : DRAG AND LIFT FORCE VALUES,24015AT5°AOA .....	152
TABLE24 : DRAG AND LIFT FORCE VALUES,24015AT5°AOA .....	152
TABLE25 : DRAG AND LIFT FORCE VALUES,24015AT10°AOA.....	158
TABLE26 : DRAG AND LIFT FORCE VALUES,24015AT10°AOA.....	158
TABLE27 : DRAG AND LIFT FORCE VALUES,24015AT15°AOA.....	164
TABLE 28 : DRAG AND LIFT FORCE VALUES,DRAG AND LIFT FORCE VALUES,24015AT15°AOA .....	165
TABLE29 : DRAG AND LIFT FORCE VALUES,24015AT20°AOA .....	171
TABLE30 : DRAG AND LIFT FORCE VALUES,24015AT20°AOA .....	171
TABLE31 : DRAG AND LIFT FORCE VALUES,24021AT0°AOA.....	184
TABLE32 : DRAG AND LIFT FORCE VALUES,24021AT0°AOA.....	184
TABLE33 : DRAG AND LIFT FORCE VALUES24021AT5°AOA .....	190
TABLE34 : DRAG AND LIFT FORCE VALUES24021AT5°AOA .....	190
TABLE35 : DRAG AND LIFT FORCE VALUES,24021AT10°AOA .....	197
TABLE36 : DRAG AND LIFT FORCE VALUES,24021AT10°AOA .....	197
TABLE37 : DRAG AND LIFT FORCE VALUES,24021AT15°AOA .....	203
TABLE38 : DRAG AND LIFT FORCE VALUES,24021AT15°AOA.....	204
TABLE39 : DRAG AND LIFT FORCE VALUES,24021AT20°AOA.....	209
TABLE40 : DRAG AND LIFT FORCE VALUES,24021AT20°AOA .....	209
TABLE 41 : FLOW SEPARATION GOOD RE-ATTACHMENT NATIONAL AERONAUTICS AND SPACEADMINISTRATIONAIRFOILS.....	228
TABLE42 : BOUNDARYCONDITIONS.....	229
TABLE43 : 21012PERCENTAGEDIFFERENCE FOR BOTH THECASESEXPERIMENTALLYAND CFD.....	242
TABLE44 : 23012PERCENTAGEDIFFERENCE FOR BOTH THECASESEXPERIMENTALLYAND CFD.....	247

## List of Figures

FIGURE 1.1 : FORCES ACTING ON AN AIRCRAFT .....	1
FIGURE 1.2 : LIFT GENERATED BY AIRFOIL THROUGH DEFLECTION OF THE FLOW .....	2
FIGURE 1.3 : AIRFOIL GEOMETRY .....	5
FIGURE 1.4 : AIRFOIL PLACED AT AN ATTACK ANGLE .....	7
FIGURE 1.5 : WINGSPAN OF BOEING 777-200ER .....	7
FIGURE 6 : DESIGN-1 .....	62
FIGURE 7 : DESIGN-2 .....	62
FIGURE 8 : DESIGN-3 .....	63
FIGURE 9 : WORKBENCH TOOL VIEW ONE .....	63
FIGURE 10 : WORKBENCH TOOL VIEW CLOSED .....	64
FIGURE 11 : AIRFOIL DESIGNING WITH VENT STEP-1 .....	65
FIGURE 12 : VENT DESIGN .....	66
FIGURE 13 : VENT DESIGN MESHING .....	66
FIGURE 14 : VENT DESIGN IN WORKBENCH .....	66
FIGURE 15 : PRESSURE AND VELOCITY FOR BOTH AT FIVE M/S .....	68
FIGURE 16 : STREAMLINE FOR BOTH AT FIVE M/S .....	68
FIGURE 18 : STREAMLINE FOR BOTH AT TEN M/S .....	69
FIGURE 19 : PRESSURE FOR BOTH AT FIFTEEN M/S .....	69
FIGURE 20 : VELOCITY FOR BOTH AT FIFTEEN M/S .....	69
FIGURE 21 : STREAMLINE FOR BOTH AT FIFTEEN M/S .....	69
FIGURE 22 : PRESSURE FOR BOTH AT TWENTY M/S .....	70
FIGURE 23 : VELOCITY PLOT FOR BOTH AT TWENTY M/S .....	70
FIGURE 24 : STREAMLINE FOR BOTH AT TWENTY M/S .....	70
FIGURE 25 : PRESSURE FOR BOTH AT TWENTY FIVE M/S .....	70
FIGURE 26 : VELOCITY FOR BOTH AT TWENTY FIVE M/S .....	71
FIGURE 27 : STREAMLINE FOR BOTH TWENTY FIVE M/S .....	71
FIGURE 28 : PRESSURE FOR BOTH THIRTY M/S .....	71
FIGURE 29 : VELOCITY FOR BOTH AT THIRTY M/S .....	72
FIGURE 30 : STREAMLINE FOR BOTH AT THIRTY M/S .....	72
FIGURE 31 : PRESSURE FOR BOTH FIFTY M/S .....	72
FIGURE 32 : VELOCITY FOR BOTH AT FIFTY M/S .....	72
FIGURE 33 : STREAMLINE FOR BOTH AT FIFTY M/S .....	72
FIGURE 34 : PRESSURE AT $5^\circ$ FOR BOTH FIVE M/S .....	74
FIGURE 35 : VELOCITY AT $5^\circ$ AT FIVE M/S .....	74
FIGURE 36 : STREAMLINE AT $5^\circ$ FOR BOTH AT FIVE M/S .....	74
FIGURE 38 : VELOCITY AT $5^\circ$ FOR BOTH TEN M/S .....	75
FIGURE 37 : PRESSURE AT $5^\circ$ FOR AT TEN M/S .....	75
FIGURE 39 : STREAMLINE AT $5^\circ$ FOR BOTH AT TEN M/S .....	75
FIGURE 41 : VELOCITY AT $5^\circ$ FOR BOTH AT FIVE M/S .....	76
FIGURE 40 : PRESSURE AT $5^\circ$ FOR BOTH AT FIVE M/S .....	76
FIGURE 42 : STREAMLINE AT $5^\circ$ FOR BOTH AT FIVE M/S .....	76
FIGURE 43 : PRESSURE AT $5^\circ$ FOR BOTH AT TWENTY M/S .....	76
FIGURE 46 : PRESSURE AT $5^\circ$ FOR BOTH AT TWENTY FIVE M/S .....	77
FIGURE 45 : STREAMLINE AT $5^\circ$ FOR BOTH AT TWENTY M/S .....	77
FIGURE 44 : VELOCITY AT $5^\circ$ FOR BOTH AT TWENTY M/S .....	77

FIGURE 47 : VELOCITY AT5° FOR BOTH TWENTY FIVE M/S.....	78
FIGURE 48 : STREAMLINE AT5° FOR BOTH ATTWENTY FIVE M/S.....	78
FIGURE 49 : PRESSURE AT5° FOR BOTH ATTHIRTY M/S .....	78
FIGURE 50 : VELOCITY AT5° FOR BOTH ATTHIRTY M/S .....	78
FIGURE 51 : STREAMLINE AT5° FOR BOTH ATTHIRTY M/S .....	79
FIGURE 52 : PRESSURE AT5° FOR BOTH AT FIFTY M/S .....	79
FIGURE 53 : VELOCITY AT5° FOR BOTH AT FIFTY M/S .....	79
FIGURE 54 : STREAMLINE AT5° FOR BOTH AT FIFTY M/S .....	79
FIGURE 55 : PRESSURE AT10° FOR BOTH ATFIVE M/S .....	80
FIGURE 56 : VELOCITY AT10° FOR BOTH AT FIVE M/S .....	81
FIGURE 57 : STREAMLINE AT10° FOR BOTH ATFIVE M/S.....	81
FIGURE 58 : PRESSURE AT10° FOR BOTH AT TEN M/S .....	81
FIGURE 59 : VELOCITY AT10° FOR BOTH AT TEN M/S .....	81
FIGURE 60 : STREAMLINE AT10° FOR BOTH AT TEN M/S.....	82
FIGURE 61 : PRESSURE AT10° FOR BOTH AT FIFTEEN M/S.....	82
FIGURE 62 : VELOCITY AT10° FOR BOTH AT FIFTEEN M/S .....	82
FIGURE 63 : STREAMLINE AT10° FOR BOTH AT FIFTEEN M/S.....	82
FIGURE 64 : PRESSURE AT10° FOR ATTWENTY M/S.....	83
FIGURE 65 : VELOCITYPLOT AT10° FOR ATTWENTY M/S .....	83
FIGURE 66 : STREAMLINE AT10° FOR ATTWENTY M/S .....	83
FIGURE 67 : PRESSURE AT10° FOR BOTH AT TWENTY FIVE M/S .....	83
FIGURE 68 : VELOCITY AT10° FOR BOTH ATTWENTY FIVE M/S .....	84
FIGURE 69 : STREAMLINE AT10° FOR BOTHAT TWENTY FIVE M/S .....	84
FIGURE 70 : PRESSURE AT10° FOR BOTH ATTHIRTY M/S .....	84
FIGURE 71 : VELOCITY AT10° FOR BOTH ATTHIRTY M/S.....	84
FIGURE 72 : STREAMLINE AT10° FOR BOTH ATTHIRTY M/S.....	85
FIGURE 73 : PRESSURE AT10° FOR BOTH AT FIFTY M/S .....	85
FIGURE 74 : VELOCITY AT10° FOR BOTH AT FIFTY M/S .....	85
FIGURE 75 : STREAMLINE AT10° FOR BOTH AT FIFTY M/S.....	85
FIGURE 76 : PRESSURE AT15° FOR BOTH ATFIVE M/S .....	86
FIGURE 77 : VELOCITY AT15° FOR BOTH AT FIVE M/S .....	86
FIGURE 78 : STREAMLINE AT15° FOR BOTH ATFIVE M/S.....	87
FIGURE 79 : PRESSURE AT15° FOR BOTH AT TEN M/S .....	87
FIGURE 80 : VELOCITY AT15° FOR BOTH AT TEN M/S .....	87
FIGURE 81 : STREAMLINE AT15° FOR BOTH AT TEN M/S .....	87
FIGURE 82 : PRESSURE AT15° FOR BOTH AT FIFTEEN M/S .....	88
FIGURE 83 : VELOCITY AT15° FOR BOTH AT FIFTEEN M/S .....	88
FIGURE 84 : STREAMLINE AT15° FOR BOTH AT FIFTEEN M/S.....	88
FIGURE 85 : PRESSURE AT15° FOR BOTH ATTWENTY M/S .....	88
FIGURE 86 : VELOCITY AT15° FOR BOTH ATTWENTY M/S .....	89
FIGURE 87 : STREAMLINE AT15° FOR BOTH ATTWENTY M/S.....	89
FIGURE 88 : PRESSURE AT15° FOR BOTH ATTWENTY-FIVE M/S.....	89
FIGURE 89 : VELOCITY AT15° FOR BOTH AT TWENTY-FIVE M/S.....	89
FIGURE 90 : STREAMLINE AT15° FOR BOTHAT TWENTY FIVE M/S.....	90
FIGURE 91 : : PRESSURE AT15° FOR BOTH ATTHIRTY M/S .....	90
FIGURE 92 : VELOCITY AT15° FOR BOTH AT THIRTY M/S .....	90
FIGURE 93 : STREAMLINE AT15° FOR BOTH ATTHIRTY M/S.....	90

FIGURE 94 : PRESSURE AT15 <sup>0</sup> FOR BOTH AT FIFTY M/S .....	91
FIGURE 95 : VELOCITY AT15 <sup>0</sup> FOR BOTH AT FIFTY M/S .....	91
FIGURE 96 : STREAMLINE AT15 <sup>0</sup> FOR BOTH AT FIFTY M/S.....	91
FIGURE 97 : PRESSURE AT20 <sup>0</sup> FOR BOTH AT FIVE M/S .....	92
FIGURE 98 : VELOCITY AT20 <sup>0</sup> FOR BOTH AT FIVE M/S .....	92
FIGURE 99 : STREAMLINE AT20 <sup>0</sup> FOR BOTH AT FIVE M/S .....	92
FIGURE 100 : PRESSURE AT20 <sup>0</sup> FOR BOTH AT TEN M/S .....	93
FIGURE 101 : VELOCITY AT20 <sup>0</sup> FOR BOTH AT TEN M/S.....	93
FIGURE 102 : STREAMLINE AT20 <sup>0</sup> FOR BOTH AT TEN M/S.....	93
FIGURE 103 : PRESSURE AT20 <sup>0</sup> FOR BOTH AT FIFTEEN M/S.....	93
FIGURE 104 : VELOCITY AT20 <sup>0</sup> FOR BOTH AT FIFTEEN M/S.....	94
FIGURE 105 : STREAMLINE AT20 <sup>0</sup> FOR BOTH AT FIFTEEN M/S.....	94
FIGURE 106 : PRESSURE AT20 <sup>0</sup> FOR BOTH AT TWENTY M/S.....	94
FIGURE 107 : VELOCITY AT20 <sup>0</sup> FOR BOTH AT TWENTY M/S.....	94
FIGURE 108 : STREAMLINE AT20 <sup>0</sup> FOR BOTH AT TWENTY M/S.....	94
FIGURE 109 : PRESSURE AT20 <sup>0</sup> FOR BOTH AT TWENTY-FIVE M/S .....	95
FIGURE 110 : VELOCITY AT20 <sup>0</sup> FOR BOTH AT TWENTY-FIVE M/S .....	95
FIGURE 111 : STREAMLINE AT20 <sup>0</sup> FOR BOTH AT TWENTY-FIVE M/S .....	95
FIGURE 112 : PRESSURE AT20 <sup>0</sup> FOR BOTH AT THIRTY M/S.....	95
FIGURE 113 : VELOCITY AT20 <sup>0</sup> FOR BOTH AT THIRTY M/S.....	96
FIGURE 114 : STREAMLINE AT20 <sup>0</sup> FOR BOTH AT THIRTY M/S .....	96
FIGURE 115 : PRESSURE AT20 <sup>0</sup> FOR BOTH AT FIFTY M/S .....	96
FIGURE 116 : VELOCITY AT20 <sup>0</sup> FOR BOTH AT FIFTY M/S.....	96
FIGURE 117 : STREAMLINE AT20 <sup>0</sup> FOR BOTH AT FIFTY M/S .....	97
FIGURE 118 : CL VERSUS ATTACK ANGLE.....	98
FIGURE 119 : CD VERSUS ATTACK ANGLE.....	98
FIGURE 120 : CL VERSUS CD .....	98
FIGURE 121 : CL VERSUS ATTACK ANGLE.....	99
FIGURE 122 : CD VERSUS ATTACK ANGLE.....	99
FIGURE 123 : CL VERSUS CD .....	99
FIGURE 124 : CL VERSUS ATTACK ANGLE.....	100
FIGURE 125 : CD VERSUS ATTACK ANGLE.....	100
FIGURE 126 : CL VERSUS CD .....	100
FIGURE 127 : CL VERSUS ATTACK ANGLE.....	101
FIGURE 128 : CD VERSUS ATTACK ANGLE.....	101
FIGURE 129 : CL VERSUS CD .....	101
FIGURE 130 : CL VERSUS ATTACK ANGLE.....	102
FIGURE 131 : CD VERSUS ATTACK ANGLE.....	102
FIGURE 132 : CL VERSUS CD .....	102
FIGURE 133 : CL VERSUS ATTACK ANGLE.....	103
FIGURE 134 : CD VERSUS ATTACK ANGLE.....	103
FIGURE 135 : CL VERSUS CD.....	103
FIGURE 136 : CL VERSUS ATTACK ANGLE.....	103
FIGURE 137 : CD VERSUS ATTACK ANGLE.....	104
FIGURE 138 : CL VERSUS CD.....	104
FIGURE 139 : PRESSURE AT0 <sup>0</sup> FOR BOTH AT FIVE M/S.....	105
FIGURE 140 : VELOCITY AT0 <sup>0</sup> FOR BOTH AT FIVE M/S .....	105

FIGURE 141 : STREAMLINE AT0 <sup>0</sup> FOR BOTH AT FIVE M/S .....	105
FIGURE 142 : PRESSURE AT0 <sup>0</sup> FOR BOTH AT TEN M/S .....	105
FIGURE 143 : VELOCITY AT0 <sup>0</sup> FOR BOTH AT TEN M/S .....	106
FIGURE 144 : STREAMLINE AT0 <sup>0</sup> FOR BOTH AT TEN M/S .....	106
FIGURE 145 : PRESSURE AT0 <sup>0</sup> FOR BOTH AT FIFTEEN M/S .....	106
FIGURE 146 : VELOCITY AT0 <sup>0</sup> FOR BOTH AT FIFTEEN M/S .....	106
FIGURE 147 : STREAMLINE AT0 <sup>0</sup> FOR BOTH AT FIFTEEN M/S.....	107
FIGURE 148 : PRESSURE AT0 <sup>0</sup> FOR BOTH AT TWENTY M/S .....	107
FIGURE 149 : VELOCITY AT0 <sup>0</sup> FOR BOTH AT TWENTY M/S .....	107
FIGURE 150 : STREAMLINE AT0 <sup>0</sup> FOR BOTH AT TWENTY M/S.....	107
FIGURE 151 : PRESSURE AT0 <sup>0</sup> FOR BOTH AT TWENTY FIVE M/S.....	108
FIGURE 152 : VELOCITY AT0 <sup>0</sup> FOR BOTH AT TWENTY-FIVE M/S.....	108
FIGURE 153 : STREAMLINE AT0 <sup>0</sup> FOR BOTH AT TWENTY FIVE M/S.....	108
FIGURE 154 : PRESSURE AT0 <sup>0</sup> FOR BOTH AT THIRTY M/S .....	108
FIGURE 155 : VELOCITY AT0 <sup>0</sup> FOR BOTH AT THIRTY M/S .....	109
FIGURE 156 : STREAMLINE AT0 <sup>0</sup> FOR BOTH AT THIRTY M/S.....	109
FIGURE 157 : PRESSURE AT0 <sup>0</sup> FOR BOTH AT FIFTY M/S .....	109
FIGURE 158 : VELOCITY AT0 <sup>0</sup> FOR BOTH AT FIFTY M/S .....	109
FIGURE 159 : STREAMLINE AT0 <sup>0</sup> FOR BOTH AT FIFTY M/S .....	110
FIGURE 160 : PRESSURE AT5 <sup>0</sup> FOR BOTH AT FIVE M/S.....	111
FIGURE 161 : VELOCITY AT5 <sup>0</sup> FOR BOTH AT FIVE M/S.....	111
FIGURE 162 : STREAMLINE AT5 <sup>0</sup> FOR BOTH AT FIVE M/S .....	111
FIGURE 163 : PRESSURE AT5 <sup>0</sup> FOR BOTH AT TEN M/S .....	111
FIGURE 164 : VELOCITY AT5 <sup>0</sup> FOR BOTH AT TEN M/S .....	112
FIGURE 165 : : STREAMLINE AT5 <sup>0</sup> FOR BOTH AT TEN M/S .....	112
FIGURE 166 : PRESSURE AT5 <sup>0</sup> FOR BOTH AT FIFTEEN M/S .....	112
FIGURE 167 : VELOCITY AT5 <sup>0</sup> FOR BOTH AT FIFTEEN M/S .....	112
FIGURE 168 : STREAMLINE AT5 <sup>0</sup> FOR BOTH AT FIFTEEN M/S.....	113
FIGURE 169 : PRESSURE AT5 <sup>0</sup> FOR BOTH AT TWENTY M/S.....	113
FIGURE 170 : VELOCITY AT5 <sup>0</sup> FOR BOTH AT TWENTY M/S .....	113
FIGURE 171 : STREAMLINE AT5 <sup>0</sup> FOR BOTH AT TWENTY M/S.....	113
FIGURE 172 : PRESSURE AT5 <sup>0</sup> FOR BOTH AT TWENTY FIVE M/S.....	114
FIGURE 173 : VELOCITY AT50 FOR BOTH AT TWENTY FIVE M/S.....	114
FIGURE 174 : STREAMLINE AT5 <sup>0</sup> FOR BOTH AT TWENTY FIVE M/S.....	114
FIGURE 175 : PRESSURE AT5 <sup>0</sup> FOR BOTH AT THIRTY M/S .....	114
FIGURE 176 : VELOCITY AT5 <sup>0</sup> FOR BOTH AT THIRTY M/S .....	115
FIGURE 177 : STREAMLINE AT50 FOR BOTH AT THIRTY M/S.....	115
FIGURE 178 : PRESSURE AT5 <sup>0</sup> FOR BOTH AT FIFTY M/S.....	115
FIGURE 179 : VELOCITY AT5 <sup>0</sup> FOR BOTH AT FIFTY M/S .....	115
FIGURE 180 : STREAMLINE AT50 FOR BOTH AT FIFTY M/S .....	116
FIGURE 181 : PRESSURE AT10 <sup>0</sup> FOR BOTH AT FIVE M/S.....	117
FIGURE 182 : VELOCITY AT10 <sup>0</sup> FOR BOTH AT FIVE M/S.....	117
FIGURE 183 : STREAMLINE AT10 <sup>0</sup> FOR BOTH AT FIVE M/S .....	117
FIGURE 184 : PRESSURE AT10 <sup>0</sup> FOR BOTH AT TEN M/S .....	117
FIGURE 185 : VELOCITY AT10 <sup>0</sup> FOR BOTH AT TEN M/S.....	118
FIGURE 186 : STREAMLINE AT10 <sup>0</sup> FOR BOTH AT TEN M/S.....	118
FIGURE 187 : PRESSURE AT10 <sup>0</sup> FOR BOTH AT FIFTEEN M/S.....	118



FIGURE 188 : VELOCITY AT10 <sup>0</sup> FOR BOTH AT FIFTEEN M/S.....	118
FIGURE 189 : STREAMLINE AT10 <sup>0</sup> FOR BOTH AT FIFTEEN M/S.....	119
FIGURE 190 : PRESSURE AT10 <sup>0</sup> FOR BOTH AT TWENTY M/S.....	119
FIGURE 191 : VELOCITY AT10 <sup>0</sup> FOR BOTH AT TWENTY M/S.....	119
FIGURE 192 : STREAMLINE AT10 <sup>0</sup> FOR BOTH AT TWENTY M/S.....	119
FIGURE 193 : PRESSURE AT10 <sup>0</sup> FOR BOTH AT TWENTY FIVE M/S.....	120
FIGURE 194 : VELOCITY AT10 <sup>0</sup> FOR BOTH AT TWENTY FIVE M/S.....	120
FIGURE 195 : STREAMLINE AT10 <sup>0</sup> FOR BOTH AT TWENTY FIVE M/S.....	120
FIGURE 196 : PRESSURE AT10 <sup>0</sup> FOR BOTH AT THIRTY M/S.....	121
FIGURE 197 : VELOCITY AT10 <sup>0</sup> FOR BOTH AT THIRTY M/S.....	121
FIGURE 198 : STREAMLINE AT10 <sup>0</sup> FOR BOTH AT THIRTY M/S.....	121
FIGURE 199 : PRESSURE AT10 <sup>0</sup> FOR BOTH AT FIFTY M/S.....	121
FIGURE 200 : VELOCITY AT10 <sup>0</sup> FOR BOTH AT FIFTY M/S.....	122
FIGURE 201 : STREAMLINE AT10 <sup>0</sup> FOR BOTH AT FIFTY M/S.....	122
FIGURE 202 : PRESSURE AT15 <sup>0</sup> FOR BOTH AT FIVE M/S.....	123
FIGURE 203 : VELOCITY AT15 <sup>0</sup> FOR BOTH AT FIVE M/S.....	123
FIGURE 204 : STREAMLINE AT15 <sup>0</sup> FOR BOTH AT FIVE M/S.....	123
FIGURE 205 : PRESSURE AT15 <sup>0</sup> FOR BOTH AT TEN M/S.....	124
FIGURE 206 : VELOCITY AT15 <sup>0</sup> FOR BOTH AT TEN M/S.....	124
FIGURE 207 : STREAMLINE AT15 <sup>0</sup> FOR BOTH AT TEN M/S.....	124
FIGURE 208 : PRESSURE AT15 <sup>0</sup> FOR BOTH AT FIFTEEN M/S.....	124
FIGURE 209 : VELOCITY AT15 <sup>0</sup> FOR BOTH AT FIFTEEN M/S.....	125
FIGURE 210 : STREAMLINE AT15 <sup>0</sup> FOR BOTH AT FIFTEEN M/S.....	125
FIGURE 211 : PRESSURE AT15 <sup>0</sup> FOR BOTH AT FIFTEEN M/S.....	125
FIGURE 212 : VELOCITY PLOT AT15 <sup>0</sup> FOR BOTH AT FIFTEEN M/S.....	125
FIGURE 213 : STREAMLINE AT15 <sup>0</sup> FOR BOTH AT FIFTEEN M/S.....	126
FIGURE 214 : PRESSURE AT15 <sup>0</sup> FOR BOTH AT TWENTY FIVE M/S.....	126
FIGURE 215 : VELOCITY AT15 <sup>0</sup> FOR BOTH AT TWENTY FIVE M/S.....	126
FIGURE 216 : STREAMLINE AT15 <sup>0</sup> FOR BOTH AT TWENTY FIVE M/S.....	127
FIGURE 217 : PRESSURE AT15 <sup>0</sup> FOR BOTH AT THIRTY M/S.....	127
FIGURE 218 : PRESSURE AT15 <sup>0</sup> FOR BOTH AT THIRTY M/S.....	127
FIGURE 219 : STREAMLINE AT15 <sup>0</sup> FOR BOTH AT THIRTY M/S.....	127
FIGURE 220 : PRESSURE AT15 <sup>0</sup> FOR BOTH AT FIFTY M/S.....	128
FIGURE 221 : VELOCITY AT15 <sup>0</sup> FOR BOTH AT FIFTY M/S.....	128
FIGURE 222 : STREAMLINE AT15 <sup>0</sup> FOR BOTH AT FIFTY M/S.....	128
FIGURE 223 : PRESSURE AT20 <sup>0</sup> FOR BOTH AT FIVE M/S.....	129
FIGURE 224 : VELOCITY PLOT AT20 <sup>0</sup> FOR BOTH AT FIVE M/S.....	130
FIGURE 225 : STREAMLINE AT20 <sup>0</sup> FOR BOTH AT FIVE M/S.....	130
FIGURE 226 : PRESSURE AT20 <sup>0</sup> FOR BOTH AT TEN M/S.....	130
FIGURE 227 : VELOCITY AT20 <sup>0</sup> FOR BOTH AT TEN M/S.....	130
FIGURE 228 : STREAMLINE AT20 <sup>0</sup> FOR BOTH AT TEN M/S.....	131
FIGURE 229 : PRESSURE AT20 <sup>0</sup> FOR BOTH AT FIFTEEN M/S.....	131
FIGURE 230 : VELOCITY AT20 <sup>0</sup> FOR BOTH AT FIFTEEN M/S.....	131
FIGURE 231 : STREAMLINE AT20 <sup>0</sup> FOR BOTH AT FIFTEEN M/S.....	131
FIGURE 232 : PRESSURE AT20 <sup>0</sup> FOR BOTH AT TWENTY M/S.....	132
FIGURE 233 : VELOCITY AT20 <sup>0</sup> FOR BOTH AT TWENTY M/S.....	132
FIGURE 234 : STREAMLINE AT20 <sup>0</sup> FOR BOTH AT TWENTY M/S.....	132

FIGURE 235 : PRESSURE AT $20^0$ FOR BOTH AT TWENTY-FIVE M/S .....	132
FIGURE 236 : VELOCITY AT $20^0$ FOR BOTH AT TWENTY-FIVE M/S.....	133
FIGURE 237 : STREAMLINE AT $20^0$ FOR BOTH AT TWENTY-FIVE M/S.....	133
FIGURE 238 : PRESSURE AT $20^0$ FOR BOTH AT THIRTY M/S.....	133
FIGURE 239 : VELOCITY AT $20^0$ FOR BOTH AT THIRTY M/S.....	133
FIGURE 240 : STREAMLINE AT $20^0$ FOR BOTH AT THIRTY M/S .....	134
FIGURE 241 : PRESSURE AT $20^0$ FOR BOTH AT FIFTY M/S.....	134
FIGURE 242 : VELOCITY AT $20^0$ FOR BOTH AT FIFTY M/S.....	134
FIGURE 243 : STREAMLINE AT $20^0$ FOR BOTH AT FIFTY M/S .....	134
FIGURE 244 : CL VERSUS ATTACK ANGLE.....	135
FIGURE 245 : CD VERSUS ATTACK ANGLE.....	136
FIGURE 246 : CL VERSUS $C_d$ .....	136
FIGURE 247 : CL VERSUS ATTACK ANGLE.....	136
FIGURE 248 : CD VERSUS ATTACK ANGLE.....	136
FIGURE 249 : CL VERSUS $C_d$ .....	137
FIGURE 250 : CL VERSUS ATTACK ANGLE.....	137
FIGURE 251 : CD VERSUS ATTACK ANGLE.....	137
FIGURE 252 : CL VERSUS $C_d$ .....	137
FIGURE 253 : CL VERSUS ATTACK ANGLE.....	138
FIGURE 254 : CD VERSUS ATTACK ANGLE.....	138
FIGURE 255 : CL VERSUS $C_d$ .....	138
FIGURE 256 : CL VERSUS ATTACK ANGLE.....	138
FIGURE 257 : CD VERSUS ATTACK ANGLE.....	139
FIGURE 258 : CL VERSUS $C_d$ .....	139
FIGURE 259 : CL VERSUS ATTACK ANGLE.....	139
FIGURE 260 : CD VERSUS ATTACK ANGLE.....	139
FIGURE 261 : CL VERSUS $C_d$ .....	140
FIGURE 262 : CL VERSUS ATTACK ANGLE.....	140
FIGURE 263 : CD VERSUS ATTACK ANGLE.....	140
FIGURE 264 : CL VERSUS $C_d$ .....	140
FIGURE 265 : PRESSURE FOR BOTH AT FIVE M/S.....	141
FIGURE 266 : VELOCITY FOR BOTH AT FIVE M/S .....	141
FIGURE 267 : STREAMLINE FOR BOTH AT FIVE M/S.....	141
FIGURE 268 : PRESSURE AT $0^0$ FOR BOTH AT TEN M/S.....	142
FIGURE 269 : VELOCITY AT $0^0$ FOR BOTH AT TEN M/S .....	142
FIGURE 270 : STREAMLINE AT $0^0$ FOR BOTH AT TEN M/S .....	142
FIGURE 271 : PRESSURE AT $0^0$ FOR BOTH AT FIFTEEN M/S .....	142
FIGURE 272 : VELOCITY AT $0^0$ FOR BOTH AT FIFTEEN M/S .....	143
FIGURE 273 : STREAMLINE AT $0^0$ FOR BOTH AT FIFTEEN M/S.....	143
FIGURE 274 : PRESSURE AT $0^0$ FOR BOTH AT TWENTY M/S.....	143
FIGURE 275 : VELOCITY AT $0^0$ FOR BOTH AT TWENTY M/S .....	143
FIGURE 276 : STREAMLINE AT $0^0$ FOR BOTH AT TWENTY M/S .....	144
FIGURE 277 : PRESSURE AT $0^0$ FOR BOTH AT TWENTY-FIVE M/S .....	144
FIGURE 278 : VELOCITY AT $0^0$ FOR BOTH AT TWENTY-FIVE M/S.....	144
FIGURE 279 : STREAMLINE AT $0^0$ FOR BOTH AT TWENTY-FIVE M/S.....	144
FIGURE 280 : PRESSURE AT $0^0$ FOR BOTH AT THIRTY M/S .....	145
FIGURE 281 : VELOCITY AT $0^0$ FOR BOTH AT THIRTY M/S .....	145

FIGURE 282 : STREAMLINE AT0 <sup>0</sup> FOR BOTH AT THIRTY M/S .....	145
FIGURE 283 : PRESSURE AT0 <sup>0</sup> FOR BOTH AT FIFTY M/S .....	145
FIGURE 284 : VELOCITY AT0 <sup>0</sup> FOR BOTH AT FIFTY M/S .....	146
FIGURE 285 : STREAMLINE AT0 <sup>0</sup> FOR BOTH AT FIFTY M/S .....	146
FIGURE 286 : PRESSURE AT5 <sup>0</sup> FOR BOTH AT FIVE M/S.....	147
FIGURE 287 : VELOCITY PRESSURE AT5 <sup>0</sup> FOR BOTH AT FIVE M/S.....	147
FIGURE 288 : STREAMLINE AT5 <sup>0</sup> FOR BOTH AT FIVE M/S .....	147
FIGURE 289 : PRESSURE AT50 FOR BOTH AT TEN M/S.....	147
FIGURE 290 : VELOCITY AT5 <sup>0</sup> FOR BOTH AT TEN M/S .....	148
FIGURE 291 : STREAMLINE AT5 <sup>0</sup> FOR BOTH AT TEN M/S .....	148
FIGURE 292 : PRESSURE AT5 <sup>0</sup> FOR BOTH VENT AT FIFTEEN M/S .....	148
FIGURE 293 : VELOCITY AT5 <sup>0</sup> FOR BOTH VENT AT FIFTEEN M/S .....	148
FIGURE 294 : STREAMLINE AT5 <sup>0</sup> FOR BOTH VENT AT FIFTEEN M/S .....	149
FIGURE 295 : PRESSURE AT5 <sup>0</sup> FOR BOTH AT TWENTY M/S .....	149
FIGURE 296 : VELOCITY AT50 FOR BOTH AT TWENTY M/S .....	149
FIGURE 297 : STREAMLINE AT5 <sup>0</sup> FOR BOTH AT TWENTY M/S.....	149
FIGURE 298 : PRESSURE AT50 FOR BOTH AT TWENTY FIVE M/S .....	150
FIGURE 299 : VELOCITY AT50 FOR BOTH AT TWENTY FIVE M/S.....	150
FIGURE 300 : STREAMLINE AT50 FOR BOTH AT TWENTY FIVE M/S.....	150
FIGURE 301 : PRESSURE AT50 FOR BOTH AT THIRTY M/S .....	150
FIGURE 302 : VELOCITY AT5 <sup>0</sup> FOR BOTH AT THIRTY M/S .....	151
FIGURE 303 : STREAMLINE AT5 <sup>0</sup> FOR BOTH AT THIRTY M/S.....	151
FIGURE 304 : PRESSURE AT5 <sup>0</sup> FOR BOTH AT FIFTY M/S.....	151
FIGURE 305 : VELOCITY AT5 <sup>0</sup> FOR BOTH AT FIFTY M/S .....	151
FIGURE 306 : STREAMLINE AT5 <sup>0</sup> FOR BOTH AT FIFTY M/S .....	152
FIGURE 307 : PRESSURE AT100 FOR BOTH AT FIVE M/S .....	153
FIGURE 308 : VELOCITY AT10 <sup>0</sup> FOR BOTH AT FIVE M/S.....	153
FIGURE 309 : STREAMLINE AT10 <sup>0</sup> FOR BOTH AT FIVE M/S .....	153
FIGURE 310 : PRESSURE AT10 <sup>0</sup> FOR BOTH AT TEN M/S .....	154
FIGURE 311 : VELOCITY AT10 <sup>0</sup> FOR BOTH AT TEN M/S.....	154
FIGURE 312 : STREAMLINE AT10 <sup>0</sup> FOR BOTH AT TEN M/S.....	154
FIGURE 313 : PRESSURE AT100 FOR BOTH AT FIFTEEN M/S.....	154
FIGURE 314 : VELOCITY AT10 <sup>0</sup> FOR BOTH AT FIFTEEN M/S.....	155
FIGURE 315 : STREAMLINE AT10 <sup>0</sup> FOR BOTH AT FIFTEEN M/S.....	155
FIGURE 316 : PRESSURE AT10 <sup>0</sup> FOR BOTH AT TWENTY M/S.....	155
FIGURE 317 : VELOCITY AT10 <sup>0</sup> FOR BOTH AT TWENTY M/S.....	155
FIGURE 318 : STREAMLINE AT10 <sup>0</sup> FOR BOTH AT TWENTY M/S.....	156
FIGURE 319 : PRESSURE AT100 FOR BOTH AT TWENTY FIVE M/S .....	156
FIGURE 320 : VELOCITY AT10 <sup>0</sup> FOR BOTH AT TWENTY FIVE M/S.....	156
FIGURE 321 : STREAMLINE AT100 FOR BOTH AT TWENTY FIVE M/S .....	156
FIGURE 322 : PRESSURE AT10 <sup>0</sup> FOR BOTH THIRTY M/S.....	157
FIGURE 323 : VELOCITY AT10 <sup>0</sup> FOR BOTH THIRTY.....	157
FIGURE 324 : STREAMLINE AT10 <sup>0</sup> FOR BOTH THIRTY M/S.....	157
FIGURE 325 : PRESSURE AT10 <sup>0</sup> FOR BOTH AT FIFTY M/S.....	157
FIGURE 326 : VELOCITY AT10 <sup>0</sup> FOR BOTH AT FIFTY M/S.....	158
FIGURE 327 : STREAMLINE AT10 <sup>0</sup> FOR BOTH AT FIFTY M/S .....	158
FIGURE 328 : PRESSURE AT15 <sup>0</sup> FOR BOTH AT FIVE M/S.....	159

FIGURE 329 : VELOCITY AT15 <sup>0</sup> FOR BOTH AT FIVE M/S.....	159
FIGURE 330 : STREAMLINE AT 15 <sup>0</sup> FOR BOTH AT FIVE M/S.....	159
FIGURE 331 : PRESSURE AT150 FOR BOTH AT TEN M/S.....	160
FIGURE 332 : VELOCITY AT15 <sup>0</sup> FOR BOTH AT TEN M/S.....	160
FIGURE 333 : STREAMLINE AT15 <sup>0</sup> FOR BOTH AT TEN M/S.....	160
FIGURE 334 : PRESSURE AT150 FOR BOTH AT FIFTEEN M/S.....	160
FIGURE 335 : VELOCITY AT15 <sup>0</sup> FOR BOTH AT FIFTEEN M/S.....	161
FIGURE 336 : STREAMLINE AT15 <sup>0</sup> FOR BOTH AT FIFTEEN M/S.....	161
FIGURE 337 : PRESSURE AT15 <sup>0</sup> FOR BOTH AT TWENTY M/S.....	161
FIGURE 338 : VELOCITY PLOT AT15 <sup>0</sup> FOR BOTH AT TWENTY M/S.....	161
FIGURE 339 : STREAMLINE AT15 <sup>0</sup> FOR BOTH AT TWENTY M/S.....	162
FIGURE 340 : PRESSURE AT15 <sup>0</sup> FOR BOTH AT TWENTY FIVE M/S.....	162
FIGURE 341 : VELOCITY AT15 <sup>0</sup> FOR BOTH AT TWENTY-FIVE M/S.....	162
FIGURE 342 : STREAMLINE AT150 FOR BOTH AT TWENTY-FIVE M/S.....	162
FIGURE 343 : PRESSURE AT15 <sup>0</sup> FOR BOTH AT THIRTY M/S.....	163
FIGURE 344 : VELOCITY AT15 <sup>0</sup> FOR BOTH AT THIRTY M/S.....	163
FIGURE 345 : STREAMLINE AT15 <sup>0</sup> FOR BOTH AT THIRTY M/S.....	163
FIGURE 346 : PRESSURE AT15 <sup>0</sup> FOR BOTH AT FIFTY M/S.....	164
FIGURE 347 : VELOCITY AT15 <sup>0</sup> FOR BOTH AT FIFTY M/S.....	164
FIGURE 348 : STREAMLINE AT15 <sup>0</sup> FOR BOTH AT FIFTY M/S.....	164
FIGURE 349 : PRESSURE AT20 <sup>0</sup> FOR AT FIVE M/S.....	165
FIGURE 350 : VELOCITY AT20 <sup>0</sup> FOR AT FIVE M/S.....	165
FIGURE 351 : STREAMLINE AT20 <sup>0</sup> FOR AT FIVE M/S.....	165
FIGURE 352 : PRESSURE AT20 <sup>0</sup> FOR BOTH AT TEN M/S.....	166
FIGURE 353 : VELOCITY AT20 <sup>0</sup> FOR BOTH AT TEN M/S.....	166
FIGURE 354 : STREAMLINE AT20 <sup>0</sup> FOR BOTH AT TEN M/S.....	166
FIGURE 355 : PRESSURE AT20 <sup>0</sup> FOR BOTH AT FIFTEEN M/S.....	166
FIGURE 356 : VELOCITY AT20 <sup>0</sup> FOR BOTH AT FIFTEEN M/S.....	167
FIGURE 357 : STREAMLINE AT20 <sup>0</sup> FOR BOTH AT FIFTEEN M/S.....	167
FIGURE 358 : PRESSURE AT20 <sup>0</sup> FOR BOTH AT TWENTY M/S.....	167
FIGURE 359 : VELOCITY AT20 <sup>0</sup> FOR AT TWENTY M/S.....	167
FIGURE 360 : STREAMLINE AT20 <sup>0</sup> FOR AT TWENTY M/S.....	168
FIGURE 361 : PRESSURE AT20 <sup>0</sup> FOR BOTH AT TWENTY FIVE M/S.....	168
FIGURE 362 : VELOCITY AT20 <sup>0</sup> FOR BOTH AT TWENTY FIVE M/S.....	168
FIGURE 363 : STREAMLINE AT20 <sup>0</sup> FOR BOTH AT TWENTY FIVE M/S.....	168
FIGURE 364 : PRESSURE AT20 <sup>0</sup> FOR BOTH AT THIRTY M/S.....	169
FIGURE 365 : VELOCITY AT20 <sup>0</sup> FOR BOTH AT THIRTY M/S.....	169
FIGURE 366 : STREAMLINE AT20 <sup>0</sup> FOR BOTH AT THIRTY M/S.....	169
FIGURE 367 : PRESSURE AT20 <sup>0</sup> FOR AT FIFTY M/S.....	170
FIGURE 368 : VELOCITY PRESSURE AT20 <sup>0</sup> FOR AT FIFTY M/S.....	170
FIGURE 369 : STREAMLINE PRESSURE AT20 <sup>0</sup> FOR AT FIFTY M/S.....	170
FIGURE 370 : CL VERSUS ATTACK ANGLE.....	171
FIGURE 371 : CD VERSUS ATTACK ANGLE.....	172
FIGURE 372 : CL VERSUS CD.....	172
FIGURE 373 : CL VERSUS ATTACK ANGLE.....	172
FIGURE 374 : CD VERSUS ATTACK ANGLE.....	173
FIGURE 375 : CL VERSUS CD.....	173

FIGURE 376 : CL VERSUS ATTACK ANGLE.....	173
FIGURE 377 : CDVERSUS ATTACK ANGLE.....	174
FIGURE 378 : CL VERSUSCd.....	174
FIGURE 379 : CLVERSUS ATTACK ANGLE.....	174
FIGURE 380 : CDVERSUS ATTACK ANGLE.....	175
FIGURE 381 : CL VERSUSCd.....	175
FIGURE 382 : CL VERSUS ATTACK ANGLE.....	175
FIGURE 383 : CDVERSUS ATTACK ANGLE.....	175
FIGURE 384 : CL VERSUSCd.....	176
FIGURE 385 : CL VERSUS ATTACK ANGLE.....	176
FIGURE 386 : CDVERSUS ATTACK ANGLE.....	176
FIGURE 387 : CL VERSUSCd.....	177
FIGURE 388 : CL VERSUS ATTACK ANGLE.....	177
FIGURE 389 : CDVERSUS ATTACK ANGLE.....	177
FIGURE 390 : CL VERSUSCd.....	177
FIGURE 391 : PRESSURE AT0 <sup>0</sup> FOR BOTH AT FIVE M/S.....	178
FIGURE 392 : VELOCITY AT0 <sup>0</sup> FOR BOTH ATFIVE M/S.....	178
FIGURE 393 : STREAMLINE AT0 <sup>0</sup> FOR BOTHATFIVE M/S.....	179
FIGURE 394 : PRESSURE AT0 <sup>0</sup> FOR BOTH AT TEN M/S.....	179
FIGURE 395 : VELOCITY AT0 <sup>0</sup> FOR BOTH VENT AT TEN M/S.....	179
FIGURE 396 : STREAMLINE AT0 <sup>0</sup> FOR BOTH AT TEN M/S.....	179
FIGURE 397 : PRESSURE AT0 <sup>0</sup> FOR BOTH AT FIFTEEN M/S.....	180
FIGURE 398 : VELOCITY AT0 <sup>0</sup> FOR BOTH AT FIFTEEN M/S.....	180
FIGURE 399 : STREAMLINE AT0 <sup>0</sup> FOR BOTHAT FIFTEEN M/S.....	180
FIGURE 400 : PRESSURE AT0 <sup>0</sup> FOR BOTH AT TWENTY M/S.....	181
FIGURE 401 : VELOCITY AT0 <sup>0</sup> FOR BOTH AT TWENTY M/S.....	181
FIGURE 402 : STREAMLINE AT0 <sup>0</sup> FOR BOTHAT TWENTY M/S.....	181
FIGURE 403 : PRESSURE AT0 <sup>0</sup> FOR BOTHAT TWENTY-FIVE M/S.....	181
FIGURE 404 : VELOCITY AT0 <sup>0</sup> FOR BOTH AT TWENTY-FIVE M/S.....	182
FIGURE 405 : STREAMLINE AT0 <sup>0</sup> FOR BOTH AT TWENTY-FIVE M/S.....	182
FIGURE 406 : PRESSURE AT0 <sup>0</sup> FOR BOTH AT THIRTY M/S.....	182
FIGURE 407 : VELOCITY AT0 <sup>0</sup> FOR BOTH AT THIRTY M/S.....	182
FIGURE 408 : STREAMLINE AT0 <sup>0</sup> FOR BOTHAT THIRTY M/S.....	183
FIGURE 409 : PRESSURE AT0 <sup>0</sup> FOR BOTH AT FIFTY M/S.....	183
FIGURE 410 : VELOCITY AT0 <sup>0</sup> FOR BOTHAT FIFTY M/S.....	183
FIGURE 411 : STREAMLINE AT0 <sup>0</sup> FOR BOTHAT FIFTY M/S.....	183
FIGURE 412 : PRESSURE AT5 <sup>0</sup> FOR ATFIVE M/S.....	184
FIGURE 413 : VELOCITY AT5 <sup>0</sup> FOR AT FIVE M/S.....	185
FIGURE 414 : STREAMLINE AT5 <sup>0</sup> FOR ATFIVE M/S.....	185
FIGURE 415 : PRESSURE AT5 <sup>0</sup> FOR BOTH AT TEN M/S.....	185
FIGURE 416 : VELOCITY AT5 <sup>0</sup> FOR BOTH AT TEN M/S.....	185
FIGURE 417 : STREAMLINE AT5 <sup>0</sup> FOR BOTH AT TEN M/S.....	186
FIGURE 418 : PRESSURE AT5 <sup>0</sup> FOR AT FIFTEEN M/S.....	186
FIGURE 419 : AT5 <sup>0</sup> FOR AT FIFTEEN M/S.....	186
FIGURE 420 : STREAMLINE AT5 <sup>0</sup> FOR AT FIFTEEN M/S.....	186
FIGURE 421 : PRESSURE AT5 <sup>0</sup> FOR AT TWENTY M/S.....	187
FIGURE 422 : VELOCITY AT5 <sup>0</sup> FOR AT TWENTY M/S.....	187

FIGURE 423 : STREAMLINE AT5 <sup>0</sup> FOR AT TWENTY M/S.....	187
FIGURE 424 : PRESSURE AT5 <sup>0</sup> FOR AT TWENTY-FIVE M/S.....	187
FIGURE 425 : VELOCITY AT5 <sup>0</sup> FOR AT TWENTY-FIVE M/S .....	188
FIGURE 426 : STREAMLINE AT5 <sup>0</sup> FOR AT TWENTY-FIVE M/S .....	188
FIGURE 427 : PRESSURE AT5 <sup>0</sup> FOR BOTH AT THIRTY M/S .....	188
FIGURE 428 : VELOCITY AT5 <sup>0</sup> FOR BOTH AT THIRTY M/S .....	188
FIGURE 429 : STREAMLINE AT5 <sup>0</sup> FOR BOTH AT THIRTY M/S.....	189
FIGURE 430 : PRESSURE AT5 <sup>0</sup> FOR AT FIFTEEN M/S.....	189
FIGURE 431 : VELOCITY AT5 <sup>0</sup> FOR AT FIFTEEN M/S.....	189
FIGURE 432 : STREAMLINE AT5 <sup>0</sup> FOR AT FIFTEEN M/S.....	189
FIGURE 433 : PRESSURE AT10 <sup>0</sup> FOR BOTH AT FIVE M/S.....	191
FIGURE 434 : VELOCITY PLOT AT10 <sup>0</sup> FOR BOTH AT FIVE M/S .....	191
FIGURE 435 : STREAMLINE AT10 <sup>0</sup> FOR BOTH AT FIVE M/S.....	191
FIGURE 436 : PRESSURE AT10 <sup>0</sup> FOR BOTH AT TEN M/S.....	192
FIGURE 437 : VELOCITY AT10 <sup>0</sup> FOR BOTH AT TEN M/S.....	192
FIGURE 438 : STREAMLINE AT10 <sup>0</sup> FOR BOTH AT TEN M/S.....	192
FIGURE 439 : PRESSURE AT10 <sup>0</sup> FOR BOTH AT FIFTEEN M/S.....	193
FIGURE 440 : VELOCITY AT10 <sup>0</sup> FOR BOTH AT FIFTEEN M/S.....	193
FIGURE 441 : STREAMLINE AT10 <sup>0</sup> FOR BOTH AT FIFTEEN M/S.....	193
FIGURE 442 : PRESSURE AT10 <sup>0</sup> FOR BOTH AT TWENTY M/S.....	193
FIGURE 443 : VELOCITY AT10 <sup>0</sup> FOR BOTH AT TWENTY M/S.....	194
FIGURE 444 : STREAMLINE AT10 <sup>0</sup> FOR BOTH AT TWENTY M/S.....	194
FIGURE 445 : PRESSURE AT10 <sup>0</sup> FOR BOTH AT TWENTY FIVE M/S .....	194
FIGURE 446 : VELOCITY PLOT AT10 <sup>0</sup> FOR BOTH AT TWENTY-FIVE M/S .....	195
FIGURE 447 : STREAMLINE AT10 <sup>0</sup> FOR BOTH AT TWENTY FIVE .....	195
FIGURE 448 : PRESSURE AT10 <sup>0</sup> FOR BOTH AT THIRTY M/S.....	195
FIGURE 449 : VELOCITY AT10 <sup>0</sup> FOR BOTH AT THIRTY M/S.....	195
FIGURE 450 : STREAMLINE AT10 <sup>0</sup> FOR BOTH AT THIRTY M/S .....	196
FIGURE 451 : PRESSURE AT10 <sup>0</sup> FOR BOTH AT FIFTY M/S.....	196
FIGURE 452 : VELOCITY AT10 <sup>0</sup> FOR BOTH AT FIFTY M/S.....	196
FIGURE 453 : STREAMLINE AT10 <sup>0</sup> FOR BOTH AT FIFTY M/S .....	196
FIGURE 454 : PRESSURE AT15 <sup>0</sup> FOR BOTH AT FIVE M/S.....	198
FIGURE 455 : VELOCITY AT15 <sup>0</sup> FOR BOTH AT FIVE M/S.....	198
FIGURE 456 : STREAMLINE AT15 <sup>0</sup> FOR BOTH AT FIVE M/S .....	198
FIGURE 457 : PRESSURE AT15 <sup>0</sup> FOR BOTH AT TEN M/S.....	199
FIGURE 458 : VELOCITY AT15 <sup>0</sup> FOR BOTH AT TEN M/S.....	199
FIGURE 459 : STREAMLINE AT15 <sup>0</sup> FOR BOTH AT TEN M/S.....	199
FIGURE 460 : PRESSURE AT15 <sup>0</sup> FOR BOTH AT FIFTEEN M/S.....	199
FIGURE 461 : VELOCITY AT15 <sup>0</sup> FOR BOTH AT FIFTEEN M/S.....	200
FIGURE 462 : STREAMLINE AT15 <sup>0</sup> FOR BOTH AT FIFTEEN M/S.....	200
FIGURE 463 : PRESSURE AT15 <sup>0</sup> FOR BOTH AT TWENTY M/S.....	200
FIGURE 464 : VELOCITY AT15 <sup>0</sup> FOR BOTH AT TWENTY M/S.....	200
FIGURE 465 : STREAMLINE AT15 <sup>0</sup> FOR BOTH AT TWENTY M/S.....	201
FIGURE 466 : PRESSURE AT15 <sup>0</sup> FOR BOTH VENT AT TWENTY-FIVE M/S .....	201
FIGURE 467 : VELOCITY AT15 <sup>0</sup> FOR BOTH VENT AT TWENTY-FIVE M/S.....	201
FIGURE 468 : STREAMLINE AT15 <sup>0</sup> FOR BOTH VENT AT TWENTY-FIVE M/S.....	201
FIGURE 469 : PRESSURE AT15 <sup>0</sup> FOR BOTH AT THIRTY M/S.....	202

FIGURE 470 : VELOCITY AT15 <sup>0</sup> FOR BOTH ATTHIRTY M/S.....	202
FIGURE 471 : STREAMLINE AT15 <sup>0</sup> FOR BOTH ATTHIRTY M/S .....	202
FIGURE 472 : PRESSURE AT15 <sup>0</sup> FOR BOTH AT FIFTY M/S .....	203
FIGURE 473 : VELOCITY AT15 <sup>0</sup> FOR BOTH AT FIFTY M/S.....	203
FIGURE 474 : STREAMLINE AT15 <sup>0</sup> FOR BOTHAT FIFTY M/S.....	203
FIGURE 475 : PRESSURE AT20 <sup>0</sup> FOR BOTH ATTWENTY M/S.....	204
FIGURE 476 : VELOCITY AT20 <sup>0</sup> FOR BOTH ATTWENTY M/S.....	204
FIGURE 477 : STREAMLINE AT20 <sup>0</sup> FOR BOTH ATTWENTY M/S.....	204
FIGURE 478 : PRESSURE AT20 <sup>0</sup> FOR BOTH AT TEN M/S.....	205
FIGURE 479 : VELOCITY AT20 <sup>0</sup> FOR BOTH AT TEN M/S.....	205
FIGURE 480 : STREAMLINE AT20 <sup>0</sup> FOR BOTH AT TEN M/S.....	205
FIGURE 481 : PRESSURE AT20 <sup>0</sup> FOR BOTH AT FIFTEEN M/S.....	205
FIGURE 482 : VELOCITY AT20 <sup>0</sup> FOR BOTH AT FIFTEEN M/S.....	206
FIGURE 483 : STREAMLINE AT20 <sup>0</sup> FOR BOTH AT FIFTEEN M/S .....	206
FIGURE 484 : PRESSURE AT20 <sup>0</sup> FOR BOTH ATTWENTY M/S.....	206
FIGURE 485 : VELOCITY AT20 <sup>0</sup> FOR BOTH ATTWENTY M/S.....	206
FIGURE 486 : STREAMLINE AT20 <sup>0</sup> FOR BOTH ATTWENTY M/S.....	207
FIGURE 487 : PRESSURE AT200 FOR BOTHAT TWENTY-FIVE M/S.....	207
FIGURE 488 : VELOCITY AT20 <sup>0</sup> FOR BOTH AT TWENTY-FIVE M/S .....	207
FIGURE 489 : STREAMLINE AT20 <sup>0</sup> FOR BOTHATTWENTY-FIVE M/S .....	207
FIGURE 490 : PRESSURE AT20 <sup>0</sup> FOR BOTH AT THIRTY M/S.....	208
FIGURE 491 : VELOCITY AT20 <sup>0</sup> FOR BOTH ATTHIRTY M/S.....	208
FIGURE 492 : STREAMLINE AT20 <sup>0</sup> FOR BOTH ATTHIRTY M/S .....	208
FIGURE 493 : PRESSURE AT20 <sup>0</sup> FOR BOTH AT FIFTY M/S.....	208
FIGURE 494 : VELOCITY AT20 <sup>0</sup> FOR BOTH AT FIFTY M/S.....	209
FIGURE 495 : STREAMLINE AT20 <sup>0</sup> FOR BOTH AT FIFTY M/S .....	209
FIGURE 496 : CL VERSUS ATTACK ANGLE.....	210
FIGURE 497 : CDVERSUS ATTACK ANGLE .....	210
FIGURE 498 : CL VERSUSCd.....	210
FIGURE 499 : CL VERSUS ATTACK ANGLE.....	211
FIGURE 500 : CdVERSUS ATTACK ANGLE .....	211
FIGURE 501 : CL VERSUSCd.....	211
FIGURE 502 : CL VERSUS ATTACK ANGLE.....	212
FIGURE 503 : CdVERSUS ATTACK ANGLE .....	212
FIGURE 504 : CL VERSUSCd.....	212
FIGURE 505 : CL VERSUS ATTACK ANGLE.....	213
FIGURE 506 : CdVERSUS ATTACK ANGLE .....	213
FIGURE 507 : CL VERSUSCd.....	213
FIGURE 508 : CL VERSUS ATTACK ANGLE.....	214
FIGURE 509 : CdVERSUS ATTACK ANGLE .....	214
FIGURE 510 : CL VERSUS CD .....	214
FIGURE 511 : CL VERSUS ATTACK ANGLE.....	214
FIGURE 512 : CdVERSUS ATTACK ANGLE .....	215
FIGURE 513 : CL VERSUSCd.....	215
FIGURE 514 : CL VERSUS ATTACK ANGLE.....	215
FIGURE 515 : CdVERSUS ATTACK ANGLE .....	216
FIGURE 516 : CL VERSUSCd.....	216

FIGURE 517 : DESIGNING WING MODEL WITH VENTS BY USING 3D PRINTING AND TEAK WOOD.....	230
FIGURE 518 : WING MODEL WITH THE STRAIGHT VENTS MAINTAIN EQUAL DISTANCE.....	231
FIGURE 519 : WING MODEL MOUNTED IN THE WIND TUNNEL SECTION 600*600MM FOR TESTING.....	231
FIGURE 520 : WIND TUNNEL SECTION 600*600MM TESTING OF AIRFOIL.....	232
FIGURE 521 : EXPERIMENTAL CL VS AOA 21012 AIRFOIL WITH AND WITHOUT VENT .....	243
FIGURE 522 : CFD FOR 21012 AIRFOIL WITH AND WITHOUT VENT AT VELOCITIES COMPARISON FIVE M/S .....	243
FIGURE 523 : FOR 21012 WITH AND WITHOUT VENT EXPERIMENTALLY AT VELOCITIES TEN M/S .....	243
FIGURE 524 : EXPERIMENTAL FOR 21012 WITH AND WITHOUT VENT.....	244
FIGURE 525 : CFD FOR 21012 WITH AND WITHOUT VENT COMPARISON .....	244
FIGURE 526 : EXPERIMENTAL FOR 21012 WITH AND WITHOUT VENT AT VELOCITIES : TWENTY M/S .....	244
FIGURE 527 : CFD FOR 21012 WITH AND WITHOUT VENT AT VELOCITIES : TWENTY M/S.....	245
FIGURE 528 : EXPERIMENTALLY FOR 21012 WITH AND WITHOUT VENT COMPARISON AT VELOCITIES TWENTY M/S .....	245
FIGURE 529 : CFD FOR 23012 WITH AND WITHOUT VENT FIVE M/S.....	247
FIGURE 530 : EXPERIMENTAL WITH AND WITHOUT VENT COMPARISON FIVE M/S .....	247
FIGURE 531 : EXPERIMENTAL FOR 23012 WITH AND WITHOUT VENT TEN M/S .....	248
FIGURE 532 : CFD FOR 23012 CL VERSUS ATTACK ANGLE CFD.....	248
FIGURE 533 : 23012 COMPARING EXPERIMENTAL WITHOUT VENT WITH VENT AT 20 M/S.....	249
FIGURE 534 : 23012 EXPERIMENTAL CL VS AOA AT TWENTY M/S .....	249
FIGURE 535 : 23012 WITHOUT VENT AND WITH VENT CFD COMPARISON TWENTY M/S.....	250
FIGURE 536 : CL VS AOA EXPERIMENTAL WITH VENT AND WITHOUT VENT AT 20 M/.....	250



## **List of Abbreviations**

**AOA** Attack angle

**P** Pressure

**V** Velocity of the Object

**L** lift

**D** Drag

**CL** Co-efficient of lift

**CD** Co-efficient of drag

**AOA** Attack angle

**P** Pressure

**Cfd**-Computational fluid dynamics

**NACA** National Advisory committee for aeronautics

**Wov** With out vent

**Wv** With vent

$\rho$  Density of the Flow

**V** velocity

**S**-Surface area of the wing

**NASA**-National aeronautics and space administration

**M**-Mach Number

The above notations are used throughout thesis unless otherwise mentioned specifically.

# Chapter1

## INTRODUCTION

### 1.1 Introduction

Birds and insects exhibit a diverse range of wing morphologies and functionalities adapted to their specific flight needs. Birds, for instance, have wings that are designed to cater to different flight styles. Soaring birds, like eagles, have long and broad wings that allow them to glide effortlessly for long distances by exploiting thermal currents. On the other hand, birds that require high maneuverability, such as sparrows and hummingbirds, have shorter wings that provide them with the ability to make rapid and precise movements.

Insects, meanwhile, possess wings that can beat at extremely high frequencies, allowing for various flight capabilities including hovering, rapid acceleration, and intricate aerial maneuvers. Dragonflies, for example, can move each of their four wings independently, granting them exceptional agility and control. This complex wing coordination is something that mechanical flight systems have yet to fully replicate but continue to draw inspiration from.

One notable bio-inspired feature is the use of winglets. Birds have evolved winglets to minimize the energy losses due as the wing creates lift, it leaves behind circular patterns of whirling air that are known as wingtip vortices. Modern aircraft have adopted this feature, leading to designs that incorporate upward-turned tips at the end of the wings, which helps in reducing drag and improving fuel efficiency.

#### **Flapping Wings (Ornithopters)**

The flapping flight of birds and insects is another area of immense interest. Birds utilize strong chest muscles and flexible wing joints to produce powerful and versatile wing strokes that generate both lift and thrust. This allows for a variety of flight behaviours, from the rapid acceleration of a falcon diving for prey to the steady endurance of a migratory bird travelling thousands of miles.

Insects, such as bees and beetles, have wings that can beat hundreds of times per second, creating lift in a manner that is highly efficient at smaller scales. This flapping mechanism has inspired the development of ornithopters mechanical devices that mimic the flapping motion. Ornithopters are

being explored for use in applications where traditional fixed-wing or rotary-wing aircraft might be less effective, such as in urban environments where agility and the ability to hover are advantageous.

**Surface Structures and Boundary Layer Control :** Another fascinating aspect of natural flight is the use of surface structures to control the boundary layer—the thin layer of fluid near the surface of an object where effects of viscosity are significant. Sharks, for example, have dermal denticles that create micro-turbulence in the water, maintaining a thin boundary layer that reduces drag. This principle is applied in the design of aircraft surfaces, aiming to replicate the drag-reducing properties seen in nature. Similarly, crocodiles have scales that help in controlling flow separation, improving their hydrodynamic efficiency. Researchers are studying these natural features to develop surfaces for aircraft that can adapt to changing flow conditions, thereby reducing drag and improving overall aerodynamic performance.

### **Characteristics of Mechanical Flight**

**Lift and Drag :**In mechanical flight, the generation of lift and the minimization of drag are fundamental concerns. Lift is generated by the airfoil shape of the wings, which create a pressure difference between the upper and lower surfaces of the wing. The angle of attack, which is the angle between the oncoming air and the wing's chord line, plays a crucial role in determining the amount of lift. As the angle of attack increases, lift increases up to a critical point before aerodynamic stall occurs. To reduce drag, aircraft designs incorporate smooth surfaces, streamlined shapes, and advanced materials. Winglets, inspired by bird wing tips, are now a common feature on modern aircraft. These winglets help to reduce induced drag by disrupting the formation of wingtip vortices, leading to improved fuel efficiency and performance.

**Power and Propulsion :** The propulsion system of an aircraft provides the necessary thrust to overcome drag and achieve flight. Traditional aircraft use either propellers or jet engines. Propellers are highly efficient at lower speeds and are commonly used in general aviation and smaller aircraft. Jet engines, on the other hand, are more suited for high-speed travel and are the standard for commercial airliners and military jets.

Research into flapping mechanisms has shown potential for developing more efficient propulsion systems, especially for small drones and unmanned aerial vehicles (UAVs). These flapping systems, inspired by the flight of birds and insects, can provide better maneuverability and efficiency at lower speeds, making them ideal for certain applications where traditional propulsion might be less effective.

**Control and Stability :** Control and stability in mechanical flight are achieved through the use of aerodynamic surfaces such as ailerons, elevators, and rudders. These control surfaces allow pilots to

adjust the aircraft's roll, pitch, and yaw, ensuring stable and controlled flight. The design and placement of these surfaces are critical for the aircraft's performance.

Bio-inspired control mechanisms are also being explored to enhance the responsiveness and efficiency of flight control systems. Birds and insects have highly adaptable and flexible control surfaces that allow for precise adjustments during flight. Incorporating similar features into aircraft design could lead to more efficient and responsive control systems.

**Materials and Structures :** Modern aircraft are constructed from advanced materials that provide high strength-to-weight ratios. Composites, such as carbon fiber reinforced polymers, are commonly used due to their lightweight and durable properties. These materials help in order to improve fuel economy by lowering the aircraft's overall weight. performance. Biomimetic structures, inspired by natural flyers, are also being investigated. for instance, the hollow bones of birds are strong yet lightweight, providing an excellent model for developing lightweight structural components for aircraft. By studying and replicating these natural structures, engineers can create more efficient and robust aircraft designs.

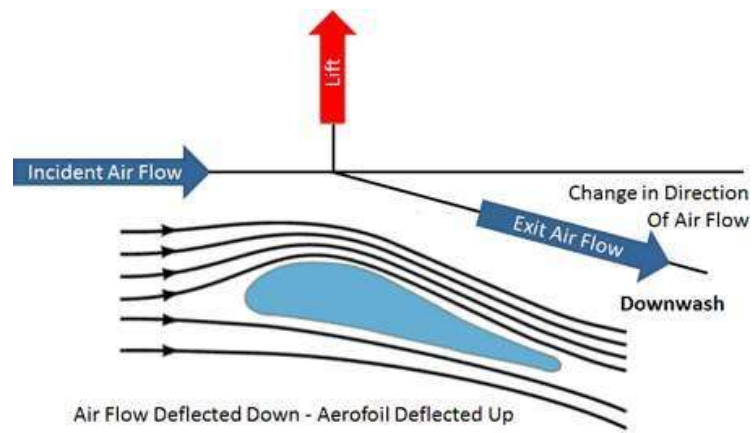
## 1.2 Fundamental forces Acting on The Object in Flight

Lift is the aerodynamic force that allows an object to fly. It is primarily generated by wings, which are designed to produce lift when they move through the air. For mechanical birds, lift is generated as they glide or fly through the air, while natural flyers like birds and insects generate lift through the flapping of their wings.



**Figure 1.1 : forces acting on an aircraft**

When air flows around a solid object, such as a wing, it gets deflected. This deflection causes a pressure differential across the surface's top and bottom halves.wing, resulting in a lift force. The shape of the object, particularly the airfoil shape of wings, is crucial in generating lift efficiently. The direction of the stream remains opposite to the lifting force, and depends on factors such as the shape of the wings, the surface area exposed to the flow, and the velocity of the object moving through the air.



**Figure 1.2 : Lift generated by airfoil through deflection of the flow**

The lift force generated by a wing is calculated by,

$$L = \frac{1}{2} \rho v^2 SC_l$$

Where, L–Force lift

$\rho$  – Density

V–Velocity

S - Surface area of the

wing  $C_l$ -Coefficient of lift

### 1.2.1 Drag

**Drag** is another aerodynamic force that resists object motion through a fluid medium. Drag always acts in the flow's parallel direction.

Drag is an aerodynamic force that opposes the motion of an object through a fluid medium, such as air or water. It always acts in the direction parallel to the flow of the fluid, effectively resisting the object's movement.

Drag is inevitable for any object moving through a fluid medium. For aircraft, the total drag force can be estimated using various expressions depending on the type of drag being considered. The general formula for calculating :

$$D = \frac{1}{2} \rho v^2 S C_d$$

$\rho$ -Density

V–Velocity

D- Drag

S–Surface area of the wing

$C_d$ –Coefficient of drag Further, the total drag coefficient  $C_d$  is estimated as,

$$C_d = C_{d0} + \frac{C_l^2}{\pi e A R}$$

## 1.2.2 Weight

### Factors Affecting Aircraft Weight

**Empty Structure:** The empty structure, also known as the basic empty weight (BEW) or operating empty weight (OEW), includes the airframe, engines, fixed equipment, and systems necessary for operation. This forms the foundation of the aircraft's total weight.

**Impact :** This weight is relatively constant and does not change during flight. It forms the baseline upon which all other weight components are added.

**Fuel :** Fuel is essential for generating the propulsion needed for flight. It is stored in various tanks within the aircraft, such as in the wings and fuselage.

**Impact :** The weight of fuel is substantial and contributes significantly to the total weight of the aircraft. Since fuel is burned to produce thrust, the weight of the aircraft decreases continuously throughout the flight. This consumption impacts the aircraft's center of gravity and overall balance, requiring careful monitoring and adjustment.

**Crew and Passengers :** This includes the pilots, flight attendants, and passengers on board. The weight of each individual is typically standardized for calculations.

**Impact :** The total weight of the crew and passengers can vary with each flight, depending on the number of people and their distribution within the aircraft. This variation affects the aircraft's center of gravity and must be considered during load planning.

**Cargo :** Cargo consists of baggage, freight, and any other goods being transported. The weight and distribution of cargo can vary significantly from flight to flight.

**Impact :** Cargo weight affects the total weight and balance of the aircraft. Proper loading and securing of cargo are crucial to maintain the aircraft's stability and performance.

**Avionic Components :** Avionic components include the electronic systems used for navigation, communication, flight control, and other operational functions.

**Impact :** While the weight of these components is relatively minor compared to other factors, they are essential for the safe and efficient operation of the aircraft. Their weight is included in the basic empty weight of the aircraft.

### Weight Fluctuation During Flight :

The weight of the aircraft fluctuates continually throughout the flight primarily due to fuel consumption. This fluctuation has several implications :

1. **Center of Gravity (CG) Management :** As fuel is burned, the CG shifts, which can affect the aircraft's stability and control. Pilots and flight management systems continuously monitor and adjust for these changes to ensure optimal performance and safety.

2. **Performance Adjustments** : Changes in weight affect the aircraft's performance characteristics, such as a cruise climbing percentage, and landing and takeoff distances efficiency. Pilots adjust their flight plans and operational parameters based on the current weight of the aircraft.
3. **Fuel Efficiency** : The reduction in weight as fuel is consumed can lead to improved fuel efficiency over the course of the flight. Lighter aircraft require less thrust to maintain altitude and speed, reducing fuel consumption rates.
4. **Load Planning and Balance** : Before takeoff, the load distribution, including passengers, cargo, and fuel, is carefully planned to ensure proper balance and stability. This planning must account for the dynamic changes in weight throughout the flight..

### 1.2.3 Thrust

Thrust is the reaction force developed by the propulsion system to push the object (aircraft) through the air and encounters the drag acting on the body. The magnitude of thrust force rests on type of propulsion system and fuel used in it. The motion of aircraft depends on the balance of these fundamental forces. They influence the direction and stability of the flight over the course of flight.

Technical description of airfoil and its characteristics

When in motion to the surrounding air, an airfoil is a 2d form that can generate an active lift force. The 2d profile of an aircraft wing is most well recognized. The cross section of the wing may be seen by cutting the wing perpendicular to the trailing and leading edges is known as an airfoil, and it has unique design requirements, as illustrated in the lower right. The chord line is a straight line traced from leading to trailing edges of the airfoil. The chord line divides airfoil into a lower and an upper surface. The mean chamber line is calculated by plotting the points halfway between the top and lower surfaces. The top side of a symmetric airfoil is a mirror of the bottom part, and the mean chamber line will fall on top of the chord line. The distance between top and bottom surfaces is specified as thickness. These values are frequently divided by the chord length to obtain a non-dimensional or "percent" sort of number. Airfoils can come in a wide range of sizes and shapes



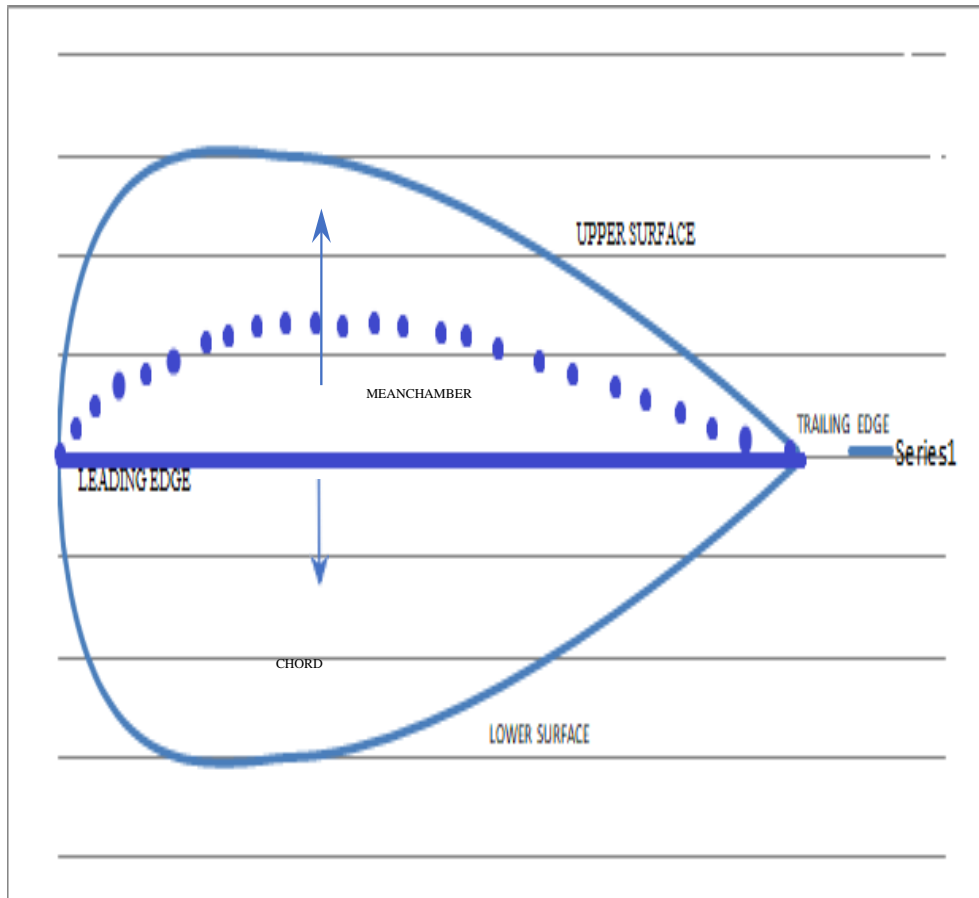


Figure 1.3 : Airfoil geometry

An aerodynamic force emerges as an airfoil-shaped object traverses through a fluid medium. The force is divided into two components : lift, which acts perpendicular to the motion, and drag, which operates parallel to it. Airfoils suited for subsonic flight have particular characteristics. These edges frequently have symmetrical curvature. Hydrofoils, on the other hand, perform similarly to airfoils but in an aquatic setting, using water as the operative fluid.

The lift produced by an airfoil is largely determined by its attack angle and form. When properly oriented, the airfoil attempts to divert incoming air (producing a downward force for fixed-wing aircraft), resulting in a force operating in the opposite direction of displacement. The aerodynamic force is divided into two components : lift and drag. Cambered airfoils may create lift even at a zero attack angle, whereas most airfoil designs require a positive attack angle to generate lift.

This occurrence involves the "circulation of air around the airfoil, leading to the creation of curved streamlines that result in reduced pressure on one side and augmented pressure on the other." Following Bernoulli's principle, the airflow encompassing the airfoil experiences greater acceleration on the top area compared to the bottom area. By amalgamating, concept of circulation with Kutta-Joukowski, lift can be directly correlated with the average flow velocity over the above and below surfaces, by passing the consideration of pressure.

NACA classifications of airfoils

NACA stand for National Advisory Committee for Aeronautics (NACA). These are distinguished by a series of numerals after the term "NACA."

**NACA four-digit series :**

The NACA defines the profile for digit wing sections as follows :

1. First digit denotes maximum camber as a percentage of the chord.
2. Second digit denotes maximum camber from the leading distance edge of the airfoil in tenths of chord.

3. Latter two values denotes maximum airfoil thickness as a percentage of chord.

The NACA Five-Digit Series defines increasingly complicated airfoil forms.

1. The coefficient of lift is produced by multiplying the first digit by 0.15.

2. When the third digits are split by two, the result is  $p$ , the maximum camber distance from the sharp end (as percent chord).

3. The fourth and fifth Figures represent the utmost airfoil

4. When the chord has normalized the chord wise location  $x$  and the ordinate  $y$ . The constant 'm' is selected to maintain the camber at  $x=p$ . Lastly,  $k_1$  is calculated to get the lift coefficient.

### 1.2.3.1 Attack angle

The angle between chord line and the relative wind. It is usually represented by  $\alpha$ .

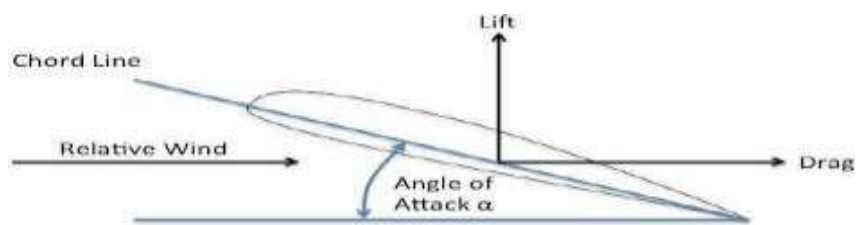


Figure 1.4 : Airfoil placed at an attack angle

### Importance of Angle of Attack

1. **Lift Generation** : The angle of attack is crucial for lift generation. As  $\alpha$  increases, the lift produced by the airfoil also increases, up to a certain point. This relationship is vital for the aircraft's ability to take off, climb, and maintain altitude.
2. **Stall** : If the angle of attack exceeds a critical value (typically around 15-20 degrees), the airflow can separate from the top area of the wing, to a stall. Stall, lift dramatically decreases, which can cause a loss of control.
3. **Flight Control** : Pilots manage the angle of attack by adjusting the aircraft's pitch. By tilting the nose up or down, they change  $\alpha$ , thus controlling the lift and the aircraft's climb or descent.
4. **Aerodynamic Efficiency** : Maintaining an optimal angle of attack is essential for aerodynamic efficiency. A low angle of attack might not produce enough lift, while a high angle can increase drag and risk a stall. Balancing  $\alpha$  ensures efficient flight performance and safety.

## 1.2.4 Wingspan

Understanding distances between points helps in optimization, navigation, and measuring spatial relationships. For example, in architecture, engineering, and navigation, accurately measuring distances between points is crucial for designing structures, planning routes, or determining the shortest path between locations.

The distance between two points along a straight line, often denoted by "b," is a fundamental concept in geometry and mathematics. It represents the length of the line segment connecting two points and has wide-ranging applications in various fields, from mathematics to real-world scenarios like navigation and engineering.

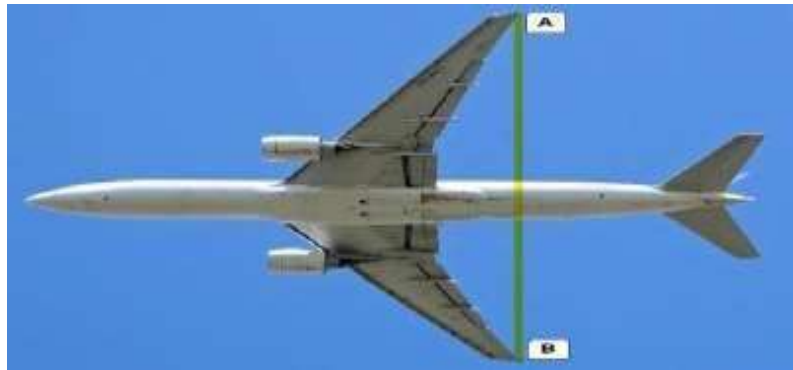


Figure 1.5 : Wingspan of Boeing 777-200ER

### 1.2.5 Aspect Ratio

The ratio of square of wingspan to surface area. It is given by,

$$AR = \frac{b^2}{S}$$

**Area** : This typically refers to the total area covered by the wings when viewed from above. It includes the area of both wings, as well as any additional surfaces like flaps or ailerons.

### 1.2.6 L/D Ratio

It is ratio of lift force developed by the aircraft to the drag developed by it. It is known as aerodynamic performance of an aircraft. Higher the value of L/D, greater is the performance. Key indicator of an aircraft's efficiency and performance. A higher L/D ratio signifies better performance, fuel efficiency, and range, making it a critical consideration in aircraft design and operation.

### 1.2.7 Wing Loading

The total weight of flying object is separated by the surface of its wings. It is an important variable in estimating several parameters such as stall speed, takeoff and landing performance. Wing loading is crucial in aviation because it affects various aspects of an aircraft's performance.

**Stall Speed** : Aircraft with higher wing loading tend to have higher stall speeds because they need more airspeed to generate enough lift to stay airborne.

**Takeoff and Landing Performance** : Higher wing loading typically requires longer runways for takeoff and landing because the aircraft needs more speed to generate lift.

**Maneuverability** : Aircraft with lower wing loading are generally more maneuverable because they can generate more lift at lower speeds, which is important for tasks like aerial combat or tight turns.

**Structural Considerations** : High wing loading can put more stress on an aircraft's structure, so engineers need to ensure the wings and other components can handle the increased loads without experiencing structural failure.

## 1.2.8 Mach Number

Mach number is a dimensionless quantity which is ratio of speed of object to speed of sound in the local medium. It is given by,

$$m = \frac{v}{a}$$

Where  $v$  is the velocity, feet per second, or other appropriate units)

$M < 1$  : Subsonic flight (speeds slower than the speed of sound).

$M = 1$  : Transonic flight (speeds approaching the speed of sound).

$M > 1$  : Supersonic flight (speeds faster than the speed of sound).

$M \gg 1$  : Hypersonic flight (speeds much greater than the speed of sound).

### 1.2.9 Reynolds Number

It is a dimensionless quantity denoted as inertial force to viscous force ratio.

This ratio is significant because it helps determine whether the flow of the fluid is primarily influenced by inertial forces. At lower Mach numbers, typically below 0.3, viscous forces dominate and the flow is often considered incompressible. At higher Mach numbers, inertial forces become more significant, and compressibility effects become apparent.

It is provided by,

$$R_e = \frac{\rho v l}{\mu}$$

Where,  $\rho$  is the fluid density

$v$  is the velocity of the flow

$l$  is the length of the object

$\mu$  is the dynamic viscosity of the fluid

# Chapter2

## LITERATUREREVIEW

### 2.1 Review of Literature

A In a scenario involving the passage of a slender airfoil through rapidly changing airflow along a linear path, researchers examined the implementation of active technique at leading point. This approach aimed to manage airflow separation, thereby preventing the occurrence of dynamic stall. Both Eulerian and Lagrangian technique were used to derive solutions for unsteady boundary layer. The study investigated the impacts of different parameters connected to a finite-length suction slot, encompassing its positioning and strength of suction. The findings reveal that significant interruptions in airflow results in separation, even with relatively modest suction, as long as the suction process is initiated early on. According to the findings, flow separation efficiently decreased by suction technique through a short slit, especially at high Reynolds numbers. ([Hediy, Walker, & David, 2005](#))

An effort has been made to make a detailed study on lift and drag coefficient of various airfoil sections. Tried to differentiate between two types of airfoils i.e., Symmetrical and asymmetrical airfoils on the basis of their lift and drag coefficients. Varying attack angle, stall angle the magnitudes coefficients were determined and evaluated. By comparing the results obtained it was found out that stall attack angle was lower for symmetric airfoil compared to asymmetric airfoil ([Shan, Jiang, Liu, Love, & Maines, 2008](#))

The study was to quantify phenomenon of subsonic flow over a NACA 0012 airfoil at a 6° attack angle. The objective was to investigate separation by using vortex generators. Three numerical simulations : an unrestrained reference situation, a restrained setting with vortex generators, another controlled arrangement with active one. The passive vortex generators revealed the ability to partially counteract airflow separation by re-joining sheared layer to airfoil across a wide region. All three cases mean flow parameters were examined using rate of time, span wise findings.



Relatively low attack angle studied here, the application of flow separation control did not lead to a noteworthy increase in lift force or a substantial drag force. However, it shows comprehension of flow controls by using active vortex generators. ([Avraham, Seifert, A., Wyganski, & Israel, 1996](#))

Experiments were conducted to showcase the efficacy of oscillatory blowing in delaying separation from a symmetrical airfoil. This technique, unlike the conventional steady blowing method, proved considerably more successful in achieving this goal. By introducing periodic, 2d oscillations, the ability to withstand more pronounced pressure gradients undergoing separation was achieved. Consequently, this approach amplified lift and curtailed drag at various angle of incidence and due to deflections where separation would otherwise occur. To achieve effective separation control, amplitude of executed oscillations should ultimate. Additionally, optimal placement actuator corresponds at this point, unless the flow within the upstream boundary layer magnifies the applied oscillations. This method's remains unaffected by factors such as inducing early transition, enhancing reynolds number. Notably, this technique differs significantly from stationary vortex generators that introduce smaller-scale stream wise vortices. ([M, Smith, Kibens, Parekh, & A, 2001](#))

Several air flow tests were carried out to investigate management flow separation unusual symmetric airfoil placing synthetic actuators. Researchers finding the effects actuation frequency, positioning, momentum coefficient at various angles of attack. Notably, these are positioned near site of separation, the momentum coefficient required to efficiently reconnect the split flow decreases. Flow reattachment is even possible by placing actuators downstream. The measurements taken offer valuable insights from a design perspective. Practical constraints prevent separation, adjusting the placement of control points (designated as  $\alpha$ ) or manipulating momentum coefficient (designated as  $C$ ) can result in optimal airfoil performance across higher AOA. ([Lin, Howard, & Selby, 1990](#))

Experiments were undertaken to analyze the efficiency of low-profile submerged vortex generators in managing moderate 2d flow separation. The study revealed that all the examined vortex generators demonstrated the ability to decrease the distance at which reattachment occurs and enhance pressure recovery, outperforming conventional vane-type vortex generators. ([Melton, Pack, Yao, & Seifert., 2006](#))

Utilizing the zero-net-mass-flux periodic excitation method, simulations were carried out across various sections on a basic high-lift system postpone onset of flow separation. Goal was to pinpoint optimal locations for the actuators by capturing detailed flow characteristics. An exceptional sensitivity to excitation placement was observed, particularly in regions where the flap exhibited significant curvature. Notably, when the flap experienced substantial deflections, the majority of alterations enhancing lift were attributed to upstream effects. Additionally, it was determined that effectively controlling boundary separation at the end point necessitates higher periodic momentum involvement. The role of curvature was emphasized with ratio between the subsequent excitation wavelength, surface's curvature radius emerging as a pertinent parameter. ([Viswanat & P., 2007](#))

The paper briefly outlines three overarching strategies for separation control. These strategies encompass methods focused on energizing the boundary layer ahead of separation, techniques aimed at modifying the bubble flow or stagnant air region, and approaches that directly impact the reattachment of the shear layer. The document provides a concise overview of various methods that offer potential solutions for the postponement of flow separation over an airfoil. ([Bur, Reynald, Coponet, & Carpels, 2003](#))

In a transonic channel, an experimental method used to manage interaction among a separated unstable boundary layer and distress wave using mechanical vortex generator devices. The spacing of these devices along the span wise direction within the channel emerged as a significant parameter for controlling the flow separation. Decreasing distance between respective device led to enhanced efficiency in merging vortices, resulting in a more effective reduction of the separation phenomenon. ([Takahashi, et al., 1991](#))

Employing active device through suction via pierced plate positioned within interaction area proved to be a more effective method for reducing shock displacement. The application of a blowing boundary layer control (BLC) implemented on outboard frontal area and ailerons of ASKA. The use of a drilled holes nozzle for BLC demonstrated effectiveness in preventing flow separation and enhancing the stall attack angle. Notably, this performance was found to be comparable to that achieved with a continuous-slot nozzle. ([Ramsay, James, Sellier, & Ho., 2020](#))

Numerical investigations were conducted to optimize scattered suction outlines preventing separation on a rounded cylinder within ( $Re < 188$ ), while minimizing control effort. These optimized suction outlines were compared by time-dependent simulations, confirming that methods successfully eradicate separation in an unsteady scenario. Non-uniform suction proved sooner in eliminating separation, through unvarying suction exhibited greater stability. The optimized results to both uniform and non-uniform suction were validated through time-dependent simulations involving their control limitations. Across entirely examined cases, suction required to suppress vortex shedding was smaller than that desirable to prevent departure. General, non-uniform dispersed suction emerged as a highly effective approach for governing the angle of separation about a cylinder. In a different study, a backward-facing step was introduced to enhance the  $L/D$  ratio of airfoil featuring separation bubble. Three different airfoils were verified, leading to assumption that step's efficacy is more pronounced for airfoil with substantial separation bubbles near mid-chord. These findings, while preliminary, underscore the need for further research to ascertain factors such as the optimal scope and placement of step, as well as influence of reestream turbulence and  $Re$ . ([Jose, Rodriguez, Rothan, & Dominique, 1993](#))

In order to understand the process for the lowering of chamber by using blowing jets positioned span-wise direction of up stream, direct aero acoustic calculations and wind tunnel experiments were both carried out. Therefore, at  $s/L = 0.1, 1.0$ , the drop of chamber one was lower. In conclusion,  $s/L = 0.05$  is an appropriate spacing for the introduction of robust longitudinal vortices into cavity flow and efficient chamber reduction. The control's projected decrease in cavity tone level and the impact of spacing on the decrease were in good alignment with the observed value ([Yokoyama, Hiroshi, Minato, Adachi, & Iida, 2017](#))

Vortex generator were employed to manage separation on suction side of a LPT airfoil. A specific case at a low  $Re = 25,000$  was studied, along with low free-stream conditions, and detailed measurements were conducted, encompassing profiles of mean and varying velocity and shear stress. The utilization of this technique exhibited success by using LPT airfoil even at extremely low

Re Figure s. When compared to a comparable scenario using passive flow management, the separation bubble was successfully minimized, resulting in fewer losses. While useful insights into the efficacy and underlying physics of synthetic vortex generating jets in LPT flows have been achieved, various problems about their adaptability under different flow conditions and optimal design parameters remain. ([Volino & J., 2009](#))

An experimental investigation was undertaken to assess relative effectiveness of various inactive method for managing, 2d, turbulent flow separation. Minor transverse and cleaned indentations, in active surfaces, large in dentations, vortex generators. Notably, transverse grooves situated region of maximum and featuring a height-to-width ratio exceeding 2.5 exhibited are duction over 50 percent in reattachment distance compared to the base line setup. Furthermore, closely spaced, large indentations positioned at X/6- 1.5 led to are duction in reattachment up to 66 percent. Conversely, all tested configurations involving passive porous surfaces tended to exacerbate separation rather than mitigate it. ([Lin, John, Howard, & Selby., 2012](#))

Aerodynamic properties of NACA 0012 airfoil were examined 0 to 180 degrees AOA. The tests are conducted using both smooth and roughened model surfaces, with the application of Carborundum granules to induce roughness on both ends. Smooth surface examine covered from 0° to 360° at a Re of around  $1.8 \times 10^6$ , and from 0° to 180° at a Re of approximately  $0.5 \times 10^6$ . for the roughened model, data were gathered from 0° to 180° at a Re of about  $1.8 \times 10^6$ . The obtained results were compared with results from other facilities and for the NACA 0015 airfoil. It was observed that introducing surface roughness and reducing the Re had minor impacts on lift coefficients within the attack angle range of 25° to 125°. However, at a 90° attack angle, both the surface condition and the Re revealed a decrease in drag. The data gained from this investigation aligned well with those obtained in a second facility using a different model of the same airfoil section. ([Chris, Critzos, Heyso, H. & Robert, 1955](#))

Active boundary layer management methods including blowing and suction were used on a symmetrical airfoil section with a 1-foot chord and 46% thickness. The tests are approved at Re  $0.7 \times 10^6$  and  $0.9 \times 10^6$ , respectively, from 0 to 15 degrees .The evaluation of flow attachment and uniformity was facilitated using yarn tufts, which were monitored in real time through a video camera. Lift force, drag, and CL were determined using pressure measurements from awake region and surface taps. Suction and blowing coefficients calculated based on venturi and plenum pressures as well as temperatures. Application of blowing with increased blowing rates exhibited capacity to delay the stall attack angle, consequently raising the CL. However, employing a large suction slot as a boundary layer

control device proved ineffective inherently low suction velocities associated with it. for the wake rake method to be employed in calculating drag. The study did not identify hysteresis effects when varying free stream velocity. Ultimately, the blowing method was deemed more effective compared to the suction slot as a boundary layer control device. [\(S, KIMMEL, SEKELSKY,& SLOMSKI, 1992\)](#)

The study aimed to study the impact of retracting flap after all boundary layer had been drawn into the slot. Variations in airfoil incidence, flap retraction, relation of suction-slot speed to free stream velocity were evaluated. Flaps including those with strips attached to bottom surface, were employed to modify the test model. Smoke tubes and tufts were used to visualize flow behavior, while awake-traverse gear was used to calculate flow characteristics. When the flap extended streamline, a stable flow was achieved. Slot entry exhibited a favorable pressure gradient, and no noticeable wake was observed downstream of the flap. Suction applied to the airfoil's rear proved effective in varying lift by governing the location of rear stagnation point. However, further retracting the flap resulted in pronounced noise and highly unsteady tunnel stream and suction flow. Visual cues from streamer that the wake in tunnel upon flap retraction. In situations where the wake brake was unnecessary, the retractable flap had extended for steady flow, leading to no additional profile drag. This study underscores the complexity of boundary layer suction and the intricate relationship between flap position and flow stability. [\(Heughan,1953\)](#)

An evaluation of transition and turbulence models is conducted to predict low Reynolds number flows involving laminar separation bubbles. The study explores the use of blowing and suction techniques to mitigate laminar separation bubbles on a single airfoil. Experiments using hot-wire anemometry on NACA 2415 airfoil at  $= 8^\circ$  and  $Re 2 \times 10^5$  demonstrate the existence of a LS bubble. Numerical simulations are performed on a NACA2415airfoil to study the control of LS bubble and conversion location. Oil flow visualization is cast-off to observe surface flow patterns. Both suction and methods manage to shift the bubble separation downstream but complete control is not achieved. Among the two methods, the suction boundary layer control proves to be more effective than the blowing jet flow control method. By simultaneously applying blowing and suction methods, the separation bubble is suppressed, resulting in increased lift and decreased drag ratios achieved through combination of jet parameters. This study demonstrates the complex interplay between various control methods and their impacts on laminar separation bubbles and airfoil performance. [\(Serdar, Ünver, & Hüseyin, 2011\)](#)

On a restricted section of the top surface of a 2D airfoil near the frontal area, within a low-speed free stream at a high attack angle, simultaneous blowing-suction control techniques are

used. The Navier-Stokes equations are used to undertake numerical research. Aerodynamic characteristics are calculated using both mass injections and suction, and numerical findings are related to investigational data. Several features flow behavior investigated, including the variation of drag and lift, power spectrum density, velocity diagrams at specific places, and instantaneous streamlines. Real frequencies improving performance lift are sub-harmonics vortex shedding of airfoil. Particularly frequency aligns with the normal frequency, airfoil presentation improves. In cases involving blowing-suction, the flow field frequency synchronizes with the forcing frequency, leading to the presence of a strong vortex on airfoil's upper surface. In scenarios without injection, the flow field frequency is semi of leading frequency, resulting in a primary leading-edge vortex that gradually moves downstream along the upper surface. The periodic blowing-suction technique yields a greater increase in lift compared to cases where no mass injection is employed. The study highlights the significance of controlling flow dynamics through simultaneous blowing and suction for enhancing airfoil performance. ([Yang, Wang, Liu, Lixian, & Sinica, 1997](#))

for a wing model composed of NATIONAL AERONAUTICS AND SPACE ADMINISTRATION 4215 airfoil sections, suction and injection control mechanisms for suppress separation bubbles laminar at low Re. The studies are carried out with various attack angles and suction-injection frequencies. Suction and injection mechanism inclined internal slots four are created. A single cylinder piston mechanism per forms simultaneous injection and suction at the boundary layer, supplying secondary fluid and sucking low-energy fluid. for different angle of attack and frequencies of injection and suction the change in pressure coefficient of top surface is calculated. Separation of boundary layer is controlled by using suction and injection mechanism. The upper surface pressure is also reduced which resulted in increase of lift and decrease of drag. Lift coefficient is increased for moderate to high attack angle. But for more higher attack angles the lift coefficient is decreased because of low interface between the disturbance and shear layer. The performance of wing is increased by lift-to-drag ratio. And stall point is also improved. ([Mashud, 2010](#))

The experiment focused on investigating the influence of various factors on the efficiency oscillatory blowing. Study specifically looked at the effect of blowing slot position, jet steady and oscillatory momentum coefficients, oscillation frequency, airfoil form, and angle of incidence. for the experiment, four alternative airfoil forms were evaluated. Through narrow slits carved into the surface of the airfoils, oscillatory blowing was introduced into the boundary layer. Roughness was provided to certain surfaces in some circumstances to cause early transition and thicken. Flow of airfoils by using slotted flaps was affected by slot geometry, Reynolds number, flap deflection (as part of the airfoil form), and other parameters. Surprisingly, early conversion, deepening of an existing disturbed boundary layer,

or changes in  $Re$  had no effect on the method's performance. The flow was insensitive to lower oscillation frequencies, and this sensitivity diminished when steady blowing or an increase in attack angle were introduced. Notably, there was no appreciable oscillatory lift or periodic vary in the center of force as a cause of the rhythmic blowing. This research highlights the complex interaction of variables situation of oscillatory blowing for separation control. ([Darabi&Wyganski, 2012](#))

The suction method is performed on NATIONAL AERONAUTICS AND SPACE ADMINISTRATION 0012 airfoil. The effect of pressure amplitude, coefficient suction, width on airfoil is examined by numerical investigation. The normal and perpendicular suction is implemented on the airfoil. Turbulent flow with Reynolds number  $5 \times 10^5$  is considered. The  $k-\omega$  SST used to remove turbulence. The relationships among  $C_L$  changes,  $C_D$  dissimilarities, and the lift to drag ratio with suction jet length at different AOA are investigated. Ratio of lift to drag raised force greater than before and separation point moved down stream. Control of flow separation at low angles, using suction had no noticeable effect on aerodynamic properties. Further more, using suction on an airfoil may cause the stall angle to increase. The lift to drag ratio increases with increase using suction jet length and separation point transferred to downstream ([Yousefi, Kianoosh, Zahedi, & Peyman, 2013](#))

The influence of tangential and perpendicular steady blowing method on flow separation management at the trailing edge of NATIONAL AERONAUTICS AND SPACE ADMINISTRATION 0012 airfoil is examined. The change in blowing amplitude and blowing coefficient parameters is numerically modeled. It is computed the influence of blowing amplitude and blowing ratio related to the lifting to drag proportion, lifting factor, and drag factor. The shear stress transfer fluctuation simulation (K-SST) of the Mentor was used for the experiment, and the flow was considered to be completely turbulent. Raising the blowing coefficient has no influence on the stall angle in tangential blowing. This approach delays separation on the airfoil. By increasing the blowing coefficient or amplitude, vortexes formed at the back of the airfoil can be minimized but not eliminated. Separation point is transferred downstream and lift to drag ratio increases with increase of blowing amplitude. In perpendicular blowing stall angle is changed. And by the increase of blowing amplitude complicates the condition and creates greater vortexes. Perpendicular blowing was only helpful at attack angles greater than the stall angle. Blowing increases, the momentum of the boundary layer and the energy given by perpendicular blowing increases turbulence. ([Yousefi, Saleh, Zahedi, & Peyman., 2013](#))

The use of synthetic jets for controlling boundary layer separation was explored in both experimental and computational contexts. The experiment was conducted over a NACA

0015airfoil within a wind tunnel setup. Large Eddy Simulations (LES) were also employed to investigate unstable flow separation over an airfoil at a high Re. The goal was to assess the effectiveness of synthetic jets as a separation control technique. The experimental study observed a notable 70% increase in the lift coefficient through the application of synthetic jets. These jets were generated through a slot that spanned the entire width of the airfoil and associated to a opening within the airfoil itself. This configuration aided in delaying the commencement of flow separation. The synthetic jet's It proved that the suction and blow phases were effective in changing the outermost layer on the airfoil's suction surface. By varying the growth, synthetic jet actuators showed the ability to maintain the boundary layer and enhance interaction among the inner and outer layers of this layer. Enhancing the downstream layer of boundaries and avoiding downstream flow separation were made feasible by blowing synthetic jets. Overall, the study illustrated the potential of synthetic jets as a viable method for mitigating boundary layer separation and improving airfoil performance.[\(D&P.,2008\)](#)



In wind tunnel studies, flow separation control was investigated using a nanosecond pulse plasma actuator. For stall conditions the lift was increased by Twenty% accompanied by drag reduction by 3times. The critical AOA shifts about 5-70. The initial experiments carried out were to demonstrate the basic belongings of actuator on dragging lifting. 3 distinct airfoil models were used : NATIONAL AERONAUTICS AND SPACE ADMINISTRATION-0015 with a 20 cm chord, NLF-MOD22A a 60 cm chord, and NATIONAL AERONAUTICS AND SPACE ADMINISTRATION 63-618 with a Twenty cm chord at flow rates of up to 80 m/s, several shapes of the actuator were evaluated. Actuator's position influence on the wing was calculated, and it was discovered that in the event of leading-edge separation, the most effective position for At the forefront is the actuator. The process of nanosecond plasma actuation has been studied through schlieren imaging experiments. It demonstrated the propagation of shock waves and the development of large-scale vortex structures in the separation zone, resulting in separation elimination. The velocity field and quantitative characteristics of vortex generation were investigated using the PIV diagnostics approach. Small-scale actuator effects were studied in flat-plate still air experiments ([Popov, et al., 2011](#))

The purpose of this work is to build a better flow mechanism by providing a single slot between the two pressure sides of an airfoil in order to overcome the major issues arising with high AOA airfoils such as separated flow, stall, drag high, short lift to drag. A computational study is performed on a NATIONAL AERONAUTICS AND SPACE ADMINISTRATION-2412 airfoil with no slot, hence the point of separation and lift coefficient are reported at various angles of attack.  $C_l$  increases with attack angle up to 180 for all air entry and exits of slots, the slotted mechanism is helpful to enhance stalling angle. For an attack angle greater than 140 wake and pressure drag are high there by flow separation is more influenced by slotted control, thus net  $C_l/C_d$  are improved. For all Attack angles, as slot hole of width 1.5% of chord will result in an increase in  $C_l/C_d$  upto 89%. As a result, slotted airfoils outperform unslotted airfoils in terms of aerodynamic performance at higher attack angles.

This study focuses on the practical use of dynamic separation flow management with three-high-lift wing-body combination in a wind tunnel operating at low speed configuration in a low-speed wind tunnel. Major goal is to prevent local flow separation by carefully positioning slot actuators. ([Paul, Ranjan, Mittal, & Jain, Slotted Flow Separation Control Over ANaca2412 Airfoil, 2012](#))

Computational Fluid Dynamics (CFD) simulations are utilized to analyze the flow characteristics over a Controlled Flow Jet (CFJ) airfoil, aiming to manage flow separation. This approach demonstrates promising results in terms of airfoil performance. The CFJ airfoil achieved more reduced pressure drag, improved stall margin, and lift at high angles of attack. In the NASA 2415 airfoil's computational performance analysis, the entire turbulent boundary layer assumption is used. The standard wall operation, a two-equation standard k-turbulent model, and limited to two dimensions compressible Navier-Stokes calculations form the basis of the solution. The CFJ airfoil technique efficiently delays flow separation, resulting in enhanced cruising aircraft efficiency and better takeoff and landing performance over shorter distances. The CFJ airfoil approach achieves benefits such as improved lift, delayed separation, and high  $cl/cd$  (lift-to-drag ratio). This translates to an expanded attack angle(AOA) operating range and increased stall margin. Due to these attributes, the CFJ airfoil is suitable for both high and low-speed aircraft. The CFJ airfoil concept involves creating an injection near leading edge, through which injected high-velocity tangentially to major flow. This transfer helps the main flow overcome an adverse pressure gradient, ultimately maintaining flow attachment and delaying separation. ([Ciobaca, et al.,2013](#))

A study involving a 150-degree sweep wing (DBD) plasma actuator has been conducted. There search focuses on flow separation control using nanosecond pulsed plasma actuation at flow rates of up to 40m/s .Experimental investigations were approved out in a wind tunnel, utilizing balanced force pressure data to analyze the impact of volt and actuator speed on the swept wing's aerodynamic characteristics. Three different actuator designs with exposed electrodes that are saw toothed and planar were evaluated for their separation flow control effectiveness. The experimentation revealed the existence of electrical energy effective short swept section stream control. Beyond this threshold, as the actuation voltage increased, the control effects improved. A 150-degreeswept wing with a DBD plasma actuator was employed, which effectively improved the aerodynamic performance of the swept wing by exciting the airflow closer to the leading edge. An optimum operational frequency for flow separation control was identified under specific conditions of optimum frequency and voltage. These optimal parameters led to the most effective flow control. As a result, the maximum lift increased by 23.1% and drag decreased by 22.4% at an angle of 14 degrees. This study highlights the potential of using DBD plasma actuators to enhance the aerodynamic performance of swept wings and control flow separation. ([Guangyin,Li, Liang, Han,&Wu, 2015](#))

The goal of this research is to create a boundary layer discovery scheme can be placed on latest planes onto on hand planes. The objective of this detection technique was to present a self-powered vortex generator system that may recognize boundary layer separation and trigger vortex producers delayed it in real time.

In order to characterize frequency domain of BL throughout a range of attack angle that includes stall, wind tunnel tests are undertaken 2D wing with a NATIONAL AERONAUTICS AND SPACE ADMINISTRATION 0012 airfoil at C Re of 500,000 and 1,000,000. Device detects a rise in acoustic output in the low region of force changes, suggesting just beginning division, using flush mounted microphones. The flow is oriented with vane-type vortex generators until the microphones detect separation. The vortex generators are then twisted to produce vortices that delay boundary layer separation at an attack angle.

Comparatively the microphones are successful to detect BL are used to activate vortex generators. These dynamic VG CL 13.8% for Re of 500,000 and 6.9% Re of 1,000,000 when compared to the maximum Cl of clean wing.[\(Jesline, Ibrahim,&New,2016\)](#)

The aerodynamic behavior of transport-type aircraft often con forms to the linear zone where the flow remains coupled and the BL. When the attack angle is raised, however, an unfavourable force incline arises on the outside, causing the flow to lose velocity and detach. This flow separation causes a large drop in lift, which eventually leads to aircraft stall incidents. A real-time pressure measuring technique has been created to overcome this issue. On the surface of the airfoil, two pitot tubes facing opposing directions are placed. The purpose of these tubes is to detect flow separation or stall situations. The position of the separation point on the surface of any particular airfoil may be connected with the attack angle at which stall occurs. As a result, separation point as measured by the pitot probes can efficiently function for stall detection and prevention. Furthermore, by watching the pressure differential between the front and backward-facing pitot tubes as the attack angle varies, it is feasible to exactly guess the performance. This method allows stall detection and avoidance tactics to be executed independent of free stream velocity fluctuations.[\(Aleman, A, Saini, &Gopalarathnam,2017\)](#)

Under low Reynolds numbers, laminar separation and transition have a substantial impact on the wing's aerodynamic characteristics. The importance of using flow control strategies to postpone and eliminate laminar separation is enormous. This study investigates the impact of using the approach in conjunction with a water tunnel test and numerical calculations. At low Reynolds numbers, suction flow management has an effect on the wing's flow state and aerodynamic force. Further investigation is underway regarding the impact of suction flow rate and suction placement on laminar separation, transition, and the aerodynamic performance of wings. Suction proves effective in mitigating laminar and transition separation when the suction orifices are positioned within the separation bubble and in close proximity to the separation point. At a Reynolds number (Re) of employing suction flow control can enhance the wing's lift-to-drag (L/D) ratio by 8.62%, thus leading to improved aerodynamic properties.. ([Jie, Yang, Li, &Cao., 2021](#))

The study findings demonstrate that applying either a single suction jet or simultaneous suction and blowing jets to an airfoil with a flap yields a more significant enhancement in the lift-to-drag ratio (CL/CD) compared to their application on an airfoil lacking a flap. The highest CL/CD ratio achieved with a single suction jet on a flapless airfoil was 73.7. Furthermore, comparing airfoils with and without flaps, the application of a single suction jet led to the most substantial increase in stall angle. This effect was particularly prominent at a suction angle of 90 degrees and a specific suction velocity 0.95. These findings highlight the effectiveness of using suction and blowing jets to improve aerodynamic efficiency and postpone flow separation, with the presence of a flap contributing to better results. ([Ali,Nichkoohi,Salarian,&Khaleghinia.,2019](#))

This study aims to develop a boundary layer separation detection system suitable for installation on new aircraft or retrofitting onto existing ones. The system, once developed, built, and implemented, showcases an autonomous vortex generator mechanism. This system can detect boundary layer separation in real-time and promptly activate vortex generators to mitigate it.

The detection system operates by monitoring changes in acoustic power within the low-frequency range of pressure fluctuations using flush-mounted microphones. When the system detects the onset of separation, vane-type vortex generators, initially aligned with the airflow, are activated. These generators are then adjusted to an optimal attack angle to generate vortices that effectively delay boundary layer separation.

Wind tunnel experiments were conducted using a 2D wing featuring a NASA 0012 airfoil design across a range of attack angles, including stall conditions, with chord Reynolds numbers set at 500,000 and 1,000,000. Remarkably, the same microphones used for boundary layer separation detection are utilized to activate the vortex generators. Comparisons with the maximum lift coefficient (CL) of the clean wing show significant improvements with active vortex generators, enhancing CL by 13.8% and 6.9% for Reynolds numbers of 500,000 and

1,000,000, respectively. ([Morice D, Geary, Baughn, Robinson, & K, 2020](#))

As the technology is developing day by day the change in loads in the increasing wing is also increasing. Increase in wind load result in formation of short waves. This will reduce the aerodynamic performance as well as propulsion system. Hence to increase flight performance many flow control methods have been introduced such as plasma actuators, synthetic jets and vortex generator etc. In this experiment an oblique jet is used to induce a streamline vortex. The results showed many disadvantages when air supply was done by pipe system. And using rod instead of jet gave the same effect on stream-line, but to gain the same effect the streamline vortex generation must be considered and the dimensions of the rod should be appropriate modeled. This paper shows the control of rod vortex generator on a stream pattern downstream by making experimental and numerical analysis. The test section nozzle is designed to give constant airflow i.e., Mach=0.3 in vortex generator. The Reynolds number offflows was 6.6x. The numerical analysis of rod vortex generator was compared with air-jets vortex generators. There were different dimensions of rods analyses for rod vortex generator. The result shows that the rod vortex generators are not far different from air-jet vortex generators. And it's easier to install rods than installing jet actuators. The rods can also be connected to MEMS actuators with an air supply system. An optimized rod vortex generators is potential of giving a similar or sometimes better performance than a air-jet vortex generators. ([Szwaba, Ryszard, Flaszynski, & Doerffer., 2019](#))

The use of passive flow control devices to improve flow quality across a flat-top carrier model was investigated. To investigate flow over the deck, a low-speed wind tunnel is employed to conduct particle image velocimetry. Control devices have been subjected both 0 and 20 degrees yaw for flow visualization analyzes spiral columnar vortex generators and flaps is arranged in different ways. Columnar vortex generators are efficient to control carriered flow separation. Low speed wind tunnel is used to experiment 1/220 scaled LHD carriers. They were installed to evaluate device performance. To gather statistics to access turbulence and vorticity level and to measure instantaneous velocity field PIV system is used. for this investigation, four devices were chosen : two for the bow and two for the longitudinal deck side margins. Because this experiment had previously been carried out on a much bigger scale. Several problems occurred during the experiment, including significant blockage due to the huge model being too large for the test section, the atmospheric boundary layer not being accurately reproduced, and the Reynolds number being too low in comparison to the full-scale vehicle. Despite this imperfection of this important details, the analyze captured the basic flow behavior. Results show that at 0- degree yaw and Twenty-degree yaw both the deck-edge flap and deck-edge columnar vortex generator reduce flight deck turbulence approximately by

a factor of twenty. The plane flap appears to be the most effective bow-only device among all of the devices tested. ([Rafael., 2020](#))

One of the most important parameters which make flying possible is Aerodynamics. Aerodynamics is important for both civil and military aircrafts, because good aerodynamic flight can make the aircraft fuel efficient and also improve its maneuverability. There fore, flow separation is an important problem in aerodynamics and boundary layer control is an important technique to solve that difficulty. NATIONAL AERONAUTICS AND SPACE ADMINISTRATION 2412 Airfoil. According to the study, design requirements such as maximum lift and drag coefficient, ratio are vital creating an appropriate wing for the needed aircraft. Geometry that a wing designer should be including are thickness, camber length, position of camber, and nose radius etc. Other design method used to make a design wing is NATIONAL AERONAUTICS AND SPACE ADMINISTRATION 4 digit or NATIONALAERONAUTICS AND SPACE ADMINISTRATION 5-digit methods, which are basically digit codes which says the dimensions and design of the airfoil geometry. Different Airfoils with dimples and with vortex generators have been designed at different attack angle. Shows the airfoil with dimples gives more coefficient of lift / coefficient of drag ratio than one with vortex generators. Although installing vortex generators increases lift it also increases drag by producing vortices, which can delay flow separation, but can increase fuel consumption because of drag. The airfoils with dimples show better result than one with vortex generators by increasing more lift and less drag. It also has more coefficient of lift /coefficient of drag than airfoil with vortex generators. Hence Airfoil with dimple will be more efficient than airfoil surface with vortex generators. ([Sonia& Bharti., 2017](#))

This paper investigates the flow structure within horizontal equilateral triangular ducts equipped with double rows of vortex generators along the slant surfaces. The experimentation utilizes a closed-loop free-surface water channel measuring 8000 x 1000 x 750 in size. Constructed from 15mm transparent Plexiglas, the channel includes a settling chamber, a honeycomb section, and a two-to-one contraction area. Water flow is supplied by a 15KW centrifugal pump with a velocity control system.

Particle velocimetry technique is employed to measure the flow field during the experiment. The study focuses on analyzing the discrepancies in the secondary flow field induced by two different types of vortex generators. End-view measurements are taken at various cross-sections of the ducts.

The results reveal that the flow behind the second pair of vortex generators is stronger compared to that behind the first pair, but its intensity diminishes in the presence of Duct1. However, the secondary flow strength in Duct2 remains consistent following both pairs of vortex generators. Both ducts demonstrate the successful generation of counter-rotating and dual foci, with Duct2 exhibiting the earlier development of a second pair of twin foci in the stream compared to Duct1. Additionally, it is observed that heat transfer increases within the induced flow field around the vortex pairs. The flow field within the vortex cores is found to be more pronounced in Duct2, resulting in more efficient heat transport compared to Duct1. In summary, the study provides insights into the flow dynamics and heat transfer characteristics within triangular ducts equipped with vortex generators, highlighting the differences between two distinct configurations..([Azize&Akçayoglu, 2011](#))

Wind tunnel experiments and numerical method analysis were done on vortex behavior of a plate on a boundary layer flow to study the importance of height of a vortex generator. Flat plate boundary layer with different H values was studied. Fluent software was used to get exact numerical calculations. for the discretization of Navier-Stokes equation with second-order accuracy difference Finite volume method was used. Mesh was divided using VCEM software in computational domain. The wind tunnel used In a closed-loop wind tunnel with a test section measuring 1.5 x 3 x 4.5, Computational Fluid Dynamics (CFD) calculations revealed that the fluid kinetic energy near the wall peaked when the vortex generator was 1.0 $\delta$  in height. Increasing the height of the vortex generator did not significantly alter the kinetic energy. Varying the height of the vortex generator ( $H=0.66\delta$ , 1.0 $\delta$ , 1.33 $\delta$ ) affected the

boundary layer thickness of the airfoil at different attack angles. The aerodynamic impact of these height variations was analyzed. Results indicated that the presence of vortex generators increased the stall angle by ten degrees. Moreover, the maximum lift coefficient of the airfoil equipped with vortex generators improved by 48.7%, while the drag coefficient decreased by 84% at an 18° attack angle. Despite this improvement, the lift-to-drag ratio decreased when vortex generators were installed compared to when they were absent. However, the best lift-to-drag ratio was achieved at a higher attack angle when vortex generators were utilized. ([Xinkai, Yang, & Wang, 2019](#))



Experimentation has been done to analyze the vortices formed on a flat plain surface installed with synthetic jet actuators. Different actuators are analyzed to find which one achieves efficient delay on the surface. A sole spherical jet controlled by actuators and an array of jets installed at the point of flow separation have been studied and analyzed through some experiments with the help of Particle image velocimetry technique. The single circular jet is installed in to boundary layer to analyze vertical flow structures and attached low momentum fluid at separation. Then the array of jets is attached at the point of separation to analyze how efficiently the vortices are achieving the reattachment of separated flow. For single circular jets the actuators are designed in such a way that its movement can be measured easily and its internal diameter is taken as 45mm and its height is 25mm. for the array of jets experiment, a rectangular hole is made to fix the orifices. Aluminum is used as test plate. It is Five mm thick and it is with elliptical LE with 1:5 thickness length. The flow is kept constant of 0.1 meters per second. Results shows that in vortex impact on boundary layer the secondary and tertiary vortices are more in off-center velocity distribution for central plain. There is so much variation caused by secondary vortex and second variation due to primary vortex. In this series of experiment the stretched and big vortices helped the flow to be attached to boundary layer for a bit longer and tilted vortices push the separation line backward ([Chaudhry,Sultan,A,Farhan,&Asim,2017](#))

Vortex generators are small vanes that help the flow to be attached on the surface by creating vortices. This research shows how this delay of flow separation is achieved at the downstream side of a car roof. Vortex generators although produce drag by producing vortices, they eliminate the bigger drag acting which is formed because of flow separation. Here we find that delta-wing shaped Vortex generators can be efficient devices for improving aerodynamic performance in various applications than bump shaped VG because of different good reasons. Flow visualization techniques are used to read the behavior fluid flow when vortex generators are installed. These techniques of flow stream are divided into three methods. And the flow is analyzed by all these methods separately. Vortex generators are installed at the rear end off the roof of the car. The delta wing vortex generators are 5mm in height, 10mm long and 2.5mm wide. The results of these research shows that the flow was getting separated when there were no vortex generators and flow was attached when there were vortex generators. Coefficient of Drag was decreasing when Reynolds number is increased. If Reynolds number is fixed then the Coefficient of drag with vortex generators is a smaller amount than Cd without vortex generators. Shows how important vortex generators are to control stability and reduce fuel economy. This research results shows the Coefficient of drag has been reduced by 0.215 when vortex generators are

installed. Hence it is proven that vortex generators help in reducing drag in cars. ([Rasedul, Hossain, Mashud, & Gias, 2013](#))

It's been a century since we started flying and still the aircrafts are not 100 percent perfect and efficient. One of such problems is solved with the help of vortex generators. Vortex generators reduce the drag caused by flow separation and increase the stability of an aircraft by creating small instabilities in the form of vortices. In this experiment, two types of vortex generators are analyzed and studied to find which type delays flow separation better. This experiment is done using a low-speed flow visualization wind tunnel. The vortex generators are installed on an aluminum plate which was painted with flat black. 3mm thick tape is used to fix the front portion of the vortex generators to the plate to prevent seepage of smoke and reduce stray filaments. The experiment was done at a high speed of 1.6 feet per second, and the specimens were placed in such a way that the flow touches them at an angle of  $0^\circ$  or  $45^\circ$ . The diameter of the vortices formed was measured using a vernier caliper, and results show that the diameter fluctuates by 85%. Errors were due to eddy currents from the wind tunnel. Optimum vortex generator placement on a wing test section will increase the stability of the flow by delaying the separation. The flow visualization shows that single winglet and Wheeler vortex generators produce vortices that break down at 86% and 55% of the distance, respectively. Perfect placement of vortex generators is found to make perfect vortices, and it is also found that pneumatically actuated vortex generators provide a 30% increase in lift/drag at more than  $12.5^\circ$  angle. ([Farokhi & Sad, 2012](#).)

Series of experiments have been conducted inside a low-speed wind tunnel on three different types of airfoils, and each airfoil was analyzed with and without vortex generators of different cross-sections. Vortex generators can be made of different shapes and sizes, but in this experiment, the researchers used rectangular-shaped vortex generators. The vortex generators could be installed parallel or in pairs to create different types of vortices. The airfoil configuration includes a 250mm chord length, 450mm span length, and 7mm thickness, and the three types of airfoils are National Aeronautics and Space Administration 3-415, NACA 63-215, and 63-430. Installing vortex generators resulted in a good lift coefficient by delaying flow separation and also decreasing the coefficient of drag. The drag increases with the increase in the size of the VG. The paper shows the importance of placing vortex generators because of the experiment, which didn't provide any improvement.

When vortex generators were fixed at Ten% distance of chord from the leading edge.

[\(Filho,Carlos,Cerón-Muñoz, &Catalano.,2013\)](#)

Experiments based on vortex generators to delay flow separation is being conducted on a deflected flap. This experiment is done on an national aeronautics and space administration 63A42 airfoil which has a easy wave also including vane type vortex generators. Flow visualization has been done for vortex generators with two different shapes and with two sizes each. The three testing methods used in the experiments are oil and thermo camera visualization, tuft filaments technique and infrared thermography. The airfoil's configuration was 250mm chord length and a span of 485mm with flap chord ratio of 30%. The two shapes of vortex generators are triangle and rectangle and each shaped vortex generators were made of two different sizes each. i.e., small vortex generators are 1.5 in height and the big ones are 3mm in height. The experiment done in Tuft filament visualization showed that the delay inflow separation was achieved only with big vortex generators with zero attack angle. The oil visualization method was done with and without flap deflection and it showed the separation bubble elimination clearly. This method showed details which weren't seen in tuft filament method. Result shows that the rectangular vortex generators were effective in all methods and small vortex generators were only useful to keep the flow attached when the flow is downstream, there fore positioning is important in case of small vortex generators. Small spacing showed good result in rectangular ones but it was opposite for triangular vortex generators. But in oil visualization technique both rectangular and triangular vortex generators behaved similarly. [\(Součkov, Kuklová, Popelka, & Matějka, 2012\)](#)

The counter rotating vane type vortex generators for transonic convex-corner flow are investigated in this experiment. The convex-corner is a cut down version of top plane of deflect tool same shock-induced BL separation. The experiment took place in a blow-down transonic wind tunnel outfitted with a cool water system, storage space tanks, air dryers, and compressors. A flat plate with and without vortex generators are used in the test model. The plane shield is 450mm extended and 150mm wide, while the instrumentation plate is 170mm long and 150mm wide. They both have a convex corner and  $\theta = 130$  and  $150$ . Upstream of the corner apex, vortex generators are situated. Surface pressure (both mean and fluctuation) is monitored. The length at flow separates was measured using oil-flow virtualization technique. The analysis proves that the high lift devices for transport aircraft can be made using deflected control surface. The mean surface pressure distribution does not affect much by sub- $\delta$  scale vortex generators. Amplitude increases when convex- corner in  $h^*$  which increases drag. This study also shows that the effect of vortex generator directly depends on the M

value. When analysis was done with  $m=0.89$  the low-pressure region downstream underwent expansion on the convex-corner. ([Kung-Ming.Su.&Chang., 2021](#))

Turbulent flow across a NATIONAL AERONAUTICS AND SPACE ADMINISTRATION 0012 airfoil is analyzed numerically by vortex generators being attached to it. Adding vortex generators at high-incident angle gave a better lift coefficient and decreased the drag coefficient. Streamline patterns and pressure coefficient is compared for airfoils with and without vortex generators. The airfoil chosen was NATIONAL AERONAUTICS AND SPACE ADMINISTRATION 0012 and triangle shaped vortex generators are used. When the attack angle of an airfoil is low the airflow is easy going but when attack angle is increased more than stalling angle the flow could not make it across the wing of an airfoil efficiently and smoothly and gets separated which produces the pressure gradient on either side of the airfoil and the flow couldn't control it and stalling happens. This is why we use vortex generators to produce vortices to keep the flow attached and to stop the growth of pressure gradient and drag coefficient. The results of comparison of streamline patterns show effective vortex generators are. It showed that at  $\alpha=11$  the streamline and vortex generators are almost same and the flow is completely attached. It is seen that the inclusion of vortex generators has reduced the poor pressure gradient on top surface of airfoil. Vortices formed from vortex generators have enough strength to delay the stalling for some angles used in this experiment. ([Gopinathan&Ganesh,2015](#))

Aviation industry is one of the many reasons for increasing the greenhouse gas, emission which is a huge threat for the future to come. Hence efforts have been taken in R and D of aircraft for building a fuel-efficient flight. Plasma Vortex generators are known for their drag reduction performance. This experiment shows us improvement in delay stall, post-stall aerodynamic efficiency and maintaining the pre-stall lift-drag ratio by using the plasma vortex generators as the leading-edge vortex generators device. This experiment is done in seven total steps including designing of airfoils, wind tunnel experimentation on all type of airfoils, data analysis, research and presentation etc. Type of airfoil used for the experiment is NATIONAL AERONAUTICS AND SPACE ADMINISTRATION 0021. The experiment airfoil was compared its performance analysis with undulated and baseline airfoil and the results were promising in post stall regime and it delayed the stall angle up to 55%. The aerodynamics of the sample was decreasing when the turbulent intensity and free stream

velocity was increasing. It can be said that plasma vortex generators can be called as leading-edge flow control device. ([Selcuk&Choi., 2017](#))

Vortex Generators were found to be the most efficient device when the scientist was working on making the flow attached to the boundary layer by creating Vortexes which can push back the high momentum separate flow to the surface. Passive and also active types of vortex generator have been used in this experiment to analyze both the Computational method and wind tunnel method. Passive vortex generators include both triangular as well as rectangular vortex generators. The wind tunnel used for this experiment was 20m long with 5m of transparent sides and the test section. Actuators are used while installing the passive vortex generators so that it rotates in counter rotating movement. After the description of the database one-point statistical analysis was done to find mean velocity in all the planes. Then spatial correction was calculated with and without actuation. The turbulent kinetic energy map was plotted and also spatial correction coefficients map. The counter rotating actuator showed a promising result by increasing the efficiency of keeping the flow attached to the boundary surface. This vortex is stronger and later mixes them in boundary layer turbulence. From the three planes analysis result shows that the vortices formed by actuator disappear down stream when the length of airfoil is long. ([Patricia,Godard,Braud,& Stanislas.,2009](#))

S duct diffusers are used in many aircraft jet air intake systems to reduce drag. Using vortex generators, the experiment examines static pressure and total pressure loss. Fox and K line on linear area ratio geometry is selected CATIA V5 and ANSYS is used to compute total pressure recovery over different Mach numbers. There vortex generators had been installed, one on plane-4 and one each on top and bottom. This type of arrangement of vortex gives the best possible performance result. The geometrical parameter includes Inlet area=65x65mm, Angle of turning. Length of center line=440mm. Radius of curvature=280mm. a ratio=1.923. Divergence angle is 7.38. Inlet conditions applied are pressure based and standard K epsilon for making mesh models. Boundary condition includes Reynolds number of 0.68x10<sup>6</sup>. Inlet flow velocity of 15.79m/s and Inlet diameter of hydraulic is 65mm and results show that static pressure recovery was positive and total pressure loss are affected by inlet flow condition. Total pressure loss is limited to 0.270 for bare S duct diffuser for maximum total pressure loss coefficient and skewed inflow profile is increased to 0.822. The S duct with and without vortex generators are analyzed with different flow velocity between Mach 0.6 and 1.0 and result show that in 0.6 Mach the flow was efficient. ([Thenambika, Ponsankar, & M,2016](#))

A Computational Design Approach for a Modified NATIONAL AERONAUTICS AND SPACE ADMINISTRATION-4415 Based on KFM for Improved Aerodynamic Efficiency. This research is based on investigation of aerodynamic characteristics of Kline fogleman airfoil. These are the airfoils which are operated at low Reynolds number. In this research two similar airfoils NATIONAL AERONAUTICS AND SPACE ADMINISTRATION 4415 and kfm2 based NATIONAL AERONAUTICS AND SPACE ADMINISTRATION 4415 is taken. This research showed that the aerodynamic performance for NATIONAL AERONAUTICS AND SPACE ADMINISTRATION 4415 kfm2 based airfoil has a reduction in drag by 24%, which also led to the reduction of lift by 11%. As the reduction of drag is higher than lift it can be considered that the aerodynamic characteristic of airfoil is improved. Thus, we can say that kfm based airfoils has better air flow characteristics when compared to NATIONAL AERONAUTICS AND SPACE ADMINISTRATION 4415 airfoil without any modifications. ([Kabir A. , Akib, Hafiz, & M., 2019](#))

This research is based on identifying the streamlined qualities of kfm based airfoils. The investigation is done on four types of airfoils at an attack angle ranging from  $0^\circ$  to  $15^\circ$ , Mach Number from 0.3 to 0.6. The aerodynamic efficiency of these four airfoils is to be measured. The NATIONAL AERONAUTICS AND SPACE ADMINISTRATION 4415 airfoil and NATIONAL AERONAUTICS AND SPACE ADMINISTRATION 4415 with kfm1, kfm 2, kfm 3 based modifications characteristics are measured by using ANSYS Fluent software. This experiment has shown that having a step on an airfoil gives us a better lift coefficient. It is seen that kfm3 based airfoil has better aerodynamic efficiency than NATIONAL AERONAUTICS AND SPACE ADMINISTRATION 4415 airfoil. This backward step introduces Vortex generators which help airfoil with better lift and drag by reducing flow separation. The kfm 3 has better aerodynamic characteristics when compared to kfm 2 and kfm1 based airfoil. ([Asi, Mehran, Jahan, Akib, & Mili., 2021](#))

In this paper air flow over a NATIONAL AERONAUTICS AND SPACE ADMINISTRATION 0012 airfoil with kfm alteration. In this study, we used four airfoils : NATIONAL AERONAUTICS AND SPACE ADMINISTRATION 0012 and NATIONAL AERONAUTICS SPACE ADMINISTRATION 0012 with kfm 1, kfm 2, and kfm 3 modifications. The computational conditions are taken as density about  $1.2043 \text{ kg/m}^3$ , Wind speed off 16 m/s, attack angle from  $-12^\circ$  to  $+12^\circ$ , the chord is of length is 1m, temperature about 293K and pressure 1atm.

This simulation gave results that by using kfm modified airfoil the air flow control can be improved. This can be seen by the improvements in aerodynamic characteristics of airfoil. The kfm 3 has better air flow properties when compared to kfm 2, kfm 1 and NATIONAL AERONAUTICS AND SPACE ADMINISTRATION 0012 airfoil. With these modifications we can increase safety of flight by preventing accidents. This method can be useful for resisting stall conditions as step take function Of Classical High Drag turbulators ([Aziz, Abdullah, & Islam., 2017](#))

In this research the control over flow separation is tested by using a slotted method. In these two airfoils NATIONAL AERONAUTICS AND SPACE ADMINISTRATION 2412 and NATIONAL AERONAUTICS AND SPACE ADMINISTRATION 2412 with slot is tested By using ANSYS fluent software. The NATIONAL AERONAUTICS AND SPACE ADMINISTRATION 2412 slotted airfoil has entry position at 10% of chord length. this slot has a width 1.5% of cord length. In this simulation the conditions taken as attack angle ranging from  $10^\circ$  to  $20^\circ$ , Reynolds number of  $1.7 \times 10^6$ , velocity of 165.4 m/s.

This simulation of NATIONAL AERONAUTICS AND SPACE ADMINISTRATION 2412 slotted airfoil has shown that using the slot, coefficient of lift increased with attack angle up to 18 degrees for all air entry and exit locations.. From this simulation we get that air entry location and exit location are best at 5% and 25% of chord length. Maximum 85% increment in CL / CD is found at 16 degrees of attack angle. This shows that NATIONAL AERONAUTICS AND SPACE ADMINISTRATION 2412 slotted airfoil has better aerodynamic performance when compared to NATIONAL AERONAUTICS AND SPACE ADMINISTRATION 2412 ([Paul, Ranjan, Mittal, & Jain., Slotted Flow Separation Control Over A Naca 2412 Airfoil." In Proceedings of 39th National Conference on Fluid Mechanics & Fluid Power \(FMFP-2012\),...2012](#))

This research investigates the delay of boundary layer separation by implementing suction slot. In this research a 2-dimensional CFD analysis is made on NATIONAL AERONAUTICS AND SPACE ADMINISTRATION 4412 airfoil and NATIONAL AERONAUTICS AND SPACE ADMINISTRATION 4412 airfoil with slots at different location. For this the parameters taken to be our attack angle ranging from  $0^\circ$  to  $16^\circ$ , Mach number 0.6, suction pressure about 65kpa to 80 Kpa. The finding of correct suction slot position and to reduce flow separation is the aim of this research.

Through a numerical investigation, the effectiveness of using slots to reduce flow separation has been examined. The study reveals that placing slots in the proximity of the trailing edge yields more significant delays in flow separation. Specifically, for an attack angle of 12 degrees, Mach number of 0.6, and positioned slot at 68% of length chord with a 2-degree angle and a suction pressure of 65 kilo pascals, the lift-to-drag ratio was approximately 2.24 higher compare to scenarios with no a suction slot. Furthermore, the investigation indicates that suction slots can enhance aerodynamic performance and delay stalling, especially a higher angles of attack. The findings demonstrate the potential benefits of incorporating suction slots to improve airflow characteristics and delay flow separation in different conditions. The simulations highlight the role of slot placement and suction parameters in achieving these enhancements in aerodynamic performance. (Azim, Ali & Mohammad, 2015)

In this research the flow separation over an airfoil is controlled by using turbulence. The comparison is made between 2 airfoils, they are NATIONAL AERONAUTICS AND SPACE ADMINISTRATION 4415 and NATIONAL AERONAUTICS AND SPACE ADMINISTRATION 4415 with turbulence. For this research particle image velocimetry technique is used. The airfoil of chord length 250 mm and span of 545 mm is used. The setup is made in low-speed wind tunnel of cross section  $0.55\text{M} \times 0.55\text{M}$ , length 1.5M, attack angle 18 degrees, Reynolds number  $1.2 \times 10^5$ , free stream velocity of 20ms. The airfoil with turbulence of wavelength about  $0.25C$  and amplitude  $0.025C$ .

This experiment revealed that applying leading-edge turbulence enhanced the chord wise extent of connected flow while decreasing the height of separated flow. When compared to the trough zone, the attached flow is stronger after the peak region. Separated flow at higher aoa is controlled by the stream wise vortices created at the leading edge. The associated flow is raised by 50%. Thus as compared to the NATIONAL AERONAUTICS AND SPACE ADMINISTRATION 4415 airfoil, the use of turbulence improved aerodynamic performance. (S & Karthikeyan, 2021)



This research shows the experimental investigation of flow separation control. In this experimental low speed wind tunnel setup is used for studying the investigation of flow separation control using spoilers at the upper surface. The conditions for this experiment are taken as attack angle about  $30^\circ$  to  $30^\circ$ , free stream velocity of 40m/Reynolds number  $2.25 \times 10^5$ . The flexible spoilers are arranged such that it is at 67%, 78%, 88% of the chord wise location stoward at trailing edge.

The study investigated the effectiveness of innovative spoilers that deploy automatically upon detecting flow separation at the wing's trailing edge. These self-activating spoilers significantly enhanced the wing's lift generation capability, as evidenced by the increased lift curve slope. Furthermore, the drag penalty associated with their deployment appears minimal. The impact of the flexible spoiler design on overall performance remains to be explored. It has been shown that it was able to produce a secondary lift peak. Thus, the Aerodynamic performance of wing is increased by using the upper surface spoilers for flow separation control.

In this research the modifications are made on airfoil at surface with an out ward direction. For the experiment we have taken two airfoils for comparison, one of NATIONAL AERONAUTICS AND SPACE ADMINISTRATION 4415 airfoil and other NATIONAL AERONAUTICS AND SPACE ADMINISTRATION 4415 with dimples. The dimples are placed at 75%, 50%, 25% of chord length. This experiment is done for a 2D airfoil in CFD software using k-epsilon turbulence model. For this we have taken airfoil of length 210mm, attack angle  $0^\circ$  to  $20^\circ$ , velocity 40ms, with viscosity being  $1.7894 \times 10^{-5}$ . ([Traub, Jaybush, & Lance Logan, 2010](#))

This CFD analysis on the 2D NATIONAL AERONAUTICS AND SPACE ADMINISTRATION 4415 airfoils with dimples and without dimples have shown the results by comparing in lift and drag coefficients. The dimple placed at 25% of chord showed it doesn't provide better result but a bad one. The dimple at 50% also didn't have a good result. But the dimple at 75% chord have shown that it increased stall angle by  $2^\circ$  and lift coefficient by 1-5% at higher attack angle than the NATIONAL AERONAUTICS AND SPACE ADMINISTRATION 4415 airfoil without any dimple. Thus, using of dimples can enhance the performance of airfoil by increasing its Aerodynamic characteristics. ([Kalkur., 2017](#))

This research aims for passive flow control on NATIONAL AERONAUTICS AND SPACE ADMINISTRATION 23012 airfoil in a subsonic flow. The passive flow control over airfoil is achieved by using slot passages cut into the body with difference of 20mm distance from each other. Three different kinds of slots are introduced. The first slot of uniform

thickness runs through the channel. The second slot has non-uniform shape and is designed as a Venturi type of route. The airfoil chord length is 20 mm, the  $Re$  is  $1.3 \times 10^5$ , and attack angle ranges from  $0^\circ$  to  $20^\circ$ .

This Computational work has shown that the usage of passive flow control device can change the unsteady 3D flow on NATIONAL AERONAUTICS AND SPACE ADMINISTRATION 23012 airfoil. This gave beneficial effects on airfoil. The different types of PFC techniques of flow accelerator prove that it can help in increasing the Aerodynamic performance of 2D streamlined bodies. The PFC device at  $20^\circ$  attack angle has shown that lift coefficient as decreased, but there is big reduction in drag. Thus, we can identify that PFC devices can benefit the NATIONAL AERONAUTICS AND SPACE ADMINISTRATION 23012 airfoil. ([Nicholas & N, 2015](#))

This research aims on reduction of skin friction drag by using Rib lets which act as passive flow control technique. for this we have chosen two airfoils NATIONAL AERONAUTICS AND SPACE ADMINISTRATIONS C(2)0610-Root and NATIONAL AERONAUTICS AND SPACE ADMINISTRATIONS C(2)0606-Tip. The conditions taken forth is experiment are as chord length of 17.7m, velocity at takeoff 0.89M and Cruising 0.85M, dynamic viscosity at sea level is  $1.783 \times 10^{-5}$  and high altitude is  $1.43610 \times 10^{-10}$  kg/ms at low Reynolds number. The arranging of zig zag patterns is made such that with height of 0.4mm, 0.6mm an  $dx/c=0.3$ . With an attack angle at  $0^\circ, 5^\circ, 10^\circ, 15^\circ, 18^\circ, 20^\circ$ .

The computational analysis of the usage of Rib lets on airfoil has shown that Self-deploying spoilers triggered by trailing edge separation yielded a moderate lift boost with minimal drag increase. This benefit likely stems from delayed flow separation, which reduces skin friction drag by avoiding a strong adverse pressure gradient. Thus the using of Rib lets of varying sizes and pattern over airfoil can be effective and improve its Aerodynamic characteristics.

In this research the study of flow field over NATIONAL AERONAUTICS AND SPACE ADMINISTRATION 23015 and NATIONAL AERONAUTICS AND SPACE ADMINISTRATION 23015 Kfm2 based airfoil is tested. For this research we have taken a wind tunnel of open cycle with intermittent suction type. The test section is of size  $600 \times 600 \times 2000$ mm, settling chamber of dimension  $1.8 \times 1.8$ m<sup>2</sup>. The parameters taken to be are airfoil of length 165mm, Span 300mm, Free stream Velocity 25m/s, Attack angle  $15^\circ$ . With this the testing of both airfoils are taken place. ([Maniwaran, 2015](#))

In this research the comparison between NATIONAL AERONAUTICS AND SPACE ADMINISTRATION 4412Kfm2 based airfoil and NATIONAL AERONAUTICS AND SPACE ADMINISTRATION 4412 Kfm3 based airfoil to find their Aerodynamic characteristics. The Kfm2 airfoil has a step at 50% of chord length with a thickness of 7-9%,Kfm3 has a step at 50%,75% of chord length with thickness of 9-12%. The 2D setup is made in CFD and analysis in ANSYS FLUENT. The conditions taken as Velocity 5m/s, Attack angle 0° to 15°, Mach number 0.3 to 0.6.

This Computational analysis has shown that Kfm had moderate lift compared to Kfm3. This Kfm3 airfoil has better lift and drag coefficients. The flow separation over Kfm3 is very less compared to Kfm2. This can increase stall angle to further high making it more stable. Thus, we can say that Kfm3 has better Aerodynamic characteristics when compared to [Kfm2 \(Kabir A., Akib, Hasan, & Islam, 2021\)](#)

In this research the performance of stepped airfoil is tested using low turbulence closed loop wind tunnel. For this experiment we have taken RG-15 airfoil and RG-15 with Kfm2 modifications. We need to find the stall resistance of stepped airfoil at different flight conditions experienced by small UAV's. The conditions for arranging this experiment are taken as Airfoil chord length 0.1m, Mach 0.0823, Velocity 4-28m/s, Reynolds Numbers as  $0.28 \times 10^7$ ,  $0.4 \times 10^7$ ,  $0.6 \times 10^7$ ,  $1 \times 10^7$ . This experiment has shown results that stall attack angle is increased by addition of step is not to be found in RG-15 airfoil. The RG-15 has better stall angle when compared to RG-15 Kfm2 based airfoil. The efficiency of RG-15 is better than RG-15 Kfm2 based airfoil. From the results gained by this investigation we have found that RG-15 Kfm2 does not form a vortex generator. Considering all these factors we have identified that the Kfm2 approach is not good for RG-15 airfoil. [\(Robert, Babel, Grzywacz, Stryczniewicz, & Kowaleczko., 2018\)](#)

Vortex generators (VG) and slot treatments are two passive flow management strategies that Bahador Bakhtiari Nia et al. investigated for reducing BL separation on airfoils. Significant improvements in aerodynamic performance were found by their investigation. (CL/CD) was enhanced by up to 112% by VGs at 16.3° incidence angle and 91% by slots at 70% chord length in post-stall situations. The combined VG and slot treatments generally outperformed the individual approaches, despite some degradation at pre-stall angles, indicating potential for optimizing wind turbine performance. [\(Nia, Ja'fari and Ranjbar\)](#)

Researchers employed Improved Delayed Detached Eddy Simulations (IDDES) to explore how flow separation behaves on a NACA0015 airfoil at high Reynolds numbers (1 million). Their focus was on the impact of varying excitation frequency and amplitude, aiming to control flow separation characteristics.

The parametric study revealed a Gaussian distribution of effective sound frequencies centered on the frequency of the primary disturbances in the baseline flow. The optimal excitation frequency ( $F^+ = 1.0$ ) with a constant excitation amplitude of  $A_m = 1.8\%$  resulted in an increase of approximately 43% in the lift-to-drag ratio. Additionally, at the highest excitation level tested ( $A_m = 10\%$ ), a fully reattached flow was achieved, leading to a 120% increase in the aerofoil's lift-to-drag coefficient.

These findings highlight the effectiveness of acoustic excitation in controlling turbulent flow separation, suggesting potential applications in aircraft and gas turbine engine flows. Over all, acoustic excitation demonstrated the ability to delay stall angles and substantially improve aerodynamic efficiency under near-stall conditions. ([Coskun, Rajendran and Pachidis](#))

Techniques for boundary layer control, or BLC, are essential for improving the lifting surfaces' aerodynamic performance. Vortex generators and roughness components are examples of passive approaches that are simple and effective, especially for low-speed flows. Numerous experts' studies have shown that they can postpone separation and lessen drag. On the other hand, whereas semi-active and active techniques like plasma actuators and synthetic jets offer more control, they can also be more expensive and complex. In order to validate the efficacy of BLC approaches and to comprehend the underlying flow mechanics, numerical simulations and experimental research have been crucial.

These studies have helped to build more effective control tactics by offering insightful information about the flow dynamics connected to various approaches. The necessity for geometry-specific optimization and the need to take cost-effectiveness into account while installing active control systems are two challenges in the sector. Subsequent avenues of inquiry seek to tackle these obstacles and enhance BLC techniques for pragmatic implementations. This entails improving energy efficiency and aerodynamic performance in a variety of operating environments, with an emphasis on creating specialized methods for particular applications and geometries. ([Svorcan, Wang and Griffin](#))

To find out how a flap a tiny gap impacts flow separation across the NPU-WA-180. This study concentrated on geometric parameters like flap gap height, angle, and position. Within a limited angle of attack (AoA) range, it was discovered that the airfoil stall characteristics were

greatly enhanced, leading to more lift and decreased drag at higher AoAs. Large gap heights, however, had a detrimental effect on stall performance augmentation. Flap angle was a major element in the features of the stall, the lift increment, and the drag decrease. Additionally, the arrangement of the flaps had a major impact on airfoil performance, with the best outcomes occurring near the separation point.

Studies conducted in low-speed wind tunnels provided empirical evidence for the usefulness of flaps. To increase airfoil aerodynamic performance. The variant that exhibited the greatest increases in maximum lift coefficient and stall characteristics was Type 1, which had a 0.5 mm gap. Though with less lift coefficient increments and drag reduction effects, smaller flap angles were linked to greater AoA ranges for stall relief and earlier stall onset. Type1 at 0.7c demonstrated the best overall impacts on lift and drag coefficients at large AoAs, while Type1 at 0.6c demonstrated improved stall delay effects. It turned out that the flap's fixing location near the dividing point was crucial. Future studies will build three-dimensional bionic airfoil wing configurations, with a special emphasis on bird wing landing configurations, and investigate dynamic flap de formation under aerodynamic stresses. ([Hao, Gao and Wei](#))

# Chapter3

## DESIGNING MODEL

### 3.1 Research gap from the findings and design implementation by using the airfoil co-ordinate values

The literature survey reveals that sudden increases in the attack angle of airfoils can lead to stalling, primarily due to higher drag and pressure differences between the upper and lower surfaces of the airfoil. Stalling occurs when the airflow over the airfoil separates, resulting in a loss of lift and an increase in drag, which can be detrimental to the aerodynamic performance of the aircraft.

To overcome stalling and maintain the coefficient of lift (CL) at certain levels, various techniques have been implemented. These techniques aim to delay or prevent flow separation and reattach the separated flow to the airfoil surface, mainly at higher attack angles.

One of the passive methods used to delay stalling involves employing techniques to reattach the separated flow to the airfoil surface. By strategically manipulating the airflow using passive methods, such as vortex generators, boundary layer suction, or vented airfoils, it is possible to maintain attached airflow over the airfoil surface, even at higher attack angles.

This approach helps to delay stalling and ensure that the airfoil continues to generate lift effectively, thereby improving aerodynamic performance and reducing the risk of stalling-induced accidents. By utilizing passive methods to delay stalling, aircraft designers can enhance the safety and efficiency of aircraft operations, particularly during critical flight phases such as takeoff, landing, and manoeuvres.

### 3.2 CATIA DESIGNING TOOL SOFTWARE :

Dassault Systèmes created CATIA, which stands for Computer Aided Three-dimensional Interactive Application, a powerful design tool. It is used in a wide range of industries, including aeronautical engineering, mechanical engineering, civil engineering, architecture, and electrical engineering.

#### Key Features and Capabilities :

- **Versatility** : CATIA offers a wide range of workbenches that can be tailored to specific design requirements. These include part design, surface design, sheet metal design, and many more, making it suitable for various engineering disciplines.
- **Parametric Modeling** : CATIA allows users to create parametric models, enabling them to modify and update designs easily as per changing requirements.
- **Integration** : Designs created in CATIA can be seamlessly transferred to various analysis software packages, including ANSYS Workbench, for further analysis. This interoperability is facilitated by converting the design files to formats such as STEP (.stp) or IGES (.igs).

### **Application in Airfoil Design :**

In the context of airfoil design, CATIA serves as a valuable tool for creating precise and intricate geometries. Designers can utilize CATIA's features to construct airfoil profiles based on different NACA (National Advisory Committee for Aeronautics) series, such as the NACA 4 and 5 series.

### **Workflow :**

1. **Spline Creation** : Airfoil profiles are often defined using mathematical equations or coordinate data. In CATIA, splines representing these profiles can be created and manipulated to generate the desired 2D airfoil shapes.
2. **3D Wing Creation** : The exported splines from external sources, such as Excel, are imported into CATIA and used to generate three-dimensional wing geometries. This process involves extruding or lofting the 2D airfoil profiles to create the complete wing structure.
3. **Export to Analysis Software** : Once the 3D wing model is finalized in CATIA, it is exported to analysis software like ANSYS Fluent for flow analysis. This export process typically involves converting the CATIA file format to a format compatible with the analysis software.

### **NACA4series :**

- a) NACA0012
- b) NACA2412
- c) NACA2418
- d) NACA2518
- e) NACA2155
- f) NACA2606

**NACA5series :**

- a. NACA23012
- b. NACA21012
- c. 23015
- d. 23021
- e. 24015
- f. 24021

**C0-ORDINATES USED FOR THE DESINING PURPOSE**

**a) NACA0012**

<b>SNO.</b>	<b>X co-ordinate</b>	<b>Y co-ordinate</b>	<b>Z co-ordinate</b>
1	1	1	0
2	0.993844	0.993844	0
3	0.975528	0.975528	0
4	0.945503	0.945503	0
5	0.904508	0.904508	0
6	0.853553	0.853553	0
7	0.793893	0.793893	0
8	0.726995	0.726995	0
9	0.654508	0.654508	0
10	0.578217	0.578217	0
11	0.5	0.5	0



12	0.421783	0.421783	0
13	0.345492	0.345492	0
14	0.273005	0.273005	0
15	0.206107	0.206107	0
16	0.146447	0.146447	0
17	0.095492	0.095492	0
18	0.054497	0.054497	0
19	0.024472	0.024472	0
20	0.006156	0.006156	0
21	0	0	0
22	0.006156	0.006156	0
23	0.024472	0.024472	0
24	0.054497	0.054497	0
25	0.095492	0.095492	0
26	0.146447	0.146447	0
27	0.206107	0.206107	0
28	0.273005	0.273005	0
29	0.345492	0.345492	0
30	0.421783	0.421783	0
31	0.5	0.5	0
32	0.578217	0.578217	0
33	0.654508	0.654508	0
34	0.726995	0.726995	0
35	0.793893	0.793893	0
36	0.853553	0.853553	0
37	0.904508	0.904508	0
38	0.945503	0.945503	0
39	0.975528	0.975528	0

40	0.993844	0.993844	0
41	1	1	0

**b) NACA2412**

<b>SNO.</b>	<b>X co-ordinate</b>	<b>Y co-ordinate</b>	<b>Z co-ordinate</b>
1	1.000084	0.001257	0
2	0.993984	0.002524	0
3	0.975825	0.006231	0
4	0.946027	0.01211	0
5	0.905287	0.019752	0
6	0.854565	0.028653	0
7	0.795069	0.03826	0
8	0.728228	0.048	0
9	0.655665	0.057302	0
10	0.579155	0.065609	0
11	0.500588	0.072381	0
12	0.421921	0.077122	0
13	0.34468	0.079198	0
14	0.271106	0.077802	0
15	0.203313	0.072947	0
16	0.143088	0.064941	0
17	0.091996	0.054325	0
18	0.051324	0.041808	0
19	0.022051	0.028152	0
20	0.004833	0.014049	0
21	0	0	0
22	0.007479	-0.01283	0

23	0.026892	-0.02341	0
24	0.057669	-0.03165	0
25	0.098987	-0.03751	0
26	0.149805	-0.04101	0
27	0.208902	-0.04235	0
28	0.274904	-0.04183	0
29	0.346303	-0.03994	0
30	0.421644	-0.03717	0
31	0.499412	-0.03349	0
32	0.577279	-0.02914	0
33	0.653352	-0.0245	0
34	0.725762	-0.01988	0
35	0.792716	-0.0155	0
36	0.852541	-0.01151	0
37	0.90373	-0.00803	0
38	0.944979	-0.00517	0
39	0.975232	-0.00304	0
40	0.993705	-0.00171	0
41	0.999916	-0.00126	0

**c) NACA2418**

<b>SNO.</b>	<b>Xco-ordinate</b>	<b>Yco-ordinate</b>	<b>Zco-ordinate</b>
1	1.000126	0.001886	0
2	0.994054	0.003582	0
3	0.975973	0.008548	0
4	0.946289	0.016431	0
5	0.905677	0.026698	0

6	0.855071	0.038694	0
7	0.795657	0.0517	0
8	0.728845	0.06497	0
9	0.656243	0.077753	0
10	0.579624	0.089296	0
11	0.500882	0.09885	0
12	0.42199	0.105696	0
13	0.344274	0.108982	0
14	0.270156	0.107711	0
15	0.201916	0.10177	0
16	0.141409	0.091429	0
17	0.090248	0.077283	0
18	0.049738	0.060173	0
19	0.020841	0.041042	0
20	0.004171	0.020768	0
21	0	0	0
22	0.008141	-0.01955	0
23	0.028102	-0.0363	0
24	0.059256	-0.05002	0
25	0.100735	-0.06047	0
26	0.151484	-0.0675	0
27	0.210299	-0.07117	0
28	0.275853	-0.07174	0
29	0.346709	-0.06973	0
30	0.421575	-0.06575	0
31	0.499118	-0.05996	0
32	0.57681	-0.05283	0
33	0.652774	-0.04495	0

34	0.725146	-0.03685	0
35	0.792128	-0.02894	0
36	0.852035	-0.02155	0
37	0.90334	-0.01498	0
38	0.944718	-0.0095	0
39	0.975084	-0.00535	0
40	0.993635	-0.00277	0
41	1.000126	0.001886	0

**d) NACA2518**

<b>SNO.</b>	<b>X co-ordinate</b>	<b>Y co-ordinate</b>	<b>Z co-ordinate</b>
1	1.000151	0.001884	0
2	0.994095	0.00366	0
3	0.976057	0.008853	0
4	0.946427	0.017076	0
5	0.905857	0.027738	0
6	0.855257	0.040113	0
7	0.795788	0.053403	0
8	0.728844	0.066788	0
9	0.656025	0.079448	0
10	0.579107	0.090579	0
11	0.5	0.09941	0
12	0.42071	0.105226	0
13	0.343283	0.107425	0
14	0.269746	0.105591	0
15	0.202041	0.099566	0
16	0.14195	0.089498	0

17	0.09103	0.075839	0
18	0.050565	0.059282	0
19	0.021525	0.040638	0
20	0.00456	0.020682	0
21	0	0	0
22	0.007751	-0.0197	0
23	0.027418	-0.03682	0
24	0.058429	-0.05104	0
25	0.099953	-0.06202	0
26	0.150944	-0.0695	0
27	0.210174	-0.07339	0
28	0.276263	-0.07384	0
29	0.3477	-0.07125	0
30	0.422855	-0.06621	0
31	0.5	-0.05941	0
32	0.577328	-0.05156	0
33	0.652992	-0.04327	0
34	0.725146	-0.03503	0
35	0.791997	-0.02722	0
36	0.85185	-0.02011	0
37	0.90316	-0.01392	0
38	0.94458	-0.00883	0
39	0.975	-0.00503	0
40	0.993594	-0.00268	0
41	0.999849	-0.00188	0

e) **NACA2606**

<b>SNO.</b>	<b>X co-ordinate</b>	<b>Y co-ordinate</b>	<b>Z co-ordinate</b>
-------------	----------------------	----------------------	----------------------

1	1.000063	0.000627	0
2	0.993948	0.001666	0
3	0.975745	0.004683	0
4	0.945876	0.009391	0
5	0.905037	0.015346	0
6	0.854189	0.021997	0
7	0.794544	0.028738	0
8	0.727534	0.034957	0
9	0.654787	0.040085	0
10	0.57816	0.043665	0
11	0.499706	0.045913	0
12	0.421217	0.046804	0
13	0.344649	0.046177	0
14	0.271918	0.043964	0
15	0.204846	0.04021	0
16	0.145111	0.03508	0
17	0.094203	0.028848	0
18	0.053382	0.021868	0
19	0.023646	0.014518	0
20	0.005711	0.007145	0
21	0	0	0
22	0.0066	-0.00633	0
23	0.025298	-0.01132	0
24	0.055612	-0.01493	0
25	0.09678	-0.01713	0
26	0.147782	-0.01794	0
27	0.207369	-0.01745	0
28	0.274091	-0.01585	0

29	0.346334	-0.01337	0
30	0.422348	-0.01033	0
31	0.500294	-0.00702	0
32	0.578275	-0.00372	0
33	0.65423	-0.00083	0
34	0.726456	0.001011	0
35	0.793241	0.001864	0
36	0.852917	0.00193	0
37	0.90398	0.001472	0
38	0.945131	0.000766	0
39	0.975311	0.000061	0
40	0.99374	-0.00044	0
41	0.999937	-0.00063	0

**a) NACA21012**

<b>SNO.</b>	<b>X co-ordinate</b>	<b>Y co-ordinate</b>	<b>Z co-ordinate</b>
1	1.000015	0.00126	0
2	0.993869	0.002193	0
3	0.975583	0.00493	0
4	0.945605	0.009298	0
5	0.904672	0.015036	0
6	0.85379	0.021827	0
7	0.794209	0.029326	0
8	0.727394	0.037168	0
9	0.654989	0.044975	0
10	0.578774	0.052337	0
11	0.500622	0.058813	0



12	0.422454	0.06394	0
13	0.346192	0.067263	0
14	0.273708	0.068388	0
15	0.206786	0.06704	0
16	0.14707	0.063111	0
17	0.096033	0.056676	0
18	0.054848	0.047974	0
19	0.019605	0.034626	0
20	0.000373	0.015489	0
21	0	0	0
22	0.011939	-0.00892	0
23	0.029339	-0.01624	0
24	0.054145	-0.02576	0
25	0.09495	-0.03542	0
26	0.145823	-0.04305	0
27	0.205429	-0.04838	0
28	0.272301	-0.0513	0
29	0.344791	-0.05188	0
30	0.421111	-0.05035	0
31	0.499378	-0.04706	0
32	0.57766	-0.04242	0
33	0.654028	-0.03685	0
34	0.726596	-0.03075	0
35	0.793576	-0.02448	0
36	0.853317	-0.01839	0
37	0.904345	-0.01279	0
38	0.945402	-0.00802	0
39	0.975474	-0.00436	0

40	0.993819	-0.00205	0
41	0.999985	-0.00126	0

**b) NACA23012**

<b>SNO.</b>	<b>X co-ordinate</b>	<b>Y co-ordinate</b>	<b>Z co-ordinate</b>
1	1.000028	0.00126	0
2	0.993891	0.002256	0
3	0.975631	0.005182	0
4	0.945694	0.009859	0
5	0.904816	0.01602	0
6	0.853997	0.023336	0
7	0.794487	0.03145	0
8	0.727745	0.039983	0
9	0.655412	0.048537	0
10	0.579263	0.056686	0
11	0.501169	0.063969	0
12	0.423045	0.069903	0
13	0.346807	0.074014	0
14	0.274326	0.075888	0
15	0.207382	0.075232	0
16	0.146288	0.071464	0
17	0.092309	0.062655	0
18	0.048932	0.048702	0
19	0.018649	0.031767	0
20	0.002449	0.014802	0
21	0	0	0

22	0.009863	-0.01117	0
23	0.030295	-0.01869	0
24	0.060061	-0.02419	0
25	0.098674	-0.02922	0
26	0.146605	-0.0347	0
27	0.204833	-0.04017	0
28	0.271683	-0.04378	0
29	0.344176	-0.04511	0
30	0.420521	-0.04437	0
31	0.498831	-0.04189	0
32	0.577171	-0.03806	0
33	0.653605	-0.03328	0
34	0.726245	-0.02793	0
35	0.793299	-0.02235	0
36	0.853109	-0.01687	0
37	0.904201	-0.0118	0
38	0.945312	-0.00745	0
39	0.975426	-0.0041	0
40	0.993797	-0.00198	0
41	0.999972	-0.00126	0

**c) NACA23015**

<b>SNO.</b>	<b>X co-ordinate</b>	<b>Y co-ordinate</b>	<b>Z co-ordinate</b>
1	1.000035	0.001575	0
2	0.993903	0.002786	0
3	0.975656	0.006342	0
4	0.945742	0.012023	0

5	0.904893	0.019497	0
6	0.854108	0.028362	0
7	0.794635	0.038175	0
8	0.727933	0.048472	0
9	0.655638	0.058764	0
10	0.579525	0.068529	0
11	0.501461	0.077201	0
12	0.42336	0.084187	0
13	0.347136	0.088904	0
14	0.274656	0.090847	0
15	0.2077	0.089657	0
16	0.146249	0.084735	0
17	0.091513	0.07414	0
18	0.047541	0.057813	0
19	0.017193	0.038075	0
20	0.001522	0.018048	0
21	0	0	0
22	0.01079	-0.01441	0
23	0.03175	-0.025	0
24	0.061452	-0.0333	0
25	0.09947	-0.04071	0
26	0.146645	-0.04797	0
27	0.204515	-0.05459	0
28	0.271353	-0.05874	0
29	0.343847	-0.06	0
30	0.420206	-0.05865	0
31	0.498539	-0.05512	0
32	0.57691	-0.0499	0

33	0.653379	-0.04351	0
34	0.726058	-0.03641	0
35	0.79315	-0.02907	0
36	0.852998	-0.02189	0
37	0.904124	-0.01528	0
38	0.945264	-0.00962	0
39	0.9754	-0.00526	0
40	0.993786	-0.00251	0
41	0.999965	-0.00158	0

**d) NACA23021**

<b>SNO.</b>	<b>X co-ordinate</b>	<b>Y co-ordinate</b>	<b>Z co-ordinate</b>
1	1.000049	0.002204	0
2	0.993926	0.003846	0
3	0.975708	0.008663	0
4	0.945838	0.016351	0
5	0.905046	0.026453	0
6	0.85433	0.038413	0
7	0.794932	0.051624	0
8	0.728307	0.065449	0
9	0.656089	0.079218	0
10	0.580048	0.092215	0
11	0.502045	0.103665	0
12	0.423991	0.112754	0
13	0.347793	0.118684	0
14	0.275317	0.120764	0
15	0.208337	0.118507	0

16	0.146169	0.111277	0
17	0.089922	0.097109	0
18	0.044759	0.076036	0
19	0.014282	0.05069	0
20	-0.00033	0.02454	0
21	0	0	0
22	0.012643	-0.02091	0
23	0.034662	-0.03762	0
24	0.064235	-0.05152	0
25	0.101061	-0.06368	0
26	0.146724	-0.07451	0
27	0.203877	-0.08344	0
28	0.270692	-0.08865	0
29	0.34319	-0.08978	0
30	0.419575	-0.08722	0
31	0.497955	-0.08158	0
32	0.576386	-0.07359	0
33	0.652928	-0.06396	0
34	0.725683	-0.05339	0
35	0.792853	-0.04252	0
36	0.852776	-0.03195	0
37	0.903971	-0.02224	0
38	0.945169	-0.01394	0
39	0.975349	-0.00758	0
40	0.993762	-0.00357	0
41	0.999951	-0.0022	0

e) **NACA24015**

<b>SNO.</b>	<b>X co-ordinate</b>	<b>Y co-ordinate</b>	<b>Z co-ordinate</b>
1	1.000043	0.001574	0
2	0.993916	0.002816	0
3	0.975685	0.006462	0
4	0.945795	0.01229	0
5	0.904978	0.019965	0
6	0.854232	0.029079	0
7	0.7948	0.039185	0
8	0.728141	0.049809	0
9	0.655889	0.060457	0
10	0.579816	0.070596	0
11	0.501786	0.079653	0
12	0.423711	0.087023	0
13	0.347502	0.092115	0
14	0.274952	0.09441	0
15	0.206369	0.092926	0
16	0.143699	0.08607	0
17	0.08984	0.07356	0
18	0.04734	0.056594	0
19	0.017905	0.037308	0
20	0.002207	0.017928	0
21	0	0	0
22	0.010104	-0.01489	0
23	0.031038	-0.02608	0
24	0.061654	-0.03445	0
25	0.101143	-0.04101	0
26	0.149194	-0.04652	0
27	0.205846	-0.05136	0

28	0.271057	-0.05516	0
29	0.343481	-0.05677	0
30	0.419855	-0.0558	0
31	0.498214	-0.05265	0
32	0.576618	-0.04782	0
33	0.653128	-0.0418	0
34	0.725849	-0.03507	0
35	0.792985	-0.02805	0
36	0.852875	-0.02117	0
37	0.904039	-0.01481	0
38	0.945211	-0.00935	0
39	0.975372	-0.00514	0
40	0.993773	-0.00248	0
41	0.999957	-0.00157	0

**f) NACA24021**

<b>SNO.</b>	<b>X co-ordinate</b>	<b>Y co-ordinate</b>	<b>Z co-ordinate</b>
1	1.00006	0.002204	0
2	0.993944	0.003876	0
3	0.975748	0.008782	0
4	0.945912	0.016617	0
5	0.905166	0.02692	0
6	0.854503	0.039129	0
7	0.795164	0.052632	0
8	0.7286	0.066784	0
9	0.656441	0.080909	0
10	0.580455	0.094279	0



11	0.502501	0.106113	0
12	0.424482	0.115586	0
13	0.348306	0.121891	0
14	0.275731	0.124324	0
15	0.206474	0.121783	0
16	0.1426	0.112589	0
17	0.087579	0.096473	0
18	0.044477	0.074804	0
19	0.015279	0.049985	0
20	0.000628	0.024492	0
21	0	0	0
22	0.011684	-0.02146	0
23	0.033665	-0.03876	0
24	0.064517	-0.05266	0
25	0.103404	-0.06392	0
26	0.150293	-0.07304	0
27	0.205741	-0.08022	0
28	0.270278	-0.08507	0
29	0.342677	-0.08654	0
30	0.419083	-0.08436	0
31	0.497499	-0.07911	0
32	0.575979	-0.0715	0
33	0.652576	-0.06225	0
34	0.725391	-0.05204	0
35	0.792622	-0.0415	0
36	0.852604	-0.03122	0
37	0.903851	-0.02176	0
38	0.945094	-0.01367	0

39	0.975309	-0.00746	0
40	0.993744	-0.00354	0
41	0.99994	-0.0022	0

### **3D Dimension Model**

Procedure : NACA series airfoil wing co-ordinates were taken from the Airfoil plotter that is CSV file of coordinates were downloaded. All the coordinates are further copied in to MS Excel and generative Shape design excel sheet was used to export all the coordinated in to CATIA.

#### **Obtaining Airfoil Coordinates :**

- Airfoil coordinates for NACA series airfoils are obtained from an Airfoil plotter tool in the form of a CSV file. These coordinates define the shape of the airfoil cross section.
- The CSV file is then imported into Microsoft Excel for further processing.

#### **Data Processing in MS Excel :**

- In Excel, all the airfoil coordinates are copied and organized appropriately for use in CATIA.
- The coordinates typically include the x and y coordinates of points along the upper and lower surfaces of the airfoil.

#### **Exporting to CATIA :**

- CATIA's Generative Shape Design module is utilized to import the airfoil coordinates.
- The Excel sheet containing the coordinates is linked or imported into CATIA's Generative Shape Design environment.

#### **Designing the Airfoil :**

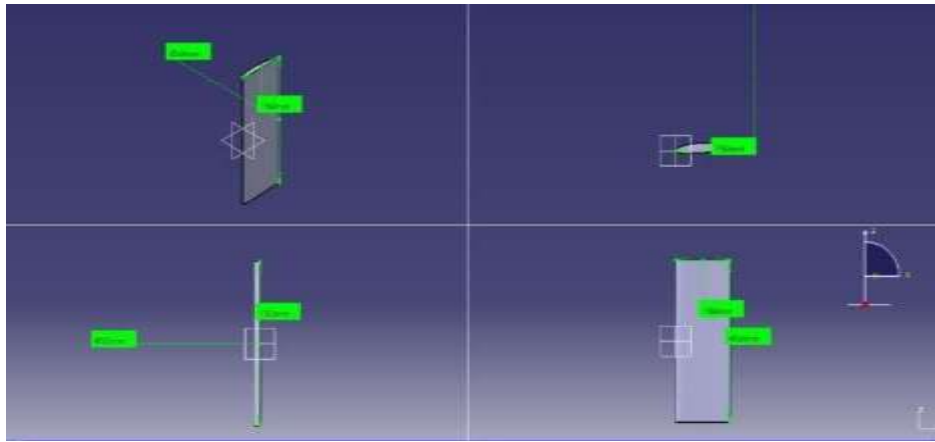
- In CATIA, the imported coordinates are used to create the airfoil profile in 2D.
- Span and chord dimensions are specified according to design requirements. For example, a span of 200mm and a chord of 100mm may be chosen.
- Using lofting or spline tools, the 2D airfoil profile is extended to create a 3D wing structure.

#### **Lofting and Spline Extraction:**

- Lofting involves creating intermediate shapes between two or more cross-sections (in this case, the airfoil profiles) to form a smooth transition between them.
- Splines are curves that smoothly interpolate between given points. In CATIA, splines can be extracted from the lofted surfaces to define the shape of the airfoil wing.

### Padding to Obtain 3D Wing :

- Padding is a CATIA feature used to extrude a profile along a path to create a solid object.
- The extracted splines are padded to obtain a 3D wing structure, with the specified span and chord dimensions.
- **Span** : 200mm **Chord** : 100mm
- Further after all the points, loft and spline are extracted into the CATIA. The Figure shows the points extracted in to CATIA and used for padding to obtain a 3Dwing.



# Chapter4

## CFD PROCEDURE

### 4.1 Computational Fluid Dynamics Overview

Three fundamental principles govern the physical properties of all fluid flows: mass conservation, Newton's second law, and energy conservation. These principles can be mathematically expressed as equations, often taking the form of partial differential equations in their most general representation. The discipline of obtaining a numerical solution to these governing equations and extending the solution across space and time to achieve a comprehensive numerical description of the entire flow area of interest is known as computational fluid dynamics (CFD).

It has revolutionized the way engineers and scientists approach the study of fluid dynamics by providing a virtual laboratory where complex fluid flow scenarios can be simulated and analyzed with high accuracy. CFD relies on solving the governing equations of fluid motion, known as the Navier-Stokes equations, using numerical methods.

We introduce CFD as a numerical simulation technique used for fluid flow analysis. We highlight its significance in understanding and predicting fluid behavior and its impact on various applications in engineering and science. The mention of solving the Navier-Stokes equations gives an initial insight into the mathematical foundation of CFD.

We delve deeper into the working principles of CFD. We explain how the fluid domain is discretized into small computational cells or grids, and the governing equations are solved

iteratively over these grids. The role of boundary conditions, fluid properties, and initial conditions is mentioned in setting up the simulations. This paragraph emphasizes the importance of numerical algorithms and grid generation in the CFD process.

We explore the diverse range of applications of CFD. We mention its ability to simulate various fluid flow scenarios, such as laminar and turbulent flows, compressible and incompressible flows, and multiphase flows. The broad scope of applications, from aerodynamics to heat transfer, weather prediction to combustion engines, is highlighted, showcasing the versatility and significance of CFD in different fields.

We discuss the advantages of using CFD in engineering and scientific research. We highlight how CFD enables engineers and scientists to gain valuable insights into fluid flow behaviors that are often challenging to study experimentally. The potential for optimizing designs, improving performance, and reducing costs associated with physical experiments is mentioned, making a case for the widespread option of CFD in various industries.

We address the importance of validation and calibration in CFD simulations. We emphasize that while CFD offers numerous benefits, accurate and reliable simulations require careful validation against experimental data. The need to ensure that CFD results align with real-world observations is crucial for obtaining meaningful insights and making informed decisions based on simulation outcomes. This paragraph highlights the importance of validating CFD models and maintaining a balance between numerical simulations and experimental data in engineering and scientific research.

The unsteady Navier-Stokes equations, which govern Newtonian fluid dynamics, Despite being known for over a century, research on the analytical reduced forms of these equations, as well as the issue of turbulent closure for the Reynolds-averaged form, is still ongoing. There has been less theoretical progress in the areas of non-Newtonian fluid dynamics, chemically reactive flows, and multiphase flows. Fluid dynamics experiments have been crucial in validating and defining the limitations of various approximations to the governing equations. The wind tunnel has proven to be an excellent experimental tool for simulating natural flows, historically offering a more cost-effective alternative to full-scale measurements. Since the 1950s, the constant growth in computer speed and accessible memory size has resulted in the emergence of computational fluid dynamics. This field of fluid dynamics supplements experimental and theoretical fluid dynamics by offering a more cost-effective method of modeling real-world flows. As such, it provides a technique of verifying theoretical breakthrough for circumstances that are not experimentally available.

The progression of more powerful computers has accelerated advancements in computational fluid dynamics. As a result, computational fluid dynamics has become the preferred method for testing alternative designs in numerous engineering applications. Before final, if any, experimental testing takes place. By adjusting the velocity and vent placement along the chord, analysis of the various flow delays for four distinct airfoils is done. There are four national aviation and space administration's for the computer analysis, five series airfoils were selected. The airfoils are designated of 4 series and 5 series. Both the conventional airfoil design and the vented airfoil designs were subjected to analysis. ANSYS 2021 R1 Software was used for the computational analysis. Software such as Fusion 360 and Catia v5 were used to generate the model.

the velocity and by varying the venting arrangement along the chord. Four airfoils of the NACA5 series have been selected for the computational analysis.

The study was performed on both the standard wing design and the vented wing design. The ANSYS 2021 R1 software was used for the computational study. Catia software was used for modeling.

Airfoil data was downloaded from the airfoil tools website. The airfoils were designed together with a 100mm chord casing. Angles of attack used were  $0^\circ$ ,  $5^\circ$ ,  $10^\circ$ ,  $15^\circ$ ,  $20^\circ$ .

## **COMPUTATIONAL ANALYSIS :**

This study primarily uses numerical simulations based on (CFD) to propose a result to the complicated physical flow phenomena. With contemporary methods and processing architecture, the dependability of CFD has risen in recent years. Nonetheless, CFD will never be able to replace pure theory or experiments; nonetheless, CFD combined with experimentation can be a dependable tool for future study. The experimental approach is largely used to validate the numerical conclusions for specific circumstances; hence the numerical methodology is discussed in depth here. The main steps for numerically solving a fluid dynamics issue include an understanding of the mathematical model, the selection of a discretization technique, the selection and production of a grid, the selection of solution methods, and the selection of temporal discretization.

In this research, the primary software utilized for the Computational Fluid Dynamics (CFD) aspect was ANSYS R21. The initial step involved importing the coordinates of the required airfoils, obtained from the airfoil plotter website. These coordinates were then used to create 3D models in CATIA V5, forming the base models for further analysis. Subsequently, these models were modified to incorporate wings both with and without vents, aimed at conducting comparative analysis.

To proceed with the computational analysis, the completed designs were exported to ANSYS Workbench. Here, they underwent extensive simulations to obtain the desired results. Before conducting the CFD analysis, the imported designs were assigned enclosures and boundary conditions, which are crucial prerequisites for accurately processing the simulations.

Furthermore, the enclosures were subjected to various flow conditions and angles of attack (AOA) to explore their effects on the designs and achieve comprehensive outcomes. The computational fluid dynamics analysis provided valuable data, such as the coefficients of lift, drag, and the ratio of lift to drag (CL/CD), for each design under different conditions.

The study commenced with importing airfoil coordinates and converting them into 3D models using CATIA V5. These models were then manipulated to create wing designs with and without vents for the subsequent analyses. ANSYS Workbench facilitated the computational simulations, where enclosures and boundary conditions were applied before subjecting the designs to various flow conditions and angles of attack. The CFD analysis yielded significant

Data on  $C_L$ ,  $C_D$ , and  $C_L/C_D$ , contributing valuable insights into the aerodynamic performance of each design.

In addition to the computational analysis, experimental investigations were conducted using the Wind Tunnel available at our college. The Wind Tunnel's specifications include [you can list the relevant specifications of the Wind Tunnel].

To begin the experimental phase, balsawood was utilized to create the physical airfoil models. These models were crafted using a CNC (Computer Numerical Control) machine, which allowed precise boring of holes and ensured the accuracy of the airfoil shapes. The production of these wooden airfoils was crucial as they formed the basis for conducting the physical tests in the Wind Tunnel.

Once the wooden airfoils were ready, they were placed inside the Wind Tunnel for testing. To measure aerodynamic forces, a six-component balance was attached to the airfoils during the experiments. This balance allowed for the accurate measurement of forces acting on the airfoils, including lift and drag, as the airflow passed over them.

During the experimental phase, various parameters were adjusted to gather comprehensive data. By systematically varying the airflow speed within the Wind Tunnel and adjusting the attack angle (AOA) of the airfoils, a wide range of test scenarios was explored. This process enabled the acquisition of detailed results for both the wings - one with vents (WV) and the other without vents (WOV). The results obtained from both the computational and experimental approaches contributed to a well-rounded and substantiated conclusion for the research project.



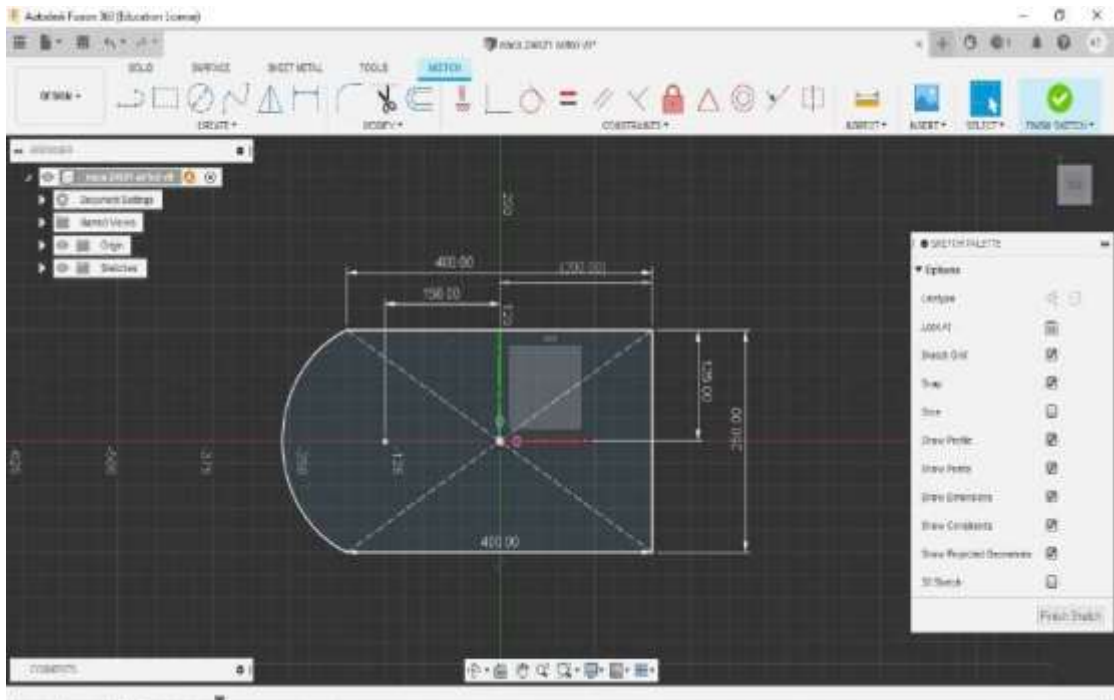


Figure 6 : Design-1

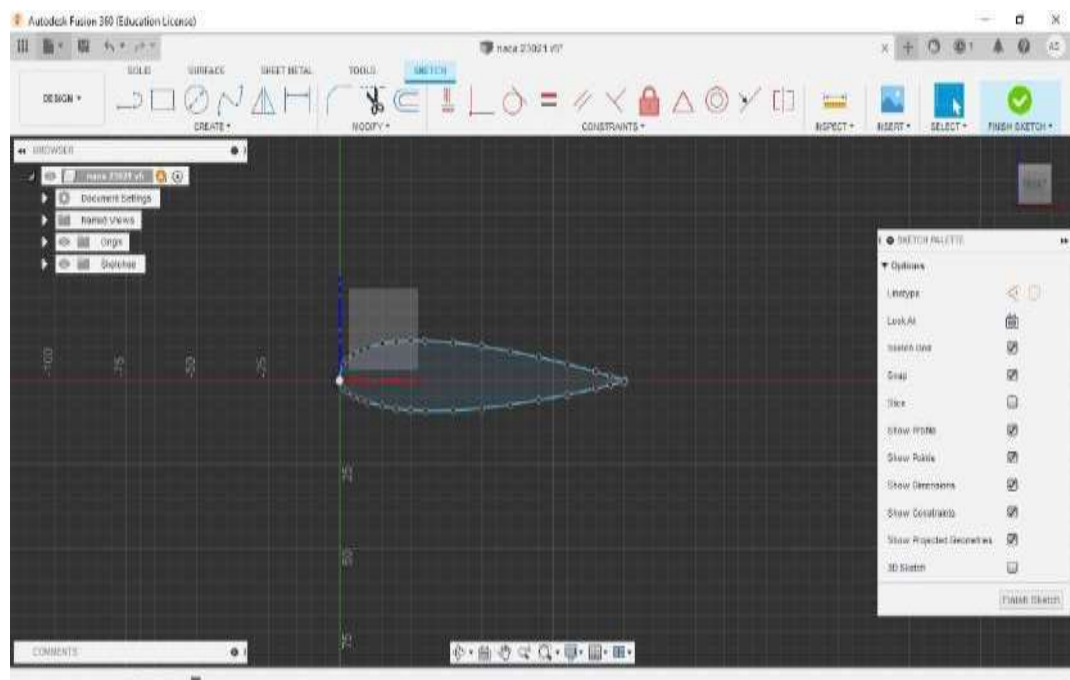


Figure 7 : Design-2

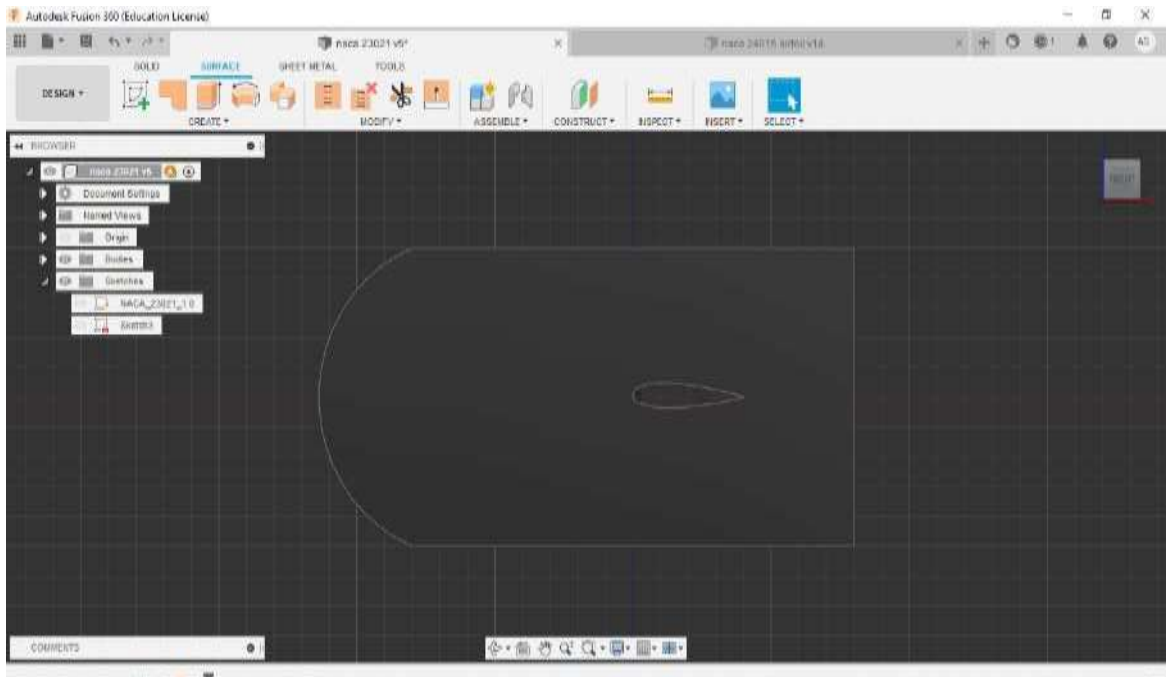


Figure 8 : Design-3

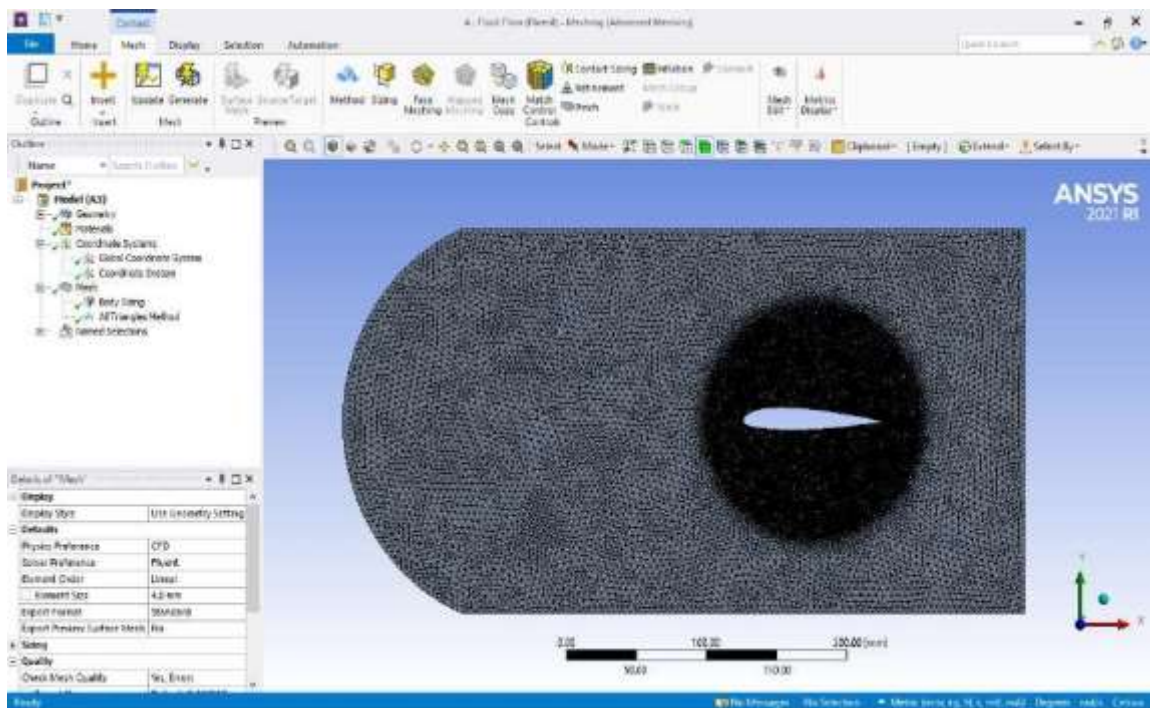


Figure 9 : Workbenchtoolviewone

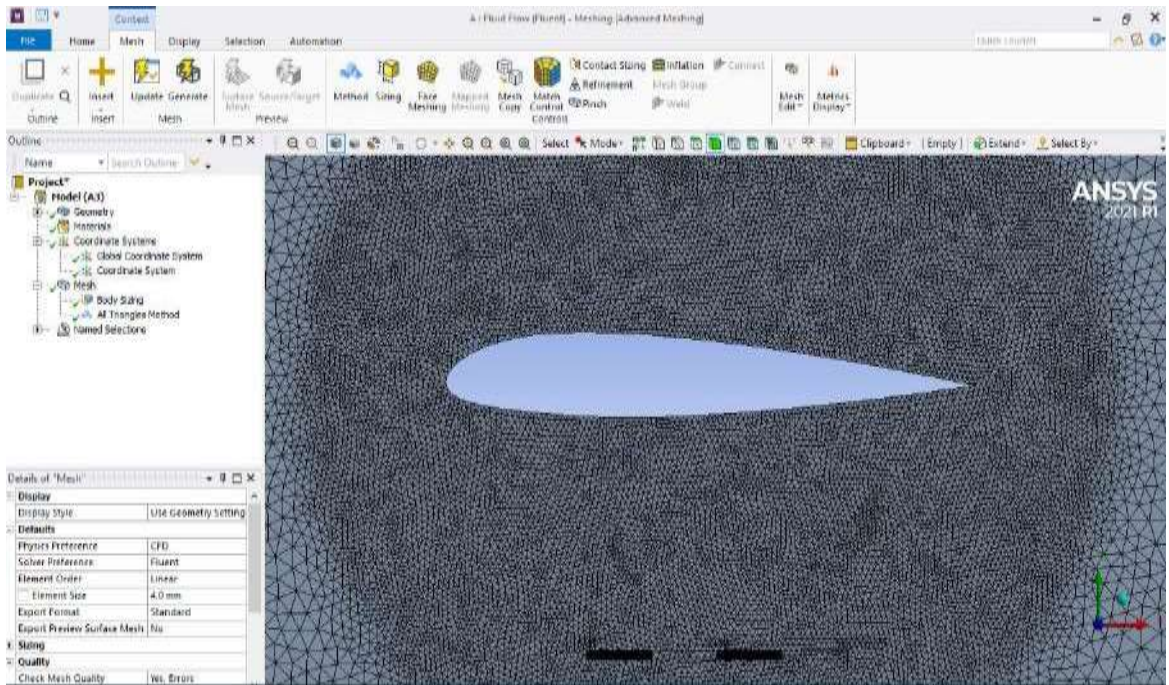


Figure 10 : workbenchtoolviewclosed

ANSYS Fluent was used to compute the Drag force, Lift force, Coefficient of Drag, and Coefficient of Lift. The Fluid flow model was utilized for 5m/s velocity, the Spalart-Allmaras model for 10m/s velocity, and the K-epsilon and K-omega models for 30m/s velocity. Mesh generation, also known as two-dimensional and three-dimensional grid generation, is the act of splitting complicated geometries into pieces that are used to discretize a domain. Mesh elements allow the governing equations to be solved on volumes that are reliably formed and mathematically specified. The equations solved on these meshes are often partial differential equations. There are different types of mesh in two-dimensional and three-dimensional. In this project a three – dimensional Tetrahedron type mesh is generated of element size 5mm and inflations are given around the wing about 15 layers with first layer thickness of 0.1mm

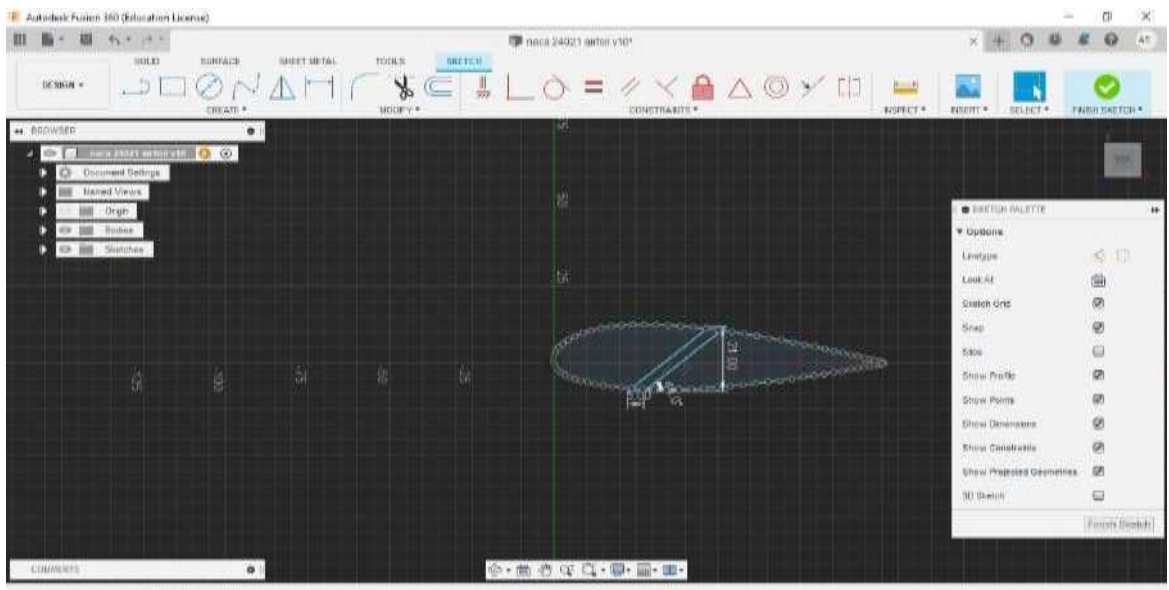


Figure 11 : AirfoilDesigningwithVentStep-1

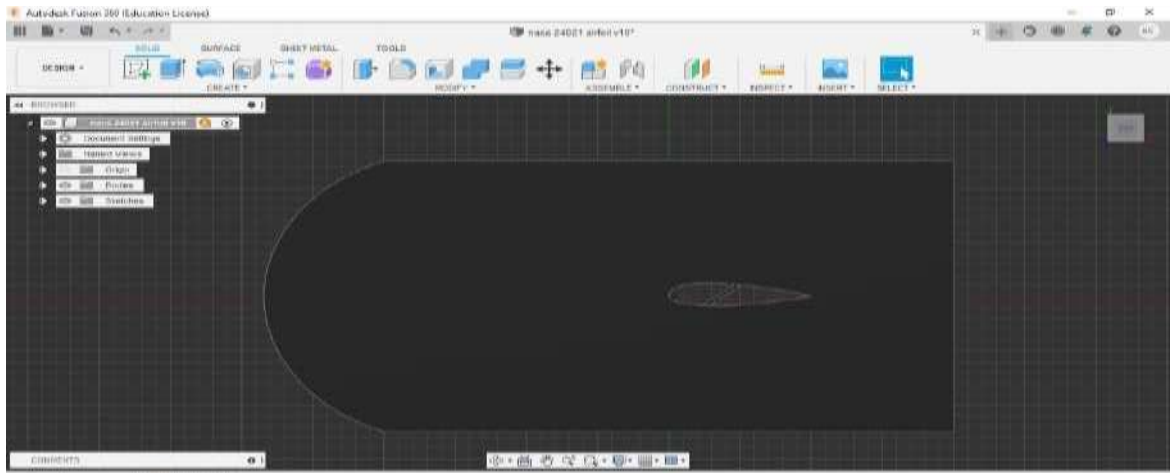


Figure 12 : Vent design

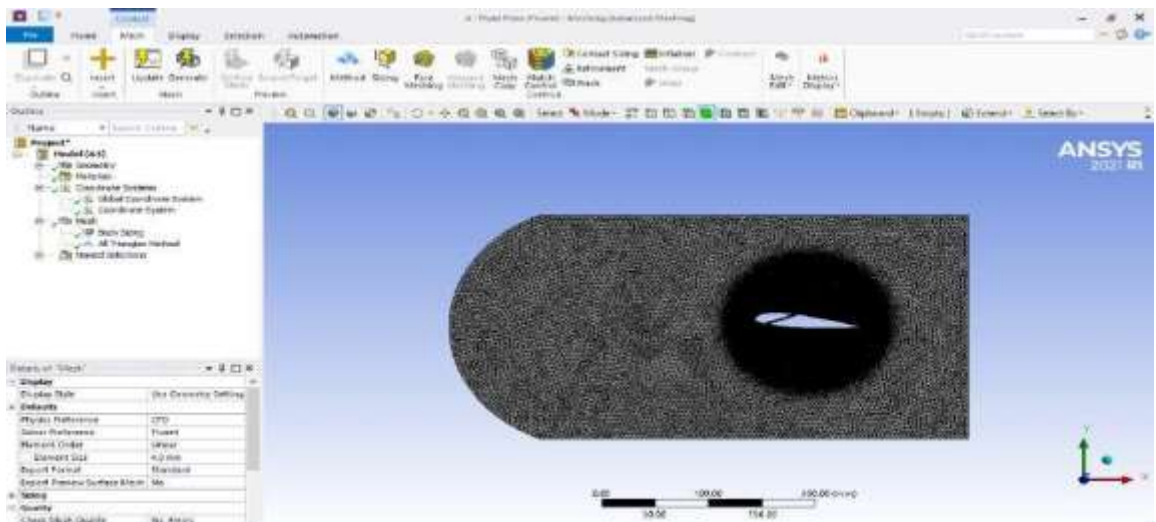


Figure 13 : Vent design meshing

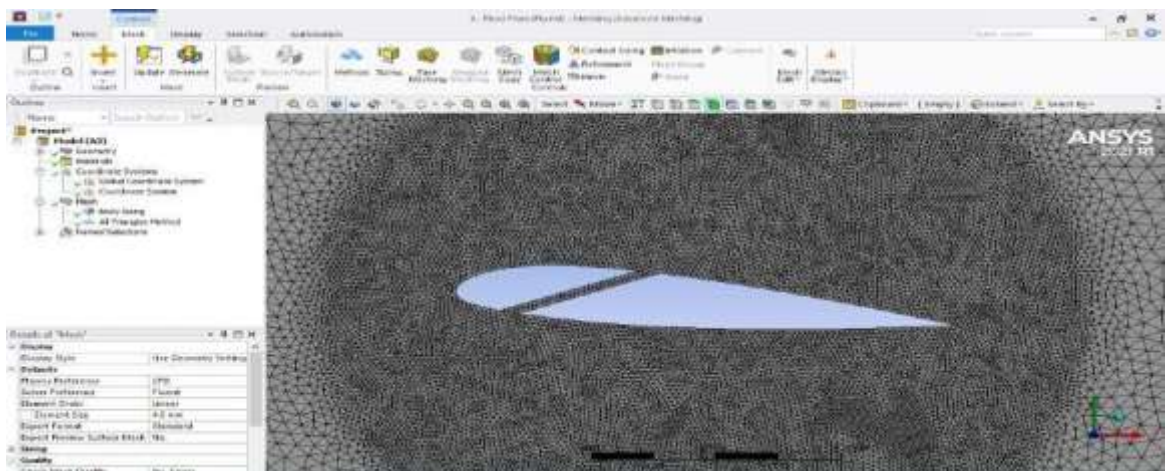


Figure 14 : Vent design in workbench

# Chapter5

## RESULT AND DISCUSION OF CFD ANALYSIS

### 5.1 RESULTS AND DISCUSSIONS

To compare the performance of normal and vented airfoils, parameters are calculated at seven different velocities and five different angles of attack (AOA). Observations for each airfoil at these varying conditions provide a comprehensive understanding of their aerodynamic characteristic. Ansys is a leading software provider for engineering simulation, enabling users to predict product performance throughout the entire product lifecycle. The software is widely used to simulate various conditions without the need for physical prototypes or crash tests.

#### Some applications include :

- Assessing how a bridge withstands long-term usage.
- Optimizing designs to minimize waste, such as in fish can production.
- Designing structures like slides with reduced material use while maintaining safety.

Ansys Fluent enhances CFD (Computational Fluid Dynamics) analysis with advanced capabilities :

- It offers a fluid simulation platform with short pre-processing and solving times, accelerating time-to-market.
- It supports limitless creativity without sacrificing accuracy, thanks to its industry-leading features.

#### Numerical Methods in Ansys Fluent

SIMPLE Algorithm

#### SIMPLE:

- A commonly utilized numerical technique for solving the Navier-Stokes equations, which govern the behavior of fluid flow.
- Transition k- $\omega$  Model

**Model Used :**

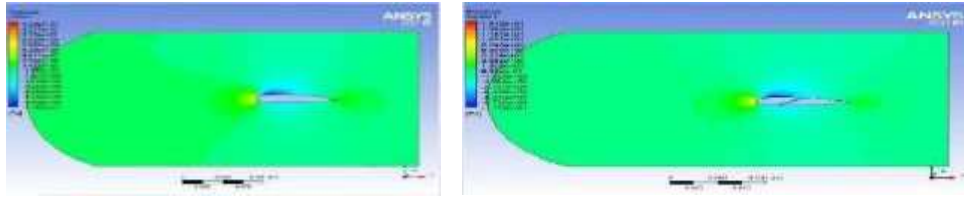
**Transition k-kl-omega :** Suitable for incompressible flows.

Particularly useful for low Reynolds numbers and transition modeling, which are critical for predicting the conversion from turbulent to laminar flow and understanding BL behavior.

**NATIONAL ADVISORY COMMITTEE FOR AERONAUTICS 23015 With vent and  
With out vent :**

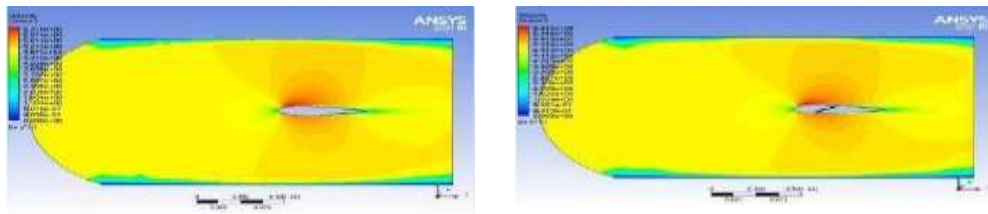
**5.2 Zero Attack angle :** - These Figures help visualize how airflow, velocity, and pressure distributions change with different attack angles, impacting lift and overall airfoil performance

### 5.3 Five m/s

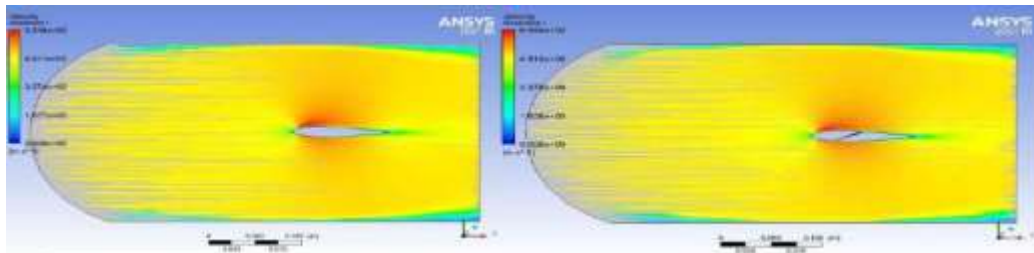


**Figure 15 :** Pressure Contours : This image depicts the pressure surrounding airfoil. The color map indicates pressure levels, with green representing lower pressures and red/yellow indicating higher pressures. The airfoil front edge experiences higher pressure, while top surface experiences lower p compared to the bottom surface with (AOA = 0°) at 5 m/s

**Figure 15 :** pressure and velocity for both at Five m/s



**Velocity Contours :** This image likely illustrates pattern velocity surrounding airfoil. colors indicate different velocities, with blue representing lower velocities and green/yellow/orange indicating higher velocities. The velocity is higher on the top surface compared to the bottom surface, which is typical for generating lift even at zero attack angle with (AOA = 0°) at 5 m/s

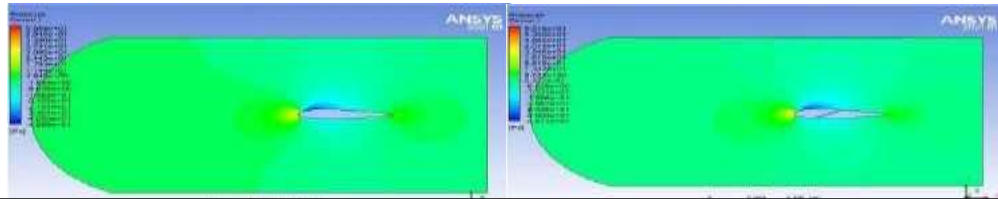


**Figure 16 :** Stream lines depicting airflow patterns showing how air flows smoothly over the airfoil or separates from the surface. Streamlines closer together indicate higher velocity regions, while separation bubbles indicate areas of flow separation. with (AOA = 0°) at 5 m/s

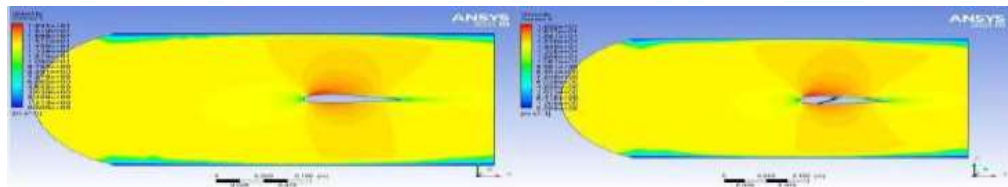
**Figure 16 :** Streamline for Both at Five m/s



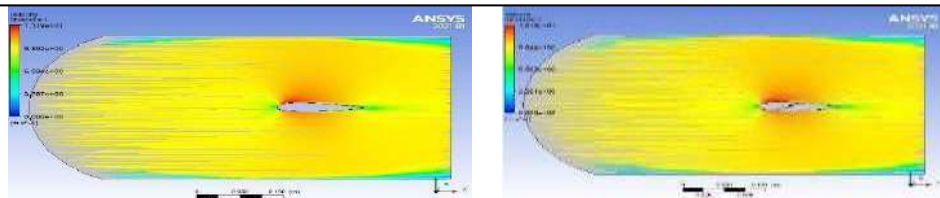
#### 5.4 Ten m/s-



Pressure Contours : This image depicts the pressure surrounding airfoil. The color map indicates pressure levels, with green representing lower pressures and red/yellow indicating higher pressures. The airfoil front edge experiences higher pressure, while top surface experiences lower p compared to the bottom surface with (AOA = 0°) at 10 m/s



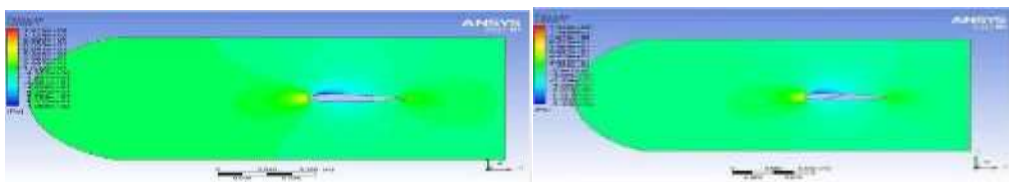
Velocity Contours : This image likely illustrates pattern velocity surrounding airfoil. colors indicate different velocities, with blue representing lower velocities and green/yellow/orange indicating higher velocities. The velocity is higher on the top surface compared to the bottom surface, which is typical for generating lift even at zero attack angle with (AOA = 0°) at 10 m/s



Stream lines depicting airflow patterns showing how air flows smoothly over the airfoil or separates from the surface. Streamlines closer together indicate higher velocity regions, while separation bubbles indicate areas of flow separation. with (AOA = 0°) at 10 m/s

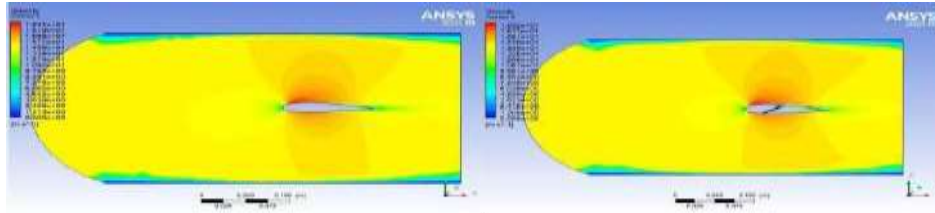
Figure 17 : Streamline for Both at Ten m/s

#### 5.5 15m/s-



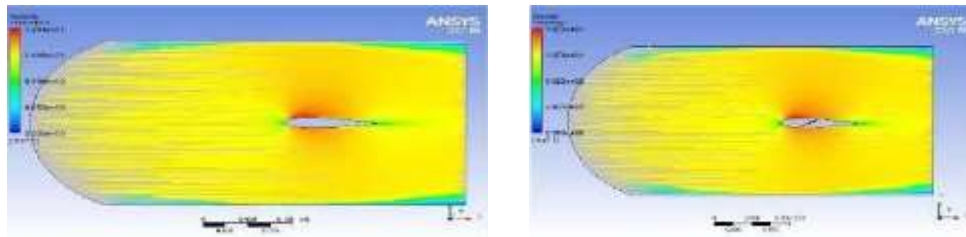
Pressure Contours : This image depicts the pressure surrounding airfoil. The color map indicates pressure levels, with green representing lower pressures and red/yellow indicating higher pressures. The airfoil front edge experiences higher pressure, while top surface experiences lower p compared to the bottom surface with (AOA = 0°) at 15 m/s

Figure 18 : Pressure for Both at fifteen m/s



Velocity Contours : This image likely illustrates pattern velocity surrounding airfoil. colors indicate different velocities, with blue representing lower velocities and green/yellow/orange indicating higher velocities. The velocity is higher on the top surface compared to the bottom surface, which is typical for generating lift even at zero attack angle with (AOA = 0°) at 15 m/s

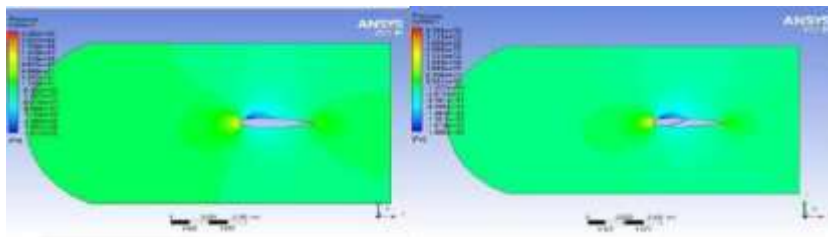
Figure 19 : Velocity for at fifteen m/s



Stream lines depicting airflow patterns showing how air flows smoothly over the airfoil or separates from the surface. Streamlines closer together indicate higher velocity regions, while separation bubbles indicate areas of flow separation. with (AOA = 0°) at 15 m/s

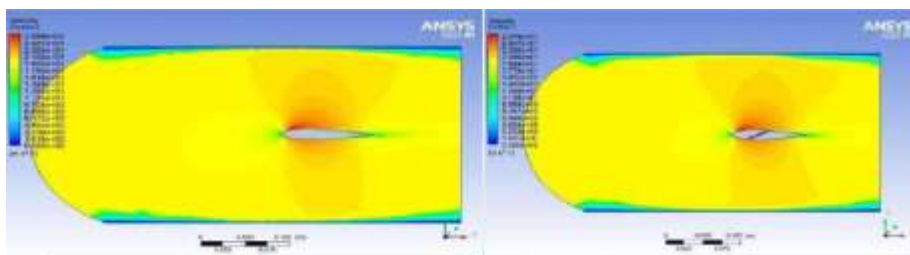
Figure 20 : Streamline for Both at fifteen m/s

## 5.6 Twenty m/s-



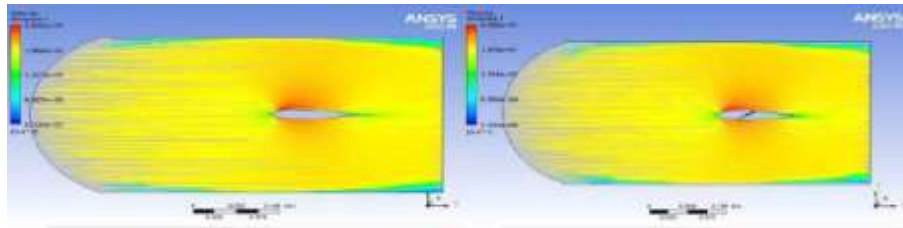
Pressure Contours : This image depicts the pressure surrounding airfoil. The color map indicates pressure levels, with green representing lower pressures and red/yellow indicating higher pressures. The airfoil front edge experiences higher pressure, while top surface experiences lower p compared to the bottom surface with (AOA = 0°) at 20 m/s

Figure 21 : Pressure for Bo that Twenty m/s



Velocity Contours : This image likely Illustrates pattern velocity surrounding airfoil. colors indicate different velocities, with blue representing lower velocities and green/yellow/orange indicating higher velocities. The velocity is higher on the top surface compared to the bottom surface, which is typical for generating lift even at zero attack angle with (AOA = 0°) at 20 m/s

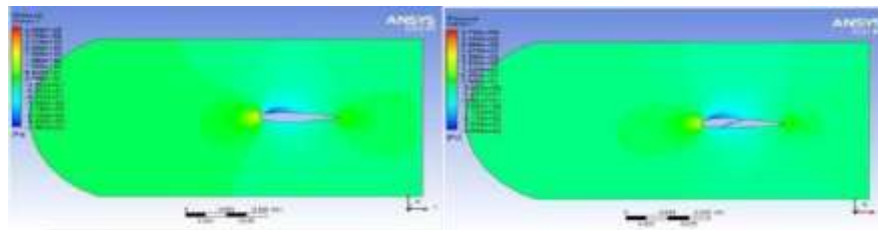
Figure 22 : Velocity Plot for Both at Twenty m/s



Stream lines depicting airflow patterns showing how air flows smoothly over the airfoil or separates from the surface. Streamlines closer together indicate higher velocity regions, while separation bubbles indicate areas of flow separation. with (AOA = 0°) at 20 m/s

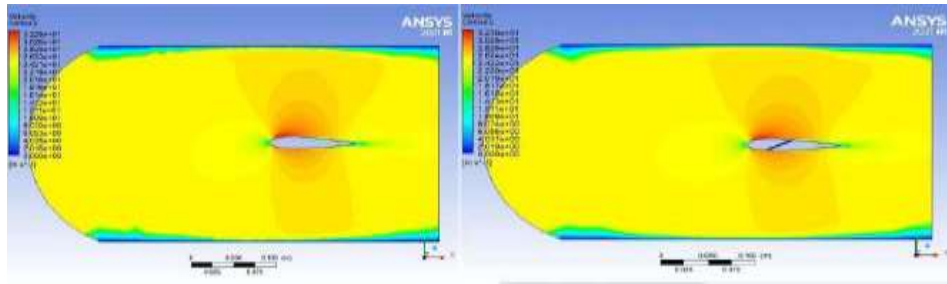
Figure 23 : Streamline for Both at Twenty m/s

### 5.7 25m/s-



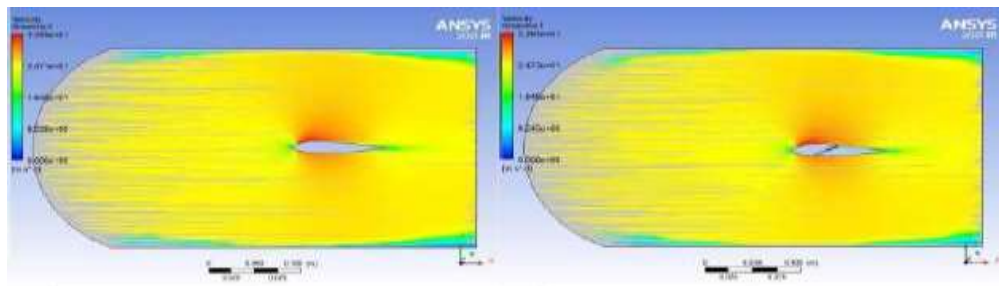
Pressure Contours : This image depicts the pressure surrounding airfoil. The color map indicates pressure levels, with green representing lower pressures and red/yellow indicating higher pressures. The airfoil front edge experiences higher pressure, while top surface experiences lower p compared to the bottom surface with (AOA = 0°) at 25 m/s

Figure 24 : Pressure for Both at twenty Five m/s



Velocity Contours : This image likely illustrates pattern velocity surrounding airfoil. colors indicate different velocities, with blue representing lower velocities and green/yellow/orange indicating higher velocities. The velocity is higher on the top surface compared to the bottom surface, which is typical for generating lift even at zero attack angle with (AOA = 0°) at 25 m/s

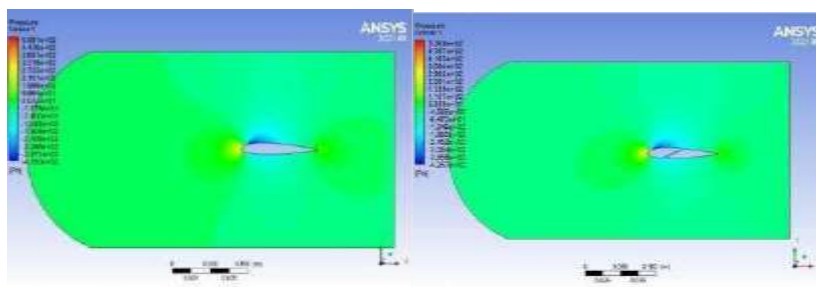
Figure 25 : Velocity for Both at twenty Five m/s



Stream lines depicting airflow patterns showing how air flows smoothly over the airfoil or separates from the surface. Streamlines closer together indicate higher velocity regions, while separation bubbles indicate areas of flow separation. with (AOA = 0°) at 25 m/s

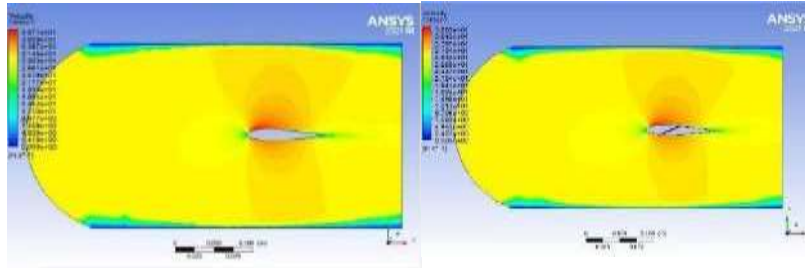
Figure 26 : Streamline for Both twenty Five m/s

### 5.8 Thirty m/s-



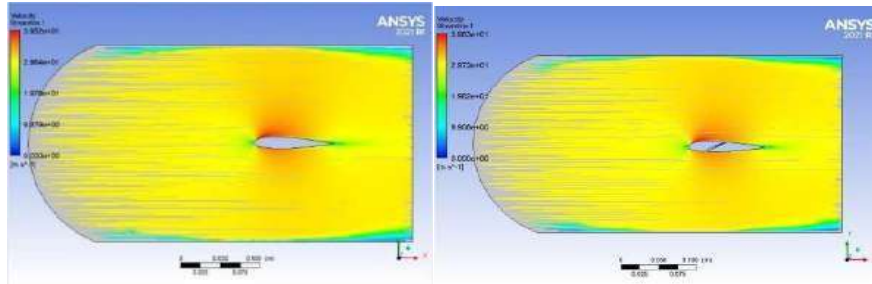
Pressure Contours : This image depicts the pressure surrounding airfoil. The color map indicates pressure levels, with green representing lower pressures and red/yellow indicating higher pressures. The airfoil front edge experiences higher pressure, while top surface experiences lower p compared to the bottom surface with (AOA = 0°) at 30 m/s

Figure 27 : Pressure for Both Thirty m/s



Velocity Contours : This image likely illustrates pattern velocity surrounding airfoil. colors indicate different velocities, with blue representing lower velocities and green/yellow/orange indicating higher velocities. The velocity is higher on the top surface compared to the bottom surface, which is typical for generating lift even at zero attack angle with (AOA = 0°) at 30 m/s

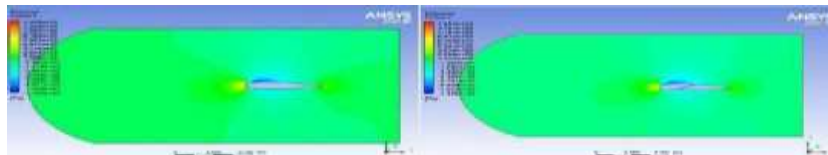
Figure 28 : Velocity for Both at Thirty m/s



Stream lines depicting airflow patterns showing how air flows smoothly over the airfoil or separates from the surface. Streamlines closer together indicate higher velocity regions, while separation bubbles indicate areas of flow separation. with (AOA = 0°) at 30 m/s

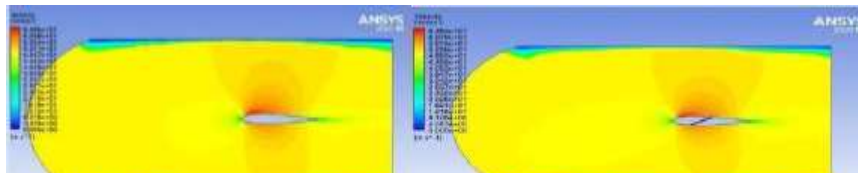
Figure 29 : Streamline for Both at Thirty m/s

## 5.9 Fifty m/s-



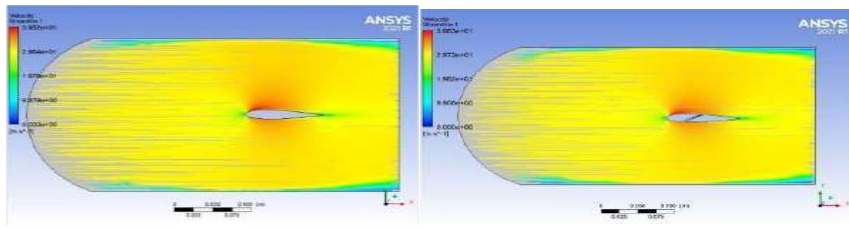
Pressure Contours : This image depicts the pressure surrounding airfoil. The color map indicates pressure levels, with green representing lower pressures and red/yellow indicating higher pressures. The airfoil front edge experiences higher pressure, while top surface experiences lower p compared to the bottom surface with (AOA = 0°) at 50 m/s

Figure 30 : Pressure for Both Fifty m/s



Velocity Contours : This image likely illustrates pattern velocity surrounding airfoil. colors indicate different velocities, with blue representing lower velocities and green/yellow/orange indicating higher velocities. The velocity is higher on the top surface compared to the bottom surface, which is typical for generating lift even at zero attack angle with (AOA = 0°) at 30 m/s

Figure 322 : Velocity for both at Fifty m/s



Stream lines depicting airflow patterns showing how air flows smoothly over the airfoil or separates from the surface. Streamlines closer together indicate higher velocity regions, while separation bubbles indicate areas of flow separation. with (AOA = 0°) at 50 m/s

Figure 313 : Streamline for Both at Fifty m/s

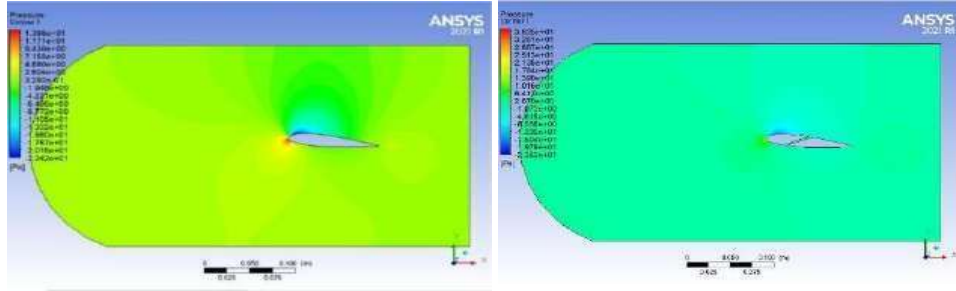
Table of Design Points									
	A	B	C	D	E	F	G	H	I
1	Name	P1 - inletvel	P2 - drag-op	P3 - drag-force-op	P4 - lift-op	P5 - lift-force-op	Retain	Retained Data	Note
2	Units	m s <sup>-1</sup>		N		N			
3	DP 0 (Current)	50	0.0018717	2.8661	0.011287	17.283	<input checked="" type="checkbox"/>	<input checked="" type="checkbox"/>	
4	DP 1	30	0.00076614	1.1732	0.0039349	6.0254	<input checked="" type="checkbox"/>	<input checked="" type="checkbox"/>	
5	DP 2	25	0.00055876	0.85559	0.0026974	4.1303	<input checked="" type="checkbox"/>	<input checked="" type="checkbox"/>	
6	DP 3	20	0.00037975	0.58149	0.0016288	2.4941	<input checked="" type="checkbox"/>	<input checked="" type="checkbox"/>	
7	DP 4	15	0.00023301	0.3568	0.00087203	1.3353	<input checked="" type="checkbox"/>	<input checked="" type="checkbox"/>	
8	DP 5	10	0.00011869	0.18174	0.00036536	0.55945	<input checked="" type="checkbox"/>	<input checked="" type="checkbox"/>	
9	DP 6	5	3.9189E-05	0.060009	8.1942E-05	0.12547	<input checked="" type="checkbox"/>	<input checked="" type="checkbox"/>	
*							<input type="checkbox"/>		

Table1 : Drag and Lift force values, 23015Airfoilat zeroAOA

Table of Design Points									
	A	B	C	D	E	F	G	H	I
1	Name	P1 - inletvel	P2 - drag-op	P3 - drag-force-op	P4 - lift-op	P5 - lift-force-op	Retain	Retained Data	Note
2	Units	m s <sup>-1</sup>		N		N			
3	DP 0 (Current)	50	0.0021536	3.2976	0.0068552	10.497	<input checked="" type="checkbox"/>	<input checked="" type="checkbox"/>	
4	DP 1	30	0.00086531	1.325	0.0023659	3.6227	<input checked="" type="checkbox"/>	<input checked="" type="checkbox"/>	
5	DP 2	25	0.00062753	0.96091	0.0016085	2.4631	<input checked="" type="checkbox"/>	<input checked="" type="checkbox"/>	
6	DP 3	20	0.00042454	0.63008	0.0010246	1.5689	<input checked="" type="checkbox"/>	<input checked="" type="checkbox"/>	
7	DP 4	15	0.0002583	0.39552	0.00052867	0.80953	<input checked="" type="checkbox"/>	<input checked="" type="checkbox"/>	
8	DP 5	10	0.00013015	0.19929	0.00018941	0.29003	<input checked="" type="checkbox"/>	<input checked="" type="checkbox"/>	
9	DP 6	5	4.2902E-05	0.065693	5.8456E-05	0.08951	<input checked="" type="checkbox"/>	<input checked="" type="checkbox"/>	
*							<input type="checkbox"/>		

Table2 : Drag and Lift force values, 23015 Air foil at zero AOA

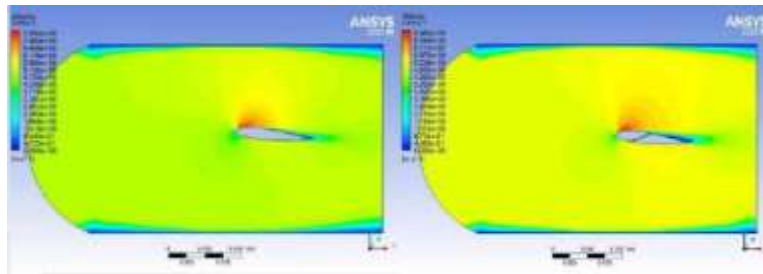
### 5.10 Five Attack angle : -



Pressure Contours : This image depicts the pressure surrounding airfoil. The color map indicates pressure levels, with green representing lower pressures and red/yellow indicating higher pressures. The airfoil front edge experiences higher pressure, while top surface experiences lower p compared to the bottom surface with (AOA = 5°) at 5 m/s

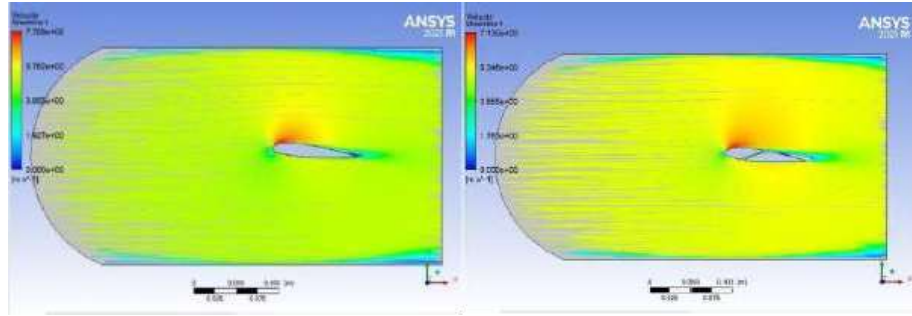
Figure 33 : Pressure at 5° for Both Five m/s

### 5.11 Five m/s



Velocity Contours : This image likely illustrates pattern velocity surrounding airfoil. colors indicate different velocities, with blue representing lower velocities and green/yellow/orange indicating higher velocities. The velocity is higher on the top surface compared to the bottom surface, which is typical for generating lift even at zero attack angle with (AOA = 5°) at 5 m/s

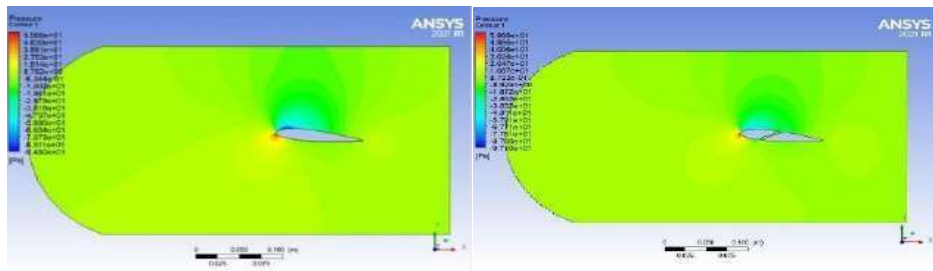
Figure 34 : Velocity at 5°at Five m/s



Stream lines depicting airflow patterns showing how air flows smoothly over the airfoil or separates from the surface. Streamlines closer together indicate higher velocity regions, while separation bubbles indicate areas of flow separation. with (AOA = 5°) at 5 m/s

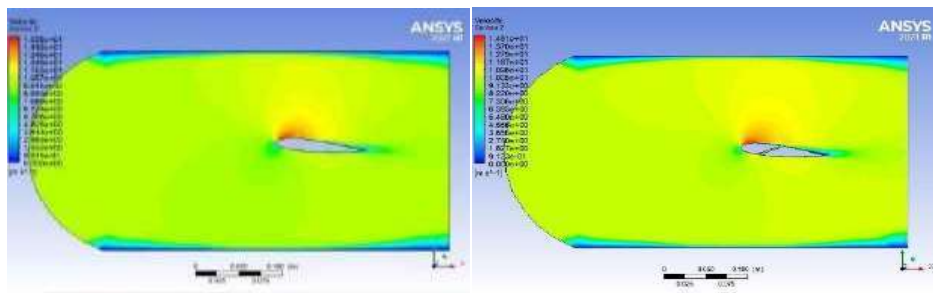
Figure 35 : Streamline at 5° for Both at Five m/s

5.12 Ten m/s-



Pressure Contours : This image depicts the pressure surrounding airfoil. The color map indicates pressure levels, with green representing lower pressures and red/yellow indicating higher pressures. The airfoil front edge experiences higher pressure, while top surface experiences lower p compared to the bottom surface with (AOA = 5°) at 10 m/s

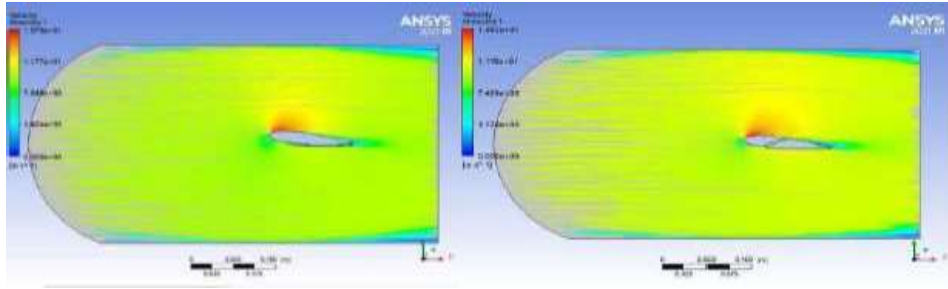
Figure 377 : Pressure at 5° for at Ten m/s



Velocity Contours : This image likely Illustrates velocity pattern surrounding airfoil. colors indicate different velocities, with blue representing lower velocities and green/yellow/orange indicating higher velocities. The velocity is higher on the top surface compared to the bottom surface, which is typical for generating lift even at zero attack angle with (AOA = 5°) at 10 m/s

Figure 368 : Velocity at 5° for Both Ten m/s

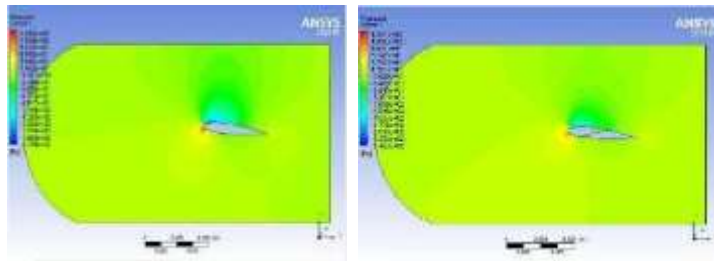




Stream lines depicting airflow patterns showing how air flows smoothly over the airfoil or separates from the surface. Streamlines closer together indicate higher velocity regions, while separation bubbles indicate areas of flow separation. with (AOA = 5°) at 5 m/s

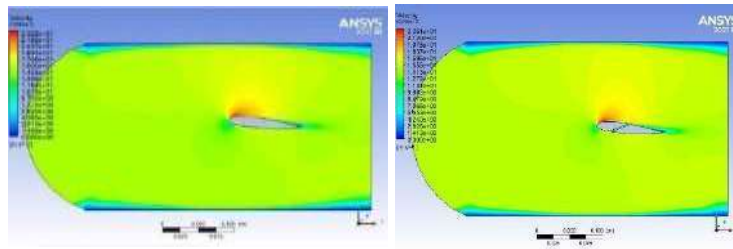
Figure 38 : Streamline at 5° for Both at Ten m/s

### 5.13 Fifteen m/s-



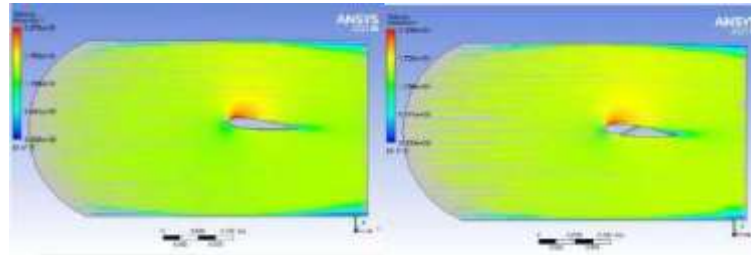
Pressure Contours : This image depicts the pressure surrounding airfoil. The color map indicates pressure levels, with green representing lower pressures and red/yellow indicating higher pressures. The airfoil front edge experiences higher pressure, while top surface experiences lower p compared to the bottom surface with (AOA = 5°) at 15 m/s

Figure 400 : Pressure at 5° for Both at Fifteen m/s



Velocity Contours : This image likely illustrates pattern velocity surrounding airfoil. colors indicate different velocities, with blue representing lower velocities and green/yellow/orange indicating higher velocities. The velocity is higher on the top surface compared to the bottom surface, which is typical for generating lift even at zero attack angle with (AOA = 5°) at 15 m/s

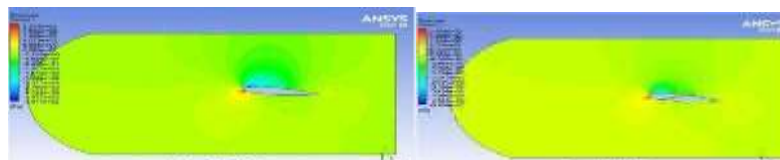
Figure 391 : Velocity at 5° for Both at Fifteen m/s



Stream lines depicting airflow patterns showing how air flows smoothly over the airfoil or separates from the surface. Streamlines closer together indicate higher velocity regions, while separation bubbles indicate areas of flow separation. with (AOA = 5°) at 15 m/s

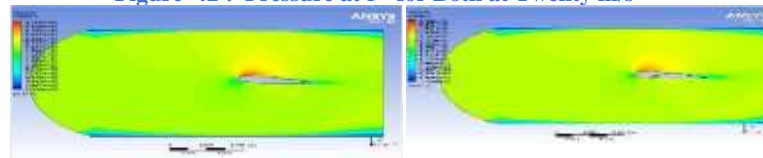
Figure 41 : Streamline at 5° for Both at Fifteen m/s

### 5.14 Twenty m/s-



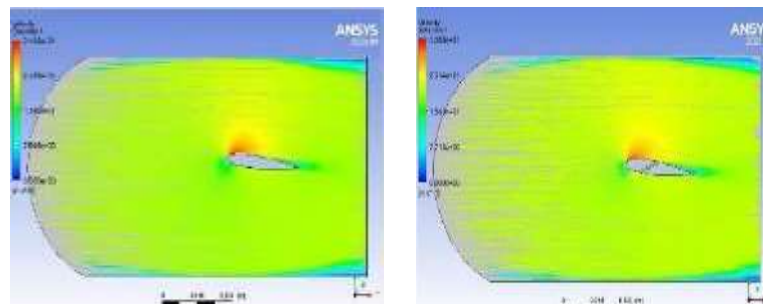
Pressure Contours : This image depicts the pressure surrounding airfoil. The color map indicates pressure levels, with green representing lower pressures and red/yellow indicating higher pressures. The airfoil front edge experiences higher pressure, while top surface experiences lower p compared to the bottom surface with (AOA = 5°) at 20 m/s

Figure 42 : Pressure at 5° for Both at Twenty m/s



Velocity Contours : This image likely illustrates pattern velocity surrounding airfoil. colors indicate different velocities, with blue representing lower velocities and green/yellow/orange indicating higher velocities. The velocity is higher on the top surface compared to the bottom surface, which is typical for generating lift even at zero attack angle with (AOA = 5°) at 20 m/s

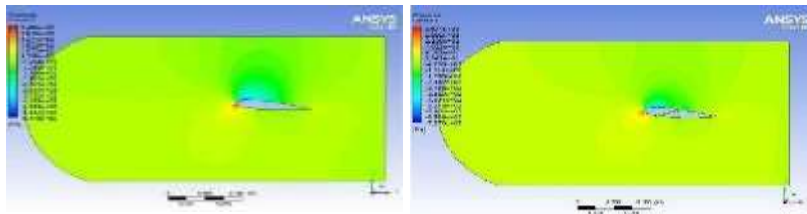
Figure 454 : Velocity at 5° for Both at Twenty m/s



Stream lines depicting airflow patterns showing how air flows smoothly over the airfoil or separates from the surface. Streamlines closer together indicate higher velocity regions, while separation bubbles indicate areas of flow separation. with (AOA = 5°) at 20 m/s

Figure 44 : Streamline at 5° for Both at Twenty m/s

### 5.15 Twenty Five m/s-



Pressure Contours : This image depicts the pressure surrounding airfoil. The color map indicates pressure levels, with green representing lower pressures and red/yellow indicating higher pressures. The airfoil front edge experiences higher pressure, while top surface experiences lower p compared to the bottom surface with (AOA = 5°) at 25 m/s

Figure 436 : Pressure at 5° for Both at twenty Five m/s

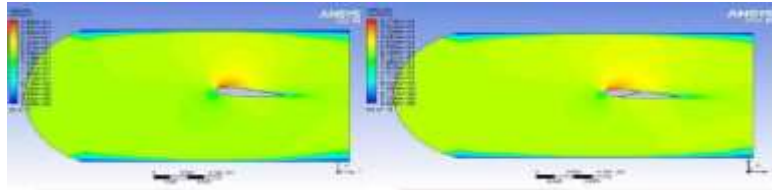
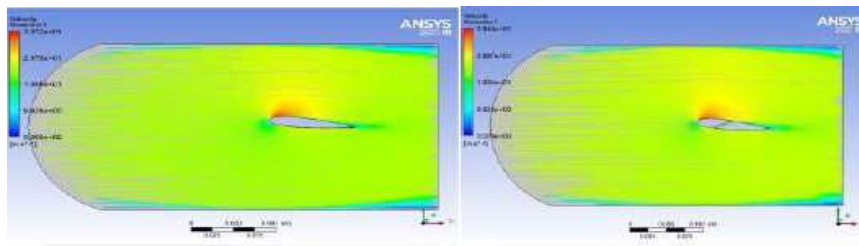


Figure 46 : Velocity at 5° for Both twenty Five m/s

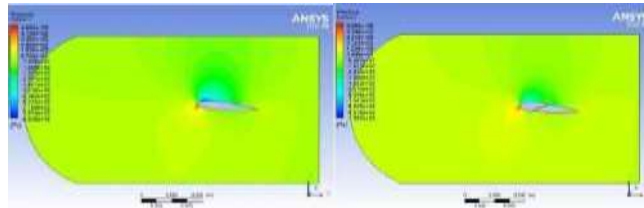
Velocity Contours : This image likely Illustrates pattern velocity surrounding airfoil. colors indicate different velocities, with blue representing lower velocities and green/yellow/orange indicating higher velocities. The velocity is higher on the top surface compared to the bottom surface, which is typical for generating lift even at zero attack angle with (AOA = 5°) at 25 m/s



Stream lines depicting airflow patterns showing how air flows smoothly over the airfoil or separates from the surface. Streamlines closer together indicate higher velocity regions, while separation bubbles indicate areas of flow separation. with (AOA = 5°) at 25 m/s

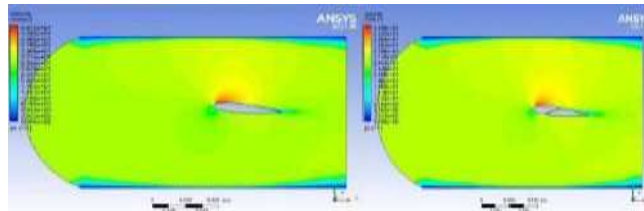
Figure 47 : Streamline at 5° for Both at twenty Five m/s

## 5.16 Thirty m/s-



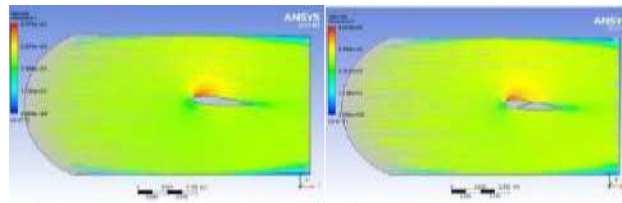
Pressure Contours : This image depicts the pressure surrounding airfoil. The color map indicates pressure levels, with green representing lower pressures and red/yellow indicating higher pressures. The airfoil front edge experiences higher pressure, while top surface experiences lower p compared to the bottom surface with (AOA = 5°) at 30 m/s

Figure 48 : Pressure at 5° for Both at Thirty m/s



Velocity Contours : This image likely illustrates pattern velocity surrounding airfoil. colors indicate different velocities, with blue representing lower velocities and green/yellow/orange indicating higher velocities. The velocity is higher on the top surface compared to the bottom surface, which is typical for generating lift even at zero attack angle with (AOA = 5°) at 30 m/s

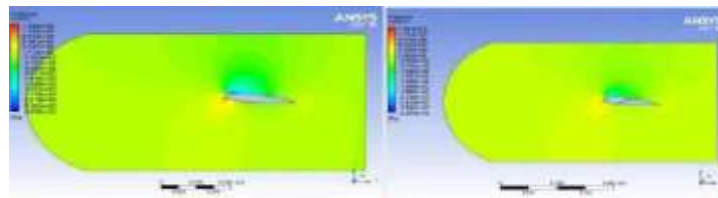
Figure 49 : Velocity at 5° for Both at Thirty m/s



Stream lines depicting airflow patterns showing how air flows smoothly over the airfoil or separates from the surface. Streamlines closer together indicate higher velocity regions, while separation bubbles indicate areas of flow separation. with (AOA = 5°) at 30 m/s

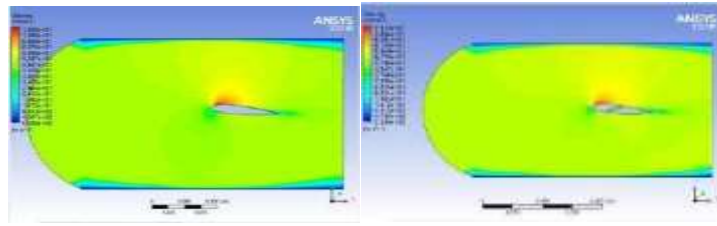
Figure 50 : Streamline at 5° for Both at Thirty m/s

## 5.17 Fifty m/s-



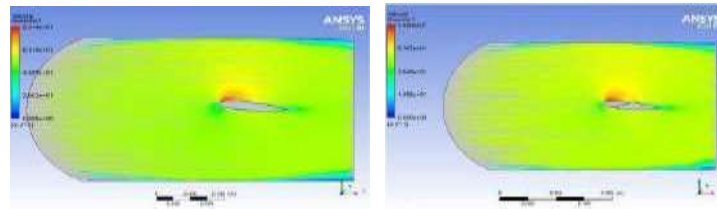
Pressure Contours : This image depicts the pressure surrounding airfoil. The color map indicates pressure levels, with green representing lower pressures and red/yellow indicating higher pressures. The airfoil front edge experiences higher pressure, while top surface experiences lower p compared to the bottom surface with (AOA = 5°) at 50 m/s

Figure 51 : Pressure at 5° for Both at Fifty m/s



Velocity Contours : This image likely illustrates pattern velocity surrounding airfoil. colors indicate different velocities, with blue representing lower velocities and green/yellow/orange indicating higher velocities. The velocity is higher on the top surface compared to the bottom surface, which is typical for generating lift even at zero attack angle with (AOA = 5°) at 50 m/s

Figure 52 : Velocity at 5° for Both at Fifty m/s



Stream lines depicting airflow patterns showing how air flows smoothly over the airfoil or separates from the surface. Streamlines closer together indicate higher velocity regions, while separation bubbles indicate areas of flow separation. with (AOA = 5°) at 50 m/s

Figure 53 : Streamline at 5° for Both at Fifty m/s

Table of Design Points									
	A	B	C	D	E	F	G	H	I
1	Name	P1 - inletvel	P2 - drag-op	P3 - drag-force-op	P4 - lift-op	P5 - lift-force-op	Retain	Retained Data	Note
2	Units	m s <sup>-1</sup>		N		N			
3	DP 0 (Current)	50	0.0022941	3.5128	0.065446	100.21	<input checked="" type="checkbox"/>	<input checked="" type="checkbox"/>	
4	DP 1	30	0.00093004	1.4241	0.022496	34.447	<input checked="" type="checkbox"/>	<input checked="" type="checkbox"/>	
5	DP 2	25	0.00067599	1.0351	0.015328	23.471	<input checked="" type="checkbox"/>	<input checked="" type="checkbox"/>	
6	DP 3	20	0.00045951	0.70377	0.0095686	14.652	<input checked="" type="checkbox"/>	<input checked="" type="checkbox"/>	
7	DP 4	15	0.00028244	0.43249	0.0051917	7.9499	<input checked="" type="checkbox"/>	<input checked="" type="checkbox"/>	
8	DP 5	10	0.00014544	0.2227	0.0021588	3.3057	<input checked="" type="checkbox"/>	<input checked="" type="checkbox"/>	
9	DP 6	5	4.8744E-05	0.07464	0.00049036	0.75086	<input checked="" type="checkbox"/>	<input checked="" type="checkbox"/>	
*							<input type="checkbox"/>		

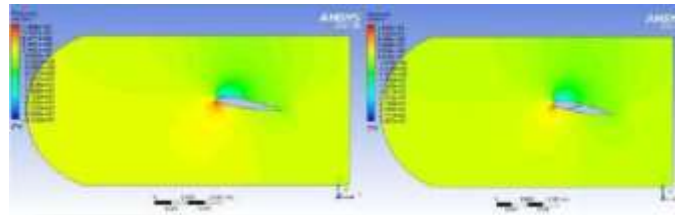
Table 3 : Drag and Lift force values,23015at5°AOA

Table of Design Points									
	A	B	C	D	E	F	G	H	I
1	Name	P1 - inletvel	P2 - drag-op	P3 - drag-force-op	P4 - lift-op	P5 - lift-force-op	Retain	Retained Data	Note
2	Units	m s <sup>-1</sup>		N		N			
3	DP 6 (Current)	50	0.0033811	5.1773	0.048956	70.37	<input checked="" type="checkbox"/>	<input checked="" type="checkbox"/>	
4	DP 7	30	0.0013338	2.0424	0.018306	23.438	<input checked="" type="checkbox"/>	<input checked="" type="checkbox"/>	
5	DP 8	25	0.00096052	1.4708	0.010289	15.724	<input checked="" type="checkbox"/>	<input checked="" type="checkbox"/>	
6	DP 9	20	0.00064492	0.98754	0.0062672	9.5965	<input checked="" type="checkbox"/>	<input checked="" type="checkbox"/>	
7	DP 10	15	0.00038863	0.59509	0.0032762	5.0167	<input checked="" type="checkbox"/>	<input checked="" type="checkbox"/>	
8	DP 11	10	0.00019358	0.29642	0.0012933	1.9804	<input checked="" type="checkbox"/>	<input checked="" type="checkbox"/>	
9	DP 12	5	6.0751E-05	0.093025	0.00025627	0.39241	<input checked="" type="checkbox"/>	<input checked="" type="checkbox"/>	
*							<input type="checkbox"/>		

Table 4 : Drag and Lift force values,23015at5°AOA

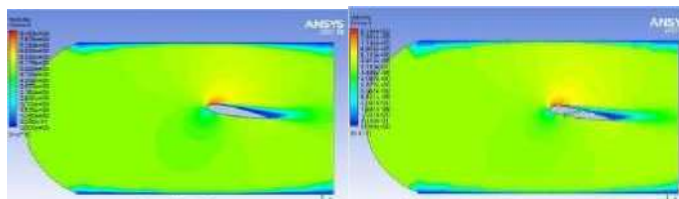
## 5.18 Ten degree Attack angle :-

5.195m/s-



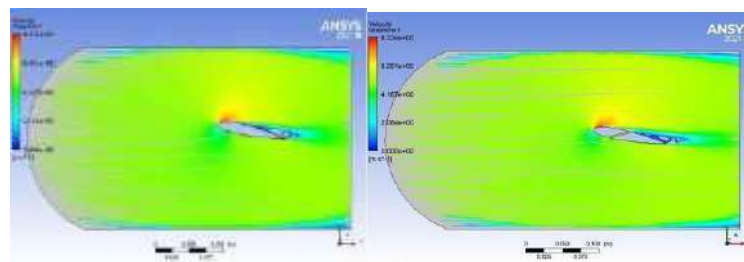
Pressure Contours : This image depicts the pressure surrounding airfoil. The color map indicates pressure levels, with green representing lower pressures and red/yellow indicating higher pressures. The airfoil front edge experiences higher pressure, while top surface experiences lower p compared to the bottom surface with (AOA = 10°) at 5 m/s

Figure 54 : Pressure at 10° for Both at Five m/s



Velocity Contours : This image likely illustrates pattern velocity surrounding airfoil. colors indicate different velocities, with blue representing lower velocities and green/yellow/orange indicating higher velocities. The velocity is higher on the top surface compared to the bottom surface, which is typical for generating lift even at zero attack angle with (AOA = 10°) at 5 m/s

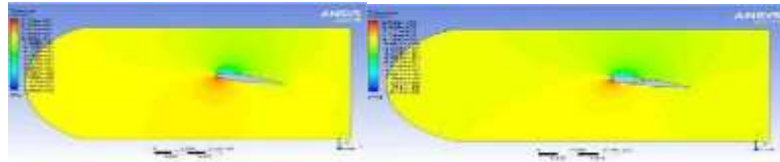
Figure 55 : Velocity at 10° for Both at Five m/s



Stream lines depicting airflow patterns showing how air flows smoothly over the airfoil or separates from the surface. Streamlines closer together indicate higher velocity regions, while separation bubbles indicate areas of flow separation. with (AOA = 10°) at 5 m/s

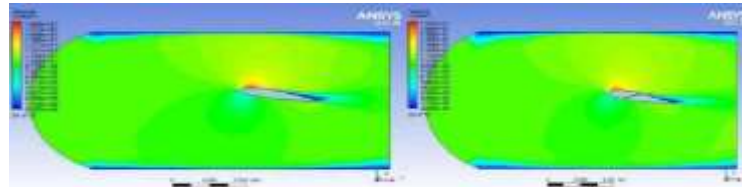
Figure 56 : Streamline at 10° for Both at Five m/s

## Ten m/s



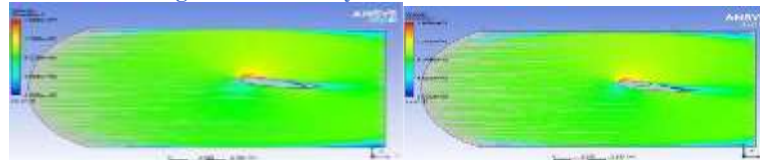
Pressure Contours : This image depicts the pressure surrounding airfoil. The color map indicates pressure levels, with green representing lower pressures and red/yellow indicating higher pressures. The airfoil front edge experiences higher pressure, while top surface experiences lower p compared to the bottom surface with (AOA = 10°) at 10 m/s

Figure 57 : Pressure at 10° for Both at Ten m/s



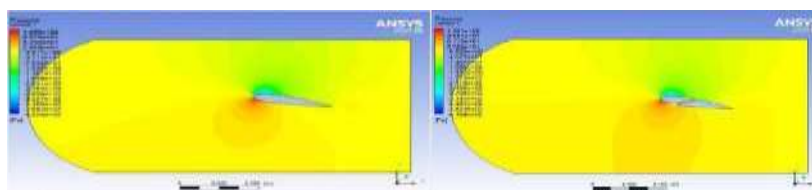
Velocity Contours : This image likely illustrates pattern velocity surrounding airfoil. colors indicate different velocities, with blue representing lower velocities and green/yellow/orange indicating higher velocities. The velocity is higher on the top surface compared to the bottom surface, which is typical for generating lift even at zero attack angle with (AOA = 10°) at 10 m/s

Figure 58 : Velocity at 10° for Both at Ten m/s



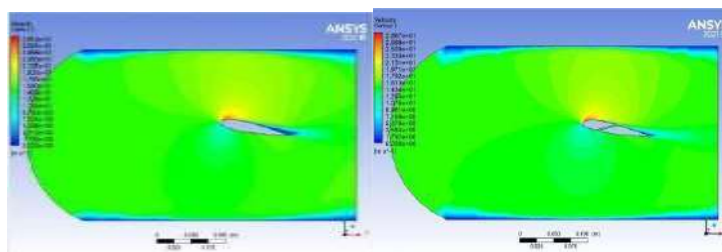
Stream lines depicting airflow patterns showing how air flows smoothly over the airfoil or separates from the surface. Streamlines closer together indicate higher velocity regions, while separation bubbles indicate areas of flow separation. with (AOA = 10°) at 10 m/s

## Fifteen m/s :



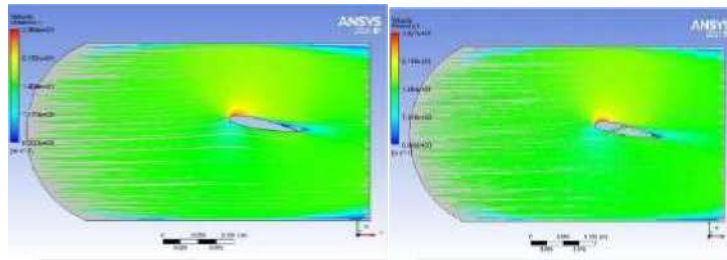
Pressure Contours : This image depicts the pressure surrounding airfoil. The color map indicates pressure levels, with green representing lower pressures and red/yellow indicating higher pressures. The airfoil front edge experiences higher pressure, while top surface experiences lower p compared to the bottom surface with (AOA = 10°) at 15 m/s

Figure 60 : Pressure at 10° for Both at fifteen m/s



Velocity Contours : This image likely Illustrates pattern velocity surrounding airfoil. colors indicate different velocities, with blue representing lower velocities and green/yellow/orange indicating higher velocities. The velocity is higher on the top surface compared to the bottom surface, which is typical for generating lift even at zero attack angle with (AOA = 10°) at 15 m/s

**Figure 61 : Velocity at 10° for Both at fifteen m/s**

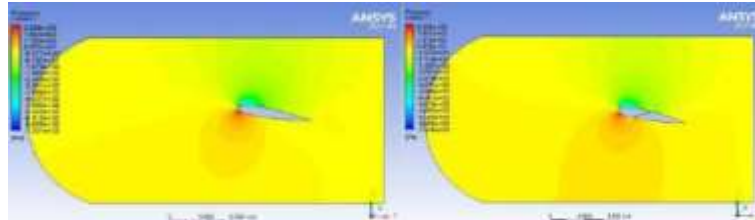


Stream lines depicting airflow patterns showing how air flows smoothly over the airfoil or separates from the surface. Streamlines closer together indicate higher velocity regions, while separation bubbles indicate areas of flow separation. with (AOA = 10°) at 15 m/s

**Figure 62 : Streamline at 10° for Both at fifteen m/s**

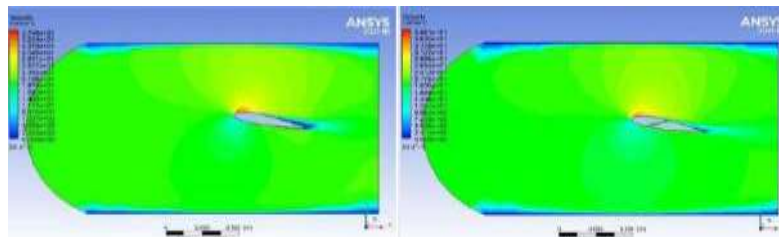


## Twenty m/s



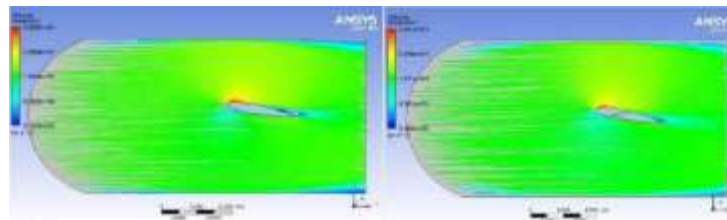
Pressure Contours : This image depicts the pressure surrounding airfoil. The color map indicates pressure levels, with green representing lower pressures and red/yellow indicating higher pressures. The airfoil front edge experiences higher pressure, while top surface experiences lower p compared to the bottom surface with (AOA = 10°) at 15 m/s

Figure 63 : Pressure at 10° for at Twenty m/s



Velocity Contours : This image likely illustrates pattern velocity surrounding airfoil. colors indicate different velocities, with blue representing lower velocities and green/yellow/orange indicating higher velocities. The velocity is higher on the top surface compared to the bottom surface, which is typical for generating lift even at zero attack angle with (AOA = 10°) at 15 m/s

Figure 64 : VelocityPlotat10° for atTwenty m/s



Stream lines depicting airflow patterns showing how air flows smoothly over the airfoil or separates from the surface. Streamlines closer together indicate higher velocity regions, while separation bubbles indicate areas of flow separation. with (AOA = 10°) at 15 m/s

Figure 65 : Stream line at 10° for at Twenty m/s

## 5.20 Twenty-Five m/s-

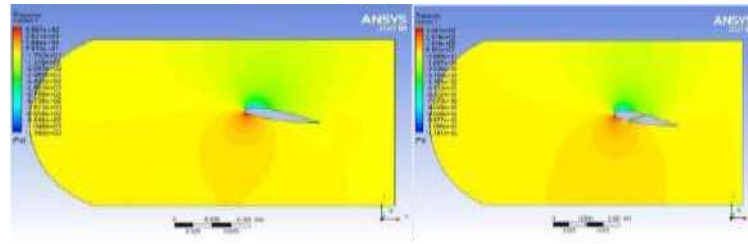
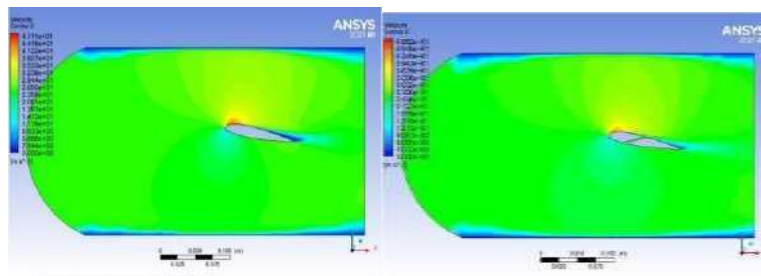


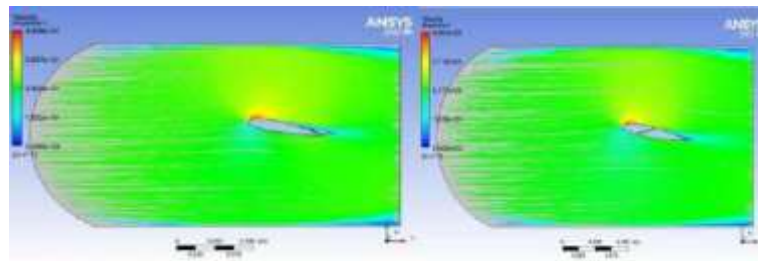
Figure 66 : Pressure at 10° for Both at twenty Five m/s

Pressure Contours : This image depicts the pressure surrounding airfoil. The color map indicates pressure levels, with green representing lower pressures and red/yellow indicating higher pressures. The airfoil front edge experiences higher pressure, while top surface experiences lower p compared to the bottom surface with (AOA = 10°) at 20 m/s



Velocity Contours : This image likely illustrates pattern velocity surrounding airfoil. colors indicate different velocities, with blue representing lower velocities and green/yellow/orange indicating higher velocities. The velocity is higher on the top surface compared to the bottom surface, which is typical for generating lift even at zero attack angle with (AOA = 10°) at 20 m/s

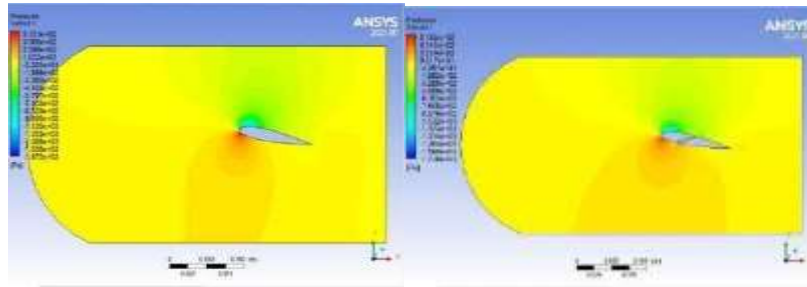
Figure 67 : Velocity at 10° for Both attwenty Five m/s



Stream lines depicting airflow patterns showing how air flows smoothly over the airfoil or separates from the surface. Streamlines closer together indicate higher velocity regions, while separation bubbles indicate areas of flow separation. with (AOA = 10°) at 20 m/s

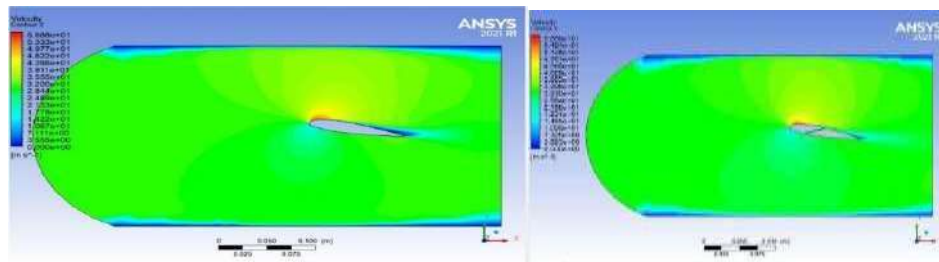
Figure 68 : Streamline at 10° for Both attwenty Five m/s

## 5.21 Thirty m/s-



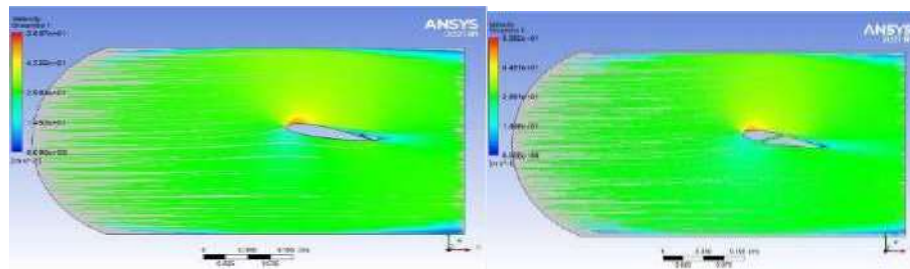
Pressure Contours : This image depicts the pressure surrounding airfoil. The color map indicates pressure levels, with green representing lower pressures and red/yellow indicating higher pressures. The airfoil front edge experiences higher pressure, while top surface experiences lower p compared to the bottom surface with (AOA = 10°) at 30 m/s

Figure 69 : Pressure at 10° for Both at Thirty m/s



Velocity Contours : This image likely illustrates pattern velocity surrounding airfoil. colors indicate different velocities, with blue representing lower velocities and green/yellow/orange indicating higher velocities. The velocity is higher on the top surface compared to the bottom surface, which is typical for generating lift even at zero attack angle with (AOA = 10°) at 30 m/s

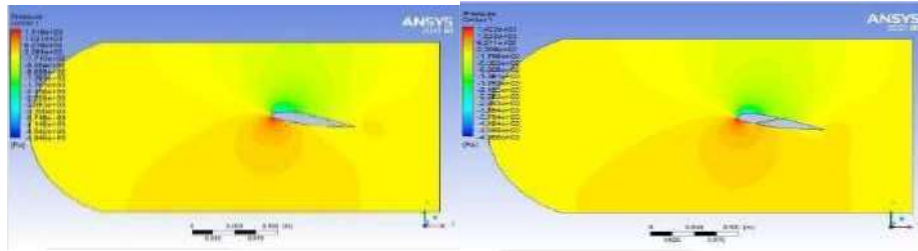
Figure 70 : Velocity at 10° for Both at Thirty m/s



Stream lines depicting airflow patterns showing how air flows smoothly over the airfoil or separates from the surface. Streamlines closer together indicate higher velocity regions, while separation bubbles indicate areas of flow separation. with (AOA = 10°) at 30 m/s

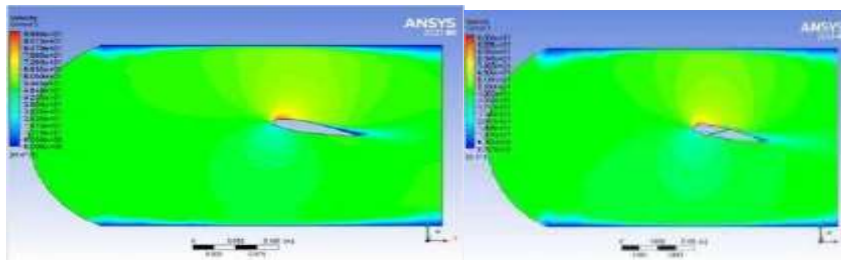
Figure 71 : Streamline at 10° for Both at Thirty m/s

## 5.22 Fifty m/s-



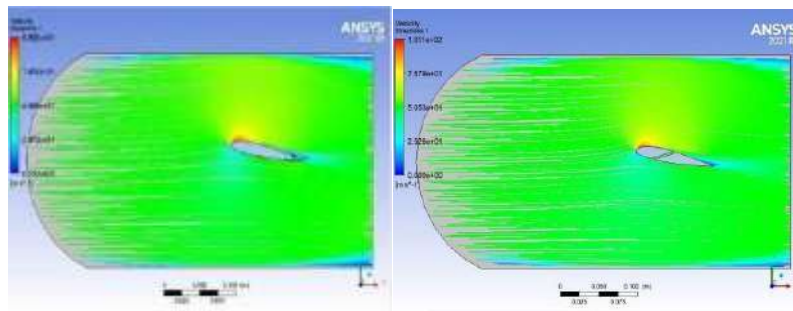
Pressure Contours : This image depicts the pressure surrounding airfoil. The color map indicates pressure levels, with green representing lower pressures and red/yellow indicating higher pressures. The airfoil front edge experiences higher pressure, while top surface experiences lower p compared to the bottom surface with (AOA = 10°) at 50 m/s

Figure 72 : Pressure at 10° for Both at Fifty m/s



Velocity Contours : This image likely illustrates pattern velocity surrounding airfoil. colors indicate different velocities, with blue representing lower velocities and green/yellow/orange indicating higher velocities. The velocity is higher on the top surface compared to the bottom surface, which is typical for generating lift even at zero attack angle with (AOA = 10°) at 50 m/s

Figure 73 : Velocity at 10° for Both at Fifty m/s



Stream lines depicting airflow patterns showing how air flows smoothly over the airfoil or separates from the surface. Streamlines closer together indicate higher velocity regions, while separation bubbles indicate areas of flow separation. with (AOA = 10°) at 50 m/s

Figure 74 : Streamline at 10° for Both at Fifty m/s

Table of Design Points									
	A	B	C	D	E	F	G	H	I
I	Name	P1 - inlets vel	P2 - drag op	P3 - drag force op	P4 - lift op	P5 - lift force op	Retain	Retained Data	Note
2	Units	m s <sup>-1</sup>		N		N			
3	DP 0 (Current)	50	0.0040105	-5.241	0.10543	161.43	<input checked="" type="checkbox"/>	<input checked="" type="checkbox"/>	
4	DP 1	30	0.0036087	-2.4534	0.036364	55.682	<input checked="" type="checkbox"/>	<input checked="" type="checkbox"/>	
5	DP 2	25	0.0011885	-1.7892	0.024799	37.974	<input checked="" type="checkbox"/>	<input checked="" type="checkbox"/>	
6	DP 3	20	0.00075945	-1.218	0.015468	23.671	<input checked="" type="checkbox"/>	<input checked="" type="checkbox"/>	
7	DP 4	15	0.00048803	-0.74729	0.0083465	12.781	<input checked="" type="checkbox"/>	<input checked="" type="checkbox"/>	
8	DP 5	10	0.00025179	-0.38555	0.0034832	5.2877	<input checked="" type="checkbox"/>	<input checked="" type="checkbox"/>	
9	DP 6	5	8.1739E-05	-0.12536	0.00075811	1.1609	<input checked="" type="checkbox"/>	<input checked="" type="checkbox"/>	
*							<input type="checkbox"/>		

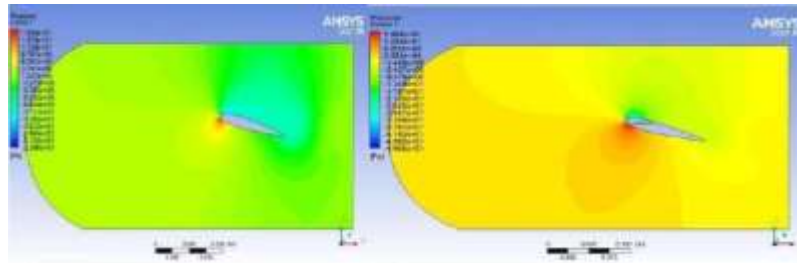
Table5 : Drag and Lift force values for23015at10°

Table of Design Points									
	A	B	C	D	E	F	G	H	I
1	Name	P1 - inlets vel	P2 - drag op	P3 - drag force op	P4 - lift op	P5 - lift force op	Retain	Retained Data	Note
2	Units	m s <sup>-1</sup>		N		N			
3	DP 6 (Current)	50	0.0048885	7.4855	0.097052	148.61	<input checked="" type="checkbox"/>	<input checked="" type="checkbox"/>	
4	DP 7	30	0.0038927	2.8962	0.033689	51.587	<input checked="" type="checkbox"/>	<input checked="" type="checkbox"/>	
5	DP 8	25	0.0013525	2.071	0.023015	35.242	<input checked="" type="checkbox"/>	<input checked="" type="checkbox"/>	
6	DP 9	20	0.00089746	1.3742	0.014405	22.058	<input checked="" type="checkbox"/>	<input checked="" type="checkbox"/>	
7	DP 10	15	0.00053321	0.81647	0.0078413	12.007	<input checked="" type="checkbox"/>	<input checked="" type="checkbox"/>	
8	DP 11	10	0.00026006	0.39822	0.0032905	5.0385	<input checked="" type="checkbox"/>	<input checked="" type="checkbox"/>	
9	DP 12	5	8.0403E-05	0.12312	0.00072216	1.1058	<input checked="" type="checkbox"/>	<input checked="" type="checkbox"/>	
*							<input type="checkbox"/>		

Table6 : Drag and Lift force values for 23015 at 10°

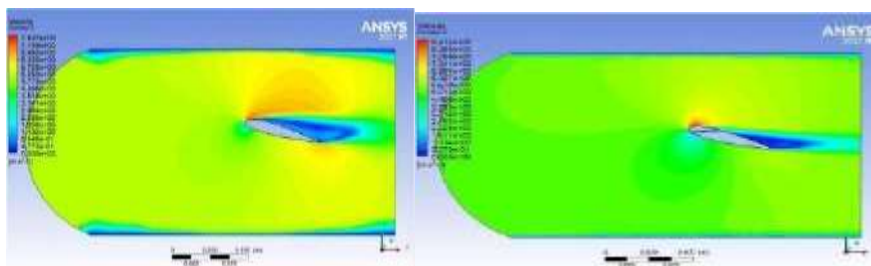
### 5.23 Fifteen Attack angle : -

### 5.24 Five m/s-



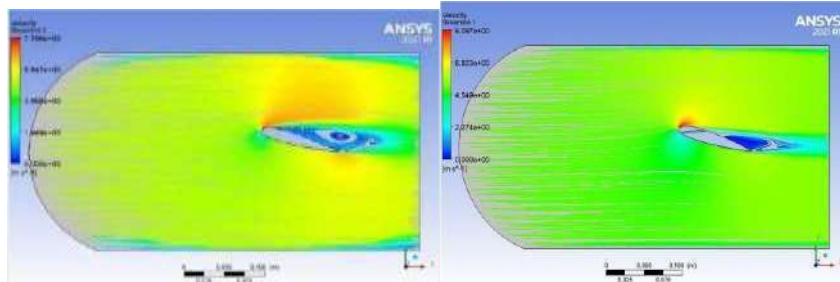
Pressure Contours : This image depicts the pressure surrounding airfoil. The color map indicates pressure levels, with green representing lower pressures and red/yellow indicating higher pressures. The airfoil front edge experiences higher pressure, while top surface experiences lower p compared to the bottom surface with (AOA = 15°) at 5 m/s

Figure 75 : Pressure at 15° for Both at Five m/s



Velocity Contours : This image likely Illustrates pattern velocity surrounding airfoil. colors indicate different velocities, with blue representing lower velocities and green/yellow/orange indicating higher velocities. The velocity is higher on the top surface compared to the bottom surface, which is typical for generating lift even at zero attack angle with (AOA = 15°) at 5 m/s

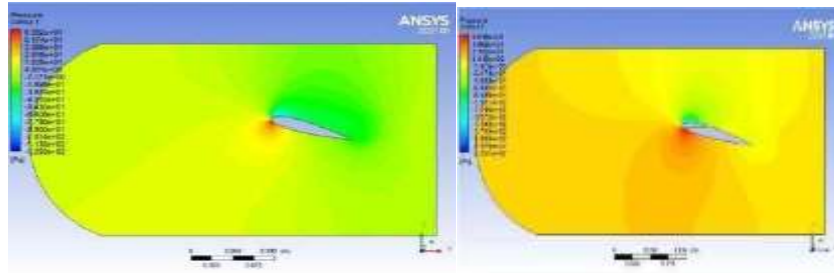
Figure 76 : Velocity at 15° for Both at Five m/s



Stream lines depicting airflow patterns showing how air flows smoothly over the airfoil or separates from the surface. Streamlines closer together indicate higher velocity regions, while separation bubbles indicate areas of flow separation. with (AOA = 15°) at 5 m/s

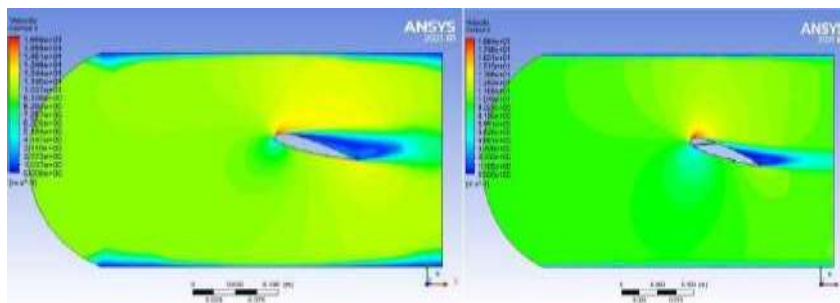
Figure 77 : Streamline at 15° for Both at Five m/s

## 5.25 Ten m/s-



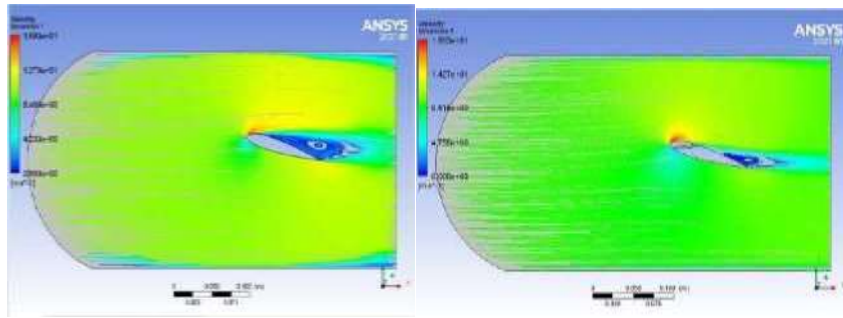
Pressure Contours : This image depicts the pressure surrounding airfoil. The color map indicates pressure levels, with green representing lower pressures and red/yellow indicating higher pressures. The airfoil front edge experiences higher pressure, while top surface experiences lower p compared to the bottom surface with (AOA = 15°) at 10 m/s

Figure 78 : Pressure at 15° for Both at Ten m/s



Velocity Contours : This image likely Illustrates pattern velocity surrounding airfoil. colors indicate different velocities, with blue representing lower velocities and green/yellow/orange indicating higher velocities. The velocity is higher on the top surface compared to the bottom surface, which is typical for generating lift even at zero attack angle with at 10 m/s

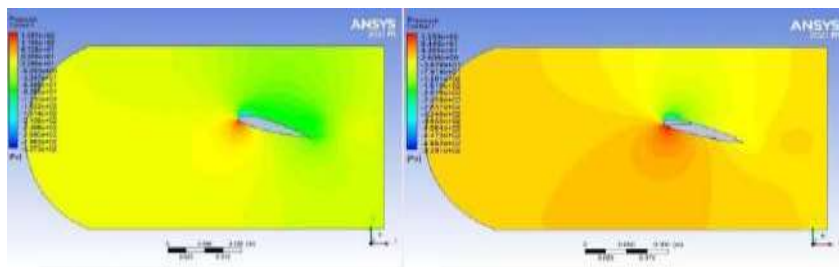
Figure 79 : Velocity at 15° for Both at Ten m/s



Stream lines depicting airflow patterns showing how air flows smoothly over the airfoil or separates from the surface. Streamlines closer together indicate higher velocity regions, while separation bubbles indicate areas of flow separation. with (AOA = 15°) at 10 m/s

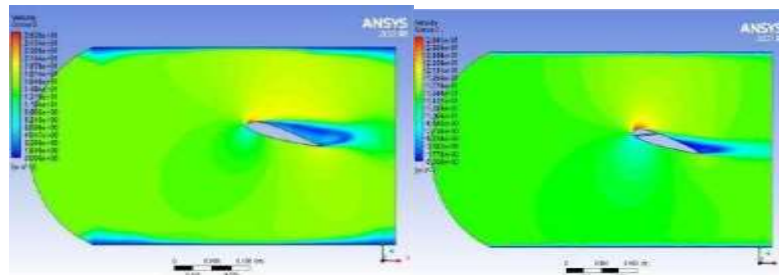
Figure 80 : Streamline at 15° for Both at Ten m/s

### 5.26 Fifteen m/s-



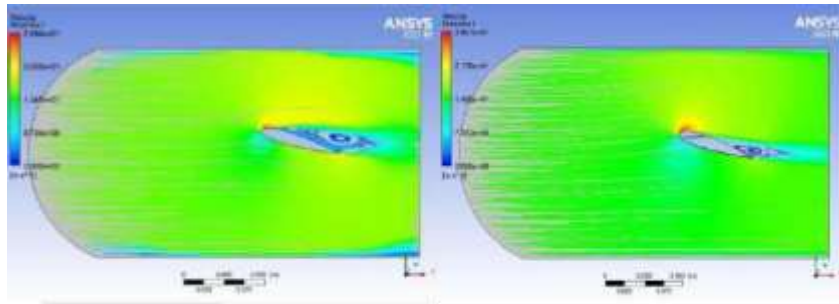
Pressure Contours : This image depicts the pressure surrounding airfoil. The color map indicates pressure levels, with green representing lower pressures and red/yellow indicating higher pressures. The airfoil front edge experiences higher pressure, while top surface experiences lower p compared to the bottom surface with (AOA = 15°) at 15 m/s

Figure 81 : Pressure at 15° for Both at fifteen m/s



Velocity Contours : This image likely illustrates pattern velocity surrounding airfoil. colors indicate different velocities, with blue representing lower velocities and green/yellow/orange indicating higher velocities. The velocity is higher on the top surface compared to the bottom surface, which is typical for generating lift even at zero attack angle with (AOA = 15°) at 15 m/s

Figure 82 : Velocity at 15° for Both at fifteen m/s

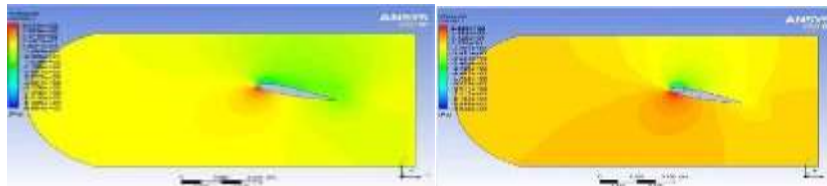


Stream lines depicting airflow patterns showing how air flows smoothly over the airfoil or separates from the surface. Streamlines closer together indicate higher velocity regions, while separation bubbles indicate areas of flow separation. with (AOA = 15°) at 15 m/s

**Figure 83 : Streamline at 15° for Both at fifteen m/s**

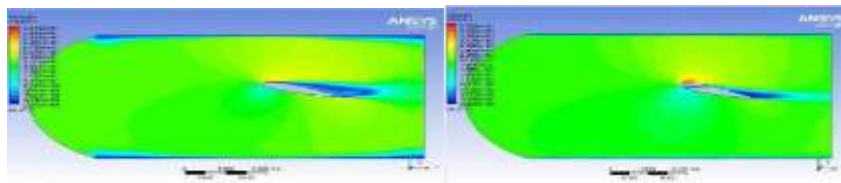


## Twenty m/s-



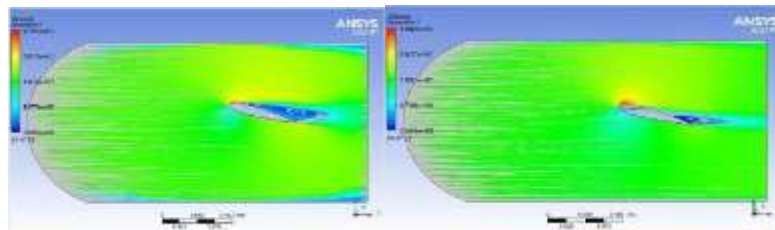
Pressure Contours : This image depicts the pressure surrounding airfoil. The color map indicates pressure levels, with green representing lower pressures and red/yellow indicating higher pressures. The airfoil front edge experiences higher pressure, while top surface experiences lower p compared to the bottom surface with (AOA = 15°) at 20 m/s

Figure 84 : Pressure at 15° for Both at Twenty m/s



Velocity Contours : This image likely illustrates pattern velocity surrounding airfoil. colors indicate different velocities, with blue representing lower velocities and green/yellow/orange indicating higher velocities. The velocity is higher on the top surface compared to the bottom surface, which is typical for generating lift even at zero attack angle with (AOA = 15°) at 20 m/s

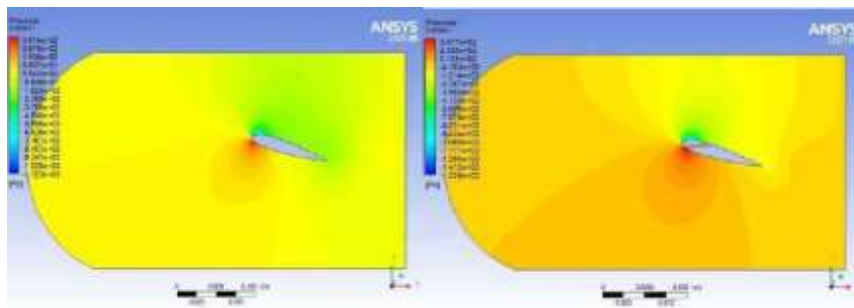
Figure 85 : Velocity at 15° for Both at Twenty m/s



Stream lines depicting airflow patterns showing how air flows smoothly over the airfoil or separates from the surface. Streamlines closer together indicate higher velocity regions, while separation bubbles indicate areas of flow separation. with (AOA = 15°) at 20 m/s

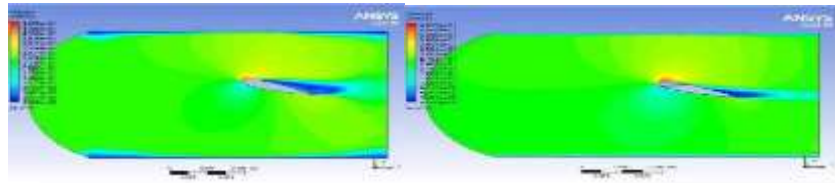
Figure 86 : Streamline at 15° for Both at Twenty m/s

## 5.27 Twenty Five m/s-



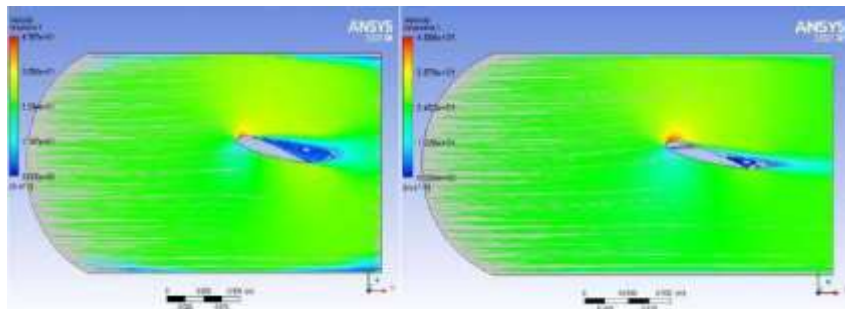
Pressure Contours : This image depicts the pressure surrounding airfoil. The color map indicates pressure levels, with green representing lower pressures and red/yellow indicating higher pressures. The airfoil front edge experiences higher pressure, while top surface experiences lower p compared to the bottom surface with (AOA = 15°) at 25 m/s

Figure 87 : Pressure at 15° for Both at twenty-Five m/s



Velocity Contours : This image likely illustrates pattern velocity surrounding airfoil. colors indicate different velocities, with blue representing lower velocities and green/yellow/orange indicating higher velocities. The velocity is higher on the top surface compared to the bottom surface, which is typical for generating lift even at zero attack angle with (AOA = 15°) at 25 m/s

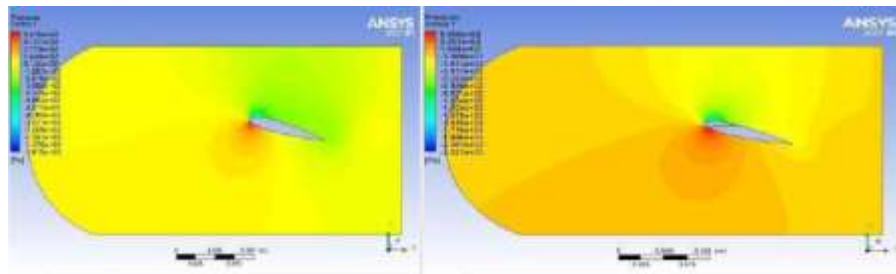
Figure 88 : Velocity at 15° for Both at twenty-Five m/s



Stream lines depicting airflow patterns showing how air flows smoothly over the airfoil or separates from the surface. Streamlines closer together indicate higher velocity regions, while separation bubbles indicate areas of flow separation. with (AOA = 15°) at 25 m/s

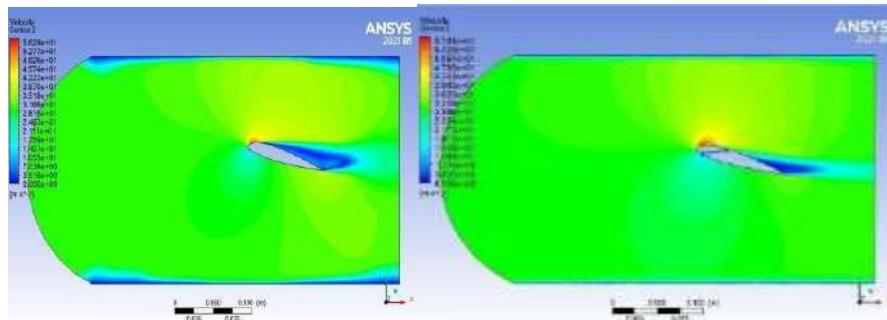
Figure 89 : Streamline at 15° for Both at twenty Five m/s

## 5.28 Thirty m/s-



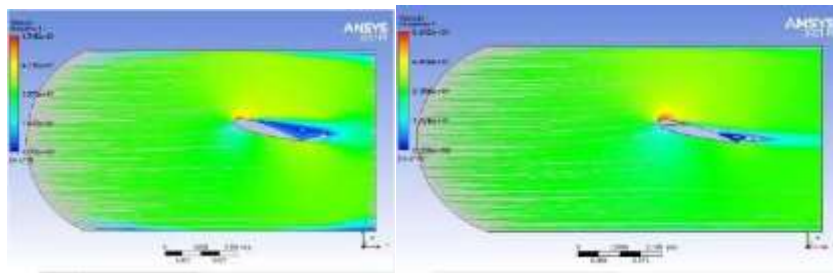
Pressure Contours : This image depicts the pressure surrounding airfoil. The color map indicates pressure levels, with green representing lower pressures and red/yellow indicating higher pressures. The airfoil front edge experiences higher pressure, while top surface experiences lower p compared to the bottom surface with (AOA = 15°) at 30 m/s

Figure 90 : Pressure at 15° for Both at Thirty m/s



Velocity Contours : This image likely illustrates pattern velocity surrounding airfoil. colors indicate different velocities, with blue representing lower velocities and green/yellow/orange indicating higher velocities. The velocity is higher on the top surface compared to the bottom surface, which is typical for generating lift even at zero attack angle with (AOA = 15°) at 30 m/s

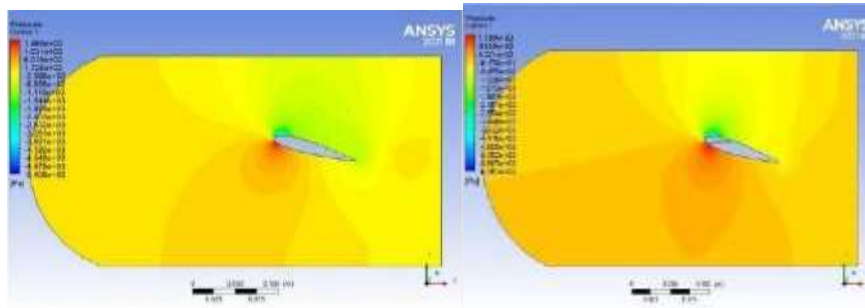
Figure 91 : Velocity at 15° for Both at Thirty m/s



Stream lines depicting airflow patterns showing how air flows smoothly over the airfoil or separates from the surface. Streamlines closer together indicate higher velocity regions, while separation bubbles indicate areas of flow separation. with (AOA = 15°) at 30 m/s

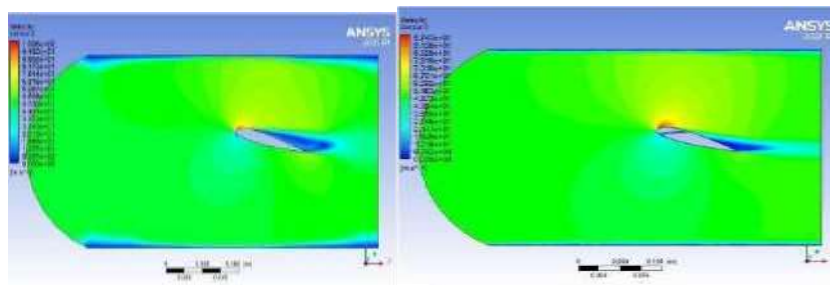
Figure 92 : Streamline at 15° for Both at Thirty m/s

## 5.29 Fifty m/s-



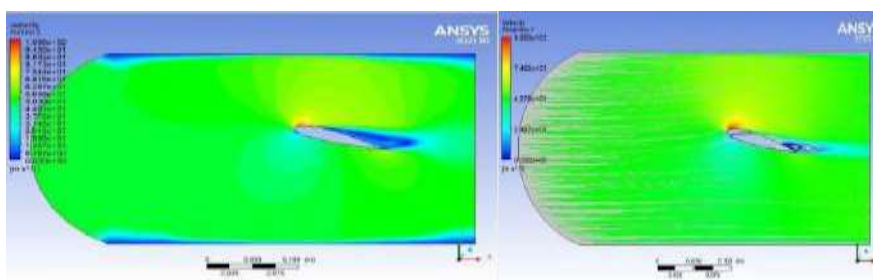
Pressure Contours : This image depicts the pressure surrounding airfoil. The color map indicates pressure levels, with green representing lower pressures and red/yellow indicating higher pressures. The airfoil front edge experiences higher pressure, while top surface experiences lower p compared to the bottom surface with (AOA = 15°) at 50 m/s

Figure 93 : Pressure at 15° for Both at Fifty m/s



Velocity Contours : This image likely illustrates pattern velocity surrounding airfoil. colors indicate different velocities, with blue representing lower velocities and green/yellow/orange indicating higher velocities. The velocity is higher on the top surface compared to the bottom surface, which is typical for generating lift even at zero attack angle with at 50 m/s

Figure 94 : Velocity at 15° for Both at Fifty m/s



Stream lines depicting airflow patterns showing how air flows smoothly over the airfoil or separates from the surface. Streamlines closer together indicate higher velocity regions, while separation bubbles indicate areas of flow separation. with (AOA = 15°) at 50 m/s

Figure 95 : Streamline at 15° for Both at Fifty m/s

Table of Design Points									
	A	B	C	D	E	F	G	H	I
1	Name	P1 - inlet vel	P2 - drag-op	P3 - drag-force-op	P4 - lift-op	P5 - lift-force-op	Retain	Retained Data	Note
2	Units	m s <sup>-1</sup>		N		N			
3	DP 0 (Current)	50	0.000611	16.247	0.10478	160.45	<input checked="" type="checkbox"/>	<input checked="" type="checkbox"/>	
4	DP 1	30	0.004164	6.3033	0.036302	55.71	<input checked="" type="checkbox"/>	<input checked="" type="checkbox"/>	
5	DP 2	25	0.0029462	4.5114	0.024829	38.019	<input checked="" type="checkbox"/>	<input checked="" type="checkbox"/>	
6	DP 3	20	0.0019677	3.013	0.015528	23.777	<input checked="" type="checkbox"/>	<input checked="" type="checkbox"/>	
7	DP 4	15	0.0011769	1.8021	0.008443	12.928	<input checked="" type="checkbox"/>	<input checked="" type="checkbox"/>	
8	DP 5	10	0.00057265	0.87717	0.003925	5.501	<input checked="" type="checkbox"/>	<input checked="" type="checkbox"/>	
9	DP 6	5	0.0001668	0.25536	0.00081349	1.2457	<input checked="" type="checkbox"/>	<input checked="" type="checkbox"/>	
*							<input type="checkbox"/>		

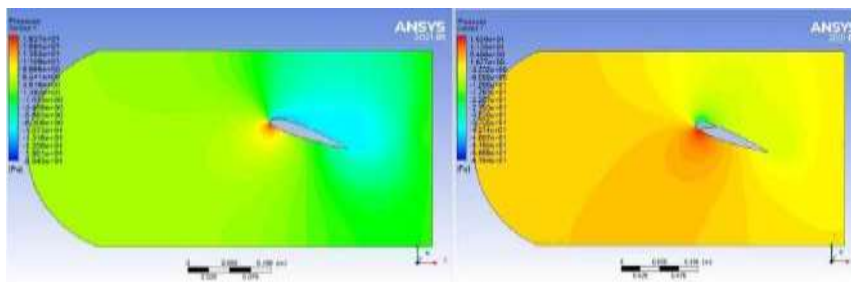
Table7 : Drag and Lift force values,23015at15°

Table of Design Points									
	A	B	C	D	E	F	G	H	I
1	Name	P1 - inlet vel	P2 - drag-op	P3 - drag-force-op	P4 - lift-op	P5 - lift-force-op	Retain	Retained Data	Note
2	Units	m s <sup>-1</sup>		N		N			
3	DP 0 (Current)	50	0.0086438	13.233	0.12016	184	<input checked="" type="checkbox"/>	<input checked="" type="checkbox"/>	
4	DP 1	30	0.0032805	5.0233	0.042127	64.507	<input checked="" type="checkbox"/>	<input checked="" type="checkbox"/>	
5	DP 2	25	0.0023283	3.5652	0.028919	44.282	<input checked="" type="checkbox"/>	<input checked="" type="checkbox"/>	
6	DP 3	20	0.001534	2.349	0.018231	27.916	<input checked="" type="checkbox"/>	<input checked="" type="checkbox"/>	
7	DP 4	15	0.00090195	1.3811	0.010012	15.331	<input checked="" type="checkbox"/>	<input checked="" type="checkbox"/>	
8	DP 5	10	0.00043238	0.66239	0.0042671	6.534	<input checked="" type="checkbox"/>	<input checked="" type="checkbox"/>	
9	DP 6	5	0.00013089	0.20043	0.00095509	1.4625	<input checked="" type="checkbox"/>	<input checked="" type="checkbox"/>	
*							<input type="checkbox"/>		

Table8 : Drag and Lift force values,23015at15°

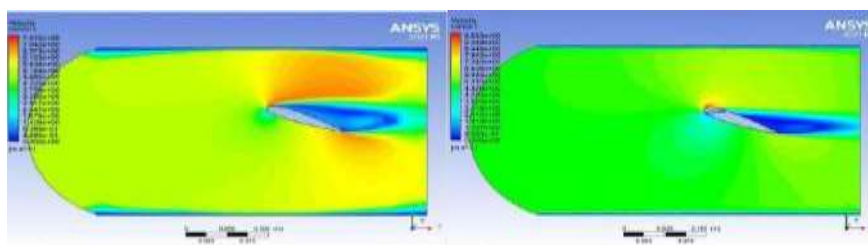
### 5.30 Twenty Attack angle : -

### 5.31 Five m/s-



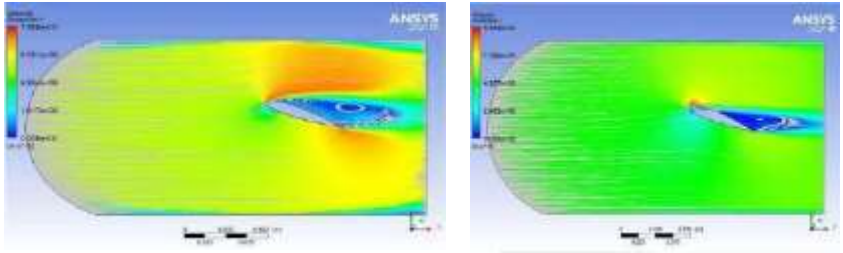
Pressure Contours : This image depicts the pressure surrounding airfoil. The color map indicates pressure levels, with green representing lower pressures and red/yellow indicating higher pressures. The airfoil front edge experiences higher pressure, while top surface experiences lower p compared to the bottom surface with (AOA = 20°) at 5 m/s

Figure 96 : Pressure at 20° for Both at Five m/s



Velocity Contours : This image likely Illustrates pattern velocity surrounding airfoil. colors indicate different velocities, with blue representing lower velocities and green/yellow/orange indicating higher velocities. The velocity is higher on the top surface compared to the bottom surface, which is typical for generating lift even at zero attack angle with (AOA = 20°) at 5 m/s

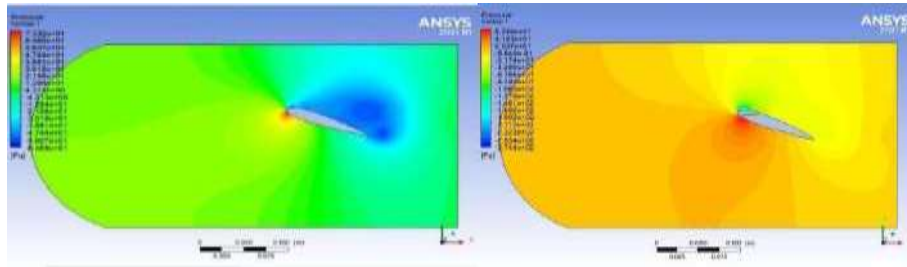
Figure 97 : Velocity at 20° for Both at Five m/s



Stream lines depicting airflow patterns showing how air flows smoothly over the airfoil or separates from the surface. Streamlines closer together indicate higher velocity regions, while separation bubbles indicate areas of flow separation. with (AOA = 20°) at 5 m/s

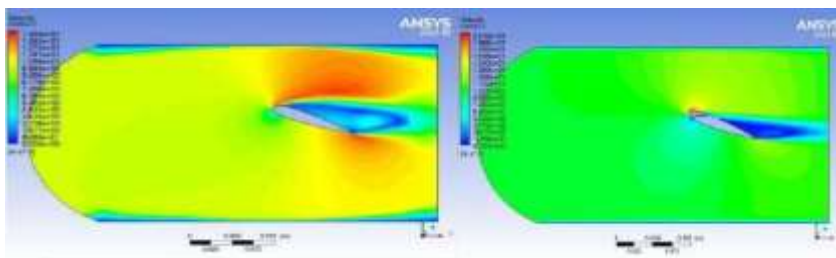
Figure 98 : Streamline at 20° for Both at Five m/s

### 5.32 Ten m/s-



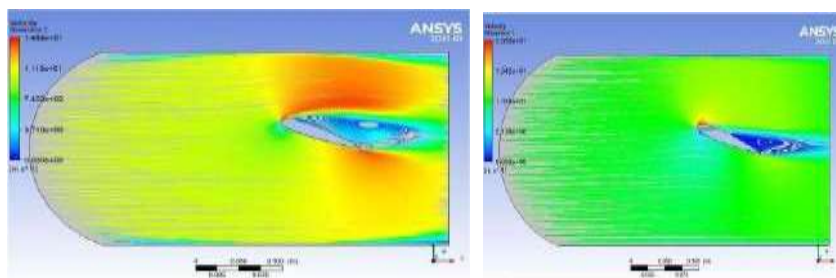
Pressure Contours : This image depicts the pressure surrounding airfoil. The color map indicates pressure levels, with green representing lower pressures and red/yellow indicating higher pressures. The airfoil front edge experiences higher pressure, while top surface experiences lower p compared to the bottom surface with (AOA = 20°) at 10 m/s

Figure 99 : Pressure at 20° for Both at Ten m/s



Velocity Contours : This image likely illustrates pattern velocity surrounding airfoil. colors indicate different velocities, with blue representing lower velocities and green/yellow/orange indicating higher velocities. The velocity is higher on the top surface compared to the bottom surface, which is typical for generating lift even at zero attack angle with (AOA = 20°) at 10 m/s

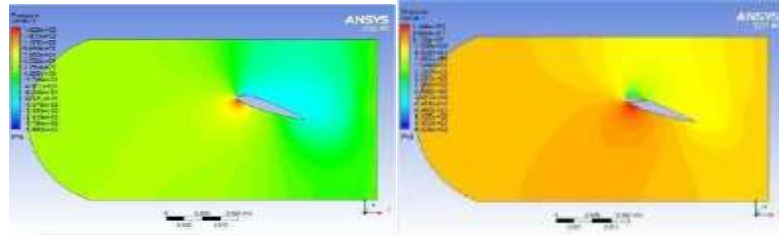
Figure 100 : Velocity at 20° for Both at Ten m/s



Stream lines depicting airflow patterns showing how air flows smoothly over the airfoil or separates from the surface. Streamlines closer together indicate higher velocity regions, while separation bubbles indicate areas of flow separation. with (AOA = 20°) at 10 m/s

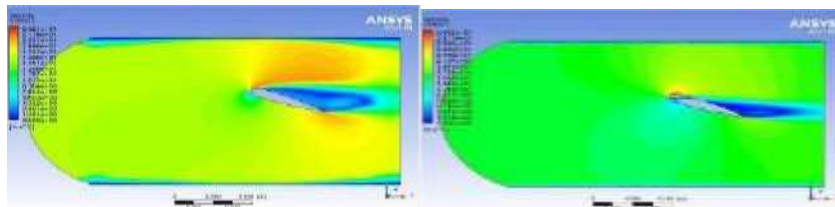
Figure 101 : Streamline at 20° for Both at Ten m/s

**Fifteen m/s :**



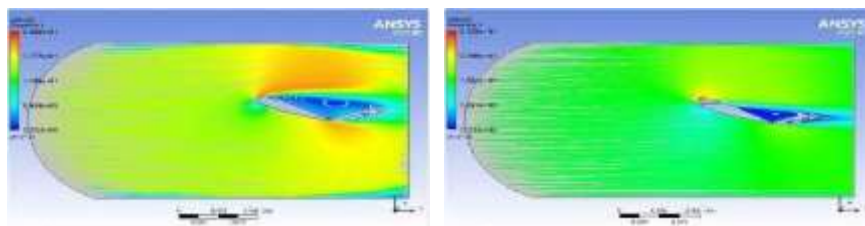
Pressure Contours : This image depicts the pressure surrounding airfoil. The color map indicates pressure levels, with green representing lower pressures and red/yellow indicating higher pressures. The airfoil front edge experiences higher pressure, while top surface experiences lower p compared to the bottom surface with (AOA = 20°) at 15 m/s

Figure 102 : Pressure at 20° for Both at fifteen m/s



Velocity Contours : This image likely illustrates pattern velocity surrounding airfoil. colors indicate different velocities, with blue representing lower velocities and green/yellow/orange indicating higher velocities. The velocity is higher on the top surface compared to the bottom surface, which is typical for generating lift even at zero attack angle with (AOA = 20°) at 15 m/s

Figure 103 : Velocity at 20° for Both at fifteen m/s

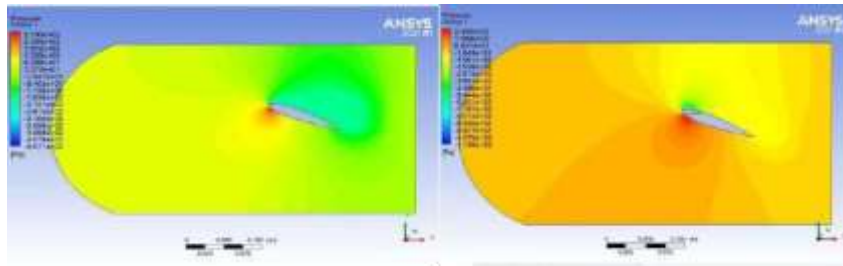


Stream lines depicting airflow patterns showing how air flows smoothly over the airfoil or separates from the surface. Streamlines closer together indicate higher velocity regions, while separation bubbles indicate areas of flow separation. with (AOA = 20°) at 15 m/s

Figure 104 : Streamline at 20° for Both at fifteen m/s

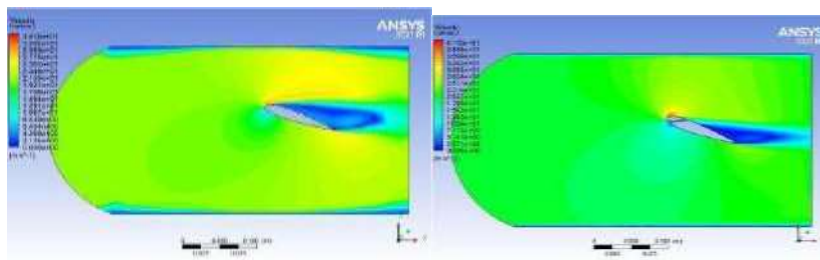


Twenty m/s-



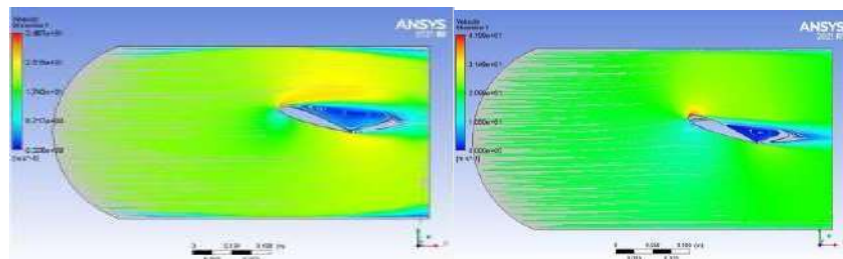
Pressure Contours : This image depicts the pressure surrounding airfoil. The color map indicates pressure levels, with green representing lower pressures and red/yellow indicating higher pressures. The airfoil front edge experiences higher pressure, while top surface experiences lower p compared to the bottom surface with (AOA = 20°) at 20 m/s

Figure 105 : Pressure at 20° for Both at Twenty m/s



Velocity Contours : This image likely illustrates pattern velocity surrounding airfoil. colors indicate different velocities, with blue representing lower velocities and green/yellow/orange indicating higher velocities. The velocity is higher on the top surface compared to the bottom surface, which is typical for generating lift even at zero attack angle with (AOA = 20°) at 20 m/s

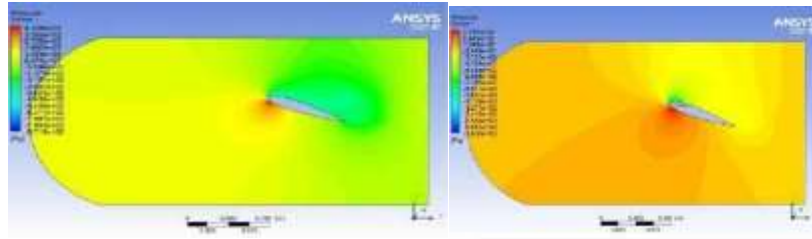
Figure 106 : Velocity at 20° for Both at Twenty m/s



Stream lines depicting airflow patterns showing how air flows smoothly over the airfoil or separates from the surface. Streamlines closer together indicate higher velocity regions, while separation bubbles indicate areas of flow separation. with (AOA = 20°) at 20 m/s

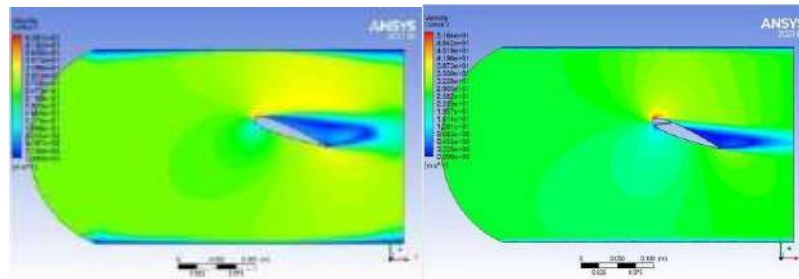
Figure 107 : Streamline at 20° for Both at Twenty m/s

## Twenty-Five m/s-



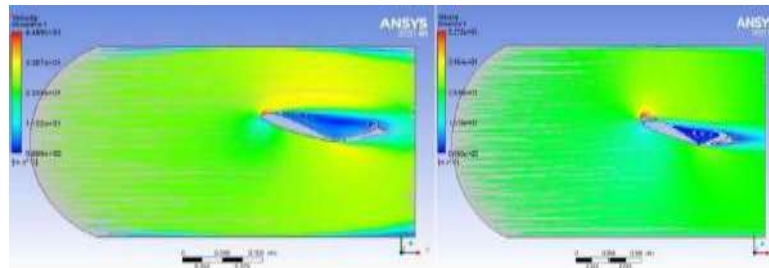
Pressure Contours : This image likely shows the pressure distribution around the airfoil. The color map indicates pressure levels, with green representing lower pressures and red/yellow indicating higher pressures. The leading edge of the airfoil experiences higher pressure, while the upper surface experiences lower pressure compared to the lower surface with (AOA = 20°) at 25 m/s

Figure 108 : Pressure at 20° for Both at twenty-Five m/s



Velocity Contours : This image likely illustrates pattern velocity surrounding airfoil. colors indicate different velocities, with blue representing lower velocities and green/yellow/orange indicating higher velocities. The velocity is higher on the top surface compared to the bottom surface, which is typical for generating lift even at zero attack angle with (AOA = 20°) at 25 m/s

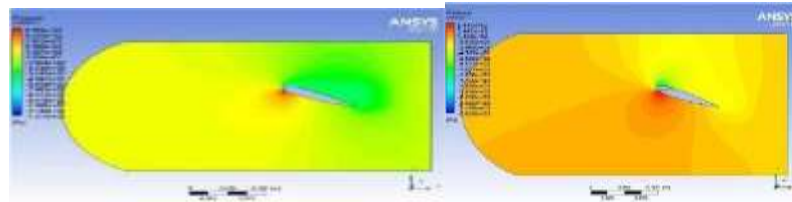
Figure 109 : Velocity at 20° for Both at twenty-Five m/s



Stream lines depicting airflow patterns showing how air flows smoothly over the airfoil or separates from the surface. Streamlines closer together indicate higher velocity regions, while separation bubbles indicate areas of flow separation. with (AOA = 20°) at 25 m/s

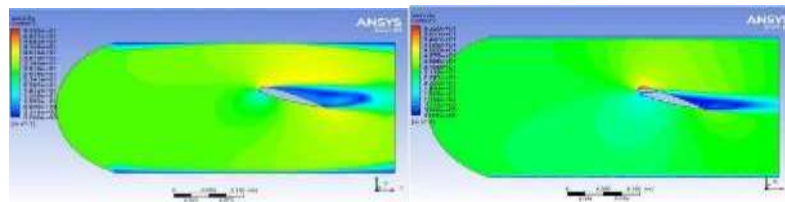
Figure 110 : Streamline at 20° for Both at twenty-Five m/s

### Thirty m/s-



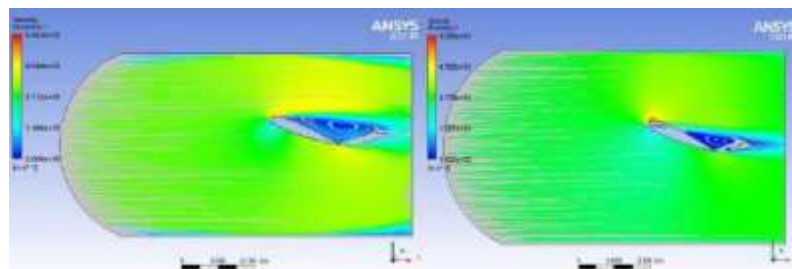
Pressure Contours : This image depicts the pressure surrounding airfoil. The color map indicates pressure levels, with green representing lower pressures and red/yellow indicating higher pressures. The airfoil front edge experiences higher pressure, while top surface experiences lower p compared to the bottom surface with (AOA = 20°) at 30 m/s

Figure 111 : Pressure at 20° for Both at Thirty m/s



Velocity Contours : This image likely illustrates pattern velocity surrounding airfoil. colors indicate different velocities, with blue representing lower velocities and green/yellow/orange indicating higher velocities. The velocity is higher on the top surface compared to the bottom surface, which is typical for generating lift even at zero attack angle with (AOA = 20°) at 30 m/s

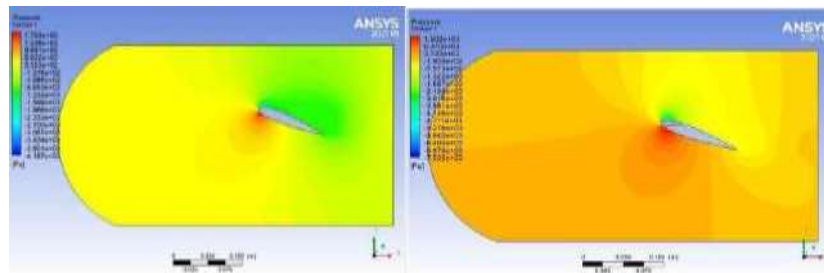
Figure 112 : Velocity at 20° for Both at Thirty m/s



Stream lines depicting airflow patterns showing how air flows smoothly over the airfoil or separates from the surface. Streamlines closer together indicate higher velocity regions, while separation bubbles indicate areas of flow separation. with (AOA = 20°) at 30 m/s

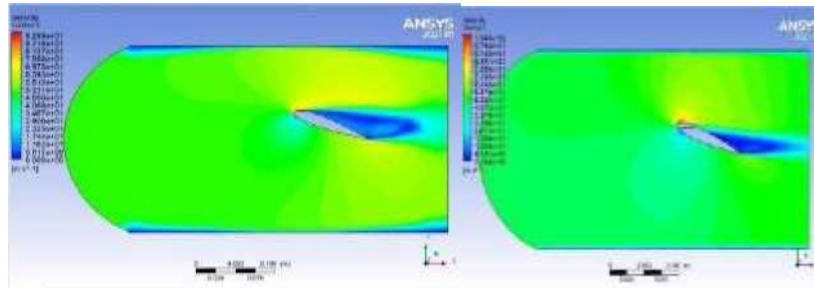
Figure 113 : Streamline at 20° for Both at Thirty m/s

### 5.33 Fifty m/s-



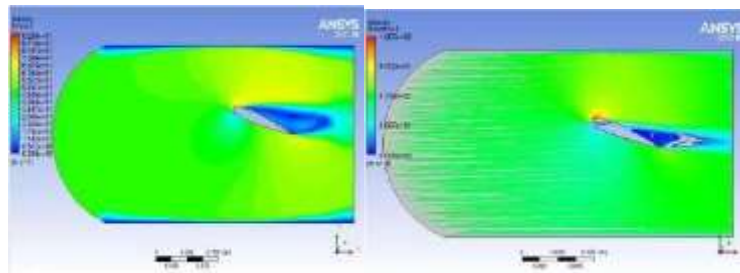
**Pressure Contours :** This image depicts the pressure surrounding airfoil. The color map indicates pressure levels, with green representing lower pressures and red/yellow indicating higher pressures. The airfoil front edge experiences higher pressure, while top surface experiences lower p compared to the bottom surface with (AOA = 20°) at 50 m/s

**Figure 114 : Pressure at 20° for Both at Fifty m/s**



**Velocity Contours :** This image likely illustrates pattern velocity surrounding airfoil. colors indicate different velocities, with blue representing lower velocities and green/yellow/orange indicating higher velocities. The velocity is higher on the top surface compared to the bottom surface, which is typical for generating lift even at zero attack angle with (AOA = 20°) at 50 m/s

**Figure 115 : Velocity at 20° for Both at Fifty m/s**



**Stream lines depicting airflow patterns** showing how air flows smoothly over the airfoil or separates from the surface. Streamlines closer together indicate higher velocity regions, while separation bubbles indicate areas of flow separation. with (AOA = 20°) at 50 m/s

**Figure 116 : Streamline at 20° for Both at Fifty m/s**

Table of Design Points									
	A	B	C	D	E	F	G	H	I
1	Name	P1 - inletvel	P2 - drag-op	P3 - drag-force-op	P4 - lift-op	P5 - lift-force-op	<input type="checkbox"/> Retain	Retained Data	Note
2	Units	m s <sup>-1</sup>		N		N			
3	DP 0 (Current)	50	0.01977	30.273	0.11954	183.04	<input checked="" type="checkbox"/>	<input checked="" type="checkbox"/>	
4	DP 1	30	0.0074525	11.412	0.04195	64.236	<input checked="" type="checkbox"/>	<input checked="" type="checkbox"/>	
5	DP 2	25	0.0052683	8.067	0.028849	44.175	<input checked="" type="checkbox"/>	<input checked="" type="checkbox"/>	
6	DP 3	20	0.0034887	5.342	0.018043	27.628	<input checked="" type="checkbox"/>	<input checked="" type="checkbox"/>	
7	DP 4	15	0.0020226	3.0972	0.009981	15.283	<input checked="" type="checkbox"/>	<input checked="" type="checkbox"/>	
8	DP 5	10	0.00094436	1.464	0.0042994	6.5834	<input checked="" type="checkbox"/>	<input checked="" type="checkbox"/>	
9	DP 6	5	0.00026429	0.4047	0.00099596	1.5251	<input checked="" type="checkbox"/>	<input checked="" type="checkbox"/>	
*							<input type="checkbox"/>		

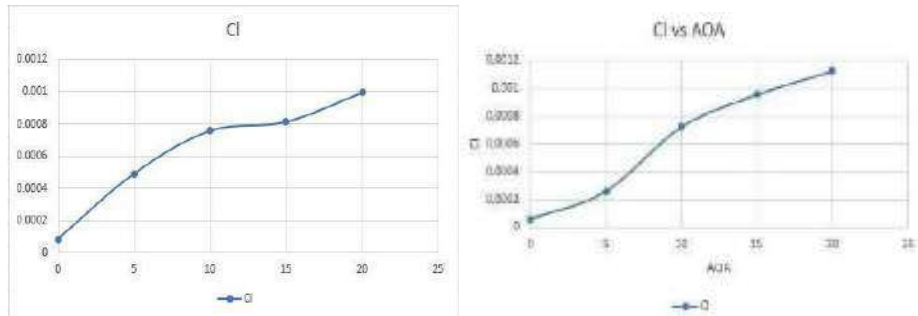
Table9 : Drag and Lift force,23015at 20°AOA

Table of Design Points									
	A	B	C	D	E	F	G	H	I
1	Name	P1 - inletvel	P2 - drag-op	P3 - drag-force-op	P4 - lift-op	P5 - lift-force-op	<input type="checkbox"/> Retain	Retained Data	Note
2	Units	m s <sup>-1</sup>		N		N			
3	DP 0 (Current)	50	0.036264	24.904	0.12547	196.72	<input checked="" type="checkbox"/>	<input checked="" type="checkbox"/>	
4	DP 1	30	0.0060534	3.2693	0.040396	69.819	<input checked="" type="checkbox"/>	<input checked="" type="checkbox"/>	
5	DP 2	25	0.0042627	6.5273	0.031435	48.155	<input checked="" type="checkbox"/>	<input checked="" type="checkbox"/>	
6	DP 3	20	0.0027784	4.2544	0.019982	30.597	<input checked="" type="checkbox"/>	<input checked="" type="checkbox"/>	
7	DP 4	15	0.0016057	2.4588	0.011126	17.037	<input checked="" type="checkbox"/>	<input checked="" type="checkbox"/>	
8	DP 5	10	0.0007511	1.2501	0.0048215	7.3829	<input checked="" type="checkbox"/>	<input checked="" type="checkbox"/>	
9	DP 6	5	0.00021949	0.3269	0.0011264	1.7246	<input checked="" type="checkbox"/>	<input checked="" type="checkbox"/>	
*							<input type="checkbox"/>		

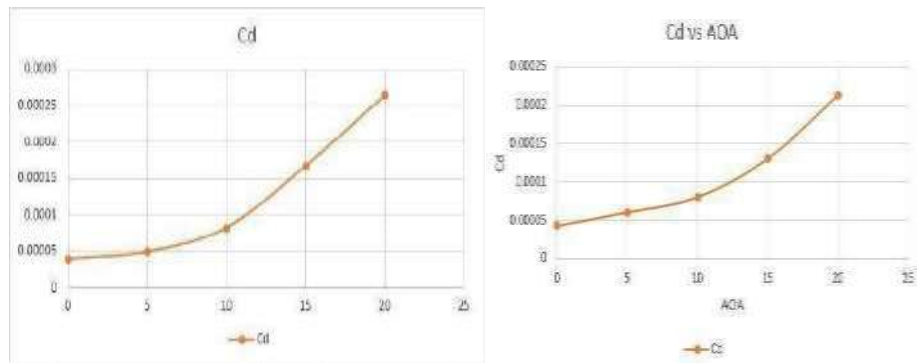
Table10 : Drag and Lift force,23015at 20°AOA

**5.34 Graphs : - for 23015 for Both vent and without vent**

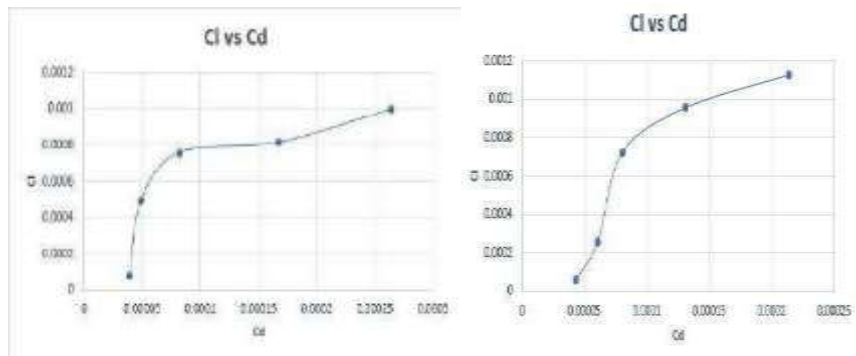
**5.35 Five m/s-**



**Figure 117 : CL versus attack angle**



**Figure 118 : Cd versus attack angle**



**Figure 119 : CL versus Cd**

### 5.36 Ten m/s-

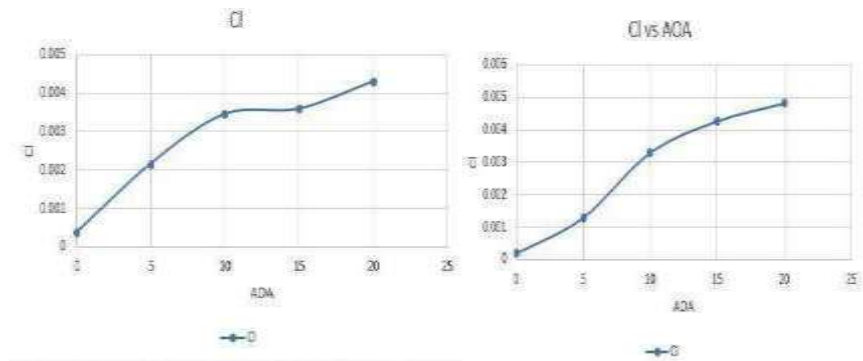


Figure 120 : CL versus attack angle

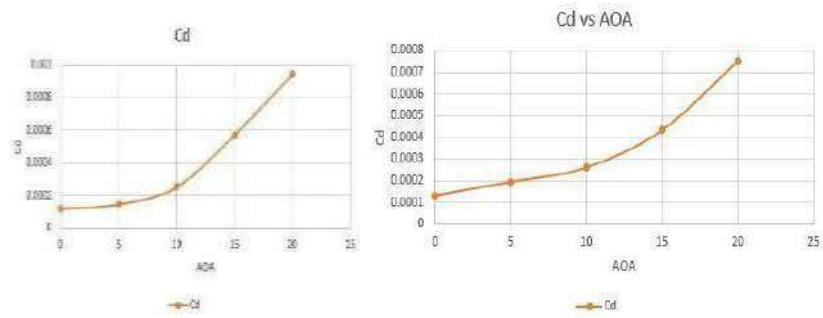


Figure 121 : Cd versus attack angle

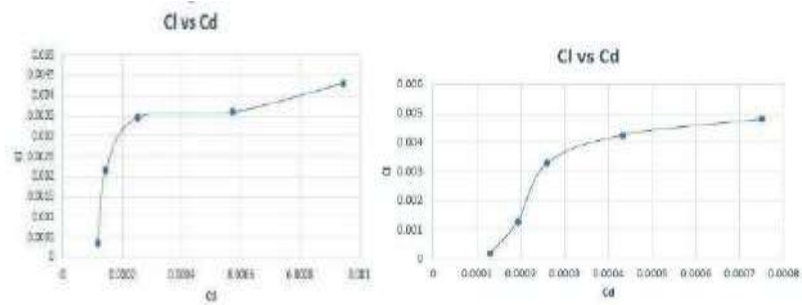


Figure 122 : CL versus Cd

### 5.37 Fifteen m/s-

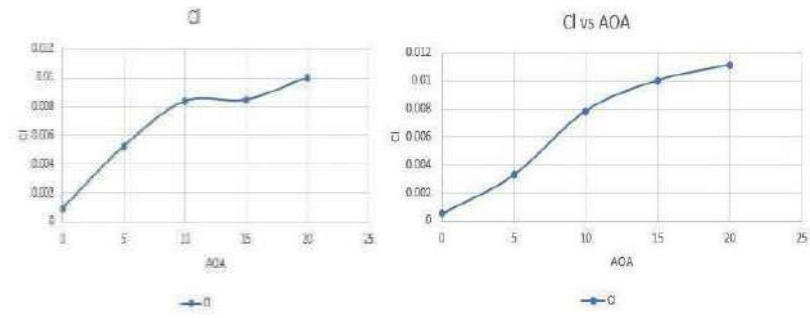


Figure 123 : CL versus attack angle

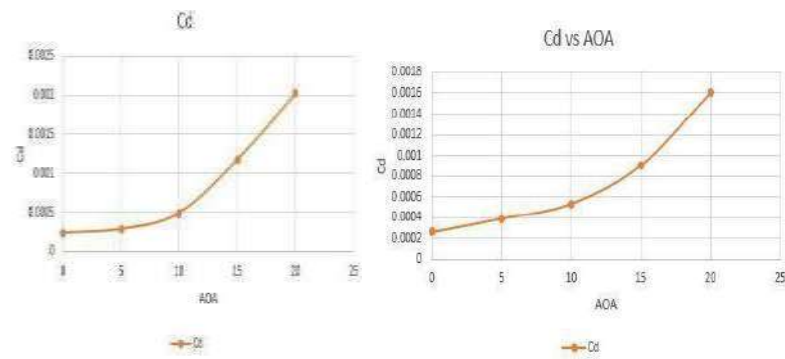


Figure 124 : Cd versus attack angle

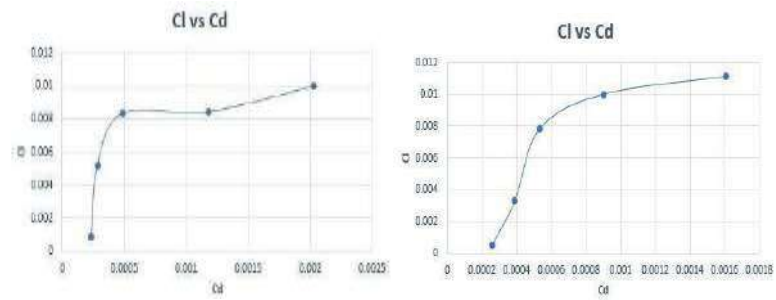


Figure 125 : CL versus Cd



### 5.38 Twenty m/s-

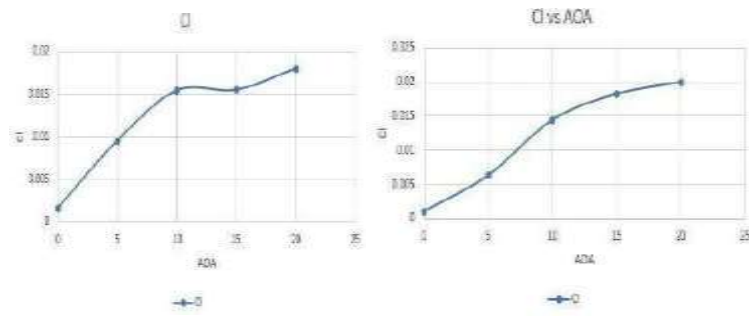


Figure 126 : CL versus attack angle

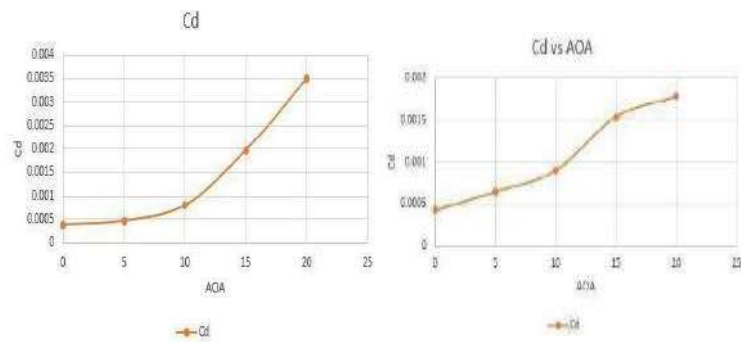


Figure 127 : Cd versus attack angle

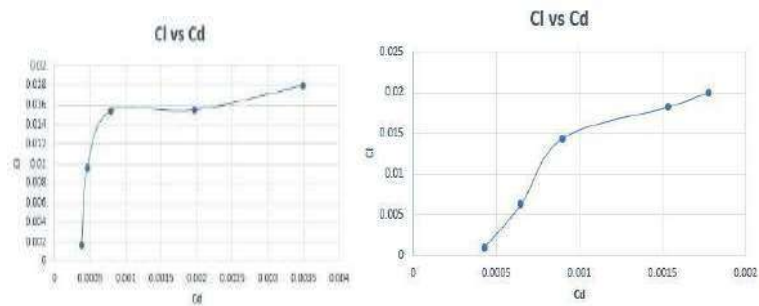


Figure 128 : CL versus Cd

### 5.39 Twenty-Five m/s-

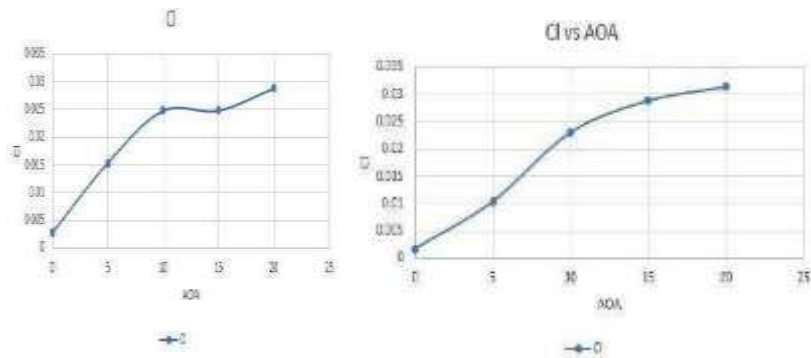


Figure 129 : CL versus attack angle

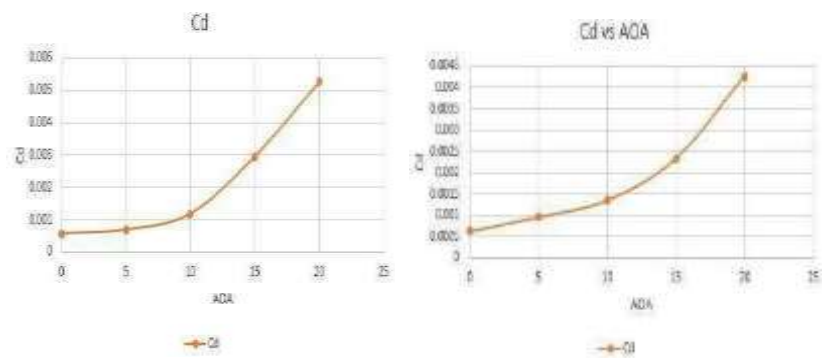


Figure 130 : Cd versus attack angle

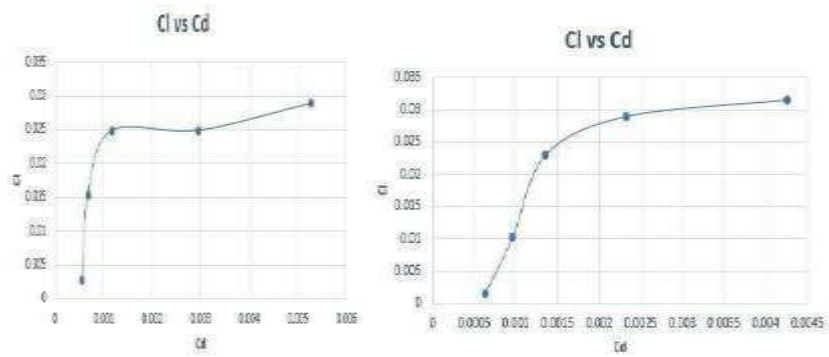


Figure 131 : CL versus Cd

### 5.40 Thirty m/s-

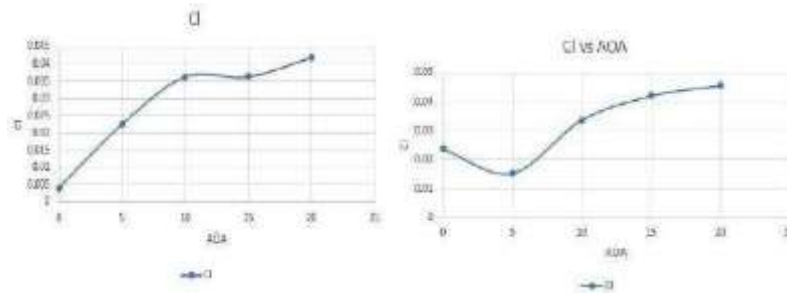


Figure 132 : Cl versus attack angle

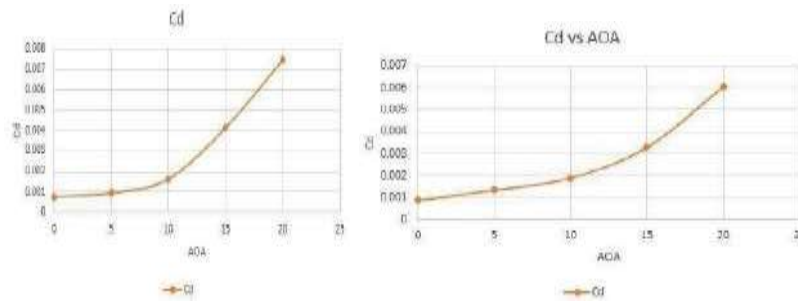


Figure 133 : Cd versus attack angle

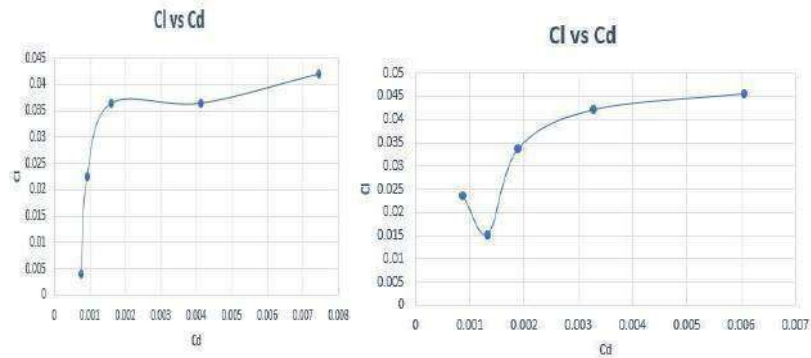


Figure 134 : Cl versus Cd

### 5.41 Fifty m/s-

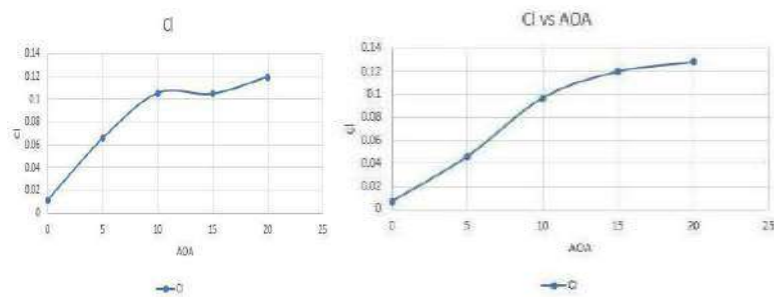


Figure 135 : CL versus attack angle

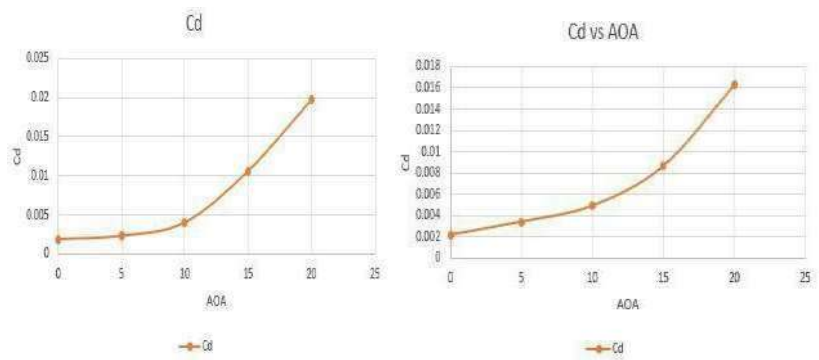


Figure 136 : Cd versus attack angle

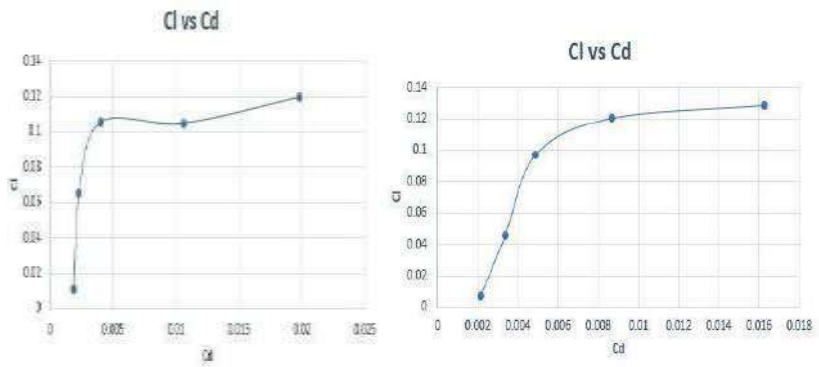


Figure 137 : Cl versus Cd

for 23021atzeroattack angle :-

#### 5.42 Five m/s-

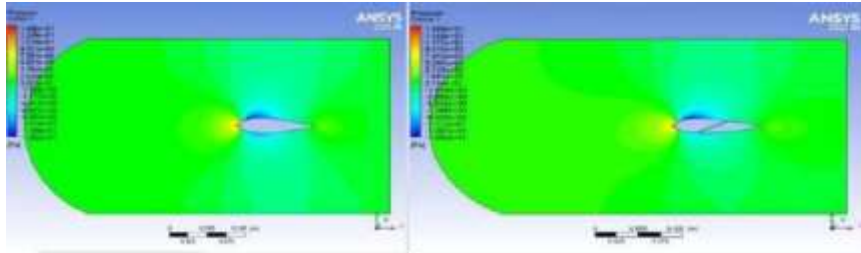


Figure 138 : Pressure at  $0^\circ$  for Both at Five m/s

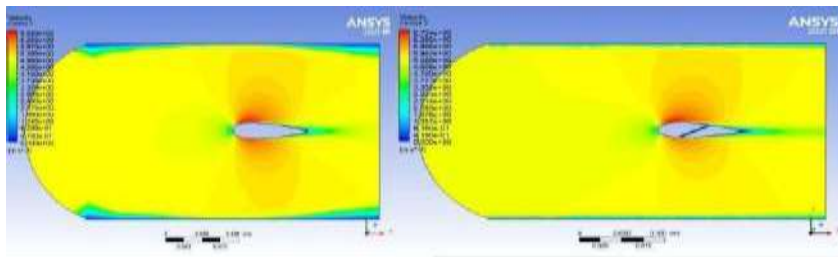


Figure 139 : Velocity at  $0^\circ$  for Both at Five m/s

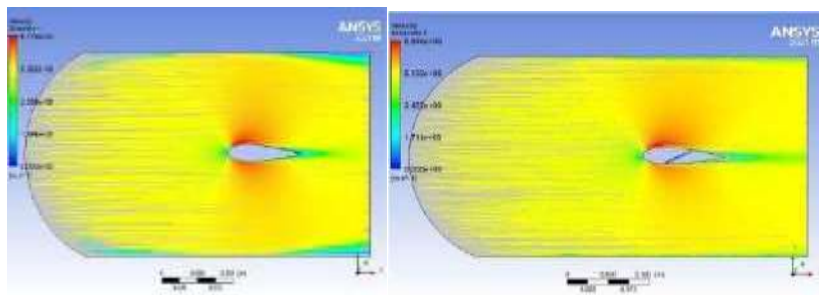


Figure 140 : Streamline at  $0^\circ$  for Both at Five m/s

#### 5.43 Ten m/s-

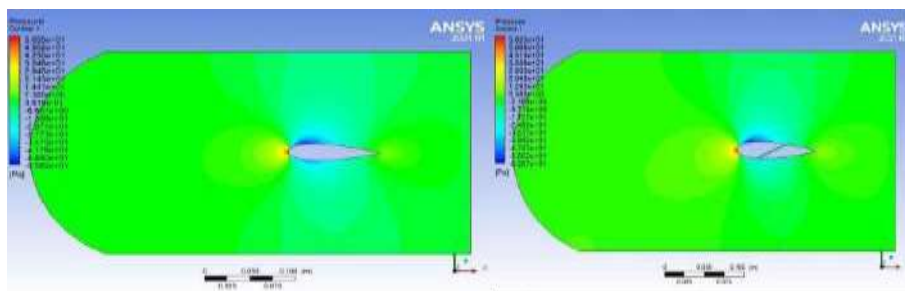


Figure 141 : Pressure at  $0^\circ$  for Both at Ten m/s

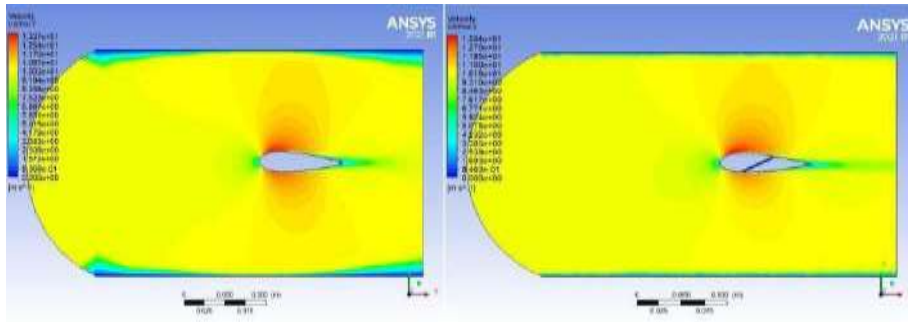


Figure 142 : Velocity at  $0^\circ$  for Both at Ten m/s

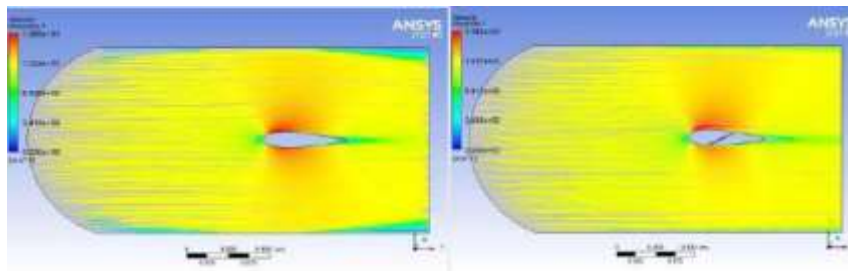


Figure 143 : Streamline at  $0^\circ$  for Both at Ten m/s

#### 5.44 Fifteen m/s-

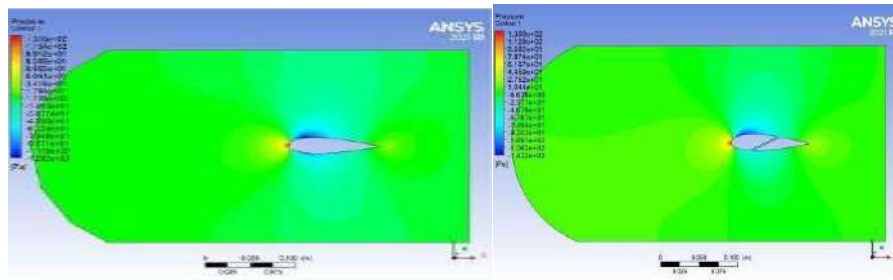


Figure 144 : Pressure at  $0^\circ$  for Both at fifteen m/s

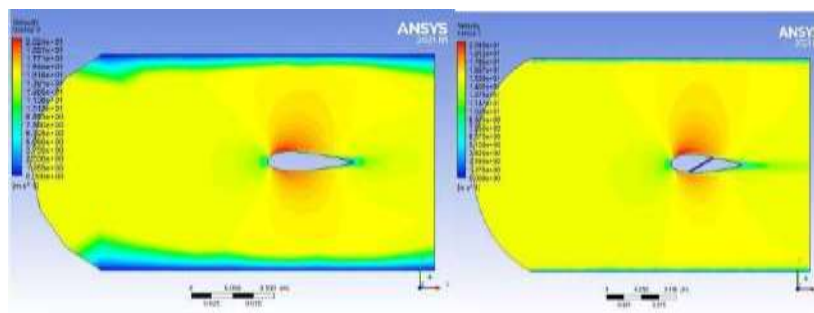


Figure 145 : Velocity at  $0^\circ$  for Both at fifteen m/s

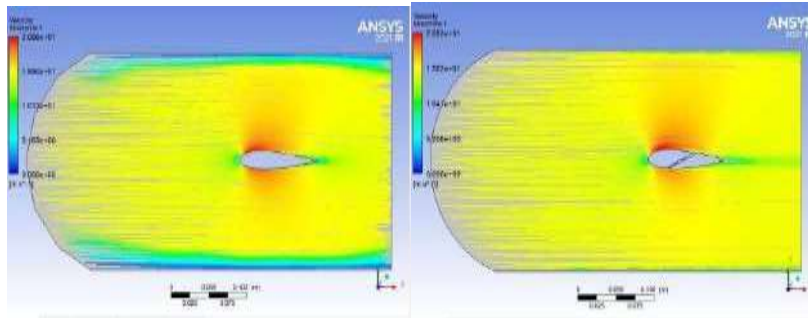


Figure 146 : Streamline at $0^{\circ}$  for Both at fifteen m/s

#### 5.45 Twenty m/s-

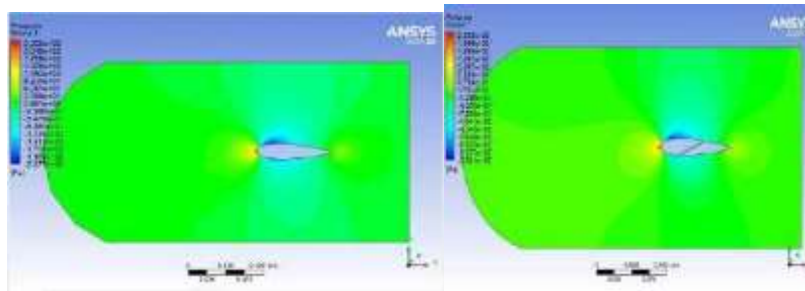


Figure 147 : Pressure at $0^{\circ}$  for Both at Twenty m/s

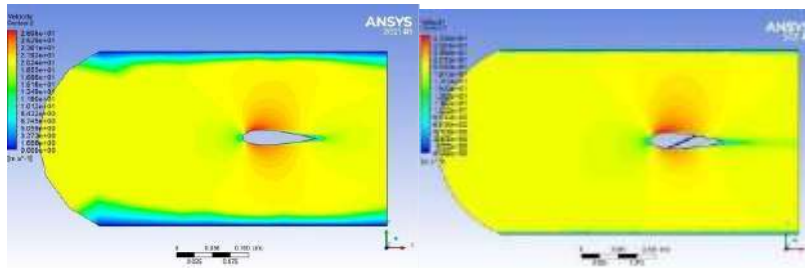


Figure 148 : Velocity at $0^{\circ}$  for Both at Twenty m/s

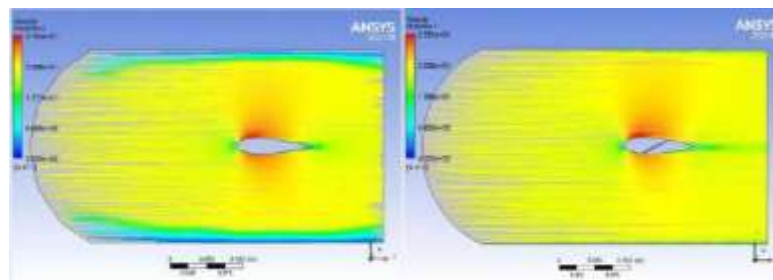


Figure 149 : Streamline at $0^{\circ}$  for Both at Twenty m/s

### 5.46 Twenty Five m/s-

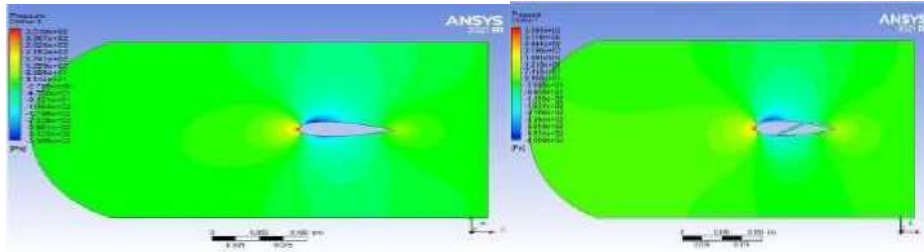


Figure 150 : Pressure at $t_0^0$  for Both at twenty Five m/s

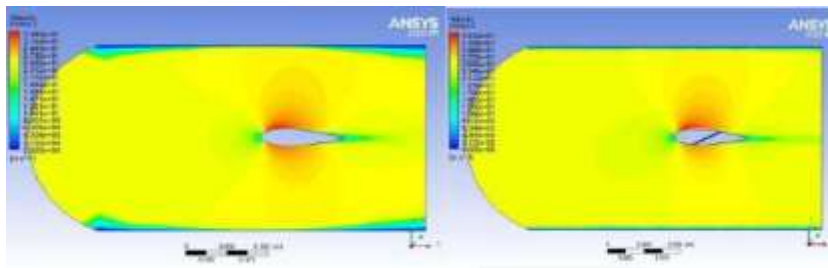


Figure 151 : Velocity at $t_0^0$  for Both at twenty-Five m/s

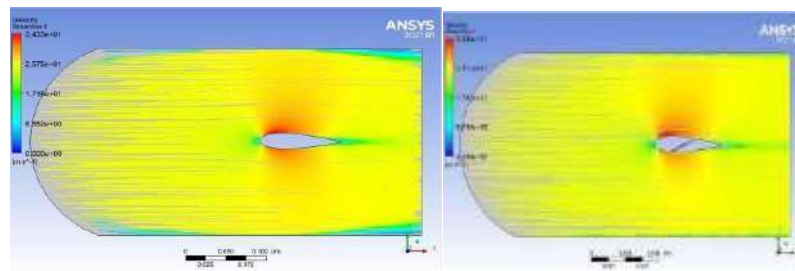


Figure 152 : Streamline at $t_0^0$  for Both at twenty Five m/s

### 5.47 Thirty m/s-

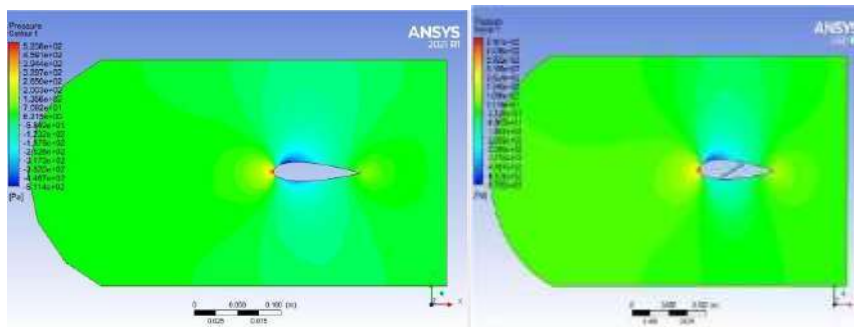


Figure 153 : Pressure at $t_0^0$  for Both at Thirty m/s



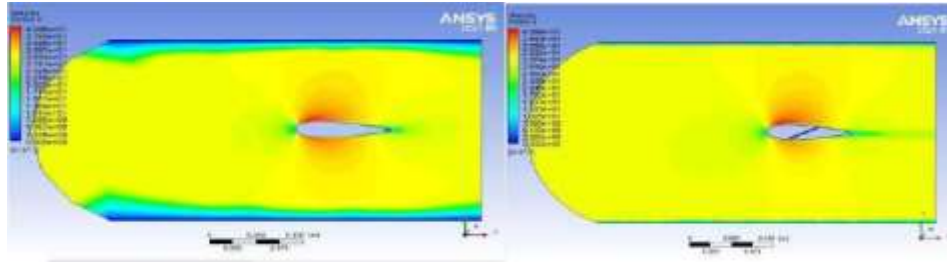


Figure 154 : Velocity at $0^{\circ}$  for Both at Thirty m/s

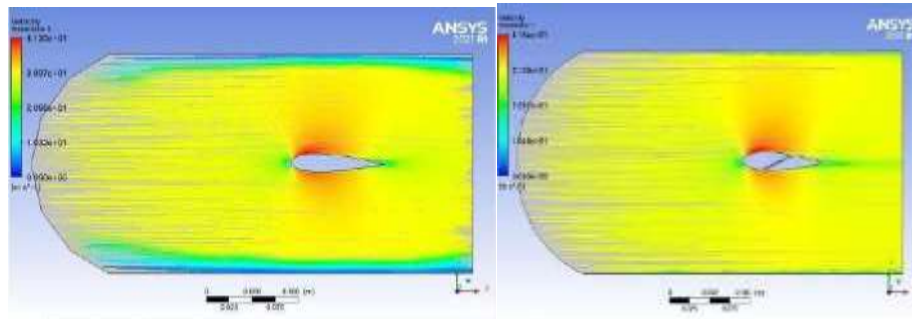


Figure 155 : Streamline at $0^{\circ}$  for Both at Thirty m/s

#### 5.48 Fifty m/s-

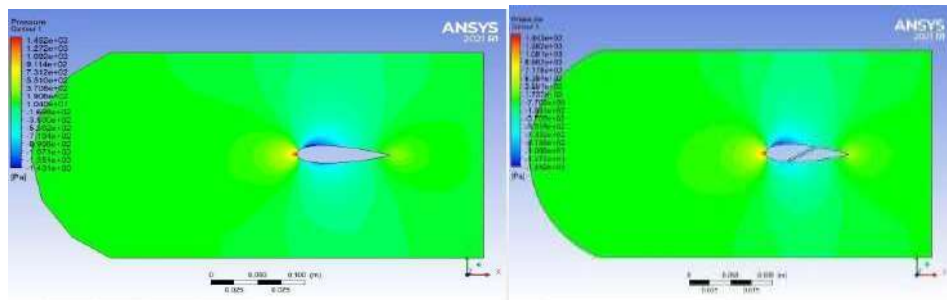


Figure 156 : Pressure at $0^{\circ}$  for Both at fifty m/s

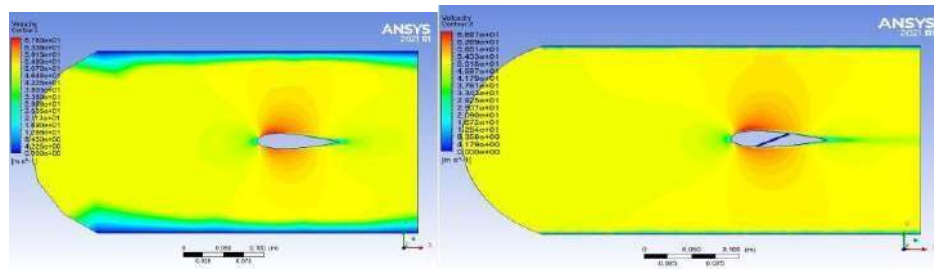


Figure 157 : Velocity at $0^{\circ}$  for Both at Fifty m/s

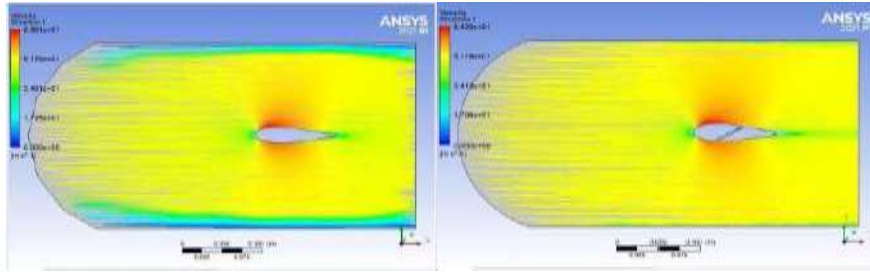


Figure 158 : Streamline at $0^\circ$  for Both at Fifty m/s

Table of Design Points									
	A	B	C	D	E	F	G	H	I
1	Name	P1 - inlet vel	P2 - drag-op	P3 - drag-force-op	P4 - lift-op	P5 - lift-force-op	Retain	Retained Data	Note
2	Units	ms <sup>-1</sup>		N		N			
3	DP 7 (Current)	50	0.0026030	3.2207	0.011002	17	<input checked="" type="checkbox"/>	<input checked="" type="checkbox"/>	
4	DP 8	30	0.0008986	1.332	0.0036718	5.6224	<input checked="" type="checkbox"/>	<input checked="" type="checkbox"/>	
5	DP 9	25	0.0005662	0.97483	0.00243	3.721	<input checked="" type="checkbox"/>	<input checked="" type="checkbox"/>	
6	DP 10	20	0.00040579	0.6673	0.0014203	2.1749	<input checked="" type="checkbox"/>	<input checked="" type="checkbox"/>	
7	DP 11	15	0.00026911	0.41206	0.00069031	0.99578	<input checked="" type="checkbox"/>	<input checked="" type="checkbox"/>	
8	DP 12	10	0.00013902	0.21387	0.0002411	0.32786	<input checked="" type="checkbox"/>	<input checked="" type="checkbox"/>	
9	DP 13	5	4.7914E-05	0.070369	6.003E-05	0.091921	<input checked="" type="checkbox"/>	<input checked="" type="checkbox"/>	
*							<input type="checkbox"/>		

Table11 : Drag and Lift force,23021

Table of Design Points									
	A	B	C	D	E	F	G	H	I
1	Name	P1 - inlet vel	P2 - drag-op	P3 - drag-force-op	P4 - lift-op	P5 - lift-force-op	Retain	Retained Data	Note
2	Units	ms <sup>-1</sup>		N		N			
3	DP 18 (Current)	50	0.0024811	3.7993	0.010469	16.031	<input checked="" type="checkbox"/>	<input checked="" type="checkbox"/>	
4	DP 19	30	0.00094796	1.4516	0.0081307	12.45	<input checked="" type="checkbox"/>	<input checked="" type="checkbox"/>	
5	DP 20	25	0.00068814	1.0537	0.0056208	8.6068	<input checked="" type="checkbox"/>	<input checked="" type="checkbox"/>	
6	DP 21	20	0.00046536	0.71258	0.0039548	5.5045	<input checked="" type="checkbox"/>	<input checked="" type="checkbox"/>	
7	DP 22	15	0.00028451	0.43566	0.0019946	3.0542	<input checked="" type="checkbox"/>	<input checked="" type="checkbox"/>	
8	DP 23	10	0.00014499	0.22202	0.0008217	1.2582	<input checked="" type="checkbox"/>	<input checked="" type="checkbox"/>	
9	DP 24	5	4.8298E-05	0.070356	0.0001668	0.25541	<input checked="" type="checkbox"/>	<input checked="" type="checkbox"/>	
*							<input type="checkbox"/>		

Table12 : Drag and Lift force,23021

5.49 Five attack angle :-

5.50 Five m/s-

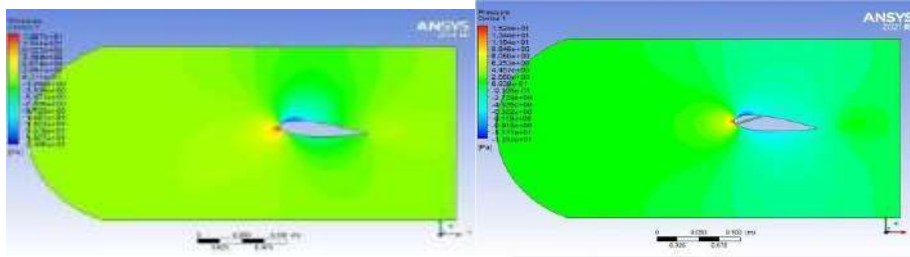


Figure 159 : Pressure at 5° for Both at Five m/s

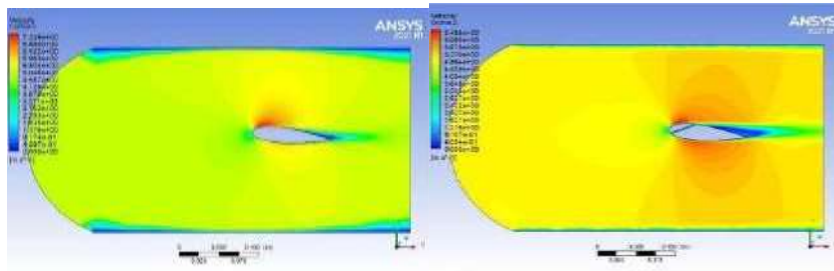


Figure 160 : Velocity at 5° for Both at Five m/s

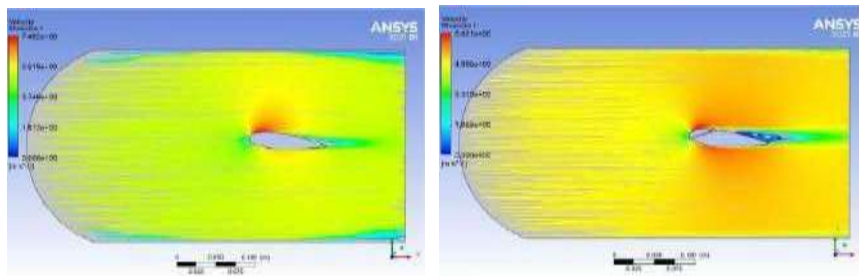


Figure 161 : Streamline at 5° for Both at Five m/s

Ten m/s-

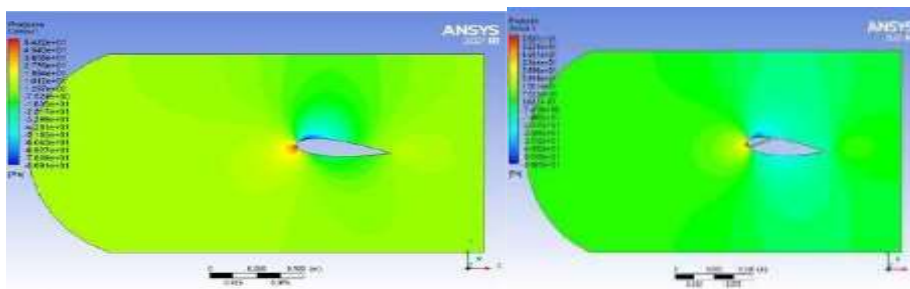


Figure 162 : Pressure at 5° for Both at Ten m/s

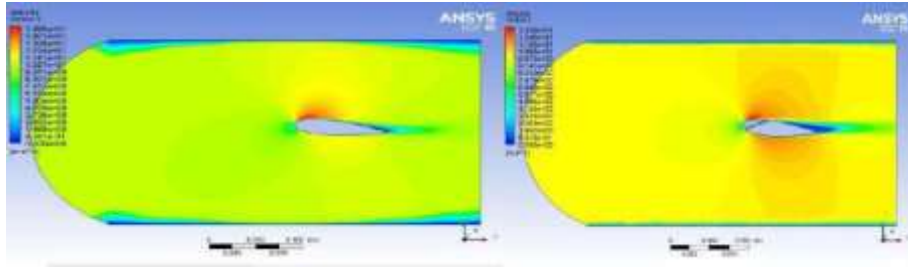


Figure 163 : Velocity at  $5^\circ$  for Both at Ten m/s

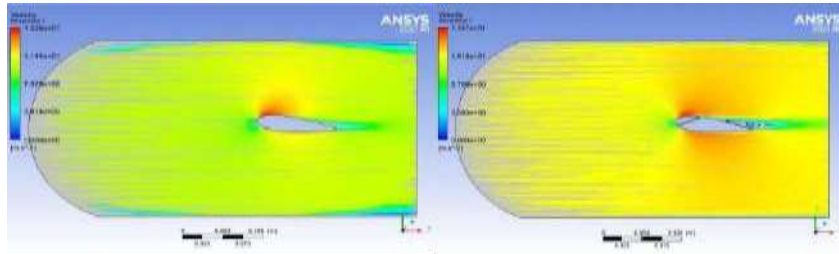


Figure 164 : : Streamline at  $5^\circ$  for Both at Ten m/s

**Fifteen m/s-**

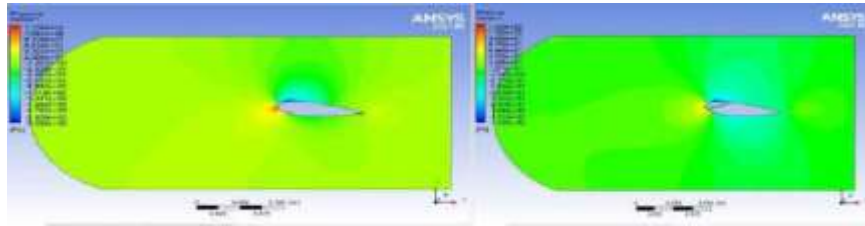


Figure 165 : Pressure at  $5^\circ$  for Both at fifteen m/s

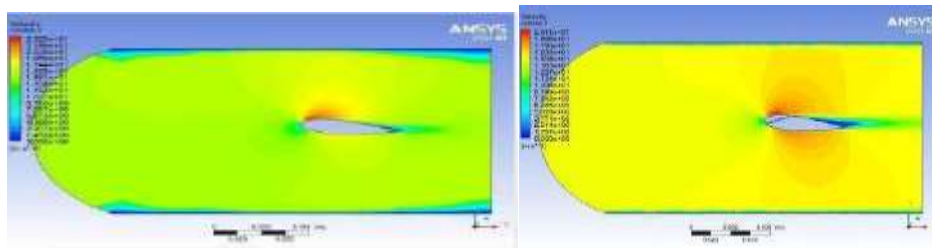


Figure 166 : Velocity at  $5^\circ$  for Both at fifteen m/s

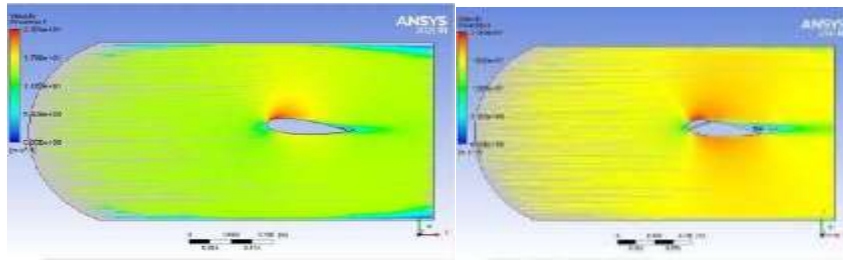


Figure 167 : Streamline at  $5^\circ$  for Both at fifteen m/s

### 5.51 Twenty m/s-

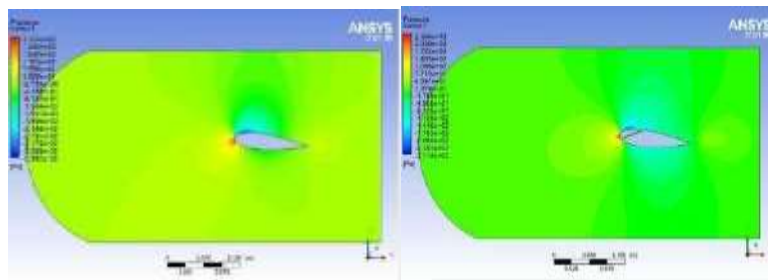


Figure 168 : Pressure at  $5^\circ$  for Both at Twenty m/s

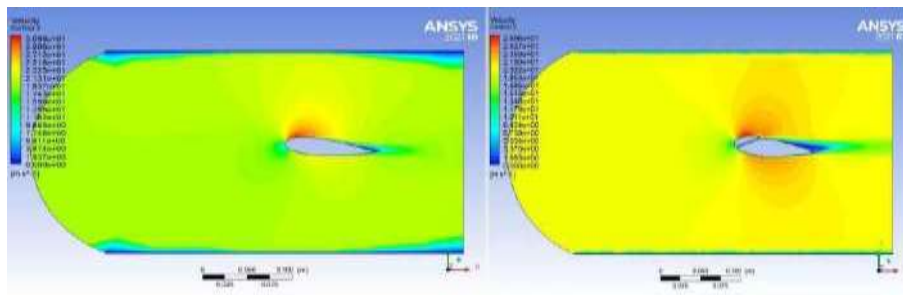


Figure 169 : Velocity at  $5^\circ$  for Both at Twenty m/s

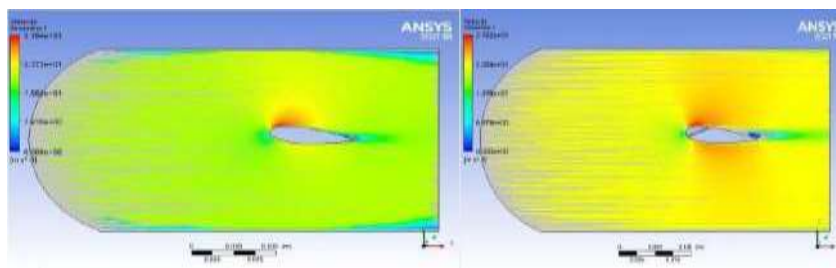


Figure 170 : Streamline at  $5^\circ$  for Both at Twenty m/s

### 5.52 Twenty Five m/s-

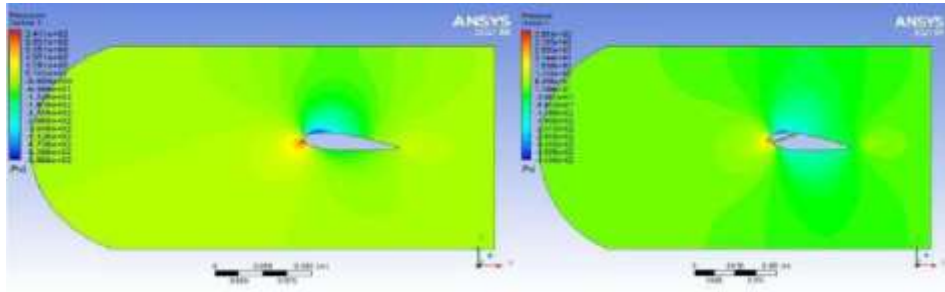


Figure 171 : Pressure at $5^0$  for Both at twenty Five m/s

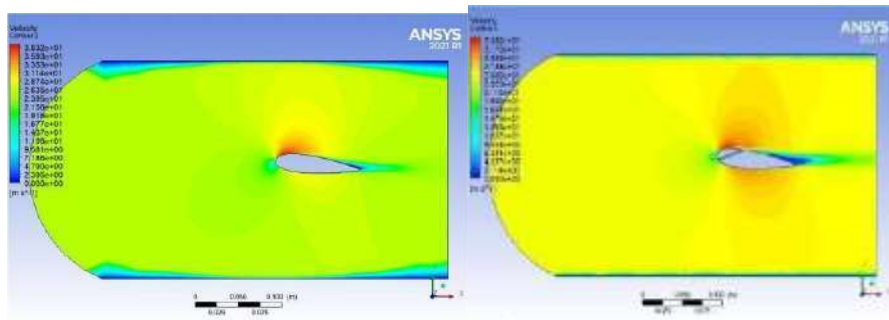


Figure 172 : Velocity at $5^0$  for Both at twenty Five m/s

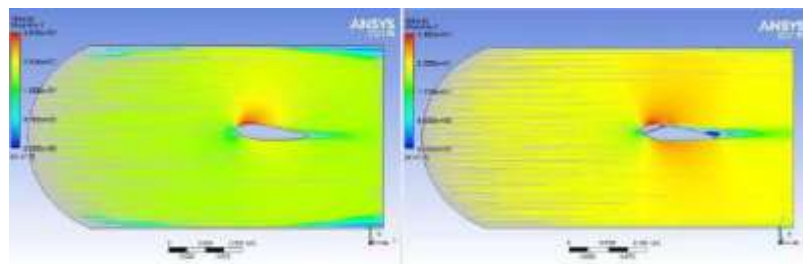


Figure 173 : Streamline at $5^0$  for Both at twenty Five m/s

### Thirty m/s-

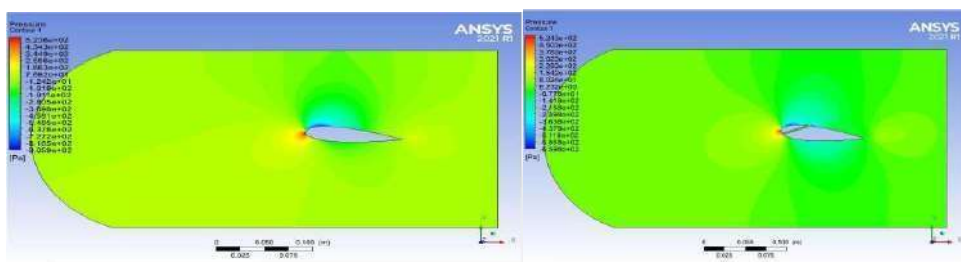


Figure 174 : Pressure at $5^0$  for Both at Thirty m/s

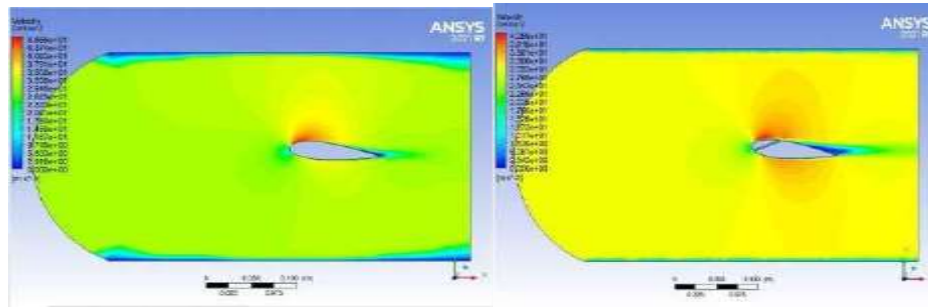


Figure 175 : Velocity at  $5^\circ$  for Both at Thirty m/s

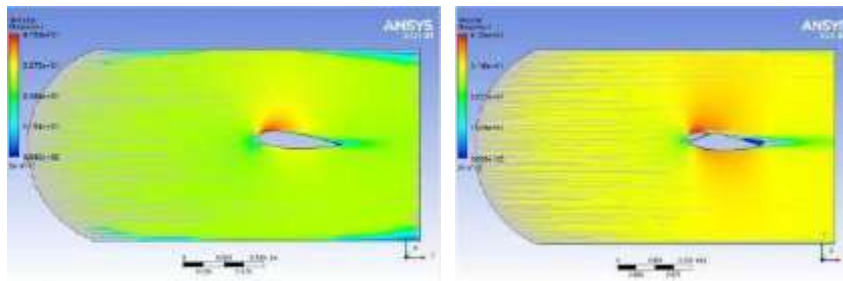


Figure 176 : Streamline at  $5^\circ$  for Both at Thirty m/s

**Fifty m/s-**

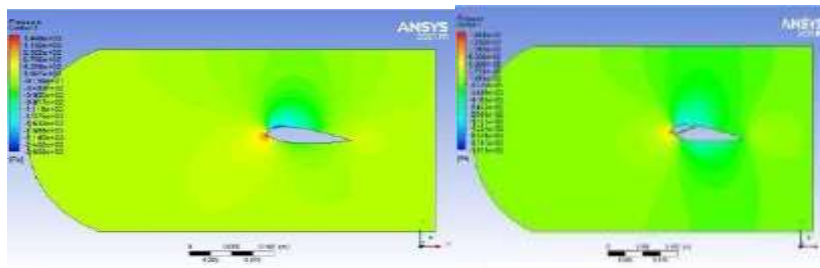


Figure 177 : Pressure at  $5^\circ$  for Both at Fifty m/s

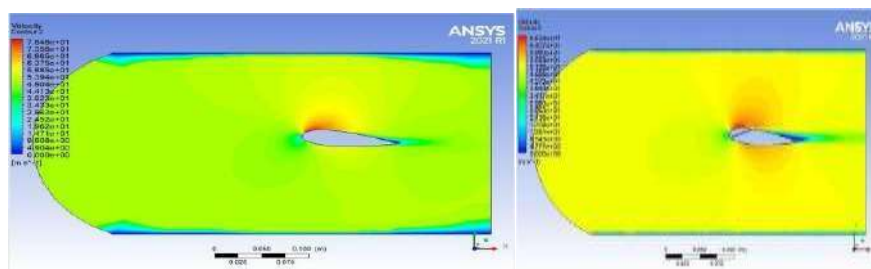


Figure 178 : Velocity at  $5^\circ$  for Both at Fifty m/s

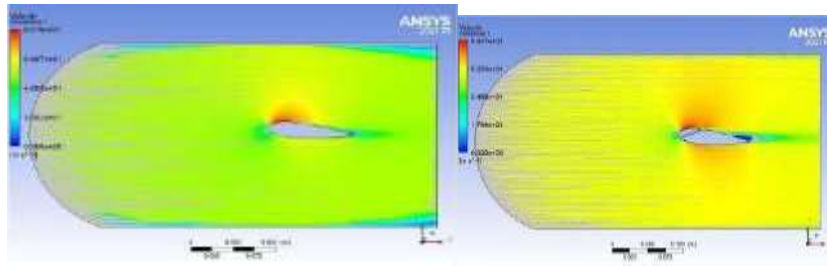


Figure 179 : Streamline at 50 for Both at Fifty m/s

Table of Design Points									
	A	B	C	D	E	F	G	H	I
1	Name	P1 - inlet vel	P2 - drag-co	P3 - drag-force-co	P4 - lift-co	P5 - lift-force-co	Retain	Retained Data	Note
2	Units	ms <sup>-1</sup>		N		N			
3	DP 7 (Current)	30	0.0025524	3.9083	0.063259	96.88	<input checked="" type="checkbox"/>	<input checked="" type="checkbox"/>	
4	DP 8	30	0.0030422	1.5959	0.020836	31.906	<input checked="" type="checkbox"/>	<input checked="" type="checkbox"/>	
5	DP 9	25	0.00076141	1.1659	0.013931	21.332	<input checked="" type="checkbox"/>	<input checked="" type="checkbox"/>	
6	DP 10	20	0.00052119	0.79808	0.009425	12.901	<input checked="" type="checkbox"/>	<input checked="" type="checkbox"/>	
7	DP 11	15	0.00032264	0.49538	0.0043066	6.5945	<input checked="" type="checkbox"/>	<input checked="" type="checkbox"/>	
8	DP 12	10	0.0001694	0.2994	0.0006687	2.54	<input checked="" type="checkbox"/>	<input checked="" type="checkbox"/>	
9	DP 13	5	6.0379E-05	0.092465	0.00031415	0.48104	<input checked="" type="checkbox"/>	<input checked="" type="checkbox"/>	
*							<input type="checkbox"/>		

Table13 : Drag and Lift force values,23021

Table of Design Points									
	A	B	C	D	E	F	G	H	I
1	Name	P1 - inlet vel	P2 - drag-co	P3 - drag-force-co	P4 - lift-co	P5 - lift-force-co	Retain	Retained Data	Note
2	Units	ms <sup>-1</sup>		N		N			
3	DP 0 (Current)	30	0.004974	7.6364	0.014251	21.822	<input checked="" type="checkbox"/>	<input checked="" type="checkbox"/>	
4	DP 1	30	0.0019608	3.0025	0.004406	6.5404	<input checked="" type="checkbox"/>	<input checked="" type="checkbox"/>	
5	DP 2	25	0.0014107	2.3501	0.003613	4.0111	<input checked="" type="checkbox"/>	<input checked="" type="checkbox"/>	
6	DP 3	20	0.00094445	1.4462	0.0014663	2.2453	<input checked="" type="checkbox"/>	<input checked="" type="checkbox"/>	
7	DP 4	15	0.00056569	0.86622	0.00067093	1.0274	<input checked="" type="checkbox"/>	<input checked="" type="checkbox"/>	
8	DP 5	10	0.00027721	0.42448	0.00023641	0.33444	<input checked="" type="checkbox"/>	<input checked="" type="checkbox"/>	
9	DP 6	5	8.4643E-05	0.12861	1.01E-05	0.015327	<input checked="" type="checkbox"/>	<input checked="" type="checkbox"/>	
*							<input type="checkbox"/>		

Table14 : Drag and Lift force values,23021



5.53 10Attack angle : -

5.54 Five m/s-

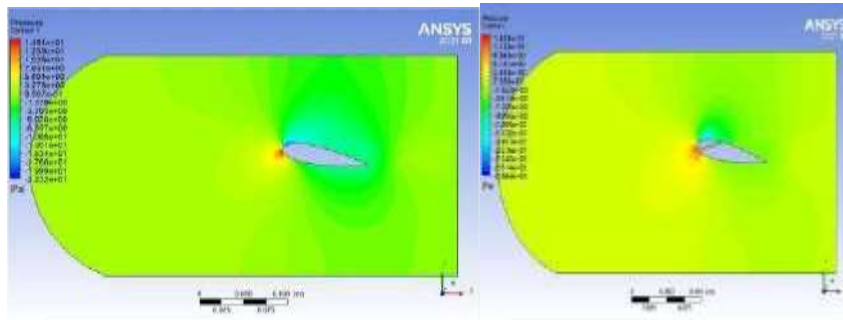


Figure 180 : Pressure at 10° for Both at Five m/s

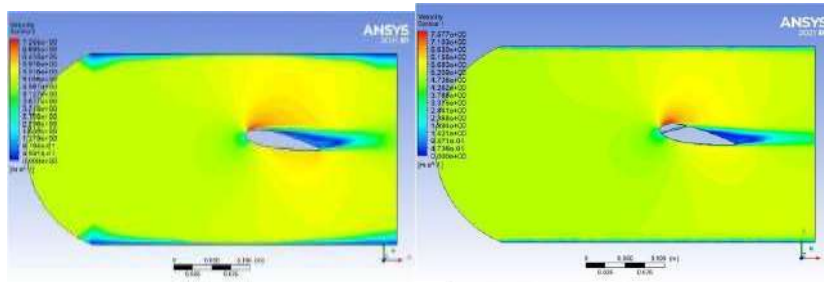


Figure 181 : Velocity at 10° for Both at Five m/s

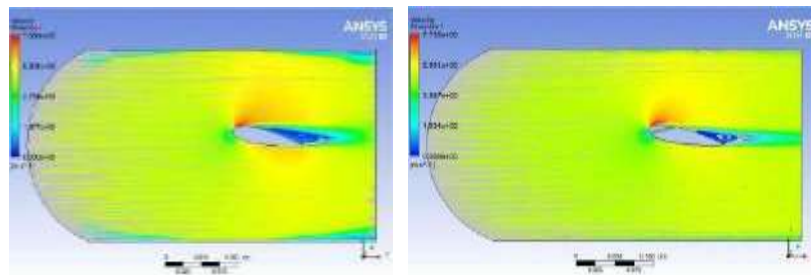


Figure 182 : Streamline at 10° for Both at Five m/s

5.55 Ten m/s-

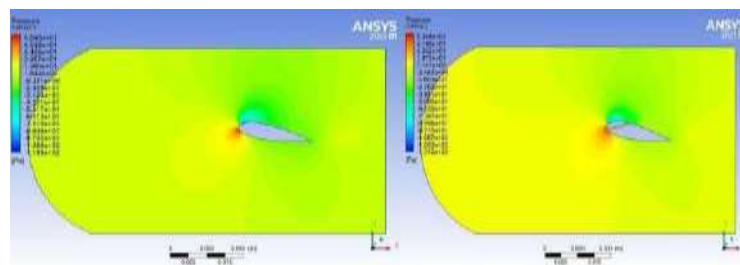


Figure 183 : Pressure at 10° for Both at Ten m/s

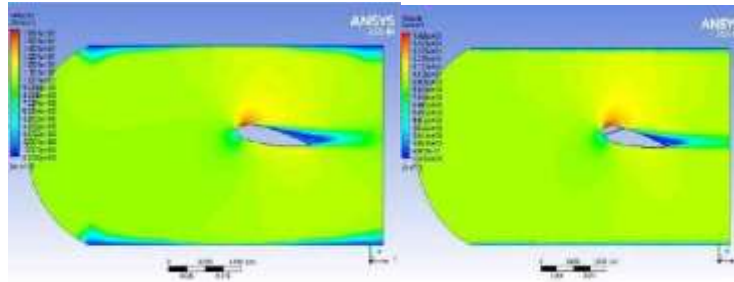


Figure 184 : Velocity at  $10^0$  for Both at Ten m/s

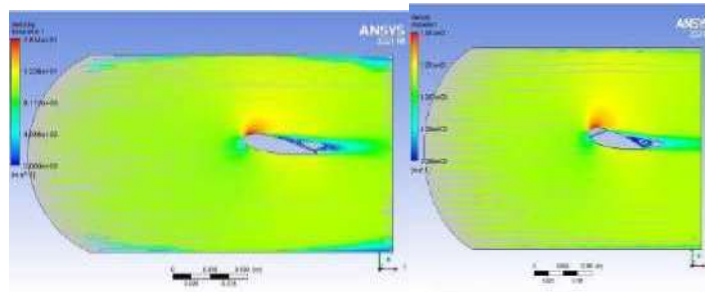


Figure 185 : Streamline at  $10^0$  for Both at Ten m/s

### 5.56 Fifteen m/s-

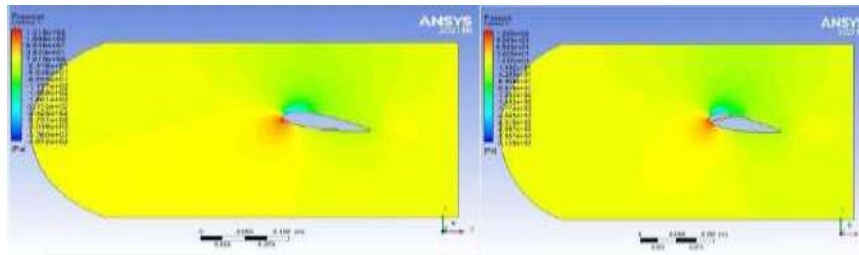


Figure 186 : Pressure at  $10^0$  for Both at fifteen m/s

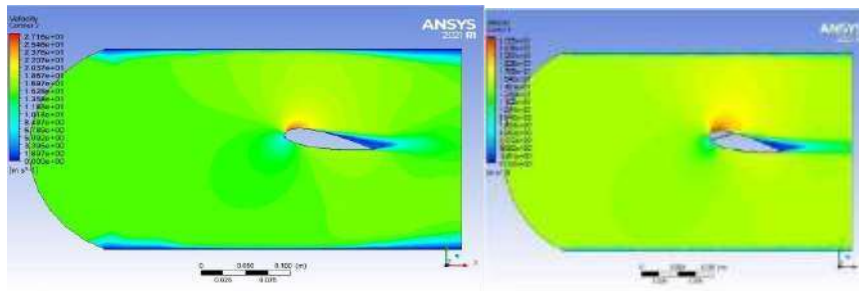


Figure 187 : Velocity at  $10^0$  for Both at fifteen m/s

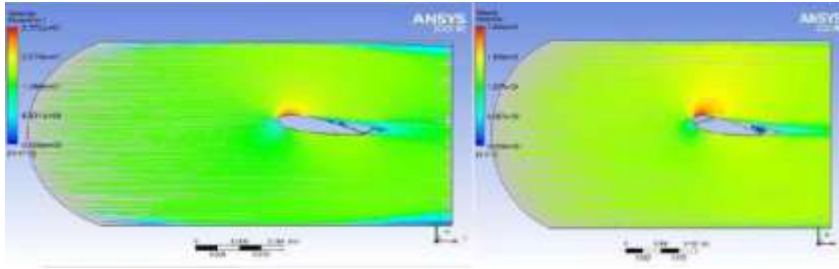


Figure 188 : Streamline at  $10^0$  for Both at fifteen m/s

### 5.57 Twenty m/s-

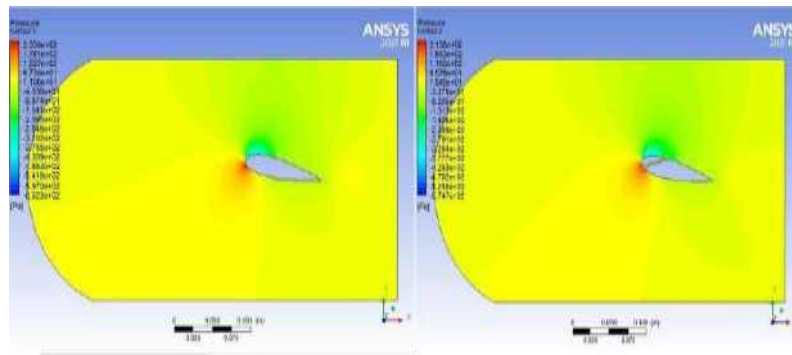


Figure 189 : Pressure at  $10^0$  for Both at Twenty m/s

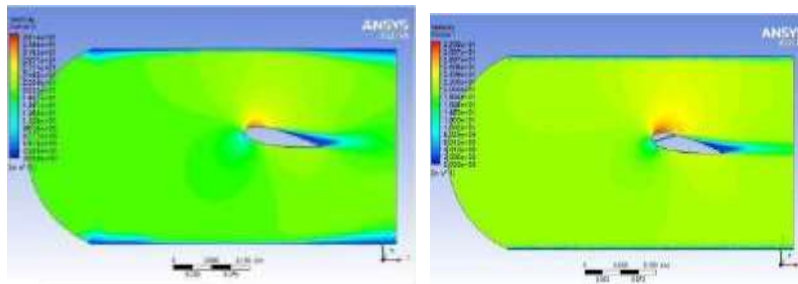


Figure 190 : Velocity at  $10^0$  for Both at Twenty m/s

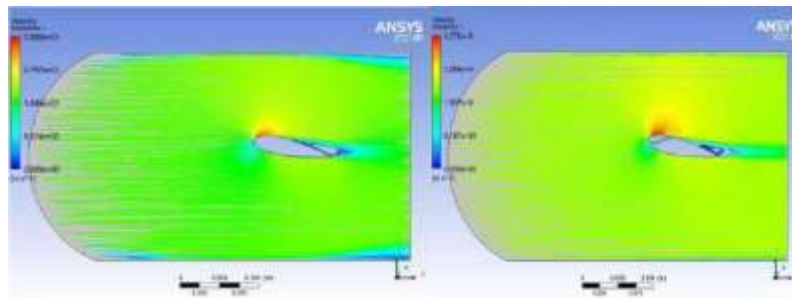


Figure 191 : Streamline at  $10^0$  for Both at Twenty m/s

### 5.58 Twenty Five m/s-

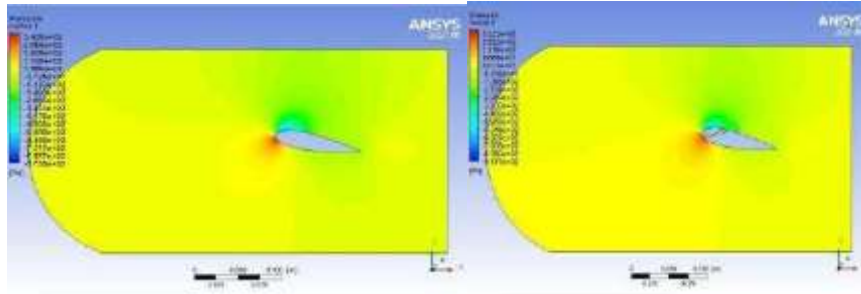


Figure 192 : Pressure at  $10^0$  for Both at Twenty Five m/s

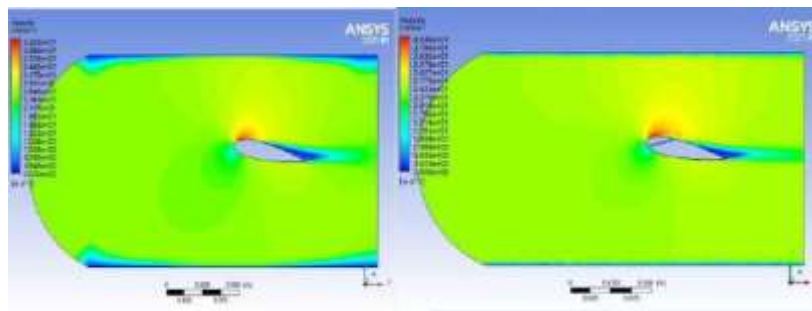


Figure 193 : Velocity at  $10^0$  for Both at Twenty Five m/s

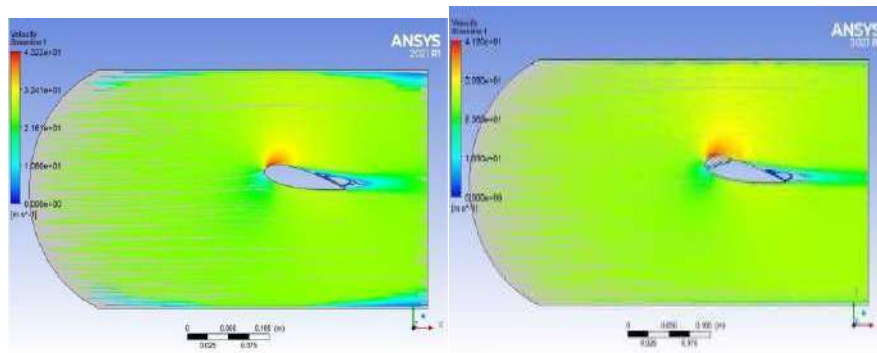


Figure 194 : Streamline at  $10^0$  for Both at Twenty Five m/s

### 5.59 Thirty m/s

### 5.60 Thirty m/s-

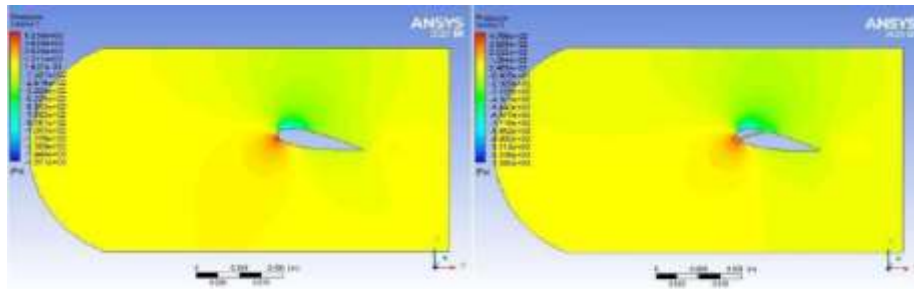


Figure 195 : Pressure at  $10^0$  for Both at Thirty m/s

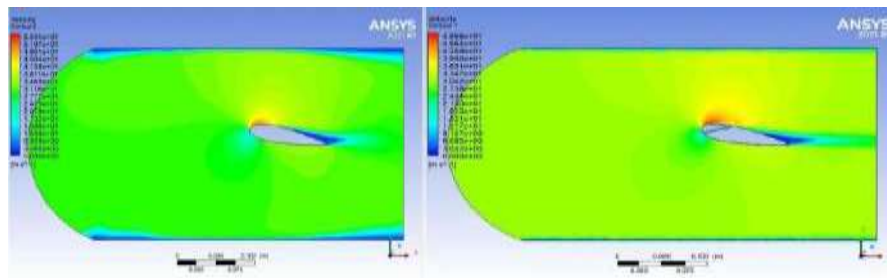


Figure 196 : Velocity at  $10^0$  for Both at Thirty m/s

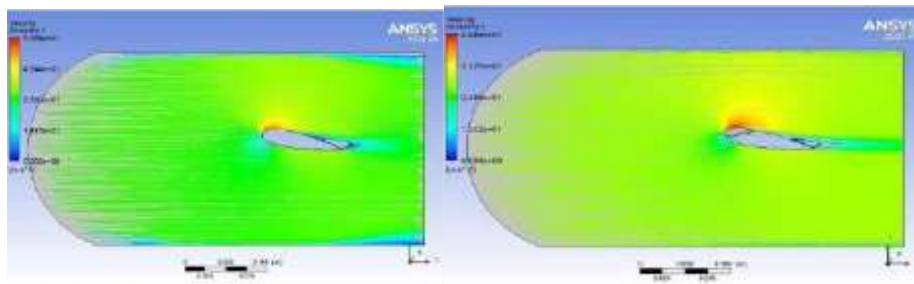


Figure 197 : Streamline at  $10^0$  for Both at Thirty m/s

### 5.61 Fifty m/s-

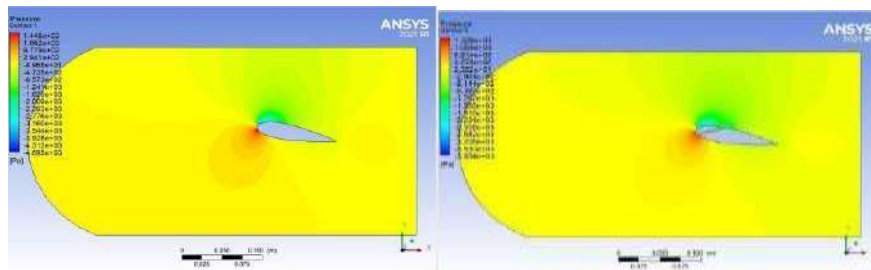


Figure 198 : Pressure at  $10^0$  for Both at Fifty m/s

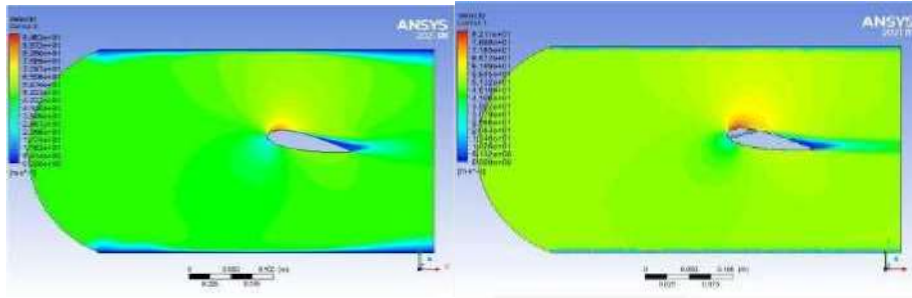


Figure 199 : Velocity at  $10^0$  for Both at Fifty m/s

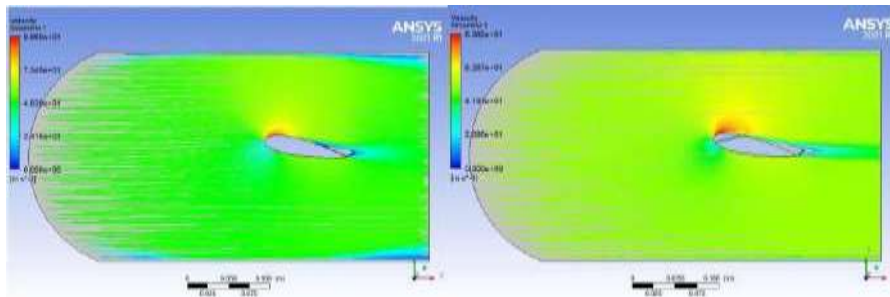


Figure 200 : Streamline at  $10^0$  for Both at Fifty m/s

Table of Design Points									
	A	B	C	D	E	F	G	H	I
1	Name	P1-inlet	P2-drag-co	P3-drag-force-co	P4-lift-up	P5-lift-force-co	Retain	Retained Data	Note
2	Units	m s <sup>-1</sup>		N		N			
3	DP 7 (Current)	30	0.0049511	7.5814	0.07835	119.97	<input checked="" type="checkbox"/>	<input checked="" type="checkbox"/>	
4	DP 8	30	0.0019911	3.0469	0.026577	40.696	<input checked="" type="checkbox"/>	<input checked="" type="checkbox"/>	
5	DP 9	25	0.0014474	2.2653	0.017973	27.521	<input checked="" type="checkbox"/>	<input checked="" type="checkbox"/>	
6	DP 10	20	0.00098484	1.506	0.011069	16.95	<input checked="" type="checkbox"/>	<input checked="" type="checkbox"/>	
7	DP 11	15	0.00060556	0.92727	0.005962	8.9762	<input checked="" type="checkbox"/>	<input checked="" type="checkbox"/>	
8	DP 12	10	0.0003683	0.47208	0.0029323	3.6219	<input checked="" type="checkbox"/>	<input checked="" type="checkbox"/>	
9	DP 13	5	0.00010266	0.1572	0.00040276	0.73922	<input checked="" type="checkbox"/>	<input checked="" type="checkbox"/>	
*							<input type="checkbox"/>		

Table15 : Drag and Lift force values,23021 at  $10^0$ AOA

Table of Design Points									
	A	B	C	D	E	F	G	H	I
1	Name	P1 - inlet vel	P2 - drag-force-op	P3 - drag-op	P4 - lift-op	P5 - lift-force-op	Retain	Retained Data	Note
2	Units	ms <sup>-1</sup>	N			N			
3	DP 0 (Current)	50	9.511	0.0062113	0.070038	107.25	<input checked="" type="checkbox"/>	<input checked="" type="checkbox"/>	
4	DP 1	30	3.6857	0.002407	0.022649	36.672	<input checked="" type="checkbox"/>	<input checked="" type="checkbox"/>	
5	DP 2	25	2.635	0.0017208	0.016271	24.915	<input checked="" type="checkbox"/>	<input checked="" type="checkbox"/>	
6	DP 3	20	1.7535	0.0011451	0.010089	15.448	<input checked="" type="checkbox"/>	<input checked="" type="checkbox"/>	
7	DP 4	15	1.0465	0.00068345	0.0053914	8.2536	<input checked="" type="checkbox"/>	<input checked="" type="checkbox"/>	
8	DP 5	10	0.50683	0.00033059	0.00221	3.384	<input checked="" type="checkbox"/>	<input checked="" type="checkbox"/>	
9	DP 6	5	0.15385	0.00010047	0.00044775	0.68562	<input checked="" type="checkbox"/>	<input checked="" type="checkbox"/>	
*							<input type="checkbox"/>		

Table16 : Drag and Lift force values,23021 at 10°AOA

## 5.62 Fifteen Attack angle : -

### 5.63 Five m/s-

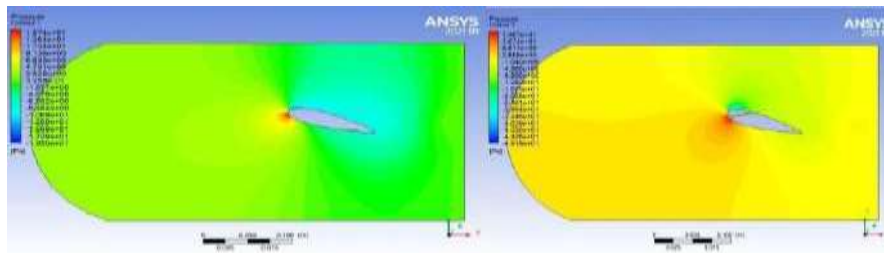


Figure 201 : Pressure at 15° for Both at Five m/s

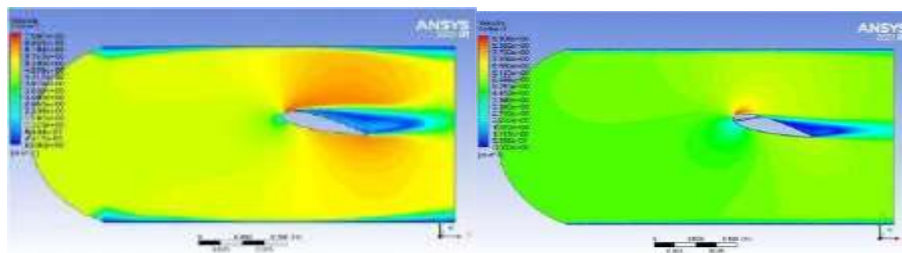


Figure 202 : Velocity at 15° for Both at Five m/s

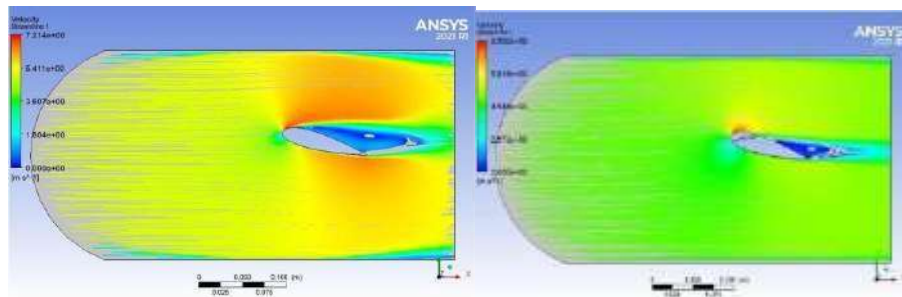


Figure 203 : Streamline at 15° for Both at Five m/s

### 5.64 Ten m/s-

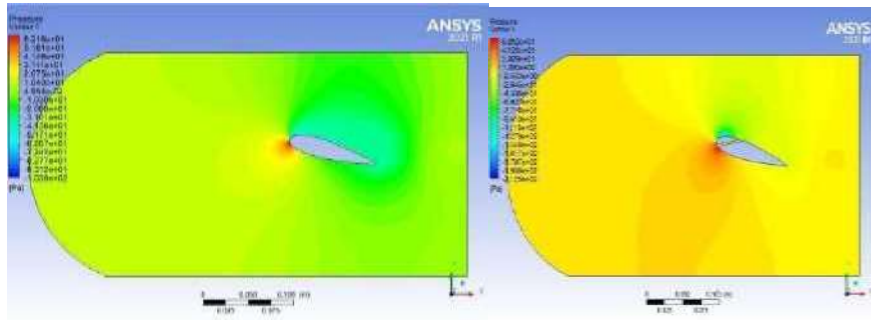


Figure 204 : Pressure at 15° for Both at Ten m/s

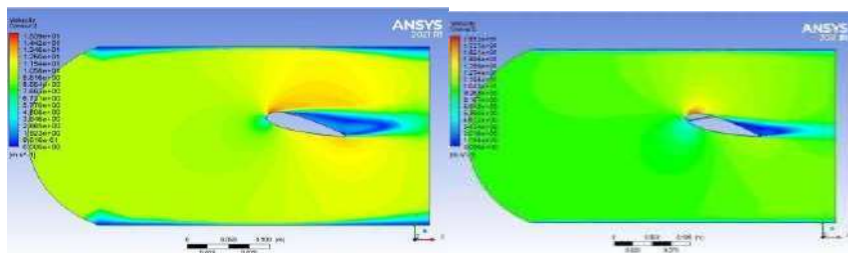


Figure 205 : Velocity at 15° for Both at Ten m/s

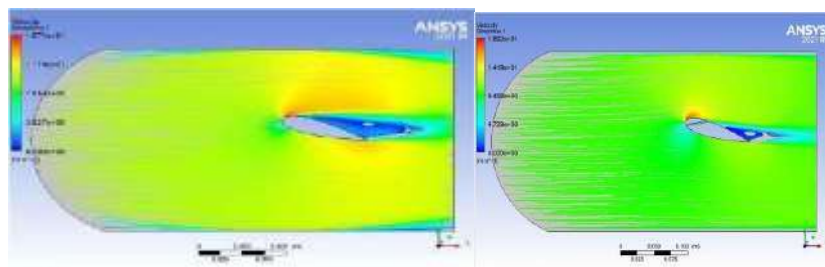


Figure 206 : Streamline at 15° for Both at Ten m/s

### 5.65 Fifteen m/s-

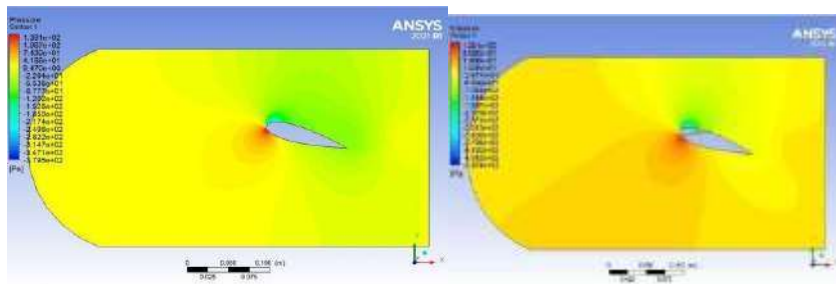


Figure 207 : Pressure at 15° for Both at fifteen m/s



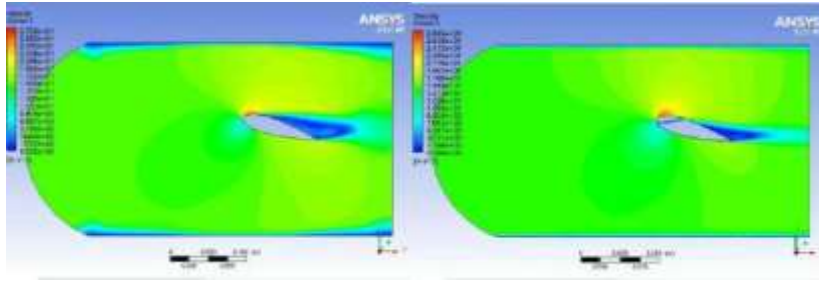


Figure 208 : Velocity at 15° for Both at fifteen m/s

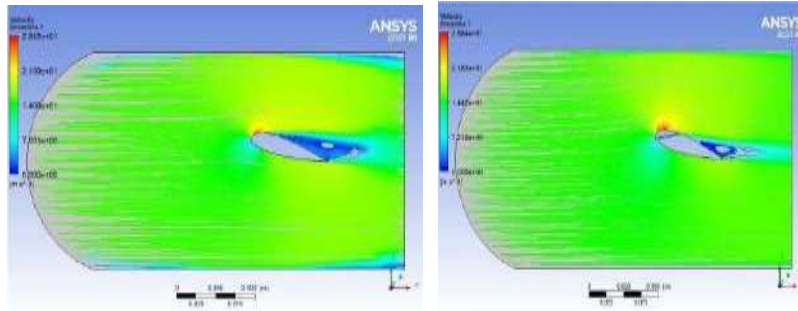


Figure 209 : Streamline at 15° for Both at fifteen m/s

### 5.66 Twenty m/s-

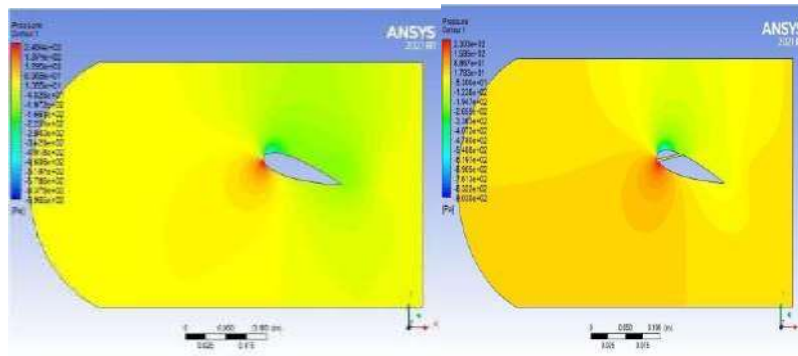


Figure 210 : Pressure at 15° for Both at fifteen m/s

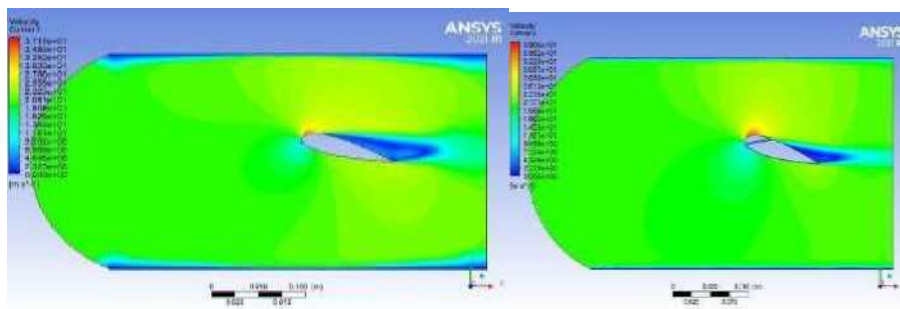


Figure 211 : Velocity Plot at 15° for Both at fifteen m/s

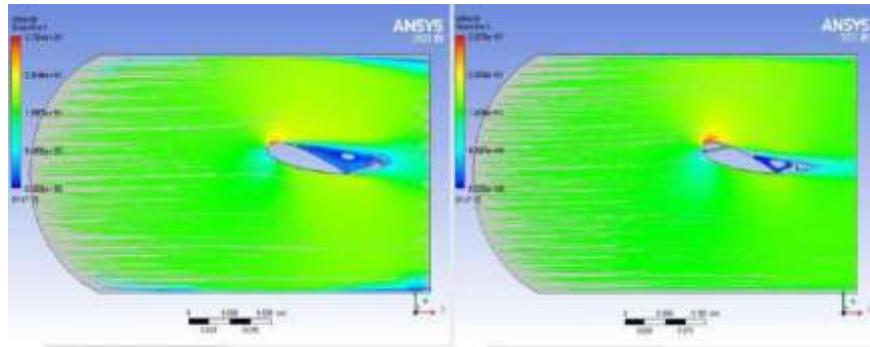


Figure 212 : Streamline at 15° for Both at fifteen m/s

### 5.67 Twenty Five m/s-

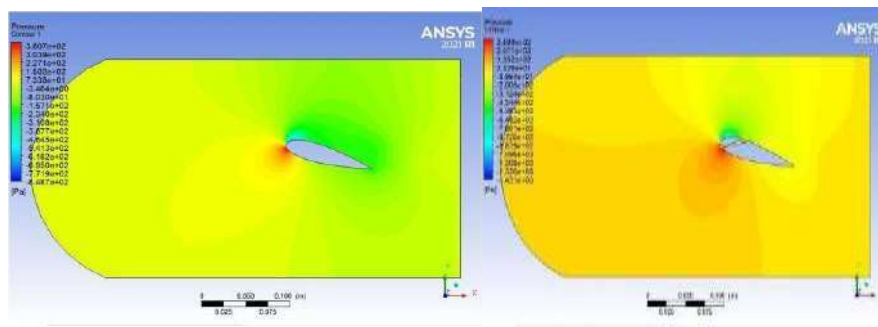


Figure 213 : Pressure at 15° for Both at twenty Five m/s

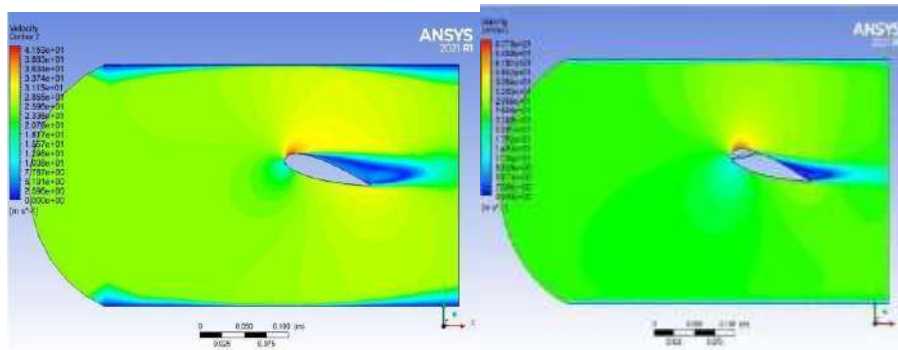


Figure 214 : Velocity at 15° for Both at twenty Five m/s

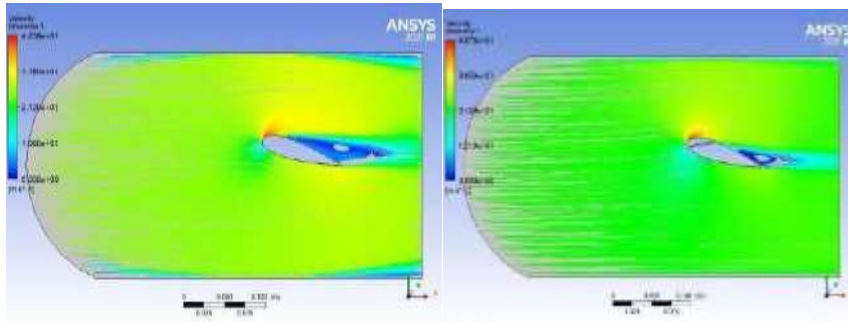


Figure 215 : Streamline at 15° for Both at twenty Five m/s

### 5.68 Thirty m/s-

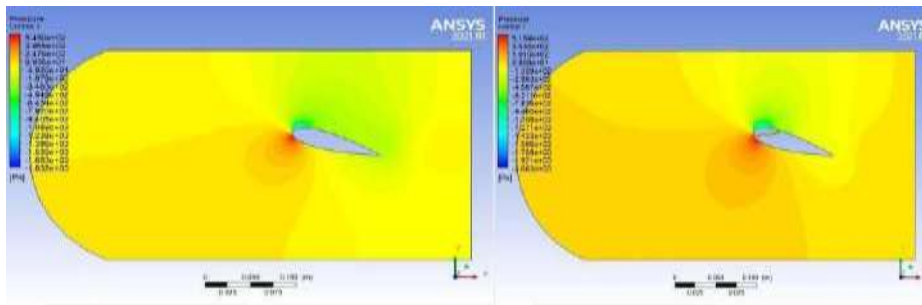


Figure 216 : Pressure at 15° for Both at Thirty m/s

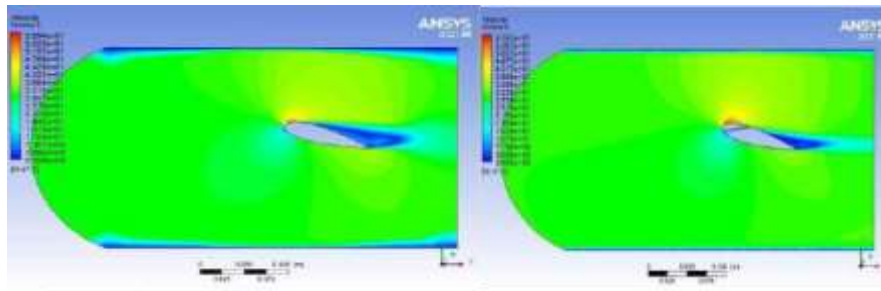


Figure 217 : Pressure at 15° for Both at Thirty m/s

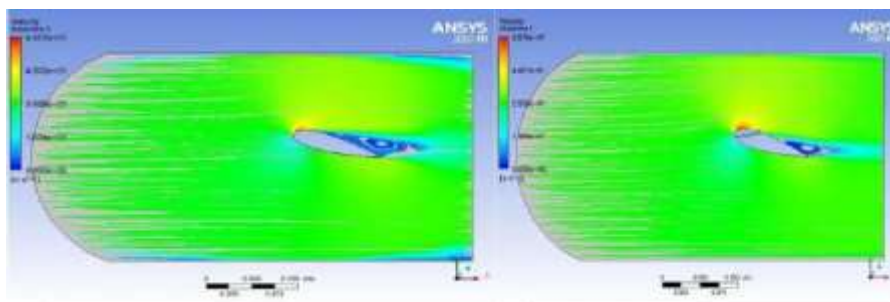


Figure 218 : Streamline at 15° for Both at Thirty m/s

### 5.69 Fifty m/s-

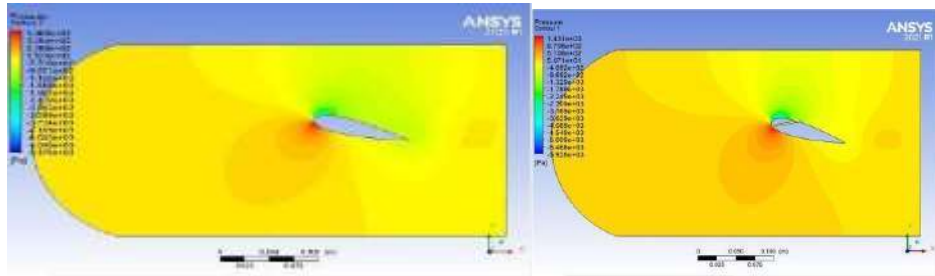


Figure 219 : Pressure at 15° for Both at Fifty m/s

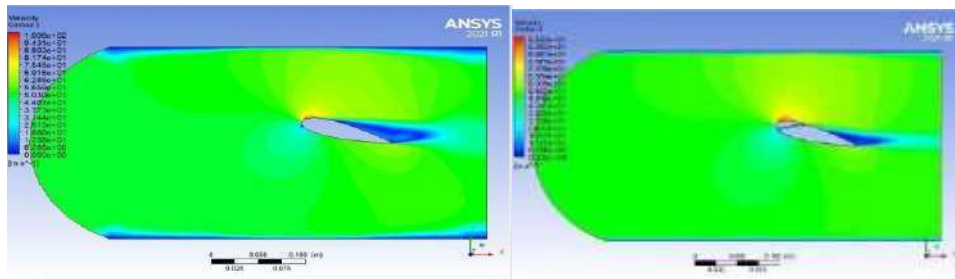


Figure 220 : Velocity at 15° for Both at Fifty m/s

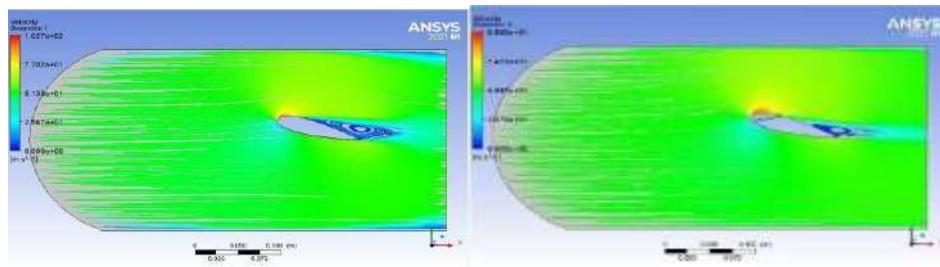


Figure 221 : Streamline at 15° for Both at Fifty m/s

Table of Design Points									
	A	B	C	D	E	F	G	H	I
1	Name	P1 - inlet vel	P2 - drag-op	P3 - drag-force-op	P4 - lift-op	P5 - lift-force-op	Retain	Retained Data	Note
2	Units	m s <sup>-1</sup>		N		N			
3	DP 7 (Current)	50	0.00749	11.469	0.12464	190.86	<input checked="" type="checkbox"/>	<input checked="" type="checkbox"/>	
4	DP 8	30	0.0030735	4.7063	0.0417	63.853	<input checked="" type="checkbox"/>	<input checked="" type="checkbox"/>	
5	DP 9	25	0.002242	3.4531	0.028157	43.084	<input checked="" type="checkbox"/>	<input checked="" type="checkbox"/>	
6	DP 10	20	0.0015271	2.3384	0.017338	26.548	<input checked="" type="checkbox"/>	<input checked="" type="checkbox"/>	
7	DP 11	15	0.0009325	1.4279	0.0092628	14.184	<input checked="" type="checkbox"/>	<input checked="" type="checkbox"/>	
8	DP 12	10	0.00047191	0.7261	0.003765	5.7652	<input checked="" type="checkbox"/>	<input checked="" type="checkbox"/>	
9	DP 13	5	0.00015179	0.23243	0.00076676	1.1741	<input checked="" type="checkbox"/>	<input checked="" type="checkbox"/>	
*							<input type="checkbox"/>		

Table17 : Drag and Lift force values,23021 at 15AOA

Table of Design Points									
	A	B	C	D	E	F	G	H	I
1	Name	P1 - inlet vel	P2 - drag-op	P3 - drag-force-op	P4 - lift-op	P5 - lift-force-op	Retain	Retained Data	Note
2	Units	m s <sup>-1</sup>		N		N			
3	DP 6 (Current)	50	0.0089373	13.685	0.098032	150.11	<input checked="" type="checkbox"/>	<input checked="" type="checkbox"/>	
4	DP 7	30	0.0033979	5.203	0.044041	52.584	<input checked="" type="checkbox"/>	<input checked="" type="checkbox"/>	
5	DP 8	25	0.002427	3.6945	0.023564	36.082	<input checked="" type="checkbox"/>	<input checked="" type="checkbox"/>	
6	DP 9	20	0.0015907	2.4357	0.014832	22.711	<input checked="" type="checkbox"/>	<input checked="" type="checkbox"/>	
7	DP 10	15	0.00093464	1.4315	0.0081456	12.473	<input checked="" type="checkbox"/>	<input checked="" type="checkbox"/>	
8	DP 11	10	0.0004814	0.68622	0.0034565	5.2927	<input checked="" type="checkbox"/>	<input checked="" type="checkbox"/>	
9	DP 12	5	0.00013449	0.20694	0.00078096	1.1959	<input checked="" type="checkbox"/>	<input checked="" type="checkbox"/>	
*							<input type="checkbox"/>		

Table18 : Drag and Lift force values,23021 at 15AOA

## 5.70 Twenty Attack angle : -

### 5.71 Five m/s-

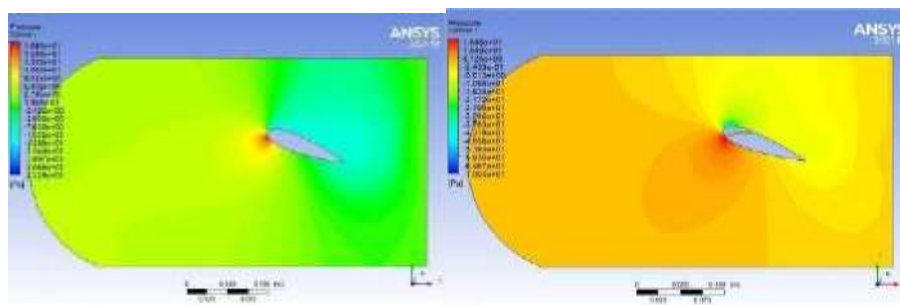


Figure 222 : Pressure at 20° for Both at Five m/s

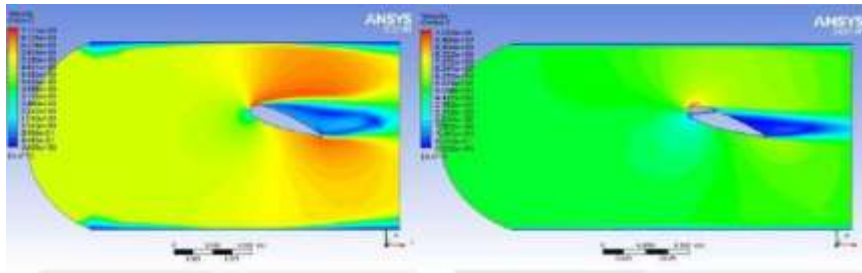


Figure 223 : Velocity Plot at  $20^\circ$  for Both at Five m/s

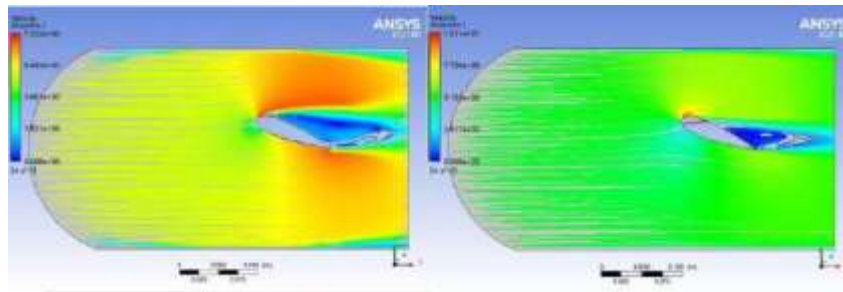


Figure 224 : Streamline at  $20^\circ$  for Both at Five m/s

### 5.72 Ten m/s-

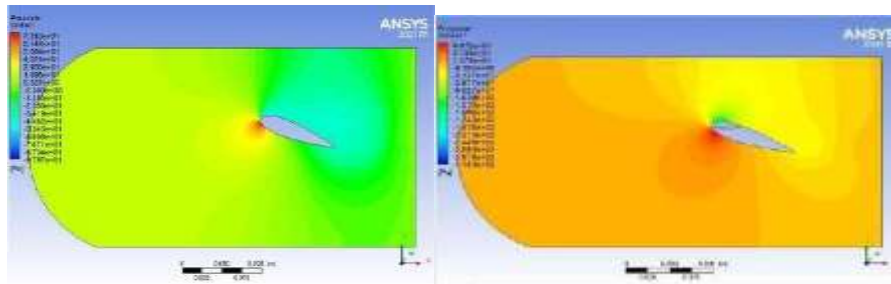


Figure 225 : Pressure at  $20^\circ$  for Both at Ten m/s

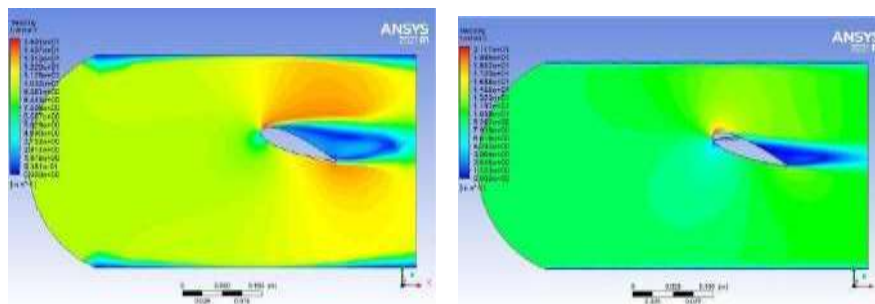


Figure 226 : Velocity at  $20^\circ$  for Both at Ten m/s

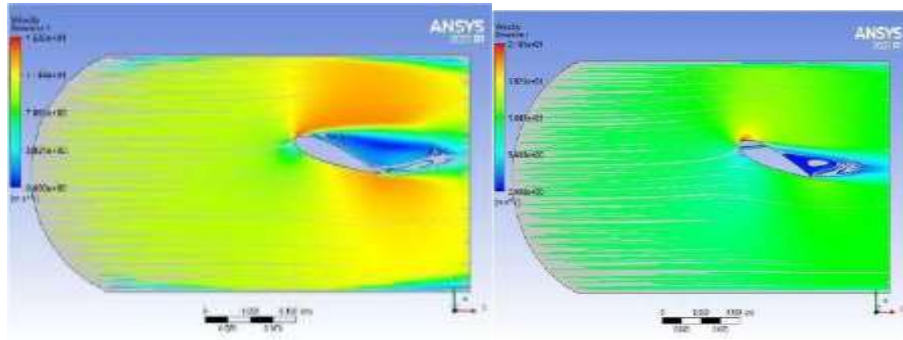


Figure 227 : Streamline at 20° for Both at Ten m/s

### 5.73 Fifteen m/s-

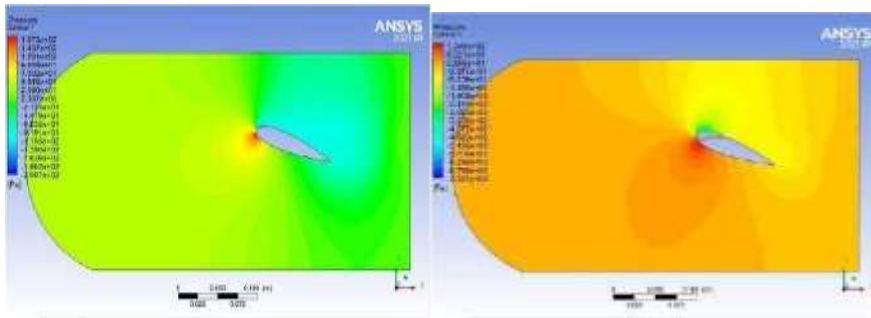


Figure 228 : Pressure at 20° for Both at Fifteen m/s

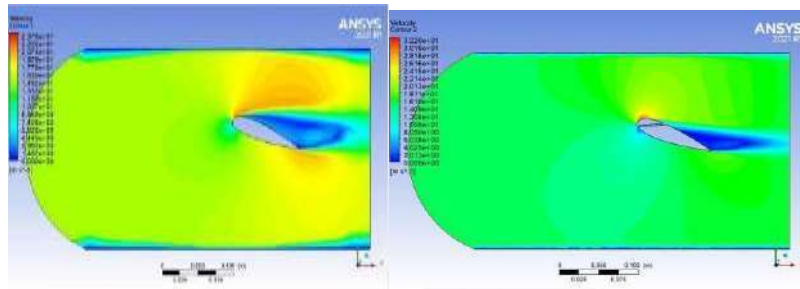


Figure 229 : Velocity at 20° for Both at fifteen m/s

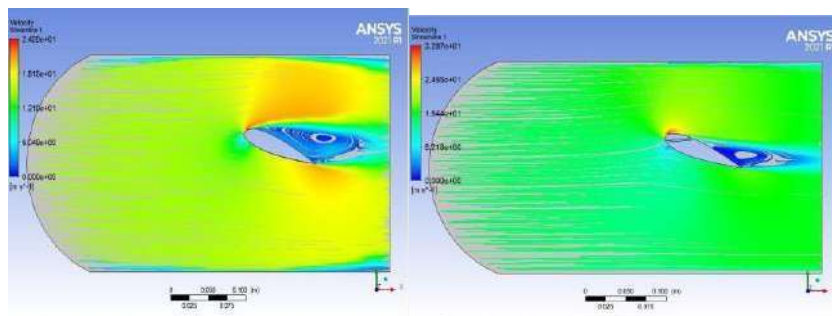


Figure 230 : Streamline at 20° for Both at fifteen m/s

### 5.74 Twenty m/s-

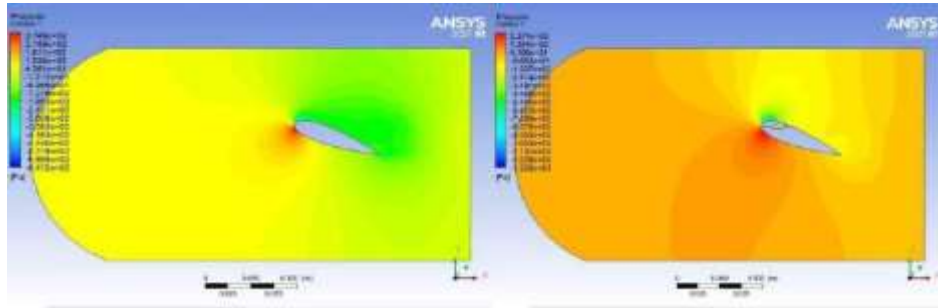


Figure 231 : Pressure at  $20^\circ$  for Both at Twenty m/s

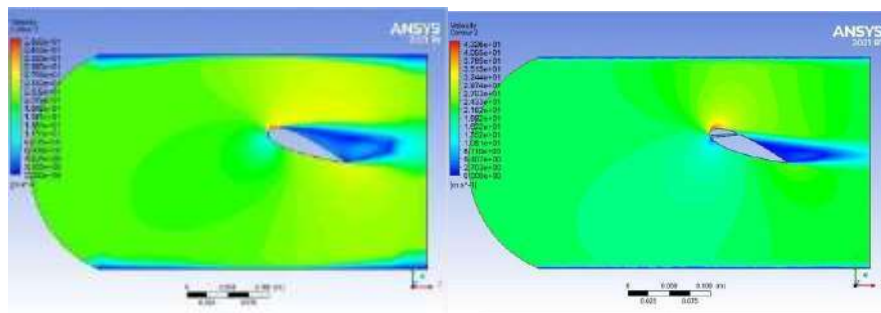


Figure 232 : Velocity at  $20^\circ$  for Both at Twenty m/s

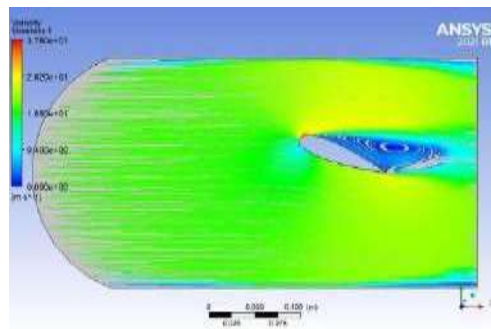


Figure 233 : Streamline at  $20^\circ$  for Both at Twenty/s

### 5.75 Twenty-Five m/s-

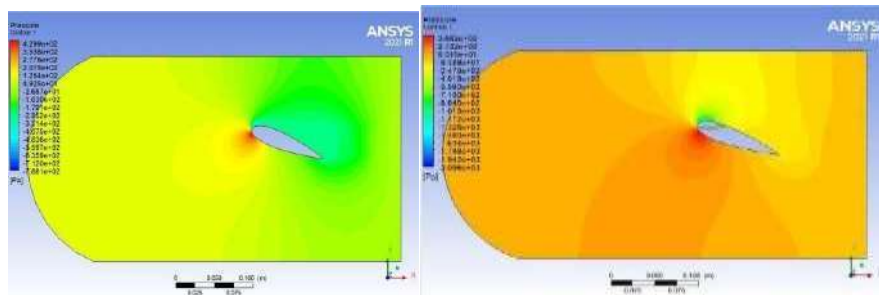


Figure 234 : Pressure at  $20^\circ$  for Both at twenty-Five m/s



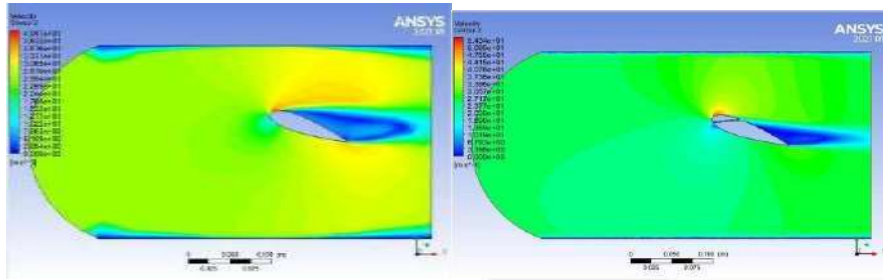


Figure 235 : Velocity at 20° for Both at twenty-Five m/s

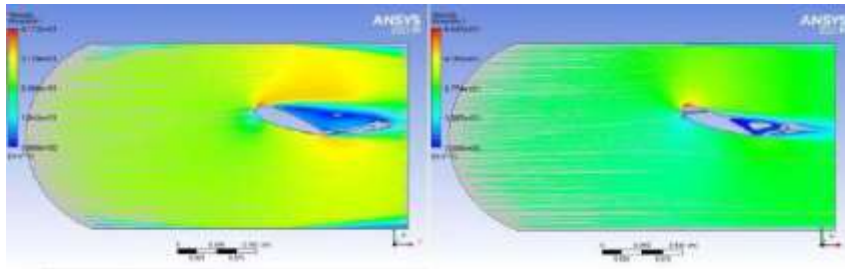


Figure 236 : Streamline at 20° for Both at twenty-Five m/s

### 5.76 Thirty m/s-

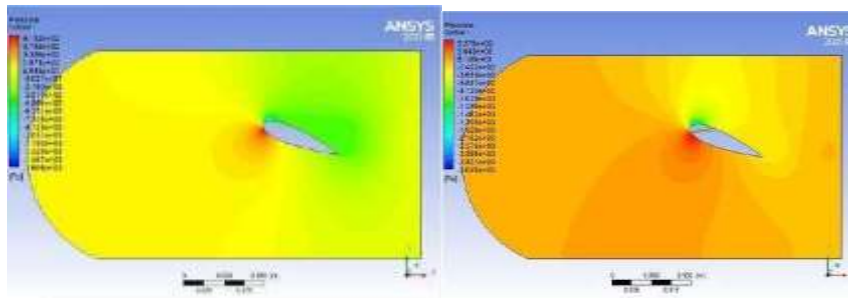


Figure 237 : Pressure at 20° for Both at Thirty m/s

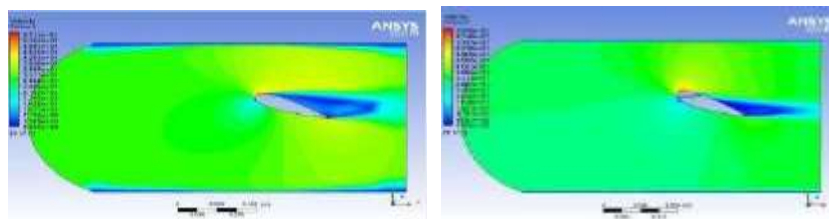


Figure 238 : Velocity at 20° for Both at Thirty m/s

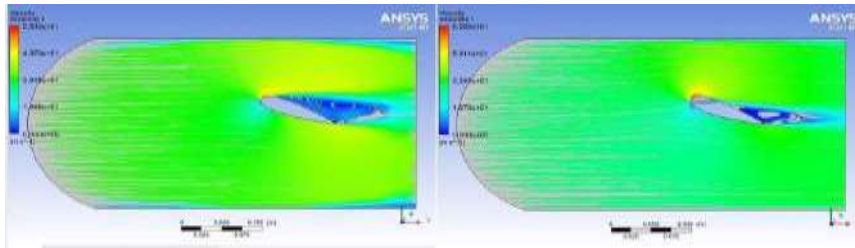


Figure 239 : Streamline at 20° for Both at Thirty m/s

### 5.77 Fifty m/s-

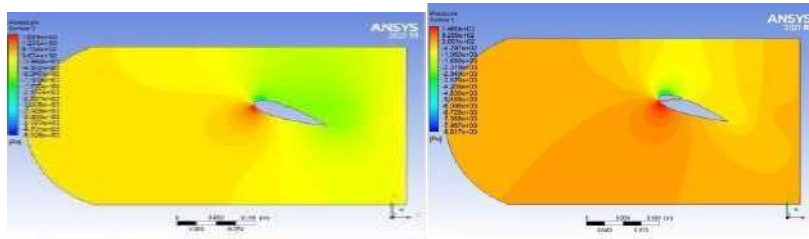


Figure 240 : Pressure at 20° for Both at Fifty m/s

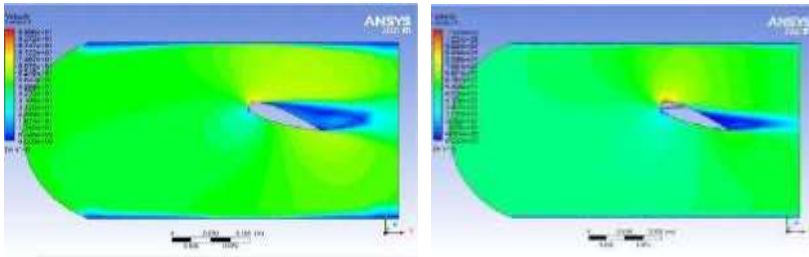


Figure 241 : Velocity at 20° for Both at Fifty m/s

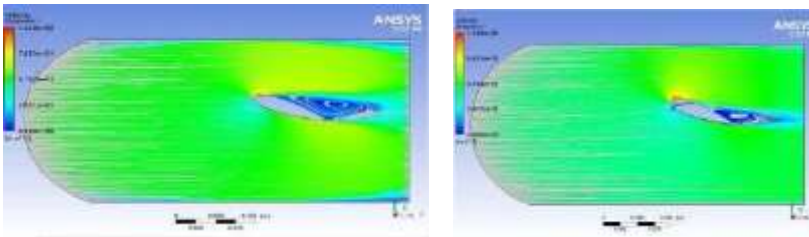


Figure 242 : Streamline at 20° for Both at Fifty m/s

	A	B	C	D	E	F	G	H	I
1	Name	P1 - inlet vel	P2 - drag-co	P3 - drag-force-op	P4 - lift-op	P5 - lift-force-op	Retain	Retained Data	Note
2	Units	m s <sup>-1</sup>		N		N			
3	DP 7 (Current)	30	0.013803	24.321	0.119	382.22	<input checked="" type="checkbox"/>	<input checked="" type="checkbox"/>	
4	DP 8	30	0.0061737	9.4504	0.04806	62.873	<input checked="" type="checkbox"/>	<input checked="" type="checkbox"/>	
5	DP 9	25	0.0044592	6.8282	0.028204	43.388	<input checked="" type="checkbox"/>	<input checked="" type="checkbox"/>	
6	DP 10	20	0.0029543	4.5137	0.017638	27.038	<input checked="" type="checkbox"/>	<input checked="" type="checkbox"/>	
7	DP 11	15	0.0017453	2.6725	0.006178	14.717	<input checked="" type="checkbox"/>	<input checked="" type="checkbox"/>	
8	DP 12	10	0.00082805	1.268	0.004121	6.3103	<input checked="" type="checkbox"/>	<input checked="" type="checkbox"/>	
9	DP 13	5	0.00024802	0.36995	0.000902	1.4038	<input checked="" type="checkbox"/>	<input checked="" type="checkbox"/>	
*							<input type="checkbox"/>		

Table19 : Drag and Lift force values,at20°

Table of Design Points									
	A	B	C	D	E	F	G	H	I
1	Name	P1 - inlet vel	P2 - drag-co	P3 - drag-force-op	P4 - lift-op	P5 - lift-force-op	Retain	Retained Data	Note
2	Units	m s <sup>-1</sup>		N		N			
3	DP 12 (Current)	50	0.014751	22.588	0.12807	196.11	<input checked="" type="checkbox"/>	<input checked="" type="checkbox"/>	
4	DP 13	30	0.0055247	8.4597	0.045318	69.392	<input checked="" type="checkbox"/>	<input checked="" type="checkbox"/>	
5	DP 14	25	0.0039028	5.9762	0.031216	47.8	<input checked="" type="checkbox"/>	<input checked="" type="checkbox"/>	
6	DP 15	20	0.0025546	3.9117	0.019767	30.258	<input checked="" type="checkbox"/>	<input checked="" type="checkbox"/>	
7	DP 16	15	0.0014652	2.2743	0.01095	16.758	<input checked="" type="checkbox"/>	<input checked="" type="checkbox"/>	
8	DP 17	10	0.00070032	1.0724	0.0047347	7.25	<input checked="" type="checkbox"/>	<input checked="" type="checkbox"/>	
9	DP 18	5	0.00020684	0.31573	0.0010684	1.6359	<input checked="" type="checkbox"/>	<input checked="" type="checkbox"/>	
*							<input type="checkbox"/>		

Table20 : Drag and Lift force values,at20°

## 5.78 Charts : - for23021 Airfoil

### 5.79 Five m/s-



Figure 243 : Cl versus attack angle

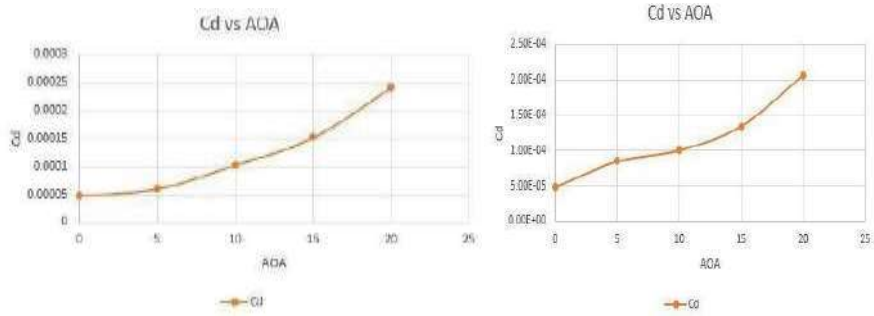


Figure 244 : Cd versus attack angle

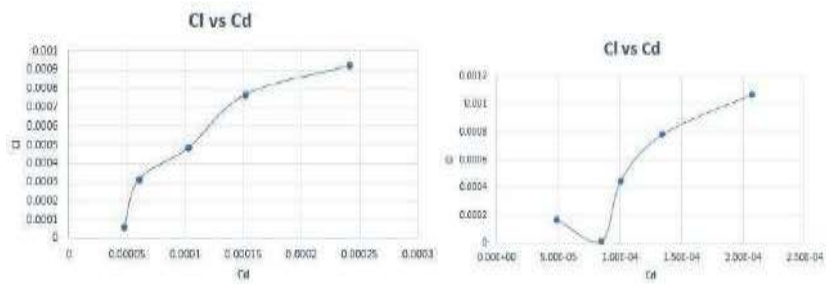


Figure 245 : Cl versus Cd

5.80 Ten m/s-

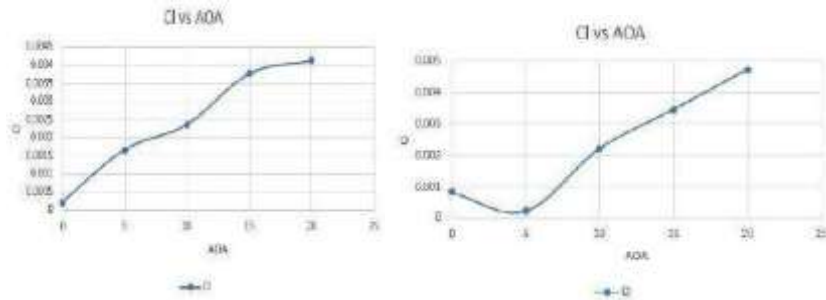


Figure 246 : Cl versus attack angle

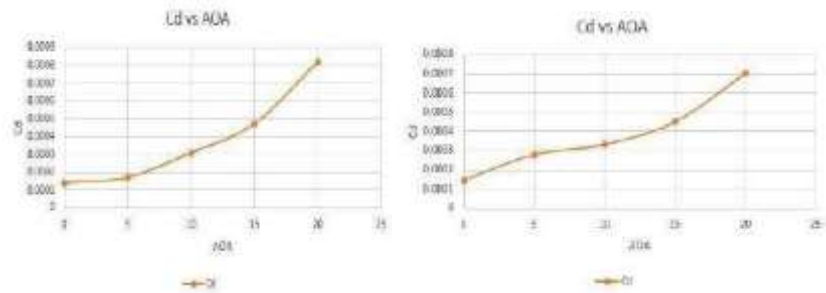


Figure 247 : Cd versus attack angle

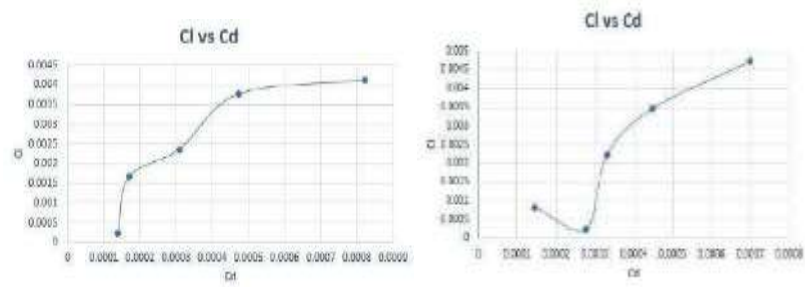


Figure 248 : Cl versus Cd

5.81 Fifteen m/s-

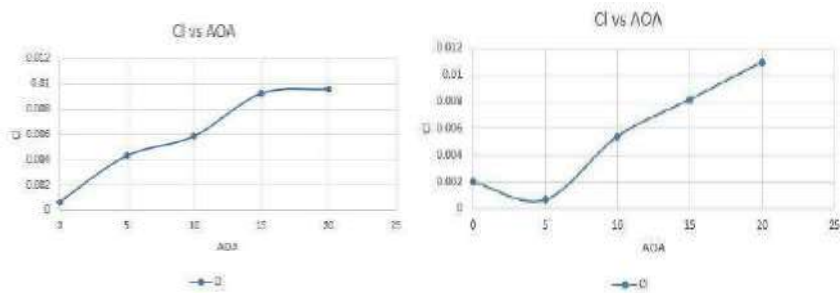


Figure 249 : Cl versus attack angle

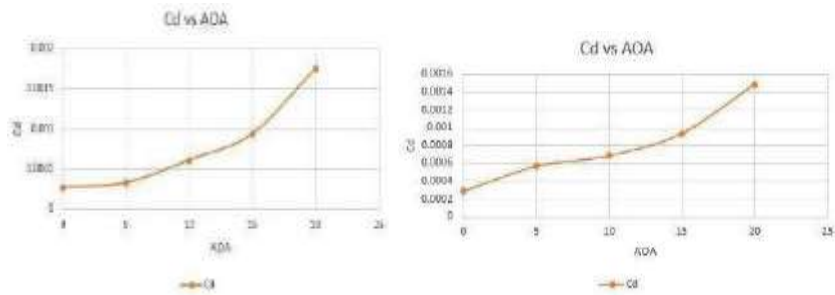


Figure 250 : Cd versus attack angle

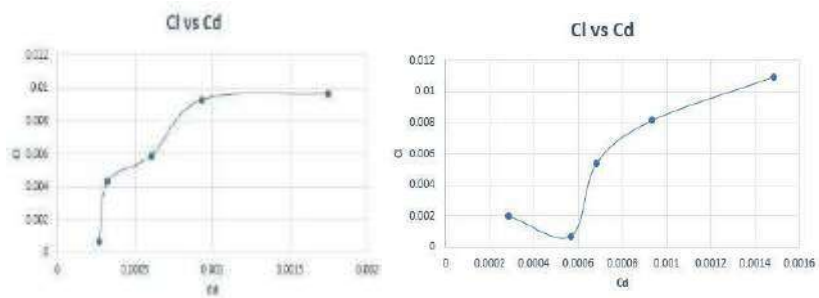


Figure 251 : Cl versus Cd

### 5.82 Twenty m/s-

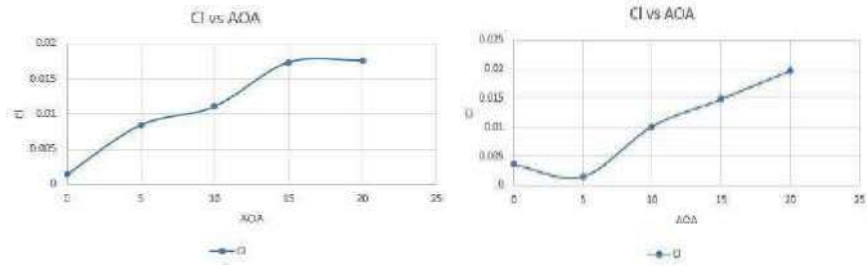


Figure 252 : Cl versus attack angle

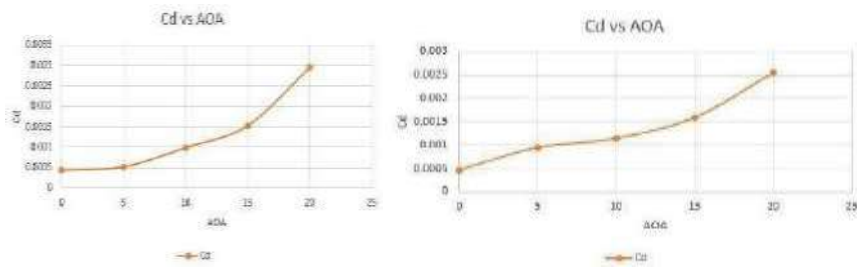


Figure 253 : Cd versus attack angle

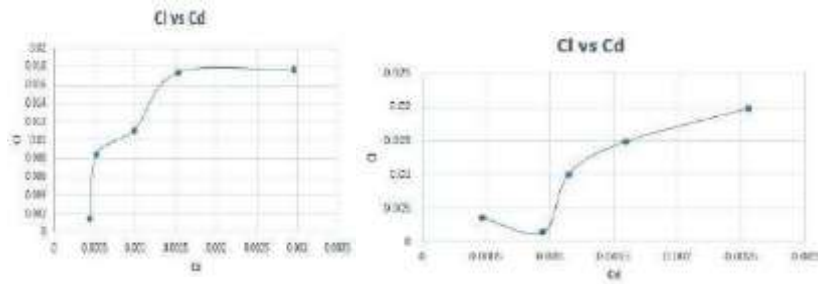


Figure 254 : Cl versus Cd

### 5.83 Twenty-Five m/s-

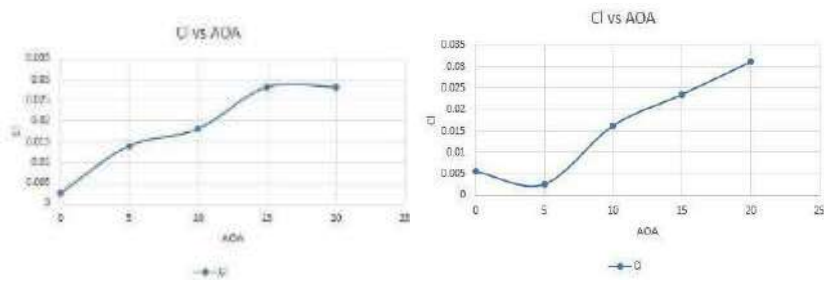


Figure 255 : Cl versus attack angle

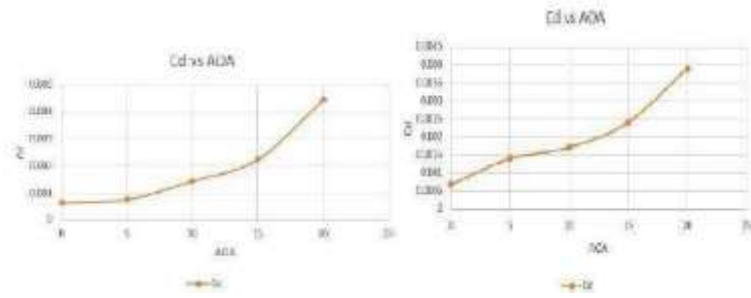


Figure 256 : Cd versus attack angle

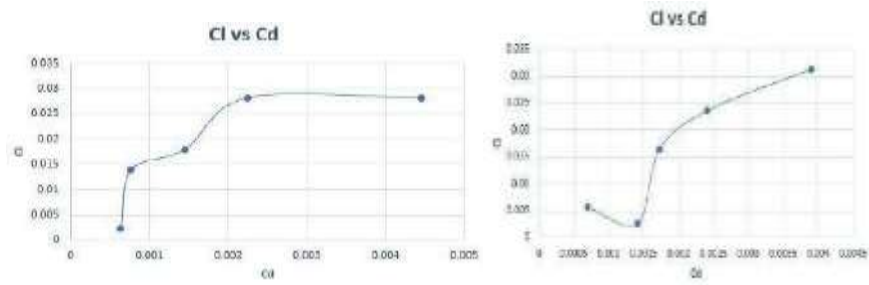


Figure 257 : Cl versus Cd

### 5.84 Thirty m/s-

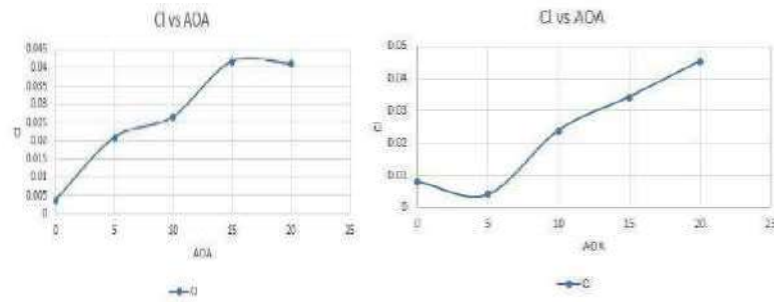


Figure 258 : Cl versus attack angle

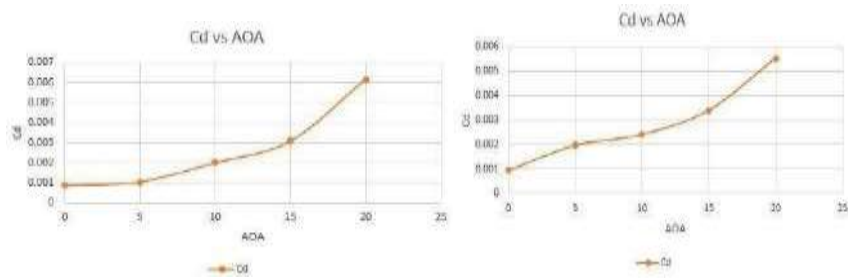


Figure 259 : Cd versus attack angle

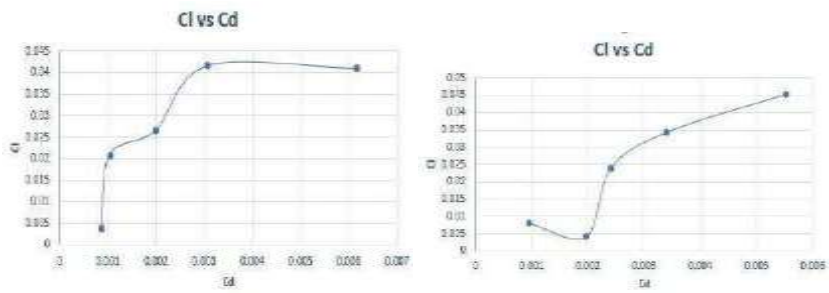


Figure 260 : Cl versus Cd

5.85 Fifty m/s-

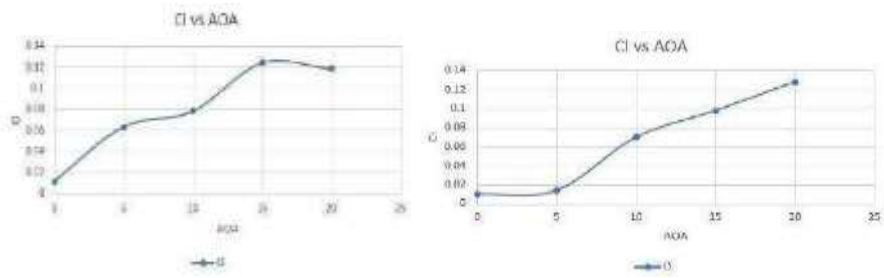


Figure 261 : Cl versus attack angle

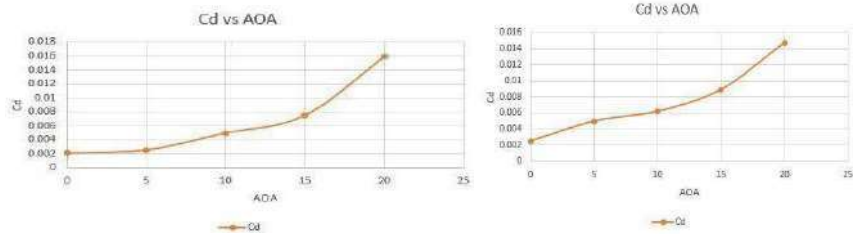


Figure 262 : Cd versus attack angle

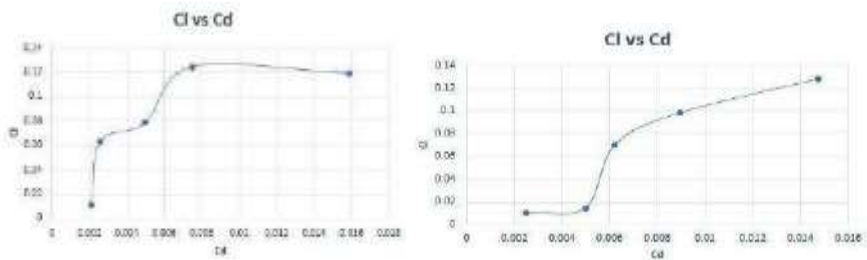


Figure 263 : Cl versus Cd



For 24015 Zero Attack angle : -

### 5.86 Five m/s-

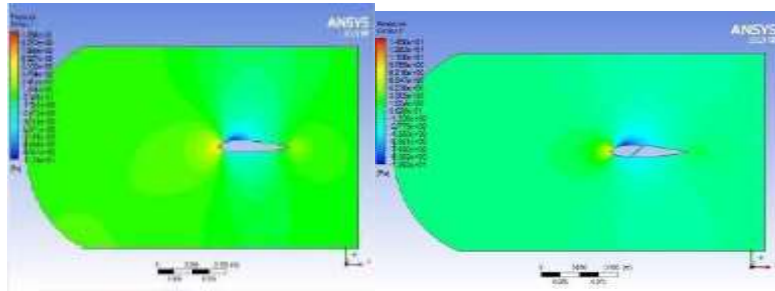


Figure 264 : Pressure for Both atFive m/s

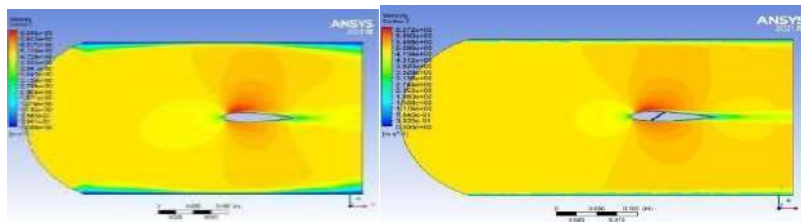


Figure 265 : Velocity for Both atFive m/s

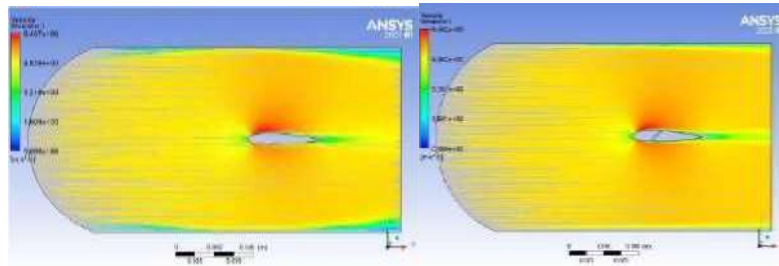


Figure 266 : Streamline for Both atFive m/s

### 5.87 Ten m/s-

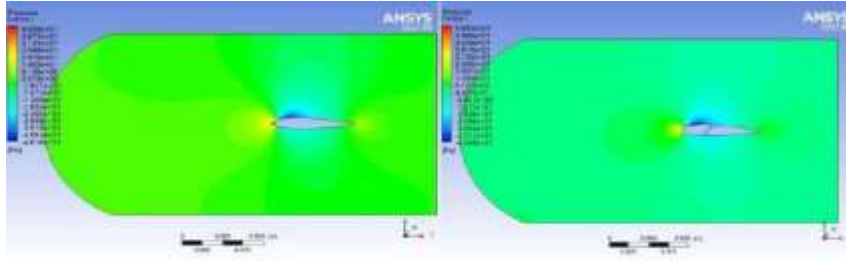


Figure 267 : Pressure at 0° for Both at Ten m/s

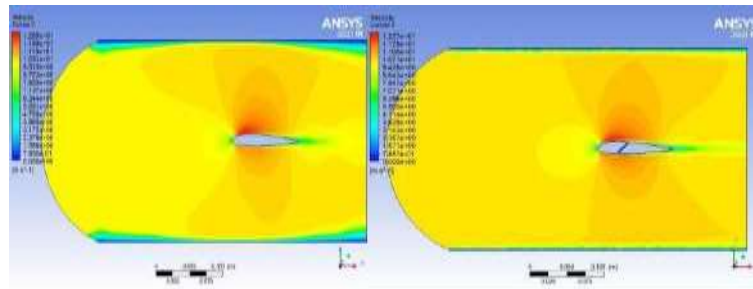


Figure 268 : Velocity at 0° for Both at Ten m/s

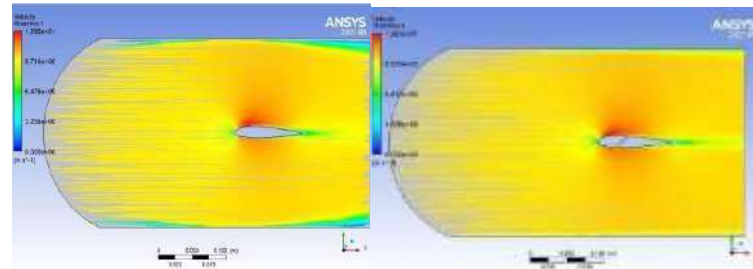


Figure 269 : Streamline at 0° for Both at Ten m/s

### 5.88 Fifteen m/s-

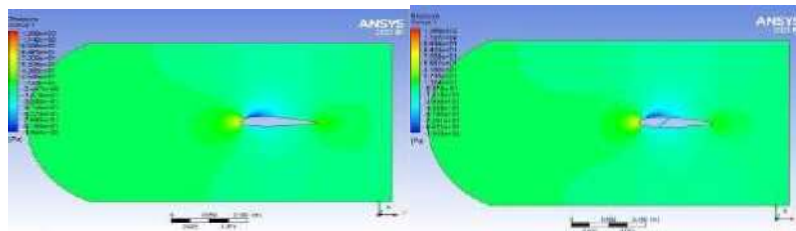


Figure 270 : Pressure at 0° for Both at fifteen m/s

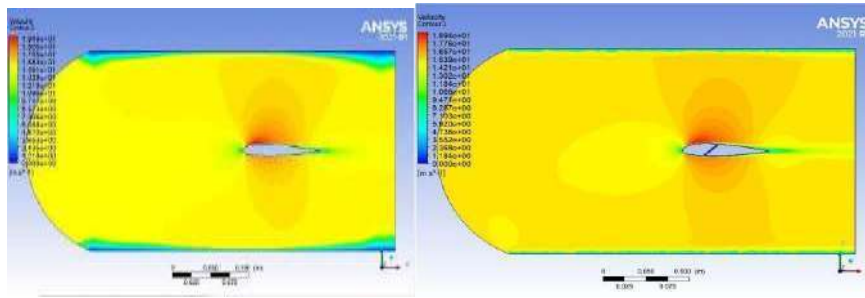


Figure 271 : Velocity at $t^0$  for Both at fifteen m/s

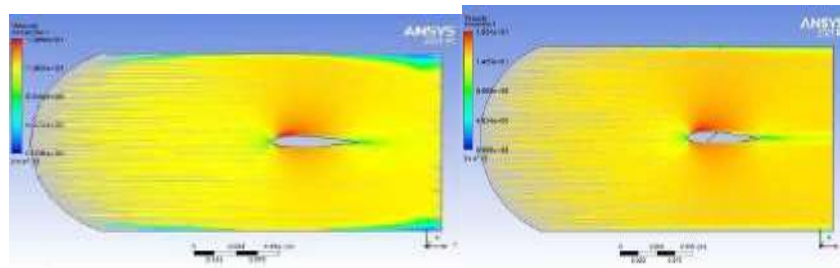


Figure 272 : Streamline at $t^0$  for Both at fifteen m/s

**Twenty m/s-**

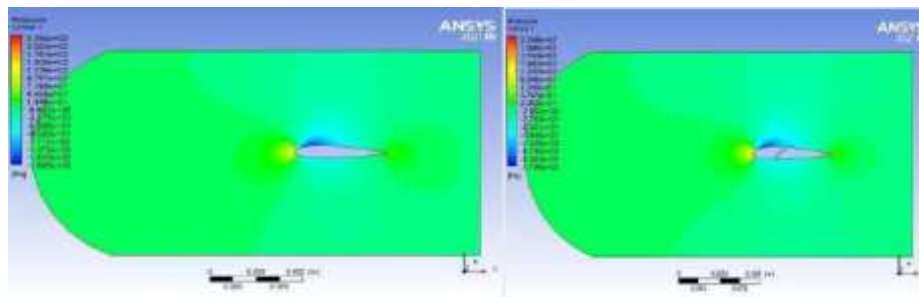


Figure 273 : Pressure at $t^0$  for Both at Twenty m/s

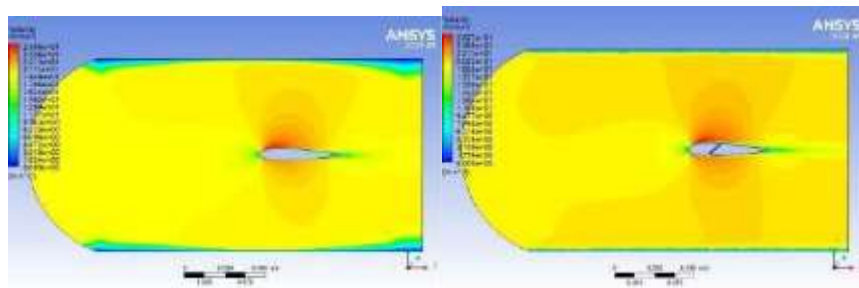


Figure 274 : Velocity at $t^0$  for Both at Twenty m/s

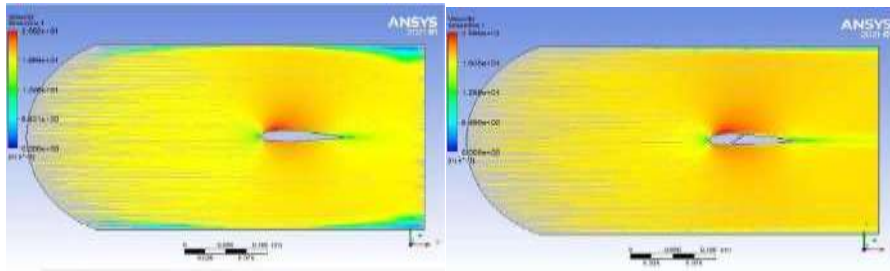


Figure 275 : Streamline at  $0^\circ$  for Both at Twenty m/s

### 5.89 Twenty-Five m/s-

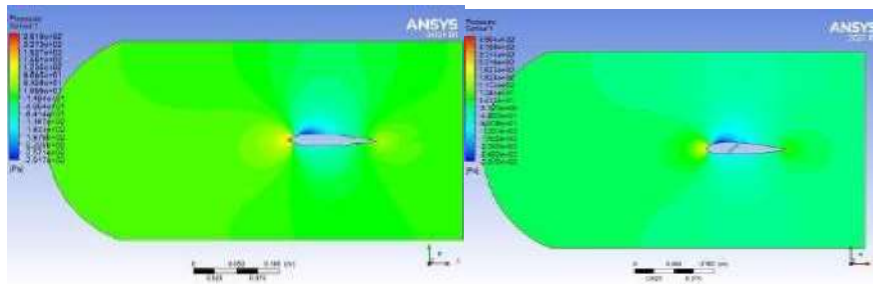


Figure 276 : Pressure at  $0^\circ$  for Both at twenty-Five m/s

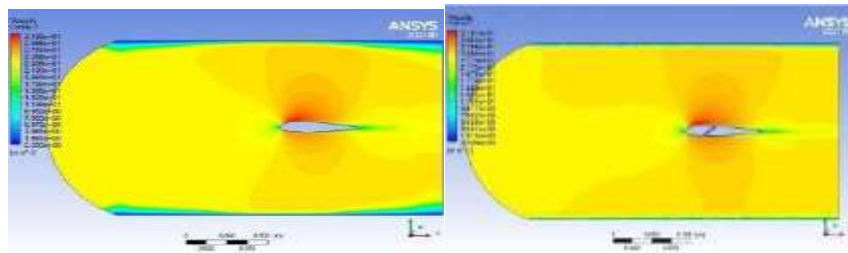


Figure 277 : Velocity at  $0^\circ$  for Both at twenty-Five m/s

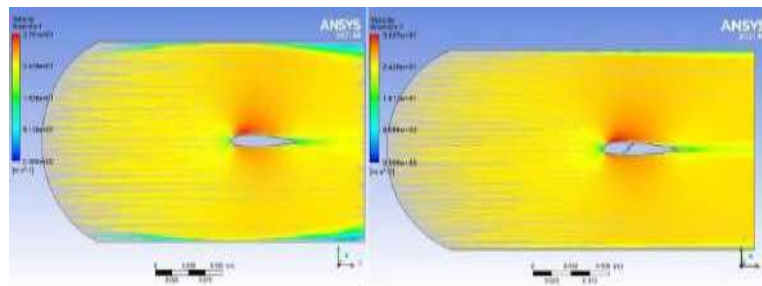


Figure 278 : Streamline at  $0^\circ$  for Both at twenty-Five m/s

### 5.90 Thirty m/s-

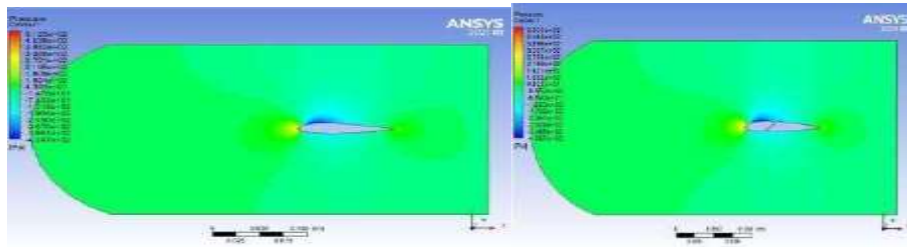


Figure 279 : Pressure at  $0^\circ$  for Both at Thirty m/s

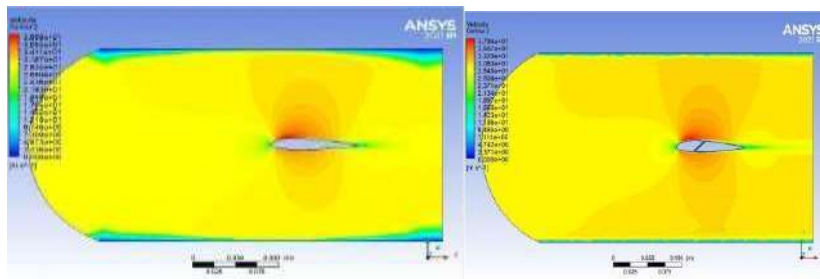


Figure 280 : Velocity at  $0^\circ$  for Both at Thirty m/s

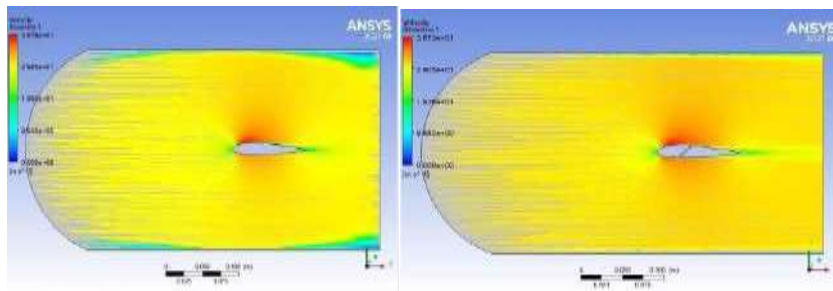


Figure 281 : Streamline at  $0^\circ$  for Both at Thirty m/s

### Fifty m/s-

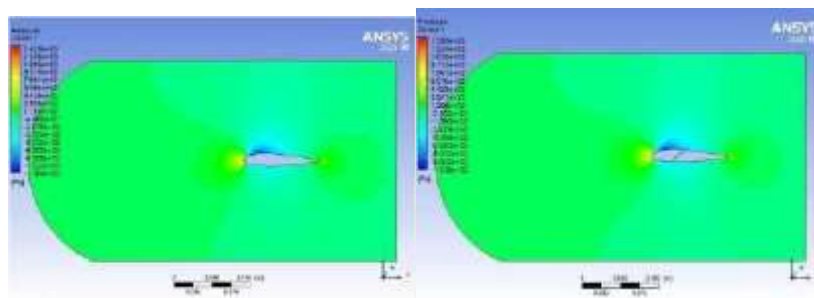


Figure 282 : Pressure at  $0^\circ$  for Both at Fifty m/s

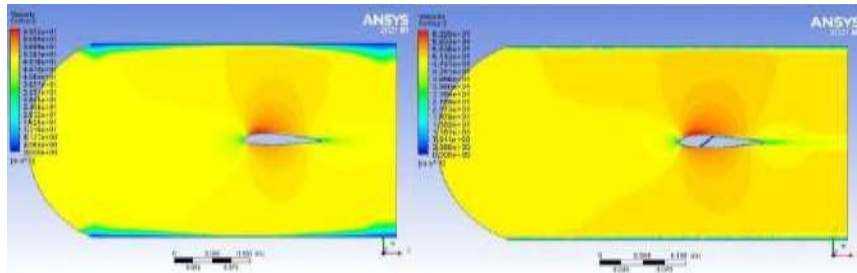


Figure 283 : Velocity at 0° for Both at Fifty m/s

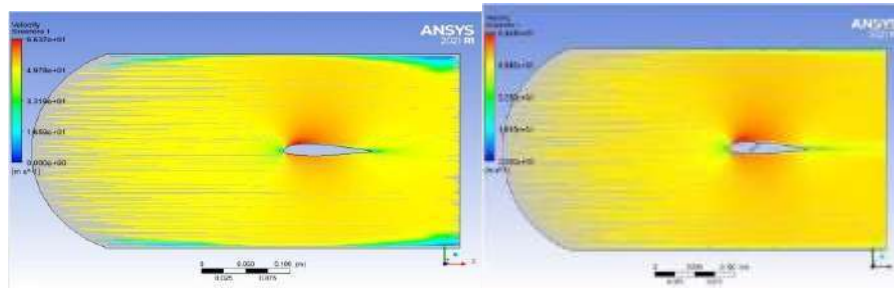


Figure 284 : Streamline at 0° for Both at Fifty m/s

Table of Design Points									
	A	B	C	D	E	F	G	H	I
1	Name	P1 - inlets	P2 - drag-up	P3 - drag-force-up	P4 - lift-up	P5 - lift-force-up	Retain	Retained Data	Note
2	Units	m/s		N		N			
3	DP 7 (Current)	50	0.0038251	3.7948	0.014048	26.512	<input checked="" type="checkbox"/>	<input checked="" type="checkbox"/>	
4	DP 8	30	0.00375182	1.1512	0.0246792	7.4712	<input checked="" type="checkbox"/>	<input checked="" type="checkbox"/>	
5	DP 9	25	0.0034933	0.94116	0.0233098	5.0681	<input checked="" type="checkbox"/>	<input checked="" type="checkbox"/>	
6	DP 10	20	0.0037513	0.57442	0.020297	3.108	<input checked="" type="checkbox"/>	<input checked="" type="checkbox"/>	
7	DP 11	15	0.0022067	0.35322	0.008607	1.6242	<input checked="" type="checkbox"/>	<input checked="" type="checkbox"/>	
8	DP 12	10	0.0011766	0.18917	0.0040193	0.61545	<input checked="" type="checkbox"/>	<input checked="" type="checkbox"/>	
9	DP 13	5	3.9051E-05	0.09844	8.0452E-05	0.13697	<input checked="" type="checkbox"/>	<input checked="" type="checkbox"/>	
*							<input type="checkbox"/>	<input type="checkbox"/>	

Table21 : Drag and Lift force values,24015 a t0° AOA

Table of Design Points									
	A	B	C	D	E	F	G	H	I
1	Name	P1 - inlets	P2 - drag-up	P3 - drag-force-up	P4 - lift-up	P5 - lift-force-up	Retain	Retained Data	Note
2	Units	m/s		N		N			
3	DP 24 (Current)	50	0.0028668	3.1647	0.010677	16.349	<input checked="" type="checkbox"/>	<input checked="" type="checkbox"/>	
4	DP 25	30	0.00382768	1.2674	0.0036847	5.5422	<input checked="" type="checkbox"/>	<input checked="" type="checkbox"/>	
5	DP 26	25	0.00359132	0.9174	0.002541	3.8936	<input checked="" type="checkbox"/>	<input checked="" type="checkbox"/>	
6	DP 27	20	0.0040324	0.61746	0.0015767	2.4144	<input checked="" type="checkbox"/>	<input checked="" type="checkbox"/>	
7	DP 28	15	0.0024382	0.37355	0.00084248	1.2801	<input checked="" type="checkbox"/>	<input checked="" type="checkbox"/>	
8	DP 29	10	0.0012317	0.1886	0.00028645	0.44957	<input checked="" type="checkbox"/>	<input checked="" type="checkbox"/>	
9	DP 30	5	4.0028E-05	0.06029	7.5622E-05	0.1158	<input checked="" type="checkbox"/>	<input checked="" type="checkbox"/>	
*							<input type="checkbox"/>	<input type="checkbox"/>	

Table22 : Drag and Lift force values,24015 at 0° AOA

### 5.91 FiveAttack angle

### 5.92 Five m/s-

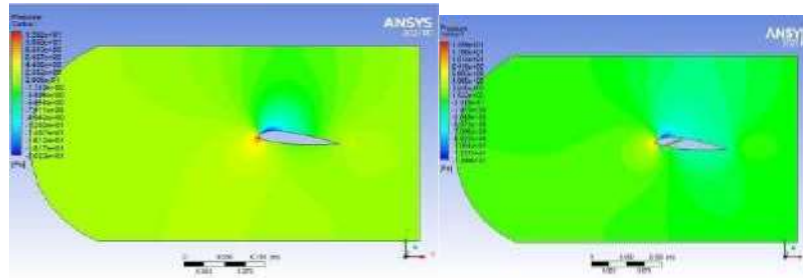


Figure 285 : Pressure at 5° for Both at Five m/s

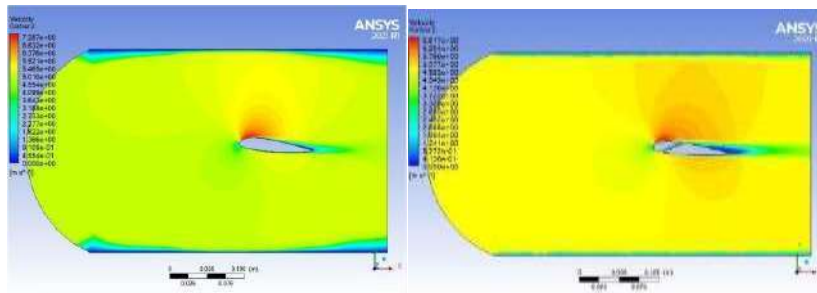


Figure 286 : Velocity Pressure at 5° for Both at Five m/s

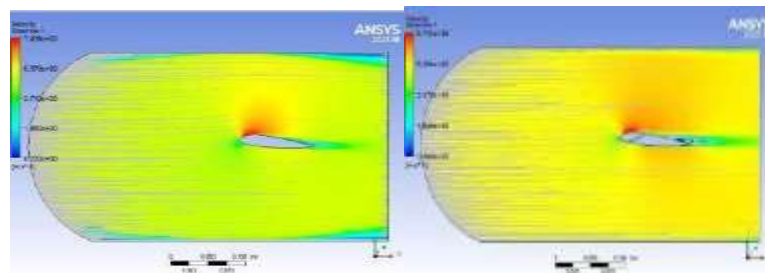


Figure 287 : Streamline at 5° for Both at Five m/s

### 5.93 Ten m/s-

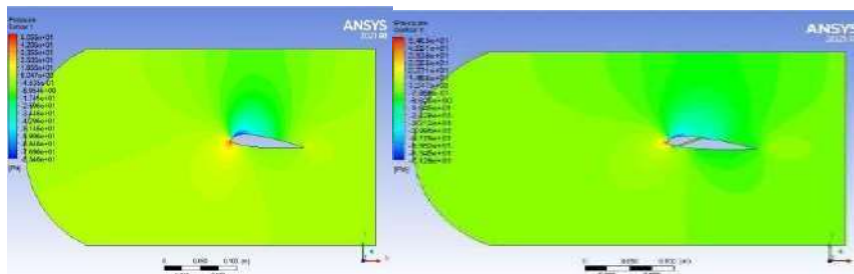


Figure 288 : Pressure at 50 for Both at Ten m/s

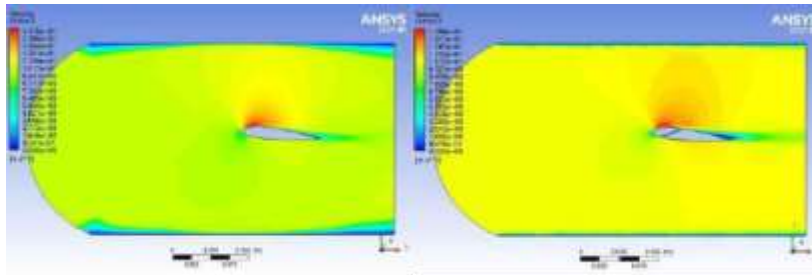


Figure 289 : Velocity at 5° for Both at Ten m/s

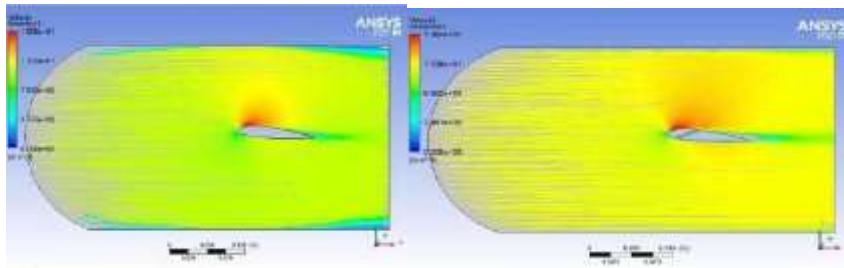


Figure 290 : Streamline at 5° for Both at Ten m/s

#### 5.94 Fifteen m/s-

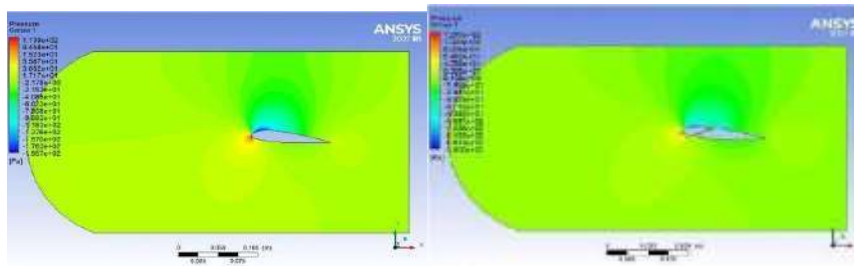


Figure 291 : Pressure at 5° for Both Ventat Fifteen m/s

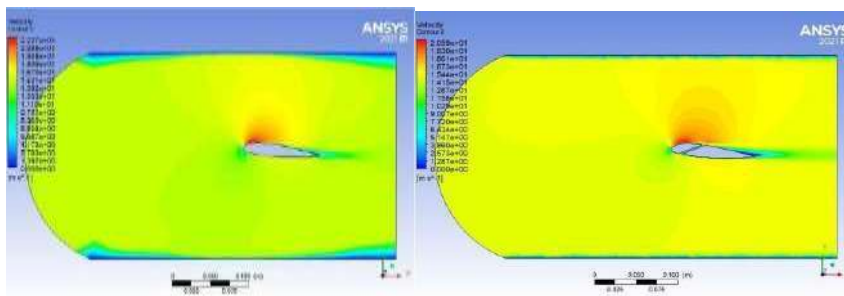


Figure 292 : Velocity at 5° for Both Vent at fifteen m/s



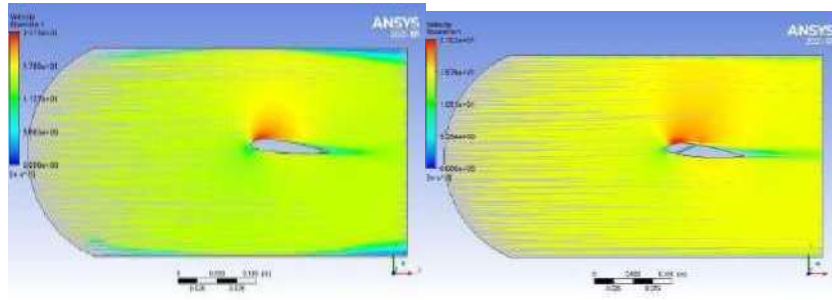


Figure 293 : Streamline at 5° for Both Vent at fifteen m/s

### 5.95 Twenty m/s-

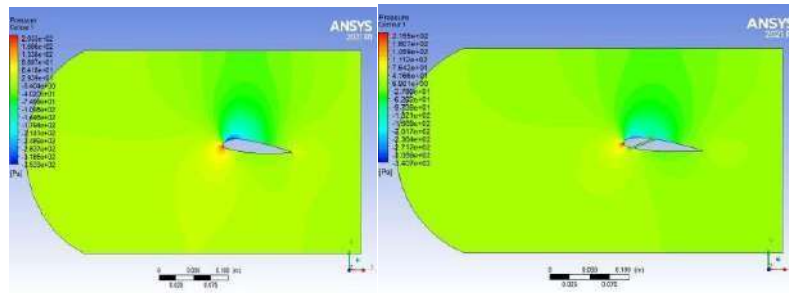


Figure 294 : Pressure at 5° for Both at Twenty m/s

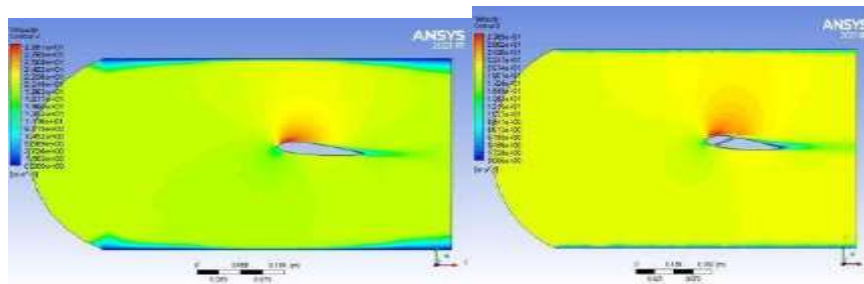


Figure 295 : Velocity at 5° for Both at Twenty m/s

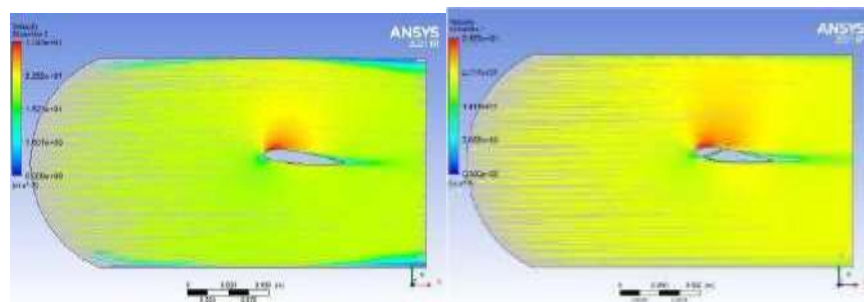


Figure 296 : Streamline at 5° for Both at Twenty m/s

### 5.96 Twenty Five m/s-

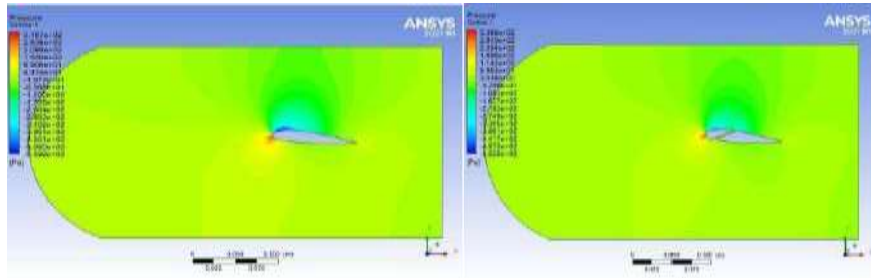


Figure 297 : Pressure at 50 for Both at twenty Five m/s

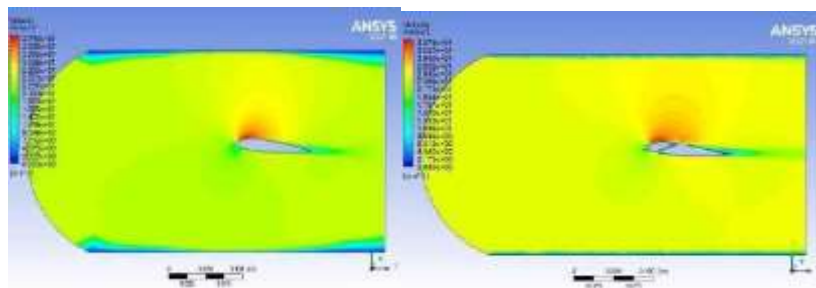


Figure 298 : Velocity at50 for Both at twenty Five m/s

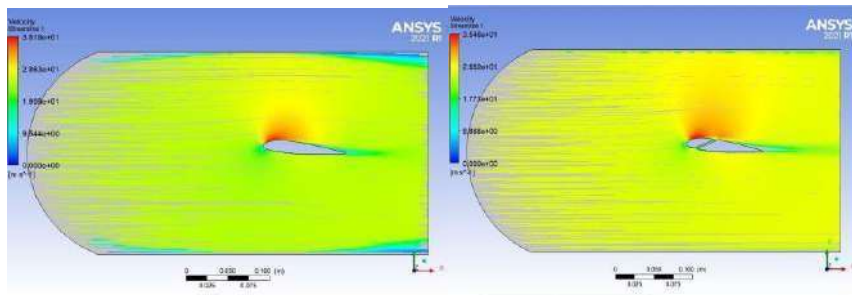


Figure 299 : Streamline at50 for Both at twenty Five m/s

### 5.97 Thirty m/s-

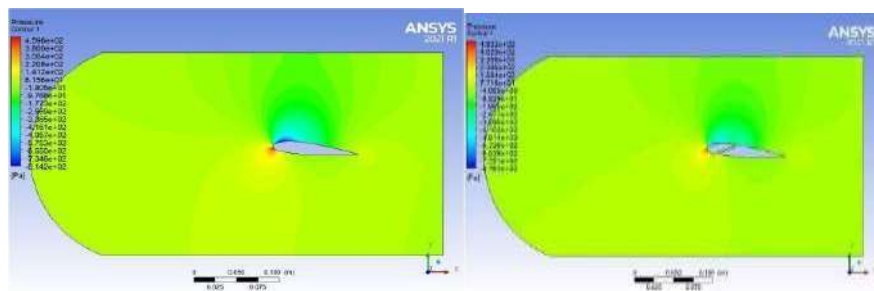


Figure 300 : Pressure at50 for Both at Thirty m/s

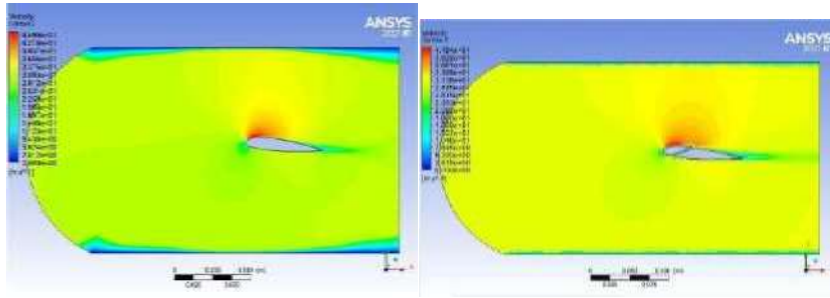


Figure 301 : Velocity at  $5^\circ$  for Both at Thirty m/s

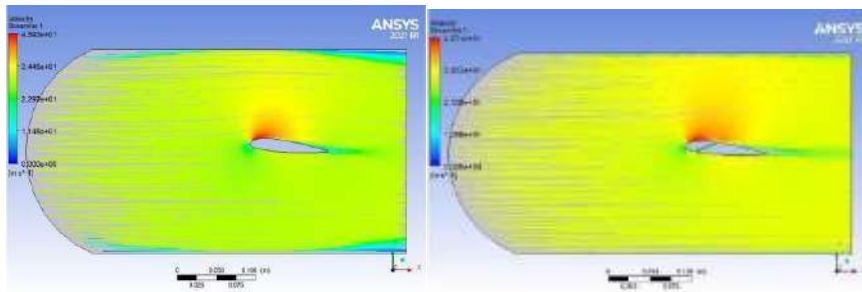


Figure 302 : Streamline at  $5^\circ$  for Both at Thirty m/s

**5.98 Fifty m/s-**

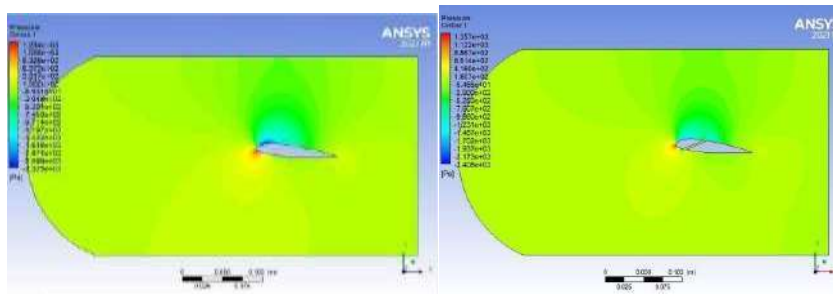


Figure 303 : Pressure at  $5^\circ$  for Both at Fifty m/s

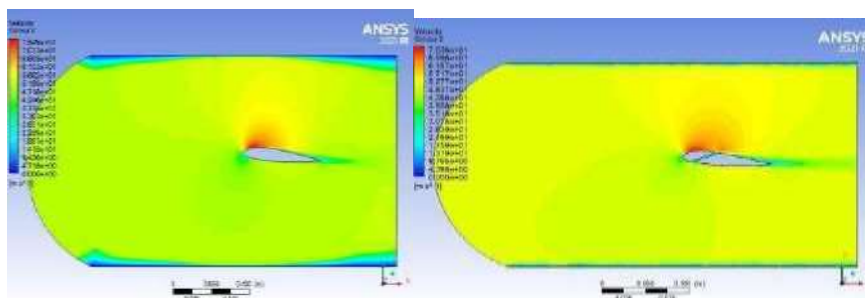


Figure 304 : Velocity at  $5^\circ$  for Both at Fifty m/s

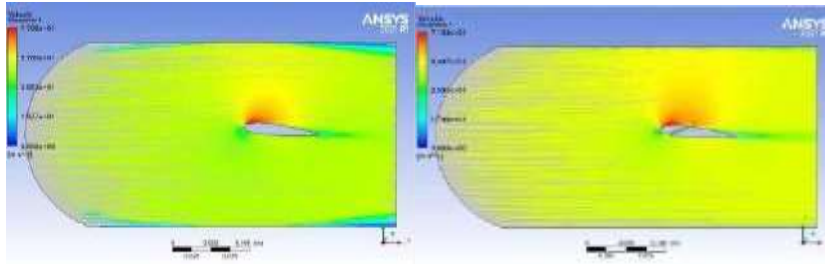


Figure 305 : Streamline at 5° for Both at Fifty m/s

Table of Design Points									
	A	B	C	D	E	F	G	H	I
1	Name	P1 - inlet vel	P2 - drag-op	P3 - drag-force-op	P4 - lift-op	P5 - lift-force-op	Retain	Retained Data	Note
2	Units	m s <sup>-1</sup>		N		N			
3	DP 7 (Current)	50	0.002281	3.4928	0.070528	108	<input checked="" type="checkbox"/>	<input checked="" type="checkbox"/>	
4	DP 8	30	0.00092219	1.4121	0.02438	37.332	<input checked="" type="checkbox"/>	<input checked="" type="checkbox"/>	
5	DP 9	25	0.00066943	1.0251	0.016601	25.421	<input checked="" type="checkbox"/>	<input checked="" type="checkbox"/>	
6	DP 10	20	0.00045378	0.69484	0.01032	15.803	<input checked="" type="checkbox"/>	<input checked="" type="checkbox"/>	
7	DP 11	15	0.00027681	0.42387	0.0055175	8.4486	<input checked="" type="checkbox"/>	<input checked="" type="checkbox"/>	
8	DP 12	10	0.00014176	0.21708	0.0022648	3.468	<input checked="" type="checkbox"/>	<input checked="" type="checkbox"/>	
9	DP 13	5	4.8079E-05	0.07362	0.00048983	0.75006	<input checked="" type="checkbox"/>	<input checked="" type="checkbox"/>	
*							<input type="checkbox"/>		

Table23 : Drag and Lift force values,24015at5°AOA

Table of Design Points									
	A	B	C	D	E	F	G	H	I
1	Name	P1 - inlet vel	P2 - drag-op	P3 - drag-force-op	P4 - lift-op	P5 - lift-force-op	Retain	Retained Data	Note
2	Units	m s <sup>-1</sup>		N		N			
3	DP 18 (Current)	50	0.0035201	5.3901	0.048055	73.585	<input checked="" type="checkbox"/>	<input checked="" type="checkbox"/>	
4	DP 19	30	0.001393	2.133	0.01582	24.224	<input checked="" type="checkbox"/>	<input checked="" type="checkbox"/>	
5	DP 20	25	0.0010049	1.5387	0.010588	16.213	<input checked="" type="checkbox"/>	<input checked="" type="checkbox"/>	
6	DP 21	20	0.00067865	1.0361	0.0064345	9.8528	<input checked="" type="checkbox"/>	<input checked="" type="checkbox"/>	
7	DP 22	15	0.0004089	0.62766	0.0033533	5.1348	<input checked="" type="checkbox"/>	<input checked="" type="checkbox"/>	
8	DP 23	10	0.00020562	0.31485	0.0013135	2.0114	<input checked="" type="checkbox"/>	<input checked="" type="checkbox"/>	
9	DP 24	5	6.5538E-05	0.10036	0.00024888	0.3811	<input checked="" type="checkbox"/>	<input checked="" type="checkbox"/>	
*							<input type="checkbox"/>		

Table24 : Drag and Lift force values,24015 at 5°AOA

### 5.99 Ten Attack angle : -

### 5.100 Five m/s-

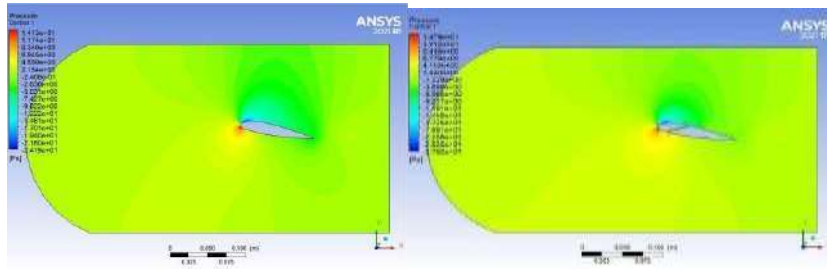


Figure 306 : Pressure at 100 for Both at Five m/s

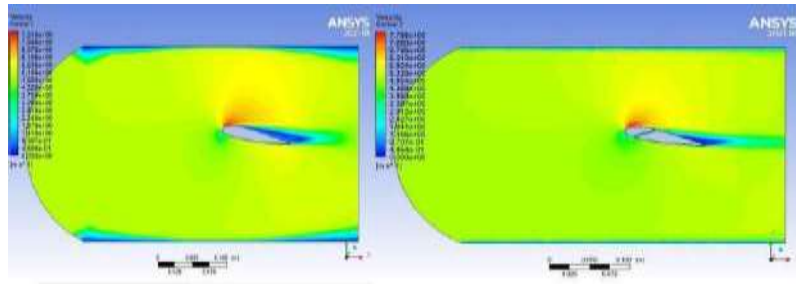


Figure 307 : Velocity at 10° for Both at Five m/s

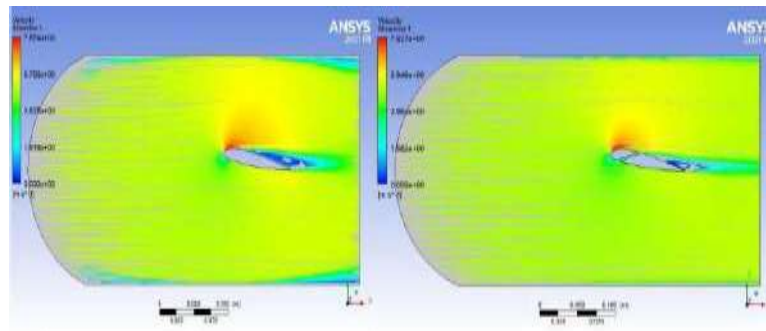


Figure 308 : Streamline at 10° for Both at Five m/s

**5.101 Ten m/s-**

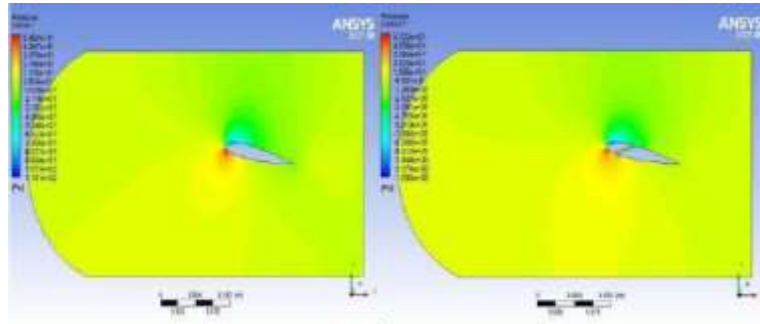


Figure 309 : Pressure at  $10^0$  for Both at Ten m/s

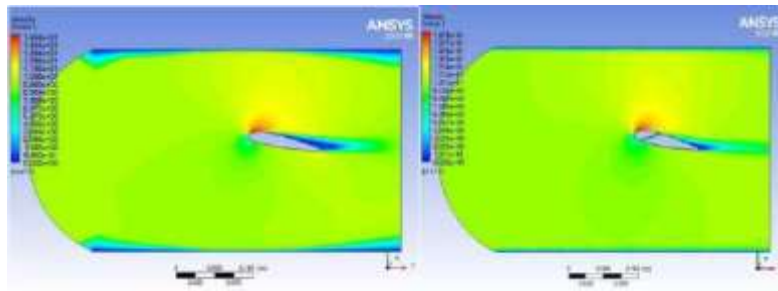


Figure 310 : Velocity at  $10^0$  for Both at Ten m/s

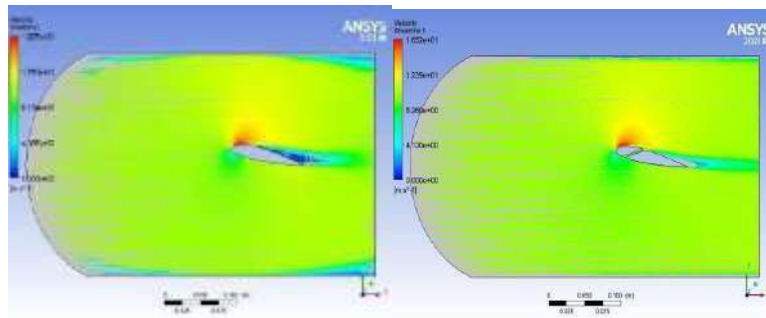


Figure 311 : Streamline at  $10^0$  for Both at Ten m/s

**Fifteen m/s-**

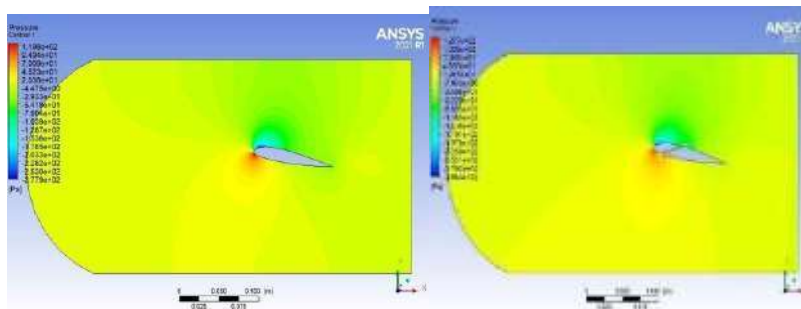


Figure 312 : Pressure at  $10^0$  for Both at fifteen m/s

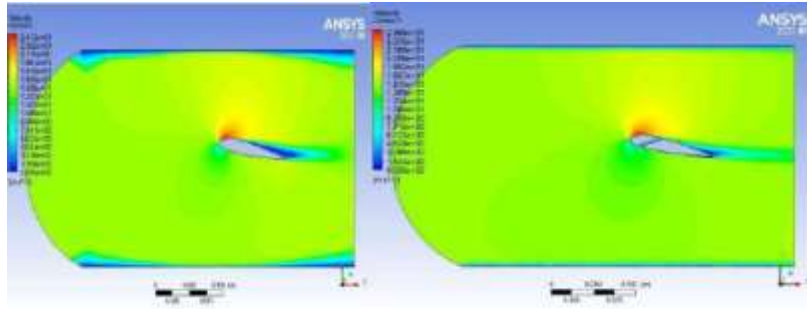


Figure 313 : Velocity at  $10^\circ$  for Both at fifteen m/s

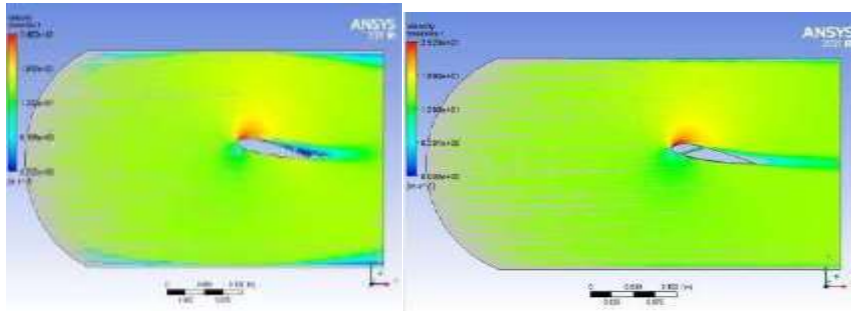


Figure 314 : Streamline at  $10^\circ$  for Both at fifteen m/s

**5.102 Twenty m/s-**

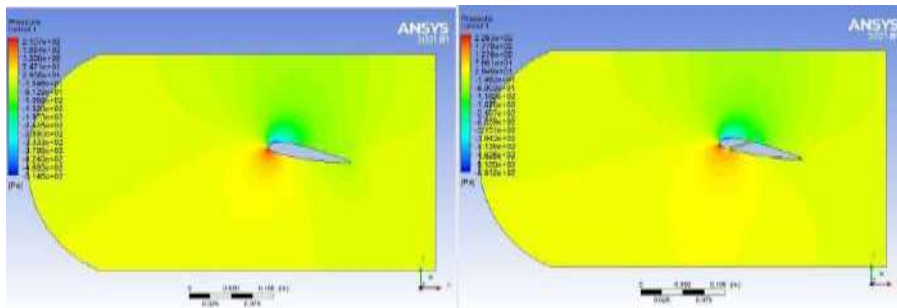


Figure 315 : Pressure at  $10^\circ$  for Both at Twenty m/s

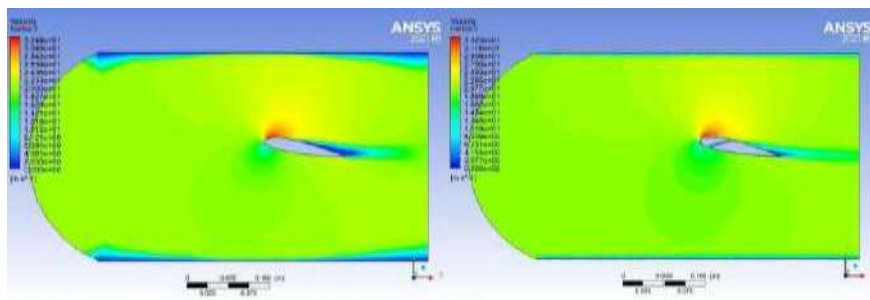


Figure 316 : Velocity at  $10^\circ$  for Both at Twenty m/s

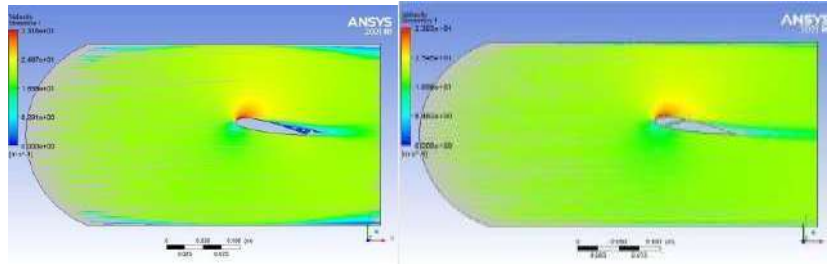


Figure 317 : Streamline at  $10^0$  for Both at Twenty m/s

Twenty Five m/s-

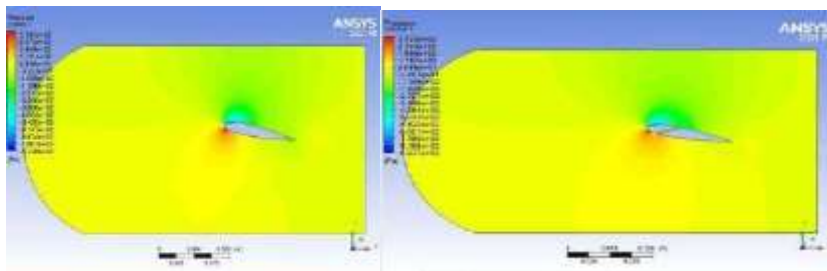


Figure 318 : Pressure at 100 for Both at twenty Five m/s

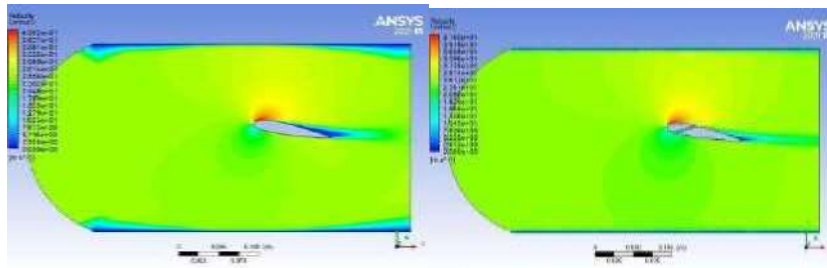


Figure 319 : Velocity at  $10^0$  for Both at twenty Five m/s

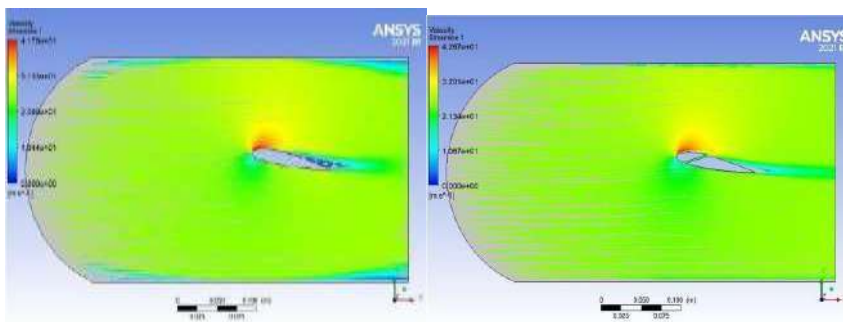


Figure 320 : Streamline at  $10^0$  for Both at twenty Five m/s



### 5.103 Thirty m/s-

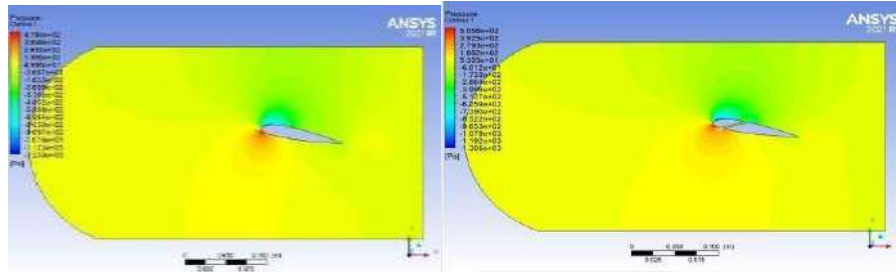


Figure 321 : Pressure at  $10^\circ$  for Both Thirty m/s

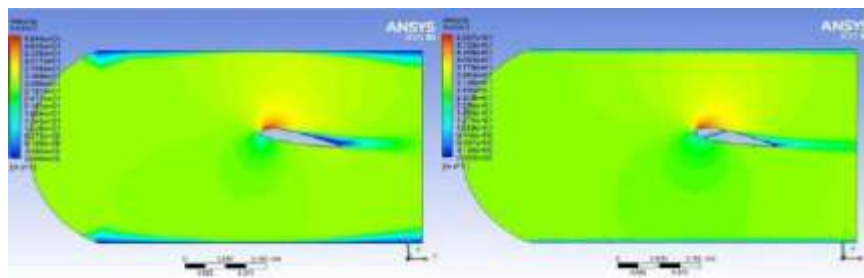


Figure 322 : Velocity at  $10^\circ$  for Both Thirty

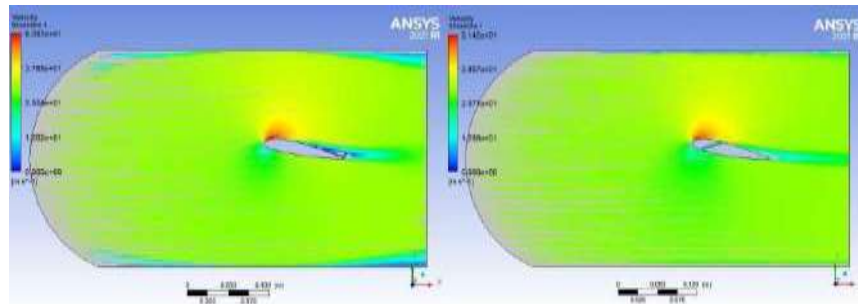


Figure 323 : Streamline at  $10^\circ$  for Both Thirty m/s

### 5.104 Fifty m/s-

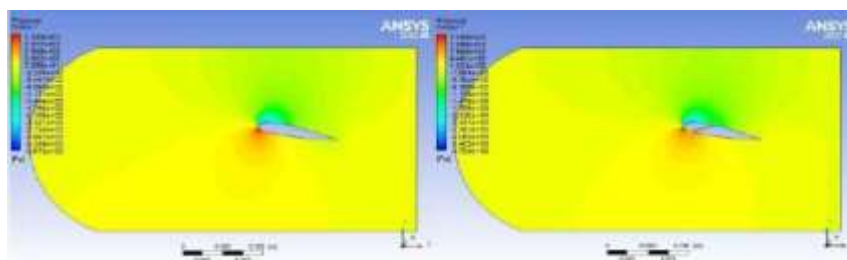


Figure 324 : Pressure at  $10^\circ$  for Both at Fifty m/s

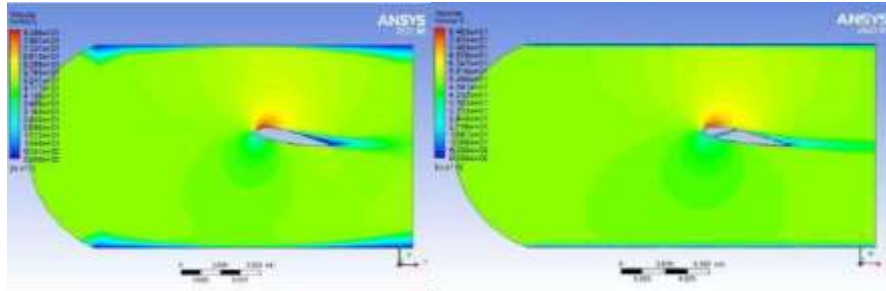


Figure 325 : Velocity at  $10^\circ$  for Both at Fifty m/s

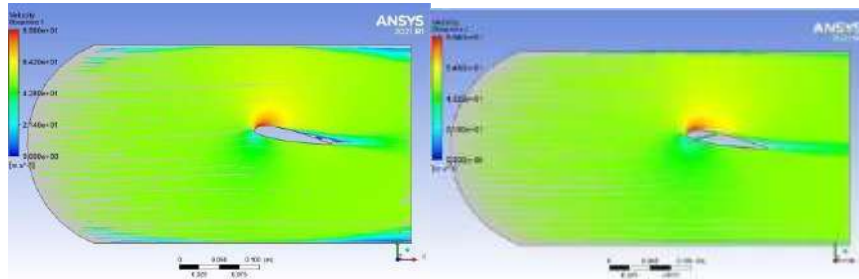


Figure 326 : Streamline at  $10^\circ$  for Both at Fifty m/s

Table of Design Points									
	A	B	C	D	E	F	G	H	I
1	Name	P1 - inlet vel	P2 - drag-op	P3 - drag-force-op	P4 - lift-op	P5 - lift-force-op	Retain	Retained Data	Note
2	Units	m s <sup>-1</sup>		N		N			
3	DP 7 (Current)	50	0.0043174	6.6111	0.10058	154.01	<input checked="" type="checkbox"/>	<input checked="" type="checkbox"/>	
4	DP 8	30	0.0017231	2.6385	0.034536	52.884	<input checked="" type="checkbox"/>	<input checked="" type="checkbox"/>	
5	DP 9	25	0.0012429	1.9032	0.023579	36.105	<input checked="" type="checkbox"/>	<input checked="" type="checkbox"/>	
6	DP 10	20	0.000839	1.2847	0.014736	22.565	<input checked="" type="checkbox"/>	<input checked="" type="checkbox"/>	
7	DP 11	15	0.00051146	0.78317	0.0079488	12.172	<input checked="" type="checkbox"/>	<input checked="" type="checkbox"/>	
8	DP 12	10	0.00025982	0.39785	0.0033124	5.0721	<input checked="" type="checkbox"/>	<input checked="" type="checkbox"/>	
9	DP 13	5	8.5701E-05	0.13123	0.0007305	1.1886	<input checked="" type="checkbox"/>	<input checked="" type="checkbox"/>	
*							<input type="checkbox"/>		

Table25 : Drag and Lift force values,24015 at  $10^\circ$  AOA

Table of Design Points									
	A	B	C	D	E	F	G	H	I
1	Name	P1 - inlet vel	P2 - drag-op	P3 - drag-force-op	P4 - lift-op	P5 - lift-force-op	Retain	Retained Data	Note
2	Units	m s <sup>-1</sup>		N		N			
3	DP 12 (Current)	50	0.0053047	8.1228	0.096399	150.21	<input checked="" type="checkbox"/>	<input checked="" type="checkbox"/>	
4	DP 13	30	0.0021378	3.1203	0.034896	52.362	<input checked="" type="checkbox"/>	<input checked="" type="checkbox"/>	
5	DP 14	25	0.0014536	2.2258	0.023349	36.753	<input checked="" type="checkbox"/>	<input checked="" type="checkbox"/>	
6	DP 15	20	0.00096329	1.475	0.014589	22.34	<input checked="" type="checkbox"/>	<input checked="" type="checkbox"/>	
7	DP 16	15	0.00057046	0.87355	0.0079052	12.105	<input checked="" type="checkbox"/>	<input checked="" type="checkbox"/>	
8	DP 17	10	0.0002771	0.42431	0.0032906	5.0389	<input checked="" type="checkbox"/>	<input checked="" type="checkbox"/>	
9	DP 18	5	8.5303E-05	0.13062	0.00065332	1.0647	<input checked="" type="checkbox"/>	<input checked="" type="checkbox"/>	
*							<input type="checkbox"/>		

Table26 : Drag and Lift force values,24015at  $10^\circ$  AOA

5.105 15Attack angle :-

5.106 Five m/s-

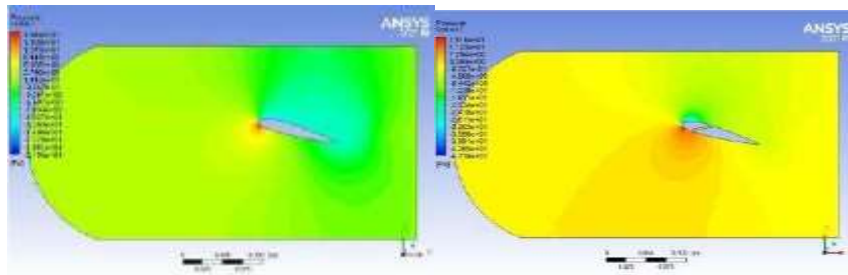


Figure 327 : Pressure at 15° for Both at Five m/s

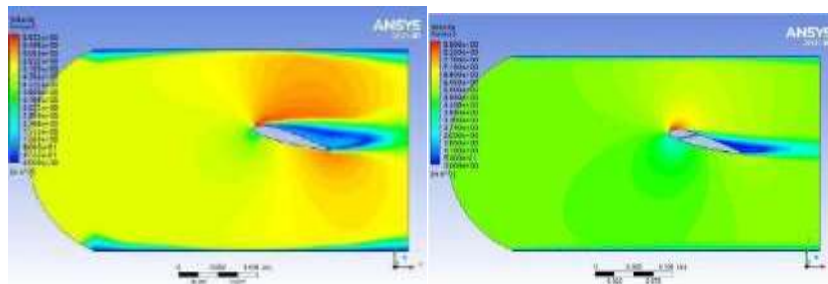


Figure 328 : Velocity at 15° for Both at Five m/s

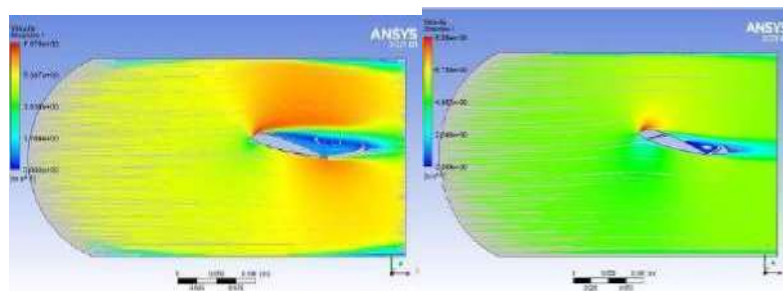


Figure 329 : Streamline at 15° for Both at Five m/s

### 5.107 Ten m/s-

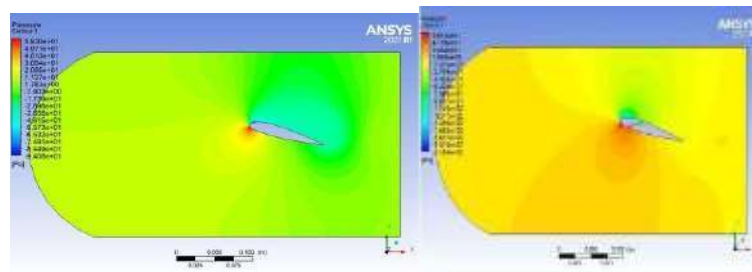


Figure 330 : Pressure at 150 for Both at Ten m/s

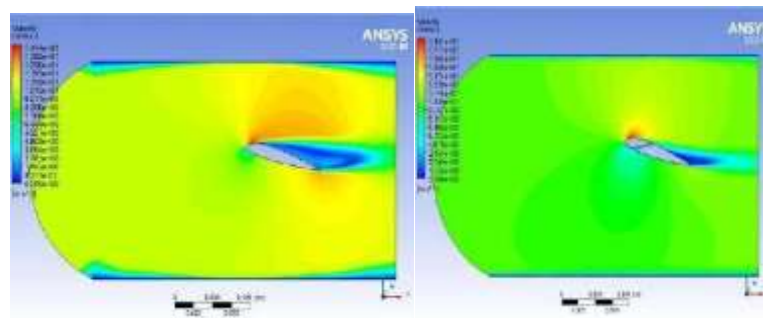


Figure 331 : Velocity at 150 for Both at Ten m/s

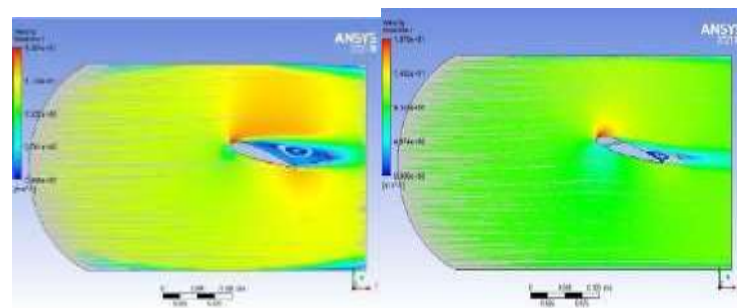


Figure 332 : Streamline at 150 for Both at Ten m/s

### 5.108 Fifteen m/s-

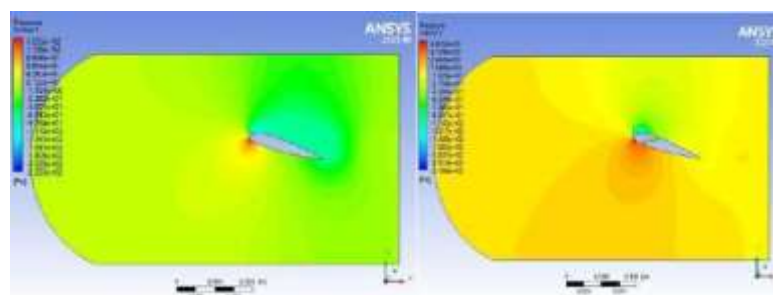


Figure 333 : Pressure at 150 for Both at fifteen m/s

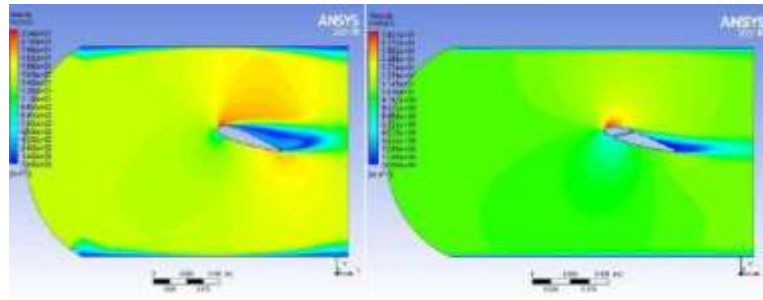


Figure 334 : Velocity at 15° for Both at fifteen m/s

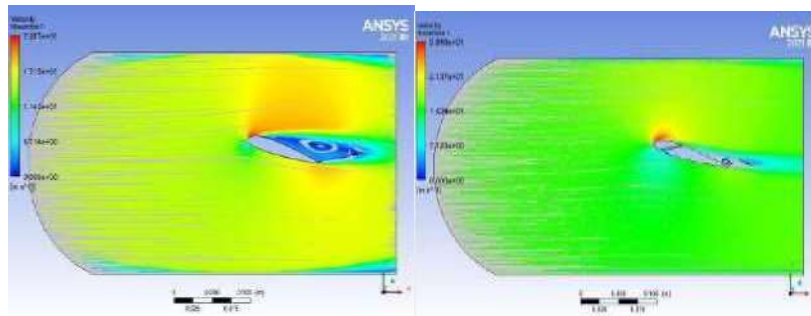


Figure 335 : Streamline at 15° for Both at fifteen m/s

### 5.109 Twenty m/s-

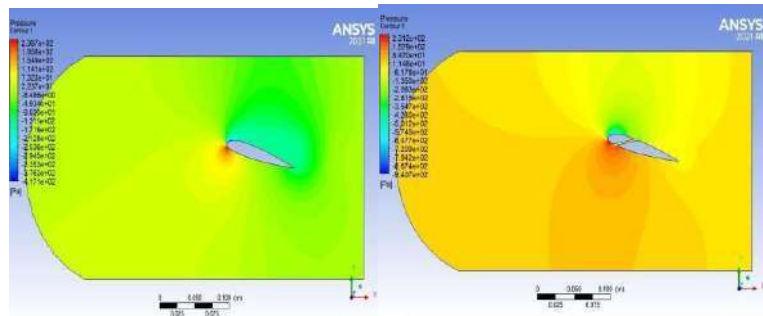


Figure 336 : Pressure at 15° for Both at Twenty m/s

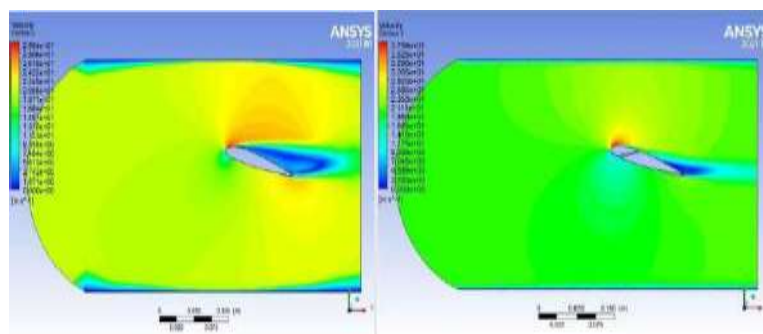


Figure 337 : Velocity Plot at 15° for Both at Twenty m/s

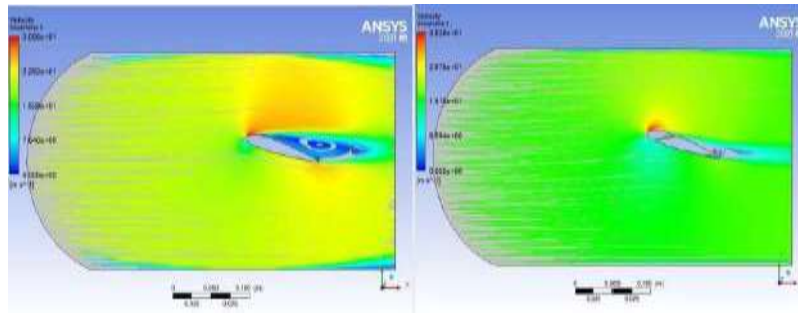


Figure 338 : Streamline at 15° for Both at Twenty m/s

**Twenty Five m/s-**

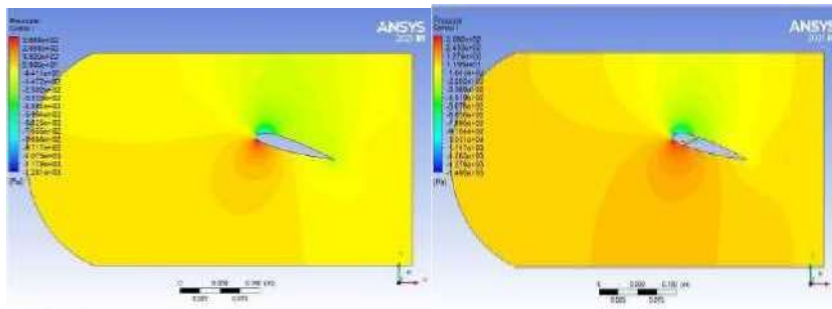


Figure 339 : Pressure at 15° for Both at twenty Five m/s

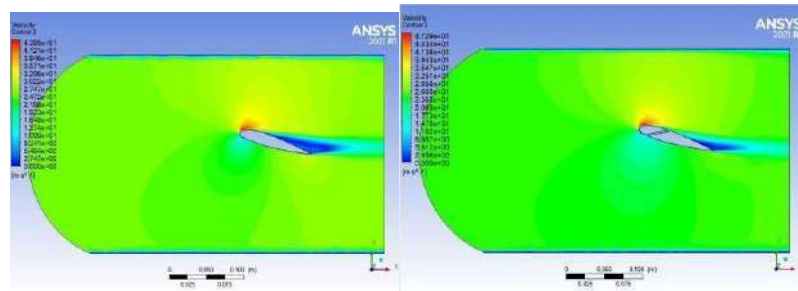


Figure 340 : Velocity at 15° for Both at twenty-Five m/s

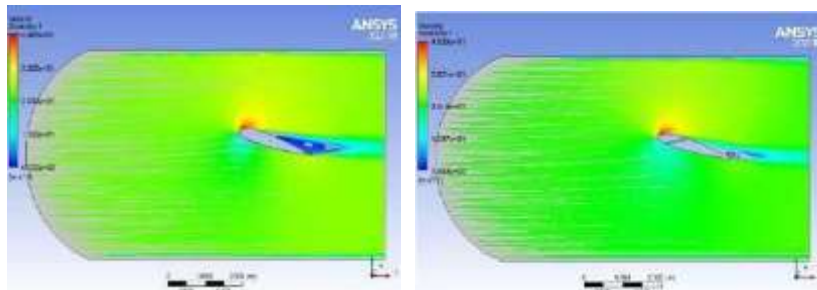


Figure 341 : Streamline at 15° for Both at twenty-Five m/s

### 5.110 Thirty m/s-

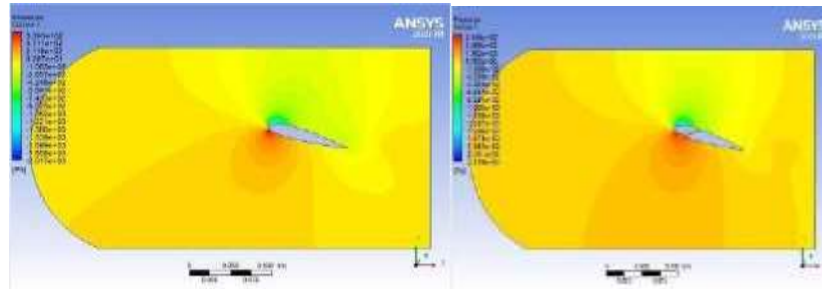


Figure 342 : Pressure at 15° for Both at Thirty m/s

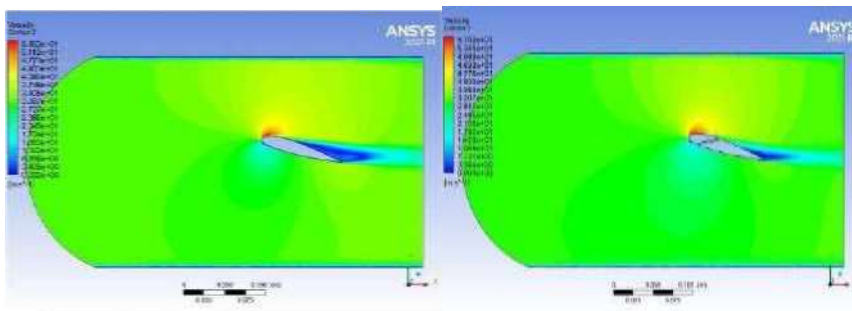


Figure 343 : Velocity at 15° for Both at Thirty m/s

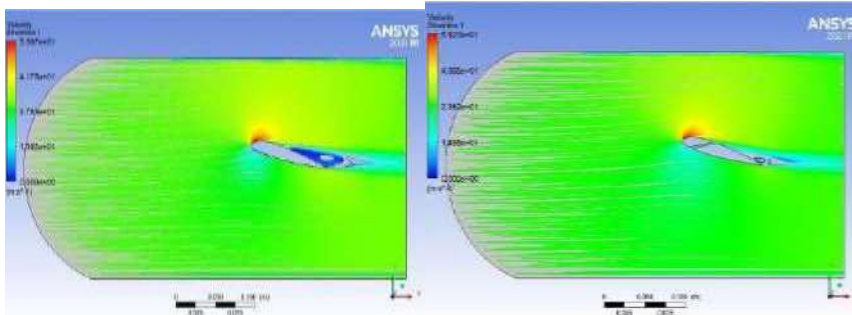


Figure 344 : Streamline at 15° for Both at Thirty m/s

### 5.111 Fifty m/s-

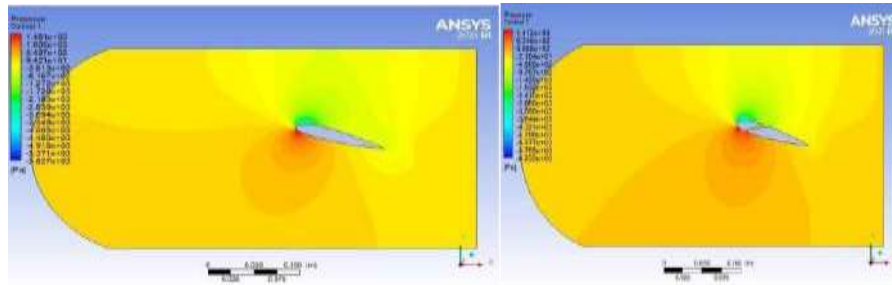


Figure 345 : Pressure at 15° for Both at Fifty m/s

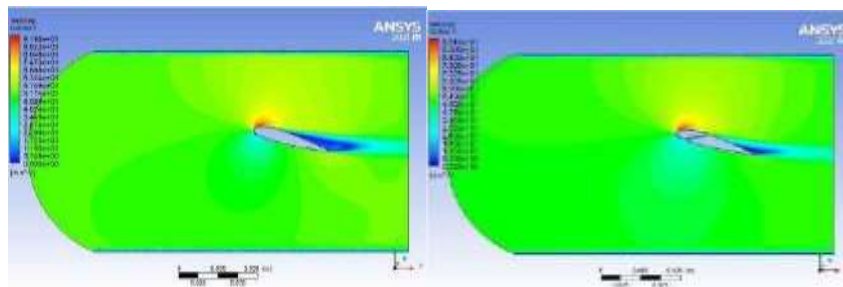


Figure 346 : Velocity at 15° for Both at Fifty m/s

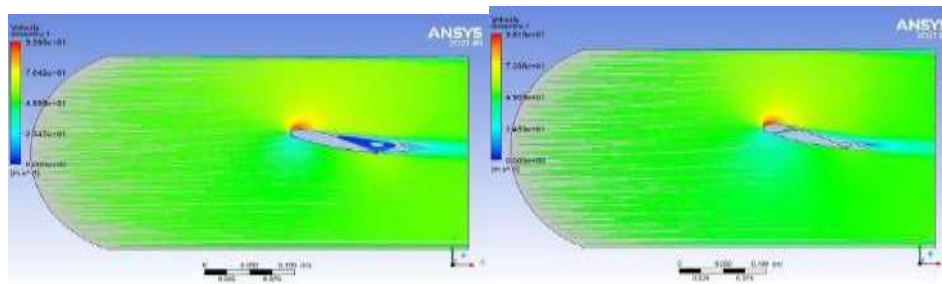


Figure 347 : Streamline at 15° for Both at Fifty m/s

	A	B	C	D	E	F	G	H	I
1	Name	P1 - inlet	F2 - drag	P3 - drag-force	P4 - lift	P5 - lift-force	Retain	Retained Data	Note
2	Units	m s <sup>-1</sup>		N		N			
3	DP 0	50	0.011197	6.1723	0.19687	58.932	<input checked="" type="checkbox"/>	<input checked="" type="checkbox"/>	
4	DP 1 (Current)	50	0.028948	15.958	0.30294	167	<input checked="" type="checkbox"/>	<input checked="" type="checkbox"/>	
5	DP 2	5	0.0004315	0.23792	0.0024658	1.3502	<input checked="" type="checkbox"/>	<input checked="" type="checkbox"/>	
6	DP 3	20	0.0014789	0.81525	0.010787	5.9462	<input checked="" type="checkbox"/>	<input checked="" type="checkbox"/>	
7	DP 4	15	0.0032948	1.796	0.025258	13.924	<input checked="" type="checkbox"/>	<input checked="" type="checkbox"/>	
8	DP 5	20	0.0052658	2.9028	0.046043	25.381	<input checked="" type="checkbox"/>	<input checked="" type="checkbox"/>	
9	DP 6	25	0.0076621	4.3851	0.075291	40.402	<input checked="" type="checkbox"/>	<input checked="" type="checkbox"/>	
*							<input type="checkbox"/>	<input type="checkbox"/>	

Table27 : Drag and Lift force values,24015 at 15°AOA



Table of Design Points									
	A	B	C	D	E	F	G	H	I
1	Name	P1 - mievel	P2 - drag-op	P3 - drag-force-op	P4 - lift-op	P5 - lift-force-op	Retain	Retained Data	Note
2	Units	m s <sup>-1</sup>		N		N			
3	DP 6 (Current)	50	0.0086316	13.217	0.1284E	196.74	<input checked="" type="checkbox"/>	<input checked="" type="checkbox"/>	
4	DP 7	30	0.0032645	4.9988	0.044979	68.874	<input checked="" type="checkbox"/>	<input checked="" type="checkbox"/>	
5	DP 8	25	0.002314	3.5433	0.030876	47.279	<input checked="" type="checkbox"/>	<input checked="" type="checkbox"/>	
6	DP 9	20	0.001523	2.3322	0.019456	29.793	<input checked="" type="checkbox"/>	<input checked="" type="checkbox"/>	
7	DP 10	15	0.00089339	1.368	0.010673	16.343	<input checked="" type="checkbox"/>	<input checked="" type="checkbox"/>	
8	DP 11	10	0.00042636	0.65318	0.0045488	6.9633	<input checked="" type="checkbox"/>	<input checked="" type="checkbox"/>	
9	DP 12	5	0.00012785	0.19577	0.000018	1.5388	<input checked="" type="checkbox"/>	<input checked="" type="checkbox"/>	
*							<input type="checkbox"/>		

Table28 : Drag and Lift force values, Drag and Lift force values,24015 at 15°AOA

### 5.112 Twenty Attack angle : -

### 5.113 Five m/s-

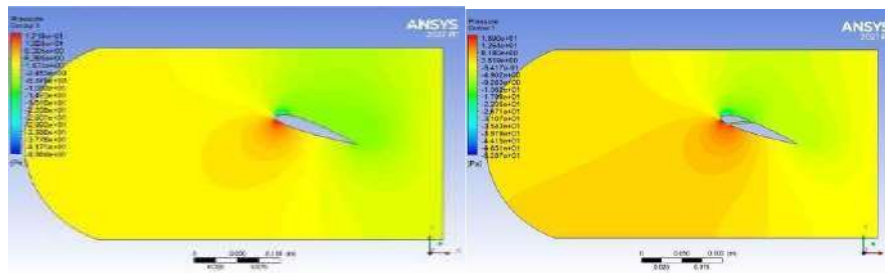


Figure 348 : Pressure at 20° for at Five m/s

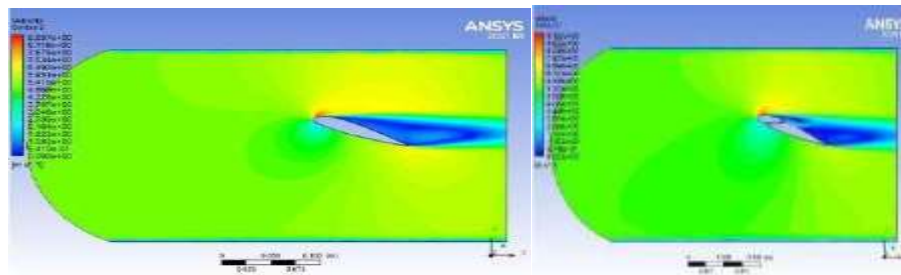


Figure 349 : Velocity at 20° for at Five m/s

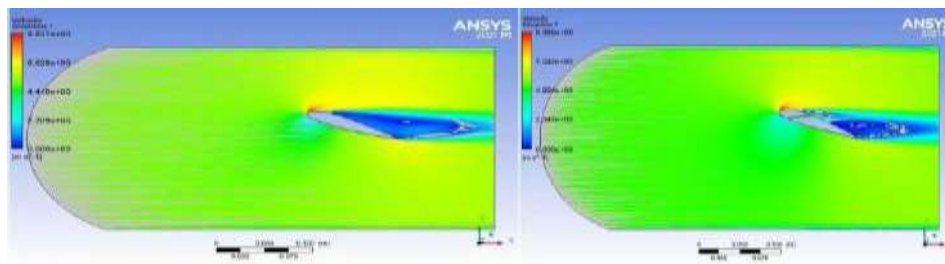


Figure 350 : Streamline at20° for at Five m/s

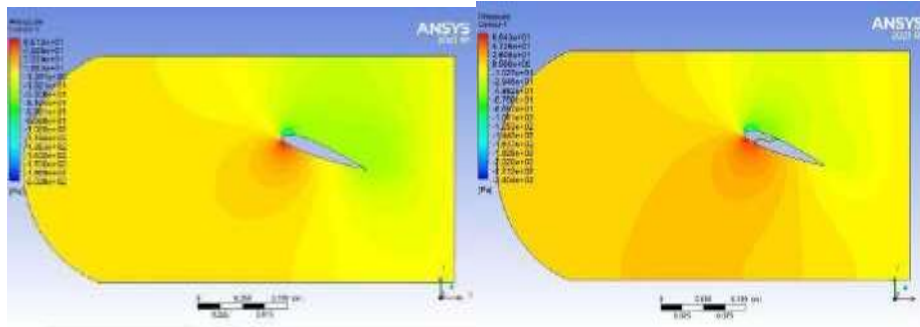


Figure 351 : Pressure at 20° for Both at Ten m/s

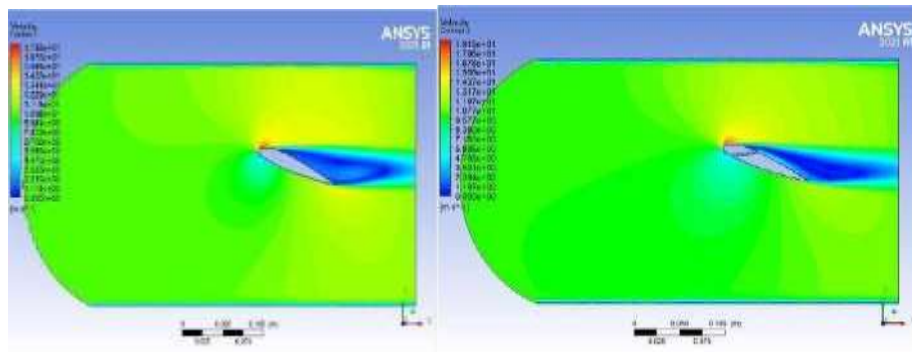


Figure 352 : Velocity at 20° for Both at Ten m/s

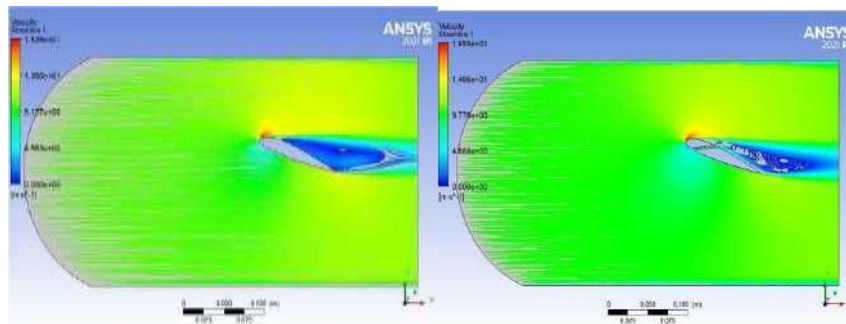


Figure 353 : Streamline at 20° for Both at Ten m/s

### 5.114 Fifteen m/s-

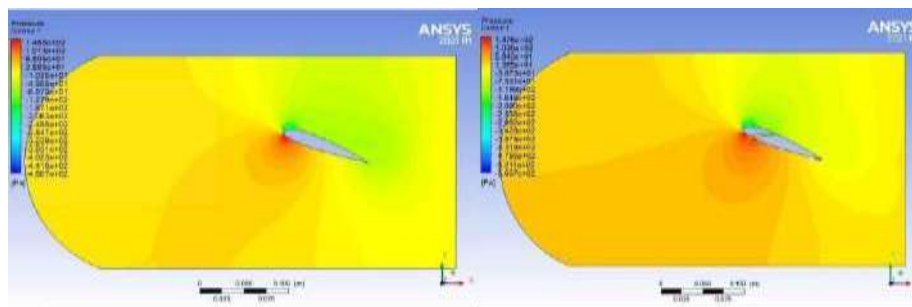


Figure 354 : Pressure at 20° for Both at fifteen m/s

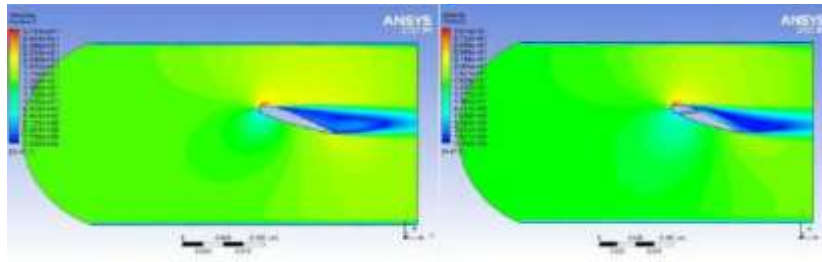


Figure 355 : Velocity at  $20^\circ$  for Both at fifteen m/s

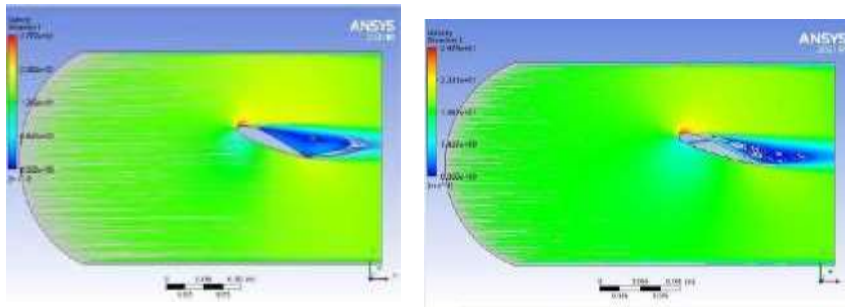


Figure 356 : Streamline at  $20^\circ$  for Both at fifteen m/s

**5.115 Twenty m/s-**

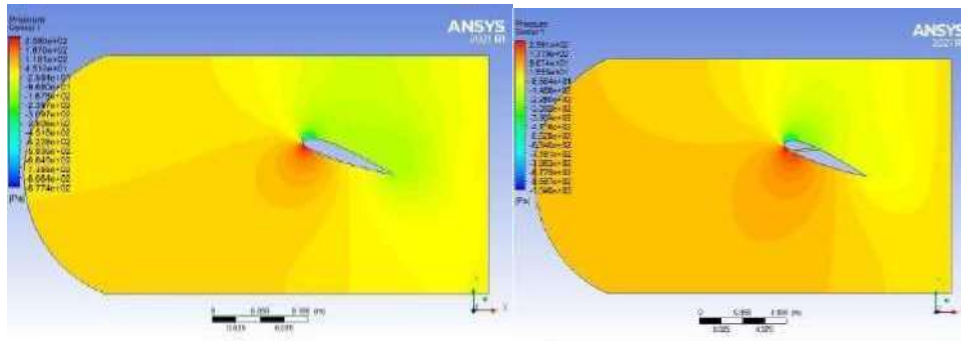


Figure 357 : Pressure at  $20^\circ$  for Both at Twenty m/s

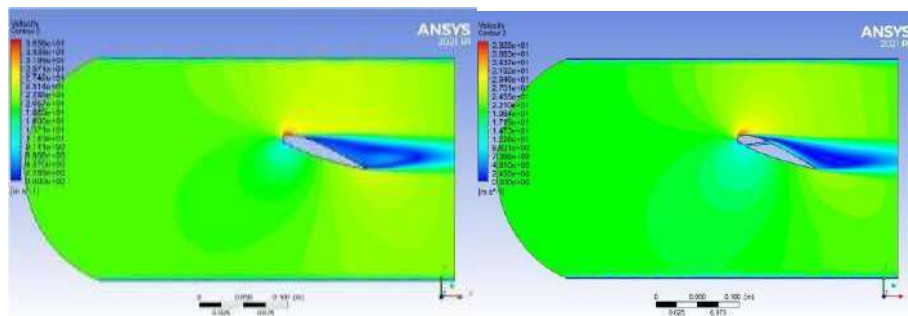


Figure 358 : Velocity at  $20^\circ$  for at Twenty m/s

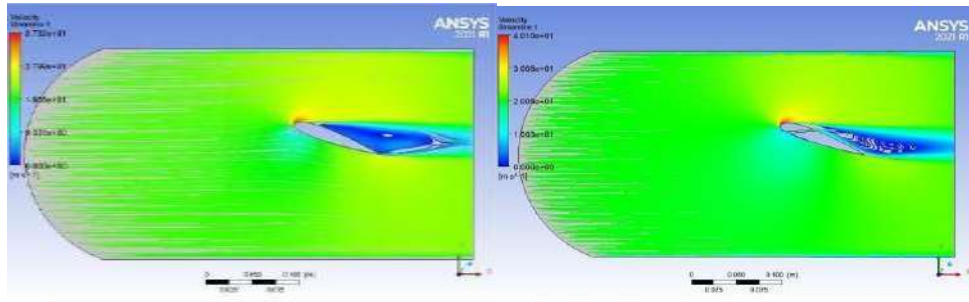


Figure 359 : Streamline at  $20^\circ$  for at Twenty m/s

### 5.116 Twenty Five m/s-

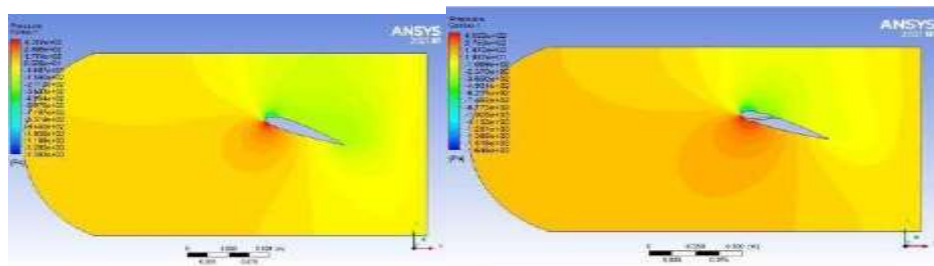


Figure 360 : Pressure at  $20^\circ$  for Both at twenty Five m/s

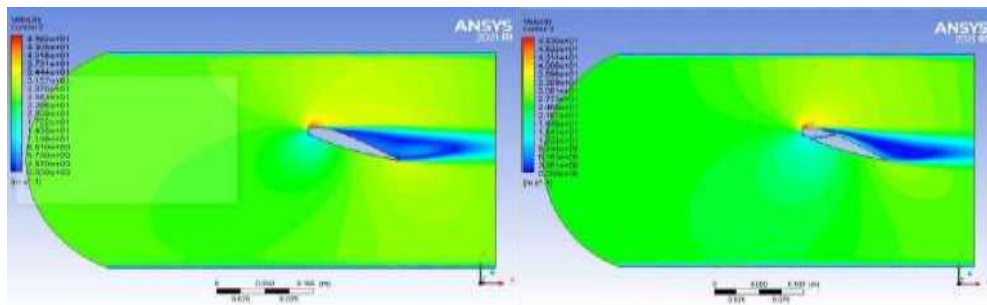


Figure 361 : Velocity at  $20^\circ$  for Both at twenty Five m/s

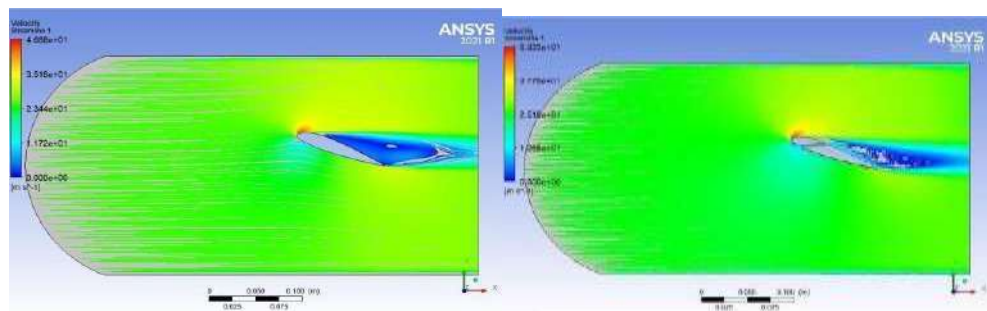


Figure 362 : Streamline at  $20^\circ$  for Both at twenty Five m/s

### 5.117 Thirty m/s-

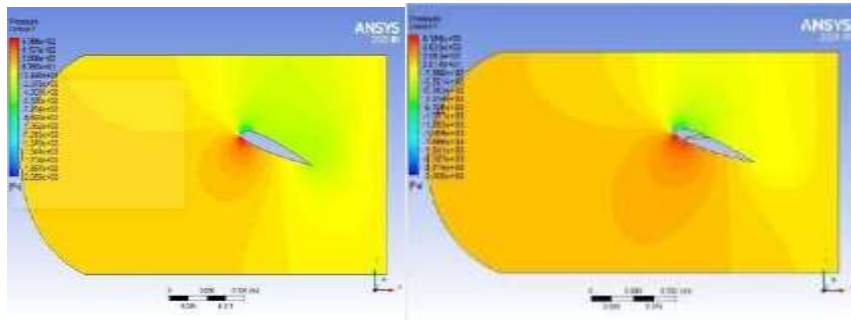


Figure 363 : Pressure at 20° for Both at Thirty m/s

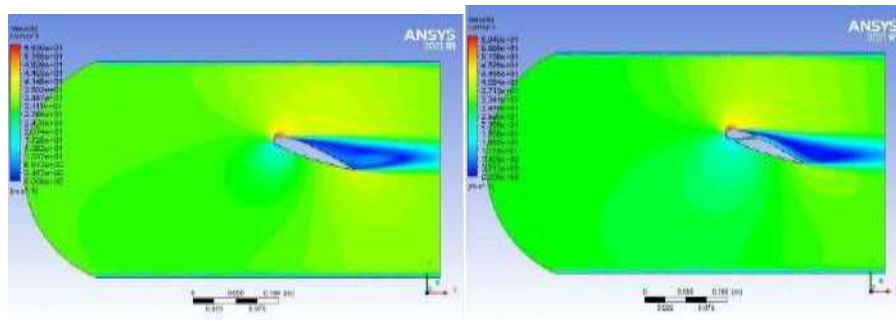


Figure 364 : Velocity at 20° for Both at Thirty m/s

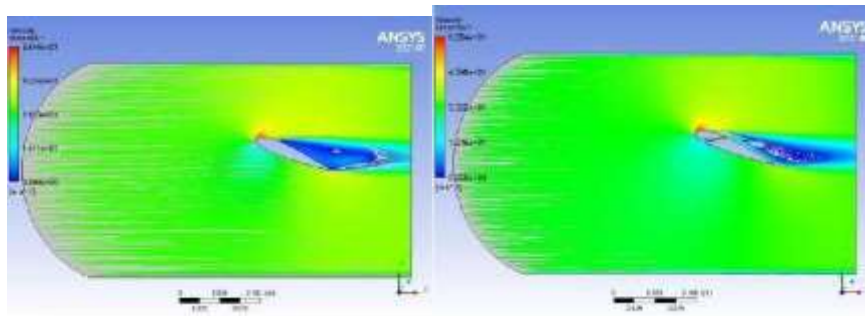


Figure 365 : Streamline at 20° for Both at Thirty m/s

### 5.118 Fifty m/s-

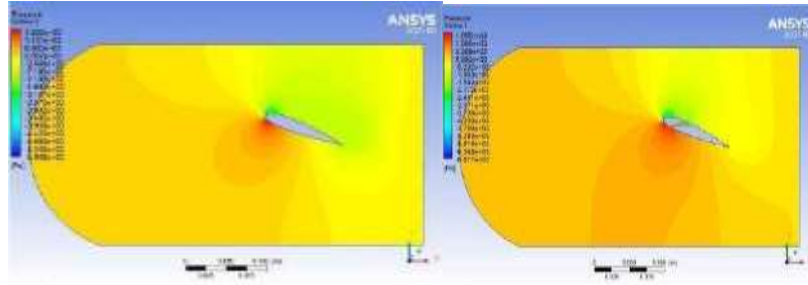


Figure 366 : Pressure at  $20^\circ$  for at Fifty m/s

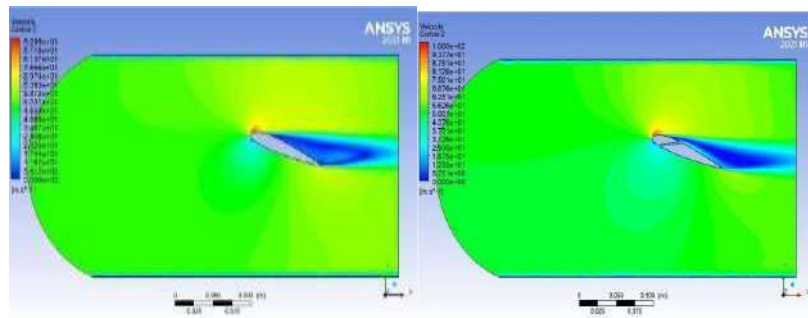


Figure 367 : Velocity Pressure at  $20^\circ$  for at Fifty m/s

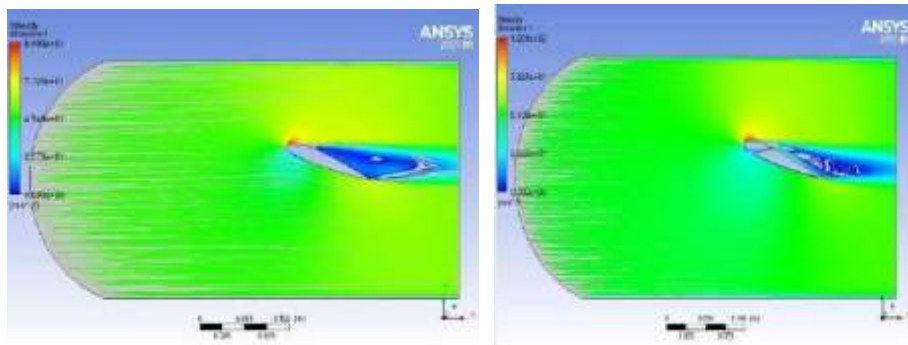


Figure 368 : Streamline Pressure at  $20^\circ$  for at Fifty m/s

Table of Design Points									
	A	B	C	D	E	F	G	H	I
1	Name	P1 - inlets	P2 - drag-op	P3 - drag-force-op	P4 - lift-op	P5 - lift-force-op	Retain	Retained Data	Note
2	Units	m s <sup>-1</sup>		N		N			
3	DP 0 (Current)	50	0.021941	32.678	0.093365	143	<input checked="" type="checkbox"/>	<input checked="" type="checkbox"/>	
4	DP 1	30	0.0075202	12.138	0.033365	50.763	<input checked="" type="checkbox"/>	<input checked="" type="checkbox"/>	
5	DP 3	25	0.0055687	8.5271	0.022915	35.089	<input checked="" type="checkbox"/>	<input checked="" type="checkbox"/>	
6	DP 4	20	0.0036233	5.5481	0.014575	22.318	<input checked="" type="checkbox"/>	<input checked="" type="checkbox"/>	
7	DP 5	15	0.0022863	3.2946	0.0081689	12.414	<input checked="" type="checkbox"/>	<input checked="" type="checkbox"/>	
8	DP 6	10	0.00096388	1.4759	0.0035341	5.4116	<input checked="" type="checkbox"/>	<input checked="" type="checkbox"/>	
9	DP 7	5	0.000263	0.40272	0.00085143	1.3038	<input checked="" type="checkbox"/>	<input checked="" type="checkbox"/>	
*							<input type="checkbox"/>		

Table29 : Drag and Lift force values, 24015 at 20°AOA

Table of Design Points									
	A	B	C	D	E	F	G	H	I
1	Name	P1 - inlets	P2 - drag-op	P3 - drag-force-op	P4 - lift-op	P5 - lift-force-op	Retain	Retained Data	Note
2	Units	m s <sup>-1</sup>		N		N			
3	DP 0 (Current)	50	0.021823	33.417	0.12986	198.84	<input checked="" type="checkbox"/>	<input checked="" type="checkbox"/>	
4	DP 1	30	0.0080666	12.352	0.045851	70.209	<input checked="" type="checkbox"/>	<input checked="" type="checkbox"/>	
5	DP 2	25	0.0056622	8.6703	0.031599	48.386	<input checked="" type="checkbox"/>	<input checked="" type="checkbox"/>	
6	DP 3	20	0.0036646	5.6114	0.020072	30.736	<input checked="" type="checkbox"/>	<input checked="" type="checkbox"/>	
7	DP 4	15	0.002114	3.237	0.011064	16.942	<input checked="" type="checkbox"/>	<input checked="" type="checkbox"/>	
8	DP 5	10	0.0009746	1.4891	0.0047882	7.332	<input checked="" type="checkbox"/>	<input checked="" type="checkbox"/>	
9	DP 6	5	0.00025382	0.38866	0.001095	1.6767	<input checked="" type="checkbox"/>	<input checked="" type="checkbox"/>	
*							<input type="checkbox"/>		

Table30 : Drag and Lift force values,24015at 20°AOA

### 5.119 Charts : - for24015

### 5.120 Five m/s-

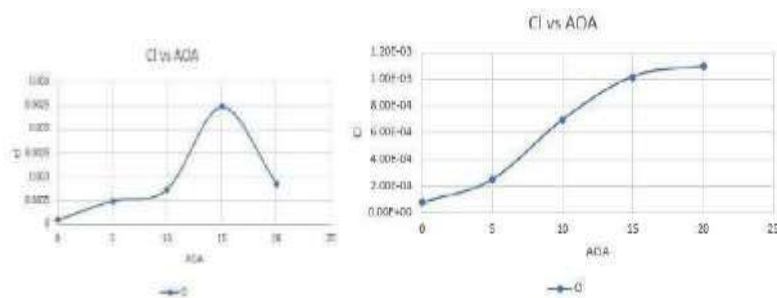


Figure 369 : Cl versus attack angle

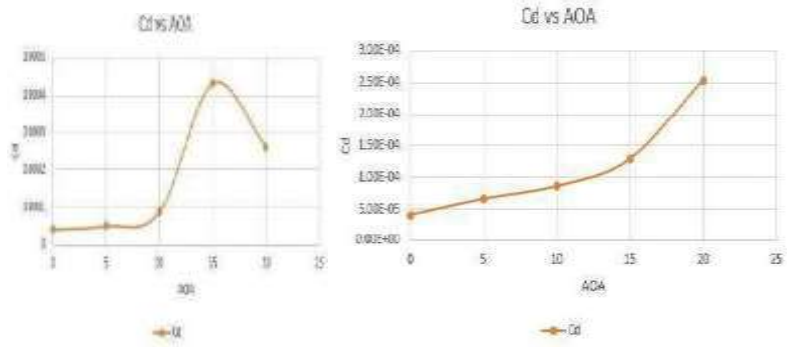


Figure 370 : Cd versus attack angle

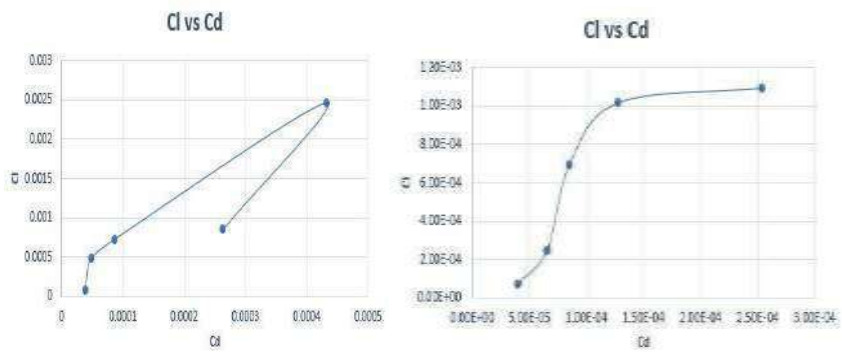


Figure 371 : Cl versus Cd

5.121 Ten m/s-

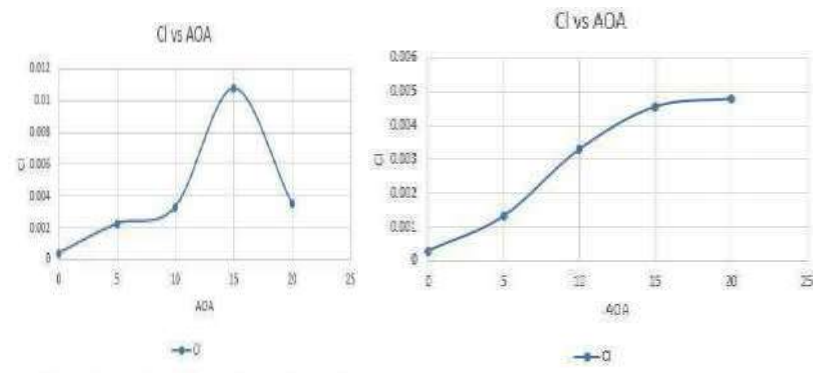


Figure 372 : Cl versus attack angle



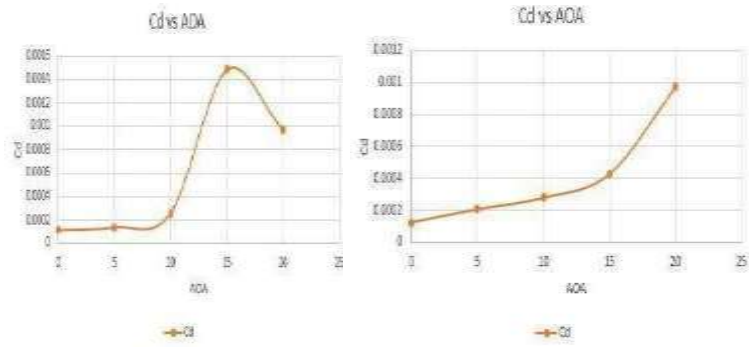


Figure 373 : Cd versus attack angle

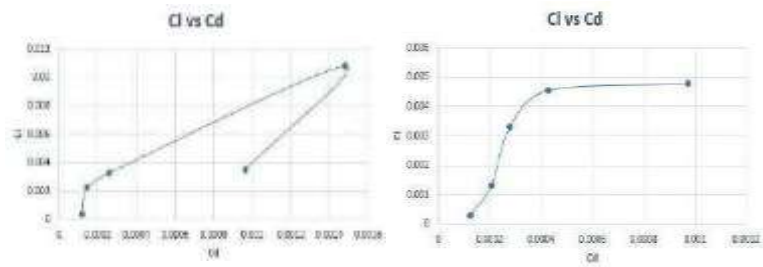


Figure 374 : Cl versus Cd

5.122 Fifteen m/s-



Figure 375 : Cl versus attack angle

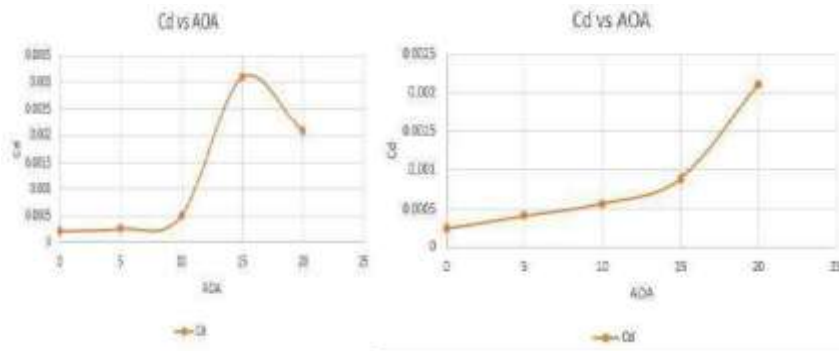


Figure 376 : Cd versus attack angle

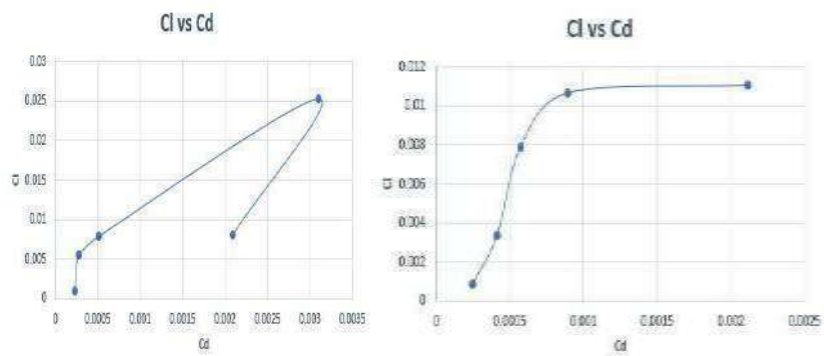


Figure 377 : Cl versus Cd

### 5.123 Twenty m/s-

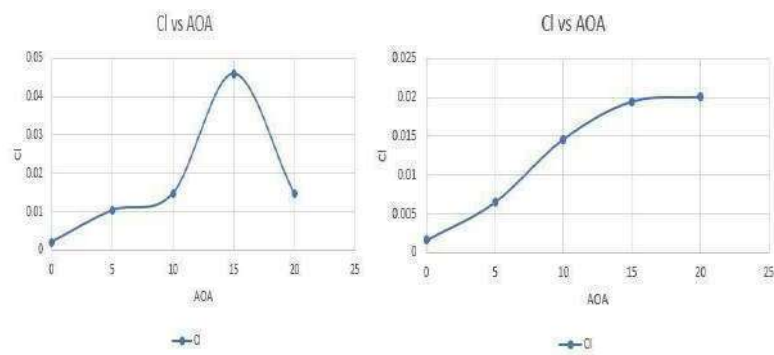


Figure 378 : CL versus attack angle

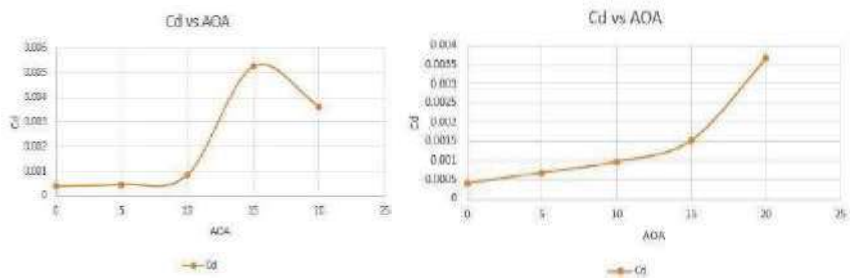


Figure 379 : Cd versus attack angle

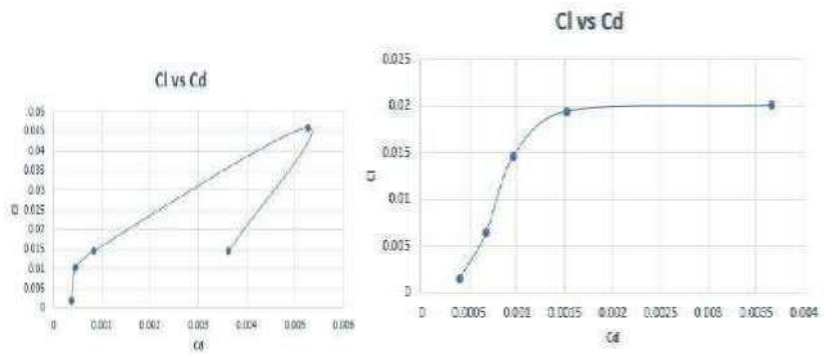


Figure 380 : Cl versus Cd

5.124 Twenty-Five m/s-

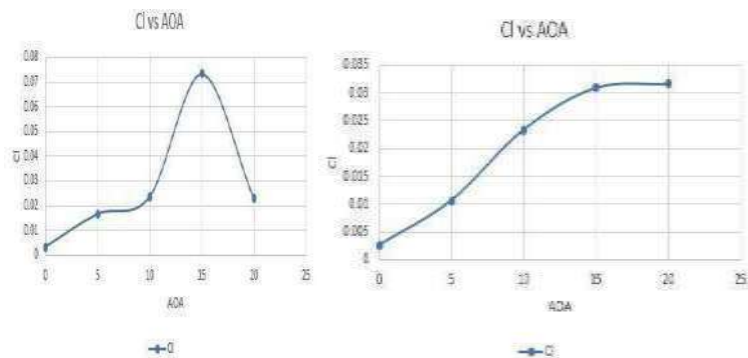


Figure 381 : Cl versus attack angle

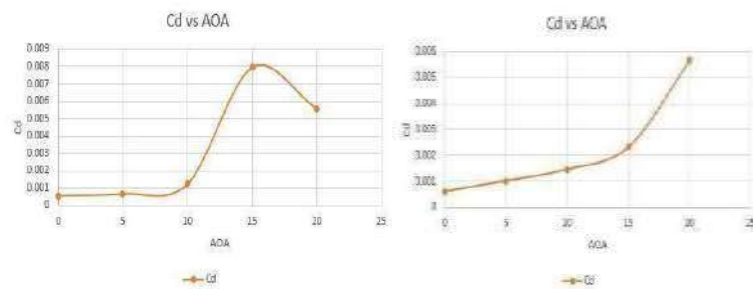


Figure 382 : Cd versus attack angle

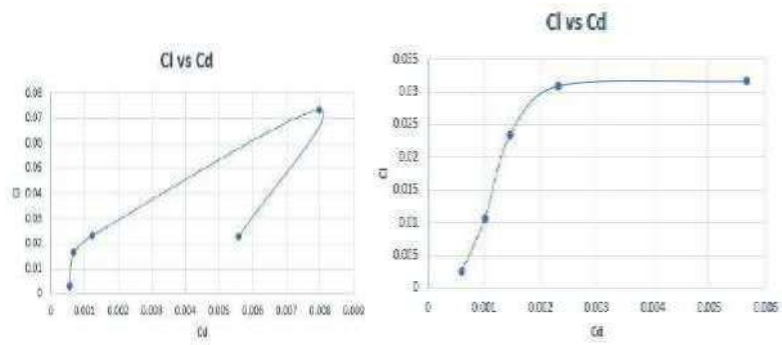


Figure 383 : Cl versus Cd

5.125 Thirty m/s-

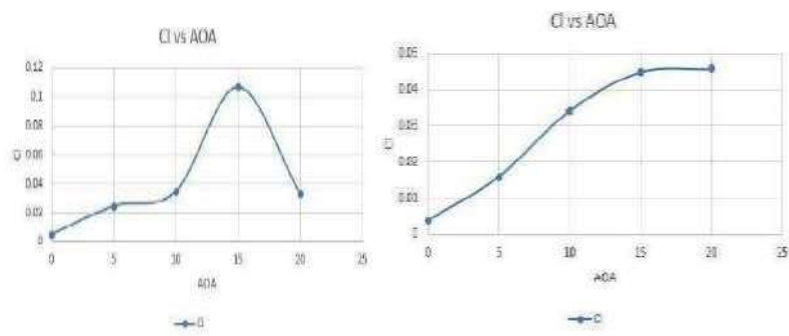


Figure 384 : Cl versus attack angle

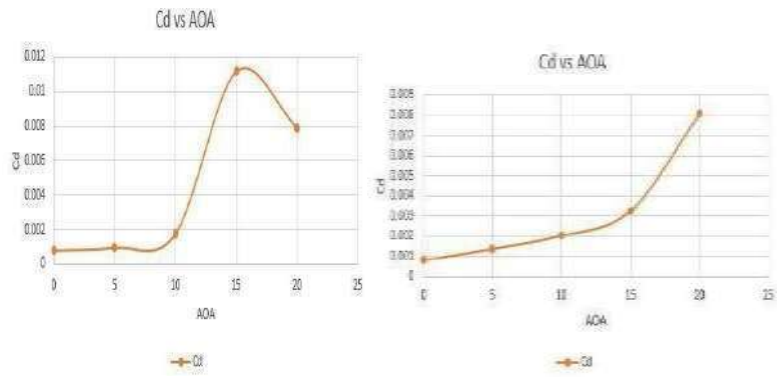


Figure 385 : Cd versus attack angle

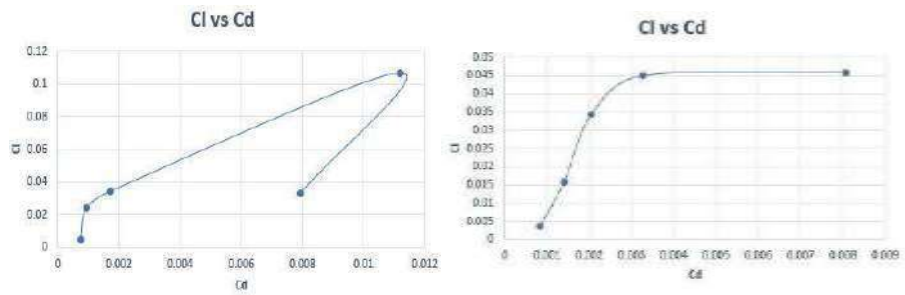


Figure 386 : Cl versus Cd

5.126 Fifty m/s-

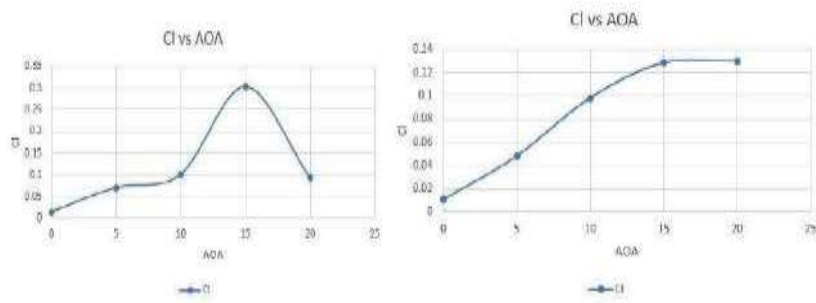


Figure 387 : Cl versus attack angle

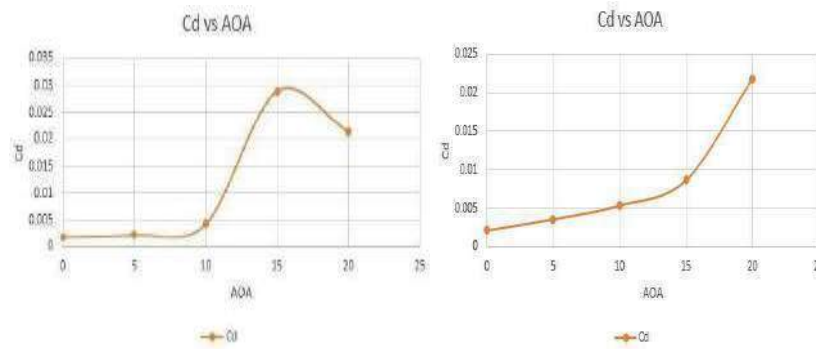


Figure 388 : Cd versus attack angle

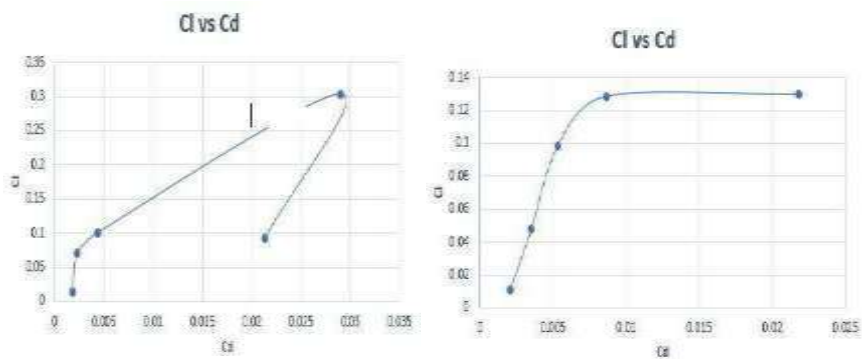
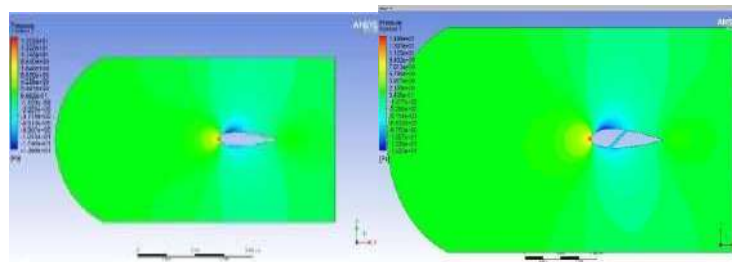


Figure 389 : Cl versus Cd

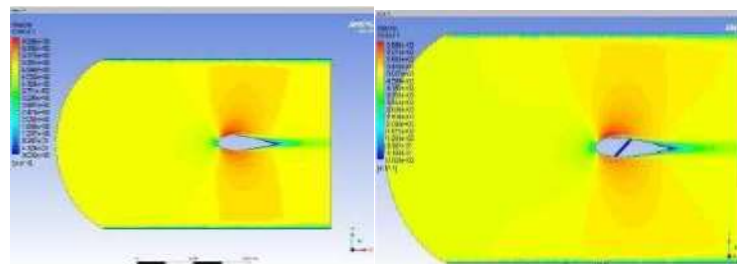
According to the fallout of the pressure plots, velocity plots, streamline, CL vs. attack angle, Cd vs attack angle, and CL against Cd graphs presented above, the vents have a greater lift force and CL than the creative designs. In comparison to the original airfoils, the vented ones create less drag force and drag coefficient. It has been shown that the vented design delays the stall, whereas the typical airfoil stops at 15° AOA and produces a rapid increase in both Lift and Drag values. According to the results, it is possible to employ the vents technique to connect the boundary layer to the top surface of an airfoil at higher aoa , increasing lift,decreasing drag.

**For 24021 Zero attack angle**

**5.127 Five m/s-**



**Figure 390 : Pressure at 0° for Both at Five m/s**



**Figure 391 : Velocity at 0° for Both at Five m/s**

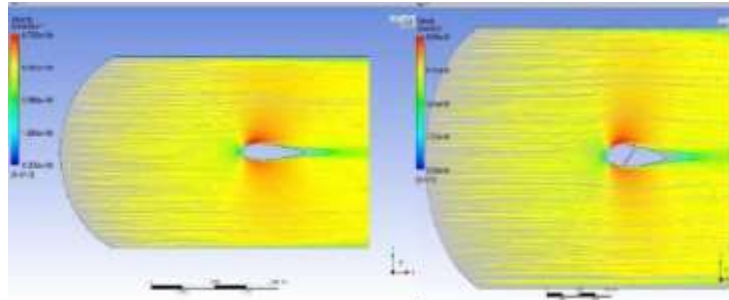


Figure 392 : Streamline at  $0^\circ$  for Both at Five m/s

5.128 Ten m/s-

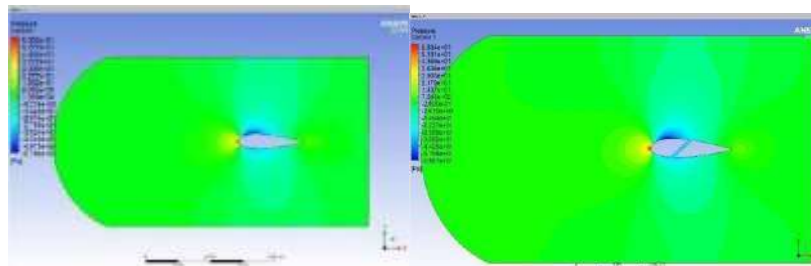


Figure 393 : Pressure at  $0^\circ$  for Both at Ten m/s

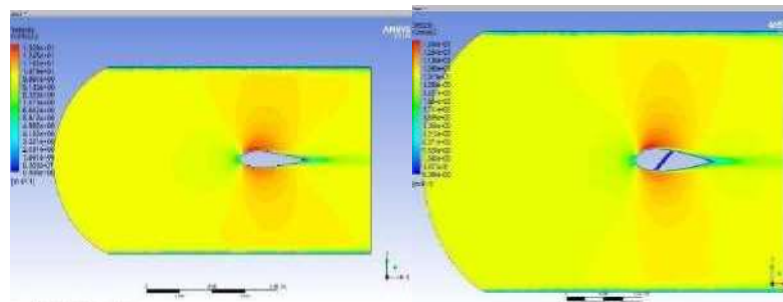


Figure 394 : Velocity at  $0^\circ$  for Both Ventat Ten m/s

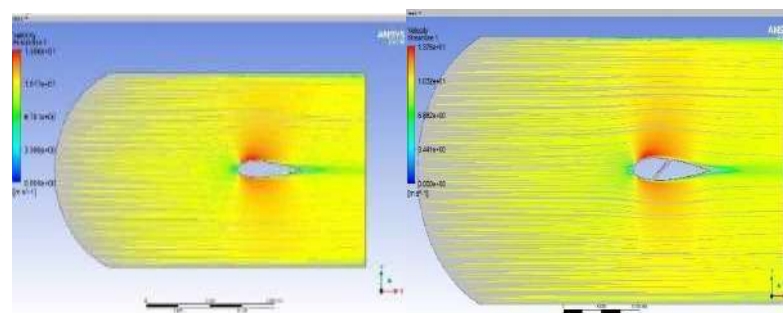


Figure 395 : Streamline at  $0^\circ$  for Both at Ten m/s

### 5.129 Fifteen m/s-

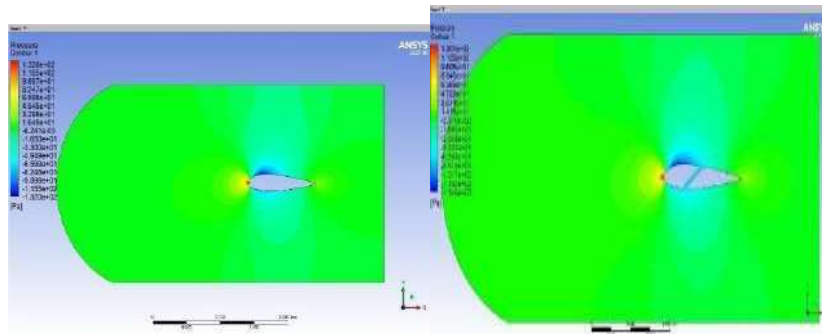


Figure 396 : Pressure at  $0^\circ$  for Both at fifteen m/s

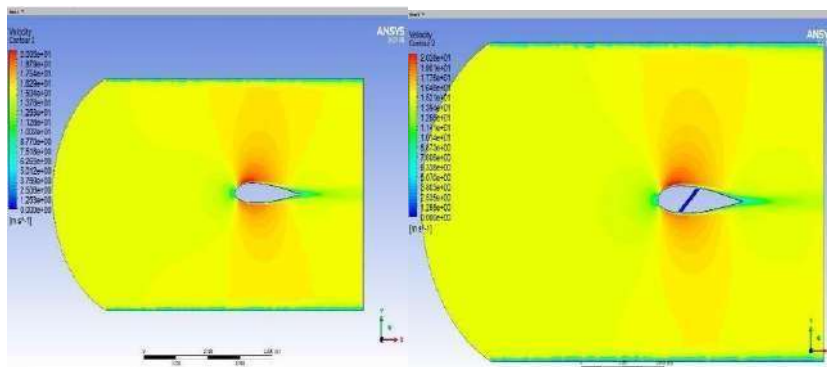


Figure 397 : Velocity at  $0^\circ$  for Both at fifteen m/s

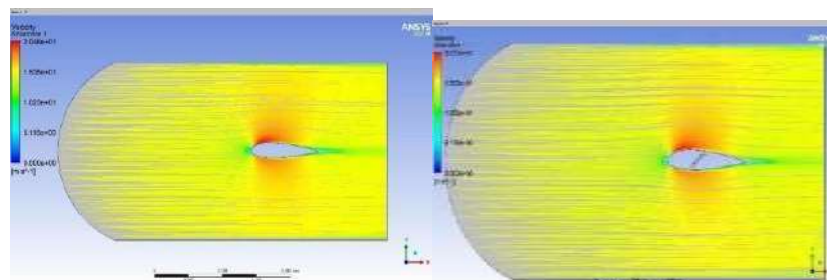


Figure 398 : Streamline at  $0^\circ$  for Both at fifteen m/s



### 5.130 Twenty m/s-

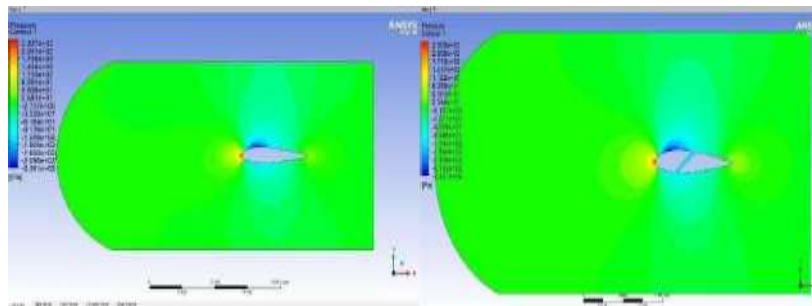


Figure 399 : Pressure at  $0^\circ$  for Both at Twenty m/s

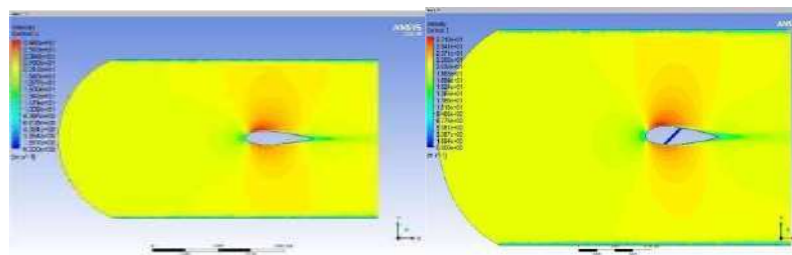


Figure 400 : Velocity at  $0^\circ$  for Both at Twenty m/s

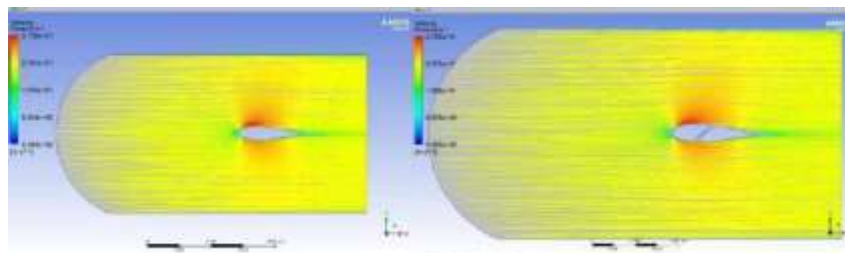


Figure 401 : Streamline at  $0^\circ$  for Both at Twenty m/s

### 5.131 Twenty Five m/s-

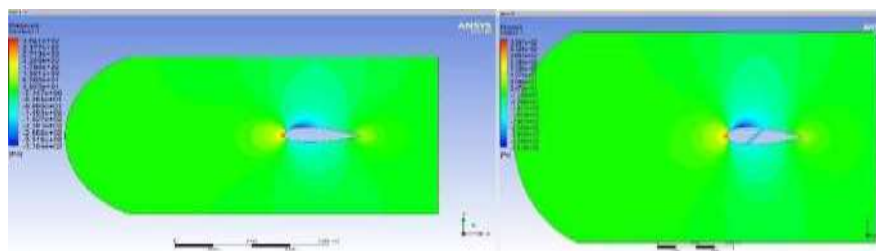


Figure 402 : Pressure at  $0^\circ$  for Both at Twenty-Five m/s

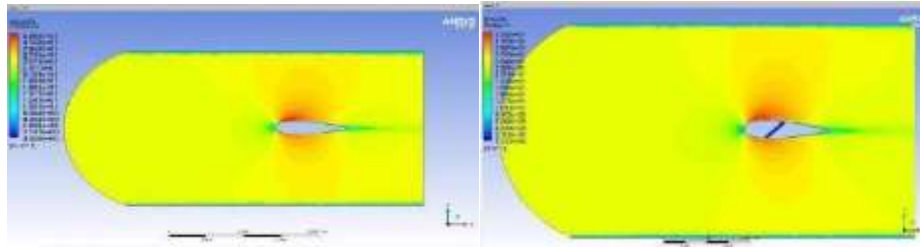


Figure 403 : Velocity at  $0^0$  for Both at Twenty-Five m/s

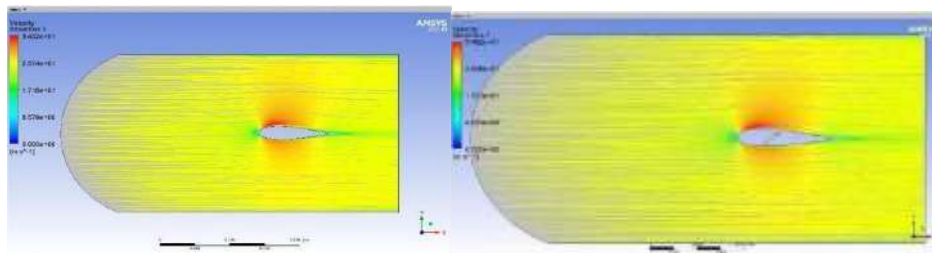


Figure 404 : Streamline at  $0^0$  for Both at Twenty-Five m/s

**5.132 Thirty m/s-**

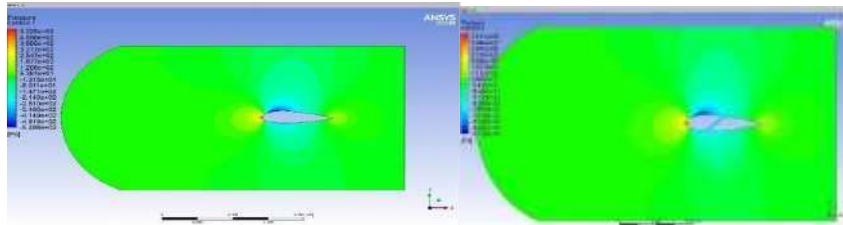


Figure 405 : Pressure at  $0^0$  for Both at Thirty m/s

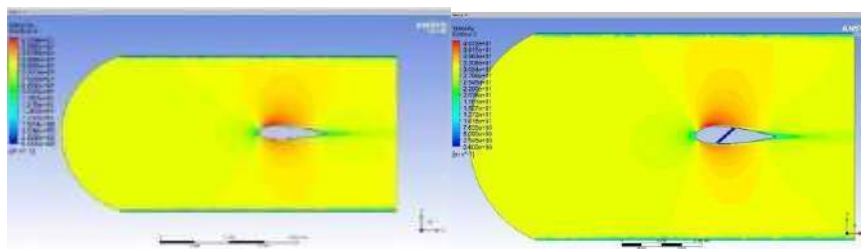


Figure 406 : Velocity at  $0^0$  for Both at Thirty m/s

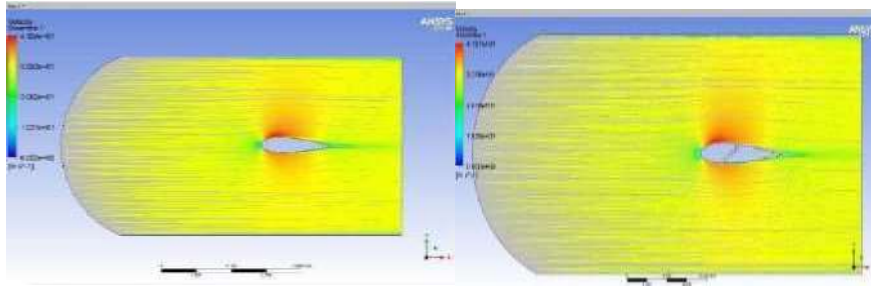


Figure 407 : Streamline at  $0^\circ$  for Both at Thirty m/s

### 5.133 Fifty m/s-

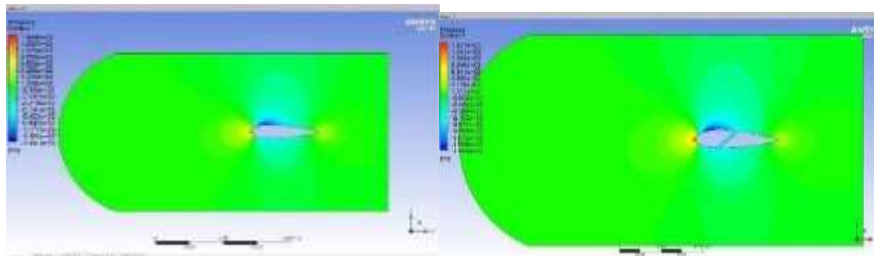


Figure 408 : Pressure at  $0^\circ$  for Both at Fifty m/s

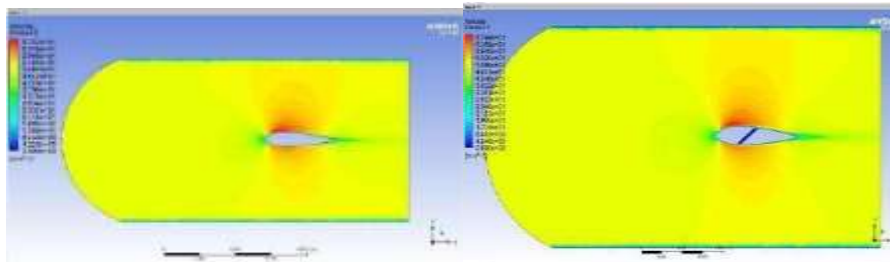


Figure 409 : Velocity at  $0^\circ$  for Both at Fifty m/s

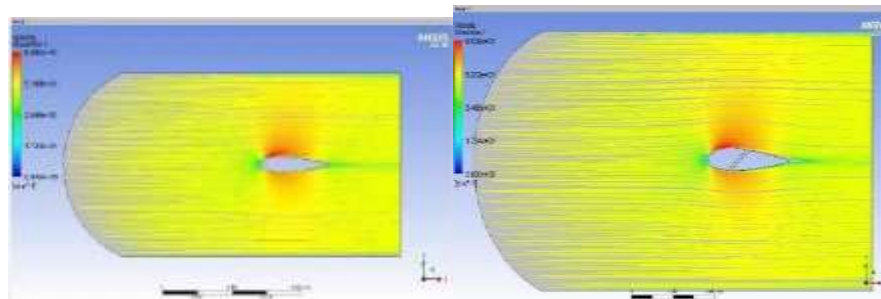


Figure 410 : Streamline at  $0^\circ$  for Both at Fifty m/s

Table of Design Points									
	A	B	C	D	E	F	G	H	I
1	Name	P1 - inletVel	P2 - drag-op	P3 - dragforce-op	P4 - lift-op	P5 - liftforce-op	Ret...	Retained Data	Note
2	Units	m s <sup>-1</sup>		N		N			
3	DP 0 (Current)	50	0.0021114	3.233	0.014856	22.748	<input checked="" type="checkbox"/>	<input checked="" type="checkbox"/>	
4	DP 1	30	0.00087359	1.3377	0.00475	7.2887	<input checked="" type="checkbox"/>	<input checked="" type="checkbox"/>	
5	DP 2	25	0.00063975	0.97961	0.0031352	4.8007	<input checked="" type="checkbox"/>	<input checked="" type="checkbox"/>	
6	DP 3	20	0.00043812	0.67067	0.0018034	2.7615	<input checked="" type="checkbox"/>	<input checked="" type="checkbox"/>	
7	DP 4	15	0.00027077	0.41462	0.00082088	1.257	<input checked="" type="checkbox"/>	<input checked="" type="checkbox"/>	
8	DP 5	10	0.0001401	0.21453	0.00025293	0.38729	<input checked="" type="checkbox"/>	<input checked="" type="checkbox"/>	
9	DP 6	5	4.8579E-05	0.074387	5.0076E-05	0.076679	<input checked="" type="checkbox"/>	<input checked="" type="checkbox"/>	
*							<input type="checkbox"/>		

Table31 : Drag and Lift force values,24021 at0° AOA

Table of Design Points									
	A	B	C	D	E	F	G	H	I
1	Name	P1 - parameter-1	P2 - drag-op	P3 - drag-force-op	P4 - lift-op	P5 - lift-force-op	Ret...	Retained Data	Note
2	Units	m s <sup>-1</sup>		N		N			
3	DP 24 (Current)	50	0.0021939	3.3594	0.013667	20.328	<input checked="" type="checkbox"/>	<input checked="" type="checkbox"/>	
4	DP 25	30	0.00089505	1.3705	0.0047027	7.2311	<input checked="" type="checkbox"/>	<input checked="" type="checkbox"/>	
5	DP 26	25	0.00065253	0.99918	0.0031635	4.8471	<input checked="" type="checkbox"/>	<input checked="" type="checkbox"/>	
6	DP 27	20	0.00044589	0.68079	0.001915	2.9323	<input checked="" type="checkbox"/>	<input checked="" type="checkbox"/>	
7	DP 28	15	0.00027337	0.4186	0.0008974	1.4696	<input checked="" type="checkbox"/>	<input checked="" type="checkbox"/>	
8	DP 29	10	0.00014071	0.21546	0.00037765	0.57827	<input checked="" type="checkbox"/>	<input checked="" type="checkbox"/>	
9	DP 30	5	4.8358E-05	0.074049	3.4724E-05	0.12573	<input checked="" type="checkbox"/>	<input checked="" type="checkbox"/>	
*							<input type="checkbox"/>		

Table32 : Drag and Lift force values, 24021 at 0°AOA

5.134 Five Attack angle : -

5.135 Five m/s-

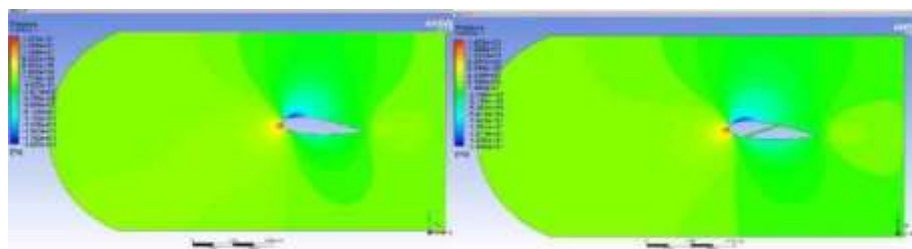


Figure 411 : Pressure at 5° for at Five m/s

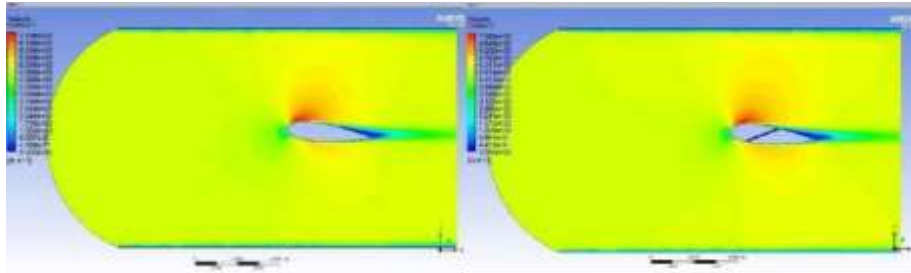


Figure 412 : Velocity at  $5^0$  for at Five m/s

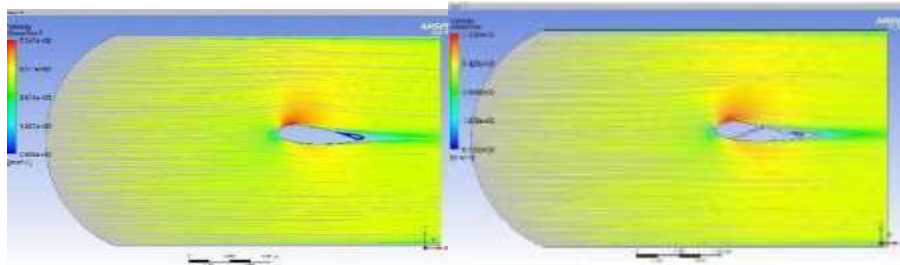


Figure 413 : Streamline at  $5^0$  for at Five m/s

**5.136 Ten m/s-**

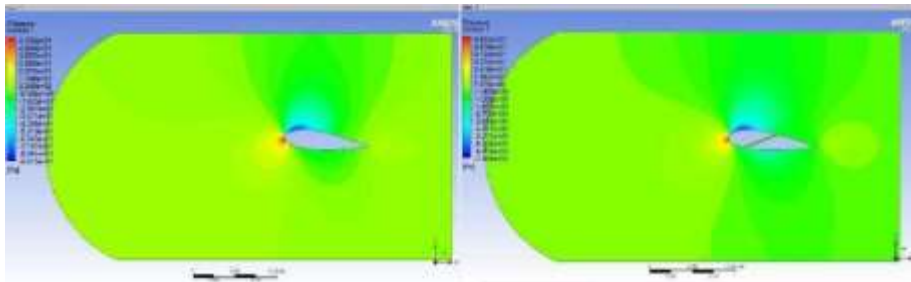


Figure 414 : Pressure at  $5^0$  for Both at Ten m/s

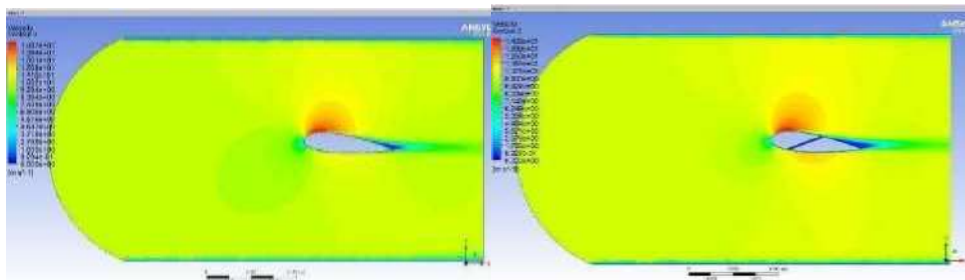


Figure 415 : Velocity at  $5^0$  for Both at Ten m/s

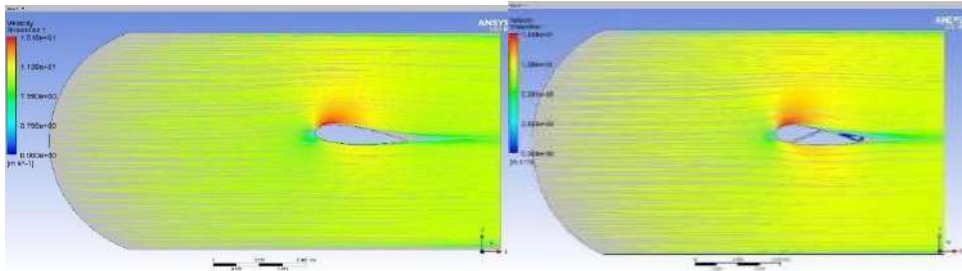


Figure 416 : Streamline at $5^{\circ}$  for Both at Ten m/s

**5.137 Fifteen m/s-**

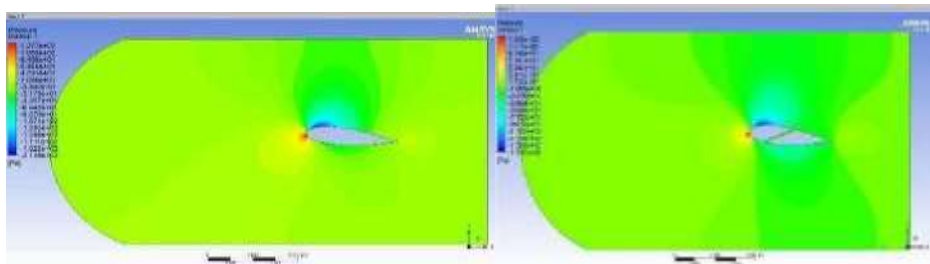


Figure 417 : Pressure at $5^{\circ}$  for at fifteen m/s

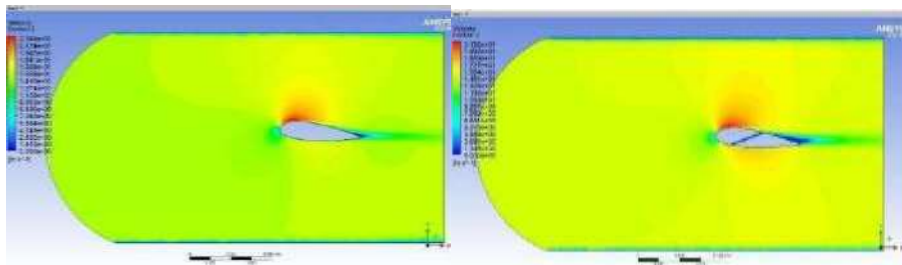


Figure 418 : at $5^{\circ}$  for at fifteen m/s

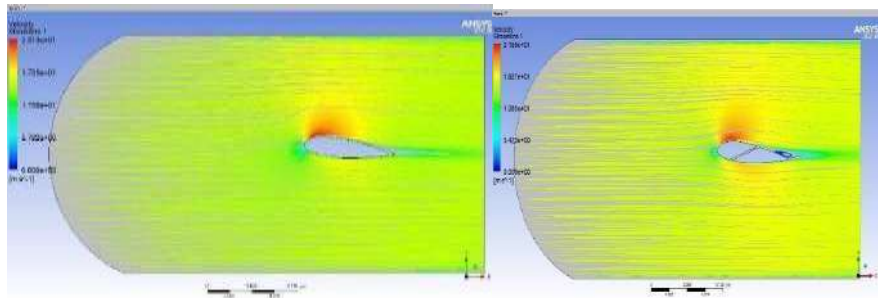


Figure 419 : Streamline at $5^{\circ}$  for at fifteen m/s

### 5.138 Twenty m/s-

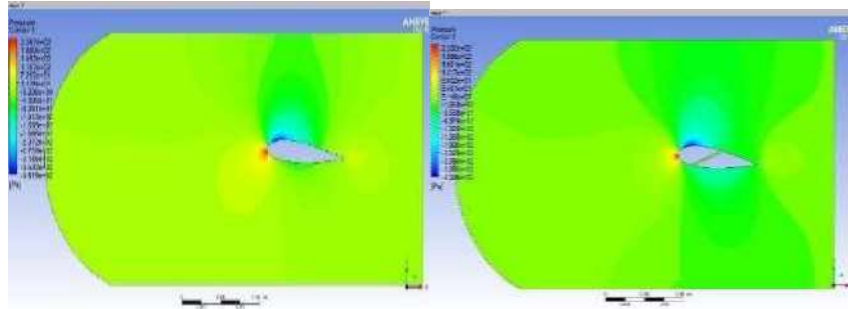


Figure 420 : Pressure at<sup>50</sup> for at Twenty m/s

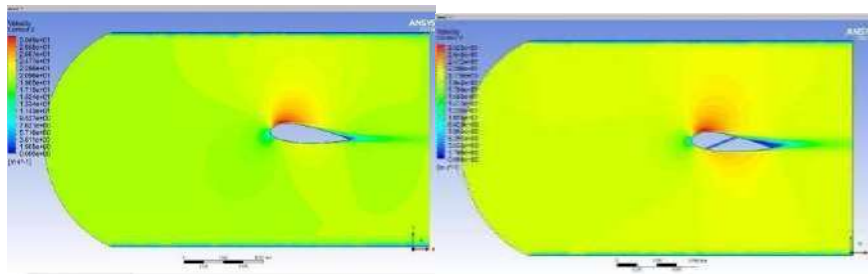


Figure 421 : Velocity at<sup>50</sup> for at Twenty m/s

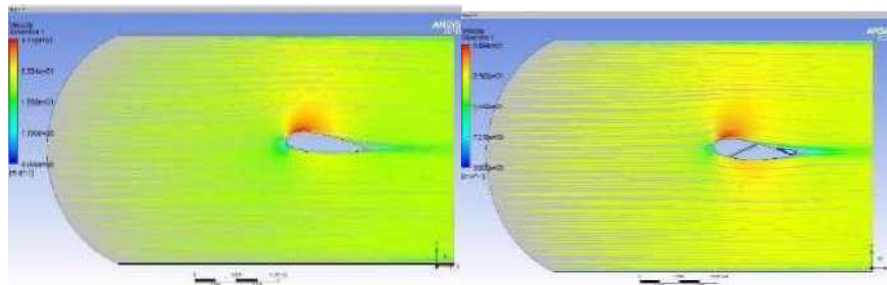


Figure 422 : Streamline at<sup>50</sup> for at Twenty m/s

### 5.139 Twenty-Five m/s-

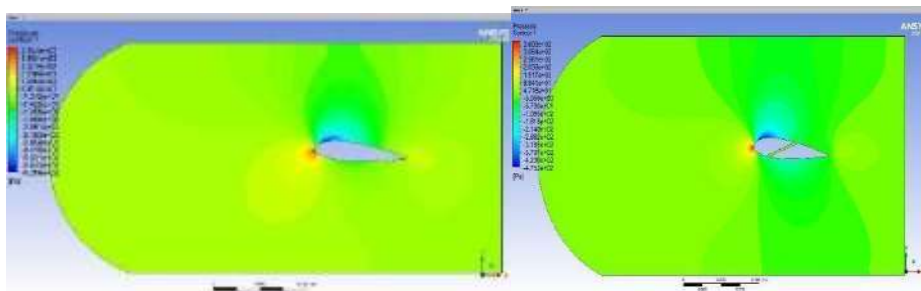


Figure 423 : Pressure at <sup>50</sup> for at twenty-Five m/s

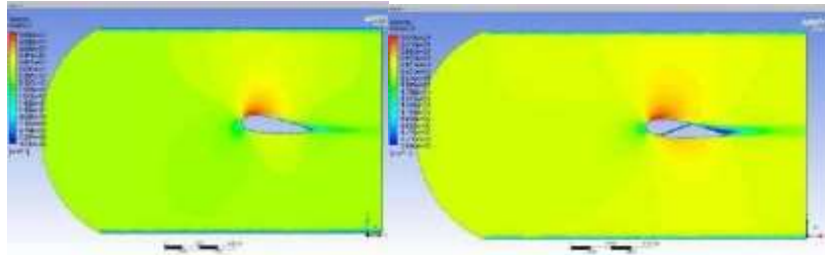


Figure 424 : Velocity at $5^0$  for at twenty-Five m/s

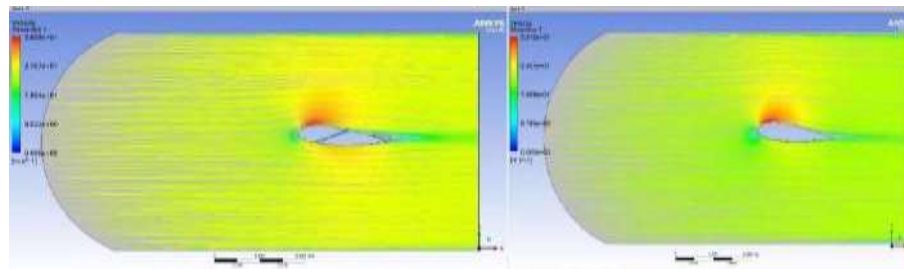


Figure 425 : Streamline at $5^0$  for at twenty-Five m/s

### 5.140 Thirty m/s-

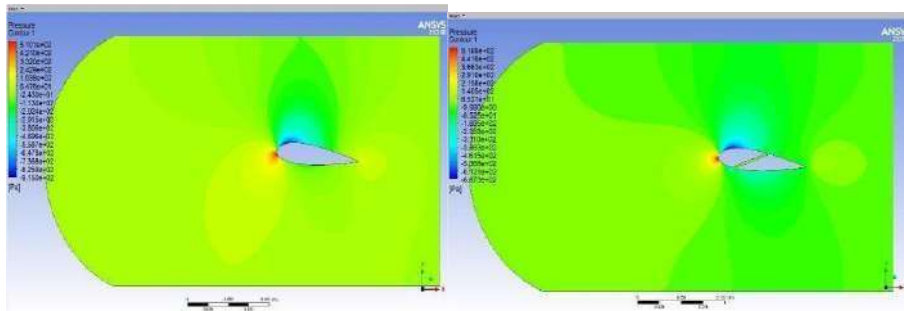


Figure 426 : Pressure at $5^0$  for Both at Thirty m/s

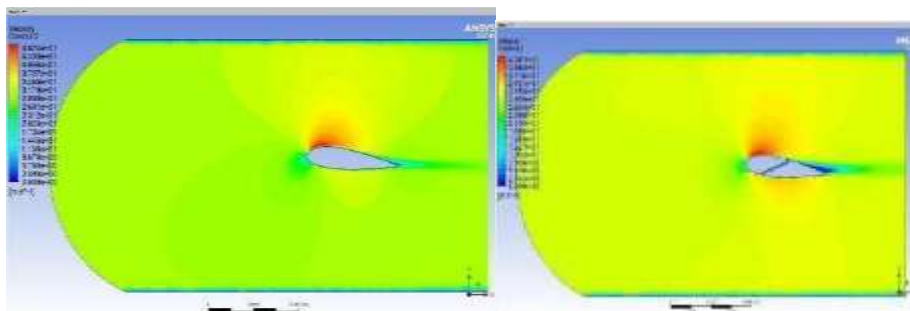


Figure 427 : Velocity at $5^0$  for Both at Thirty m/s



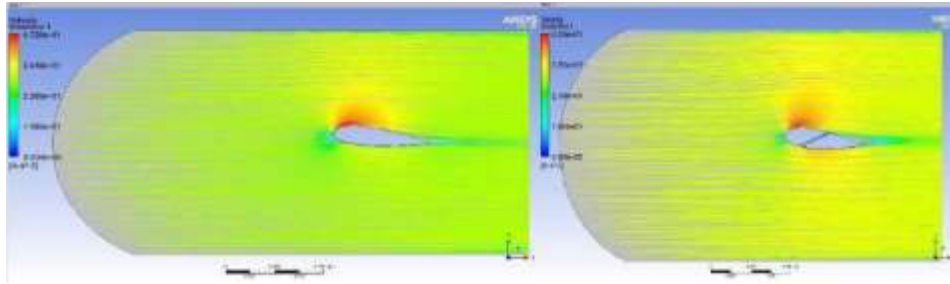


Figure 428 : Streamline at  $5^\circ$  for Both at Thirty m/s

**5.141 Fifteen m/s-**

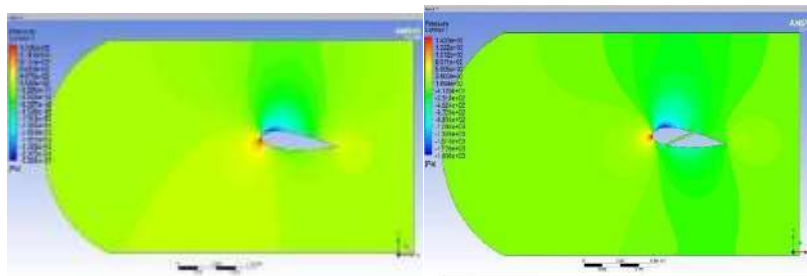


Figure 429 : Pressure at  $5^\circ$  for at fifteen m/s

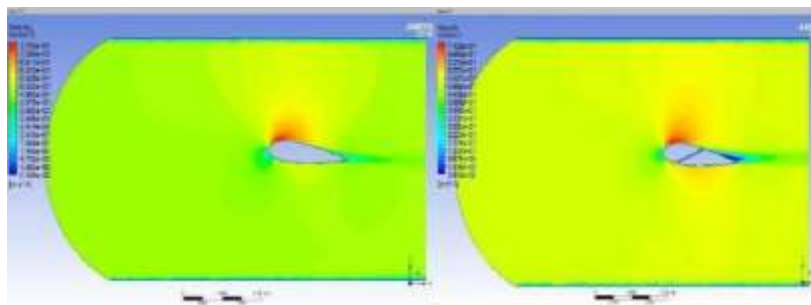


Figure 430 : Velocity at  $5^\circ$  for at fifteen m/s

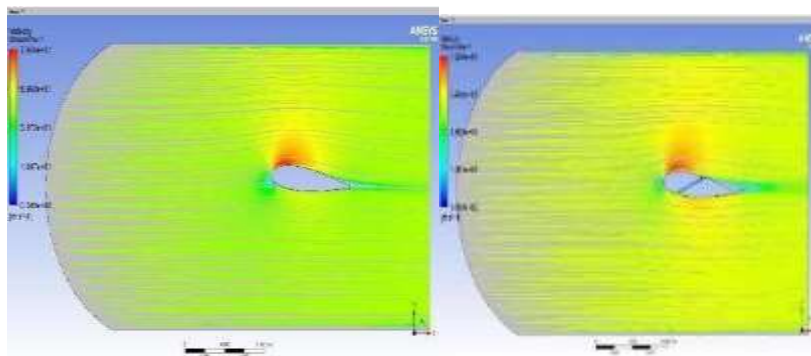


Figure 431 : Streamline at  $5^\circ$  for at fifteen m/s

Table of Design Points									
	A	B	C	D	E	F	G	H	
1	Name	P1 - parameter-1	P2 - drag-op	P3 - drag-force-op	P4 - lift-op	P5 - lift-force-op	Ret...	Retained Data	Note
2	Units	ms <sup>-1</sup>		N		N			
3	DP 0 (Current)	50	0.00251	3.8435	0.362906	97.397	<input checked="" type="checkbox"/>	<input checked="" type="checkbox"/>	
4	DP 1	30	0.001035	1.5949	0.021999	32.308	<input checked="" type="checkbox"/>	<input checked="" type="checkbox"/>	
5	DP 2	25	0.00075889	1.1521	0.014069	21.543	<input checked="" type="checkbox"/>	<input checked="" type="checkbox"/>	
6	DP 3	20	0.00052236	0.79989	0.0084867	12.998	<input checked="" type="checkbox"/>	<input checked="" type="checkbox"/>	
7	DP 4	15	0.0003652	0.49998	0.0049901	6.7223	<input checked="" type="checkbox"/>	<input checked="" type="checkbox"/>	
8	DP 5	10	0.0002791	0.25476	0.001889	2.5652	<input checked="" type="checkbox"/>	<input checked="" type="checkbox"/>	
9	DP 6	5	6.1462E-05	0.094112	0.00010075	0.47584	<input checked="" type="checkbox"/>	<input checked="" type="checkbox"/>	
*							<input type="checkbox"/>		

Table33 : Drag and Lift force values 24021 at 5°AOA

Table of Design Points									
	A	B	C	D	E	F	G	H	
1	Name	P1 - parameter-1	P2 - drag-op	P3 - drag-force-op	P4 - lift-op	P5 - lift-force-op	Ret...	Retained Data	Note
2	Units	ms <sup>-1</sup>		N		N			
3	DP 0 (Current)	50	0.0039277	6.0142	0.021585	33.052	<input checked="" type="checkbox"/>	<input checked="" type="checkbox"/>	
4	DP 1	30	0.0015344	2.3495	0.0072304	11.072	<input checked="" type="checkbox"/>	<input checked="" type="checkbox"/>	
5	DP 2	25	0.0010986	1.6822	0.0049165	7.5284	<input checked="" type="checkbox"/>	<input checked="" type="checkbox"/>	
6	DP 3	20	0.00075135	1.1199	0.003083	4.7209	<input checked="" type="checkbox"/>	<input checked="" type="checkbox"/>	
7	DP 4	15	0.00042932	0.6574	0.0018485	2.8306	<input checked="" type="checkbox"/>	<input checked="" type="checkbox"/>	
8	DP 5	10	0.00020203	0.32936	0.00099029	1.5164	<input checked="" type="checkbox"/>	<input checked="" type="checkbox"/>	
9	DP 6	5	6.2329E-05	0.095441	0.00024558	0.37604	<input checked="" type="checkbox"/>	<input checked="" type="checkbox"/>	
*							<input type="checkbox"/>		

Table34 : Drag and Lift force values 24021 at 5°AOA

5.142 Ten Attack angle : -

5.143 Five m/s-

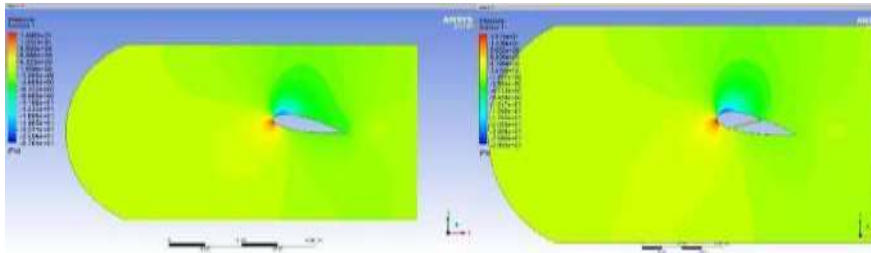


Figure 432 : Pressure at  $10^0$  for Both at Five m/s

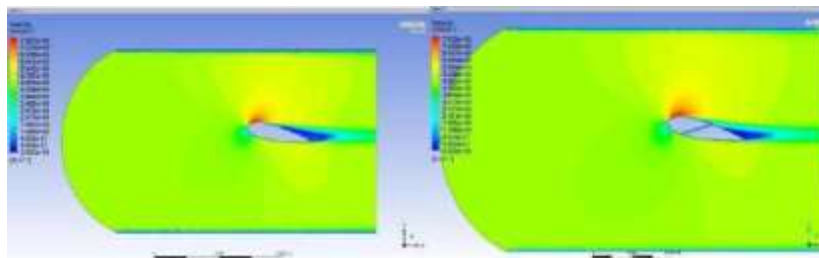


Figure 433 : VelocityPlot at  $10^0$  for Both at Five m/s

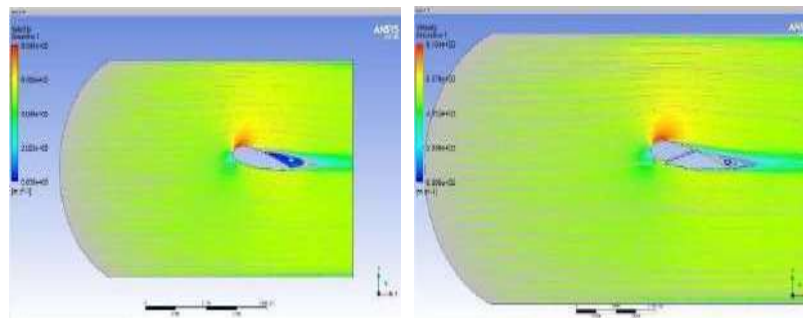
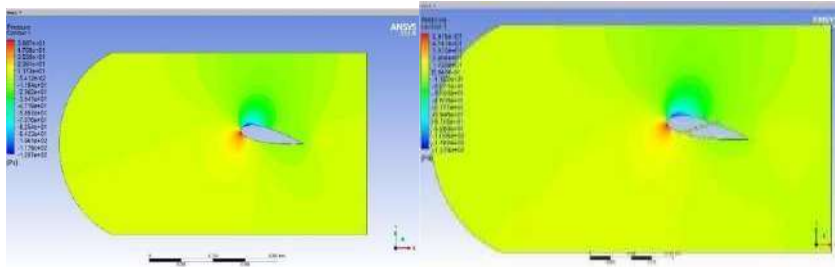
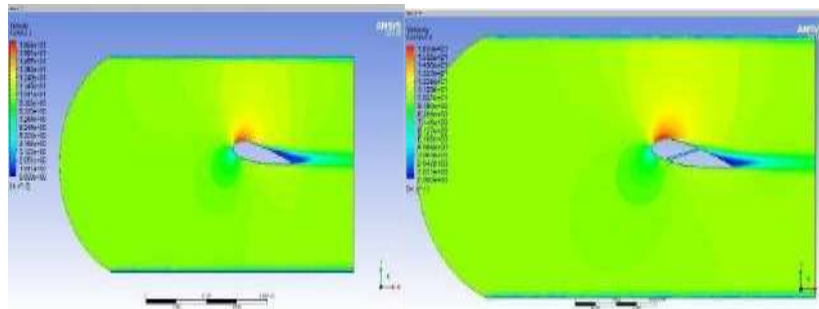


Figure 434 : Streamline at 100 for Both at Five m/s

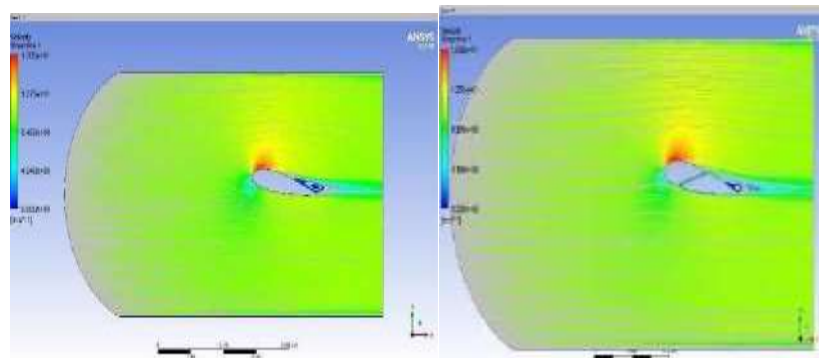
**5.144 Ten m/s-**



**Figure 435 : Pressure at $10^0$  for Both at Ten m/s**

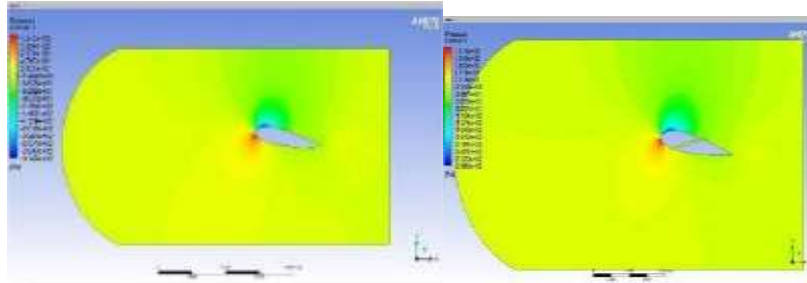


**Figure 436 : Velocity at $10^0$  for Both at Ten m/s**

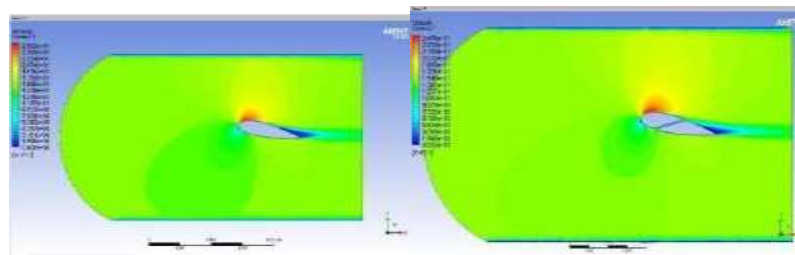


**Figure 437 : Streamline at $10^0$  for Both at Ten m/s**

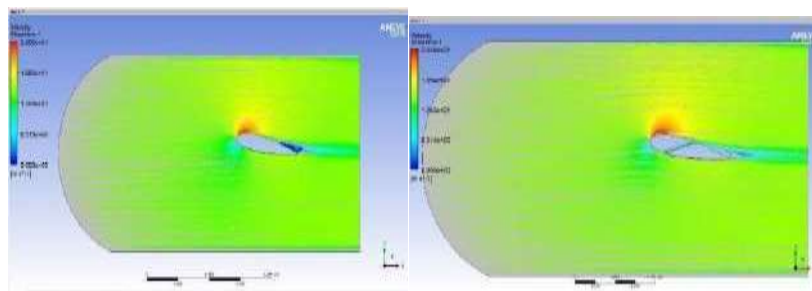
**5.145 Fifteen m/s-**



**Figure 438 : Pressure at $10^0$  for Both at fifteen m/s**

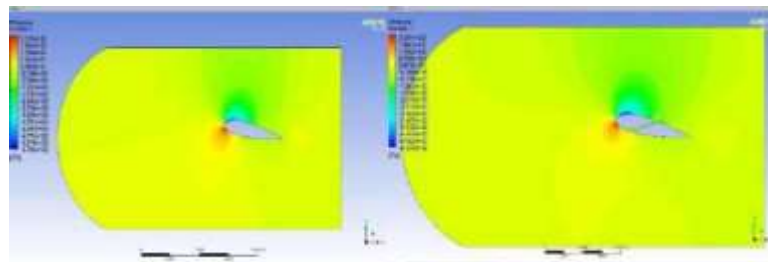


**Figure 439 : Velocity at $10^0$  for Both at fifteen m/s**



**Figure 440 : Streamline at $10^0$  for Both at fifteen m/s**

**5.146 Twenty m/s-**



**Figure 441 : Pressure at $10^0$  for Both at Twenty m/s**

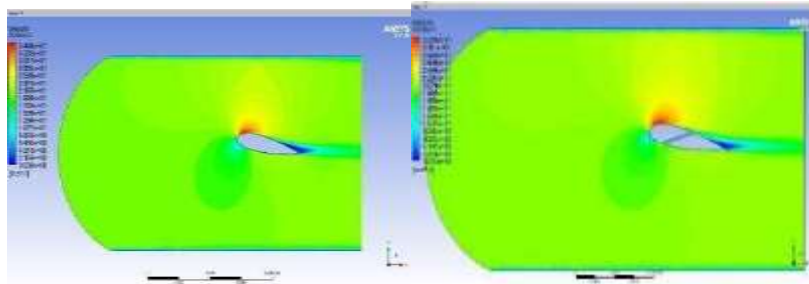


Figure 442 : Velocity at  $10^0$  for Both at Twenty m/s

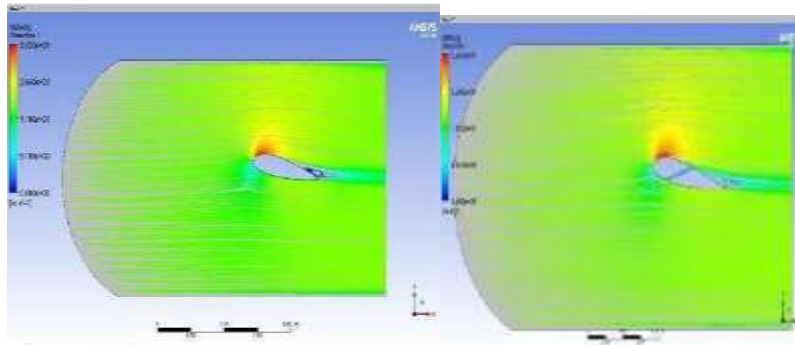


Figure 443 : Streamline at  $10^0$  for Both at Twenty m/s

**5.147 Twenty Five m/s-**

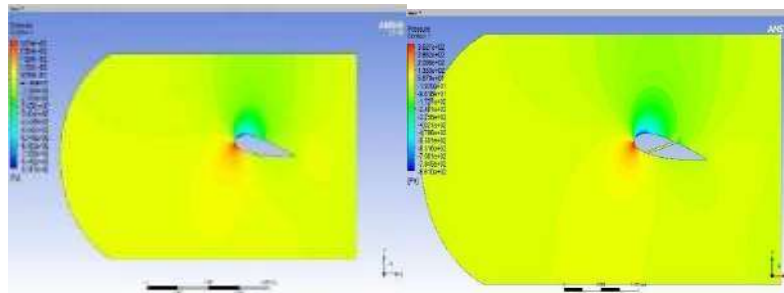


Figure 444 : Pressure at  $10^0$  for Both at twenty Five m/s

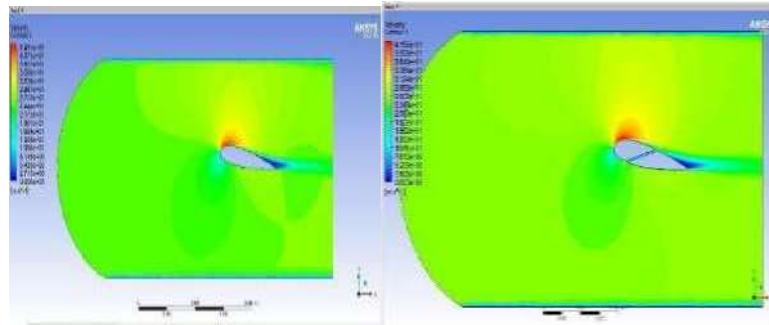


Figure 445 : VelocityPlot10<sup>0</sup> for Both at twenty-Five m/s

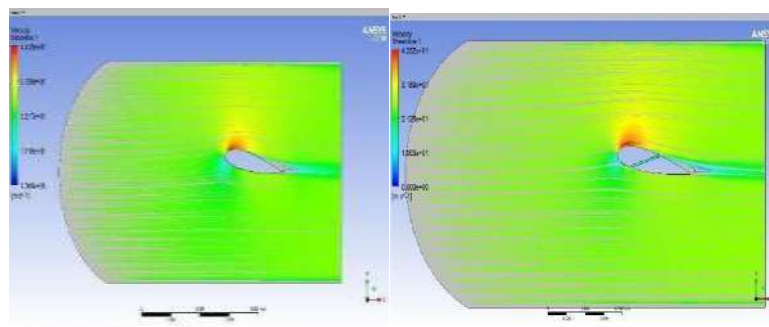


Figure 446 : Streamline atPlot10<sup>0</sup> for Both at twenty Five

**5.148 Thirty m/s-**

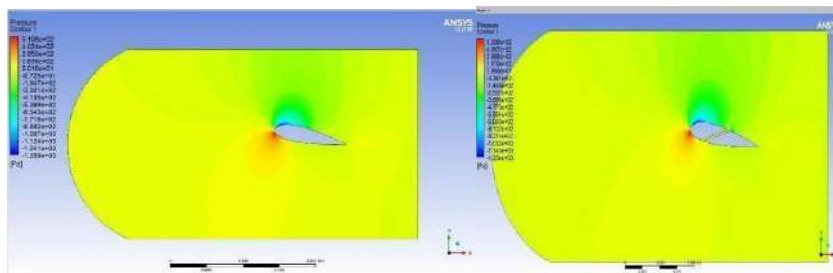


Figure 447 : Pressure at10<sup>0</sup> for Both at Thirty m/s

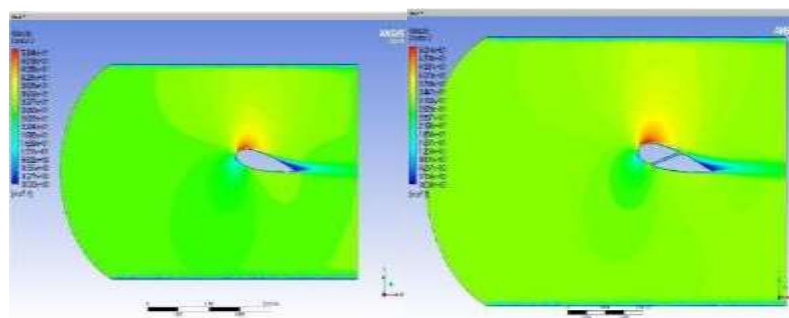


Figure 448 : Velocity at 10<sup>0</sup> for Both at Thirty m/s

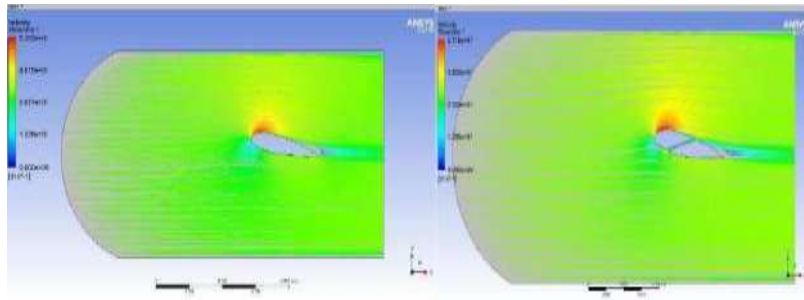


Figure 449 : Streamline at  $10^0$  for Both at Thirty m/s

**5.149 Fifty m/s-**

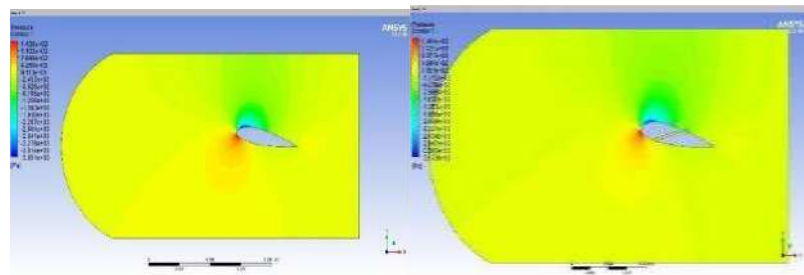


Figure 450 : Pressure at  $10^0$  for Both at Fifty m/s

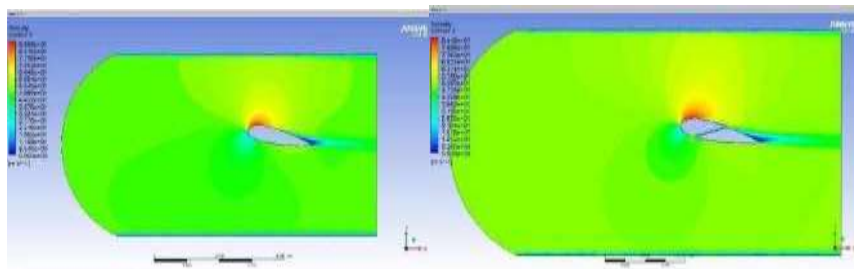


Figure 451 : Velocity at  $10^0$  for Both at Fifty m/s

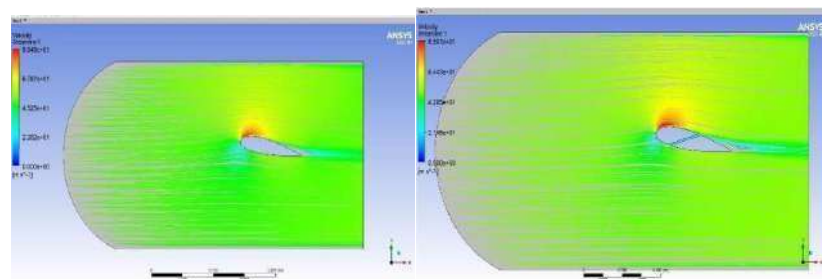


Figure 452 : Streamline at  $10^0$  for Both at Fifty m/s



Table of Design Points									
	A	B	C	D	E	F	G	H	I
1	Name	P1-inletVel	P2-drag-op	P3-dragforce-op	P4-lift-op	P5-liftforce-op	Ret...	Retained Data	Note
2	Units	m s <sup>-1</sup>		N		N			
3	DP 0 (Current)	50	0.004251	6.4697	0.197219	148.67	<input checked="" type="checkbox"/>	<input checked="" type="checkbox"/>	
4	DP 1	30	0.0017899	2.6627	0.12541	46.828	<input checked="" type="checkbox"/>	<input checked="" type="checkbox"/>	
5	DP 2	25	0.0012714	1.9469	0.12363	33.615	<input checked="" type="checkbox"/>	<input checked="" type="checkbox"/>	
6	DP 3	20	0.00087045	1.3329	0.113504	20.678	<input checked="" type="checkbox"/>	<input checked="" type="checkbox"/>	
7	DP 4	15	0.00053935	0.82588	0.1071244	10.909	<input checked="" type="checkbox"/>	<input checked="" type="checkbox"/>	
8	DP 5	10	0.00027897	0.42717	0.1028467	4.3544	<input checked="" type="checkbox"/>	<input checked="" type="checkbox"/>	
9	DP 6	5	9.4712E-05	0.14426	0.100599	0.15734	<input checked="" type="checkbox"/>	<input checked="" type="checkbox"/>	
*							<input type="checkbox"/>		

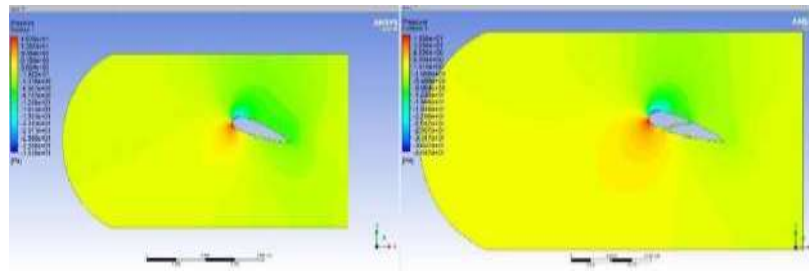
Table35 : Drag and Lift force values,24021 at 10° AOA

Table of Design Points									
	A	B	C	D	E	F	G	H	I
1	Name	P1-parameter-1	P2-drag-op	P3-dragforce-op	P4-lift-op	P5-liftforce-op	Ret...	Retained Data	Note
2	Units	m s <sup>-1</sup>		N		N			
3	DP 6 (Current)	50	0.0045673	7.6062	0.08418	128.9	<input checked="" type="checkbox"/>	<input checked="" type="checkbox"/>	
4	DP 7	30	0.0019476	2.9623	0.029133	44.61	<input checked="" type="checkbox"/>	<input checked="" type="checkbox"/>	
5	DP 8	25	0.0013991	2.1424	0.019882	30.445	<input checked="" type="checkbox"/>	<input checked="" type="checkbox"/>	
6	DP 9	20	0.00093628	1.4307	0.012423	19.023	<input checked="" type="checkbox"/>	<input checked="" type="checkbox"/>	
7	DP 10	15	0.00056084	0.85878	0.006769	10.365	<input checked="" type="checkbox"/>	<input checked="" type="checkbox"/>	
8	DP 11	10	0.00027709	0.42429	0.0034395	4.3547	<input checked="" type="checkbox"/>	<input checked="" type="checkbox"/>	
9	DP 12	5	8.6576E-05	0.12563	0.00060066	0.92006	<input checked="" type="checkbox"/>	<input checked="" type="checkbox"/>	
*							<input type="checkbox"/>		

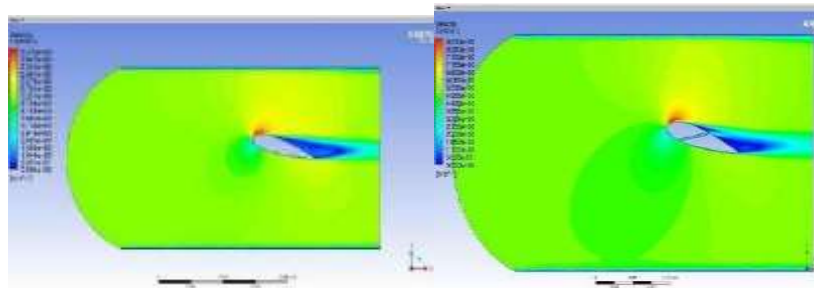
Table36 : Drag and Lift force values,24021 at 10° AOA

**5.150 Five attack angle : -**

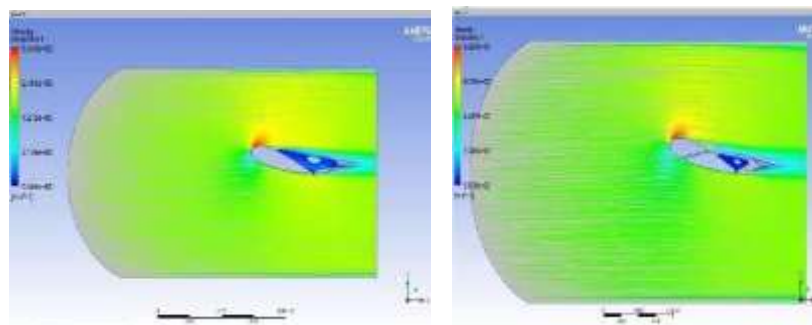
**5.151 Five m/s-**



**Figure 453 : Pressure at15° for Both atFive m/s**

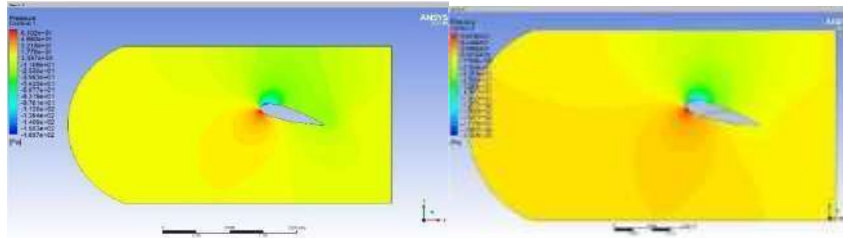


**Figure 454 : Velocity at15° for Both atFive m/s**

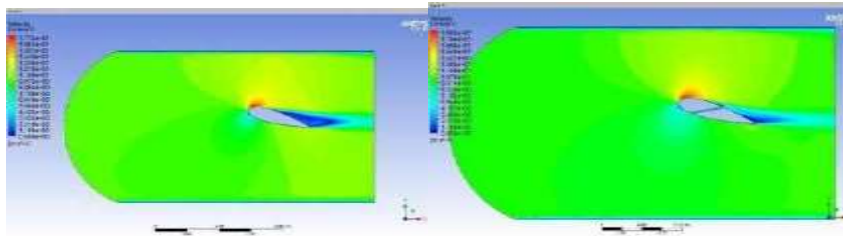


**Figure 455 : Streamline at15° for Both atFive m/s**

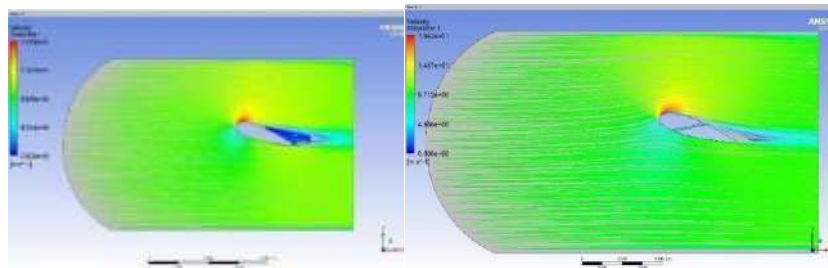
**5.152 Ten m/s-**



**Figure 456 : Pressure at15° for Both at Ten m/s**

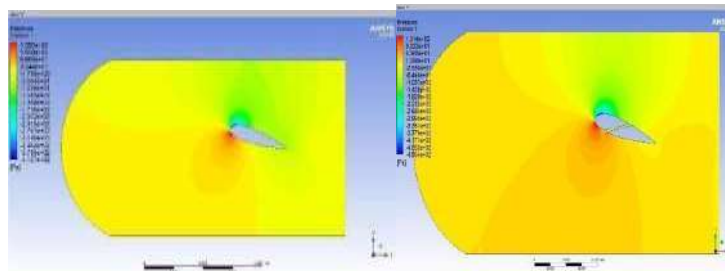


**Figure 457 : Velocity at15° for Both at Ten m/s**



**Figure 458 : Streamline at15° for Both at Ten m/s**

**5.153 Fifteen m/s-**



**Figure 459 : Pressure at15° for Both at fifteen m/s**

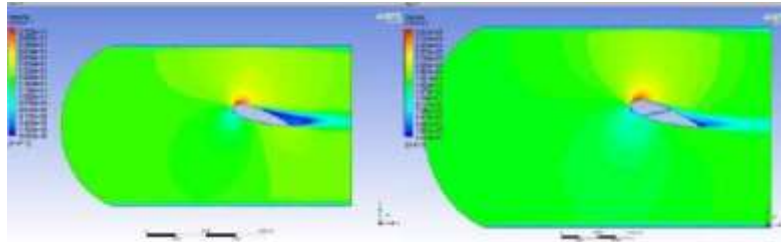


Figure 460 : Velocity at  $15^\circ$  for Both at fifteen m/s

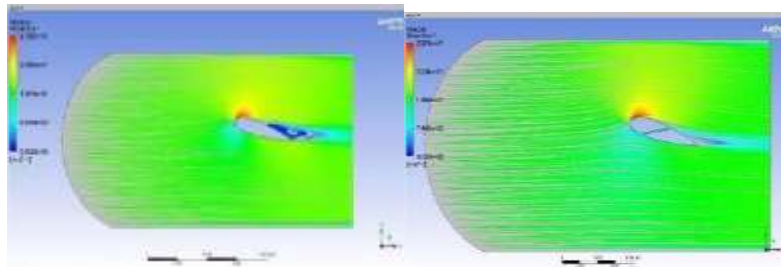


Figure 461 : Streamline at  $15^\circ$  for Both at fifteen m/s

**5.154 Twenty m/s-**

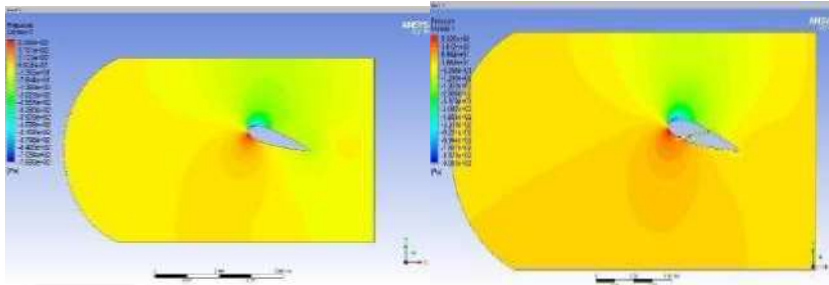


Figure 462 : Pressure at  $15^\circ$  for Both at Twenty m/s

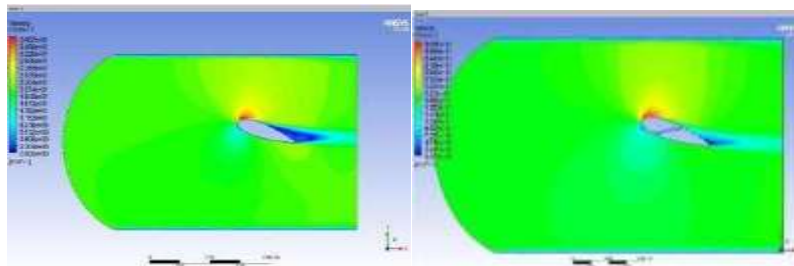


Figure 463 : Velocity at  $15^\circ$  for Both at Twenty m/s

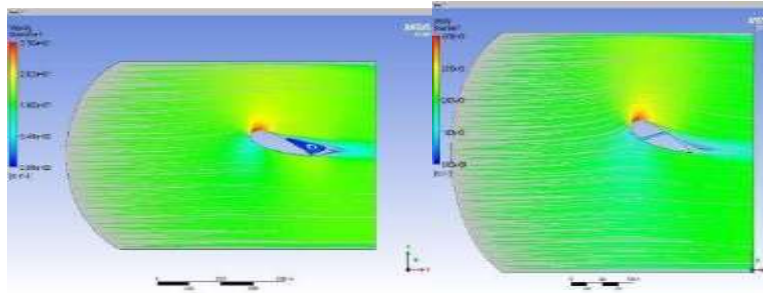


Figure 464 : Streamline at 15° for Both at Twenty m/s

**5.155 Twenty Five m/s-**

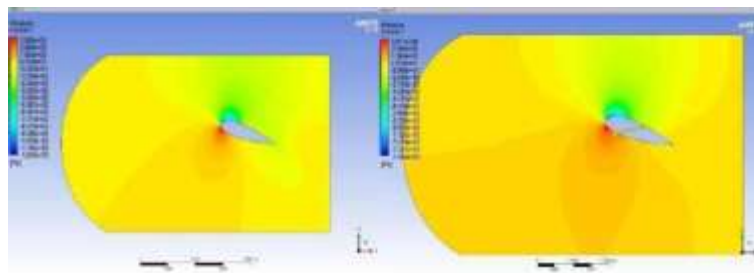


Figure 465 : Pressure at 15° for Both Vent at twenty-Five m/s

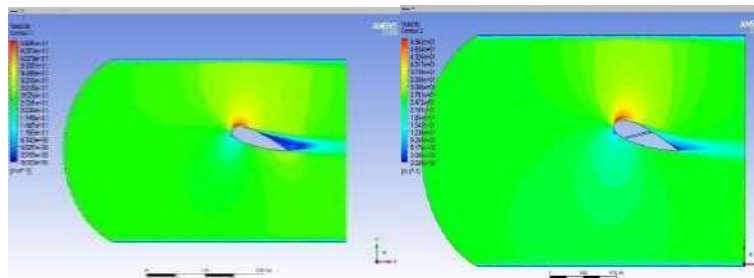


Figure 466 : Velocity at 15° for Both Vent at twenty-Five m/s

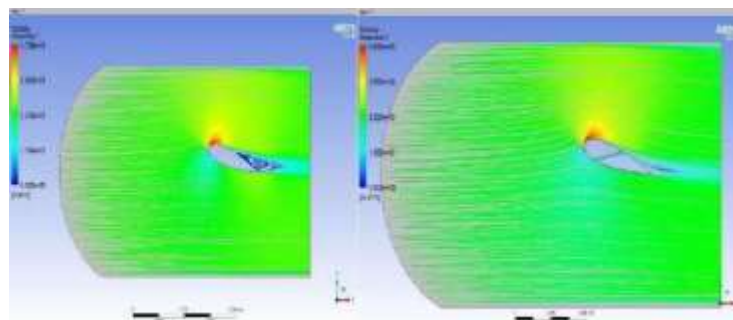


Figure 467 : Streamline at 15° for Both Vent at twenty-Five m/s

### 5.156 Thirty m/s-

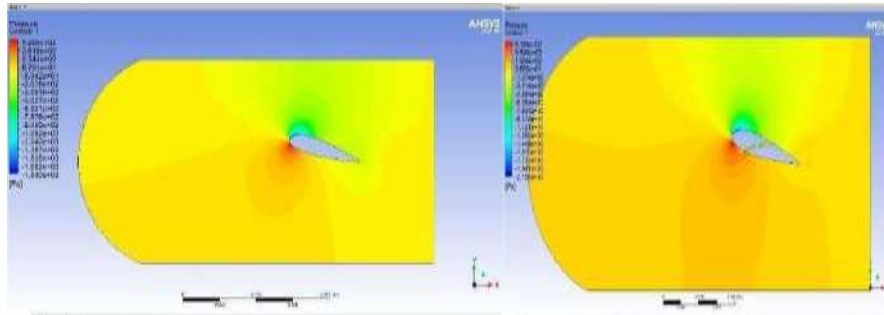


Figure 468 : Pressure at 15° for Both at Thirty m/s

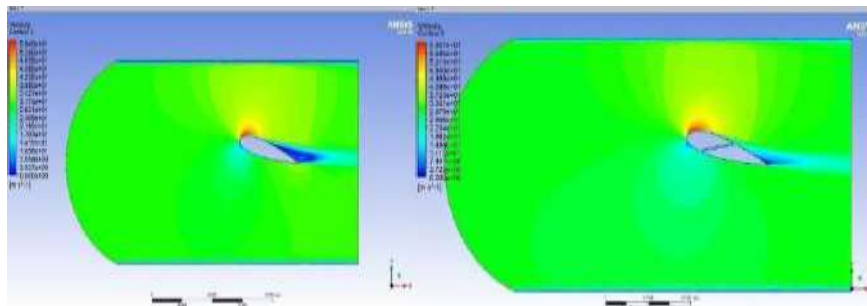


Figure 469 : Velocity at 15° for Both at Thirty m/s

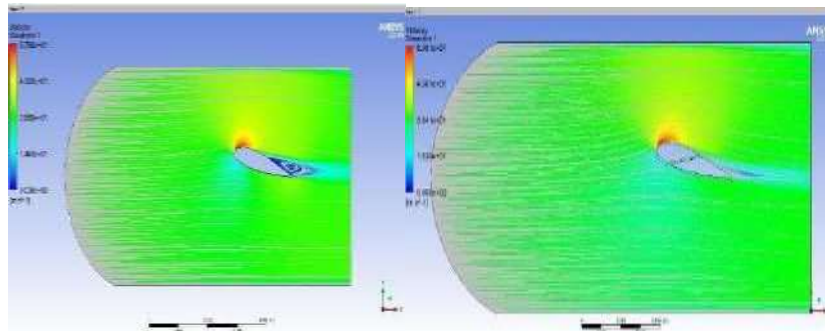


Figure 470 : Streamline at 15° for Both at Thirty m/s

### 5.157 Fifty m/s-

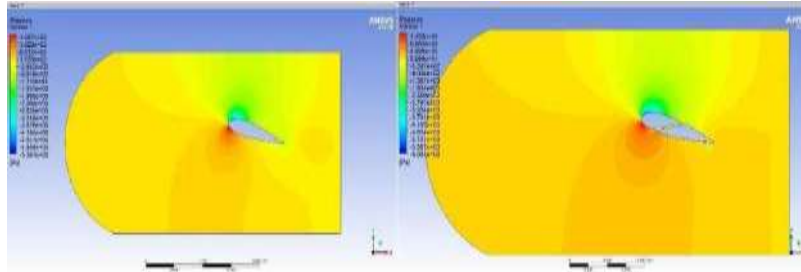


Figure 471 : Pressure at 15° for Both at Fifty m/s

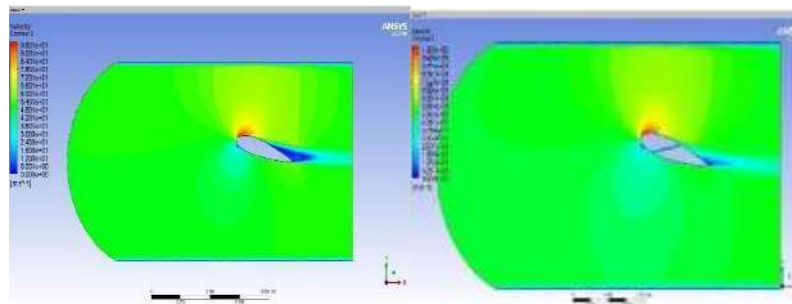


Figure 472 : Velocity at 15° for Both at Fifty m/s

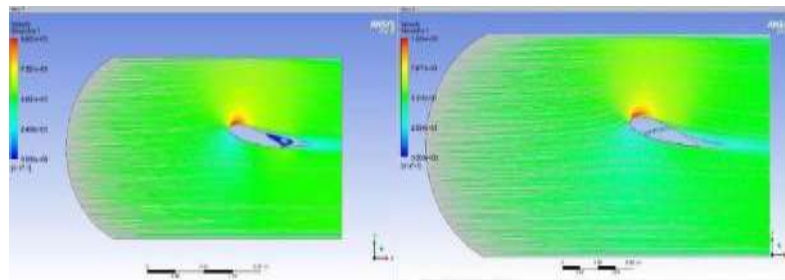


Figure 473 : Streamline at 15° for Both at Fifty m/s

Table of Design Points									
	A	B	C	D	E	F	G	H	I
1	Name	P1 - inlets	P2 - drag-co	P3 - drag force-co	P4 - lift-co	P5 - lift force-co	Ret...	Retained Data	Note
2	Units	m s <sup>-1</sup>		N		N			
3	DP 1 (Linear)	50	0.002409	12.623	0.118	180.59	<input checked="" type="checkbox"/>	<input checked="" type="checkbox"/>	
4	DP 1	30	0.003312	5.0715	0.039627	60.966	<input checked="" type="checkbox"/>	<input checked="" type="checkbox"/>	
5	DP 2	25	0.0024004	3.5756	0.02691	41.205	<input checked="" type="checkbox"/>	<input checked="" type="checkbox"/>	
6	DP 3	20	0.0016264	2.4904	0.016602	25.401	<input checked="" type="checkbox"/>	<input checked="" type="checkbox"/>	
7	DP 4	15	0.00096694	1.5113	0.008736	13.588	<input checked="" type="checkbox"/>	<input checked="" type="checkbox"/>	
8	DP 5	10	0.00046394	0.75615	0.003623	5.5477	<input checked="" type="checkbox"/>	<input checked="" type="checkbox"/>	
9	DP 5	5	0.00015638	0.23945	0.00074637	1.1459	<input checked="" type="checkbox"/>	<input checked="" type="checkbox"/>	
=							<input type="checkbox"/>	<input type="checkbox"/>	

Table37 : Drag and Lift force values,24021 at 15° AOA

Table of Design Points										
	A	B	C	D	E	F	G	H		
1	Name	P1 - parameter-1	P2 - drag-op	P3 - drag-force-op	P4 - lift-op	P5 - lift-force-op	Ret...	Retained Data	Not	
2	Units	m s <sup>-1</sup>		N		N				
3	DP 12 (Current)	50	0.00704	10.78	0.14114	216.12	<input checked="" type="checkbox"/>	<input checked="" type="checkbox"/>		
4	DP 13	30	0.0027272	4.176	0.049139	75.244	<input checked="" type="checkbox"/>	<input checked="" type="checkbox"/>		
5	DP 14	25	0.0019532	2.9908	0.033641	51.513	<input checked="" type="checkbox"/>	<input checked="" type="checkbox"/>		
6	DP 15	20	0.0013042	1.9971	0.021111	32.326	<input checked="" type="checkbox"/>	<input checked="" type="checkbox"/>		
7	DP 16	15	0.00078061	1.1953	0.011455	17.541	<input checked="" type="checkbox"/>	<input checked="" type="checkbox"/>		
8	DP 17	10	0.00039138	0.5993	0.0046816	7.1688	<input checked="" type="checkbox"/>	<input checked="" type="checkbox"/>		
9	DP 18	5	0.00013793	0.21121	0.00090507	1.3859	<input checked="" type="checkbox"/>	<input checked="" type="checkbox"/>		
*							<input type="checkbox"/>	<input type="checkbox"/>		

Table38 : Drag and Lift force values,24021 at 15°AOA

### 5.158 Twenty attack angle : -

### 5.159 Five m/s-

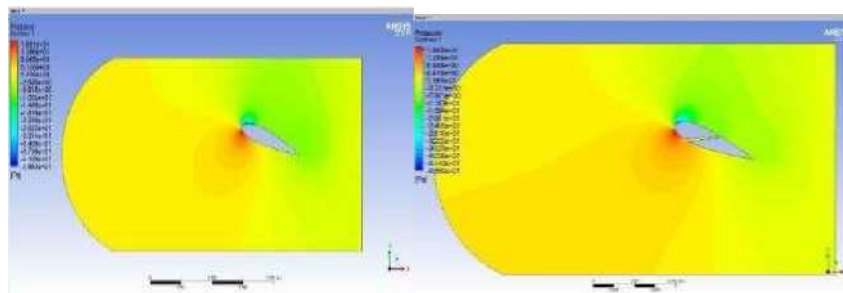


Figure 474 : Pressure at 20° for Both at Twenty m/s

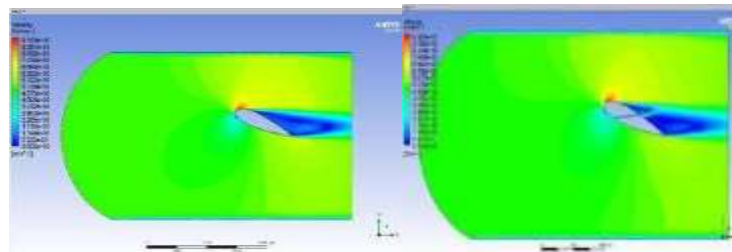


Figure 475 : Velocity at 20° for Both at Twenty m/s

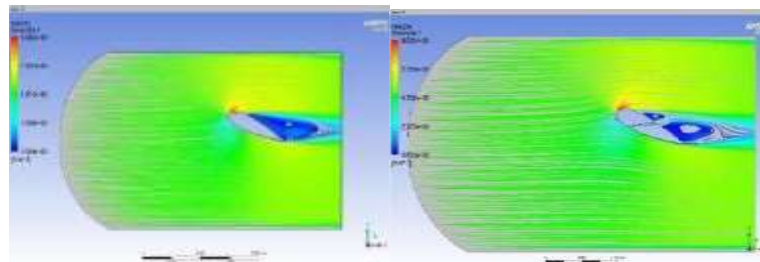
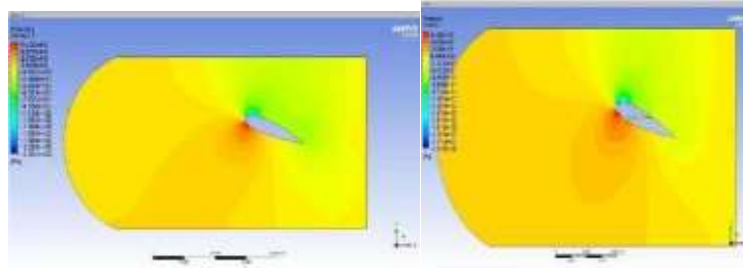


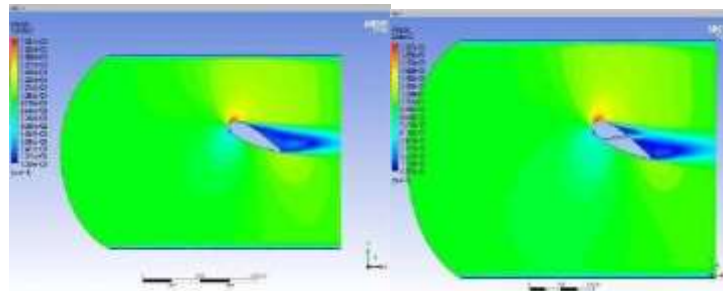
Figure 476 : Streamline at 20° for Both at Twenty m/s



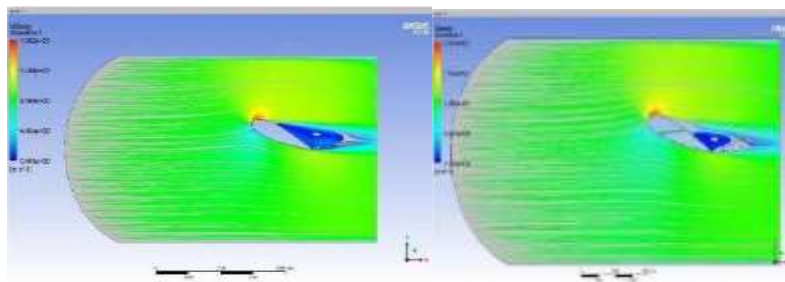
**5.160 Ten m/s-**



**Figure 477 : Pressure at $20^\circ$  for Both at Ten m/s**

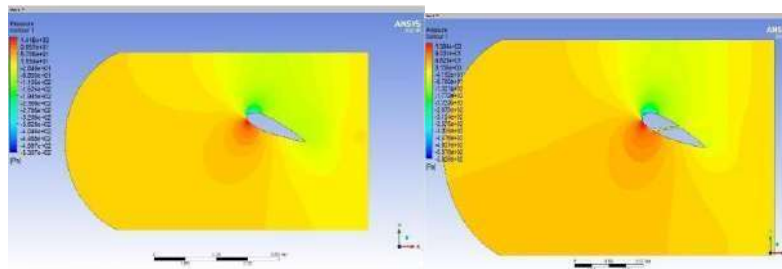


**Figure 478 : Velocity at $20^\circ$  for Both at Ten m/s**



**Figure 479 : Streamline at $20^\circ$  for Both at Ten m/s**

**5.161 Fifteen m/s-**



**Figure 480 : Pressure at $20^\circ$  for Both at fifteen m/s**

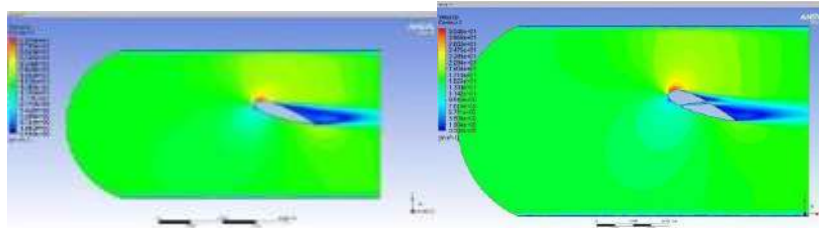


Figure 481 : Velocity at  $20^\circ$  for Both at fifteen m/s

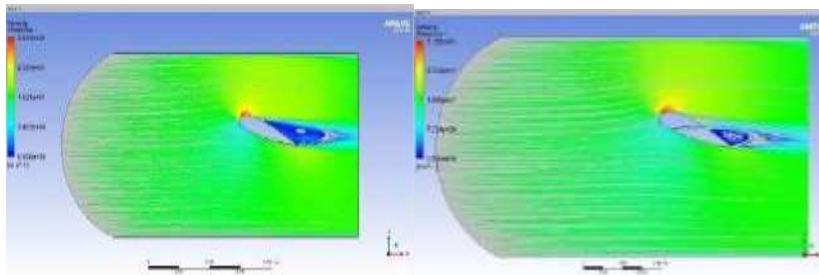


Figure 482 : Streamline at  $20^\circ$  for Both at fifteen m/s

### 5.162 Twenty m/s-

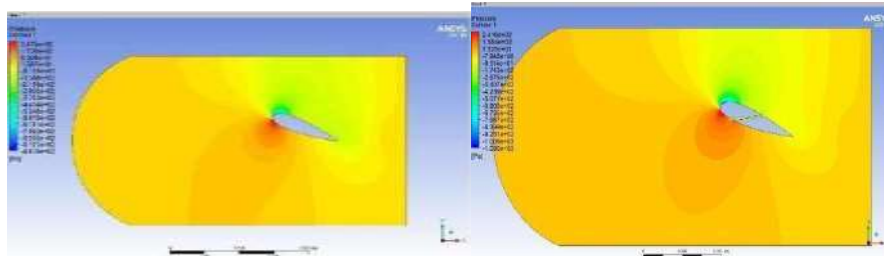


Figure 483 : Pressure at  $20^\circ$  for Both at Twenty m/s

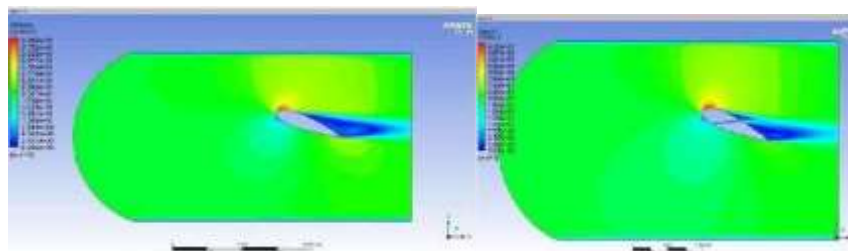


Figure 484 : Velocity at  $20^\circ$  for Both at Twenty m/s

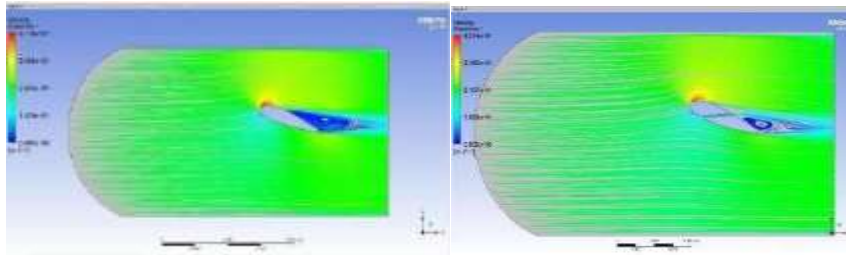


Figure 485 : Streamline at 20° for Both at Twenty m/s

### 5.163 Twenty Five m/s-

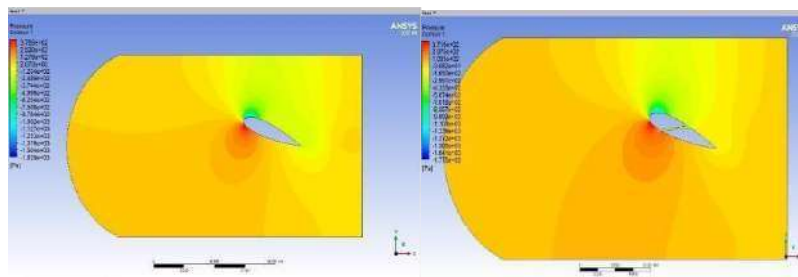


Figure 486 : Pressure at 200 for Both at twenty-Five m/s

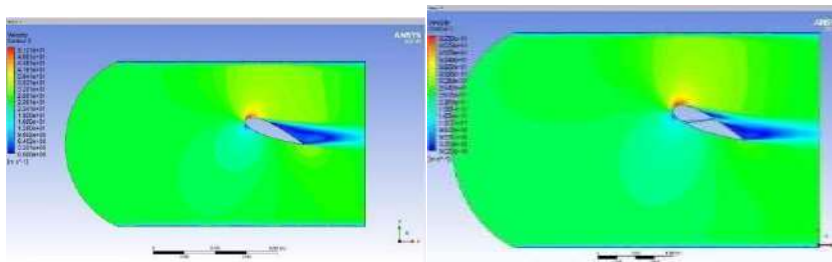


Figure 487 : Velocity at 20° for Both at twenty-Five m/s

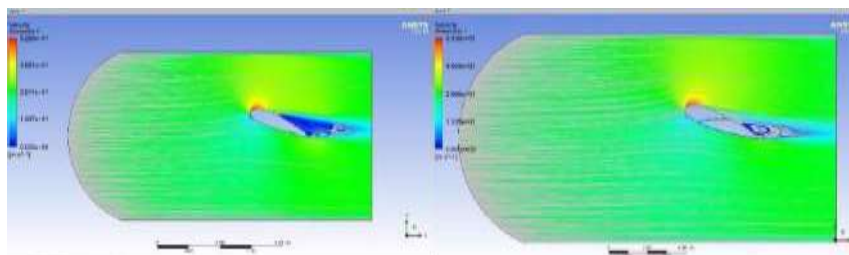


Figure 488 : Streamline at 20° for Both at twenty-Five m/s

**5.164 Thirty m/s-**

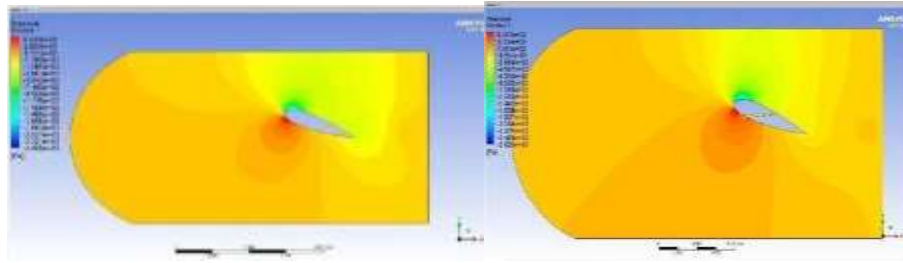


Figure 489 : Pressure at  $20^\circ$  for Both at Thirty m/s

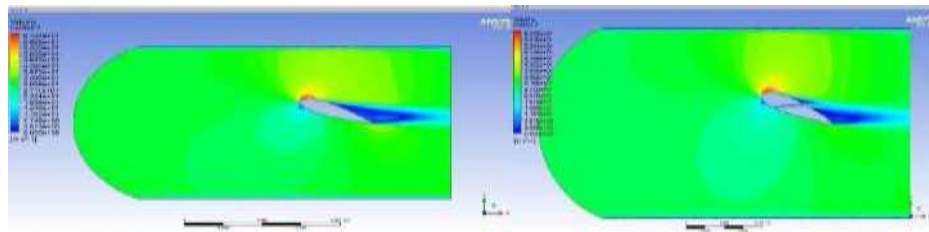


Figure 490 : Velocity at  $20^\circ$  for Both at Thirty m/s

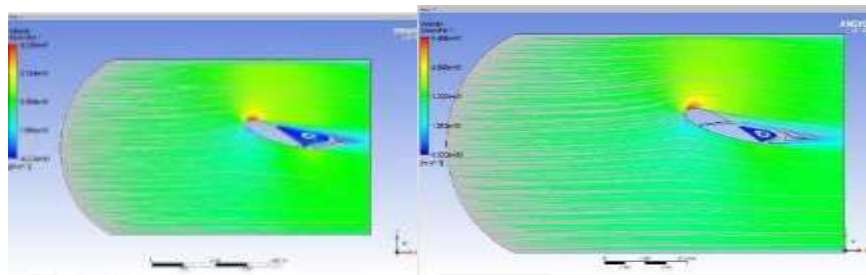


Figure 491 : Streamline at  $20^\circ$  for Both at Thirty m/s

**5.165 Fifty m/s**

**5.166 Fifty m/s-**

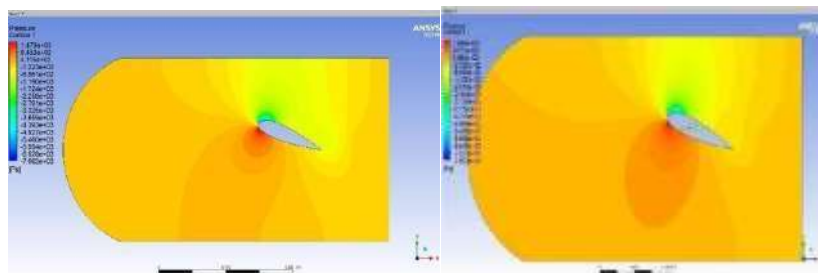


Figure 492 : Pressure at  $20^\circ$  for Both at Fifty m/s

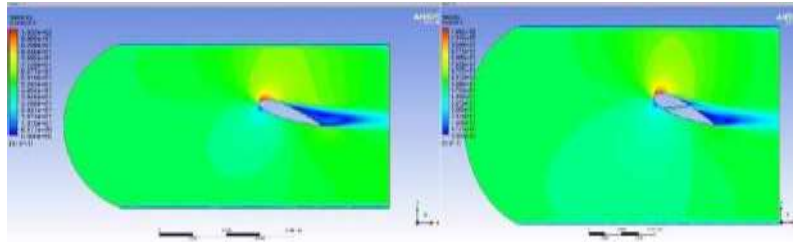


Figure 493 : Velocity at 20° for Both at Fifty m/s

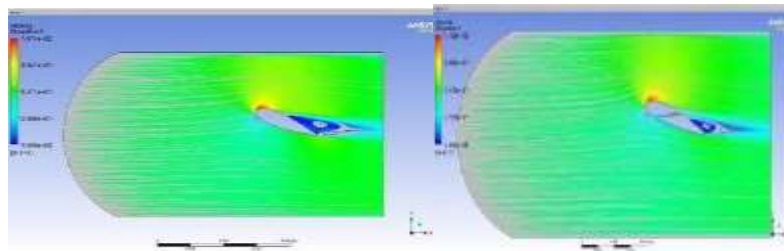


Figure 494 : Streamline at 20° for Both at Fifty m/s

Table of Design Points										
	A	B	C	D	E	F	G	H	I	
1	Name	P1 - inlebel	P2 - drag-op	P3 - drag-force-op	P4 - lift-op	P5 - lift-force-op	Ret...	Retained Data	Note	
2	Units	m s <sup>-1</sup>		N		N				
3	DP 0 (Current)	50	0.014769	22.616	0.13181	201.83	<input checked="" type="checkbox"/>	<input checked="" type="checkbox"/>		
4	DP 1	30	0.0057759	8.8444	0.045143	69.126	<input checked="" type="checkbox"/>	<input checked="" type="checkbox"/>		
5	DP 2	25	0.0041517	6.3573	0.030673	46.967	<input checked="" type="checkbox"/>	<input checked="" type="checkbox"/>		
6	DP 3	20	0.0028364	4.3432	0.018705	28.643	<input checked="" type="checkbox"/>	<input checked="" type="checkbox"/>		
7	DP 4	15	0.0016899	2.5677	0.010124	15.503	<input checked="" type="checkbox"/>	<input checked="" type="checkbox"/>		
8	DP 5	10	0.00081304	1.245	0.0042596	6.5225	<input checked="" type="checkbox"/>	<input checked="" type="checkbox"/>		
9	DP 6	5	0.00024043	0.36816	0.00093039	1.4247	<input checked="" type="checkbox"/>	<input checked="" type="checkbox"/>		
*							<input type="checkbox"/>	<input type="checkbox"/>		

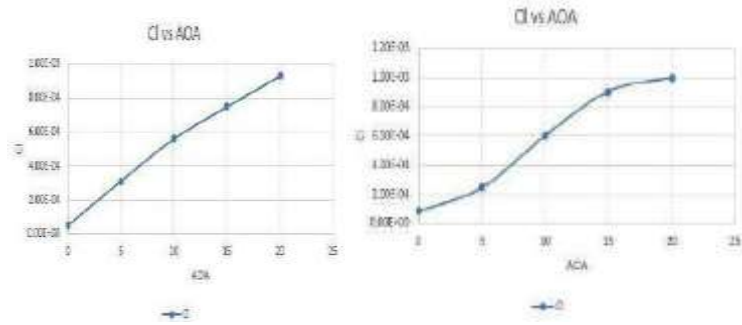
Table39 : Drag and Lift force values,24021 at 20°AOA

Table of Design Points										
	A	B	C	D	E	F	G	H	I	
1	Name	P1 - parameter-1	P2 - drag-op	P3 - drag-force-op	P4 - lift-op	P5 - lift-force-op	Ret...	Retained Data	Note	
2	Units	m s <sup>-1</sup>		N		N				
3	DP 18 (Current)	50	0.01267	19.707	0.14715	225.32	<input checked="" type="checkbox"/>	<input checked="" type="checkbox"/>		
4	DP 19	30	0.0051134	7.8299	0.046799	76.255	<input checked="" type="checkbox"/>	<input type="checkbox"/>		
5	DP 20	25	0.0036933	5.6553	0.033768	51.707	<input checked="" type="checkbox"/>	<input type="checkbox"/>		
6	DP 21	20	0.0024865	3.8074	0.020803	31.855	<input checked="" type="checkbox"/>	<input type="checkbox"/>		
7	DP 22	15	0.0014958	2.2904	0.011214	17.171	<input checked="" type="checkbox"/>	<input type="checkbox"/>		
8	DP 23	10	0.00073815	1.1303	0.00465	7.1203	<input checked="" type="checkbox"/>	<input type="checkbox"/>		
9	DP 24	5	0.00022703	0.34764	0.00099994	1.5312	<input checked="" type="checkbox"/>	<input type="checkbox"/>		
*							<input type="checkbox"/>	<input type="checkbox"/>		

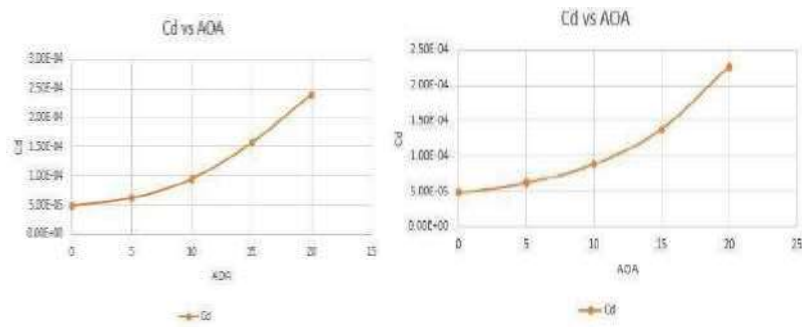
Table40 : Drag and Lift force values,24021 at 20°AOA

**5.167 Charts : -  
for24021**

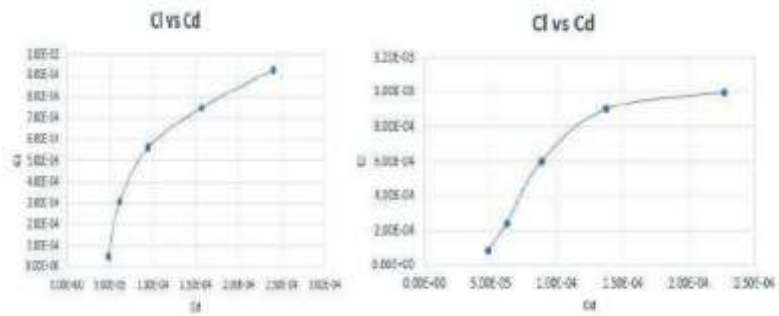
**5.168 Five m/s-**



**Figure 495 : Cl versus attack angle**



**Figure 496 : Cd versus attack angle**



**Figure 497 : Cl versus Cd**

5.169 Ten m/s-

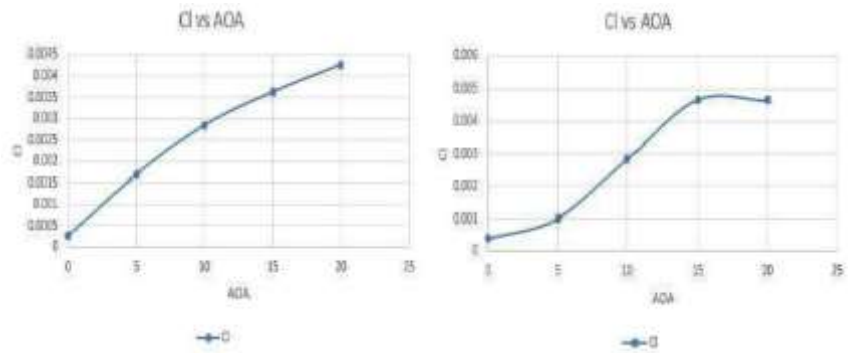


Figure 498 : Cl versus attack angle

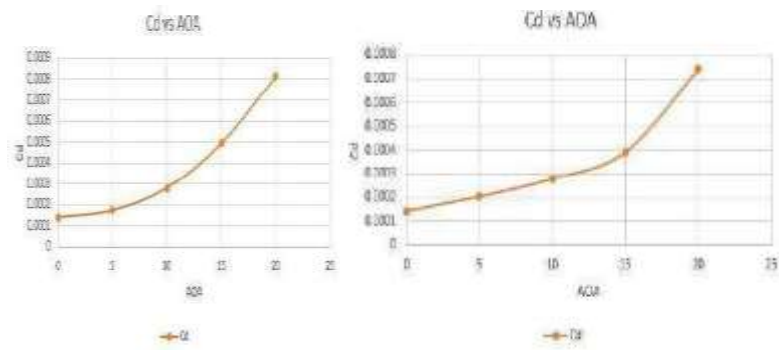


Figure 499 : Cd versus attack angle

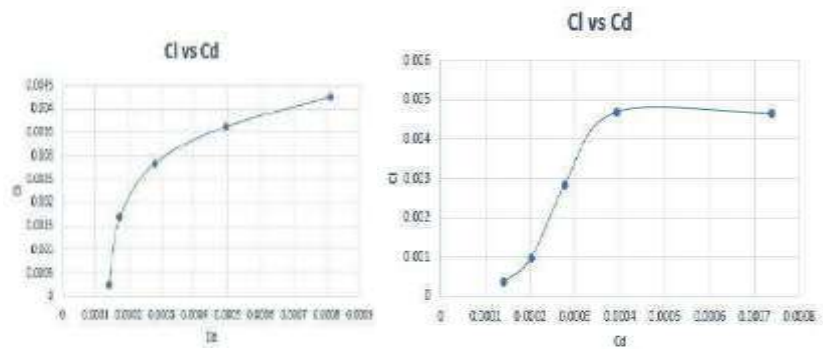


Figure 500 : Cl versus Cd

5.170 Fifteen m/s-

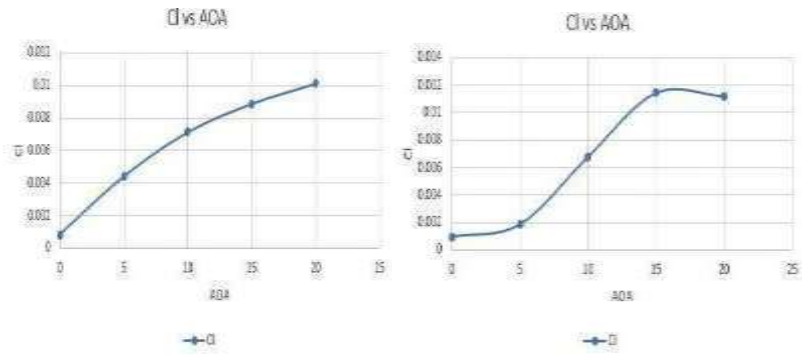


Figure 501 : Cl versus attack angle

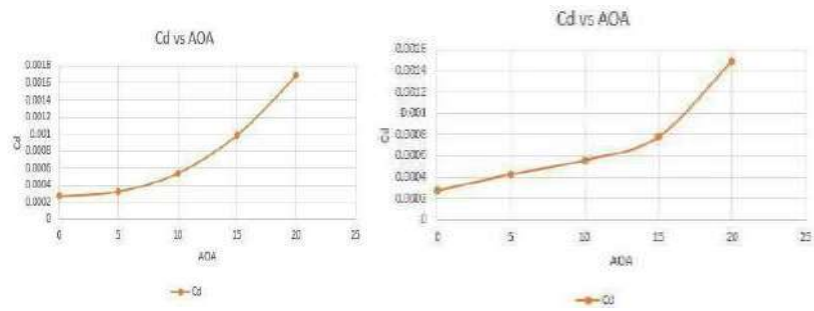


Figure 502 : Cd versus attack angle

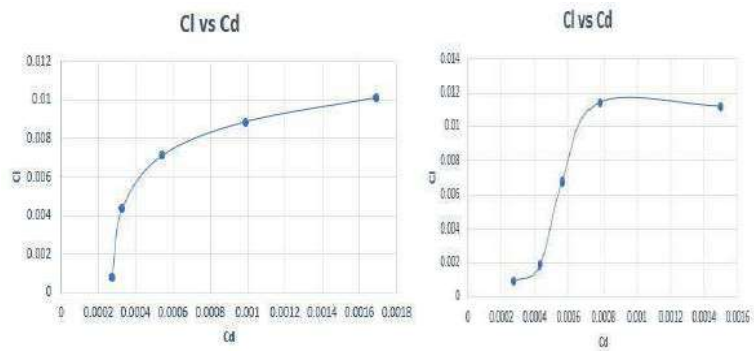


Figure 503 : Cl versus Cd



5.171 Twenty m/s-

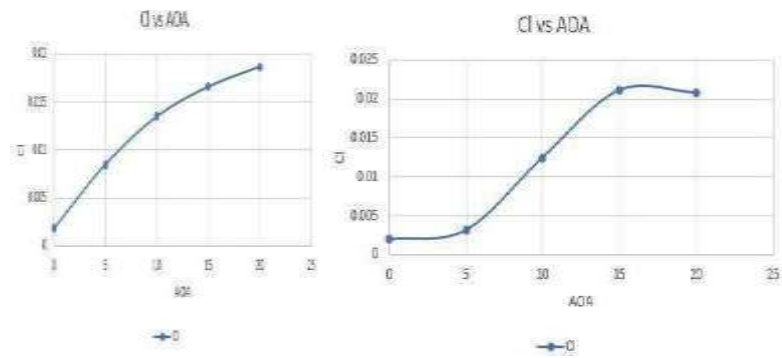


Figure 504 : Cl versus attack angle

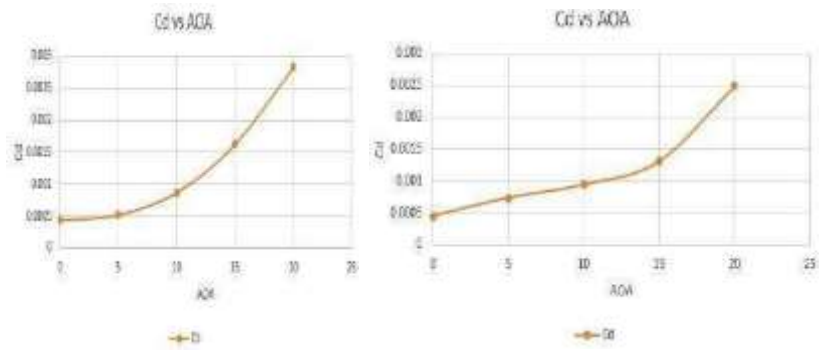


Figure 505 : Cd versus attack angle

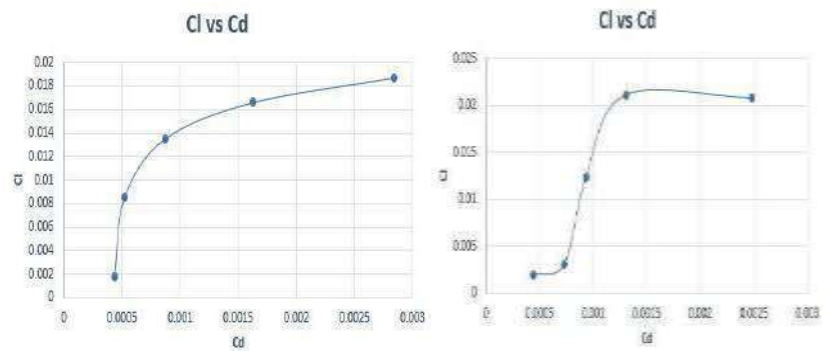
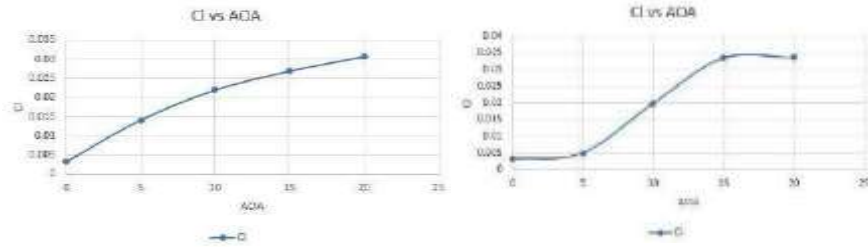
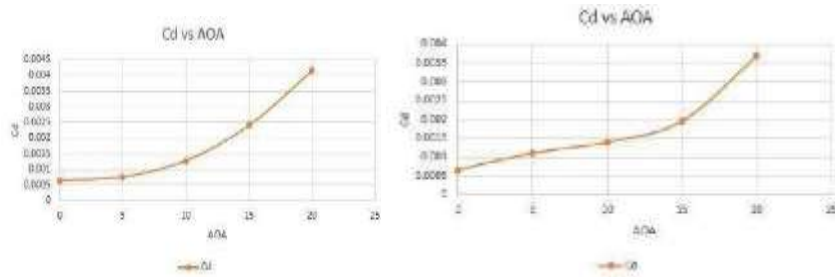


Figure 506 : Cl versus Cd

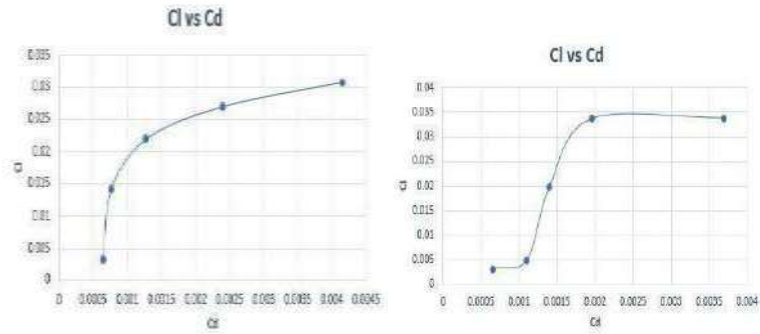
**5.172 Twenty Five m/s-**



**Figure 507 : Cl versus attack angle**

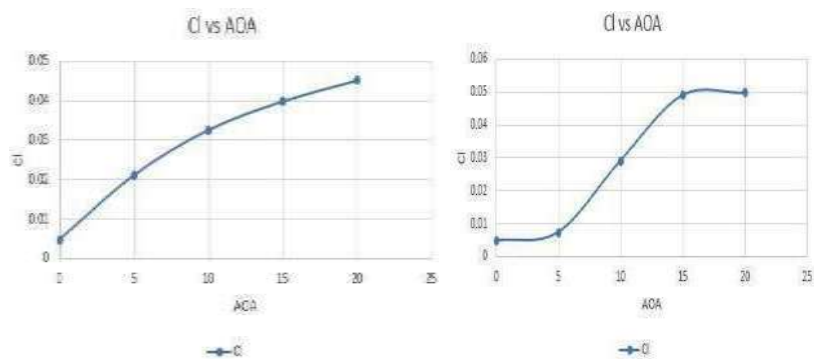


**Figure 508 : Cd versus attack angle**



**Figure 509 : Cl versus Cd**

**5.173 Thirty m/s-**



**Figure 510 : Cl versus attack angle**

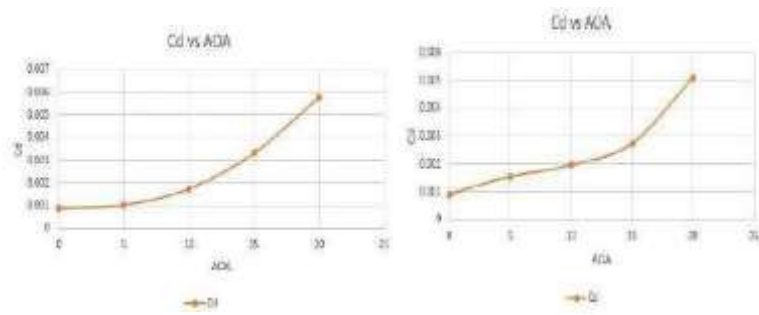


Figure 511 : Cd versus attack angle

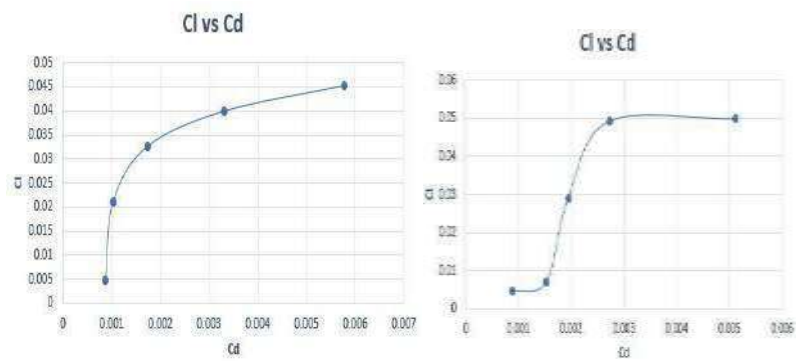


Figure 512 : Cl versus Cd

5.174 Fifty m/s-

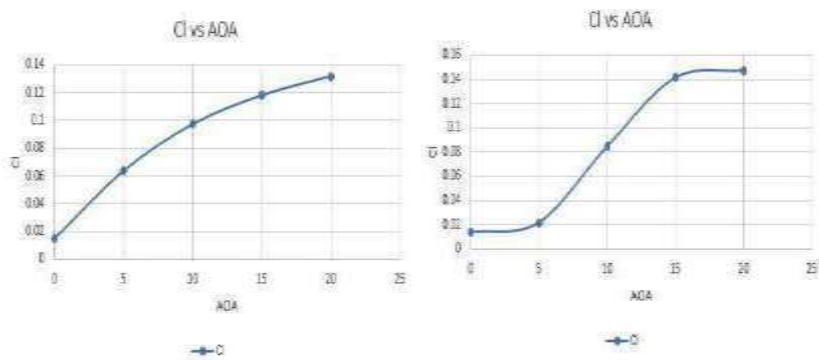


Figure 513 : Cl versus attack angle

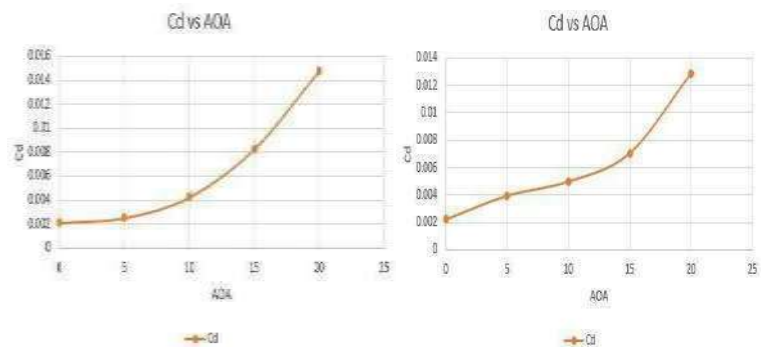


Figure 514 : Cd versus attack angle

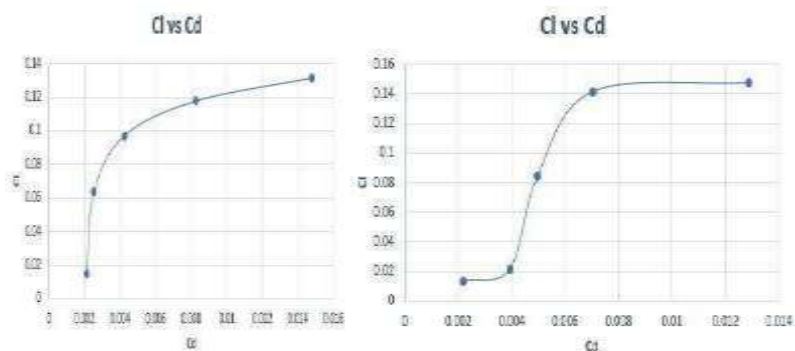
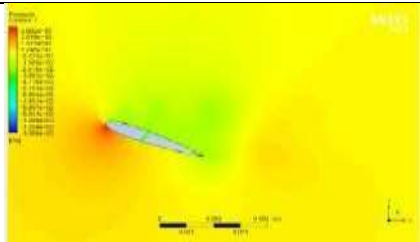
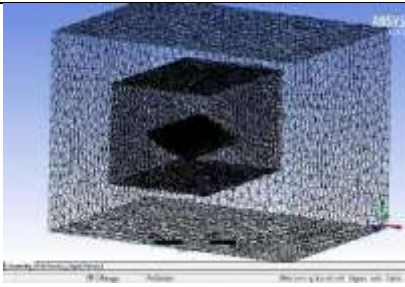
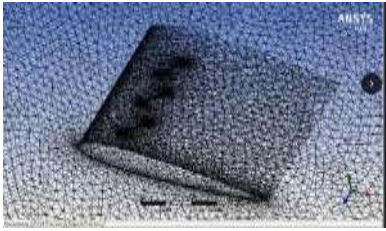
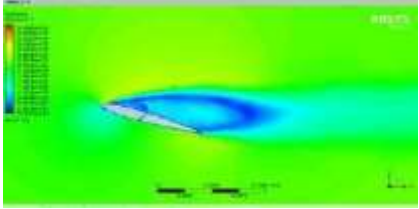
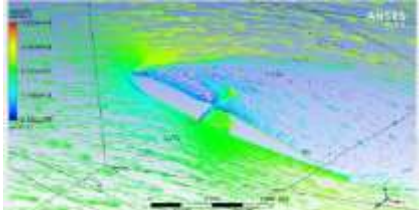
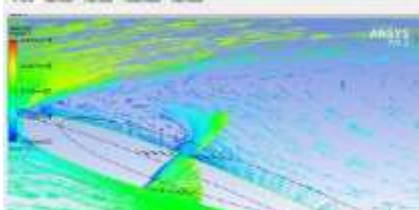
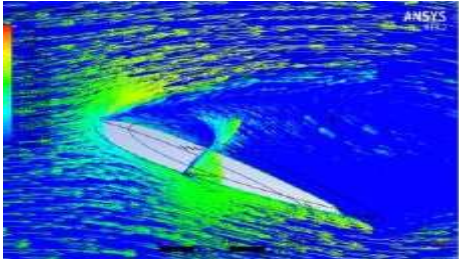
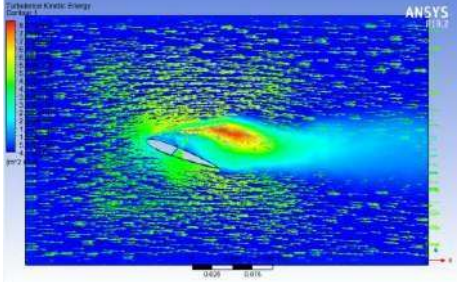
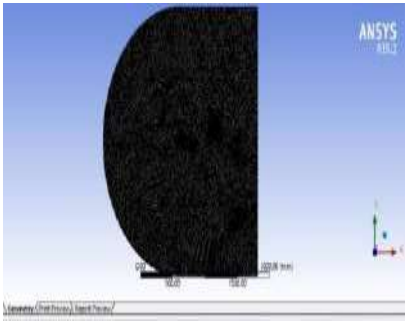
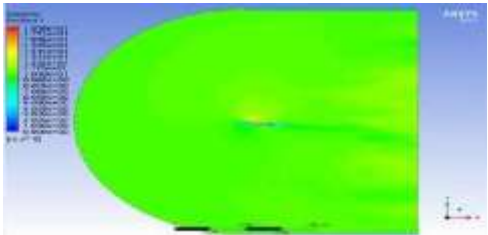
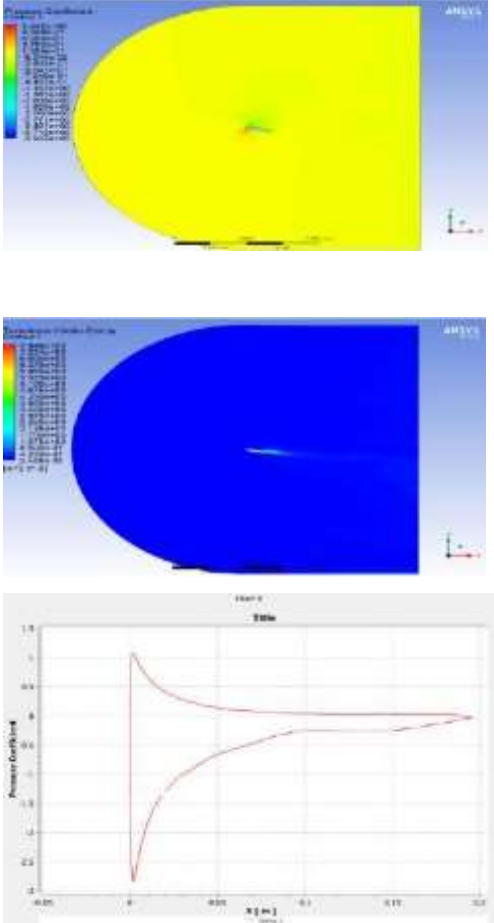
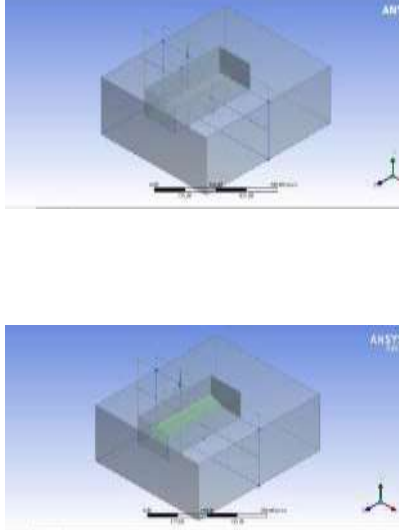
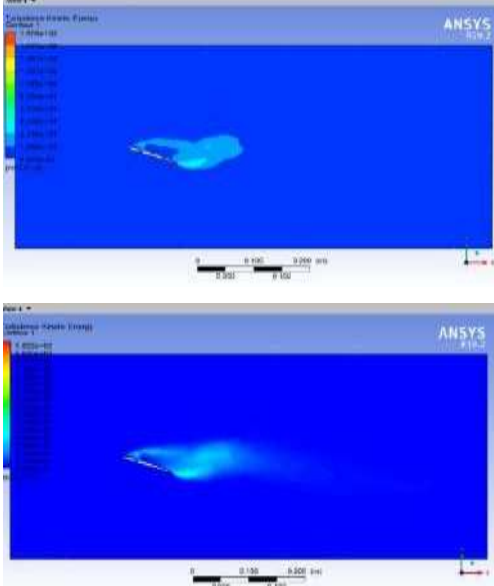



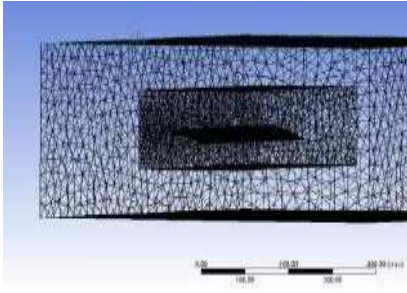
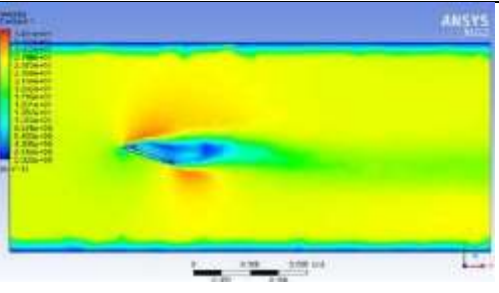
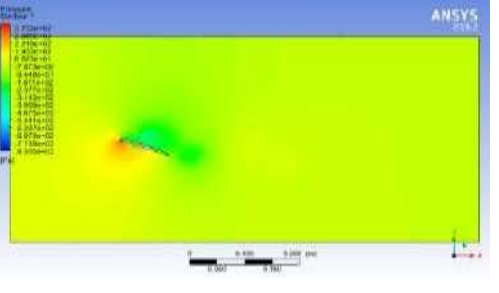
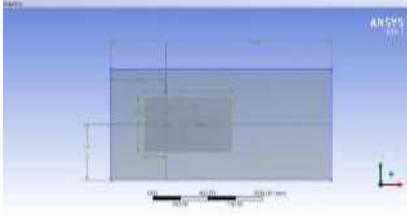
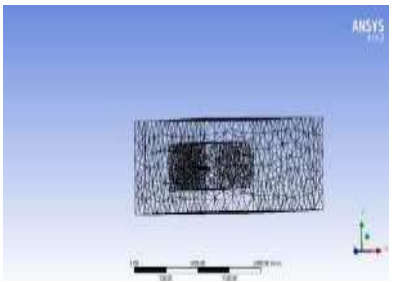
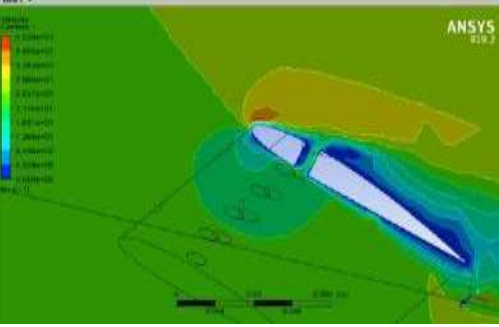
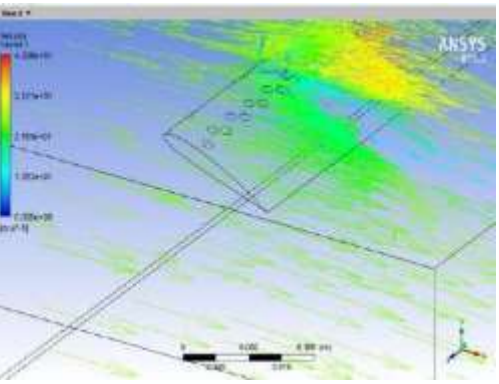
Figure 515 : Cl versus Cd

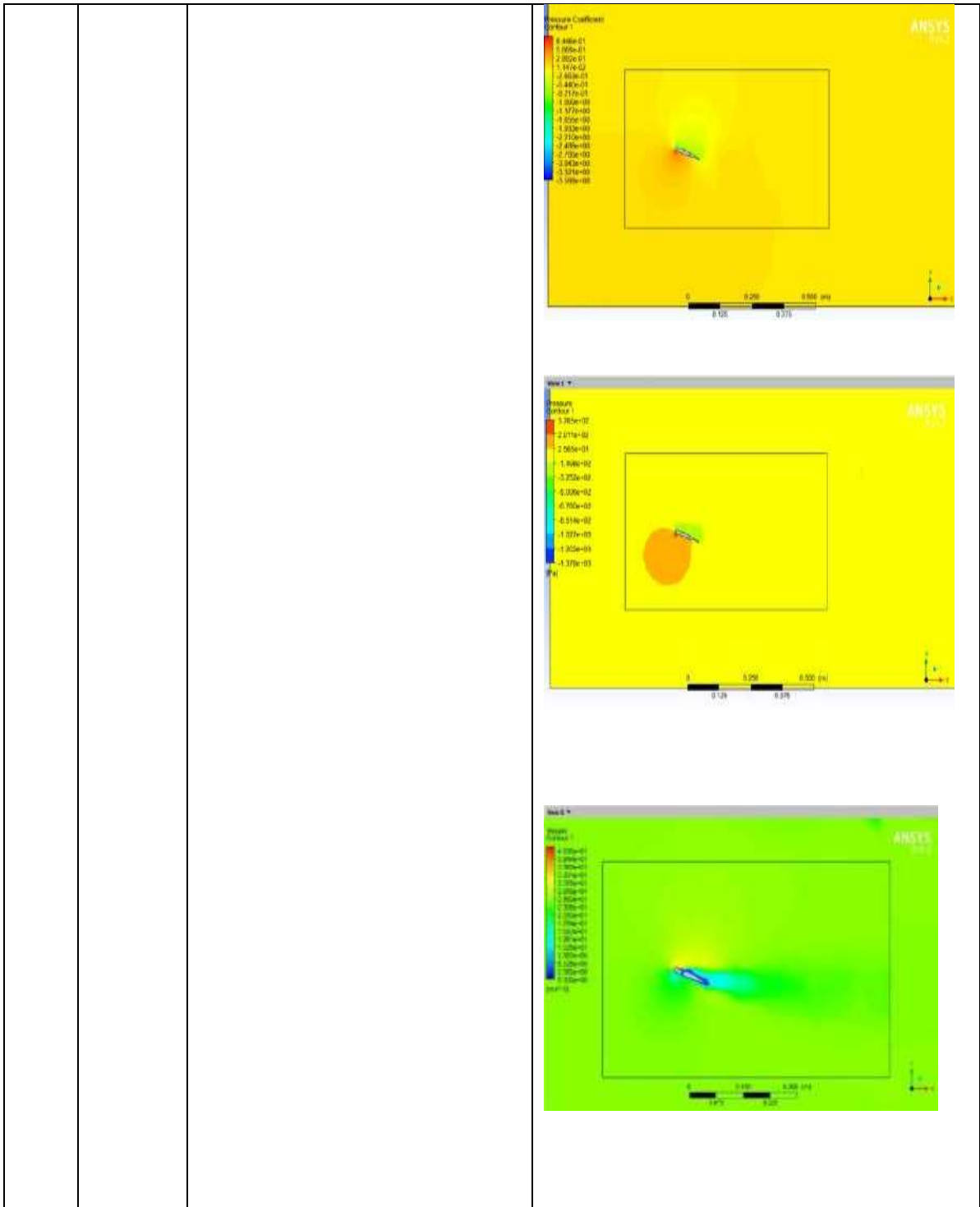
Airfoils with vents clearly show higher lift forces and coefficients of lift than the original designs, as evidenced by the results shown in the pressure plots, velocity plots, streamlines, lift coefficient vs attack angle, and drag coefficient versus attack angle graphs mentioned above. Furthermore, compared to previous versions, vented airfoils have a slightly lower coefficient of drag and drag force. These findings imply that the addition of vents may successfully link the boundary layer to the airfoil's upper surface, especially at greater angles of attack, increasing lift, decreasing drag.

S.N	Airfoil series	Mesh type element nodes	Pressure plot WV velocity turbulence
1	NACA 0012		

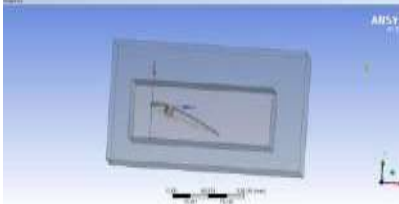
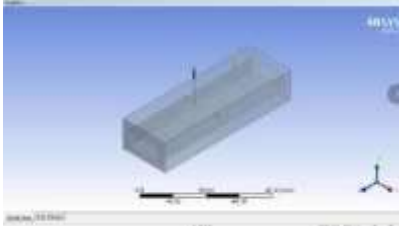


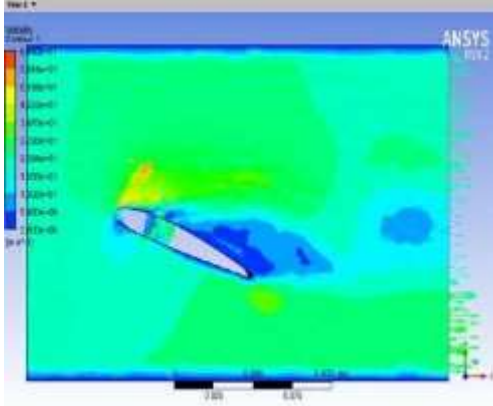
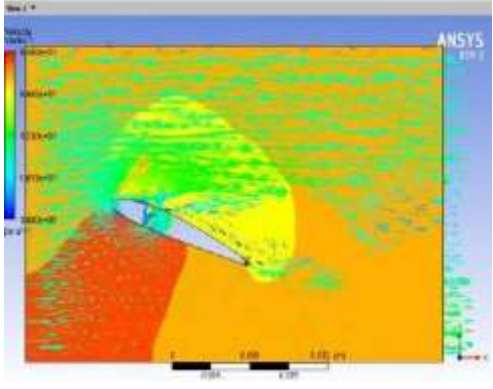
		  <p>Nodes- 244939Elements- 1225369</p>	    
2	NACA 0012 WOV		

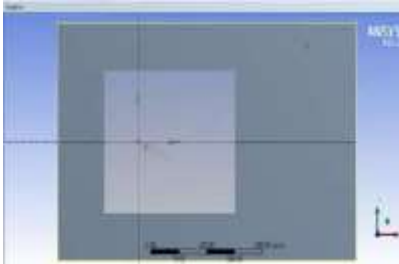
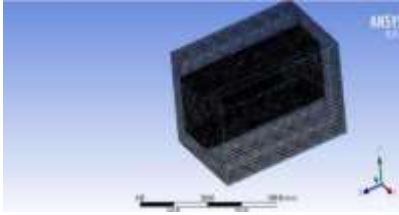
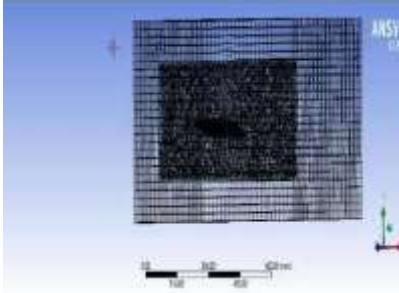
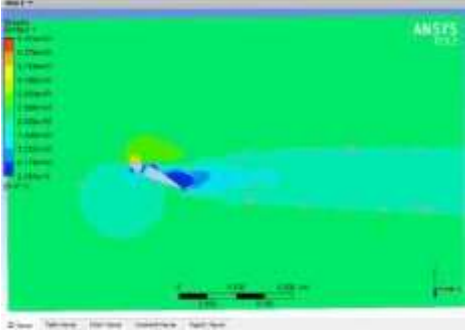
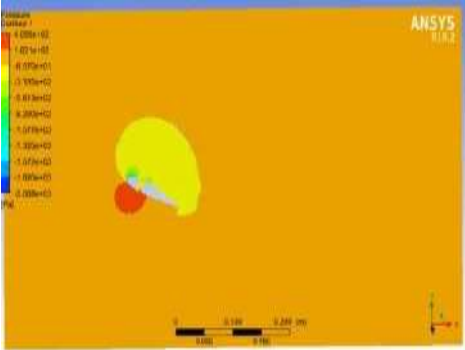
		<p>Nodes : 326677 Elements : 1523445</p>	
3	NACA 2606 WV		

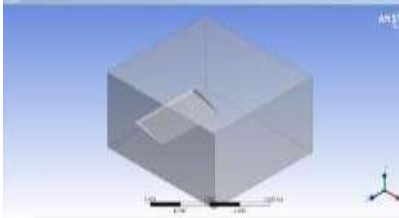
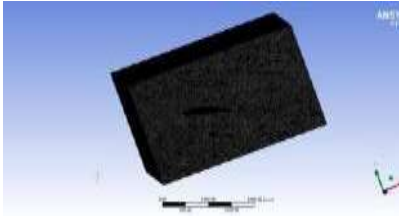
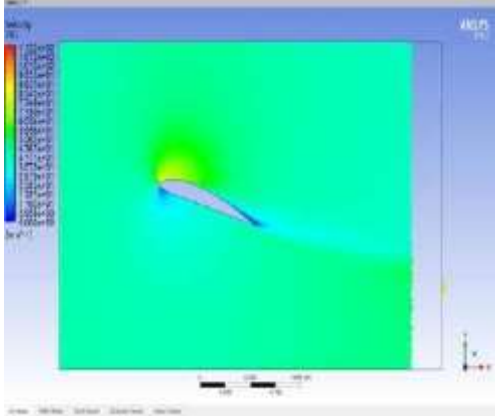
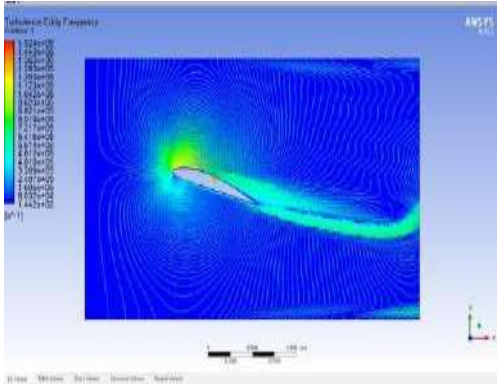
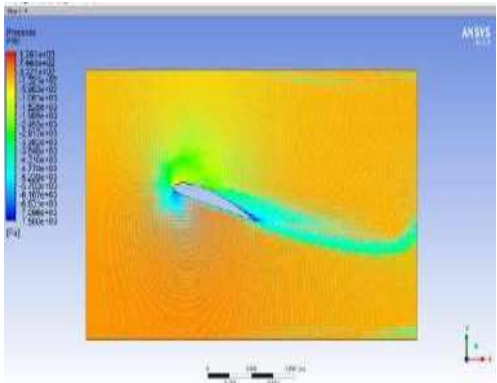
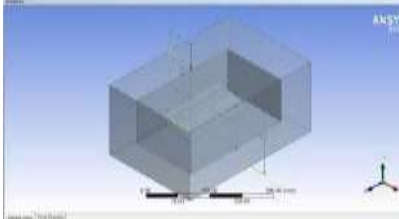
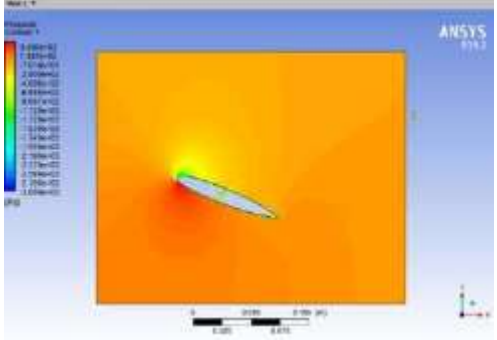
		 	 
4	NACA 2512 WV	 	 

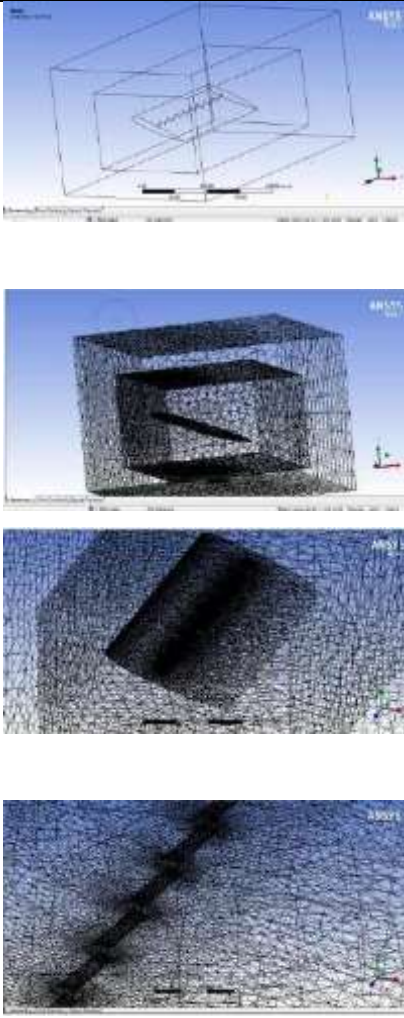
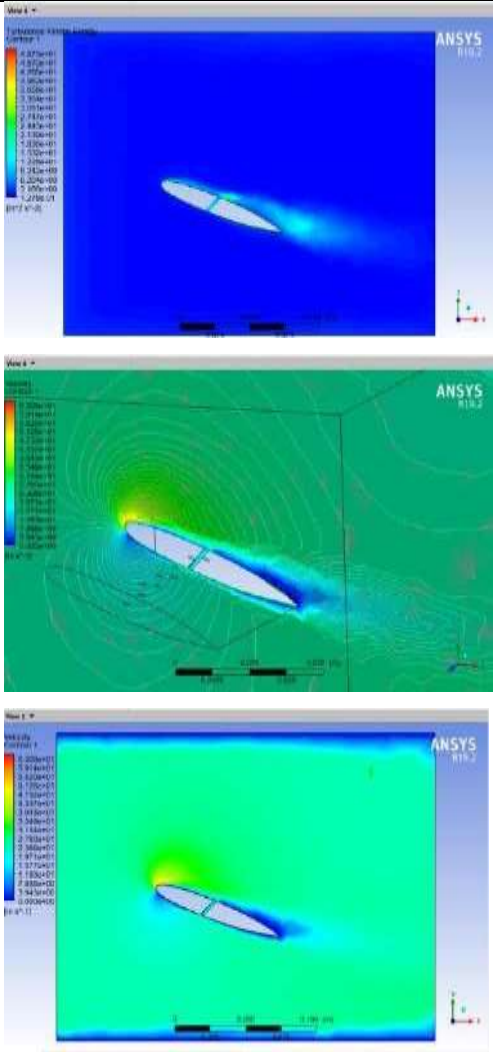
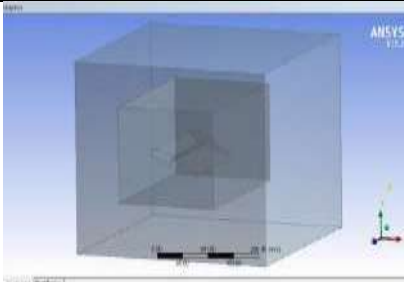
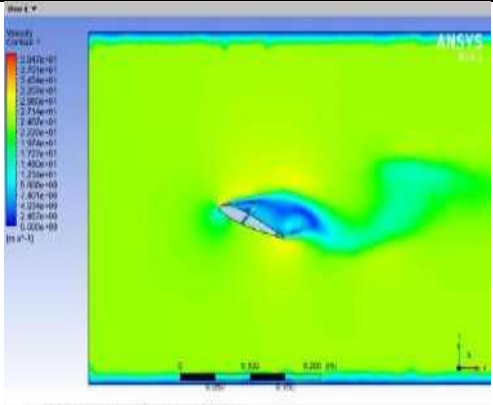


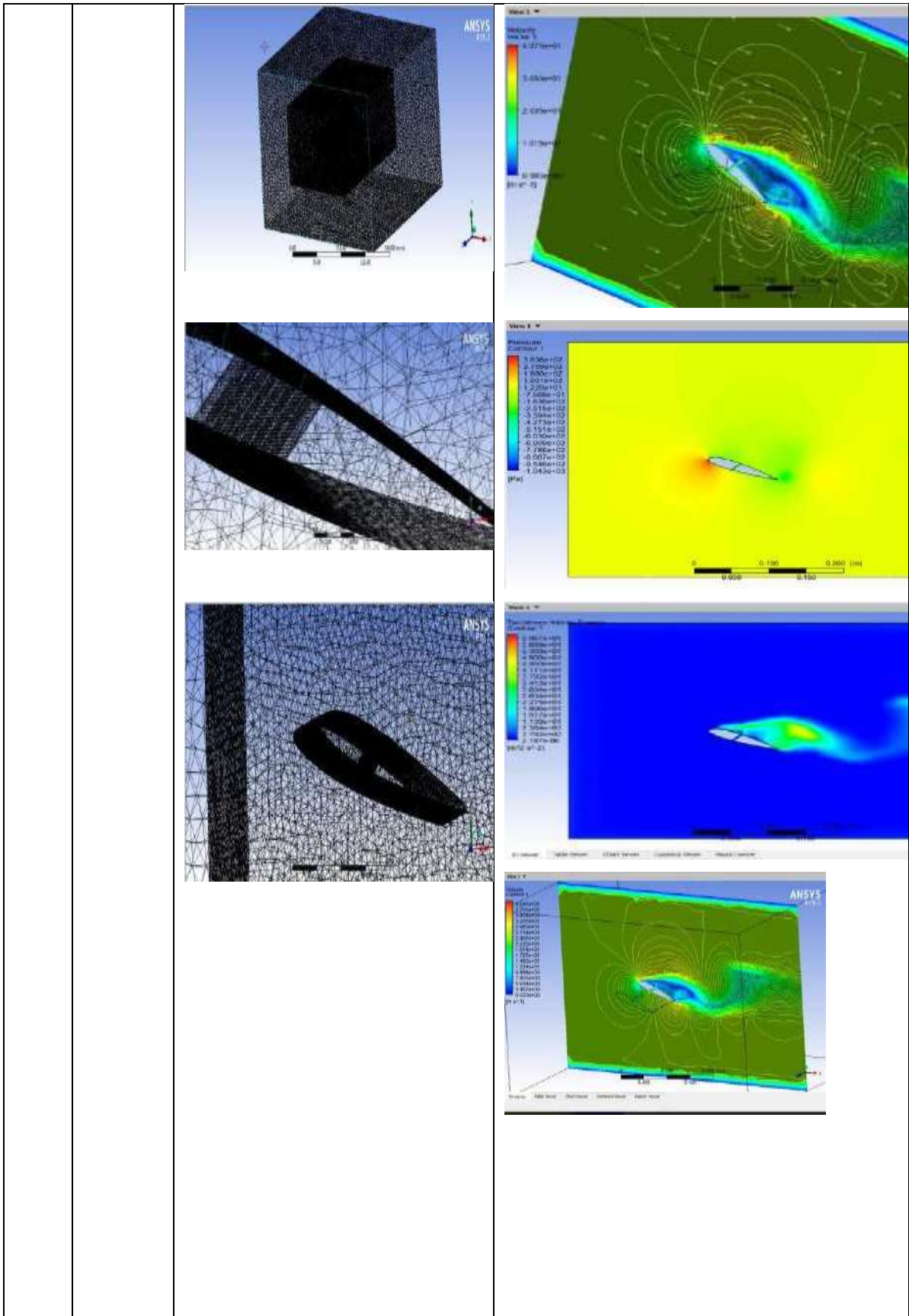


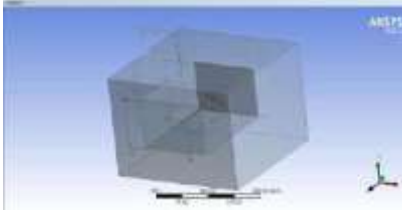
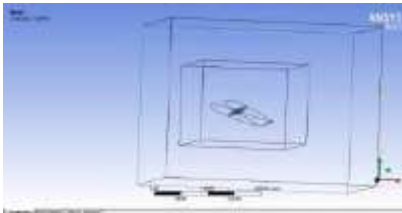
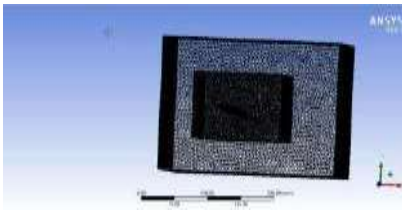
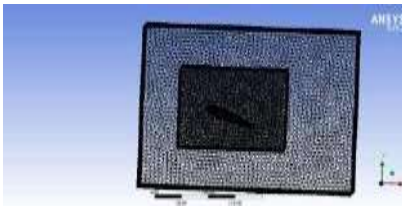

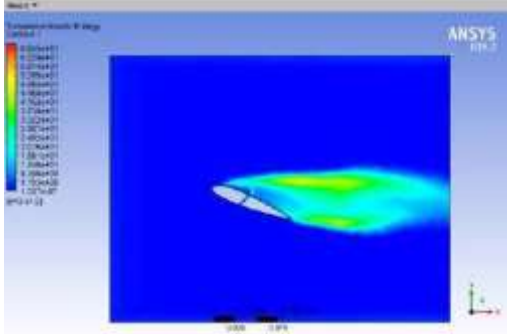
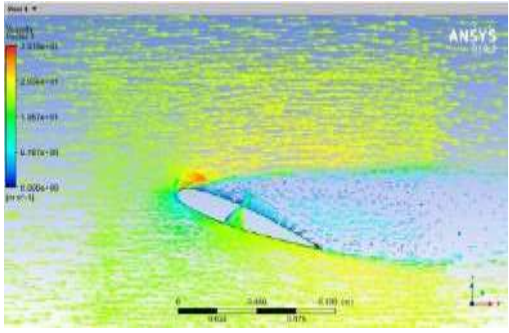
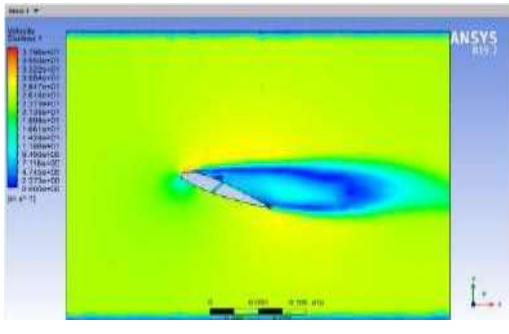
5	NACA 2412 WV	    <p data-bbox="496 1675 719 1756">Nodes : 198897 Elements : 251433</p>	 
---	--------------------	--	--

6	NACA 2418 wv	   <p data-bbox="496 1424 735 1503">Nodes : 147660 Elements : 5998978</p>	 
---	-----------------	---	--

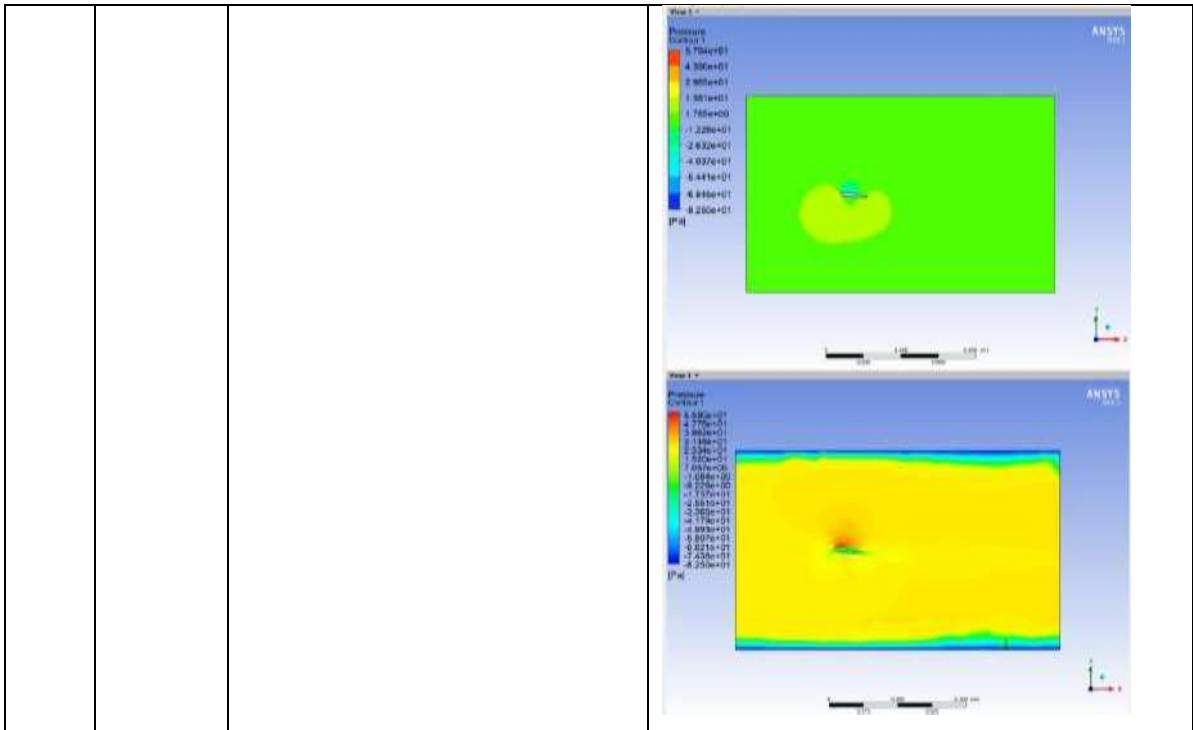
7	NACA 4412 wov	 	  
8	NACA 21012 wv		

		 <p>Nodes : 144586 Elements : 752952</p>	
9	NACA 23015 wv		



		<p>Nodes : 618713 Elements : 2151549</p>	
10	NACA 23012 wv	    	  

11	NACA215 wov	 	  



**Table41 : Flow separation good re-attachment national aeronautics and space administration airfoils**



# Chapter6

## EXPERIMENTAL ANALYSIS WITH WING MODELS

### 6.1 EXPERIMENTAL BOUNDARY CONDITIONS

S.No	Parameter	Value
1	Flow medium	Air
2	Density	1.225kg/m <sup>3</sup>
3	Viscosity	1.7894e-05kg/ms
4	Flow velocity	Inlet5,10,15,20,25m/s
5	Chord length	100mm
6	Attack angle	0-25°
7	Model	K-epsilonomega-sst

Table42 : Boundary conditions



Figure 516 : Designing wing model with vents by using 3d printing and teakwood



Figure 517 : Wing model with the straight vents maintain equal distance

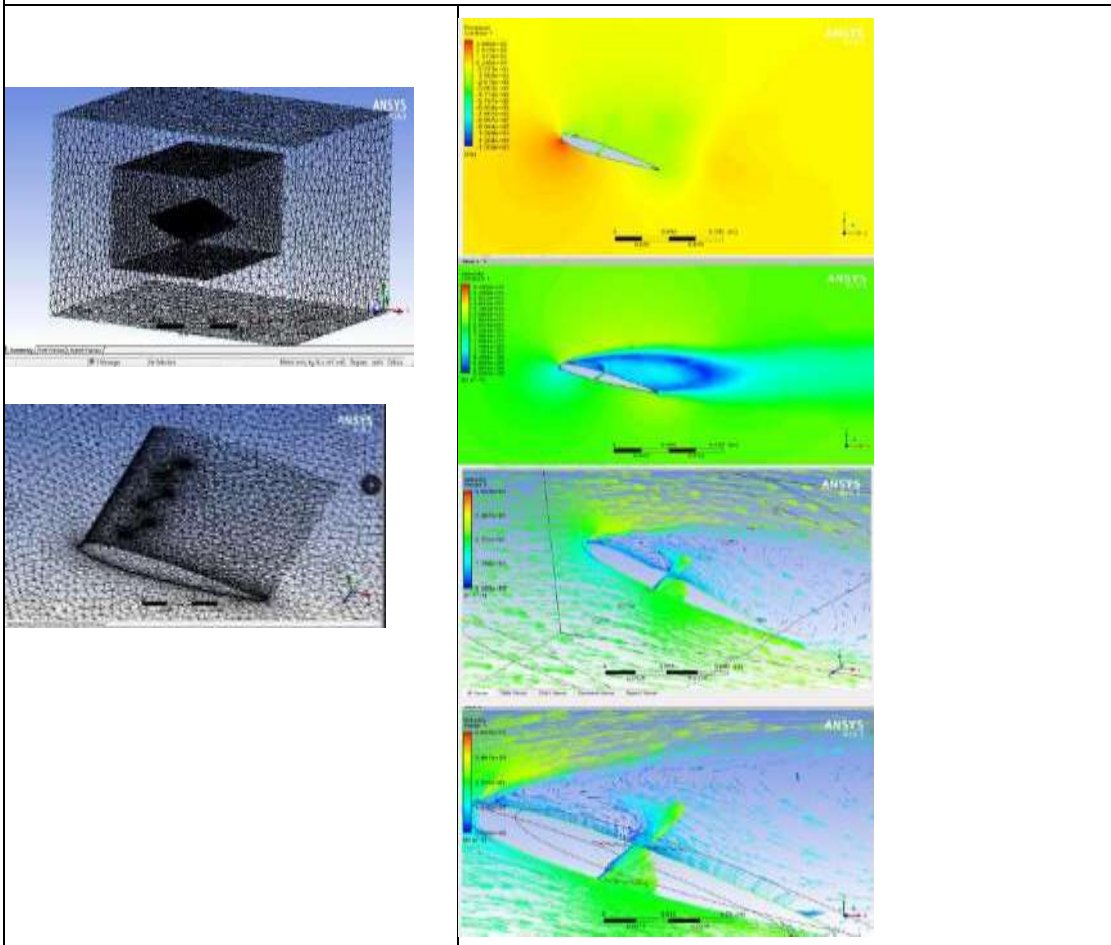


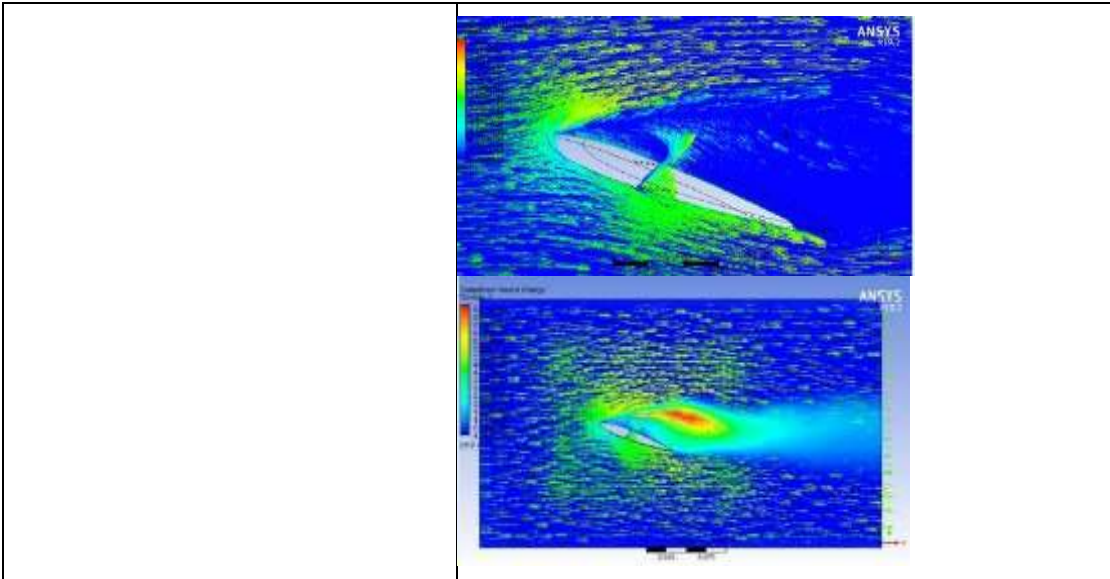
Figure 518 : Wing model mounted in the wind tunnel section 600\*600mm for testing



Figure 519 : wind tunnel section 600\*600mm testing of airfoil

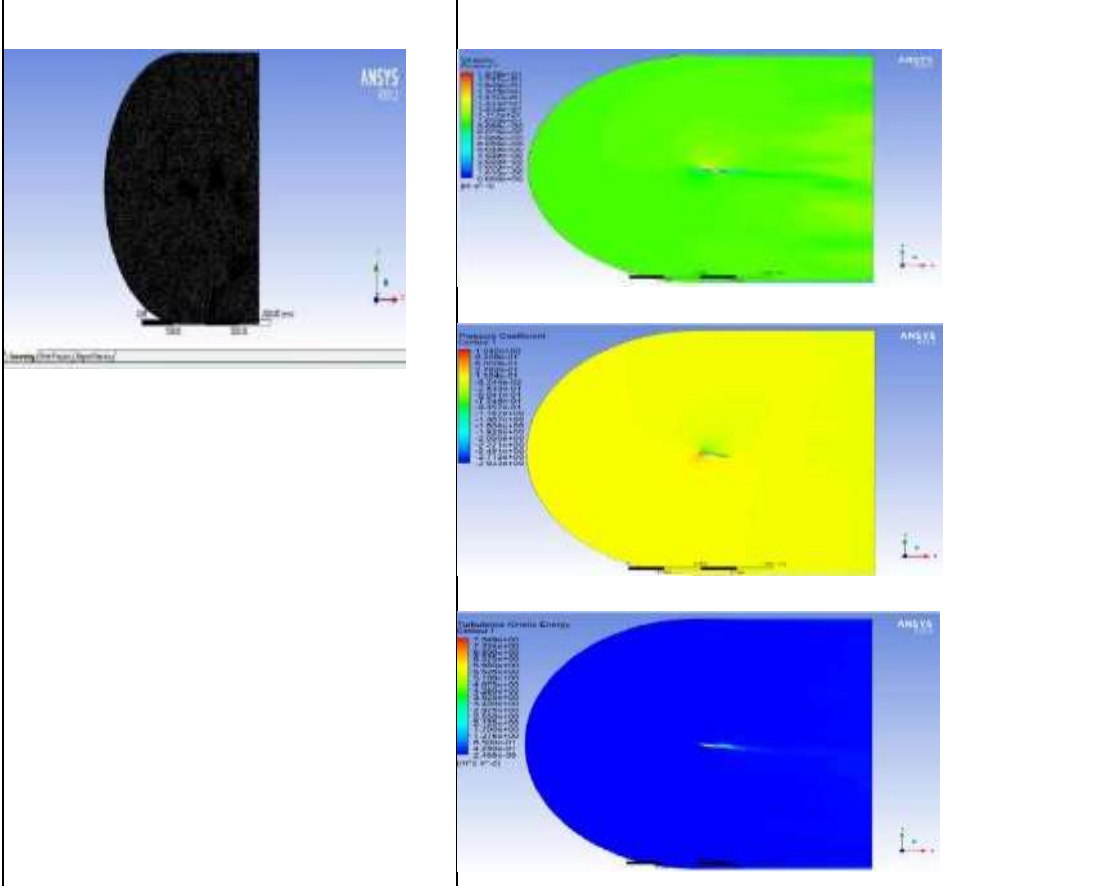
➤ DETAILING OF FLOW SEPERATION NACA0012

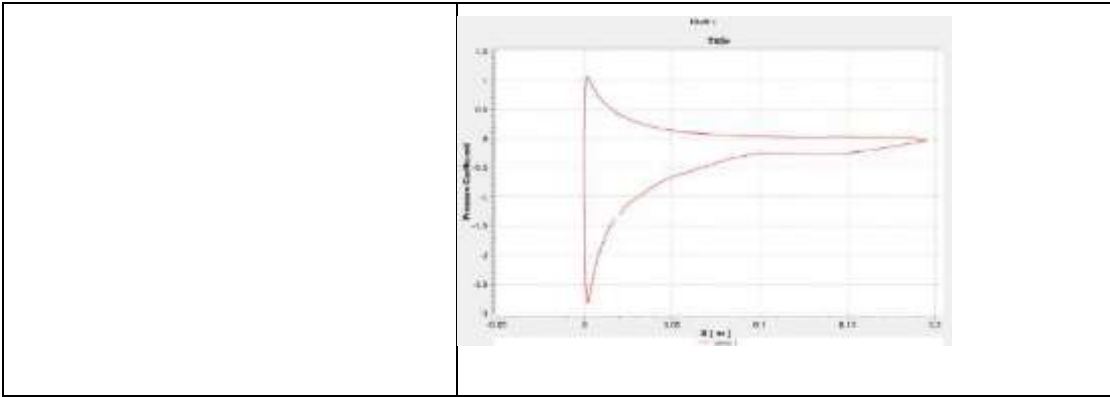




Nodes-244939 Elements-1225369 Pressure plot WV velocity turbulence

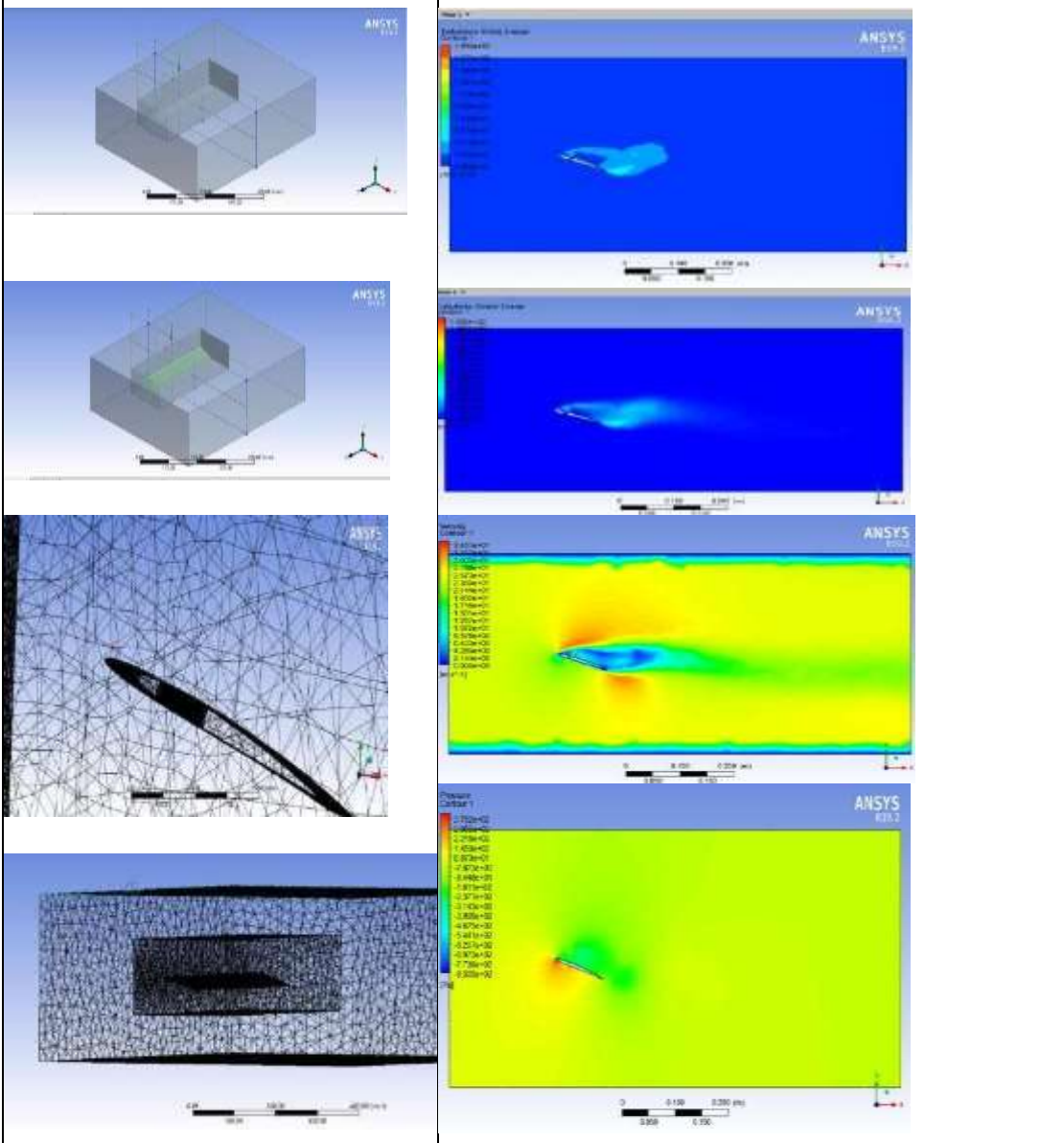
➤ FLOW SEPERATION OF NACA0012 WOV





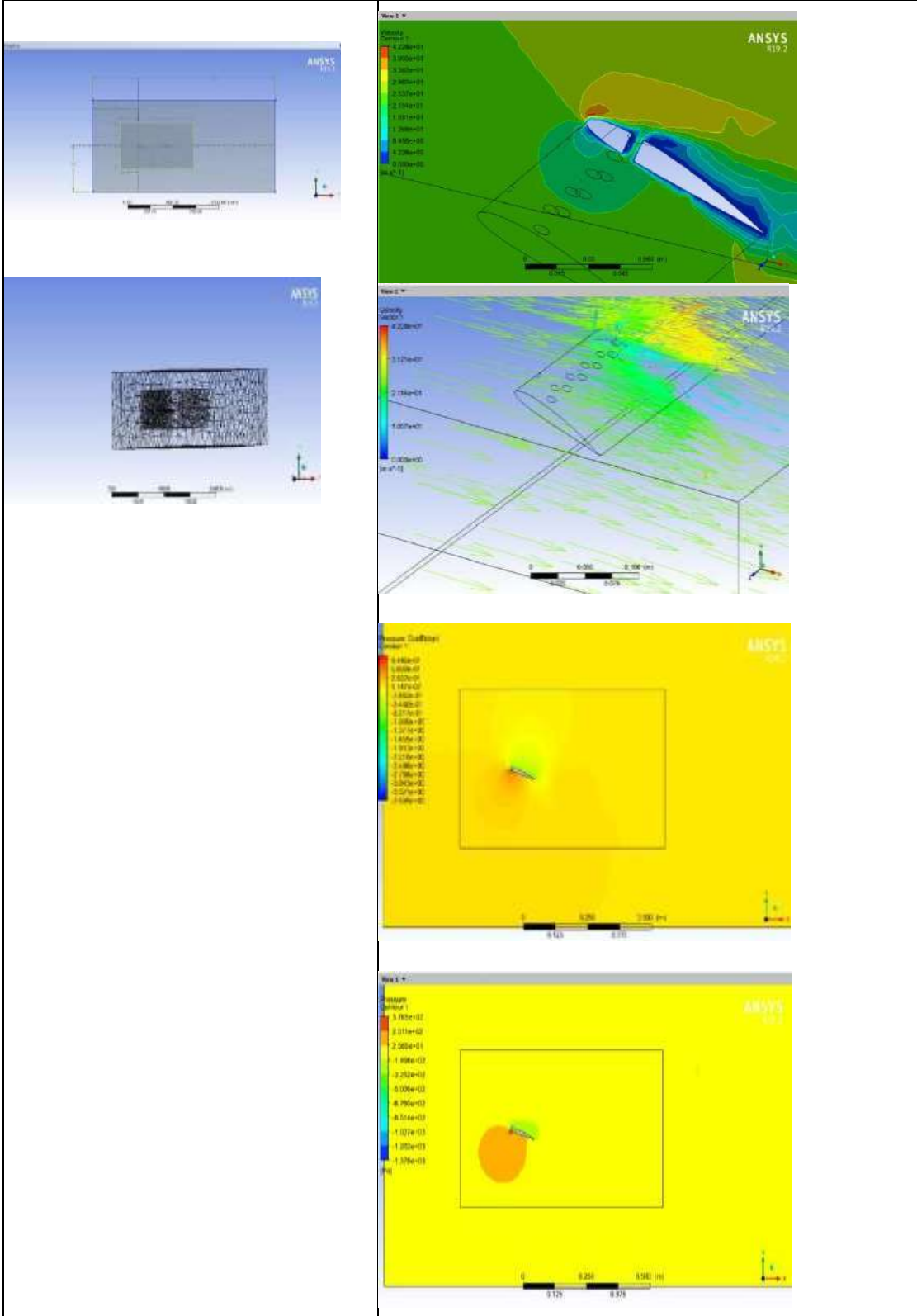
Nodes : 326677 Elements : 1523445 Pressure plot WV velocity turbulence

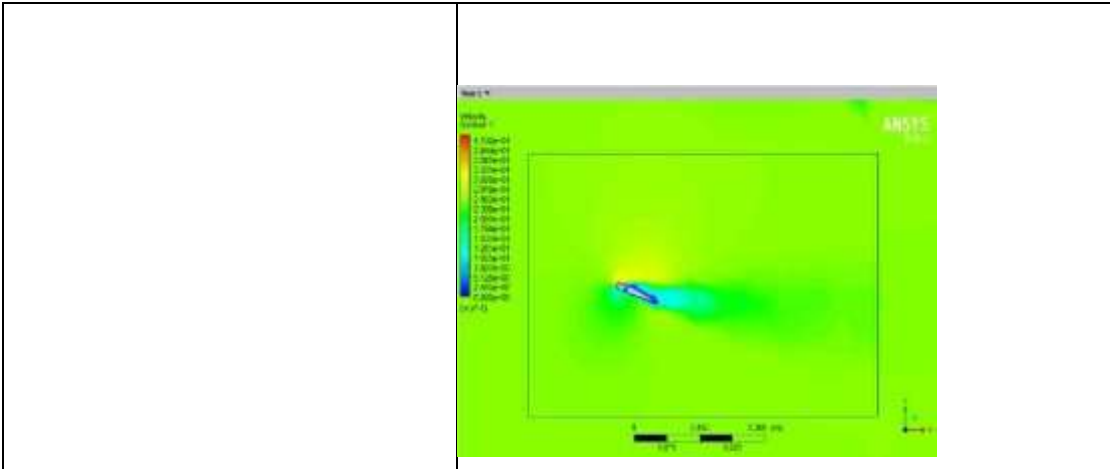
➤ FLOW SEPERATION OF NACA2606WV



Nodes : 189897 Elements : 261423 Pressure plot WV velocity turbulence

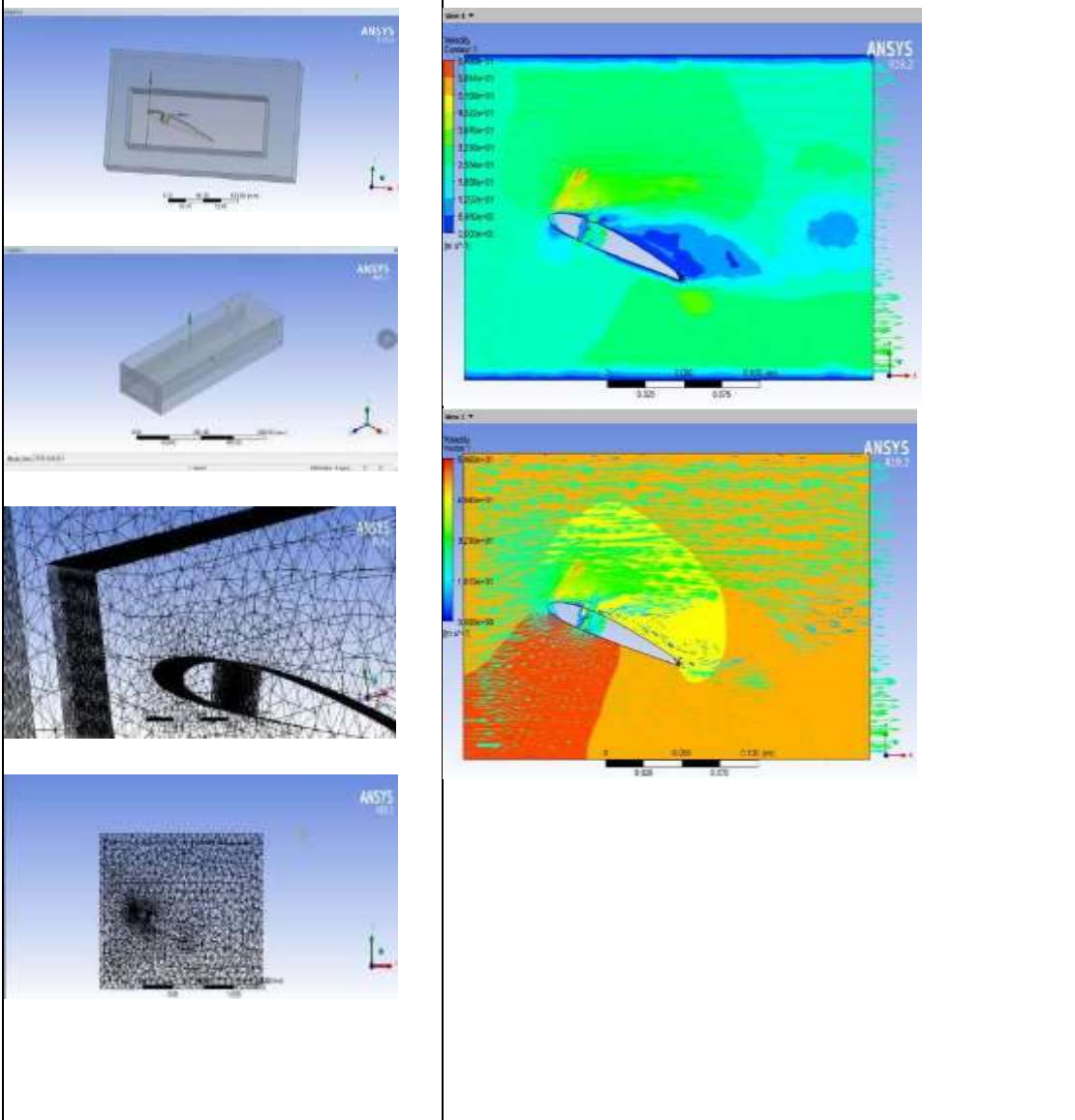
➤ FLOWSEPERATION OFNACA2512WV





Nodes : 198897 Elements : 251433 Pressure plot WV velocity turbulence

➤ FLOWSEPERATIONOF NACA2512WV

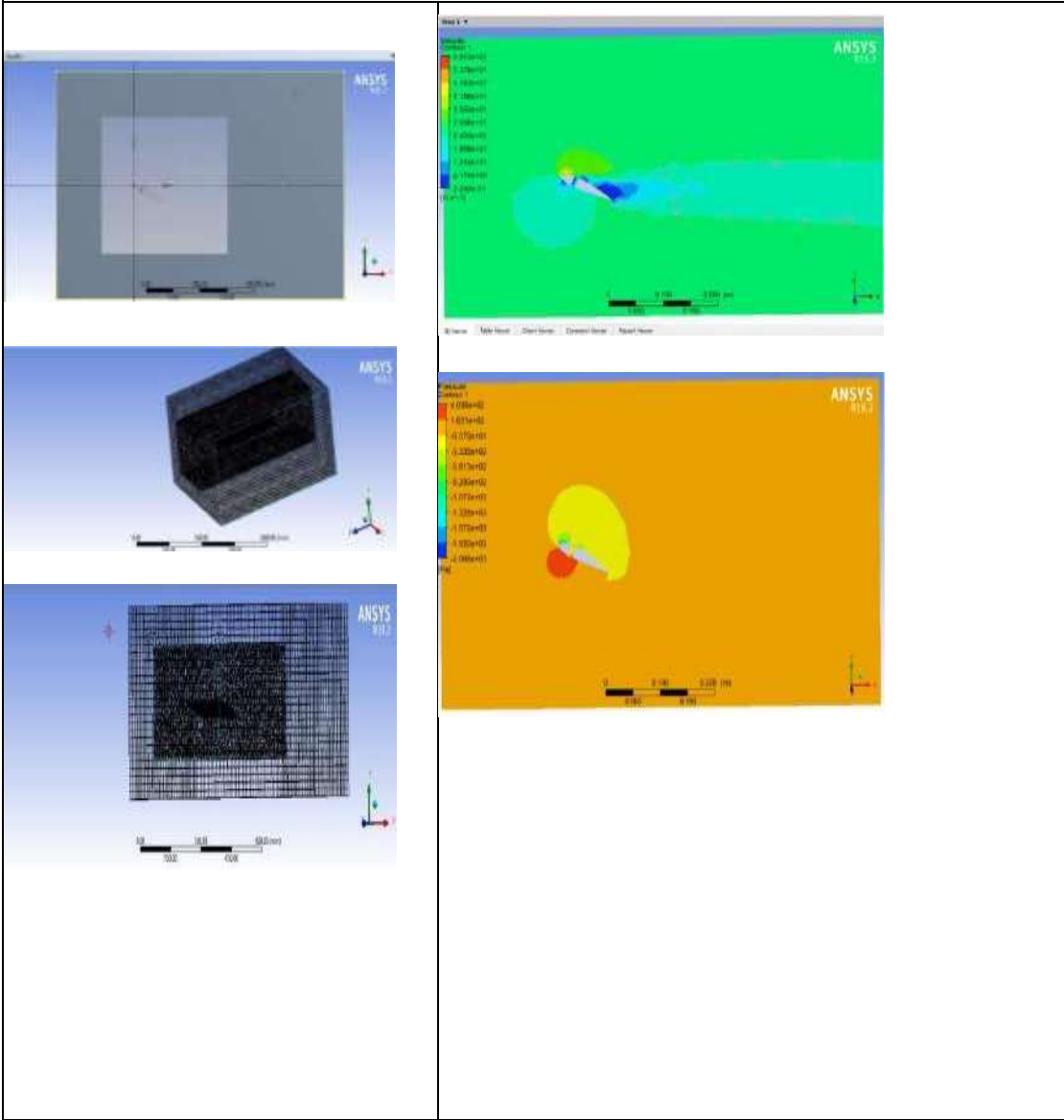




--	--

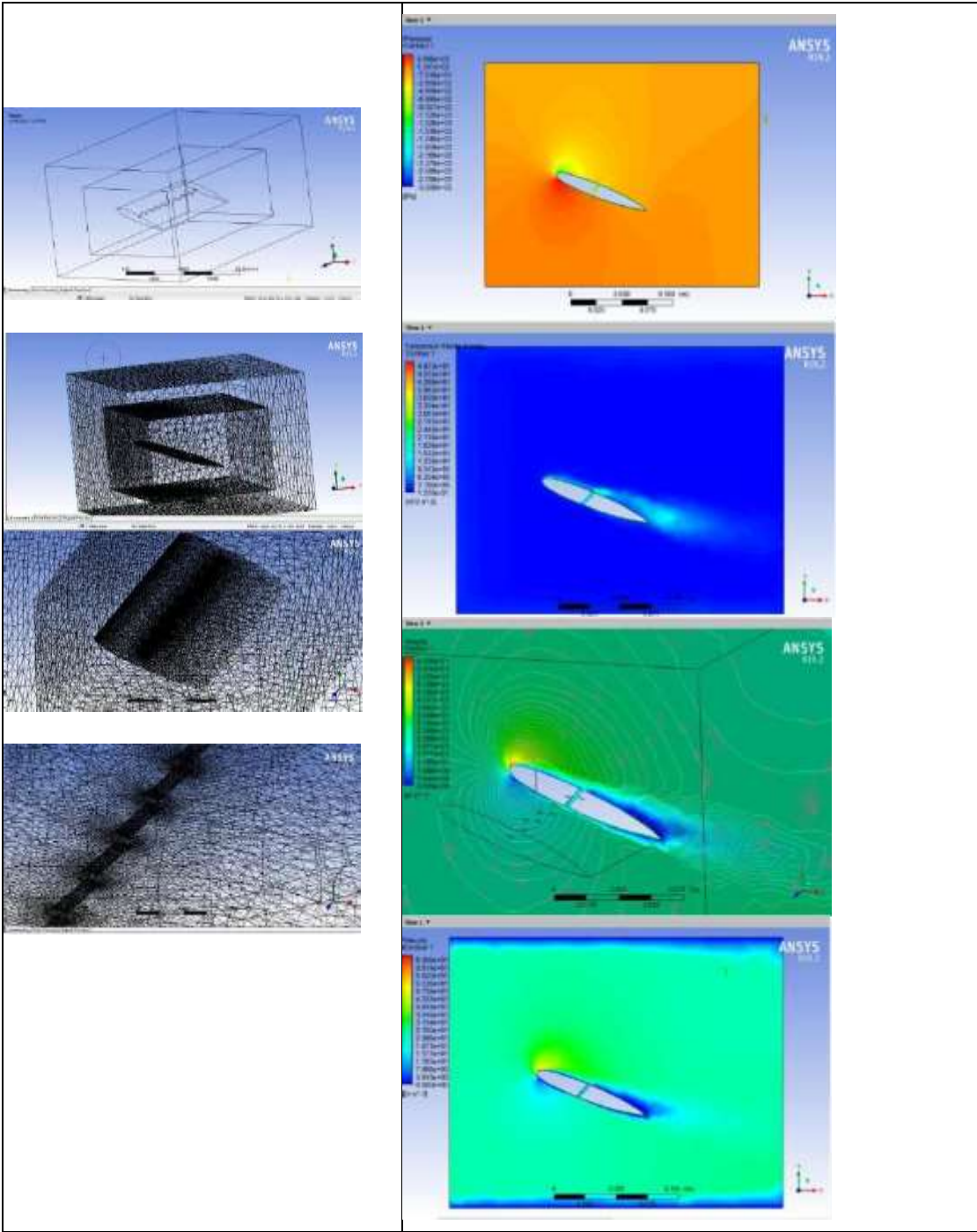
Nodes : 198897 Elements : 251433 Pressure plot WV velocity turbulence

➤ FLOW SEPERATION OF NACA2418 WV



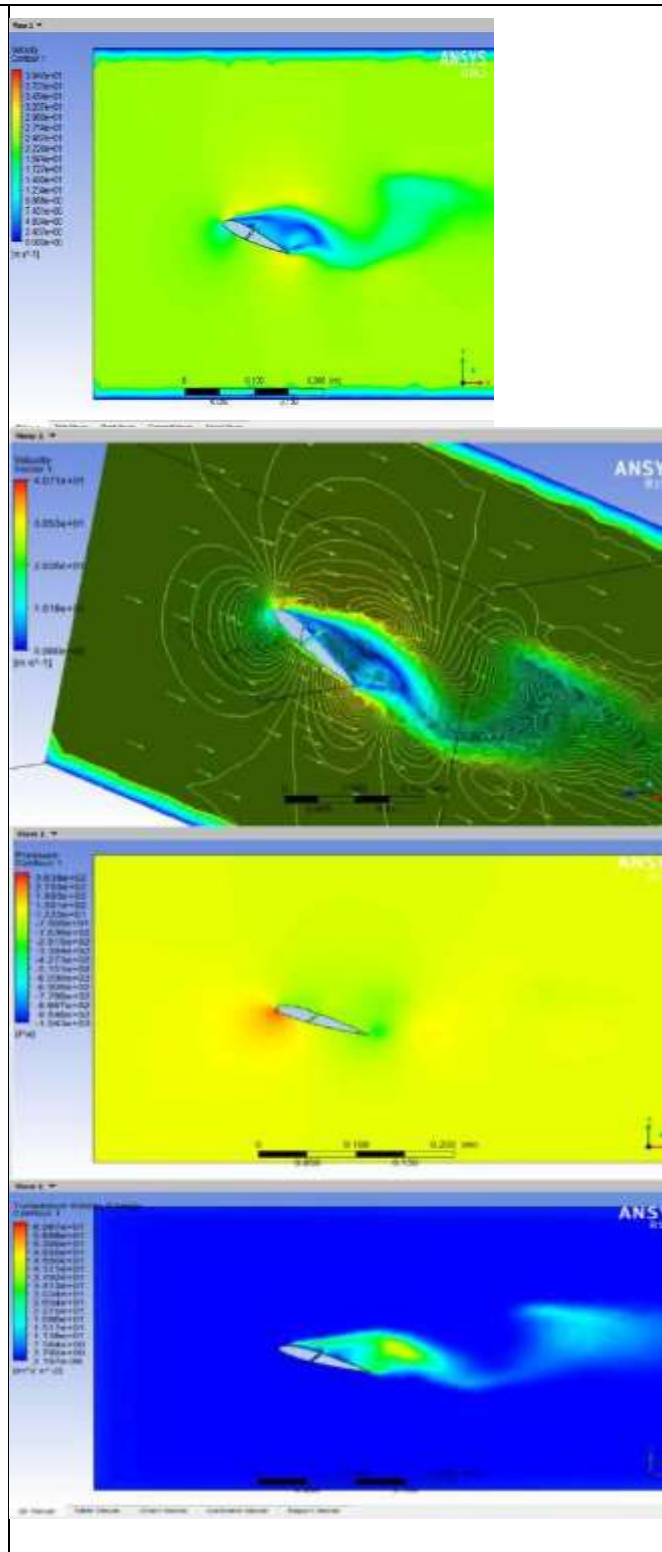
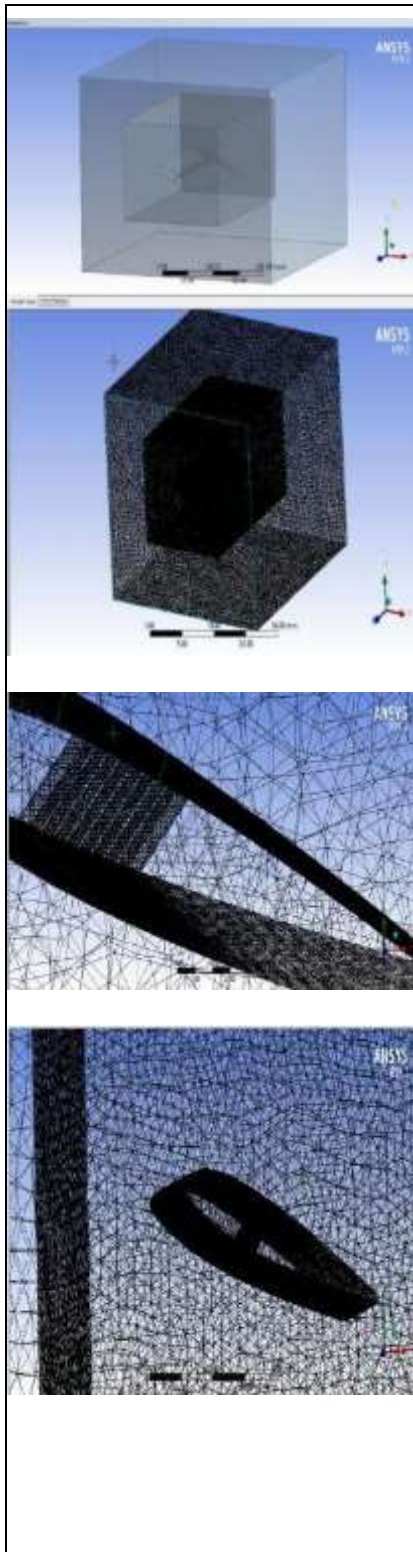
Nodes : 147660 Elements : 5998978 Pressure plot WV velocity turbulence

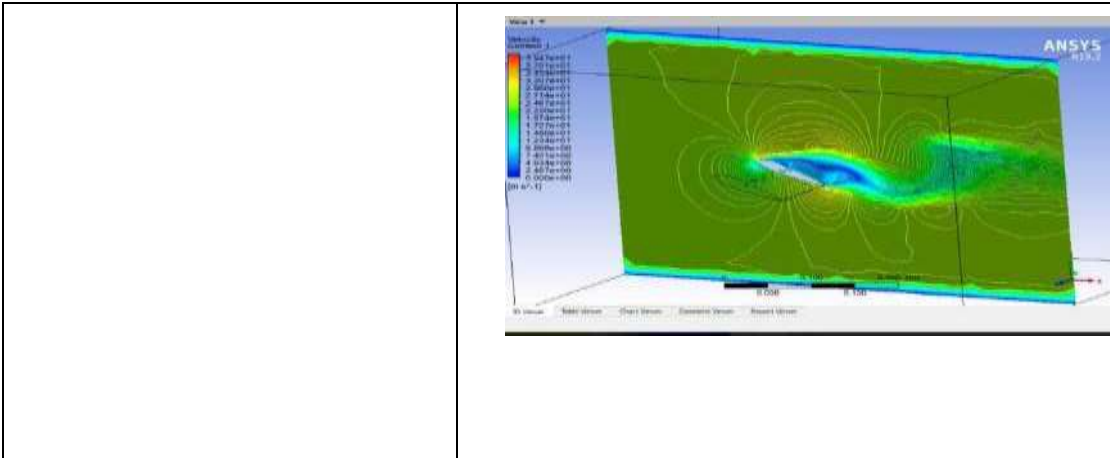
➤ FLOW SEPERATION OF NACA21012 WV



Nodes : 144586 Elements : 752952 velocity vector plot WV

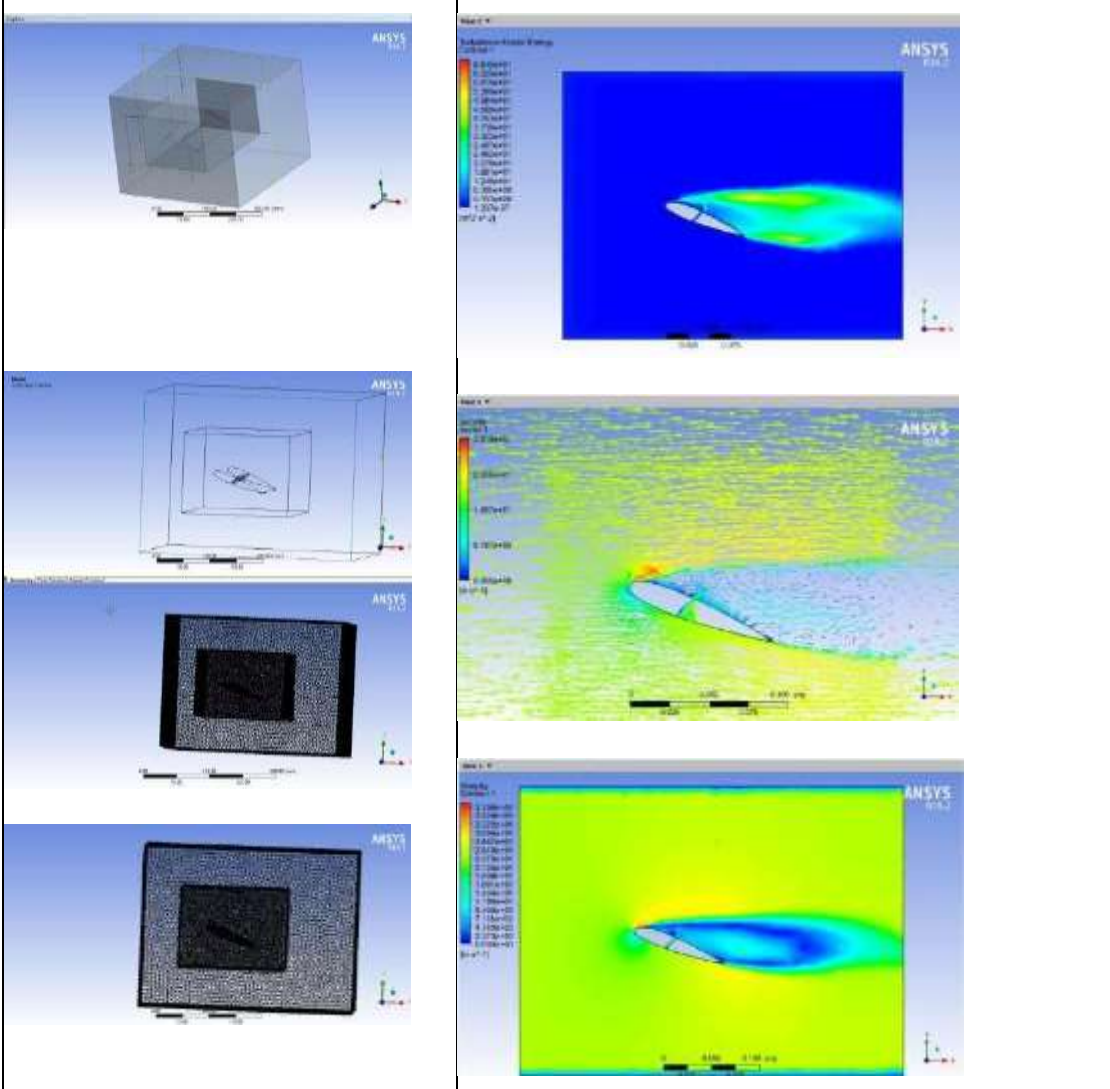
➤ FLOW SEPEARTION OF NACA23015WV

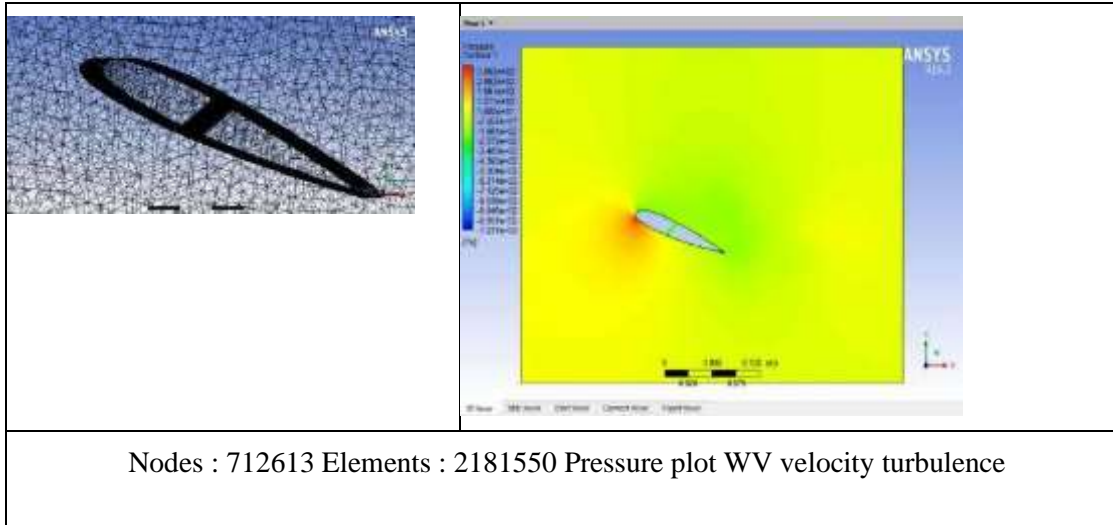




Nodes : 618713 Elements : 2151549 Pressure plot WV velocity turbulence

➤ FLOWSEPERATIONOF NACA23012WV





Considering the best airfoils the below given data are validated.

21012			WVOV CFD		WVOV EXP		WVCFD		WVEXP		CFDVSEXPPwv	WVOV EXP vsWVEXP	DIFF
S.NO	AO A	V	CL	CD	CL	CD	CL	CD	CL	CD	%ofdiffernce	%ofdiffernce	DIFF
1	0	5	0.02	0.3	0.03	0.0418	0.05	0.0479	0.052	0.048	3.921568627	53.658536 F59	0.022
2	5	5	0.36	0.035	0.38	0.0421	0.41	0.0481	0.42	0.0485	2.409638554	10	0.04
3	10	5	0.6	0.054	0.72	0.0648	0.69	0.0674	0.73	0.068	5.633802817	1.3793103 45	0.01
4	15	5	0.72	0.132	0.74	0.139	0.75	0.124	0.78	0.129	3.921568627	5.2631578 95	0.04
5	20	5	0.48	0.184	0.49	0.188	0.81	0.1794	0.82	0.182	1.226993865	50.381679 39	0.33
6	25	5	0.39	0.196	0.4	0.203	0.71	0.187	0.72	0.193	1.398601399	57.142857 14	0.32
7	0	10	0.05	0.0221	0.06	0.0227	0.08	0.031	0.083	0.032	3.680981595	32.167832 17	0.023
8	5	10	0.42	0.0225	0.44	0.0229	0.49	0.0314	0.51	0.0322	4	14.736842 11	0.07
9	10	10	0.98	0.0345	0.99	0.0353	1.11	0.0451	1.14	0.0459	2.666666667	14.084507 04	0.15
10	15	10	1.05	0.064	1.08	0.0657	1.15	0.0821	1.18	0.0827	2.575107296	8.8495575 22	0.1
11	20	10	0.85	0.087	0.89	0.0889	1.21	0.0794	1.23	0.0817	1.639344262	32.075471 7	0.34
12	25	10	0.69	0.103	0.7	0.109	0.72	0.124	0.75	0.128	4.081632653	6.8965517 24	0.05

13	0	15	0.1	0.024	0.13	0.0228	0.14	0.03	0.2	0.0321	3.29411765	42.424242 42	0.07
14	5	15	0.55	0.026	0.57	0.029	0.58	0.0314	0.6	0.0322	3.38983508	5.1282512 8	0.03
15	10	15	1.16	0.043	1.18	0.049	1.18	0.0541	1.2	0.0549	1.680672269	1.6806722 69	0.02
16	15	15	1.21	0.073	1.25	0.077	1.26	0.0842	1.29	0.0848	2.352941176	3.1496062 99	0.04
17	20	15	0.74	0.106	0.78	0.112	1.28	0.103	1.31	0.107	2.316602317	50.717703 35	0.53
18	25	15	0.7	0.126	0.71	0.129	0.75	0.142	0.79	0.146	5.194805195	10.666666 67	0.08
19	0	20	0.13	0.017	0.18	0.0193	0.19	0.016	0.2	0.018	2.12825128	10.526315 79	0.02
20	5	20	0.62	0.018	0.66	0.0194	0.65	0.0168	0.67	0.0184	3.030303	1.5037593 98	0.01
21	10	20	1.2	0.029	1.23	0.03	1.24	0.031	1.26	0.034	1.6	2.4096385 54	0.03
22	15	20	1.21	0.063	1.28	0.0641	1.3	0.0784	1.32	0.084	1.526717557	3.0769230 77	0.04
23	20	20	0.79	0.094	0.88	0.0952	1.35	0.0846	1.36	0.0984	0.73800738	42.857142 86	0.48
24	25	20	0.71	0.106	0.78	0.119	0.87	0.113	0.91	0.125	4.494382022	15.384615 38	0.13
25	0	25	0.15	0.014	0.19	0.018	0.2	0.028	0.21	0.029	4.87804878	10	0.02
26	5	25	0.69	0.016	0.7	0.0183	0.71	0.0284	0.73	0.0291	2.777777778	4.1958041 96	0.03
27	10	25	1.23	0.014	1.25	0.016	1.24	0.0278	1.28	0.0283	3.174603175	2.3715415 02	0.03
28	15	25	1.25	0.011	1.2	0.013	1.29	0.0272	1.35	0.0278	4.545454545	11.764705 88	0.15
29	20	25	0.8	0.009	0.83	0.011	1.3	0.0267	1.33	0.0272	2.281368821	46.296296 3	0.5
30	25	25	0.7	0.007	0.81	0.009	0.79	0.264	0.82	0.271	3.726708075	1.2269938 65	0.01

**Table43 : 21012 Percentage difference for Both the cases Experimentally and Cfd**

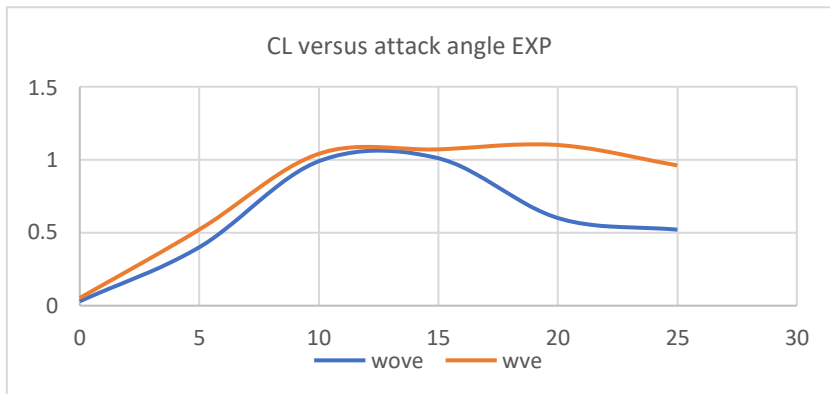


Figure 520 : Experimental CL vs AOA 21012 Airfoil with and with outvent.

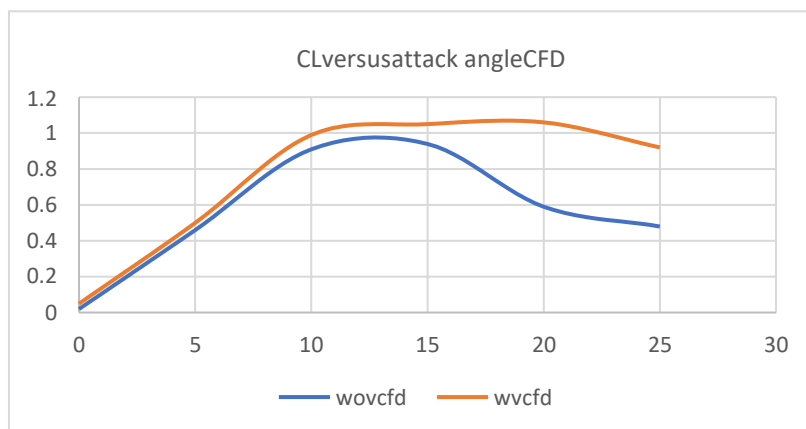


Figure 521 : CFD for 21012 Airfoil with and with out vent at velocities Comparison Five m/s

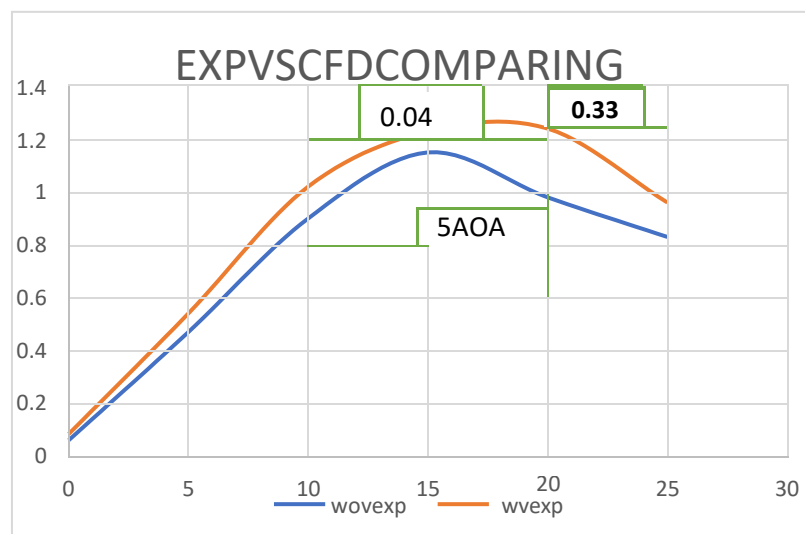


Figure 522 : 21012 with and with out vent experimentally at velocities Ten m/s

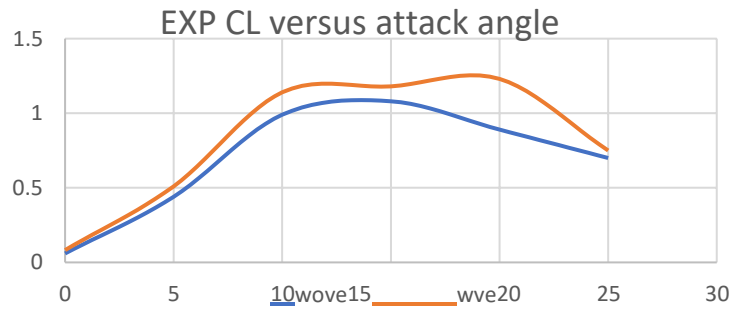


Figure 523 : Experimental for 21012 with and withoutvent

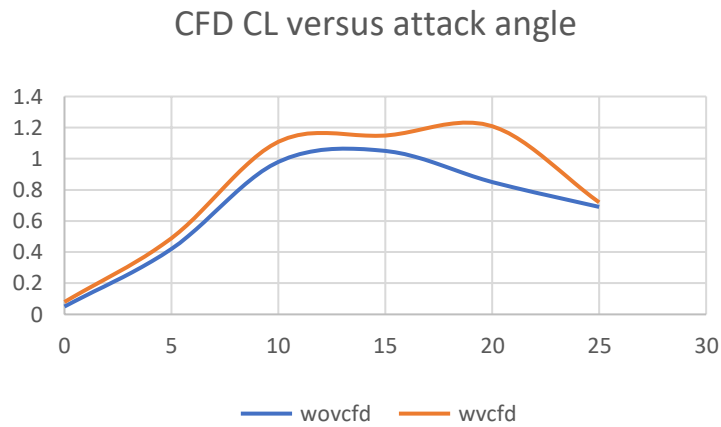


Figure 524 : CFD for21012 with and with out vent comparison

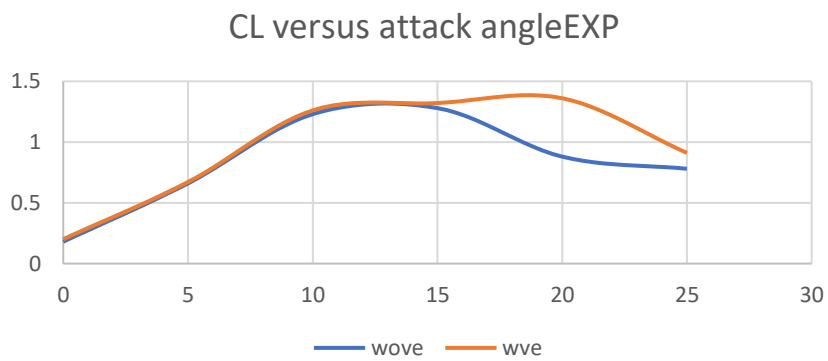


Figure 525 : Experimental for21012 with and without vent at velocities Twenty m/s



### CL VERSUS ATTACK ANGLECFD

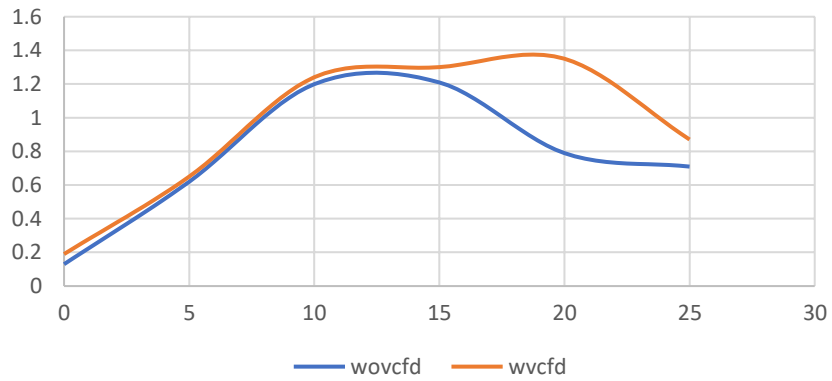


Figure 526 : Cfd for 21012 with and with out vent at velocities : Twenty m/s

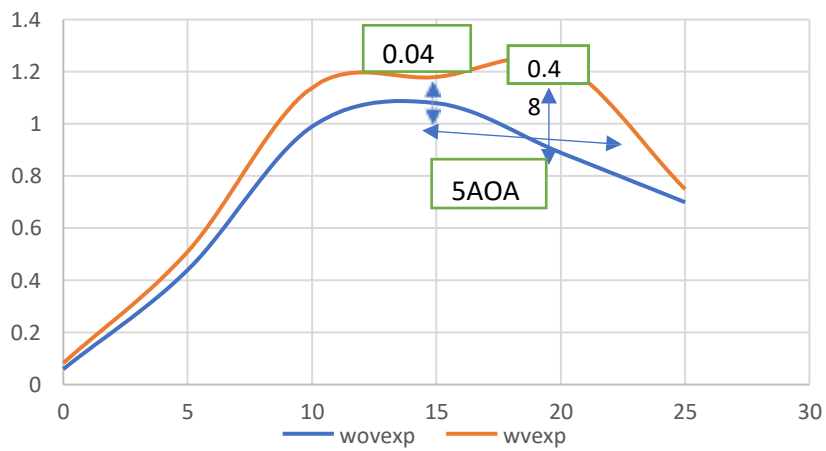


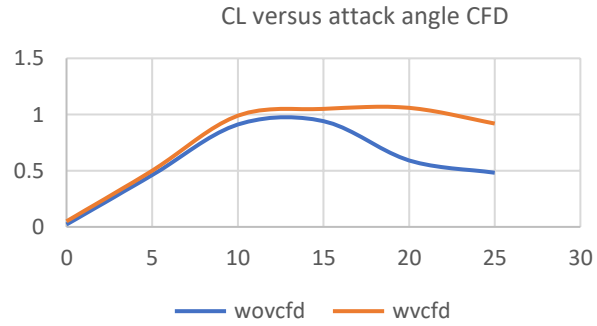
Figure 527 : Experimentally for 21012 with and with outvent comparison at velocities Twenty m/s

S.NO	AOA	V	WOV CFD		WOV EXP		WVCFD		WVEXP		CFDVSEXP <sub>wv</sub>	WOV EXP vsWVEXP	DIFF
			CL	CD	CL	CD	CL	CD	CL	CD			
1	0	5	0.02	0.3	0.03	0.0418	0.05	0.0479	0.051	0.048	1.98019802	51.85185185	0.021
2	5	5	0.46	0.026	0.4	0.029	0.5	0.032	0.52	0.058	3.921568627	26.08695652	0.12
3	10	5	0.91	0.043	0.99	0.052	0.99	0.054	1.04	0.064	4.926108374	4.926108374	0.05
4	15	5	0.94	0.13	1.01	0.098	1.05	0.18	1.07	0.194	1.886792453	5.769230769	0.06

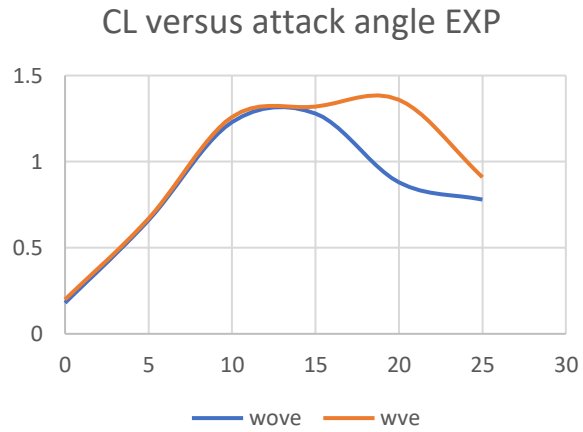
5	20	5	0.59	0.23	0.6	0.24	1.06	0.26	1.1	0.276	3.703703704	58.82352941	0.5
6	25	5	0.48	0.32	0.52	0.35	0.92	0.39	0.96	0.365	4.255319149	59.45945946	0.44
7	0	10	0.05	0.0221	0.06	0.0227	0.08	0.031	0.083	0.032	3.680981595	32.16783217	0.023
8	5	10	0.45	0.019	0.47	0.021	0.52	0.027	0.54	0.0386	3.773584906	13.86138614	0.07
9	10	10	0.89	0.025	0.9	0.028	0.99	0.037	1.02	0.0485	2.985074627	12.5	0.12
10	15	10	0.95	0.086	1.15	0.094	1.18	0.098	1.23	0.0957	4.149377593	6.722689076	0.08
11	20	10	0.61	0.16	0.98	0.13	1.21	0.17	1.24	0.19	2.448979592	23.42342342	0.26
12	25	10	0.49	0.23	0.83	0.28	0.93	0.32	0.96	0.39	3.174603175	14.52513966	0.13
13	0	15	0.1	0.024	0.13	0.0228	0.14	0.03	0.2	0.0321	35.29411765	42.42424242	0.07
14	5	15	0.56	0.018	0.59	0.012	0.69	0.021	0.71	0.0354	2.857142857	18.46153846	0.12
15	10	15	1	0.032	1.05	0.027	1.09	0.039	1.13	0.058	3.603603604	7.339449541	0.08
16	15	15	1.07	0.058	1.1	0.049	1.16	0.062	1.21	0.0795	4.219409283	9.523809524	0.11
17	20	15	0.98	0.116	0.99	0.13	1.23	0.18	1.28	0.21	3.984063745	25.55066079	0.29
18	25	15	0.86	0.24	0.96	0.192	1.1	0.213	1.13	0.22	2.69058296	16.26794258	0.17
19	0	20	0.13	0.017	0.18	0.0193	0.19	0.016	0.2	0.018	5.12820128	10.52631579	0.02
20	5	20	0.63	0.015	0.67	0.017	0.77	0.024	0.8	0.0289	3.821656051	17.68707483	0.13
21	10	20	1.1	0.021	1.15	0.026	1.4	0.0286	1.45	0.0348	3.50877193	23.07692308	0.3
22	15	20	1.15	0.043	1.32	0.048	1.35	0.058	1.37	0.0684	1.470588235	3.717472119	0.05
23	20	20	0.99	0.058	1.31	0.06	1.36	0.068	1.39	0.0798	2.181818182	5.925925926	0.08
24	25	20	0.89	0.065	0.97	0.069	1.1	0.072	1.15	0.0895	4.444444444	16.9811328	0.18
25	0	25	0.15	0.014	0.19	0.018	0.2	0.028	0.21	0.029	4.87804878	10	0.02
26	5	25	0.79	0.025	0.83	0.021	0.92	0.027	0.95	0.029	3.2855615	13.48314607	0.12
27	10	25	0.89	0.031	0.9	0.028	1.05	0.0316	1.11	0.0384	5.555556	20.89552239	0.21
28	15	25	0.75	0.048	0.77	0.052	1.08	0.062	1.13	0.068	4.224886878	37.89473684	0.36

29	20	25	0.73	0.058	0.75	0.064	1.12	0.069	1.16	0.072	3.50877193	42.931937 17	0.41
30	25	25	0.64	0.128	0.7	0.07	1.03	0.078	1.06	0.83	2.870813397	40.909090 91	0.36

**Table44 : 23012 Percentage difference for Both the cases Experimentally and Cfd**



**Figure 528 : Cfd for 23012withand with out vent Five m/s**



**Figure 529 : Experimental with and without vent comparison Five m/s**

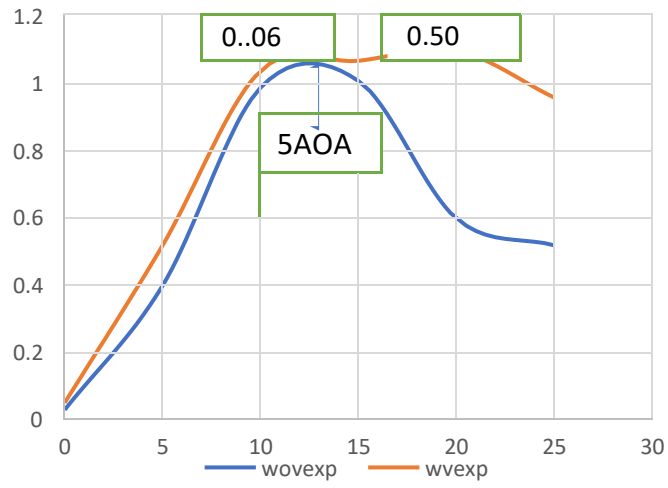


Figure 530 : Experimental for 23012 with and without vent Ten m/s

### CL versus attack angle CFD

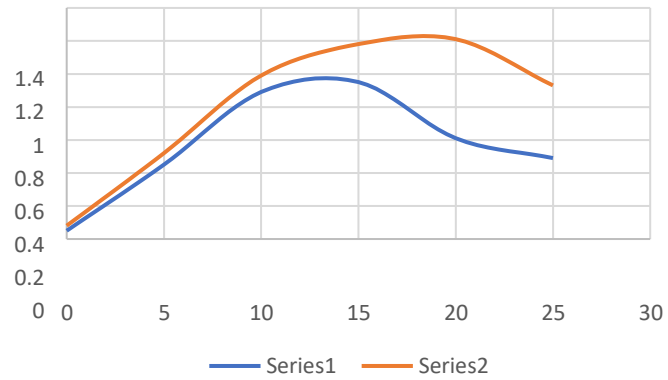


Figure 531 : Cfd for 23012 CL versus attack angle CFD

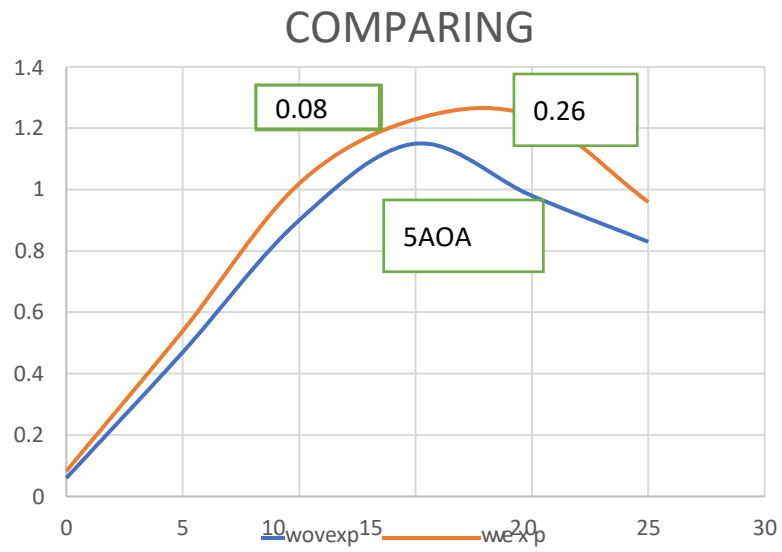


Figure 532 : 23012 Comparing Experimental without vent with vent at 20m/s

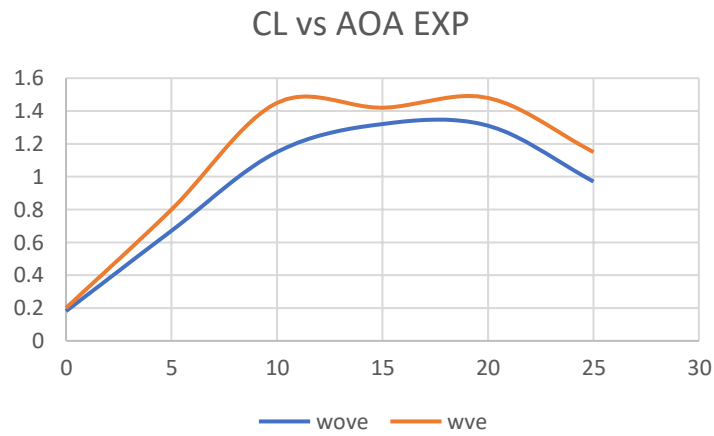


Figure 533 : 23012 Experimental CL vs AOA Twenty m/s

### CL versus attack angle CFD

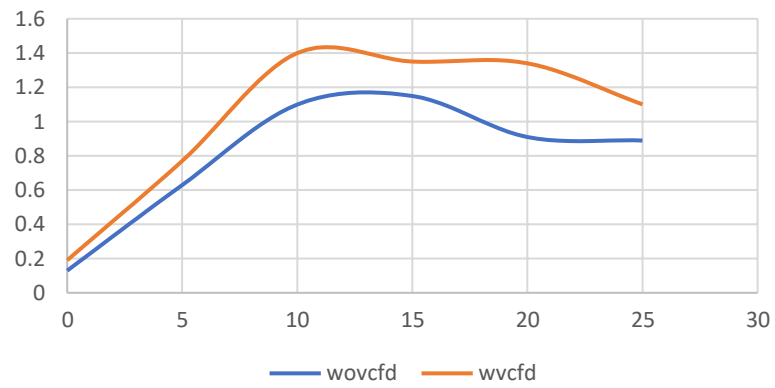


Figure 534 : 23012withoutventandwithventcfddcomparisonTwenty m/s

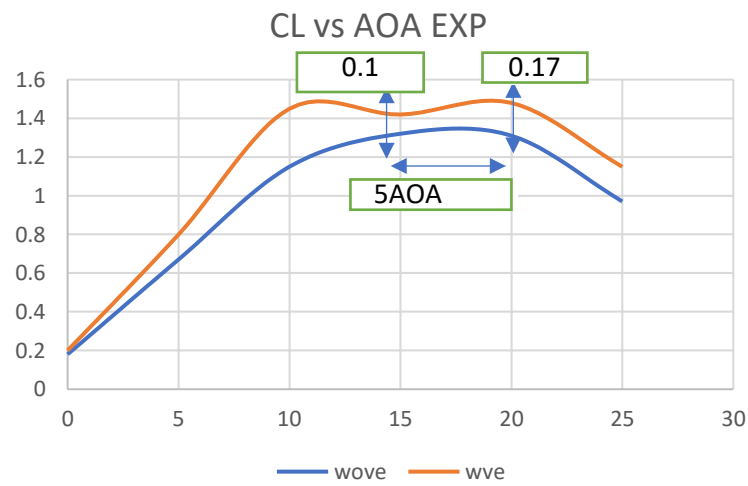


Figure 535 :CL vs AOA Experimental with vent and without vent at 20m/s

# Chapter7

## RESULTS AND DISCUSSION

### 7.1 RESULTS AND DISCUSSIONS

The velocity and pressure contours are described using the concepts that specify the air's velocity is carried through the domain in positive X direction, the air strike occurs at leading edge. The flow then travelled all across airfoil as a result velocity and pressure are dramatically lowered.

The pressure at the nose of the airfoil is three to four times that of the surrounding atmosphere. The top surface airflow is greater than the lower; the top surface generates a low pressure, while the lower creates a high amount of pressure.

Whenever the attack angle is raised, the lift force is increased continually until the stalling position is attained.

It is determined throughout the methodological process that the coefficient lift and lift force on vented airfoil sections raise while the coefficient of drag and drag force decrease. The passive technique, which employs airfoil vents, is beneficial for reattaching the separated boundary layer, allowing the airfoil to generate additional lift at 20° without the usage of high lift devices.

The vented airfoils are less effective at lower attack angle because the flow is de formed bythe vent, which reduces lift force and lift coefficient and increases drag force and drag coefficient. Inferring that the boundary layer is effectively reattached to the vented airfoils at higher attack angles compared to the original airfoil sections from the fact that vented airfoils are more useful at higher attack angles than lower. Only the vents efficient design and location are seen.

As this research primarily focuses on the ascent phase of an aircraft's mission profile, when take-off speed and attack angle are not very high, the AOAs and Velocities were constrained.

# Chapter8

## CONCLUSION

### 8.1 CONCLUSION

for all instances, the flow simulation through multiple airfoils is effective. The drag force, lift force, and parameters are effectively accomplished. for each case of observation, a plot for the velocity and pressure varies over the whole area.

This research aims to investigate a theoretical study on turbulence delay that covers ways applying passive techniques. This research thoroughly examines the suction approach, making boundary layer detachment simple. The flow delay of unique airfoils is tested by modifying velocities and vent locations in chord wise.

The beneficial location of vents found was nearly 1/4th of a chord wise. Vented aerofoil are beneficial at greater angles of attack. Only the specifications set and positioning of the vents were demonstrated in the outcomes.

According to the data, airfoils featuring vents exhibit lift force will greater, higher coefficient of lift compare to contemporary design. Vented airfoils also generate reduced drag force and a lower coefficient of drag when compared to their original counterparts. These findings suggest that at higher aoa, there appears a connection between upper surface of airfoil and employment of vent techniques, resulting in an enhancement of lift and a reduction in drag.

Research investigates methods for delaying turbulence in airflow over airfoils through passive techniques, with a focus on suction-based approaches. By preventing boundary layer separation using suction, the study aims to improve the Aerofoil performance particularly at high angles of attack where flow separation is more prevalent.

The study involves modifying velocities and vent locations along the chord wise direction of unique airfoils to determine the most effective configuration for turbulence delay. Through comprehensive flow simulations, the researchers analyse the effects of these modifications on lift force, drag force, and other aerodynamic parameters.

Results indicate that positioning vents approximately 1/4th of chord wise distance from LE of the airfoil yields most beneficial effects in terms of delaying turbulence. This positioning



helps maintain attached airflow over the airfoil surface, reducing flow separation and improving aerodynamic performance.

Furthermore, the study finds that airfoils featuring vents exhibit greater lift force and higher coefficients of lift compared to conventional designs. Additionally, vented airfoils demonstrate reduced drag force and lower coefficients of drag, indicating improved overall aerodynamic efficiency.

The findings suggest that employing vent techniques on airfoils can enhance lift and reduce drag, particularly at higher angles of attack. This connection between vent positioning and aerodynamic performance underscores the potential of passive techniques for improving the efficiency and effectiveness of airfoil designs in various applications, from aircraft wings to turbine blades.

## 8.2 FUTURE PERSPECTIVE

The flow simulation across the various airfoils comprises several situations observing at a greater attack angle, i.e., 25 degrees, to analyze coefficients of lift and drag in connection to the precise efficiency of results produced by vented airfoils against conventional airfoils. Making a 3D model of the vented airfoil to compare its performance to that of a standard wing. The study focusing on flow simulations across various airfoils, particularly at a high attack angle of 25 degrees, presents a significant step forward in understanding aerodynamic behaviors and optimizing airfoil designs. As we look ahead, several future perspectives emerge that could further enhance our understanding and application of aerodynamics.

**1. Advanced Computational Techniques:** Advancements in (CFD) and numerical method offer opportunities refine and expand scope aerodynamic simulations. High-fidelity simulations with improved accuracy and computational efficiency will enable more detailed analysis of complex flow phenomena, including turbulence, separation, and vortex shedding, thereby providing deeper insights into airfoil performance.

**2. Multi-Objective Optimization:** Future research can focus on Utilizing multi-objective optimization methods to optimize multiple performance metrics simultaneously such as lift-to-drag ratio, stall margin, and structural integrity. By considering a broader range of design objectives, including aerodynamic efficiency, stability, and structural robustness, engineers can develop airfoil designs that offer superior overall performance across various operating conditions.

**3. Active flow control :** Investigating potential of this control techniques, such as boundary layer suction, plasma actuators, and synthetic jets, could lead to innovative approaches for enhancing airfoil performance. By dynamically manipulating the airflow surrounding the airfoil surface, active flow control mechanisms can mitigate flow separation, delay stall onset, and improve overall aerodynamic efficiency, particularly at high angles of attack.

**4. Experimental Validation :** While computational simulations provide valuable insights, experimental validation remains essential for verifying and refining numerical models. Future research efforts should focus on conducting comprehensive wind tunnel tests and flight trials to validate the findings of computational studies and assess the real-world performance of vented airfoils under varying operating conditions.

**5. Integration with Additive Manufacturing:** The advent of additive manufacturing technologies opens new possibilities for rapid prototyping and customization of airfoil designs. By integrating advanced manufacturing techniques with aerodynamic analysis tools, engineers can explore novel geometries and configurations that were previously impractical

or impossible to manufacture, thereby unlocking new frontiers in airfoil design and optimization.

**6. Application in (UAVs) and (UAM) :** As the demand for unmanned aerial vehicles (UAVs) and (UAM) platforms continues to grow, there is a pressing need for aerodynamically efficient airfoil designs tailored to the unique requirements of these emerging applications. Future research can focus on developing specialized airfoils optimized for UAVs and UAM vehicles, considering factors such as agility, stability, and energy efficiency in urban environments.

**7. Environmental Considerations:** With increasing emphasis on sustainability and environmental stewardship, future airfoil designs will likely prioritize energy efficiency and reduced environmental impact. Research efforts can explore innovative materials, coatings, and design concepts aimed at minimizing drag, reducing fuel consumption, and mitigating emissions, contributing to a more sustainable aviation industry.

Researchers and engineers can continue to push the boundaries of airfoil design and optimization, driving progress in aerospace engineering and shaping the future of flight.

APPENDIX1

Figure 7.1 Wing model with the inclined vents maintain equal distance



APPENDIX2



Figure 7.2 Wing model with the straight vents maintain equal distance facility

# **Annexures**

## **A.References**

- 1 Aleman, A. M., Saini, A., &Gopalarathnam, a. A. (2017). Airfoil Flow-Separation and Stall Detection Using Surface-Mounted Pitot Tubes. In p. 3. In 35th AIAA Applied Aerodynamics Conference(Ed.).doi : <https://doi.org/10.2514/6.2017-3749>
- 2 Ali, F. E., Nichkoochi, L., Salarian, H., &Khaleghinia., a. J. (2019). Comparative study of flow separation control using suction and blowing over an airfoil with/without flap.*Springer*,220(15),5674-5688.doi : [10.1177/0954410019854628](https://doi.org/10.1177/0954410019854628)
- 3 Asi, K., M. I., Jahan, N., Akib, Y. M., & Mili., a. M. (2021). Numerical Simulation and Comparative Study of Aerodynamic Performance of Kline Fogle man Modified Backward Stepped Airfoils and the NACA 4415 Airfoil. *Bangladesh Maritime Journal (BMJ)*, 5(1),97-110.
- 4 Avraham, Seifert, A., D., Wyganski, & Israel. (1996). Delay of airfoil stall by periodic excitation *Journal ofaircraft*,33.4,691-698.
- 5 Azim, R. M., Ali, M., & Mohammad, a. H. (2015). Numerical investigation on the delay of boundary layer separation by suction for NACA 4412. *ELSEVIER*, 105, 329-334.doi : [10.1016/j.proeng.2015.05.013](https://doi.org/10.1016/j.proeng.2015.05.013)
- 6 Aziz, B., Abdullah, M., & Islam., a. M. (2017). Effect of Lower Surface Modification on Aerodynamic Characteristics of an Airfoil. International Conference on Mechanical Engineering and RenewableEnergy.
- 7 Azize,&Akçayoglu.(2011).Flowpastconfineddelta-wingtypevortexgenerators. *Elsevier*,35(1),112-120.doi : [10.1016/j.expthermflusci.2010.08.012](https://doi.org/10.1016/j.expthermflusci.2010.08.012)
- 8 Bur, Reynald, Coponet, D., & Carpels, a. Y. (2003). Separation control by vortex generator devices in a transonic channel flow. *Shock Waves* 19, no. 6, 521-530.doi : [10.1007/s00193-009-0234-6](https://doi.org/10.1007/s00193-009-0234-6)
- 9 Chaudhry, I. A., Sultan, T., A, S. F., Farhan, M., & Asim, M. (2017). The flow separation delay in the boundary layer by induced vortices. *springer*, 20(7), 251-261.doi : [10.1007/s12650-016-0396-0](https://doi.org/10.1007/s12650-016-0396-0)
- 10 Chris, Critzos, C., Heyso, H, H., & Robert, W. B. (1955). Aerodynamic characteristics ofNACA 0012 airfoil section at angles of attack from 0 degrees to 180 degrees No. NACA-TN-3361). *NATIONAL ADVISORY COMMITEE FOR AERONAUTICS TECHNICAL NOTE3361*,pp.1-21.
- 11 Ciobaca, V., Kühn, T., Rudnik, R., Bauer, M., Gölling, B., & Breitenstein, W. &. (2013).Active Flow-Separation Control on aHigh-Lift.50no1,5672.doi : [10.2514/1.C031659](https://doi.org/10.2514/1.C031659)
- 12 D, Y., & P., M. (2008). Active control of flow separation over an airfoil using synthetic jets. *Journal of Fluids and Structures*, 24(8), 1349–1357.doi : [10.1016/j.jfluidstructs.2008.06.017](https://doi.org/10.1016/j.jfluidstructs.2008.06.017)

- 13 Darabi, A., &Wyganski. (2012). Delay of airfoil stall by periodic excitation. *Journal of Aircraft.Aerospacere searchcentral,33(4),691–698*.doi : 10.2514/3.47003
- 14 Farokhi, & Sad, R. B. (2012.). ON THE AERODYNAMICS AND PERFORMANCE OF ACTIVEVORTEX GENERATORS. (pp. 376-386). 1th Applied Aerodynamics Conference, p. 3447.doi : 10.2514/6.1993-3447
- 15 Filho, D., Carlos, A., Cerón- Muñoz, H., & Catalano., a. F. (2013). Experimental study ofthe influence of vortex generators on airfoils for wind turbines. (pp. 1-12). In VI Congreso Internacional de Ingenieria Mecanica y IV de Ingenieria Mecatronica IV Congreso Internacional de Materiales, Energiay Medio Ambiente..
- 16 Gopinathan, T., & Ganesh, V. M. (2015). Passive Flow Control over NACA0012 Aerofoilusing Vortex Generators. *International Journal of Engineering Research & Technology,4(9),674-678*.
- 17 Guangyin, Z., Li, Y., Liang, H., Han, M., & Wu, a. Y. (2015). Flow separation control onswept wing with nanosecond pulse driven DBD plasma actuators. *Chinese Journal ofAeronautics,28,no.2,368-376*.
- 18 Hedy, A., Walker, & David. (2005). Boundary-layer separation control using localsuctionandinjection.*4thAIAAtheoretical FluidMechanics Meeting*.
- 19 Heughan, D. M. (1953). An Experimental Study of a Symmetrical Aerofoil with a Rear Suction Slot and a Retractable Flap. *The Aeronautical Journal 57, no. 514, 627-645*.doi : 10.1017/S0368393100126719
- 20 Jesline, J., Ibrahim, I. H., & New, a. T. (2016). Numerical investigation on flow separation control of low Reynolds number sinusoidal aerofoils. *In 46th AIAA Fluid DynamicsConference,p.3949*.doi : <https://doi.org/10.2514/6.2016-3949>
- 21 Jie, T., Yang, Y., Li, Y., & Cao., a. D. (2021). A 6-DOF micro-vibration isolation plat formbasedonthequasi-zero-stiffnessisolator.235(22).doi : 10.1177/0954406221101083
- 22 Jose, Rodriguez, Rothan, & Dominique. (1993). Low Reynolds Number Laminar Separation Bubble Control Using a Backward Facing Step. *SAE Transactions, 1892-1900*.doi : 10.4271/932572
- 23 Kabir, A., Akib, M., Hafiz, Y. A., & M, I. (2019). Comparison between two Kline Fogleman Modified (KFm) based Stepped Airfoils for better Aerodynamic Performance. *IEEEExplore*. doi : 10.1109/ICIET48527.2019.9290506

- 24 Kabir, A., Akib, Y. M., Hasan, M., & Islam, a. M. (2021). Comparison between two Kline–Fogleman Modified (KFm) based Stepped Airfoils for better Aerodynamic Performance. *IEEE*, 2324(1). doi : 10.1063/5.0037582
- 25 Kalkur., M. A. (2017). Enhancement of Aerodynamics of Airfoils by Surface Modifications – Numerical Study. *International Journal of Scientific Development and Research*, 2(8), 169-173.
- 26 Kung-Ming, C., Su, K.-C., & Chang., a. K.-C. (2021). The effect of vortex generators on shock-induced boundary layer separation in a transonic convex-corner flow. 8(6), 2-11. doi : 10.3390/aerospace8060157
- 27 Lin, J. c., Howard, F. G., & Selby, G. (1990). Small submerged vortex generators for turbulent flow separation control. *Journal of Spacecraft and Rockets*, 503-507. doi : 10.2514/3.26172
- 28 Lin, John, Howard, F., & Selby., a. G. (2012). Turbulent flow separation control through passive techniques. *2nd shear flow conference*, (p. 976). Aerospace research centralsociety. doi : 10.2514/6.1989-976
- 29 M, A., Smith, Kibens, D. R., Parekh, V., & A, D. E. (2001). Aerodynamic flow control over an unconventional airfoil using synthetic jet actuators. *AIAA Journal*, 39(3), 361-370.
- 30 Maniiarasan, P. (2015). Reduction of Skin Friction Drag in Wings by Employing Riblets. *International Journal of Engineering Research & Technology*, 4(7), 46-51.
- 31 Mashud, M. &. (2010). Experimental Study of Flow Separation Control of an Airfoil by Suction and Injection. *Proceedings of the 13th Asian Congress of Fluid Mechanics*, 166-169.
- 32 Melton, Pack, L., Yao, C. S., & Seifert., a. A. (2006). Active control of separation from the flap of a supercritical airfoil. *AIAA Journal* 44, no1, 34-41. doi : 10.2514/1.12225
- 33 Morice D, S. G., Geary, K., Baughn, S., Robinson, J., & K, a. S. (2020). Detection of Boundary Layer Separation and Implementation of Autonomous Vortex Generators. *In AIAA Scitech 2020 forum*, p. 0788., 1-9. doi : /10.2514/6.2020-0788
- 34 Nicholas, & N, F. (2015). Passive Flow Control Applied to a NACA23012 Airfoil In A Subsonic Flow. *AIAA Aviation American Institute of Aeronautics and Astronautics*, 1-15. doi : 10.2514/6.2015-2729
- 35 Patricia, C., Godard, G., Braud, C., & Stanislas., a. M. (2009). The flow structure behind vortex generators embedded in a decelerating turbulent boundary layer. *Journal of turbulence Taylor & Francis*, 10(N42). doi : 10.1080/14685240903273881



- 36 Paul, Ranjan, A., Mittal, A., & Jain, a. A. (2012). Slotted Flow Separation Control Over ANaca 2412 Airfoil. 39. At NIT, Surat, Gujarat, In Proceedings of 39th National Conference on Fluid Mechanics & Fluid Power.
- 37 Paul, Ranjan, A., Mittal, A., & Jain., a. A. (2012). Slotted Flow Separation Control Over ANaca 2412 Airfoil." In Proceedings of 39th National Conference on Fluid Mechanics & Fluid Power (FMFP-2012),39. NIT, Surat, Gujarat : Proceedings of the Thirty Ninth National Conference on Fluid Mechanics and Fluid Power.
- 38 Popov, Giuseppe, C., Ilya, R., Aleksandr, S., Andrei, H., Steven, V., & Leo. (2011). Flow Separation Control on Airfoil with Pulsed Nanosecond Discharge Actuator. *AIAA Aerospace research central*.doi : 10.2514/6.2011-1079
- 39 Rafael., B. (2020). Optimization of a columnar vortex generator installed over an aircraft carrier ski-jump ramp. *Proceedings of the Institution of Mechanical Engineers, Part M : Journal of Engineering for the Maritime Environment*, 234(1), 223-230.doi : 10.1177/147509021983890
- 40 Ramsay, James, Sellier, M., & Ho., a. W. (2020). Eliminating Boundary Layer Separation on a Cylinder with Non uniform Suction. *International Journal of Aerospace Engineering*.doi : 10.1155/2020/9137369
- 41 Rasedul, I. M., Hossain, M. A., Mashud, M., & Gias, a. M. (2013). Drag reduction of a carby using vortex generator. *International Journal of Scientific & Engineering Research*,4(7),1298-1302.
- 42 Robert, S., Babel, R., Grzywacz, A., Stryczniewicz, W., & Kowaleczko., a. G. (2018). The effect of using the Kline-Fogleman modification upon the coefficient characteristics of aerodynamic forces in the airfoil. *Sciend*, 25(2), 350-356.doi :10.5604/01.3001.0012.2854
- 43 S, D., KIMMEL, SEKELSKY, A. K., & SLOMSKI, J. (1992). Experimental evaluation of a 50-percent thick airfoil with blowing and suction boundary layer control. [*American Institute of Aeronautics and Astronautics Astrodynamics Conference*. - Hilton Head Island, SC,U.S.A.
- 44 S, S., & Karthikeyan, a. N. (2021). Flow Separation Control on a NACA-4415 Airfoil at Low Reynolds Number. *Proceedings of 16th Asian Congress of Fluid Mechanics*, 323-334.doi : 10.1007/978-981-15-5183-3\_35
- 45 Selcuk, S., & Choi., a. K.-S. (2017). *Active Leading-Edge Undulations Based on Plasma Vortex Generators*.
- 46 Serdar, G. M., Ünver, K., & Hüseyin, Y. (2011). Performance of transition model for predicting low aeroflow flows without/with single and simultaneous blowing and suction. , 30(2), 218–235. doi : .*European Journal of Mechanics-B/Fluids*, 30(2), 218-235.doi : 10.1016/j.euromechflu.2010.11.001

- 47 Shan, H., Jiang, L., Liu, C., Love, M., & Maines, B. (2008). Numerical study of passive and active flow separation control over a NACA0012 airfoil. *Computers and fluids*, 975-992.
- 48 Sonia, C., & Bharti., a. M. (2017). Design and Analysis of Vortex Generator and Dimple over an Airfoil Surface to Improve Aircraft Performance. 3(4), 173-181.
- 49 Součkov, N., Kuklová, J., Popelka, L., & Matějka, a. M. (2012). Visualization of flow separation and control by vortex generators on a single flap in landing configuration. In EPJ Web of Conferences (Ed.). 25 , pp. 02026-p2-p11. EPJ Web conferences. doi : 10.1051/epjconf/20122502026
- 50 Szwaba, Ryszard, Flaszynski, P., & Doerffer., a. P. (2019). Streamwise vortex generation by the rod. *Chinese Journal of Aeronautics*, 32(8), 1903-1911. doi : 10.1016/j.cja.2019.03.033
- 51 Takahashi, F., Hirotooshi, H., Miyashita, Miyamoto, J. Y., Sakai, K., Morita, & Yoshio. (1991). Aerodynamic Development of Boundary Layer Control System for NAL QSTOL Research Aircraft ASKA (No. 912010). *SAE Technical Paper*. doi : 10.4271/912010
- 52 The nambika, V., Ponsankar, S., & M, K. P. (2016). Design and flow analysis of S duct diffuser with submerged vortex generators. *International Journal of Engineering Research and Applications*, 6(2), 79-84. Retrieved from [https://www.ijera.com/papers/Vol6\\_issue2/Part%20-%205/N62057984.pdf](https://www.ijera.com/papers/Vol6_issue2/Part%20-%205/N62057984.pdf)
- 53 Traub, W., Jaybush, & Lance Logan, a. (2010). Experimental investigation of separation control using upper-surface spoilers. *Journal of aircraft*, 47(2), 714-718. doi : 10.2514/1.45434
- 54 Viswanat, & P. R. (2007). Some thoughts on separation control strategies. *Sadhana* 32, no. 1, 89-92.
- 55 Volino, & J, R. (2009). Separation control on low-pressure turbine airfoils using synthetic vortex generator jets. 36886, 845-859. doi : 10.1115/GT2003-38729
- 56 Xinkai, L., Yang, K., & Wang, a. X. (2019). Experimental and numerical analysis of the effect of vortex generator height on vortex characteristics and airfoil aerodynamic performance. 12(5). doi : 10.3390/en12050959
- 57 Yang, G., Wang, S., Liu, N., Lixian, Z., & Sinica, A. M. (1997). Control of unsteady vertical lift on an airfoil by leading-edge blowing-suction. *SPRINGER*, 13, 304-312. doi : 10.1007/bf02487189
- 58 Yokoyama, Hiroshi, Minato, T., Adachi, R., & Iida, a. A. (2017). Experimental and numerical investigations on control methods of cavity tone by blowing jet in an

upstream boundary layer. *INTER-NOISE and NOISE-CON Congress and Conference*, 254, no2, pp.168-176.

- 59 Yousefi, Kianoosh, S., Zahedi, R., & Peyman. (2013). Numerical Investigation of Suction and Length of Suction Jet on Aerodynamic Characteristics of the NACA 0012 Airfoil. *International Journal of Materials Mechanics and Manufacturing*, 1(2),10-24.
- 60 Yousefi, Saleh, K. &, Zahedi, R. &, & Peyman. (2013). Numerical Study of Flow Separation Control by Tangential and Perpendicular Blowing on the NACA 0012 Airfoil. *International Journal of Engineering. International Journal of Engineering (IJE)*, 7(1), 10-24.
- 61 Coskun, S., et al. "Control of Flow Separation over an airfoil by External Acoustic Excitation at a High Reynolds Number." *Physics of Fluids*, 36(1) (2024).
- 62 Hao, L., Y. Gao and B. Wei. "Experimental Investigation of Flow Separation Control over Airfoil by Upper Surface Flap with a Gap." *International Journal of Aeronautical and Space Sciences*, 23(5) (2022) : 859-869).
- 63 Nia, B. B., et al. "Passive control of boundary layer flow separation on a wind turbine airfoil using vortex generators and slot." *Ocean Engineering*, 283, 115170 (2023).
- 64 Svorcan, J., J. M. Wang and K. P. Griffin. "Current state and future trends in boundary layer control on lifting surfaces." *Advances in Mechanical Engineering*, 14(7), 16878132221112161. (2022).

## CERTIFICATE



Complete Training Solution to Aviation Industry  
(An ISO 9001 : 2015 Certified Aviation)

29-03-2022

**To whomsoever it may concern**

This is to certify that the vented hole Airfoils designed and developed by Ms. K Sai Priyanka research scholar Lovely professional University, has been manufactured, and tested in our facility.

Test carried out during the period - March 26<sup>th</sup> to 27<sup>th</sup> 2022

Wish her all success

A handwritten signature in black ink, appearing to be 'EPA', is written over a faint circular stamp.

**For Aerozjet  
Proprietor**

#261 C, 4th Phase, 407 Scheme, Yelahanka New Town, Bangalore-64  
#7 kaveri street, Vasanth Nagar, muthialpet, pondicherry-605003 india  
support@aerozjet.com, ceo@aerozjet.com  
8050020076, 8973021173

# PATENT

(12) PATENT APPLICATION PUBLICATION	(21) Application No.202211063303 A
(19) INDIA	
(22) Date of filing of Application :05/11/2022	(43) Publication Date : 18/11/2022
(54) Title of the invention : A SYSTEM OF FLOW SEPARATION DELAY VENT TECHNIQUE FOR AIRFOIL TO INCREASE ANGLE OF ATTACK	
(51) International classification :G01M0009040000, G01M0009060000, G01M0009020000, F03D0003060000, F03D0009250000	(71)Name of Applicant : <b>1)LOVELY PROFESSIONAL UNIVERSITY</b> Address of Applicant :JALANDHAR-DELHI G.T. ROAD, PHAGWARA, PUNJAB-144 411, INDIA. PHAGWARA
(86) International Application No :NA Filing Date :NA	Name of Applicant : NA Address of Applicant : NA
(87) International Publication No : NA	(72)Name of Inventor : <b>1)DR. J V MURUGA LAL JEYAN</b> Address of Applicant :LOVELY PROFESSIONAL UNIVERSITY, JALANDHAR-DELHI G.T. ROAD, PHAGWARA, PUNJAB-144 411, INDIA. PHAGWARA
(61) Patent of Addition to Application Number :NA Filing Date :NA	<b>2)MS. K.SAI PRIYANKA</b> Address of Applicant :LOVELY PROFESSIONAL UNIVERSITY, JALANDHAR-DELHI G.T. ROAD, PHAGWARA, PUNJAB-144 411, INDIA. PHAGWARA
(62) Divisional to Application Number :NA Filing Date :NA	
(57) Abstract : In this invention wind tunnels are used for flow analysis on a flying object for testing. The flow in the test section has to be uniformly streamlined and has to be parallel to the axis of the wind tunnel. The change in flow properties inside the tunnel with respect to the time should be negligible. However, prior to conducting a test process, the calibration of wind tunnel has to be done. Normally, calibration of subsonic wind tunnel is done by the vented wing models. By using this vented technique, it can delay stall at higher angle of attacks to get the positive lift and reduce drag. Henceforth, a new vented technique with varying distance between them holes are designed by overcoming the limitations.	
No. of Pages : 18 No. of Claims : 3	